Scientific Foundations

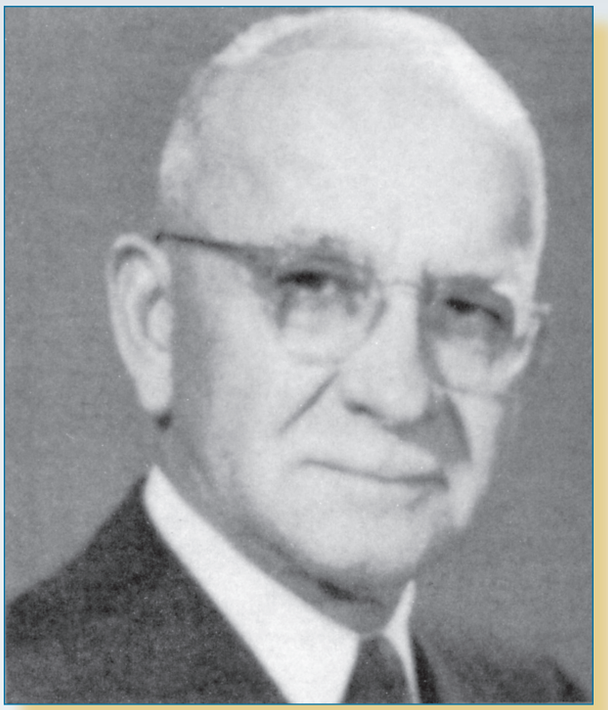

THEODORE H. BAST (1890–1959) • First described the utriculo-endolymphatic valve.

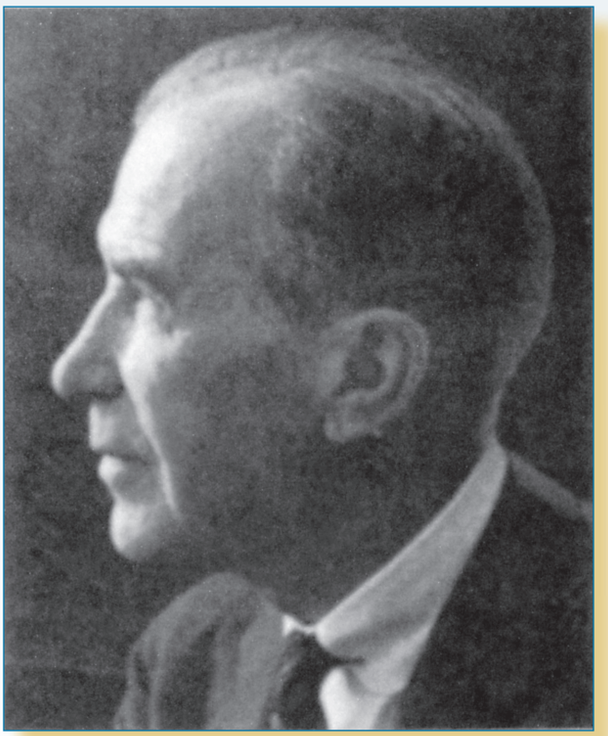

BARRY J. ANSON (1894–1974) • Student and investigator par excellence of the gross and microscopic anatomy of the temporal bone.

Developmental Anatomy of the Temporal Bone and Skull Base

1

Aina Julianna Gulya, MD, FACS

The complexity of nature's machinations is exemplified in the development of the ear, both in phylogenetic and ontogenetic terms. The labyrinth represents a parsimonious salvage and modification of the lateral line system of fish, whereas the ossicles originally participated in the masticatory apparatus of ancestral vertebrates.

As intriguing as the phylogeny of the ear is in an abstract sense, knowledge of its embryologic development is of crucial, concrete importance to the modern-day neurotologic surgeon. Management of major malformations of the ear, such as the manifestations of aural dysmorphogenesis, obviously demands such knowledge if a rational approach to the alleviation of associated hearing handicaps is to prevail. The surgeon who is able to anticipate more subtle irregularities of development, such as persistent stapedial arteries and high jugular bulbs, can confidently negotiate such potential hazards rather than fall prey to them.

This chapter presents a focused discussion of the development of the ear, emphasizing those features of particular surgical importance. The discussion begins with the most lateral structures of the temporal bone and progresses medially, just as a surgeon encounters these structures. The fetal ages are based on conversion of crown-rump measurements to postconceptual ages and thus may show some variations from figures based on alternative dating methods.

The reader interested in reviewing the pioneer works of Bast, Anson, Donaldson, Streeter, and Padget is referred to their referenced works. Comprehensive overviews of both phylogeny and anatomy are extant in such works as those by Gulya and Schuknecht,[1] Anson and Donaldson,[2] Pearson,[3] and Bast and Anson.[4]

DEVELOPMENT OF THE EXTERNAL EAR AND TEMPORAL BONE

External Ear

The development of the pinna commences at 4 weeks as tissue condensations of the mandibular and hyoid arches appear at the distal portion of the first branchial groove. Within 2 weeks, six ridges, known as the hillocks of His, arise from the tissue condensations (Figure 1–1). The significance of these hillocks varies, according to the investigator, from coincidental to integral to the development of the pinna. Accompanying these divergent views are studies that, on the one hand, suggest that the entire pinna except the tragus and anterior external auditory canal (of mandibular arch origin) arises from the hyoid (second branchial) arch.[5] Other studies demonstrate a balanced participation of both the first and second branchial arches in the development of the pinna.[3,6]

The hillocks fuse into an anterior fold of mandibular arch origin and a posterior fold of hyoid arch origin, oriented about the first branchial groove. The folds unite at the upper end of this groove (Figure 1–2).

Adult configuration (Figure 1–3) is achieved by the fifth month, independent of developmental progress in the middle

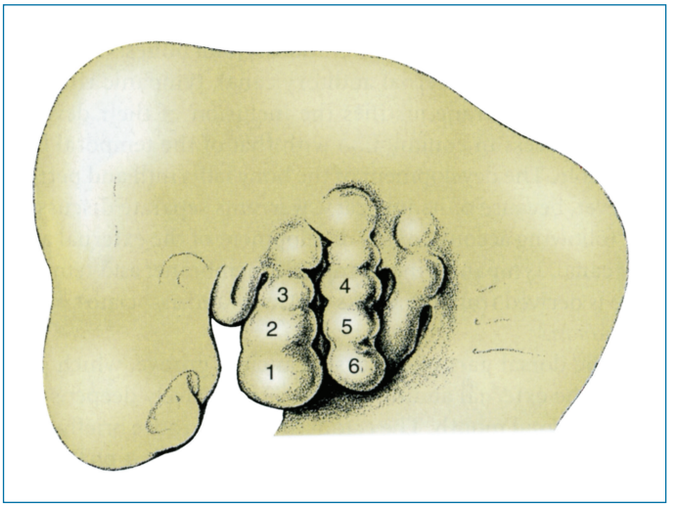

FIGURE 1-1 • The six hillocks of His at approximately 6 weeks. *After Levine.[6] Reproduced with permission from Gulya AJ. Gulya and Schuknecht's anatomy of the temporal bone with surgical implications. 3rd ed. New York: Informa Healthcare USA; 2007.*

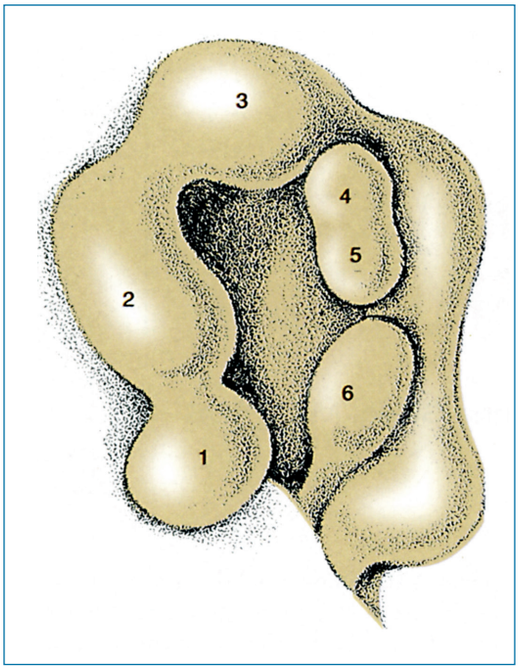

FIGURE 1–2 • At approximately 7 weeks, the six hillocks are fusing to form two folds, which will later fuse superiorly. *After Levine.*[6] *Reproduced with permission from Gulya AJ. Gulya and Schuknecht's anatomy of the temporal bone with surgical implications. 3rd ed. New York: Informa Healthcare USA; 2007.*

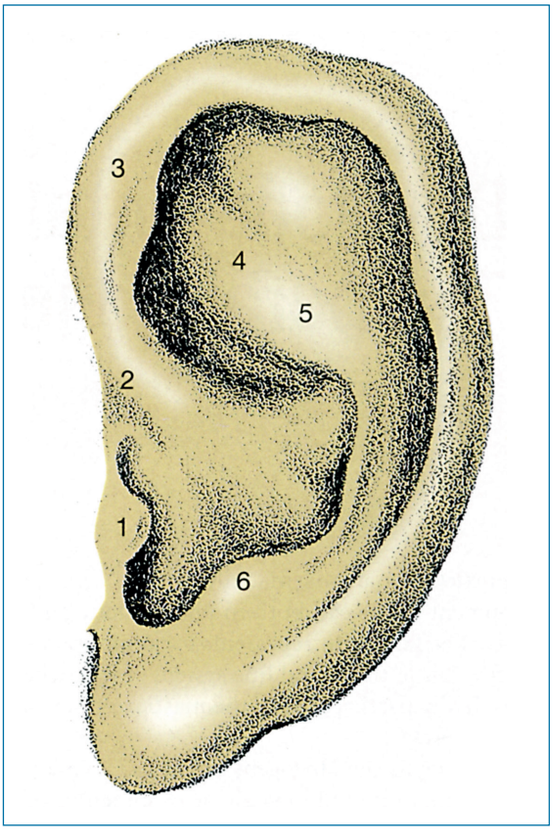

FIGURE 1–3 • The adult auricle with the derivatives of the six hillocks numbered. *After Levine.*[6] *Reproduced with permission from Gulya AJ. Gulya and Schuknecht's anatomy of the temporal bone with surgical implications. 3rd ed. New York: Informa Healthcare USA; 2007.*

and inner ears. The Darwinian tubercle, corresponding to the tip of the pinna in lower mammals, makes its appearance at roughly 6 months.

Temporal Bone, External Auditory Canal, Tympanic Ring, and Tympanic Membrane

The adult temporal bone is an amalgam of the squamous, petrous, mastoid, tympanic, and styloid bones. The close association of the external auditory canal, tympanic ring, and tympanic membrane justifies the inclusion of their developmental process in conjunction with that of the temporal bone as a whole. The development of the bony labyrinth and petrosa, however, because of its intricacy, warrants separate discussion. The following account of the development of the external auditory canal, tympanic ring, tympanic membrane, and temporal bone is derived from the works of Anson and associates[7] as well as Pearson.[3]

The dorsal part of the first branchial groove, which gives rise to the external auditory canal, progressively deepens during the second month. The ectoderm of the groove briefly abuts on the endoderm of the tubotympanic recess (first pharyngeal pouch), but during the sixth week, a mesodermal ingrowth breaks this contact. Beginning at 8 weeks, the inferior portion of the first branchial groove deepens again, forming the primary external auditory canal, which corresponds to the fibrocartilaginous canal of the adult. At the same time, development of the squama begins, marked by the appearance of a membranous bone ossification center. In the next week of development, a cord of epithelial cells at the depths of the primary external auditory canal grows medially into the mesenchyme to terminate in a solid (meatal) plate (Figure 1–4). The mesenchyme adjacent to the meatal plate gives rise to the lamina propria (fibrous layer) of the tympanic membrane and at 9 weeks is surrounded by the four membranous bone ossification centers of the tympanic ring. In addition to supporting the tympanic membrane, it has been theorized that the tympanic ring also functions to inhibit inward epithelial migration. Failure of this function may lead to cholesteatoma formation (ie, congenital cholesteatoma) at the junction of the first and second branchial arches.[8]

By the 10th week, the tympanic ring elements fuse except superiorly, where a defect remains, the notch of Rivinus. These elements then expand, accompanied by growth of the solid epithelial cord of cells. It is not until after the fifth month that the cord splits open, initially at its medial terminus, forming the bony external auditory canal by the seventh month. The cells remaining at the periphery form the epithelial lining of the bony external auditory canal, whereas those remaining medially form the superficial layer of the tympanic membrane. The medial layer of the tympanic membrane derives from the epithelial lining of the first pharyngeal pouch. These developmental changes in the external auditory canal occur at a time when the outer, middle, and inner ears are already well developed.

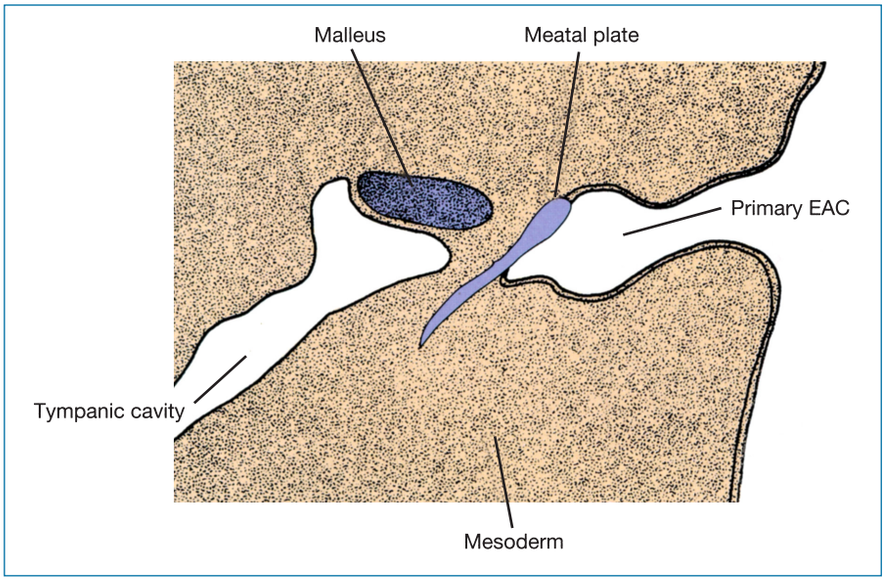

FIGURE 1–4 • The primary external auditory canal (EAC) is formed at 9 weeks with deepening of the first branchial groove. The meatal plate develops as epithelial cells grow medially toward the tympanic cavity. *After Anson and Donaldson.[2] Reproduced with permission from Gulya AJ. Gulya and Schuknecht's anatomy of the temporal bone with surgical implications. 3rd ed. New York: Informa Healthcare USA; 2007.*

Meanwhile, beginning at 4 months, the squama projects posterior to the tympanic ring, forming what will become the lateral (squamous) portion of the mastoid, roof of the external auditory canal, and lateral wall of the antrum. The medial (petrous) portion of the mastoid develops as air cells invade the periosteal layer of the bony labyrinth. The external petrosquamous fissure marks the junction of the petrosa with the squama and generally disappears by the second year of life.

The hypotympanum develops between 22 and 32 weeks as a tripartite bony amalgam[9] composed of the tympanic bone (membranous bone), the canalicular otic capsule (enchondral bone), and a petrosal ledge (periosteal bone). This variegated structure is thought to predispose this area to anomalous development, such as that which leaves bare the jugular bulb in the middle ear.

After the eighth month, the tympanic ring begins to fuse with the otic capsule, a process that is not completed until birth. Postnatally, lateral extensions of the tympanic ring and the squama (Figure 1–5) extend the external auditory canal and carry the tympanic membrane from the horizontal angulation of the neonate to the acute angulation of the adult (see Figure 1–5). The styloid process does not make its appearance until after birth, arising in an ossification center at the upper aspect of Reichert's cartilage.

Microtia, anotia, and aberrant positioning of the pinna derive from abnormal development of the first and second branchial arches. Developmental failure of the first branchial groove results in stenosis or atresia of the external auditory canal, based on either a lack of canalization of the meatal plate or a deficiency in epithelial ingrowth. The presence or absence of accompanying defects in the middle and inner ears depends on the time period at which development was disrupted.

Postnatal Development of the Temporal Bone

Although inner and middle ear structures have completed development long before birth, the mastoid and tympanic bones, in particular, manifest postnatal growth and development. Knowledge of these developmental changes is imperative for the otologic surgeon contemplating operative intervention in the very young pediatric patient or cochlear implantation in the profoundly deaf infant or child.

In the neonate, the squama is disproportionately large in comparison with that of the adult (Figure 1–6). The mastoid process is essentially nonexistent, and the tympanic bone is a relatively flat ring, rather than a cylinder. The relative position of the entire temporal bone in the neonate (see Figure 1–6) is inferolateral in comparison with the temporal bone in the adult and its more lateral orientation.

The facial nerve, in the absence of a mastoid process, exits the stylomastoid foramen to emerge on the lateral aspect of the skull and thus is especially vulnerable to injury if a standard postauricular incision is performed. After the first year of life, the mastoid process begins development both laterally and inferiorly, with the mastoid tip deriving from the petrous portion of the mastoid.[10] Similarly, the tympanic ring extends laterally, completing the formation of the bony external auditory canal, the sheath of the styloid process, and the nonarticular part of the glenoid fossa (see Figure 1–5). In the 1-year-old infant, opposing spurs of growing bone at the ventral aspect of the bony external auditory canal fuse, dividing the original external auditory canal into the adult external auditory canal and an inferior channel, known as the foramen of Huschke. The adult external auditory canal is cranial to, and larger than, the foramen of Huschke (see Figure 1–5). This secondary foramen closes in late childhood.[7] With these changes in the mastoid and tympanic bones, the lateral aspect of the temporal bone is vertically oriented, and the facial nerve is buried beneath the protective barrier of the mastoid process. The lateral growth of the tympanic ring, as mentioned previously, carries the tympanic membrane from the nearly horizontal orientation of the neonate to the adult angulation by age 4 or 5 years.

With a view toward cochlear implantation in the infant or young child, one study suggested that the dimensions that show

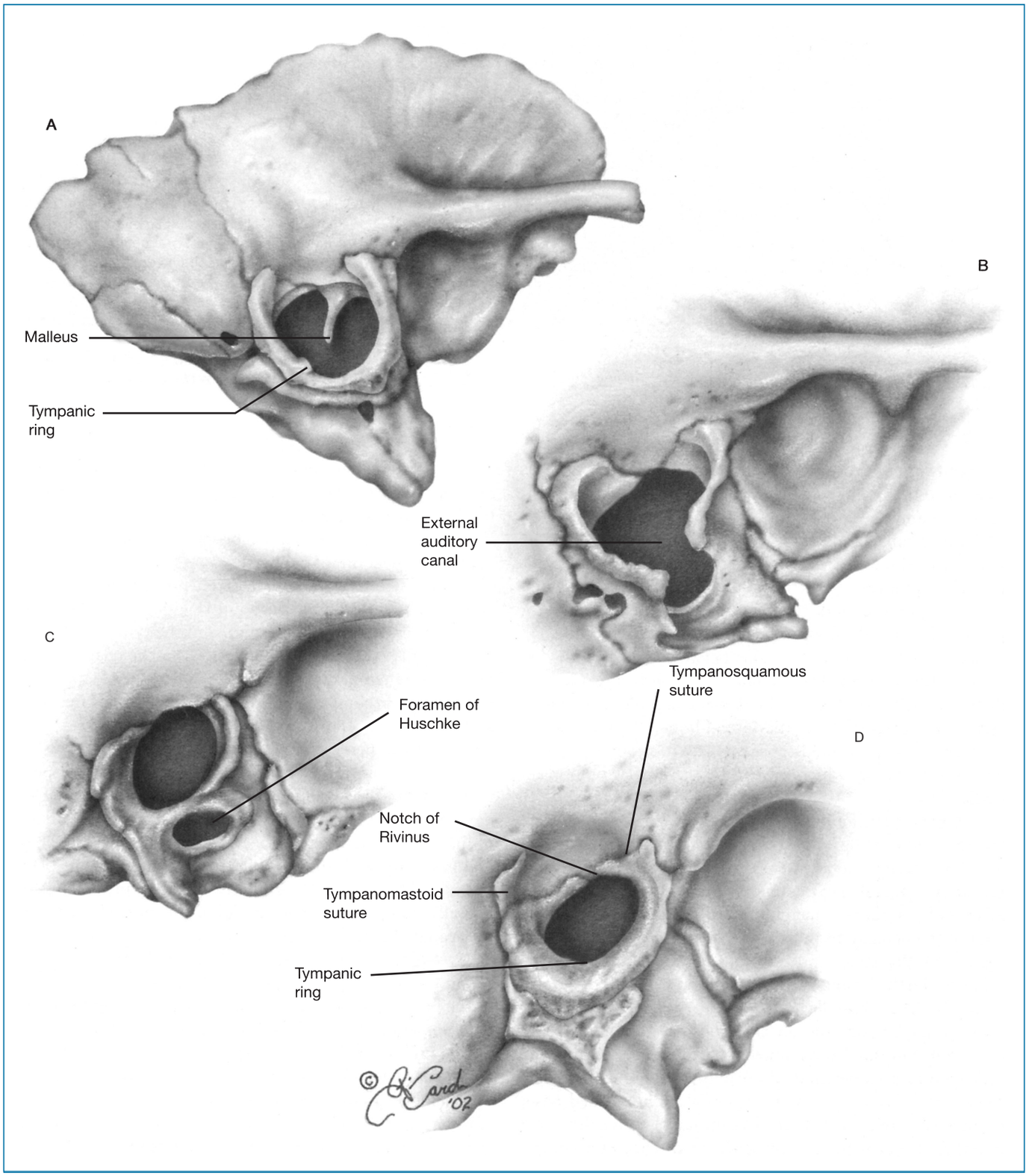

FIGURE 1–5 • Postnatal development of the tympanic portion of the temporal bone. *A*, Neonate. Note the flat tympanic ring and the exposed stylomastoid foramen. *B*, Infant, 11 months. The notch of Rivinus and the foramen of Huschke are becoming evident. *C*, Infant, 1 year. *D*, Adolescent. *After Anson BJ, Donaldson JA. Surgical anatomy of the temporal bone and ear. Philadelphia: WB Saunders; 1981.*

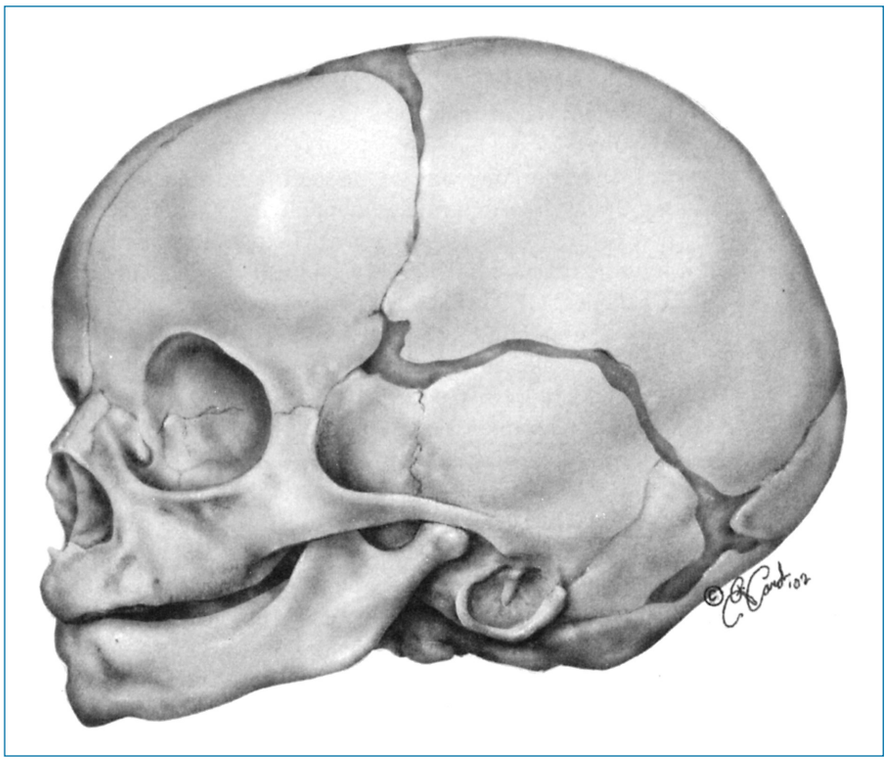

FIGURE 1–6 • The temporal bone of the infant, absent a mastoid process and laterally extending external auditory canal, is located more inferiorly on the skull than that of the adult.

significant growth, continuing into the teenage years, include the depth of the tympanic cavity (as measured by the distance between the tympanic membrane and the stapes footplate) and the length, width, and depth of the mastoid.[11] Cochlear wires, if reaching to the lateral skull, should be placed with approximately 2.5 cm of slack to accommodate anticipated growth. The facial recess, on the other hand, should be adult size at birth.[12]

DEVELOPMENT OF THE TYMPANOMASTOID COMPARTMENT AND EUSTACHIAN TUBE

The tympanomastoid compartment represents the phylogenetic salvage and functional adaptation of the aquatic gill apparatus, which transiently appears in the ontogeny of the human. As life forms evolved from a water environment to a terrestrial environment, a mechanism for matching the sound impedance of water with that of air became essential to auditory function. The middle ear and its contained ossicular chain serve this purpose. The first vestige of such an impedance-matching mechanism emerged as the spiracular diverticulum of the eusthenopteron (a crossopterygian fish).[13]

In the developing human, the tympanomastoid compartment appears at the 3-week stage as an outpouching of the first pharyngeal pouch known as the tubotympanic recess. The endodermal tissue of the dorsal end of this pouch eventually becomes the eustachian tube and tympanic cavity (Hammar, as cited in Proctor[14]). Expansion of the pouch begins at the inferior aspect of the definitive tympanic cavity and progresses by invasion of the adjacent mesenchyme, a loose, gelatinous derivative of mesoderm. By 7 weeks, concomitant growth of the second branchial arch constricts the midportion of the tubotympanic recess; according to Hammar (as cited in Proctor[14]), the primary tympanic cavity lies lateral and the primordial eustachian tube lies medial to this constriction. The terminal end of the first pharyngeal pouch buds into four sacci (anticus, posticus, superior, and medius[14]), which expand to progressively pneumatize the middle ear and the epitympanum. Expansion of the sacci envelops the ossicular chain and lines the tympanomastoid compartment, whereas the interface between two sacci gives rise to mesentery-like mucosal folds, transmitting blood vessels.

The further development of the eustachian tube is marked by its lengthening and narrowing, with mesodermal chondrification establishing the fibrocartilaginous eustachian tube. By the 21st week, pneumatization reaches the antrum. Although the tympanic cavity is essentially complete by 30 weeks, some configurational changes occur with finalization of the bony hypotympanum (see above).

Mastoid pneumatization is evident as early as 33 weeks and proceeds by well-established tracts.[15] Heredity, environment, nutrition, bacterial infection, and adequate ventilation provided by the eustachian tube are all thought to play a role in the interindividual variability of temporal bone pneumatization.[1]

By birth, the antrum approximates that of the adult. However, mesenchymal resolution may continue as late as 1 year postnatally,[16] or even later in some rare cases. Remnants of embryonic connective tissue in the adult are manifest as connective tissue strands draped over the oval and round windows.[10] Similarly, the mastoid continues to grow for up to 19 years after birth.[11]

Epitympanic fixation of the head of the malleus is a clinically encountered condition rooted in the incomplete pneumatization of the epitympanum.[17] Such bony fixation of the malleus is a normal occurrence in certain mammals.[18]

Alternative theories for the development of the middle ear have been proposed. Fraser (cited in Proctor[14]) suggested that the first, second, and third branchial arches, as well as the second branchial groove, give rise to the primitive tympanic cavity. Other workers suggested that the first pharyngeal pouch forms only the eustachian tube, whereas the remainder of the tympanomastoid compartment develops by the cavitation of mesenchyme.[19] In this scheme, mesenchymal derivatives, rather than the respiratory mucosa of the first pharyngeal pouch, form the lining of the middle ear.

DEVELOPMENT OF THE OSSICULAR CHAIN

The ossicular chain, a functional component of the middle ear impedance-matching mechanism, for the most part traces its phylogenetic roots to the branchial arch (gill slit) apparatus. In early vertebrates, the mesenchyme of branchial arches I (Meckel's cartilage, mandibular arch) and II (Reichert's cartilage, hyoid arch) was destined to become part of the masticatory apparatus. Evolutionary modifications that reduced the stresses on the jaw rendered certain of its components, namely, the articular and the quadrate, superfluous.[20] The malleus and the incus, respectively, are derived from these jaw components, whereas the origin of the stapes has been traced back to the columella auris of reptiles.

The first evidence of ossicular development in the human embryo occurs at approximately 4 weeks as an interbranchial bridge appears, connecting the upper end of that portion of the first branchial arch referred to as the mandibular visceral bar and the central region of the hyoid (second branchial arch) visceral bar. It is this condensed mesenchymal bridge, consisting of both first and second branchial arch elements, that through cartilaginous differentiation gives rise to the primordial malleus and incus.[21] All of the stapes blastema derives from the hyoid bar except for the medial surface of the footplate and its annular ligament, which are of otic capsular (lamina stapedialis) origin (Gradenigo, 1889, cited in Gulya and Schuknecht[1]) (Figure 1–7).

Over the following 11 weeks, the future ossicular chain continues growth and development as a cartilaginous model (see Figure 1–7); such formation of bone from a cartilage model is termed enchondral bone development (see "DEVELOPMENT OF THE OTIC CAPSULE"). The anterior process of the malleus is unique in that it develops as membranous bone without a cartilaginous model. Development of the stapes blastema involves progressive encirclement of the stapedial artery. The obturator foramen represents the completed ring left empty after the stapedial artery involutes (see "DEVELOPMENT OF THE ARTERIES"). Growth of the lamina stapedialis, an otic capsule structure, involves retrogressive changes in the cartilaginous rim of the oval window.

By 15 weeks, the ossicles have attained adult size, and ossification soon begins, first in the incus, then in the malleus, and finally in the stapes. As the footplate attains adult size, tissue at the oval window rim develops into the fibrous tissue of the annular ligament. During the same time frame, the tensor tympani and stapedius muscles develop from the mesenchyme of the first and second branchial arches, respectively. The ossicles assume their adult configuration by 20 weeks, although the megalithic stapes of the fetus continues to lose bulk well into the 32nd week. Otherwise, the endochondral bone of the ossicles, similar to that of the otic capsule, undergoes little change over the lifetime of the individual and demonstrates poor reparative capacity in response to trauma.

Meanwhile, pneumatization of the tympanic cavity extends into the epitympanum and antrum, and the ossicles are enveloped in the mucous membrane lining of the tubotympanic recess.

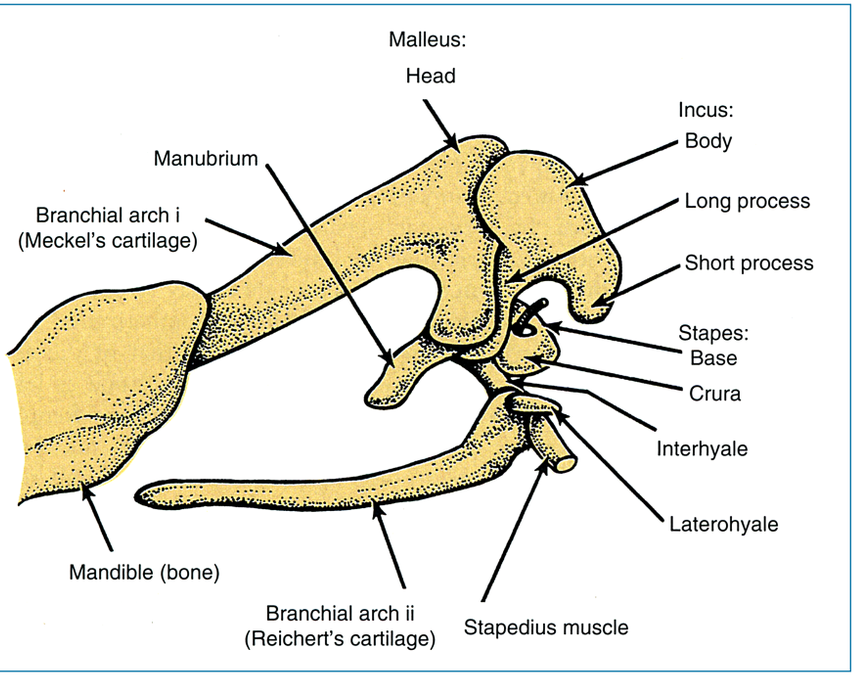

FIGURE 1–7 • The branchial arch origin of the ossicles at 8 to 9 weeks as seen in a left lateral view. The interhyale marks the site of development of attachment of the stapedius tendon, which is its derivative. The laterohyale, eventually migrating to lie posterior to the stapes, temporarily acts as part of the facial nerve canal. *After Hanson and colleagues.*[21] *Reproduced with permission from Gulya AJ. Gulya and Schuknecht's anatomy of the temporal bone with surgical implications. 3rd ed. New York: Informa Healthcare USA; 2007.*

DEVELOPMENT OF THE OTIC LABYRINTH

The precursor of the mammalian otic labyrinth is the cranial portion of the lateral line system of fish,[22] a water- motion detection system. This system of fluid-filled pits (ampullae) features epidermal placode derivation; innervation by cranial nerves VII, IX, and X; and a functional architecture consisting of hair cells, supporting cells, and surrounding fluid (sea water), recapitulated in the mammalian inner ear. Enclosure of the lateral line system, separating it from the ocean environment, is first seen in the hagfish (Myxinoidea) and results in the formation of the first true vestibular mechanism.[22] Ascending the vertebrate ladder, the vestibular mechanism becomes increasingly complex as it changes from a structure consisting of a utricle and two semicircular canals (the superior and posterior) by adding the endolymphatic duct passages; a third semicircular canal (the lateral), the saccule; and an outgrowth of the saccule, the lagena, which eventually gives rise to the cochlea. Endolymph replaced seawater as the surrounding fluid as the lateral line system evolved from use in aquatic to terrestrial organisms.

The development of the otic labyrinth in the human embryo faithfully follows much the same sequence as did the development of the mechanism in our vertebrate ancestors; hence, the phylogenetically older semicircular canals and utricle (pars superior) precede the development of the saccule and the cochlear duct (pars inferior). The phylogenetic seniority of the pars superior is thought to underlie its relative resistance to developmental malformations when contrasted with the newer pars superior.

The otic placode, a plaquelike thickening of surface ectoderm dorsal to the first branchial groove, appears at the end of the third week. Invagination into the underlying mesenchyme occurs within days, forming the auditory pit (Figure 1–8). The endolymphatic appendage appears at this stage, considerably in advance of the semicircular and cochlear ducts.[23] Expansion of the auditory pit and fusion of overlying tissue create the otocyst (otic vesicle), separated from the surface. The mesenchymal tissue that surrounds and differentiates in conjunction with the otocyst is the future otic capsule (bony labyrinth). By the fourth week, two flanges (the future semicircular ducts) arise from the otocyst. Development then involves elongation of the otocyst and the appearance of three deepening folds (I, II, and III), which demarcate the utricle with its three semicircular ducts, the endolymphatic duct and sac, and the saccule with its cochlear duct (Figure 1–9). The utriculoendolymphatic valve (of Bast) is a derivative of fold III, functionally separating the utricle and the dilated proximal aspect, or sinus, of the endolymphatic duct.[24]

In the 6-week embryo, the lumina of the semicircular ducts have formed, and the macula communis (the primordial macula at the medial wall of the otocyst) has divided into superior and inferior segments. The macula of the utricle and the ampullary crests of the superior and lateral semicircular ducts are derivatives of the superior segment, whereas the macula of the saccule and the ampullary crest of the posterior semicircular duct are derived from the inferior segment. At the same time, the cochlear duct has extended from the saccule, completing one turn during the course of the week.

As the semicircular ducts increase in both the radius of the arc of curvature and in luminal diameter (Figure 1–10), progressive deepening of the three folds (Figure 1–11) delineates the ductal connections of the utricle, saccule, and endolymphatic sac as well as of the cochlea and saccule. Meanwhile, the cochlear duct continues its spiraling growth, rapidly completing its 2½ turns by the eighth week (see Figure 1–8). A number of cochlear anomalies are recognized and are believed to reflect the stage at which normal development is disrupted.[25]

Between 8 and 16 weeks, the otic labyrinth approaches its adult configuration (Figure 1–12). The epithelium of the cristae ampullaries of the semicircular ducts differentiates to a sensory neuroepithelium with hair cells and gelatinous cupula as the semicircular ducts continue expansion. Similarly, the maculae of the otolithic organs (utricle and saccule) differentiate as hair

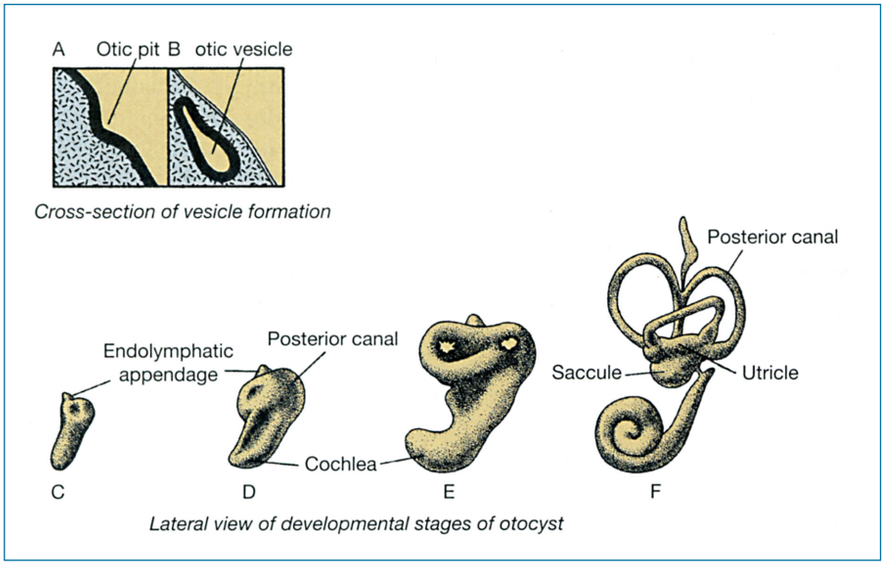

FIGURE 1–8 • The evolution of the endolymphatic (otic) labyrinth. *A*, 22 days, *B*, 4 weeks, *C*, 4½ weeks, *D*, 5½ weeks, *E*, 6 weeks, and *F*, 8+ weeks. *After Streeter.*[23] *Reproduced with permission from Gulya AJ. Gulya and Schuknecht's anatomy of the temporal bone with surgical implications. 3rd ed. New York: Informa Healthcare USA; 2007.*

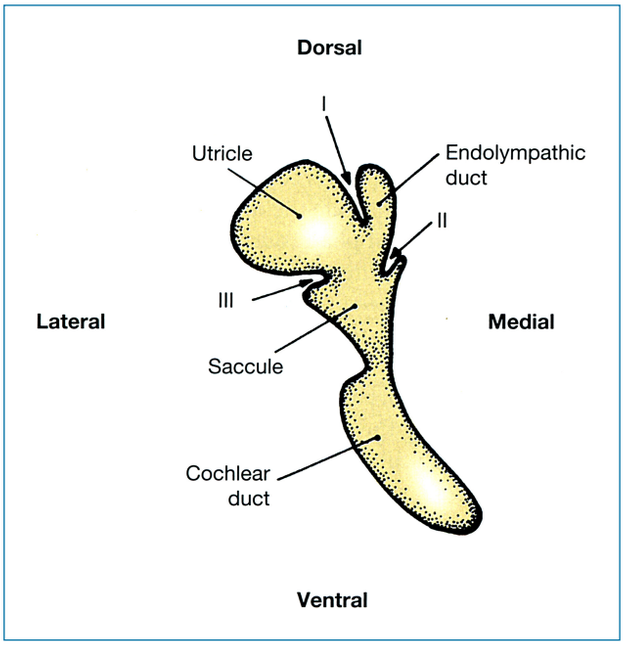

FIGURE 1–9 • The otic labyrinth at the 6- to 8-week stage. Folds I, II, and III begin to indent the otocyst. *After Bast and Anson.[4] Reproduced with permission from Gulya AJ. Gulya and Schuknecht's anatomy of the temporal bone with surgical implications. 3rd ed. New York: Informa Healthcare USA; 2007.*

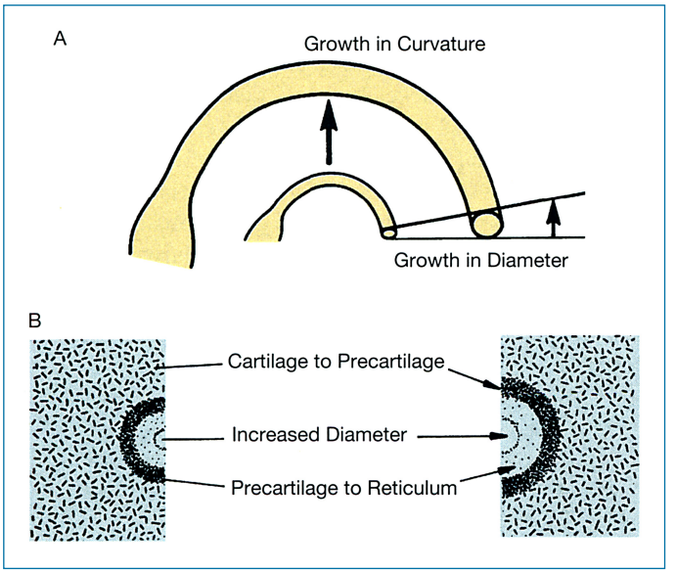

FIGURE 1–10 • Growth of the semicircular ducts involves retrogressive changes in the surrounding cartilage and precartilage. *After Pearson.[3] Reproduced with permission from Gulya AJ. Gulya and Schuknecht's anatomy of the temporal bone with surgical implications. 3rd ed. New York: Informa Healthcare USA; 2007.*

cells and otolithic membranes appear. The proximal endolymphatic sac begins to develop a rugose epithelium. The primitive circular cochlear duct assumes a more triangular outline as the neuroepithelium of the basal turn begins to differentiate into the organ of Corti (Figure 1–13).

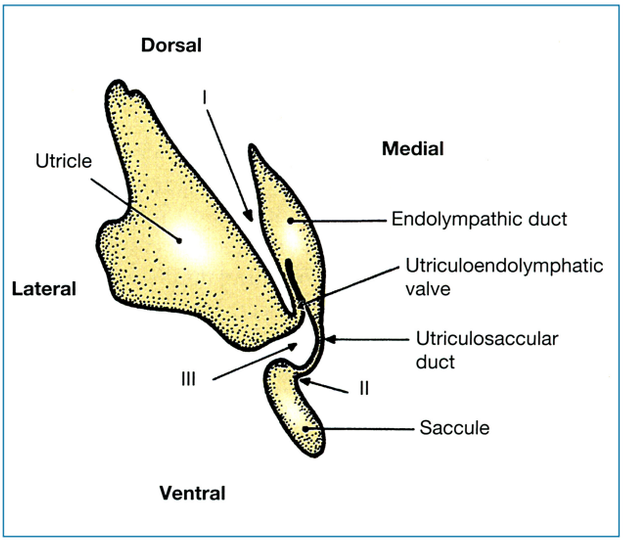

FIGURE 1–11 • The otic labyrinth at 9 weeks. Deepening of folds I, II, and III (compare with Figure 1–9) more clearly distinguishes the utricle, saccule, and endolymphatic duct. *After Bast and Anson.[4] Reproduced with permission from Gulya AJ. Gulya and Schuknecht's anatomy of the temporal bone with surgical implications. 3rd ed. New York: Informa Healthcare USA; 2007.*

At 20 weeks, the superior semicircular duct has reached adult size. In a phylogenetically determined sequence, the posterior and lateral ducts complete growth, and the cristae ampullares are completely differentiated. The endolymphatic duct, up to this stage, has followed a straight course, paralleling the crus commune to reach the endolymphatic sac; now the duct begins to develop a bend as it is dragged inferiorly and laterally along with the endolymphatic sac by the continuing growth of the sigmoid sinus and posterior fossa. The first part of the endolymphatic duct, then, is an anatomically constant structure in close relationship to the crus commune; the distal duct and sac, however, vary in position according to the degree of sigmoid sinus migration and posterior fossa development.[1] The sac continues to grow, with its size at term attaining quadruple that seen at midterm and with its lining further differentiating. The lining epithelium of the saccular, utricular, and endolymphatic ducts ranges from simple squamous to cuboidal. As demonstrated by Lundquist,[26] the proximal endolymphatic sac (Figure 1–14), located within the vestibular aqueduct, and the distal third, completely enveloped in dura adjacent to the lateral venous sinus, similarly possess a simple cuboidal lining. In contrast, the intermediate one-third, or rugose portion, which lies partly within the vestibular aqueduct and partly within folds of dura mater, has a highly differentiated epithelium. The tall, cylindrical cells of the epithelium possess microvilli and pinocytotic vesicles, are ruffled into papillae and crypts, and overlie a rich, subepithelial capillary network.

All of these features suggest resorptive and phagocytic functions, with the latter function providing for local immune defense.[27]

The organ of Corti is differentiated to such a degree by 20 weeks that the fetus can "hear" and respond to fluid-borne sounds.[28] The organ of Corti approximates the adult structure by 25 weeks.[3]

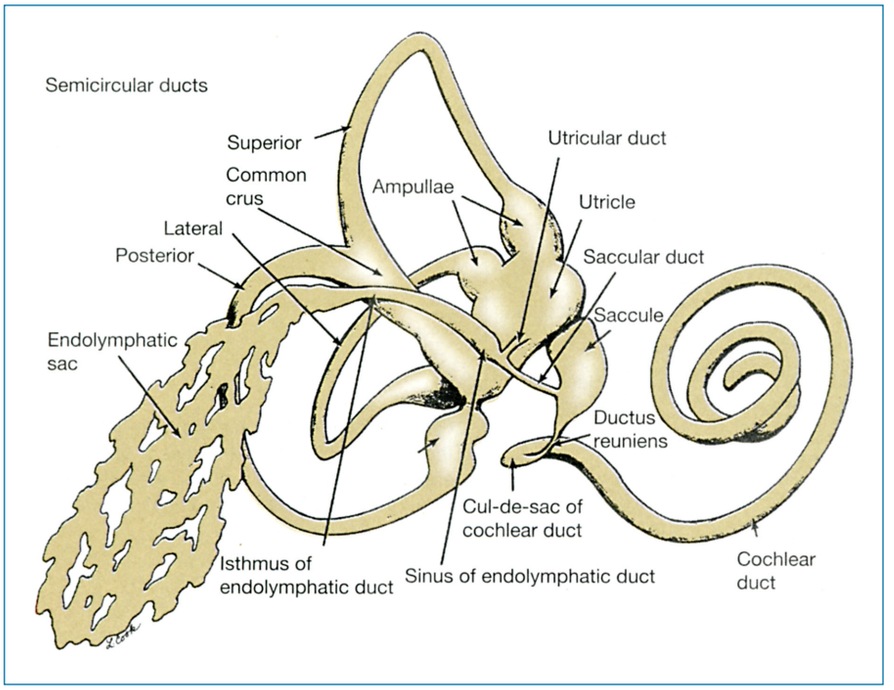

FIGURE 1–12 • The adult membranous labyrinth, medial aspect. The endolymphatic duct initially parallels the common crus and posterior semicircular duct but then diverges to the posterior cranial fossa location of the endolymphatic sac. *After Anson and Donaldson.*[2] *Reproduced with permission from Gulya AJ. Gulya and Schuknecht's anatomy of the temporal bone with surgical implications. 3rd ed. New York: Informa Healthcare USA; 2007.*

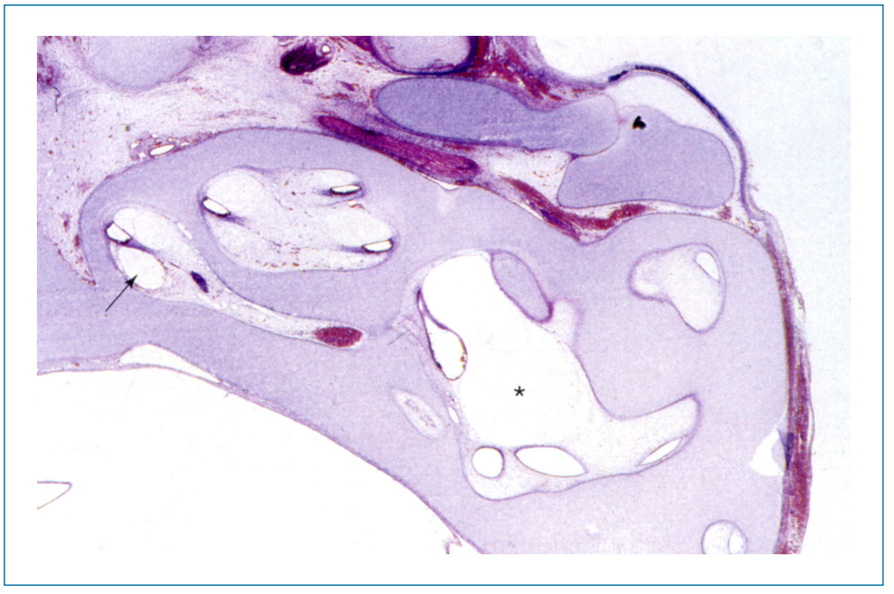

FIGURE 1–13 • In this 12-week fetus, the vestibule (asterisk) is advanced in development and the scala tympani (arrow) is evident in the basal turn of the cochlea. The cochlear duct of the basal turn assumes a more triangular configuration, whereas the apical turn still retains its circular outline. *Reproduced with permission from Gulya AJ. Gulya and Schuknecht's anatomy of the temporal bone with surgical implications. 3rd ed. New York: Informa Healthcare USA; 2007.*

DEVELOPMENT OF THE PERILYMPHATIC (PERIOTIC) LABYRINTH

The perilymphatic (periotic) labyrinth comprises the fluid-tissue space interposed between the membranous otic (or endolymphatic) labyrinth and its bony covering—the otic capsule. The perilymphatic cistern (of the vestibule), scala tympani, scala vestibuli, perilymphatic space of the semicircular canals, fissula ante fenestram, fossula post fenestram, and periotic duct are all considered part of the perilymphatic labyrinth.

It is not until the 8th week that the first sign of perilymphatic space formation is seen. Mesodermal tissue surrounding the membranous labyrinth (ie, the future otic capsule) retrogressively dedifferentiates from precartilage into a loose, vascular reticulum, initially around the ampullae of the semicircular ducts and in the region of the perilymphatic cistern of the vestibule. The scala tympani starts its emergence from precartilage as an area of retrogressive rarefaction in the precartilage just under the round window.

Rapidly changing over the next several weeks, the reticulum of the primordial perilymphatic labyrinth becomes highly vacuolated, its spaces traversed by supporting fibers for the walls of the saccule and the utricle and for the vascular and neural supplies of the inner ear.[3] The perilymphatic cistern of the vestibule, adjacent to the oval window, is the first recognizable space of the perilymphatic labyrinth, appearing late in the 12th week (see Figure 1–13). The scala tympani appears soon afterward, with the scala vestibuli appearing somewhat later as a diverticulum

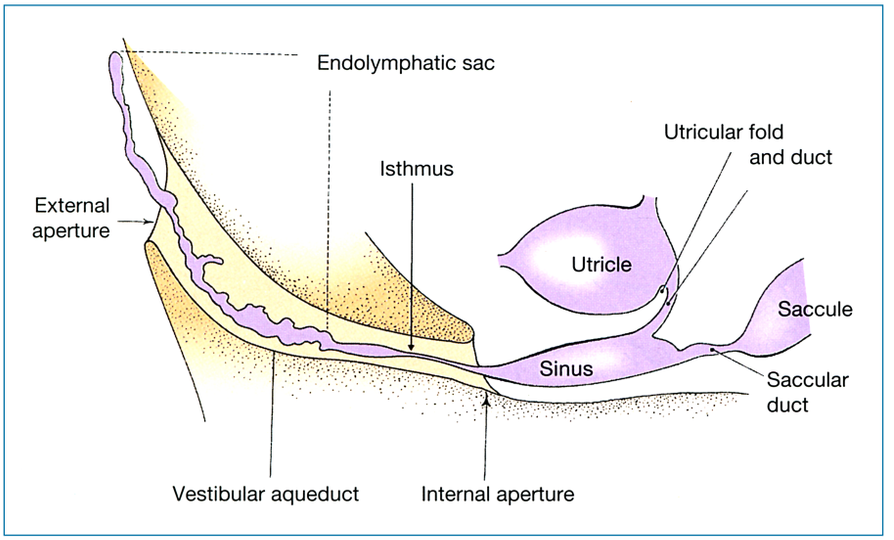

FIGURE 1–14 • The osseous relationships of the endolymphatic duct and sac. *After Anson and Donaldson.[2] Reproduced with permission from Schuknecht HF. Pathology of the ear. Ontario: BC Decker; 1974.*

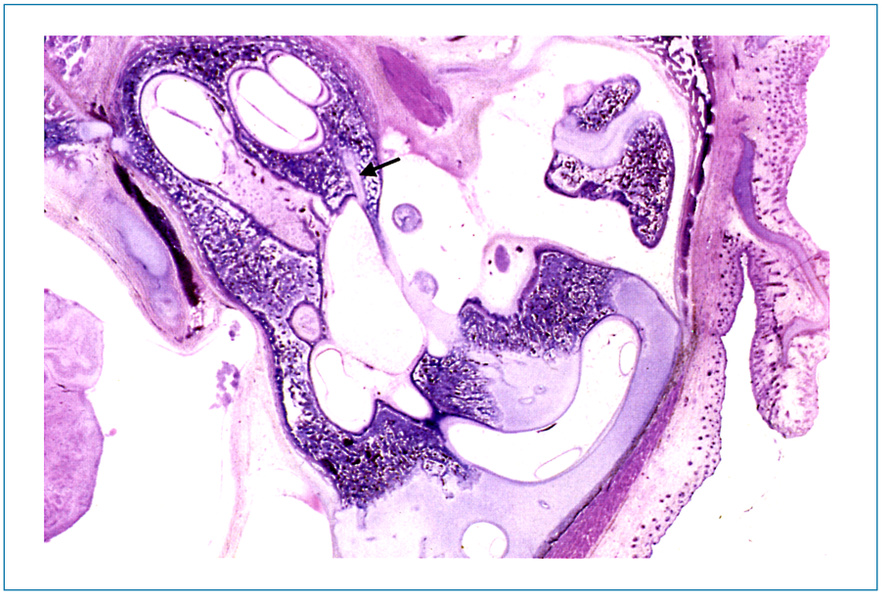

FIGURE 1–15 • This photomicrograph, from a 16-week specimen, shows the fissula ante fenestram (arrow). *Reproduced with permission from Gulya AJ. Gulya and Schuknecht's anatomy of the temporal bone with surgical implications. 3rd ed. New York: Informa Healthcare USA; 2007.*

of the perilymphatic cistern near the oval window. The expansion of both scalae is closely linked to that of the developing cochlear duct and cochlea. The canalicular portion of the perilymphatic labyrinth is relatively delayed in development. Only at 16 weeks does vacuolization begin; however, development is usually completed by 20 weeks.

Fissula Ante Fenestram

The fissula ante fenestram and the fossula post fenestram, although part of the perilymphatic labyrinth, undergo a different developmental sequence and hence merit separate discussion (Figure 1–15).

Apparently, the fissula ante fenestram is unique to humans, although Anson and Bast[10] detected a rudimentary, incomplete fissula in the rhesus monkey. The fissula is first apparent in the 9-week embryo as a strip of precartilage in the lateral wall of the cartilaginous otic capsule immediately anterior to the oval window (*ante* is Latin for "in front of," *fenestram* is Latin for "window"). In the course of the next 3 weeks, this extension of periotic tissue stretches as a connective tissue ribbon from the vestibule to the middle ear. Vertically, the ribbon extends from the scala vestibuli to the tympanic cavity, near the cochleariform process. The fissula continues to grow until midfetal life (about 21 weeks), at which time the ossification of the otic capsule is nearing completion.

Although the fissula is a constant tract in humans, it shows interindividual variation both in capacity and in form and undergoes alteration of its lining cartilage over the life of the individual. The cartilage border that separates the connective tissue of the fissula from the bone of the otic capsule is gradually replaced by intrachondral bone (see "Development of the Otic Capsule").[29]

Fossula Post Fenestram

The fossula post fenestram, an evagination of periotic tissue from the vestibule into the otic capsule (see Figure 1–15) posterior to the oval window, undergoes a developmental sequence similar to

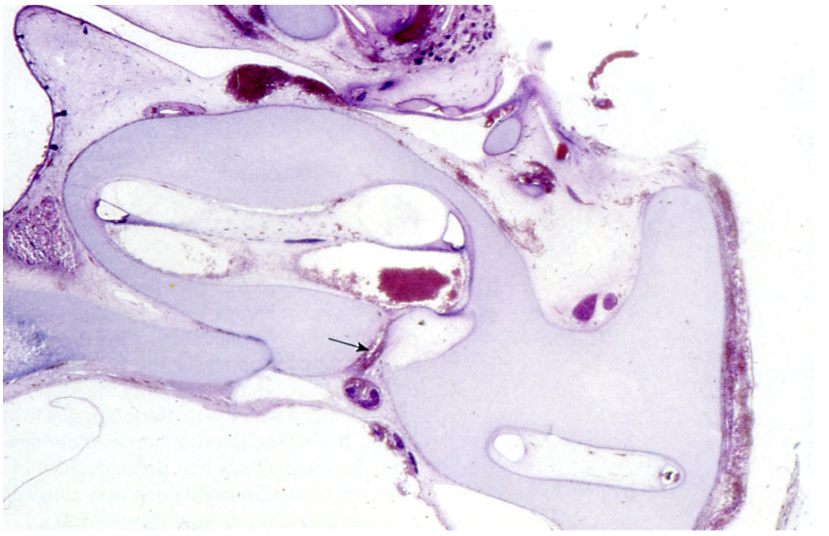

FIGURE 1–16 • As seen in a 12-week fetus, the cochlear aqueduct (arrow) reaches from the posterior cranial fossa to the scala tympani of the basal turn. *Reproduced with permission from Gulya AJ. Gulya and Schuknecht's anatomy of the temporal bone with surgical implications. 3rd ed. New York: Informa Healthcare USA; 2007.*

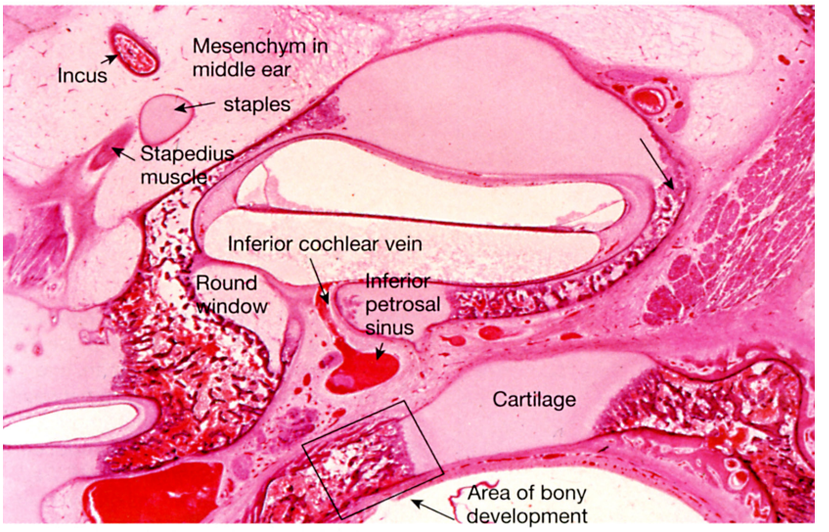

FIGURE 1–17 • The inferior cochlear vein occupies the primitive cochlear aqueduct, as seen in a fetus of approximately 17 weeks. The boxed area is enlarged in Figure 1–22. *Reproduced with permission from Gulya AJ. Gulya and Schuknecht's anatomy of the temporal bone with surgical implications. 3rd ed. New York: Informa Healthcare USA; 2007.*

that of the fissula ante fenestram. The fossula (*fossula* is Latin for "little ditch," *post* is Latin for "behind") is first seen in the fetus of 10½ weeks as an area of dedifferentiating precartilage. As early as 4½ weeks later, the fossula can be distinguished as a zone of connective tissue, which soon becomes surrounded by the bone of the otic capsule. Differing from the fissula, the fossula is an inconstantly occurring structure found in only 67% of all ears studied and extends through the otic capsule to the tympanic cavity in only 25% of those ears with a fossula.[4]

Although the fossula is an area of histologic instability for reasons similar to those for the fissula, cartilaginous and bony changes affect only 5% of all fossulae.[4]

Cochlear Aqueduct

The primordial (bony) cochlear aqueduct first appears at 7 weeks as a rarefaction of precartilage at the medial wall of the cochlear basal turn. The cochlear aqueduct extends from the area of the developing round window to the posterior cranial fossa. The reticulum of the primordial aqueduct links the loose mesenchyme of the round window niche with the connective tissue of the posterior cranial fossa dura, ninth cranial nerve, and inferior petrosal sinus (Figure 1–16).

By the 9th week, the inferior cochlear vein emerges from the syncytium of the cochlear aqueduct. Meanwhile, a cartilaginous bar, as it extends from the round window niche and ampulla of the posterior canal toward the opening of the cochlear aqueduct, gives rise to the floor and medial rim of the round window.

The development of the periotic duct and surroundings in the 16- to 40-week period has been detailed by Spector and associates.[30] In the 16- to 18-week stage (Figure 1–17), three structures are seen in the primitive cochlear aqueduct: the inferior cochlear vein (vein at the cochlear aqueduct), the tympanomeningeal hiatus (Hyrtl's fissure), and the periotic duct. There is still connective tissue continuity between the posterior cranial fossa

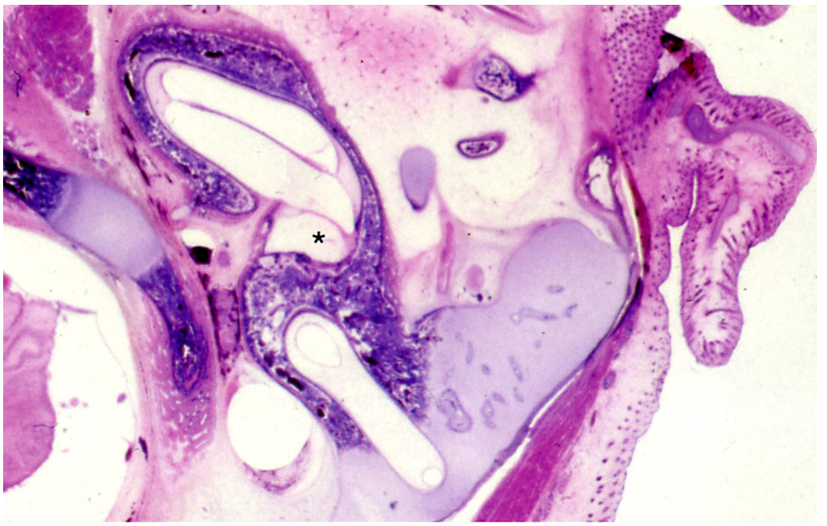

FIGURE 1–18 • Although younger than the fetus shown in Figure 1–17, this fetus shows more advanced ossification of the rim of the round window niche (asterisk) in particular, breaking the communication of the round window niche with the posterior cranial fossa (fetus, 16 weeks). *Reproduced with permission from Gulya AJ. Gulya and Schuknecht's anatomy of the temporal bone with surgical implications. 3rd ed. New York: Informa Healthcare USA; 2007.*

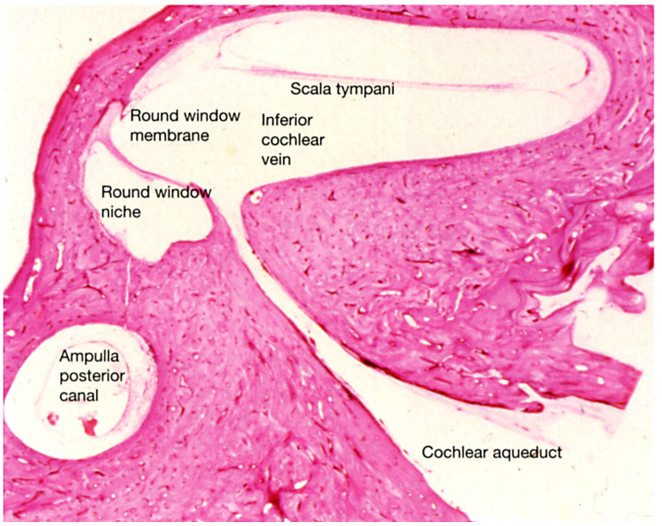

FIGURE 1–19 • The widely patent cochlear aqueduct is thought to underlie the "perilymph oozer" seen in stapes surgery (man, age 67 years). A microfissure is visible between the posterior semicircular canal ampulla and the round window niche. *Reproduced with permission from Schuknecht HF, Seifi AE. Experimental observations on the fluid physiology of the inner ear. Ann Otol Rhinol Laryngol 1963;72:687.*

and the tissue of the round window niche, especially through Hyrtl's fissure.

Ossification of the otic capsule, progressing to the round window by the 18- to 26-week stage (Figure 1–18), fuses the cochlear and canalicular segments of the otic capsule, caps Hyrtl's fissure, and relegates the round window niche to the tympanic cavity. The inferior cochlear vein is segregated into its own canal (of Cotugno) at 20 weeks through further growth and ossification of the otic capsule.

Completion of the cochlear aqueduct occurs between 32 and 40 weeks and entails elongation of the cochlear aqueduct with its contained periodic duct, widening of the cranial apertures of the cochlear aqueduct and periotic duct, and ingrowth of arachnoid tissue, which forms a lining membrane and meshwork. A widely patent cochlear aqueduct (Figure 1–19) is thought to underlie the "perilymph oozer"[1] occasionally encountered in stapes surgery. A persistent tympanomeningeal hiatus represents incomplete ossification. The hiatus extends from the depths of the round window niche to the posterior cranial fossa at the junction of the inferior petrosal sinus and jugular bulb (Figure 1–20).[1] The hiatus is a potential route that cerebrospinal fluid and brain tissue may follow to the middle ear.[30–33]

DEVELOPMENT OF THE OTIC CAPSULE

The otic capsule develops from the precartilage (compacted mesenchyme that is differentiating into embryonic cartilage) surrounding it. Eventually, the otic capsule becomes the petrous portion of the temporal bone.[4] The initial step in development of the otic capsule, as described by Bast and Anson,[4] occurs at the end of the 4th week as the cell density of the mesenchyme enveloping the otic capsule increases. By the 8th week, the

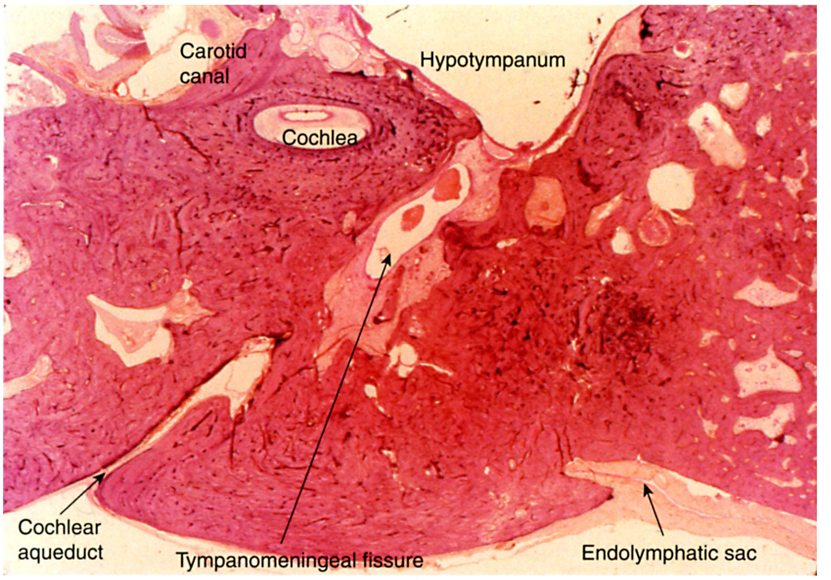

FIGURE 1–20 • The tympanomeningeal fissure (hiatus), occasionally persisting in the adult, is paralleled by the cochlear aqueduct (man, age 44 years). *Reproduced with permission from Gulya AJ. Gulya and Schuknecht's anatomy of the temporal bone with surgical implications. 3rd ed. New York: Informa Healthcare USA; 2007.*

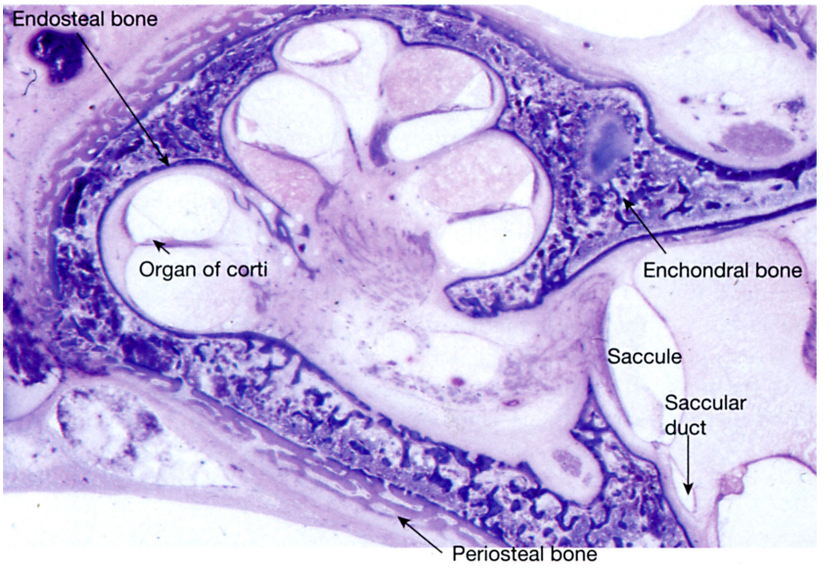

FIGURE 1–21 • With ossification of the otic capsule, three layers of bone are created (fetus, 16 weeks). *Reproduced with permission from Gulya AJ. Gulya and Schuknecht's anatomy of the temporal bone with surgical implications. 3rd ed. New York: Informa Healthcare USA; 2007.*

mesenchymal condensation has formed a cartilaginous model of the otic capsule. At this stage, although the membranous labyrinth, which the cartilaginous otic capsule surrounds, has attained adult configuration, it does not attain adult size until nearly midterm. Retrogressive dedifferentiation of otic capsular cartilage to a loose reticulum accommodates the expansion of the membranous labyrinth. Redifferentiation to cartilage occurs at the inner, trailing edge of the semicircular ducts (see Figure 1–10).

According to Bast and Anson,[4] the first ossification center of the otic capsule appears at the region of the cochlea only as the contained membranous labyrinth reaches adult size, usually by 16 weeks. A total of 14 centers eventually appear and fuse to complete the ossification of the otic capsule despite its small size. The last ossification center appears at 20 to 21 weeks in the posterolateral region of the posterior semicircular canal. The only areas that remain cartilaginous are those at the region of the fissula ante fenestram and an area that overlies part of the posterior and lateral semicircular ducts, where ossification does not begin until 2 weeks later.[4]

A detailed discussion of the ossification sequence of the otic capsule is beyond the scope of this chapter, and the interested reader is referred to Bast and Anson[4] and Gulya and Schuknecht[1] for a more detailed discussion. However, several unique features of the bone of the otic capsule are of clinical significance and are outlined below.

Three layers of bone emerge from the ossification of the cartilaginous otic capsule (Figure 1–21). The perichondrial

membrane lining the external and the internal (facing the membranous labyrinth) surfaces of the otic capsule becomes a periosteal membrane as newly differentiated osteoblasts deposit calcium. The periosteal and endosteal bone layers are thus formed.

The endosteal layer does not significantly change throughout adult life, although in response to infection or trauma (including perhaps electrical stimulation), it may proliferate to such a degree as to obliterate the lumen of the labyrinth.[1] Alternatively, it has been proposed that undifferentiated mesenchymal cells, located around capillaries, are the true source of such obliterative, bony growths.[34] The periosteal layer, in contrast, does change, by lamellar addition of bone and by pneumatization, until early adult life.[10] This layer has the capability of good osteogenic repair in response to trauma and infection and remodels throughout life, similar to periosteal bone elsewhere in the body.

Sandwiched between the endosteal and periosteal layers of bone is the enchondral layer, consisting of both intrachondral (intrachondrial) and endochondral bone. Intrachondral bone (globuli interossei) comprises persistent islands of calcified hyaline cartilage, the lacunae of which are occupied by osteocytes and on which endochondral bone is deposited. Initial steps in the formation of intrachondral bone (Figure 1–22) are hypertrophy of cartilage cells in their lacunae, calcification of the cartilaginous matrix, and vascular bud invasion. Much of the calcified cartilage is removed, but scattered islands remain. Osteocytes repopulate the formerly cartilaginous lacunae and begin bone deposition.

Osteoblasts lining the surface of the calcified cartilage islands deposit layers of endochondral bone. This bone deposition nearly obliterates the vascular spaces and establishes the layer of very dense, poorly vascular bone characteristic of the petrous (rocklike) pyramid known as the enchondral layer.

The enchondral layer, similar to the endosteal layer, once formed in midfetal life undergoes little change save for conversion to increasingly dense bone.[10] Enchondral bone, also similar to endosteal bone, exhibits a minimal reparative response to insults, such as trauma and infection, at best healing by fibrous union. Because of the poor reparative capacity of the endosteal and enchondral layers, the ravages of stress and trauma leave indelible marks on the architecture of the bony labyrinth. Major trauma, sufficient to fracture the temporal bone, results in large fissures that may traverse the entire temporal bone.

The so-called microfissures are commonly encountered disruptions in the endosteal and enchondral layers of the bony labyrinth.[1] A microfissure found in all ears after the age of 6 years is located between the round window niche and the ampulla of the posterior canal (see Figure 1–19).[35] Additionally, microfissures can be found about the oval window region in 25% of ears examined, usually extending vertically above and below the oval window without involving the footplate, more commonly after the age of 40 years.[36] Typically, these microfissures are obstructed by fibrous tissue in association with an acellular matrix resembling osteoid. Why these microfissures occur remains unclear. It has been hypothesized that the microfissures represent stress fractures resulting from structural changes of the labyrinth[45] or from the transferred stresses of mastication.[37] Alternatively, the microfissures bridging the round window niche and the posterior canal ampulla may be related to an embryologic communication.[35] Although, by term, cartilage replaces the mesenchyme of this transient channel, this area may remain structurally weak and readily fractured.

The microfissures of the bony labyrinth have been thought to play a role in the contamination of the inner ear by inflammatory processes or ototoxic substances applied to the middle ear. Similarly, these microfissures have been theorized to give rise to spontaneous perilymph fistulae.

Attaching such clinical implications to microfissures remains a matter of conjecture. In an examination of 34 temporal bones, El Shazly and Linthicum were unable to find any relationship between the presence or absence of microfissures to sudden sensorineural hearing loss.[38]

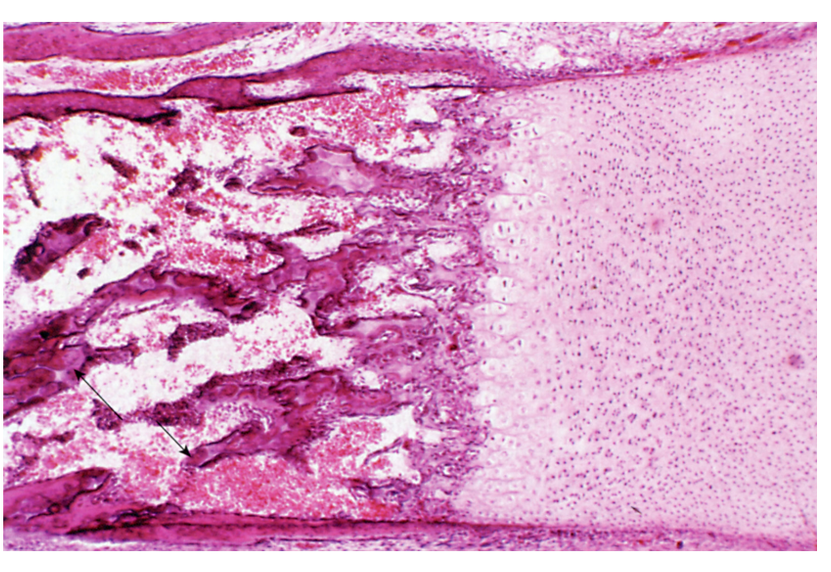

FIGURE 1–22 • This detailed view of the boxed area of Figure 1–17 illustrates the steps of enchondral bone formation. Going from right to left, cartilage cells multiply, enlarge, and are ossified. Globuli interossei (arrows) represent persisting islands of cartilage (fetus, age 17 weeks). *Reproduced with permission from Gulya AJ. Gulya and Schuknecht's anatomy of the temporal bone with surgical implications. 3rd ed. New York: Informa Healthcare USA; 2007.*

Distinct from and independent of the formation of the otic capsule from a cartilaginous model is the formation of the cochlear modiolus as membranous bone. The deposition of bone within the modiolus, housing the cochlear nerve, first occurs at 20 to 21 weeks in the region between the basal and second turns.[4] By 25 weeks, modiolar ossification is nearly complete.

Osseous extensions of the cochlear otic capsule, known as interscalar septa, serve to anchor the modiolus. The first septa appear in the 22nd week and within 5 weeks have stabilized the cochlear modiolus from base to apex. Following a similar time frame, the osseous spiral lamina begins ossification in the 23rd week and completes this process by the 25th.

Aberrations in the finer developmental steps of the cochlea may appear as structural anomalies that occasionally attain surgical importance. Partial absence of the interscalar septum (scala communis) is a relatively common developmental anomaly that does not interfere with normal cochlear function (Figure 1–23). Absence of the modiolus results in a wide communication between the subarachnoid space of the internal auditory canal and the scala vestibuli of the basal turn. This anomaly may represent the anatomic correlate of the "perilymph gusher," the voluminous outflow occasionally encountered in stapes surgery (Figure 1–24).

DEVELOPMENT OF THE ACOUSTIC NERVE AND GANGLION

The acoustic nerve, ganglion, and Schwann sheath cells begin development in the 4th week as cells of otic placode derivation begin to stream ventrally between the epithelium of the otocyst and its basement membrane. After penetrating the basement membrane, these cells reach the area at which the acoustic ganglion forms,[3,39] ventral and slightly medial to the otocyst.[40]

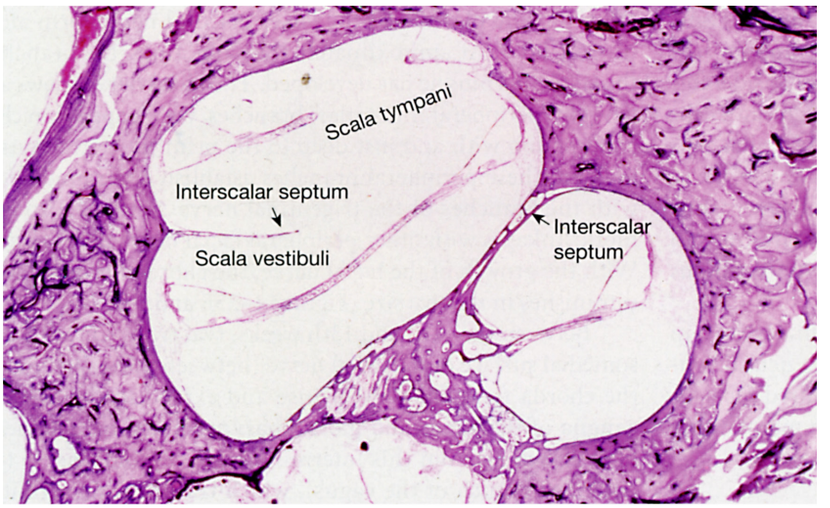

FIGURE 1–23 • Partial absence of the interscalar septum, as shown in this micrograph, is known as scala communis (woman, age 63 years). *Reproduced with permission from Gulya AJ. Gulya and Schuknecht's anatomy of the temporal bone with surgical implications. 3rd ed. New York: Informa Healthcare USA; 2007.*

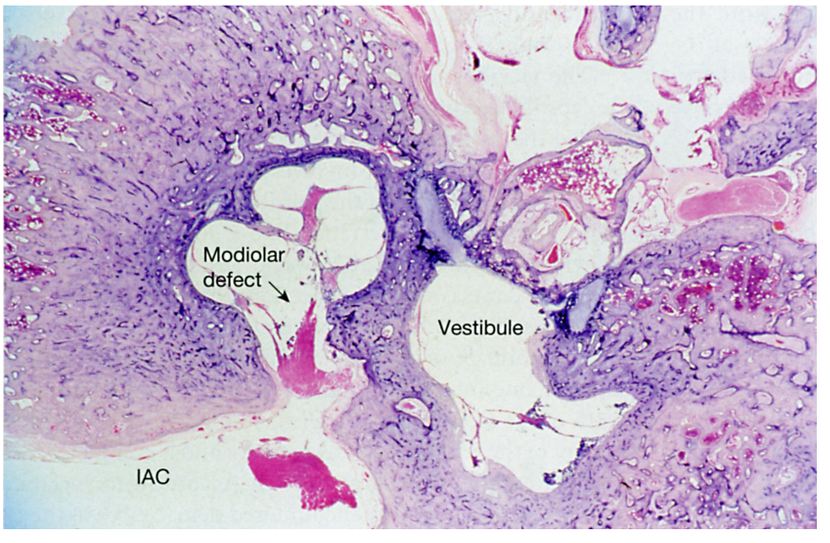

FIGURE 1–24 • The modiolar defect in the cochlea of this 2½-year-old child with a congenital conductive hearing loss results in a wide communication of the subarachnoid space of the internal auditory canal (IAC) with the scala vestibuli of the basal turn. Stapedectomy in such cases results in a "perilymph gusher." *Reproduced with permission from Shi S-R. Temporal bone findings in a case of otopalatodigital syndrome. Arch Otolaryngol 1985;111:120. Copyright 1985, American Medical Association.*

Over the remainder of the 4th and 5th weeks, the acoustic ganglion divides into superior and inferior segments.[23] The superior segment gives rise to the fibers that innervate the crista of the superior and lateral semicircular ducts as well as the utricular macula. Slightly later, the inferior segment divides into upper and lower portions. The upper portion supplies fibers to the saccular macula and to the crista of the posterior semicircular duct, whereas the lower portion innervates the organ of Corti.

By the end of 8 weeks, the acoustic nerve approaches full maturity. The ganglia of the vestibular division are spread along the nerve trunks, and its terminal branches, derived from the bipolar ganglion cells, develop as fairly long, discretely individual nerve fibers. The cochlear ganglion, in contrast, ends up at the distal terminus of the nerve trunk, and its terminal branches are short, anastomosing fibers.[23] Similarly, central connections (to the brainstem) are established, initially by the vestibular nerve and then later by the cochlear nerve fibers.[40] As soon as central connections (to the brainstem) are established, migration of glial cells from the brain tube begins to envelop the proximal portion of the acoustic nerve fibers, but it is only later in development that Schwann cells begin to migrate centrally. Thus, the central glial sheath extends for a considerable distance laterally along the acoustic nerve before Schwann cells migrate medially. Moreover, the distance covered by glial cells is greater on the vestibular nerve than on the cochlear nerve because of the earlier initiation of migration, the former when compared with the latter.[40] The junction of the Schwann cell and glial sheaths occurs variably about the region of the fundus of the internal auditory canal.

It is thought that the sensory neuroepithelium develops in those areas of the membranous labyrinth at which neural contact is established.[3] Such contact may not be required for neuroepithelial differentiation but may play a role in maintaining such specialization.[41,42]

DEVELOPMENT OF THE FACIAL NERVE AND GENICULATE GANGLION

At about 4 weeks, the facial nerve and its geniculate ganglion begin to develop from primordial tissue, arising from the rhombencephalon, which impinges on the deep aspect of the second branchial arch epibranchial placode,[43] a thickened area of surface ectoderm just caudal to the first branchial groove (Figures 1–25A and B, and 1–26A and B).

The later stages of facial nerve and geniculate ganglion development have been described by Gasser and colleagues.[43–45] Neuroblast differentiation in the region at which the primordial facial nerve tissue is in contiguity with the epibranchial placode results in a distinguishable geniculate ganglion by 6 weeks (Figures 1–25C and 1–26C). Meanwhile, the chorda tympani nerve, the first branch of the facial nerve to appear, is clearly evident. At approximately the same time, the facial motor nucleus appears in the future metencephalon; its intramedullary fibers are displaced by the abducens nucleus as the metencephalon grows, creating the internal genu of the facial nerve.

The chorda tympani nerve, at 6 weeks approximating the size of the facial nerve, dives into the mandibular arch to terminate in the same region as the lingual nerve ends and the submandibular ganglion develops.

The chorda tympani and lingual nerves clearly unite just proximal to the ganglion by the 7th week (Figures 1–25D and 1–26D). Also at approximately 6 weeks, the greater petrosal nerve, the second branch of the facial nerve to form, develops from the ventral aspect of the geniculate ganglion. The nervus intermedius (nerve of Wrisberg, the sensory fibers of the facial nerve) develops independently from the geniculate ganglion and extends to the brainstem bordered by the motor root of the facial nerve and the eighth cranial nerve. The main trunk of the facial nerve establishes its definitive intratemporal relationships within the cartilaginous otic capsule.

In sequence, the posterior auricular nerve and the fibers to the posterior belly of the digastric muscle appear. Branches of the posterior auricular nerve communicate with nerves of the second and third cervical ganglia, resulting in the formation of the transverse cervical and lesser occipital nerves.

At 7 weeks, a ventral offshoot from the geniculate ganglion reaches the glossopharyngeal ganglion. In the next week, the tympanic plexus and the lesser petrosal nerve form along this offshoot. At approximately the same time, the branch to the stapedius muscle has developed. The facial nerve grows and develops peripheral (muscular) branches, which appear in close conjunction with and just deep to the primitive facial muscle masses. These peripheral branches establish communications with the branches of the trigeminal nerve. Similarly, anastomotic linkages with other peripheral facial nerve fibers appear. With the growth of the facial nerve, the chorda tympani nerve diminishes in relative size (Figures 1–25E and 1–26E).

Between the 12th and 13th weeks, two twigs from the dorsomedial surface of the facial nerve (between the stapedius and the chorda tympani nerves) fuse and extend to the superior ganglia of the vagus and glossopharyngeal nerves. The nerve fiber emerging from this intermingling is Arnold's nerve (the auricular branch of the vagus), which traverses the primitive tympanomastoid fissure to innervate the subcutaneous tissue of the posterior aspect of the external auditory canal.

By 17 weeks, the definitive communications of the facial nerve, including those with the second and third cervical nerves, the three divisions of the trigeminal nerve, and the vagus and the glossopharyngeal nerves, are established.

The facial canal, originally a sulcus in the cartilaginous otic capsule, becomes a bony canal as it ossifies. Spector and Ge detailed the ossification of the tympanic segment of the fallopian canal, a process that involves two ossification centers: an anterior one developing at the apical cochlear ossification center at the end of 20 weeks gestation and a posterior one arising at the pyramidal eminence at 25 weeks gestation.[46] Each ossification center emits two bony projections that (ideally) encircle the facial nerve in its entirety. Each ossification center also extends from its point of origin, the anterior one posteriorly and the posterior one inferiorly, to envelop progressively more of the length of the facial nerve. By term, about 80% of the tympanic segment of the fallopian canal is present and is completely developed by roughly 3 months after birth. According to Spector and Ge, most of the surgically encountered dehiscences of the tympanic segment of the fallopian canal can be related to varying

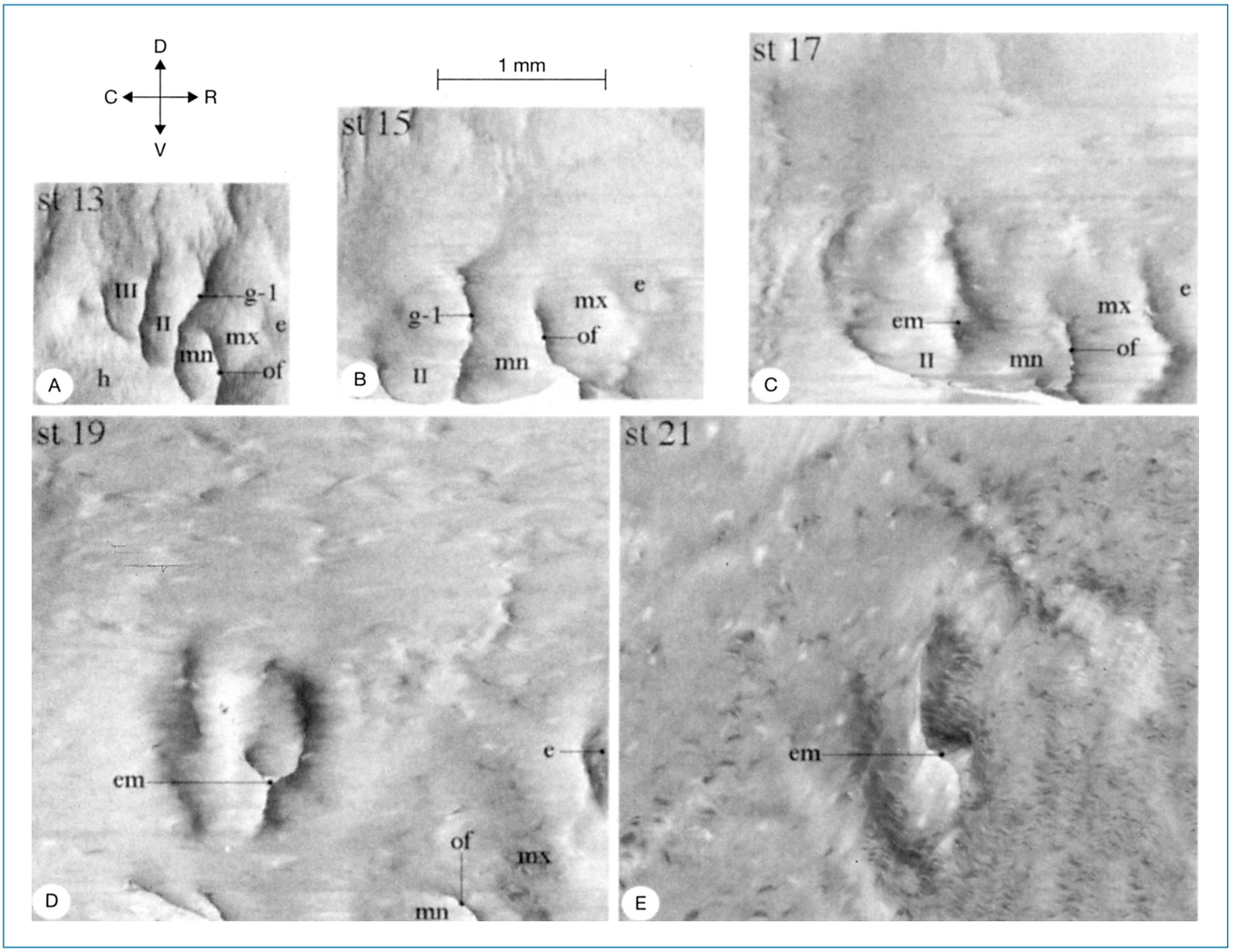

FIGURE 1–25 • Computer reconstructions of the ectoderm of the right external ear region at approximate ages 28 days (*A*), 33 days (*B*), 41 days (*C*), 48 days (*D*), and 52 days (*E*). Dorsal is superior, ventral is inferior, rostral is to the right, and caudal is to the left. This view, companion to Figure 1–26, reveals the structures anatomically related to the lateral aspect of the developing facial nerve. II, second arch; III, third arch; e, eye; em, external auditory meatus; g-1, first groove; h, heart; mn, mandibular part of first arch; mx, maxillary part of first arch; of, oral fissure. *Reproduced with permission from Gasser RF, Shigihara S, Shimada K. Three-dimensional development of the facial nerve path through the ear region in human embryos. Ann Otol Rhinol Laryngol 1994;103:395–403.*

degrees of failure of fusion of the two ossification centers and to failure of fusion of their bony projections.[46] Additionally, they report that the pattern of ossification of the tympanic segment is symmetric in 80% of the paired bones studied.

The mastoid process and tympanic ring grow postnatally, medially displacing and thus protecting the facial nerve.

DEVELOPMENT OF THE ARTERIES

The fetal circulatory system first appears in the 3rd week of development as mesenchymal vascular islands coalesce.[47] The primordial vascular supply to the brain derives from presegmental branches of the paired ("dorsal") aortae. A total of six aortic arches arise successively from the dilated region of the truncus arteriosus known as the aortic sac and course ventrally through their corresponding branchial arches into the ipsilateral dorsal aorta.[47] The primitive internal carotid artery is a branch of the first aortic arch. During this branchial phase of arterial development, there is a correspondence between each branchial arch and its aortic arch. However, not all of the aortic arch arteries exist at the same time. The first and second arch arteries disappear before the more caudal arch arteries develop. The following details of cranial arterial development are based on the comprehensive study of Padget.[48]

In the 4th week, as the first and second aortic arches begin to involute, they leave behind dorsal fragments, the mandibular and hyoid arteries, respectively, and the portion of the paired dorsal aortae extending anteriorly from the third arch artery becomes the adult internal carotid artery (Figure 1–27). In the hindbrain region, the bilateral longitudinal neural arteries

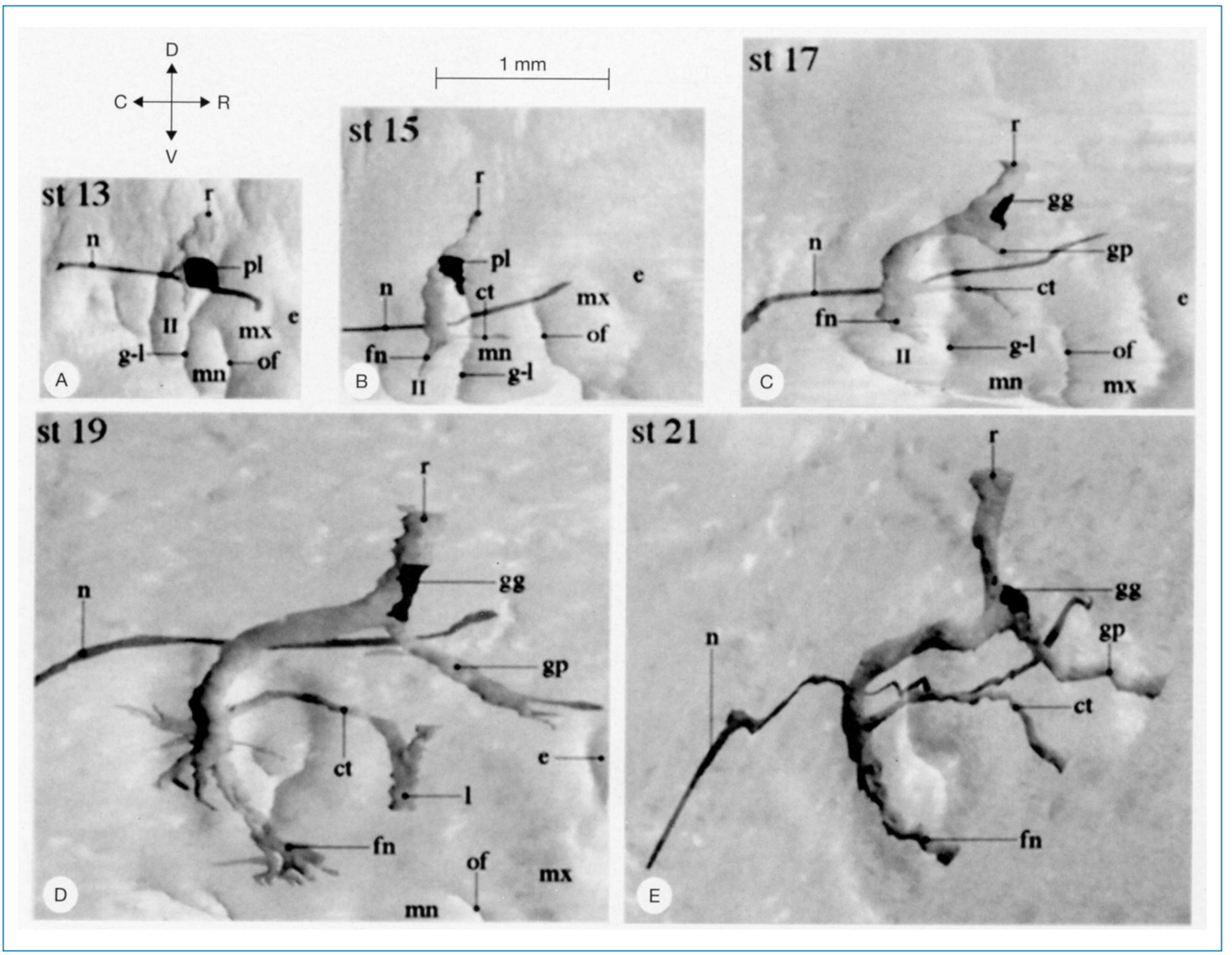

FIGURE 1–26 • Same specimens as Figure 1–25 but with *computer reconstruction making the surface ectoderm* relatively transparent, allowing visualization of the developing facial nerve. II, second arch; III, third arch; ct, chorda tympani nerve; e, eye; fn, facial nerve; g-1, first groove; gg, geniculate ganglion; gp, greater petrosal nerve; l, lingual nerve; mn, mandibular part of first arch; mx, maxillary part of first arch; of, oral fissure; pl, placode; n, notocord; r, facial nerve root. *Reproduced with permission from Gasser RF, Shigihara S, Shimada K. Three-dimensional development of the facial nerve path through the ear region in human embryos. Ann Otol Rhinol Laryngol 1994;103:395–403.*

emerge, supplied at the level of the otocyst and acoustic nerve by the primitive otic artery, a remnant of a presegmental branch of the paired aortae (see Figure 1–27).

In the 4- to 5-week stage, the ventral pharyngeal artery, which parallels the internal carotid artery, arises in the area formerly occupied by the ventral aspects of the first and second arch arteries. This artery supplies the bulk of the first two pharyngeal bars and subsequently is involved in the formation of the stapedial and external carotid arteries. At the same time, the bilateral longitudinal neural arteries fuse to form the basilar artery.

At 6 weeks, as the transition from branchial phase to postbranchial phase takes place, the stapedial artery appears as a small offshoot of the hyoid artery and passes through the stapes blastema to enter the mandibular bar; here the stapedial artery anastomoses with the distal remnant of the shrinking ventral pharyngeal artery. The maxillomandibular division of the stapedial artery is the result of this anastomosis, and it divides into maxillary and mandibular branches. The proximal remnant of the ventral pharyngeal artery evolves into the root of the external carotid artery, whereas the common carotid artery develops from the ventral union of the third and fourth arch arteries.

The development of the labyrinthine and anterior inferior cerebellar arteries during the 4th through 6th weeks passes through a ring configuration, with the abducens nerve in the center. Whether the labyrinthine artery arises from the anterior inferior cerebellar artery or from the basilar artery is determined by the point at which the vascular ring atrophies.

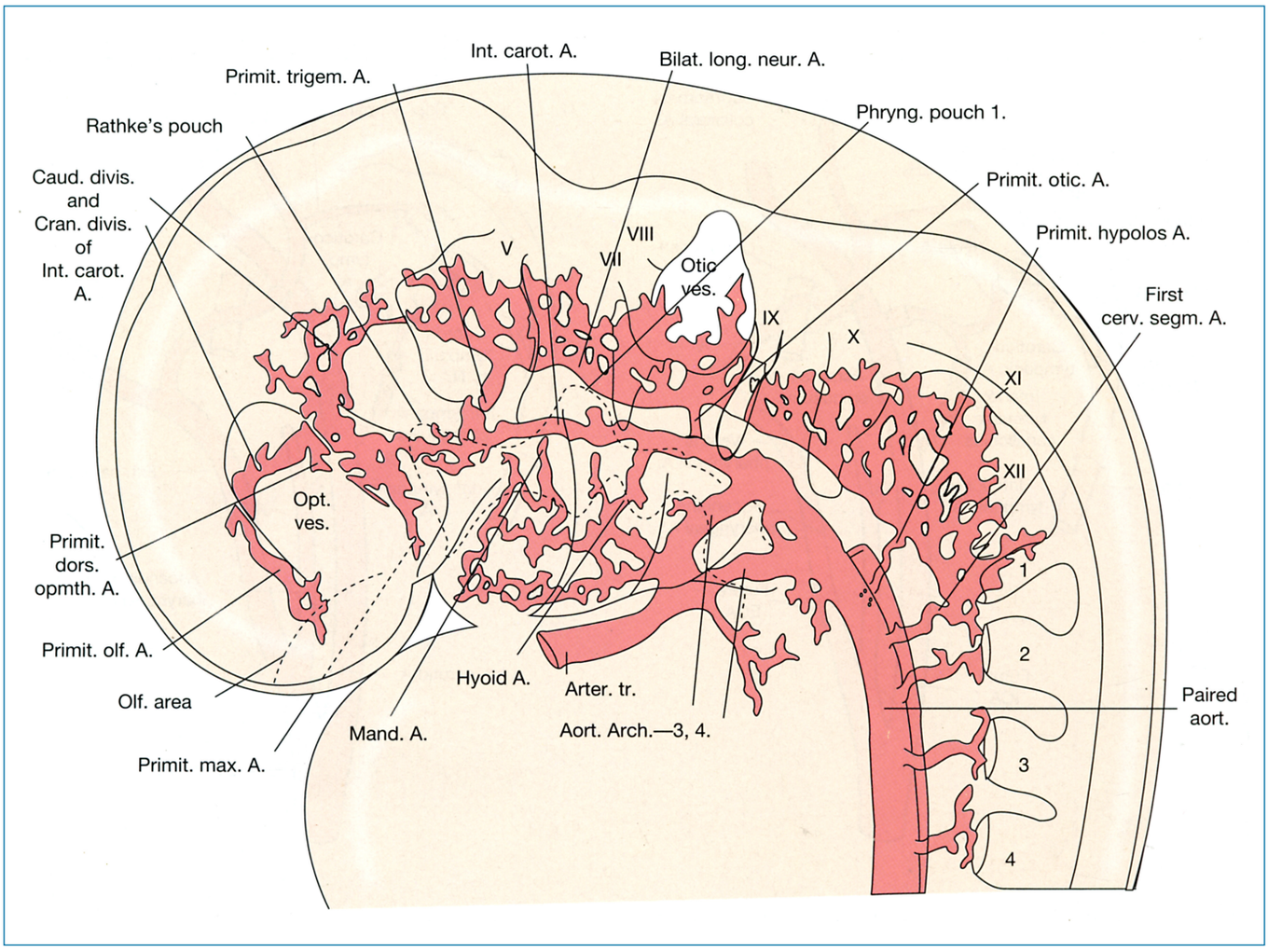

FIGURE 1–27 • Graphic reconstruction of the cranial arteries in a 4-week embryo. The mandibular and hyoid arteries are remnants of the first two aortic arches; the internal carotid artery originates from the third arch, and the bilateral neural arteries are starting to emerge. *Reproduced with permission from Padget DH. The development of the cranial arteries in the human embryo. Contrib Embryol 1948;32:205.*

The stapedial artery reaches the height of its development at 7 weeks (Figure 1–28A) and has two divisions, the maxillomandibular and the supraorbital; the latter division supplies the primitive orbit. Branches of the external carotid artery that can be identified now are the thyroid, lingual, occipital, and external maxillary arteries. Over the next week, the two major divisions of the stapedial artery are annexed by the internal maxillary artery of the external carotid artery and the ophthalmic artery, respectively. The trunk of the maxillomandibular division becomes the stem of the middle meningeal artery (Figure 1–28B). As the stapedialartery withers proximal to the stapes, its more distal stem becomes the superior tympanic branch of the adult middle meningeal artery. The hyoid artery, which originally gave rise to the stapedial artery, dwindles to a mere twig and is partially retained as a caroticotympanic branch of the adult internal carotid artery (Figure 1–28C). Remnants of the stapedial artery also are thought to play a role in the development of the caroticotympanic arteries, anterior tympanic artery, and superior petrosal artery (Tandler, as cited in Gulya and Schuknecht[1] and Altmann[49]).

The subarcuate artery, traversing the subarcuate fossa, develops as a branch of either the labyrinthine or anterior inferior cerebellar artery by the end of the eighth week and supplies part of the otic capsule and mastoid. The adult pattern of origin of all of the cranial arteries is visible by the ninth week.

The stapedial artery, usually a transient structure, may abnormally persist into adulthood, interfering with stapes operations especially (Figure 1–29). After passing through the stapes, the stapedial artery branches; bifurcation of the stapedial artery proximal to the stapes, with both branches penetrating the stapes blastema, may give rise to a three-legged stapes.[50] The stapedial artery, either directly or indirectly through a branch, may fix the developing internal carotid artery so as to pull it into the middle ear (Figure 1–30A and B) more posteriorly and laterally than it ordinarily would run.[50] Such aberrant internal

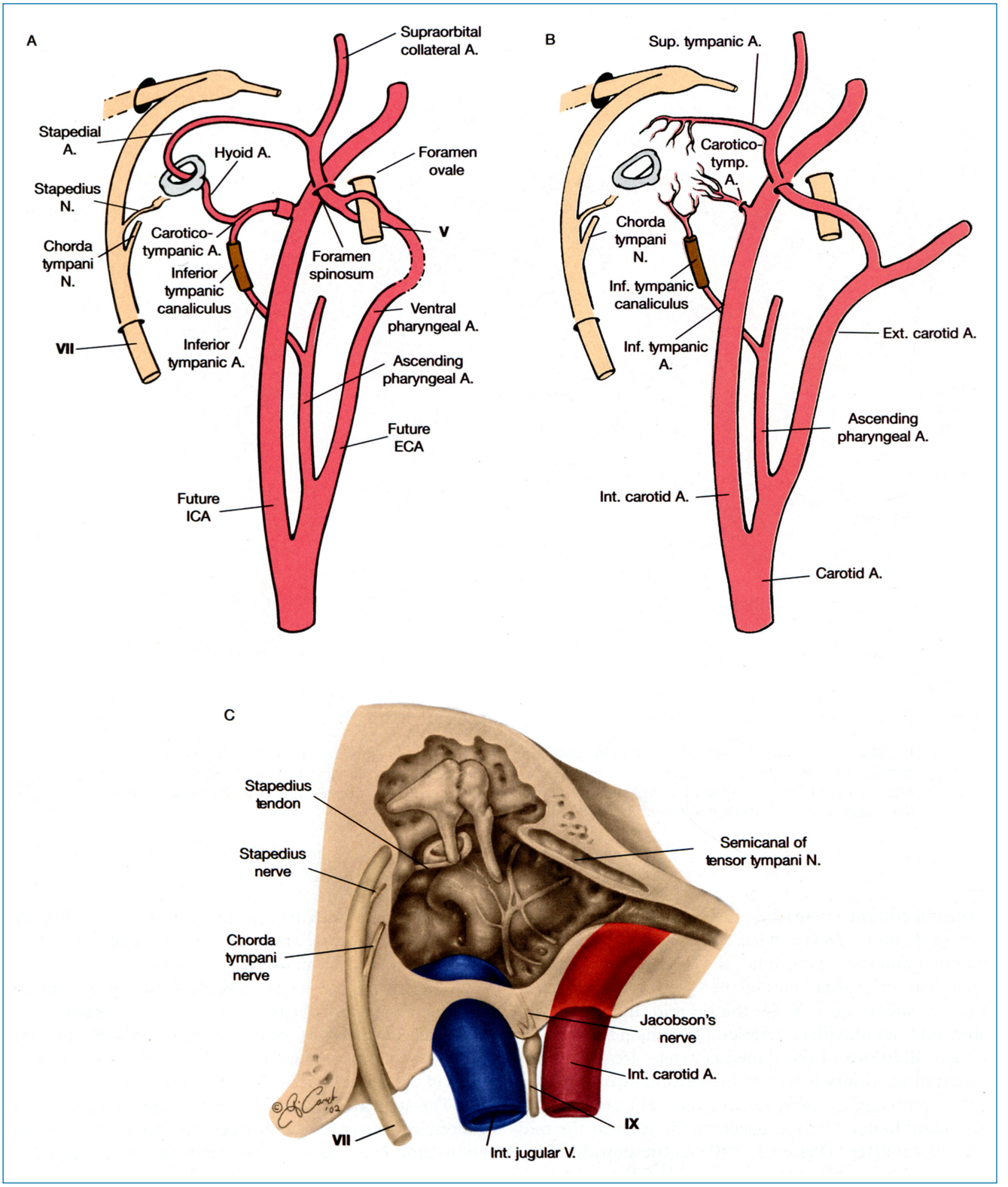

FIGURE 1–28 • Development of the cranial arteries. *A*, Approximately 7 weeks. *B*, Adult configuration. *C*, The internal carotid artery, internal jugular vein, and their interrelationships with the tympanomastoid compartment. *After Moret and colleagues. Abnormal vessels in the middle ear. J Neuroradiol 1982;9:227.*

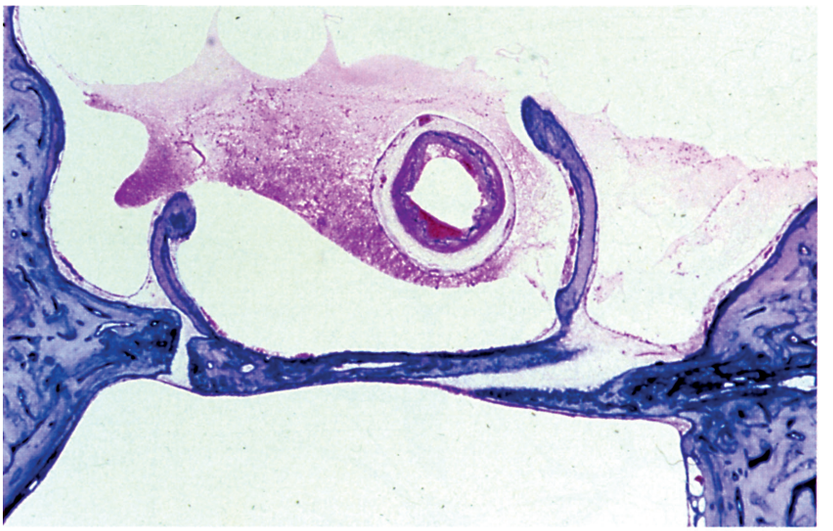

FIGURE 1–29 • The persistent stapedial artery traverses the obturator foramen (man, age 84 years). Reproduced with permission from Gulya AJ. Gulya and Schuknecht's anatomy of the temporal bone with surgical implications. 3rd ed. New York: Informa Healthcare USA; 2007.

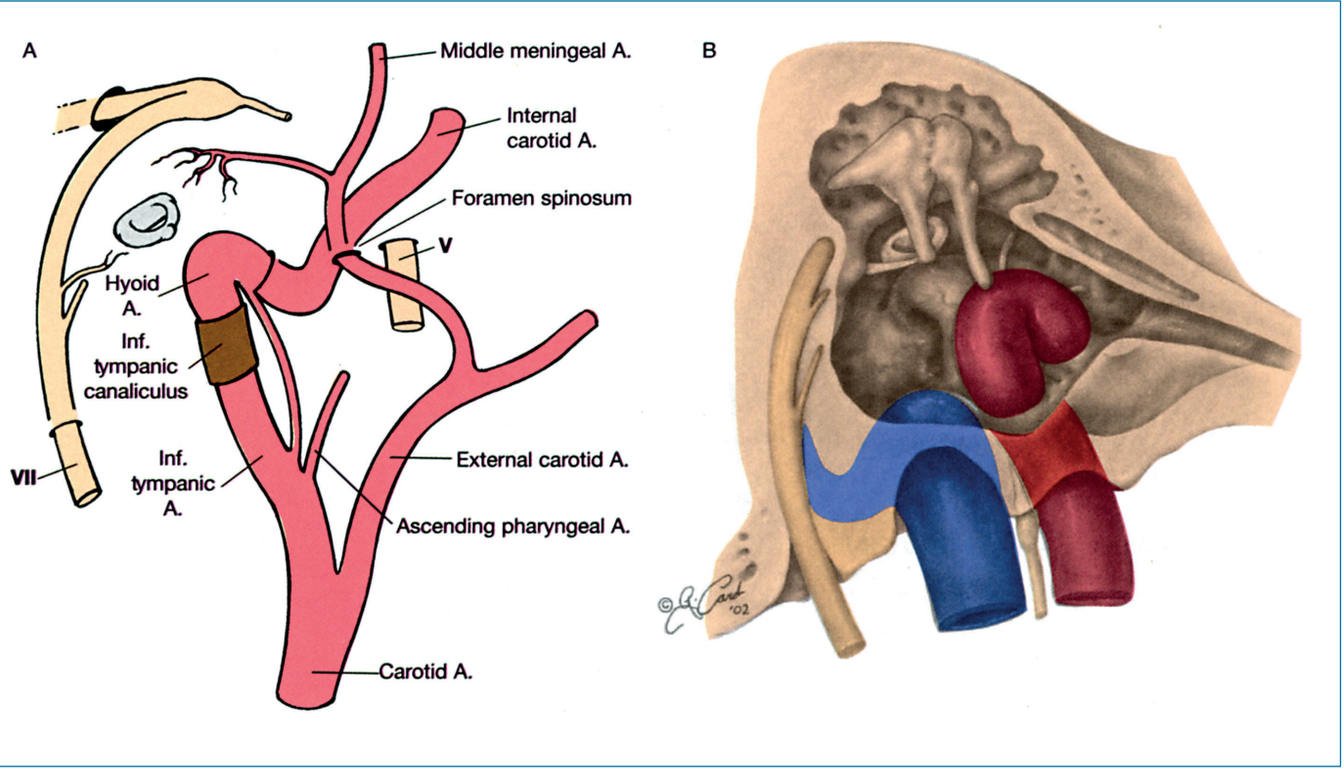

FIGURE 1–30 • *A,* The aberrant internal carotid artery, feeding into the horizontal portion of the intrapetrous internal carotid artery, is seen in association with the inferior tympanic artery and a persisting hyoid artery. *B*, The aberrant internal carotid artery is seen protruding into the tympanic cavity. *After Moret and colleagues. Abnormal vessels in the middle ear. J Neuroradiol 1982;9:227.*

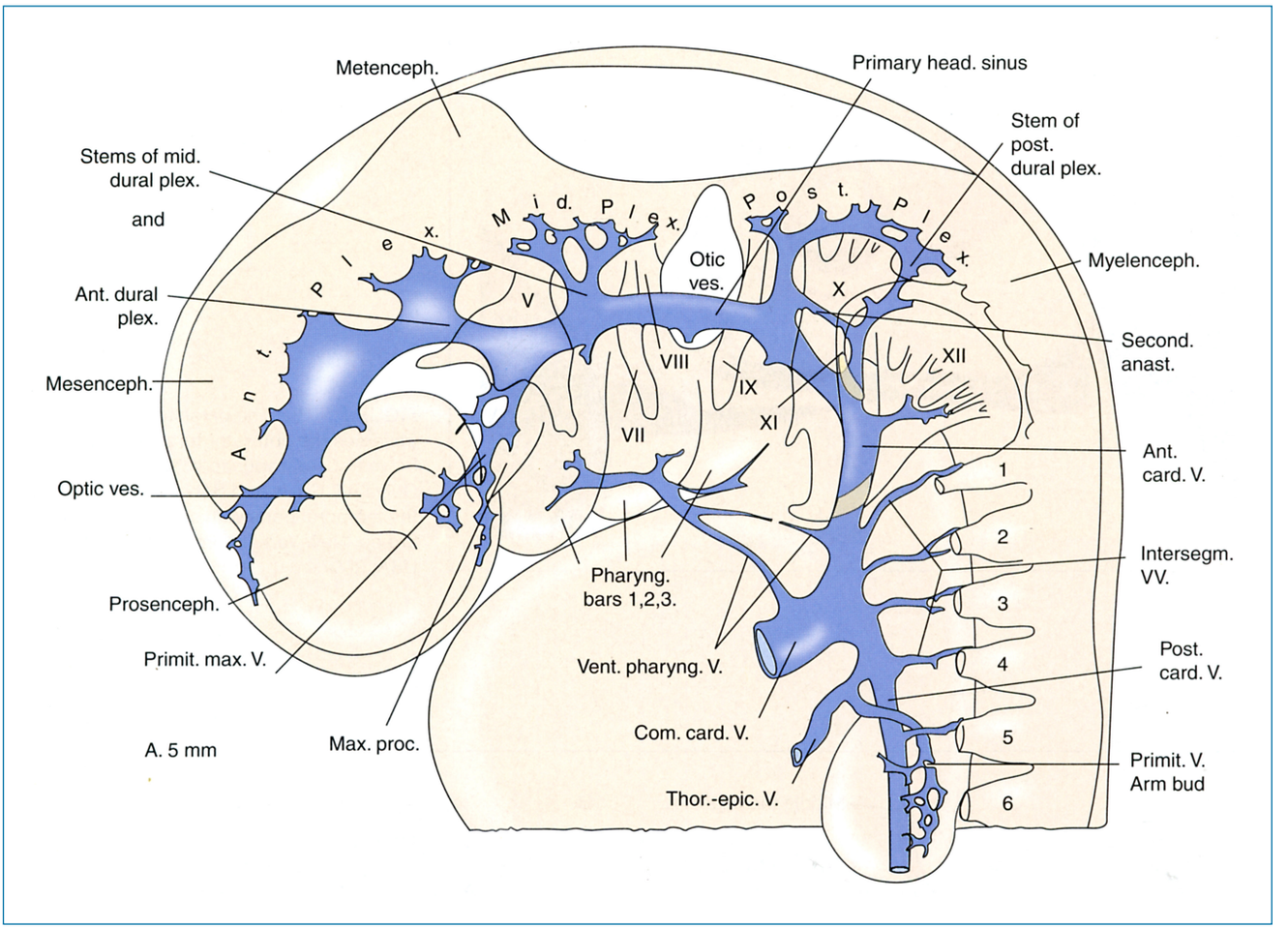

FIGURE 1–31 • The cranial venous system at approximately 4 weeks. Venous blood of the brain drains to the primary head sinus through three stems. The primary head sinus is in continuity with the anterior cardinal vein. *Reproduced with permission from Padget DH. Development of the cranial venous system in man, from the viewpoint of comparative anatomy. Contrib Embryol 1957;36:79.*

carotid arteries occasionally are encountered clinically as pulsatile middle ear masses.

DEVELOPMENT OF THE VEINS

The following account of the development of the venous circulation of the human is largely based on the exhaustive reviews of Padget.[51,52] In general, the venous system lags behind the arterial system in approaching adult configuration; in fact, adult configuration of the cranial venous system is not usually present at birth.[52]

In the developing human of 3 to 4 weeks, most of the neural tube is covered by a primitive capillary plexus, which drains dorsolaterally into a more superficial plexus. Through anterior, middle, and posterior venous stems, the superficial plexus drains into the primary head sinus (also known as the lateral capital vein), a channel that is medial to cranial nerves V and X and lateral to cranial nerves VII, VIII, and IX and the otocyst. The primary head sinus is the first true drainage channel of the craniocervical region and is present by 4 weeks (Figure 1–31). The primary head sinus is continuous with the anterior cardinal vein (the primitive internal jugular vein), which lies medial to cranial nerves X, XI, and XII. The anterior cardinal vein joins the posterior cardinal vein to form the common cardinal vein (duct of Cuvier), draining into the sinus venosus of the embryonic heart.

In the 5th and 6th weeks of development, the primary head sinus encircles and then completes its migration to lie lateral to the vagus nerve. The medial aspect of the ring around the vagus nerve forms the ventral myelencephalic vein. As the primary head sinus moves laterally, the posterior stem moves caudally, becoming continuous with the primitive internal jugular vein and thus constituting the caudal end of the definitive sigmoid sinus. The anterior cardinal (internal jugular) vein also moves to lie lateral to cranial nerves X, XI, and XII.

The jugular foramen, demarcating the internal jugular vein inferiorly and the sigmoid sinus superiorly, is completed by the 7th week. At the same time, a plexiform channel

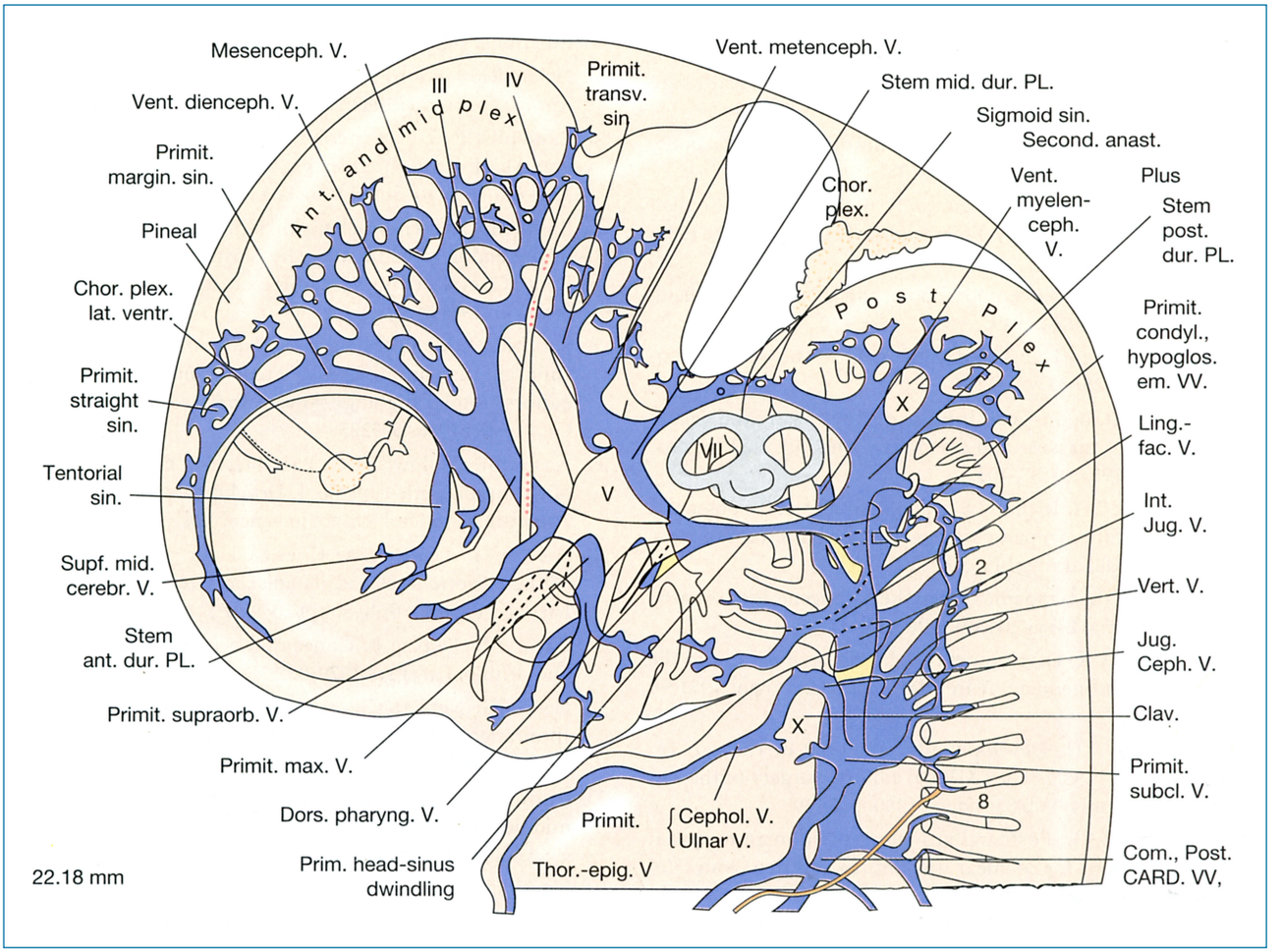

FIGURE 1–32 • The venous system at approximately 8 weeks shows the development of the sigmoid sinus from the anastomotic linkage of the middle and posterior dural plexuses. *Reproduced with permission from Padget DH. Development of the cranial venous system in man, from the viewpoint of comparative anatomy. Contrib Embryol 1957;36:79–140.*

develops, parallel and dorsal to the primary head sinus. This channel links the anterior, middle, and posterior stems and lies dorsal to the trigeminal nerve and the otocyst. Also during the 7th week, the primary head sinus begins to involute, being replaced by the dorsal channel, and the direction of flow reverses in the middle stem as it becomes the pro-otic sinus (Figure 1–32). The definitive sigmoid sinus is composed of the channel connecting the middle and posterior stems and the ventral remainder of the posterior stem. The transverse sinus develops from the anastomotic channel between the anterior and middle stems.

In embryos of approximately 8 weeks, the primary head sinus has essentially disappeared except for three remnants. The cranial remnant medial to the trigeminal nerve (part of the pro-otic sinus) becomes the lateral wing of the cavernous sinus. A caudal remnant contributes to the formation of the veins accompanying the superficial petrosal and stylomastoid arteries and draining the middle ear region, whereas yet another remnant of the primary head sinus accompanies the facial nerve extracranially, ventral to the otic capsule. Also at this stage, for the first time, the tendency of the venous drainage to pass more to the right than to the left is apparent and is accompanied by greater developmental maturity of the venous system of the right side when compared with that of the left side.

In the 9th and 10th weeks, the ventral myelencephalic vein receives the hypoglossal emissary and inferior cochlear veins. The inferior petrosal sinus is thus established.

By 12 weeks, cerebral expansion pushes the transverse sinus into its adult position. A medial tributary of the pro-otic sinus, the ventral metencephalic vein, becomes recognizable as the superior petrosal sinus.

After birth, anastomoses develop that add cavernous and inferior petrosal sinus drainage routes to the drainage of the cerebral and cerebellar veins into the junction of the transverse and sigmoid sinuses.[52]

References

1. Gulya AJ, Schuknecht H.F. Anatomy of the temporal bone with surgical implications. 3rd ed. New York: Informa Healthcare USA; 2007.
2. Anson BJ, Donaldson JA. Surgical anatomy of the temporal bone. 3rd ed. Philadelphia: WB Saunders; 1981.
3. Pearson AA. Developmental anatomy of the ear. In: English GM, editor. Otolaryngology. Philadelphia: Harper & Row; 1984. p. 1–68.
4. Bast TH, Anson BJ. The temporal bone and the ear. Springfield, IL: Charles C. Thomas; 1949.
5. Wood-Jones F, Wen I-C. The development of the external ear. J Anat 1934;68:525–33.
6. Levine H. Cutaneous carcinoma of the head and neck: Management of massive and previously uncontrolled lesions. Laryngoscope 1983;93:87–105.
7. Anson BJ, Bast TH, Richany SF. The fetal and early postnatal development of the tympanic ring and related structures in man. Ann Otol Rhinol Laryngol 1955;64:802–23.
8. Aimi K. Role of the tympanic ring in the pathogenesis of congenital cholesteatoma. Laryngoscope 1983;93:1140–6.
9. Spector GJ, Ge X-X. Development of the hypotympanum in the human fetus and neonate. Ann Otol Rhinol Laryngol 1981;90 Suppl 88:2–20.
10. Anson BJ, Bast TH. Developmental anatomy of the ear. In: Shambaugh GE Jr, Glasscock ME III, editors. Surgery of the ear. 3rd ed. Philadelphia: WB Saunders; 1980. p. 5–29.
11. Eby TL, Nadol JB Jr. Postnatal growth of the human temporal bone: Implications for cochlear implants in children. Ann Otol Rhinol Laryngol 1986;95:356–64.
12. Eby TL. Development of the facial recess: Implications for cochlear implantation. Laryngoscope 1996;106 Suppl 80:1–7.
13. van Bergeijk WA. Evolution of the sense of hearing in vertebrates. Am Zoologist 1966;6:371–7.
14. Proctor B. Embryology and anatomy of the eustachian tube. Arch Otolaryngol 1967;86:503–14.
15. Allam AF. Pneumatization of the temporal bone. Ann Otol Rhinol Laryngol 1969;78:49–64.
16. Takahara T, Sando I, Hashida Y, Shibahara Y. Mesenchyme remaining in human temporal bones. Otolaryngol Head Neck Surg 1986;95:349–57.
17. Davies DG. Malleus fixation. J Laryngol Otol 1968;82:331–51.
18. Pye A, Hinchcliffe R. Comparative anatomy of the ear. In: Hinchcliffe R, Harrison D, editors. Scientific foundations of otolaryngology. London: William Heinemann Medical Books; 1976.
19. Marovitz WF, Porubsky ES. The embryological development of the middle ear: A new concept. Ann Otol Rhinol Laryngol 1971;80:384–9.
20. Van de Water TR, Maderson PFA, Jaskoll TF. The morphogenesis of the middle and external ear. Birth Defects 1980;16:147–80.
21. Hanson JR, Anson BJ, Strickland EM. Branchial sources of the auditory ossicles in man. Part II: Observations of embryonic stages from 7 mm to 28 mm (CR length). Arch Otolaryngol 1962;76:200–15.
22. Guggenheim L. Phylogenesis of the ear. Culver City, CA: Murray and Gee; 1948.
23. Streeter GL. On the development of the membranous labyrinth and the acoustic and facial nerves in the human embryo. Am J Anat 1906;6:139–65.
24. Schuknecht HF, Belal AA. The utriculoendolymphatic valve: Its functional significance. J Laryngol Otol 1975;89:985–96.
25. Jackler RK, Luxford WM. Congenital malformations of the inner ear. Laryngoscope 1987;97 Suppl 40:2–14.
26. Lundquist P-G. The endolymphatic duct and sac in the guinea pig: An electron microscopic and experimental investigation. Acta Otolaryngol Suppl (Stockh) 1965;201:1–108.
27. Rask-Andersen H, Bredberg G, Stahle J. Structure and function of the endolymphatic duct. In: Vosteen K-H, Schuknecht HF, Pfaltz C, et al, editors. Meniere's disease. New York: Thieme-Stratton; 1981.
28. Smith RJH. Medical diagnosis and treatment of hearing loss in children. In: Cummings CW, Fredrickson JM, Harker LA, et al, editors. Otolaryngology—head and neck surgery. St. Louis: CV Mosby; 1986. p. 3225–46.
29. Anson BJ, Cauldwell EW, Bast TH. The fissula ante fenestram of the human otic capsule. I. Developmental and normal adult structure. Ann Otol Rhinol Laryngol 1947;56:957–85.
30. Spector GJ, Lee D, Carr C, et al. Later stages of development of the periotic duct and its adjacent area in the human fetus. Laryngoscope 1980;90 Suppl 20:1–31.
31. Gacek RR, Leipzig B. Congenital cerebrospinal otorrhea. Ann Otol Rhinol Laryngol 1979;88:358–65.
32. Neely JG, Neblett CR, Rose JE. Diagnosis and treatment of spontaneous cerebrospinal fluid otorrhea. Laryngoscope 1982;92:609–12.
33. Gulya AJ, Glasscock ME III, Pensak ML. Neural choristoma of the middle ear. Otolaryngol Head Neck Surg 1987;97:52–6.
34. Schuknecht HF. Pathology of the ear. Cambridge, MA: Harvard University Press; 1974.
35. Okano Y, Myers EN, Dickson DB. Microfissure between the round window niche and posterior canal ampulla. Ann Otol Rhinol Laryngol 1977;86:49–57.
36. Harada T, Sando I, Myers EN. Microfissure in the oval window area. Ann Otol Rhinol Laryngol 1981;90:174–80.
37. Proops DW, Hawke WM, Berger G. Microfractures of the otic capsule: The possible role of masticatory stress. J Laryngol Otol 1986;100:749–58.
38. El Shazly MAR, Linthicum FH Jr. Microfissures of the temporal bone: Do they have any clinical significance? Am J Otol 1991;12:169–71.
39. Batten EH. The origin of the acoustic ganglion in sheep. J Embryol Exp Morph 1958;6:597–615.
40. Skinner HA. The origin of acoustic nerve tumors. Br J Surg 1928–1929;16:440–63.
41. Van De Water TR, Ruben RJ. Organogenesis of the ear. In: Hinchcliffe R, Harrison D, editors. Scientific foundations of otolaryngology. London: William Heinemann Medical Books; 1976. p. 173–84.
42. Hilding DA. Electron microscopy of the developing hearing organ. Laryngoscope 1969;79:1691–704.
43. Gasser RF, Shigihara S, Shimada K. Three-dimensional development of the facial nerve path through the ear region in human embryos. Ann Otol Rhinol Laryngol 1994;103:395–403.
44. Gasser RF. The development of the facial nerve in man. Ann Otol Rhinol Laryngol 1967;6:37–56.
45. Gasser RF, May M. Embryonic development of the facial nerve. In: May M, editor. The facial nerve. New York: Thieme; 1986. p. 3–19.

46. Spector JG, Ge X. Ossification patterns of the tympanic facial canal in the human fetus and neonate. Laryngoscope 1993;103:1052–65.
47. Pansky B. Review of medical embryology. New York: Macmillan; 1982.
48. Padget DH. The development of the cranial arteries in the human embryo. Contrib Embryol 1948;32:205–61.
49. Altmann F. Anomalies of the internal carotid artery and its branches. Their embryological and comparative anatomical significance. Report of a new case of persistent stapedial artery in man. Laryngoscope 1947;57:313–39.
50. Steffen TN. Vascular anomalies of the middle ear. Laryngoscope 1968;78:171–97.
51. Padget DH. Development of the cranial venous system in man, from the viewpoint of comparative anatomy. Contrib Embryol 1957;36:79–140.
52. Padget DH. The cranial venous system in man in reference to development, adult configuration, and relation to the arteries. Am J Anat 1956;98:307–55.

Anatomy of the Temporal Bone and Skull Base

2

Aina Julianna Gulya, MD, FACS

The temporal bone is a fascinating, intricate, and complex structure, and developing a three-dimensional appreciation of the anatomic interrelationships of its components is an intellectually demanding task. To the otologic/neurotologic surgeon, such a three-dimensional grasp is critical to understanding the pathophysiology of, and skillfully diagnosing and managing, otologic disorders. This chapter presents a brief overview of those features of the anatomy of the temporal bone and its environs critical to the otologist; the interested reader is referred to *Anatomy of the Temporal Bone with Surgical Implications*[1] for detail beyond the scope of this chapter. In addition, since there is (as yet) no substitute for supplementing the acquisition of anatomic facts by careful dissection of a wide variety of temporal bone specimens, the reader is strongly encouraged to review the Appendix, "Surgical Anatomy of the Temporal Bone through Dissection," and to practice the described dissections.

PINNA AND EXTERNAL AUDITORY CANAL

Pinna

The pinna acts to focus and aid in the localization of sound. Its shape, showing considerable interindividual variability, reflects its multicomponent embryologic origin. Nonetheless, there are constant features.

The contour of the pinna is determined by the configuration of its elastic cartilage frame. The lateral surface of the pinna is dominated by concavities, in particular the concha (Figure 2–1). The skin of the lateral and medial surfaces of the pinna possesses hair and both sebaceous and sudoriferous glands; however, the attachment of the skin differs, being tightly bound down to the perichondrium on the lateral aspect and only loosely attached on the medial.

The pinna is securely attached to the tympanic bone by the continuity of its cartilage with that of the cartilaginous external auditory canal (EAC). Otherwise, the pinna loosely attaches to the skull by its skin, connective tissue, ligaments, and three extrinsic and six intrinsic muscles. A branch of the facial nerve, the posterior auricular nerve, innervates the intrinsic muscles, in general poorly developed in the human.

External Auditory Canal

The lateral one-third of the EAC comprises a continuation of the cartilage of the pinna and is deficient superiorly at the incisura terminalis (see Figure 2–1); the extracartilaginous endaural incision for access to the underlying temporal bone capitalizes on this gap. The two or three variably present perforations in the anterior aspect of the cartilaginous canal are the fissures of Santorini. The remaining medial two-thirds of the approximately 2.5-cm length of the canal are bony. The isthmus, the narrowest portion of the EAC, lies just medial to the junction of the bony and cartilaginous canals.

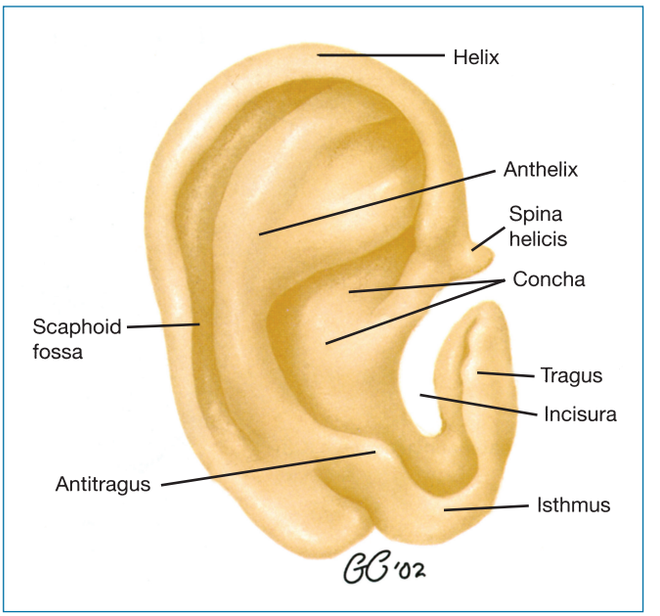

FIGURE 2–1 • Auricular cartilage.

The skin of the cartilaginous canal has a substantial subcutaneous layer, replete with hair follicles, sebaceous glands, and cerumen glands. The skin of the osseous canal, in contrast, is very thin and its subcutaneous layer is bereft of the usual adnexal structures. Accordingly, the absence of hair serves to distinguish the bony and cartilaginous canals.

Innervation

The auriculotemporal branch of the trigeminal nerve, greater auricular nerve (a branch of C3), lesser occipital nerve (of C2 and C3 derivation), auricular branch of the vagus nerve (Arnold's nerve), and twigs from the facial nerve all contribute to the sensory innervation of the pinna and EAC (Figures 2–2 and 2–3).

Effective local anesthesia can be obtained by 1 to 2% lidocaine infiltration of the postauricular region accompanied by infiltration of the cartilaginous canal in a four-quadrant (ie, at the 2, 4, 8, and 10 o'clock positions) fashion. Infiltration of the bony canal must be done gently to avoid troublesome bleb formation; if done properly, the anchoring of the skin of the bony EAC "outlines" the tympanomastoid and tympanosquamous sutures, which are the landmarks for the "vascular strip" incisions (see below). Inflammation, as with infection of the middle ear or external ear, reduces the efficacy of local anesthesia.

Vascular Supply

Two branches of the external carotid artery, the posterior auricular artery and the superficial temporal artery, are the sources of arterial blood supply to the pinna and EAC (see Figure 2–2). The posterior auricular artery, as it courses superiorly on the mastoid portion of the temporal bone, supplies the skin of the pinna and the skin and bone of the mastoid; its stylomastoid branch enters the fallopian canal to supply the inferior segment of the facial nerve. Anteriorly, a few twigs of the superficial temporal artery provide additional supply to the pinna and EAC. The veins accompanying the arteries drain into the internal jugular vein by either the facial or external jugular veins.

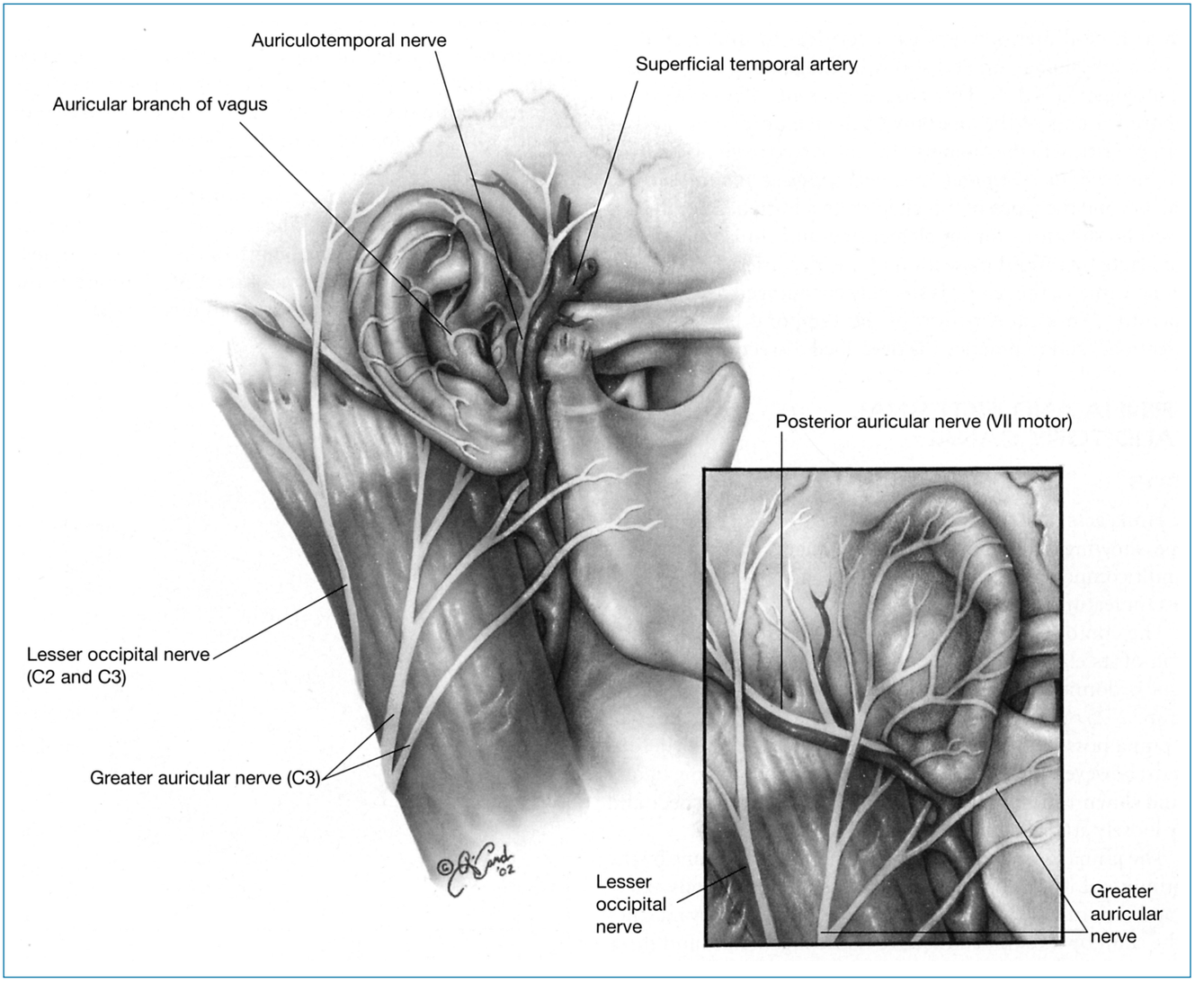

FIGURE 2–2 • Innervation of the external ear (lateral view). The inset shows the innervation of the posterior aspect of the pinna.

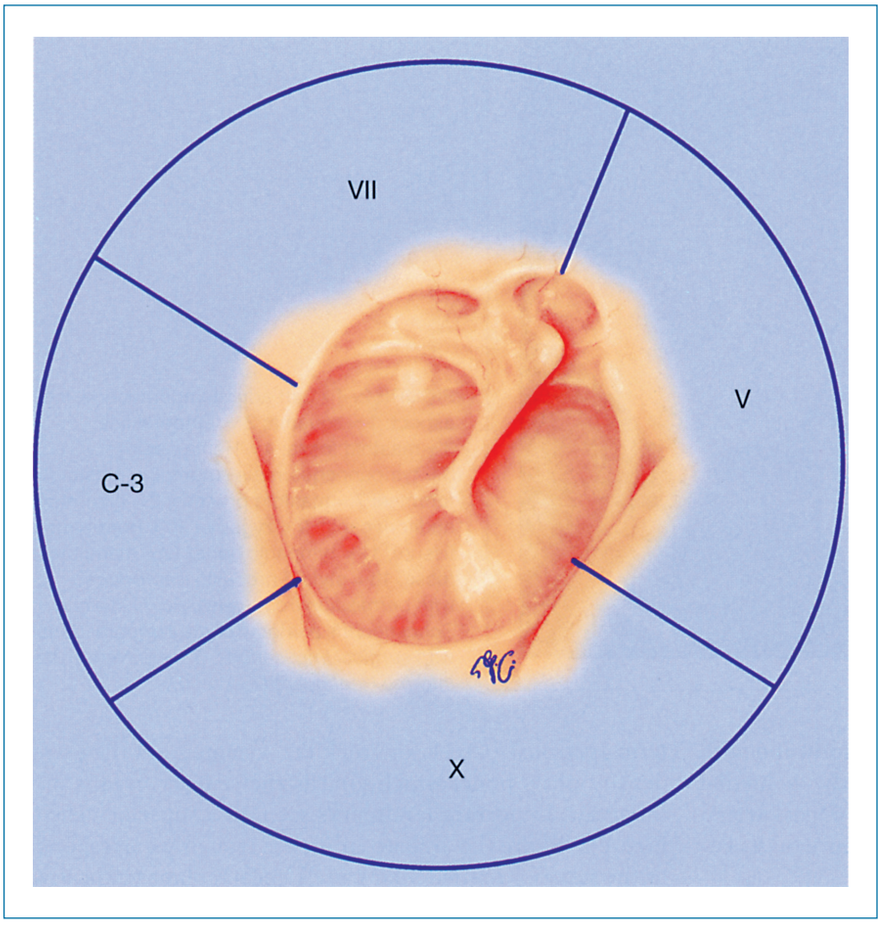

FIGURE 2–3 • The innervation of the external auditory canal.

TEMPORAL BONE, SKULL BASE, AND RELATED STRUCTURES

Temporal Bone and Skull Base

The temporal bone is a composite structure consisting of the tympanic bone, mastoid process, squama (also known as the squamous portion of the temporal bone), and petrosa (also known as the petrous portion of the temporal bone). Although the styloid process is closely related to the temporal bone, it is not considered a portion of it.

The tympanic, squamous, and mastoid portions of the temporal bone are evident on a lateral view (Figure 2–4). The tympanic bone forms the anterior, inferior, and parts of the posterior wall of the EAC. It interfaces with the squama at the tympanosquamous suture, the mastoid at the tympanomastoid suture, and the petrosa at the petrotympanic fissure and constitutes the posterior wall of the glenoid fossa for the temporomandibular joint (TMJ). The tympanomastoid suture is traversed by Arnold's nerve, whereas the chorda tympani nerve, anterior process of the malleus, and anterior tympanic artery traverse the petrotympanic fissure. Henle's spine is a projection of variable prominence at the posterosuperior aspect of the EAC. Inferiorly, the vaginal process, a projection of tympanic bone, forms the sheath of the styloid bone. Laterally, the tympanic bone borders the cartilaginous EAC, whereas medially it bears a circular groove, the annular sulcus. The annular sulcus houses the annulus of the tympanic membrane except superiorly, where it is deficient; at this point, known as the notch of Rivinus, the tympanic membrane attaches directly to the squama.

The tympanosquamous and tympanomastoid sutures are landmarks for the "vascular strip" incisions used in tympanomastoid surgery. The elevation of EAC skin and periosteum at these two sutures often requires sharp dissection to divide the contained periosteum, particularly at the tympanosquamous suture. Elevation of the tympanic membrane, as for a transcanal exploratory tympanotomy, typically commences just above the notch of Rivinus; the surgeon is thus able to identify and elevate the annulus in continuity with the tympanic membrane. The apparent size of the EAC may be diminished by excessive prominence of the bone at the tympanosquamous suture; access to the EAC in such cases can be improved by removal of the offending spur. Henle's spine marks the anterior limit of dissection in a canal wall up mastoidectomy. On occasion, posterior bulging of the anterior canal wall may obscure full visualization of the tympanic membrane. Anterior canalplasty can improve surgical visualization but if overzealous may result in prolapse of the TMJ into the EAC with, eg, opening the mouth. Temporomandibular joint dysfunction, as well as disease of the molar teeth, may manifest in referred otalgia, owing both to the proximity of the EAC and the shared innervation by the mandibular division of the trigeminal (fifth cranial) nerve.

The squamous portion of the temporal bone serves as the lateral wall of the middle cranial fossa and (see Figures 2–4

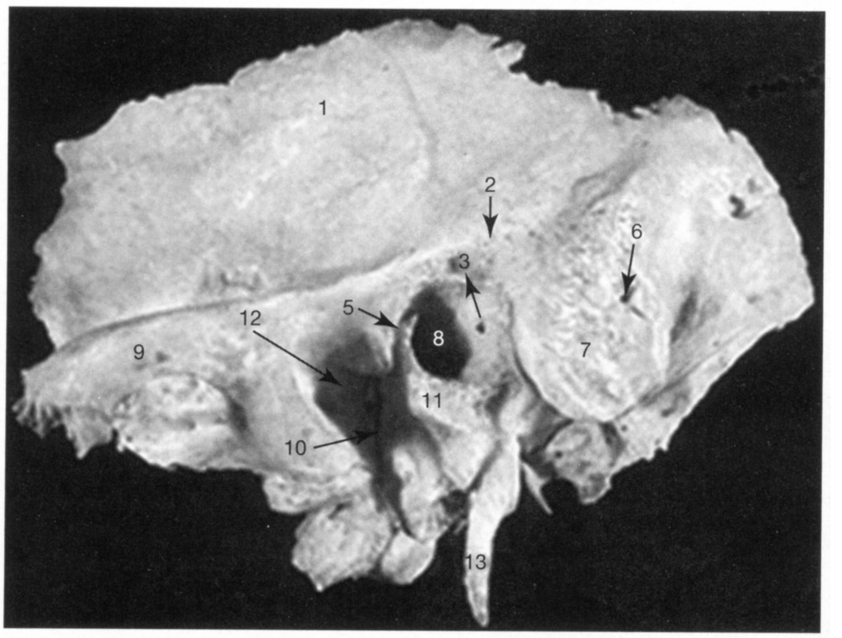

FIGURE 2–4 • Left adult temporal bone, lateral aspect. 1 = squama; 2 = temporal line; 3 = mastoid fossa; 4 = Henle's spine; 5 = tympanosquamous suture; 6 = mastoid foramen; 7 = mastoid process; 8 = external auditory canal; 9 = zygoma; 10 = petrotympanic fissure; 11 = tympanic bone; 12 = mandibular fossa; 13 = styloid process. *Reproduced with permission from Gulya, AJ. Gulya and Schuknecht's anatomy of the temporal bone with surgical implications. 3rd ed. New York: Informa Healthcare USA; 2007.*

and 2–5) interfaces with the parietal bone superiorly and with the zygomatic process and the sphenoid anteriorly. Its medial surface is grooved by a sulcus for the middle meningeal artery, whereas the middle temporal artery runs in a groove on its lateral aspect.

The mastoid portion of the temporal bone (see Figure 2–4) is the inferiorly extending projection seen on the lateral surface of the temporal bone. It is composed of a squamous portion (laterally) and a petrous portion (medially) separated by Körner's (petrosquamous) septum. The fossa mastoidea (Macewen's triangle) is defined by the linea temporalis (temporal line), a ridge of bone extending posteriorly from the zygomatic process (marking the lower margin of the temporalis muscle and approximating the inferior descent of the middle cranial fossa dura), the posterosuperior margin of the EAC, and a tangent to the posterior margin of the EAC. The fossa mastoidea, a cribrose (cribriform) area, is identified by its numerous, perforating small blood vessels.

The mastoid foramen, located posteriorly on the mastoid process, is traversed by the mastoid emissary vein and one or two mastoid arteries. Inferiorly, the sternocleidomastoid muscle attaches to the mastoid tip.

The linea temporalis is an avascular plane, a feature that makes it an ideal location for the superior limb of the "T" musculoperiosteal incision used in the postauricular approach to the tympanomastoid compartment. The fossa mastoidea is an important surgical landmark as it laterally overlies the mastoid antrum. The mastoid antrum, medial to the fossa mastoidea (Macewen's triangle), develops in the earliest stages of mastoid pneumatization and is ordinarily present in even the least pneumatized temporal bones. Therefore, the fossa mastoidea is the site at which mastoid drilling ordinarily commences.

The petrosa (see Figures 2–5, 2–6, and 2–7) is evident on superior, medial, and posterior views of the temporal bone; the term "petrous" (Greek for "rocklike") stems from the extreme density of its bone, which guards the sensory organs of the inner ear. Important landmarks seen on a superior view (see Figure 2–6) are the arcuate eminence (roughly corresponding to the superior semicircular canal), meatal plane (indicative of the internal auditory canal), foramen spinosum for the middle meningeal artery, and facial hiatus (marking the departure of the greater petrosal nerve from the anterior aspect of the geniculate ganglion). The lesser petrosal nerve, accompanied by the superior tympanic artery, occupies the superior tympanic canaliculus, lying lateral to and paralleling the path of the greater petrosal nerve to the petrous apex. The petrous apex points anteromedially and is marked by the transition of the intrapetrous to the intracranial internal carotid artery, orifice of the bony eustachian tube, and, anterolaterally, ganglion of the trigeminal nerve in Meckel's cave.

The medial view of the temporal bone (see Figure 2–5) features the porus of the internal auditory canal (IAC). The foramen seen at the petrous apex is the internal carotid foramen, by which the internal carotid artery exits the temporal bone. The sigmoid portion of the lateral venous sinus runs in the deep sulcus seen posteriorly, whereas the superior petrosal sinus runs in the sulcus located at the junction of the posterior and middle fossa faces of the temporal bone.

The vertically oriented posterior face of the petrosa dominates the posterior view of the temporal bone (see Figure 2–7) as it delimits the anterolateral aspect of the posterior cranial fossa and lies between the superior and inferior petrosal sinuses. The porus of the IAC, operculum, endolymphatic fossette cradling the endolymphatic sac, and subarcuate fossa are the key anatomic features on this surface.

The inferior surface of the temporal bone (Figure 2–8) figures prominently in skull base anatomy as it interfaces with the sphenoid and occipital bones. It provides attachment for the deep muscles of the neck and is perforated by a multitude

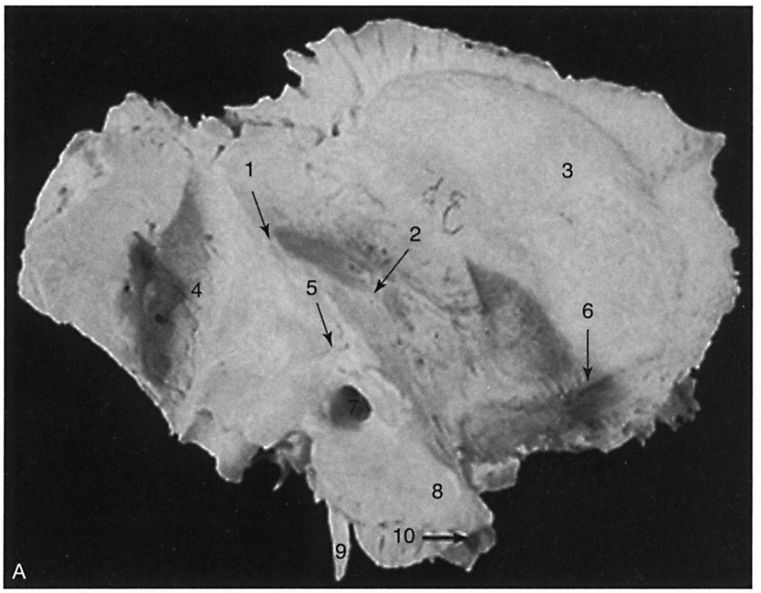

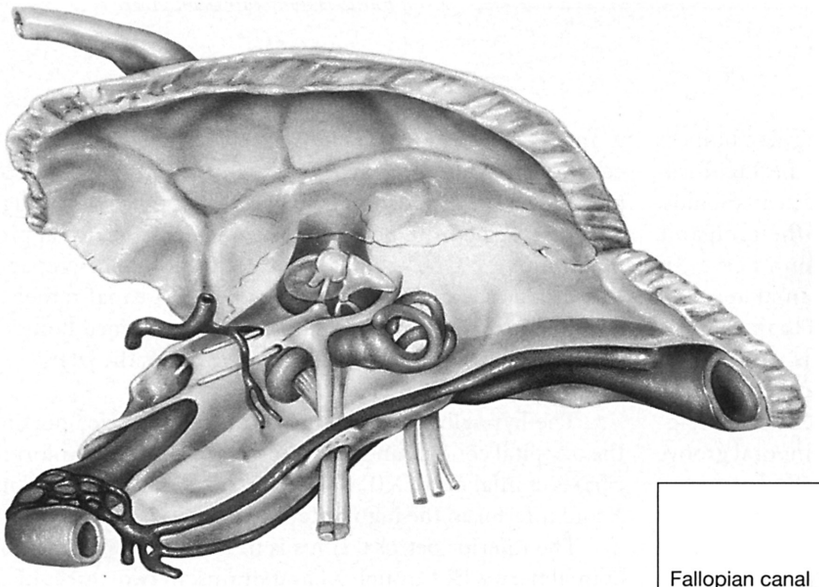

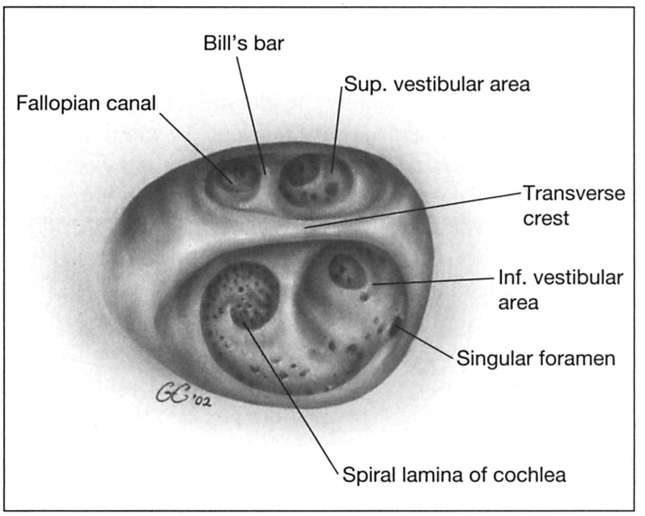

B

FIGURE 2–5 • *A*, Left adult temporal bone, medial aspect. 1 = superior petrosal sulcus; 2 = arcuate eminence; 3 = squama; 4 = sigmoid sulcus; 5 = petromastoid canal; 6 = middle meningeal artery sulcus; 7 = internal auditory canal; 8 = petrous apex; 9 = styloid process; 10 = internal carotid artery foramen. *Reproduced with permission from Gulya, AJ. Gulya and Schuknecht's anatomy of the temporal bone with surgical implications. 3rd ed. New York: Informa Healthcare USA; 2007. B*, Drawing indicating approximate anatomic relationships of the internal carotid artery, superior petrosal sinus, facial nerve, bony labyrinth, and ossicular chain (right temporal bone). Inset shows the anatomic interrelationships at the fundus of the internal auditory canal.

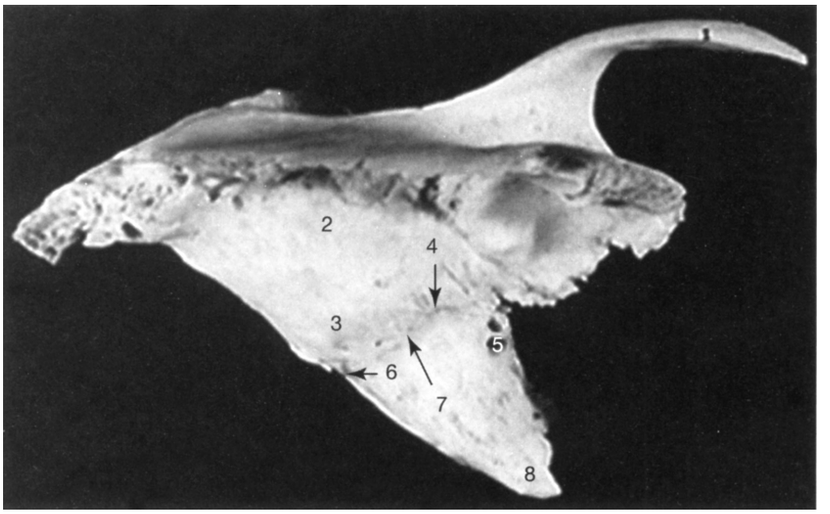

FIGURE 2–6 • Left adult temporal bone, superior aspect. 1 = zygoma; 2 = tegmen; 3 = arcuate eminence; 4 = lesser superficial petrosal canal; 5 = internal carotid artery foramen; 6 = internal audotory canal; 7 = facial hiatus; 8 = petrous apex. *Reproduced with permission from Gulya, AJ. Gulya and Schuknecht's anatomy of the temporal bone with surgical implications. 3rd ed. New York: Informa Healthcare USA; 2007.*

of foramina. The jugular fossa, housing the jugular bulb, is separated from the internal carotid artery by the jugulocarotid crest. The aperture of the inferior tympanic canaliculus, traversed by the inferior tympanic artery and the tympanic branch of the glossopharyngeal nerve (Jacobson's nerve), is sited in the jugulocarotid crest, whereas the cranial aperture of the cochlear aqueduct is located anteromedial to the jugular fossa. The groove for the inferior petrosal sinus can be seen near the petrous apex. The stylomastoid foramen of the facial nerve is located just posterior to the styloid process. The occipital artery and the digastric muscle occupy the temporal groove and the mastoid incisure, respectively, at the medial aspect of the tip.

The jugular foramen is of particular importance in skull base surgery as it is traversed by the glossopharyngeal (ninth), vagus (tenth), and spinal accessory (eleventh) cranial nerves as they exit the skull (Figures 2–9, 2–10, and 2–11). In the course of posterolateral skull base exposure, decortication and fibrous tissue dissection reveal the internal jugular vein, its bulb, and the internal carotid artery. Posterior retraction of the internal jugular vein and resection of the jugular bulb allow visualization of the lower cranial nerves exiting the skull (see Figure 2–11), the most anterior and lateral of which is cranial nerve IX, as it passes just posterior to the jugulocarotid crest.[2,3] Cranial nerves X and XI are located progressively more posterior (and medial) to cranial nerve IX. Cranial nerve XI is generally identified as it crosses over the internal jugular vein in the neck and the lateral process of the atlas; however, it is important to recognize that nearly as often cranial nerve XI can pass medial to the internal jugular vein.[4]

Contradictory reports exist in the literature regarding the bony/fibrous compartmentalization of the jugular foramen and the distribution of contained neurovascular structures; in the compartmentalized jugular foramen, cranial nerve IX is found in the anteromedial compartment, whereas cranial nerves X and XI and the jugular bulb are located posterolaterally. The contradiction appears particularly when contrasting neurosurgical studies, which use an intracranial approach to the jugular foramen, to neurotologic studies, in which a lateral approach predominates. One suggested resolution to the discrepancy is to consider the jugular foramen as a "short canal rather than a simple foramen"[4] in which a medially positioned bony/thick fibrous tissue septum thins as one approaches the lateral aspect of the foramen.

The hypoglossal canal, located in the anterior portion of the occipital condyle and anteroinferior to the jugular foramen, carries cranial nerve XII, which courses medial to cranial nerve X and inferior to the jugular foramen.[3]

The inferior petrosal sinus is in close anatomic relation to cranial nerves IX through XI as it drains, in two-thirds of cases via multiple openings, into the anterior aspect of the jugular bulb (see Figure 2–10). Most commonly, the inferior petrosal sinus runs inferior and medial to cranial nerve IX and superior and lateral to cranial nerves X and XI.[4] The condylar emissary vein, draining the suboccipital plexus, opens into the jugular bulb inferiorly and posteriorly, in proximity to cranial nerves X and XI.[4]

The cochlear aqueduct, carrying the periotic (or perilymphatic) duct, is an important landmark for the neuro-otologist. As the cochlear aqueduct runs from the medial aspect of the scala tympani of the basal cochlear turn to terminate anteromedial to the jugular bulb, it parallels, and lies inferior to, the IAC. From the transmastoid perspective, the aqueduct is encountered when drilling medial to the jugular bulb; opening the aqueduct results in the flow of cerebrospinal fluid into the mastoid, a useful maneuver in translabyrinthine cerebellopontine angle tumor surgery as it decompresses cerebrospinal fluid pressure. In addition, cranial nerve IX, the inferior petrosal sinus, and, in some cases, cranial nerves X and XI can be found immediately inferior to the lateral terminus of the cochlear aqueduct.[5]

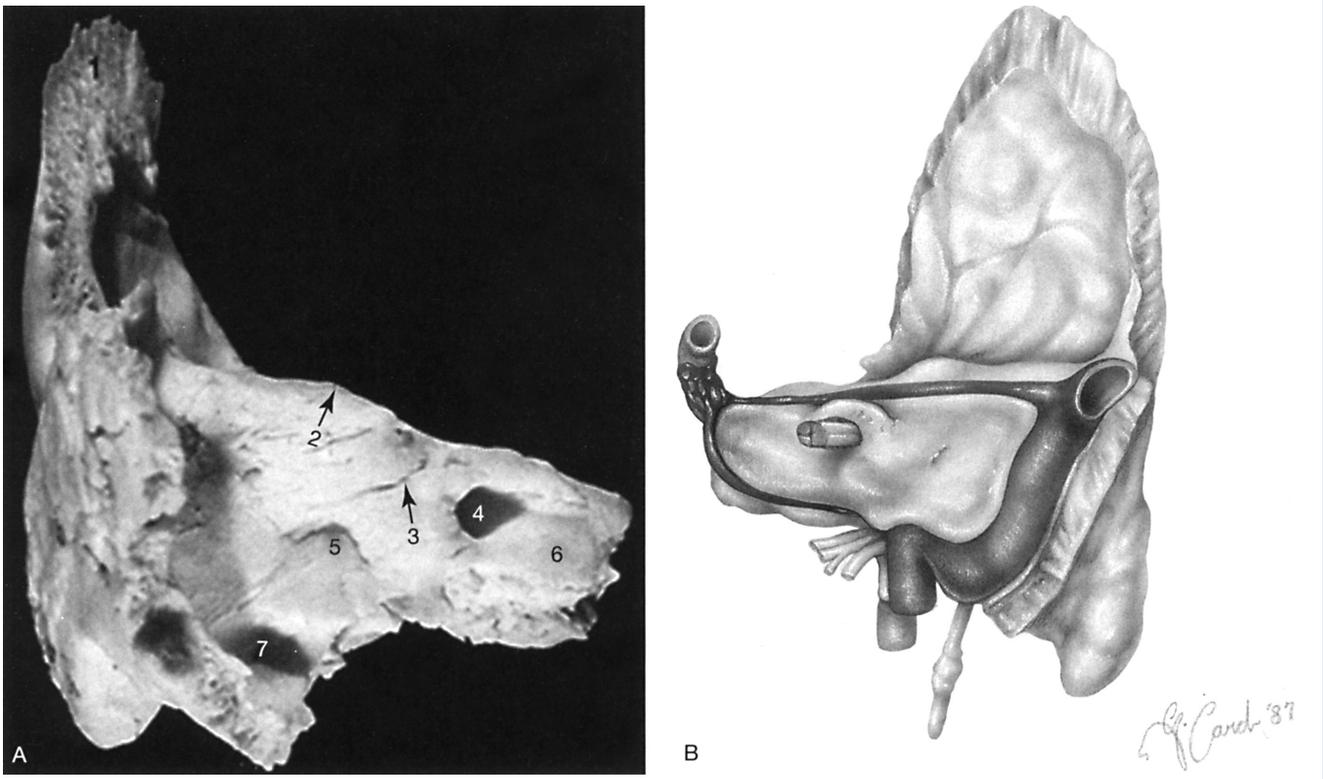

FIGURE 2–7 • *A*, Left adult temporal bone, posterior aspect. 1 = squama; 2 = arcuate eminence; 3 = petromastoid canal; 4 = internal auditory canal; 5 = endolymphatic fossette; 6 = petrous apex; 7 = sigmoid sulcus. *Reproduced with permission from Gulya, AJ. Gulya and Schuknecht's anatomy of the temporal bone with surgical implications. 3rd ed. New York: Informa Healthcare USA; 2007. B*, Artist's depiction of the posterior aspect of the right temporal bone, with neovascular structures.

Therefore, the cochlear aqueduct can be used as a guide to the lower limits of IAC dissection in, eg, the translabyrinthine approach as it allows full exposure of the IAC without risking the lower cranial nerves.

Related Structures

Tympanic Membrane

The tympanic membrane (see Figure 2–3) emulates an irregular cone, the apex of which is formed by the umbo (at the tip of the manubrium). The adult tympanic membrane is about 9 mm in diameter and subtends an acute angle with respect to the inferior wall of the EAC. The fibrous annulus of the tympanic membrane anchors it in the tympanic sulcus. In addition, the tympanic membrane firmly attaches to the malleus at the lateral process and at the umbo; between these two points, only a flimsy mucosal fold, the plica mallearis, connects the tympanic membrane to the malleus.

The tympanic membrane is separated into a superior pars flaccida (Shrapnell's membrane) and a pars inferior by the anterior and posterior tympanic stria, which run from the lateral process of the malleus to the anterior and posterior tympanic spines, respectively. Shrapnell's membrane serves as the lateral wall of Prussak's space (the superior recess of the tympanic membrane); the head and neck of the malleus, the lateral malleal ligament, and anterior and posterior malleal folds form the medial, anterosuperior, and inferior limits of Prussak's space.

The tympanic membrane is a trilaminar structure. The lateral surface is formed by squamous epithelium, whereas the medial layer is a continuation of the mucosal epithelium of the middle ear. Between these layers is a fibrous layer, known as the pars propria. The pars propria at the umbo splits to envelop the distal tip of the manubrium.

Ossicles

The ossicular chain (Figure 2–12), made up of the malleus, incus, and stapes, serves to conduct sound from the tympanic membrane to the cochlea.

The malleus, the most lateral of the ossicles, has a head (caput), manubrium (handle), neck, and anterior and lateral

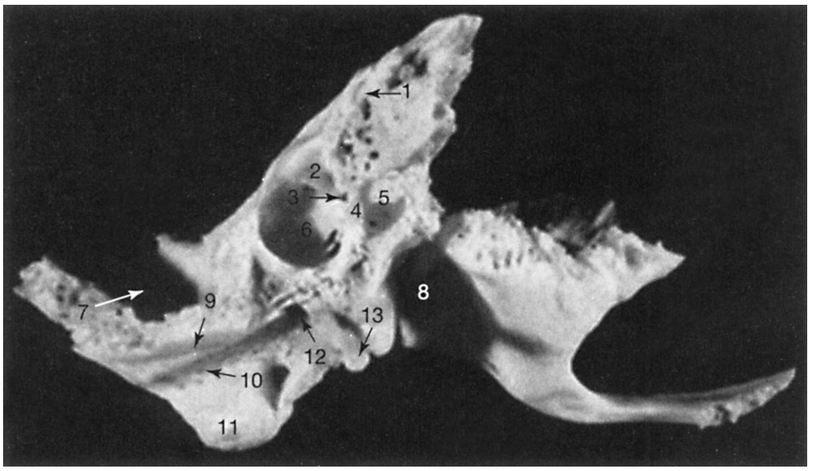

FIGURE 2–8 • Left adult temporal bone, inferior aspect. 1, inferior petrosal sulcus; 2, cochlear aqueduct; 3, inferior tympanic canaliculus; 4, jugulocarotid crest; 5, internal carotid artery formaen; 6, jugular fossa; 7, sigmoid sulcus; 8, mandibular fossa; 9, temporal groove; 10, mastoid incisure; 11, mastoid tip; 12, stylomastoid foramen; 13, styloid process. *Reproduced with permission from Gulya, AJ. Gulya and Schuknecht's anatomy of the temporal bone with surgical implications. 3rd ed. New York: Informa Healthcare USA; 2007.*

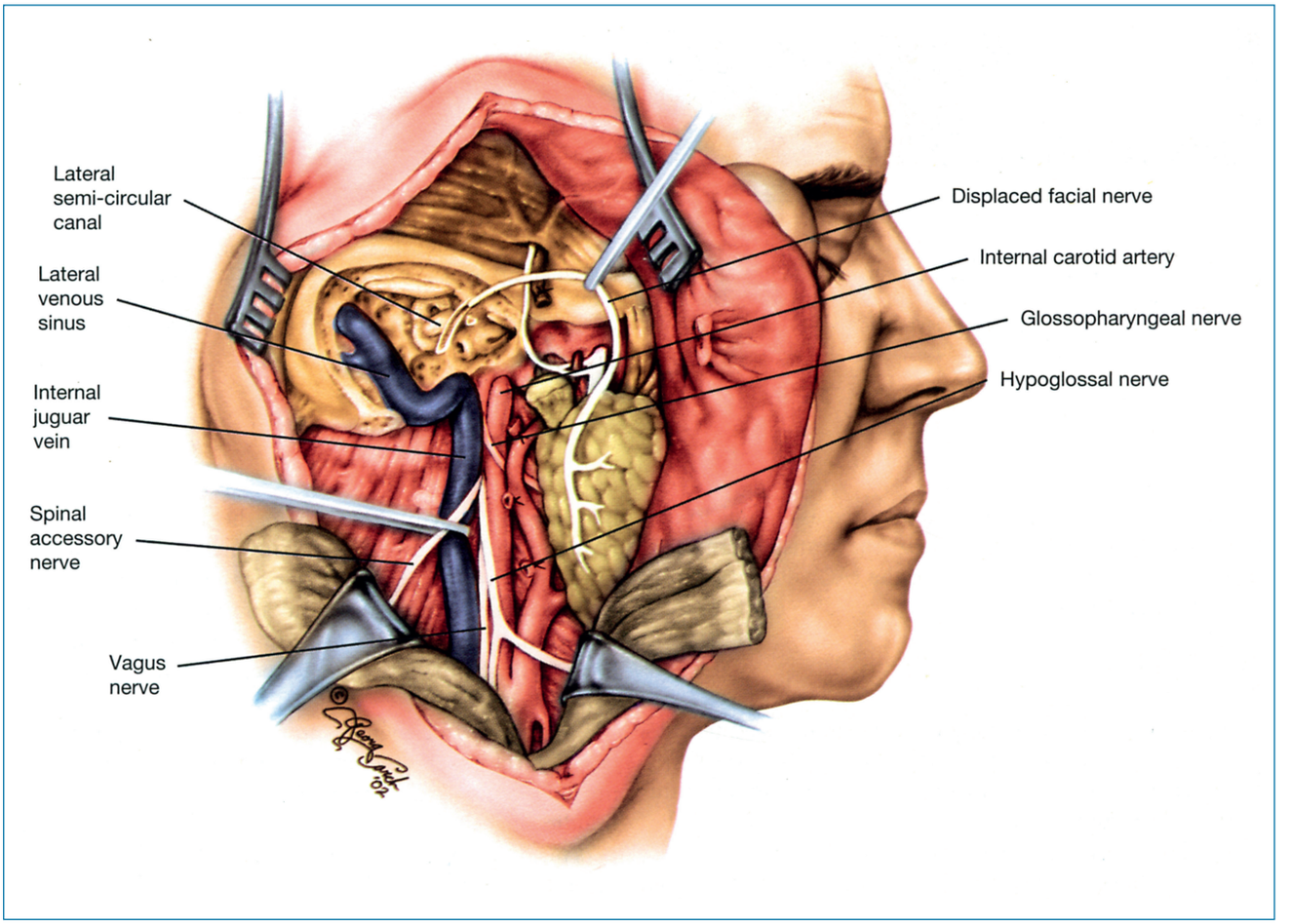

FIGURE 2–9 • Skull base dissection, right. A radical mastoidectomy and neck dissection have been done. The sigmoid sinus and internal carotid artery (ICA) have been decorticated, and the cochlea has been partially removed. The facial nerve has been rerouted anteriorly, and the lower cranial nerves are seen emerging from the crevice between the ICA and the internal jugular vein. *After Goldenberg RA. Surgeon's view of the skull base from the lateral approach. Laryngoscope 1984;94:1–21.*

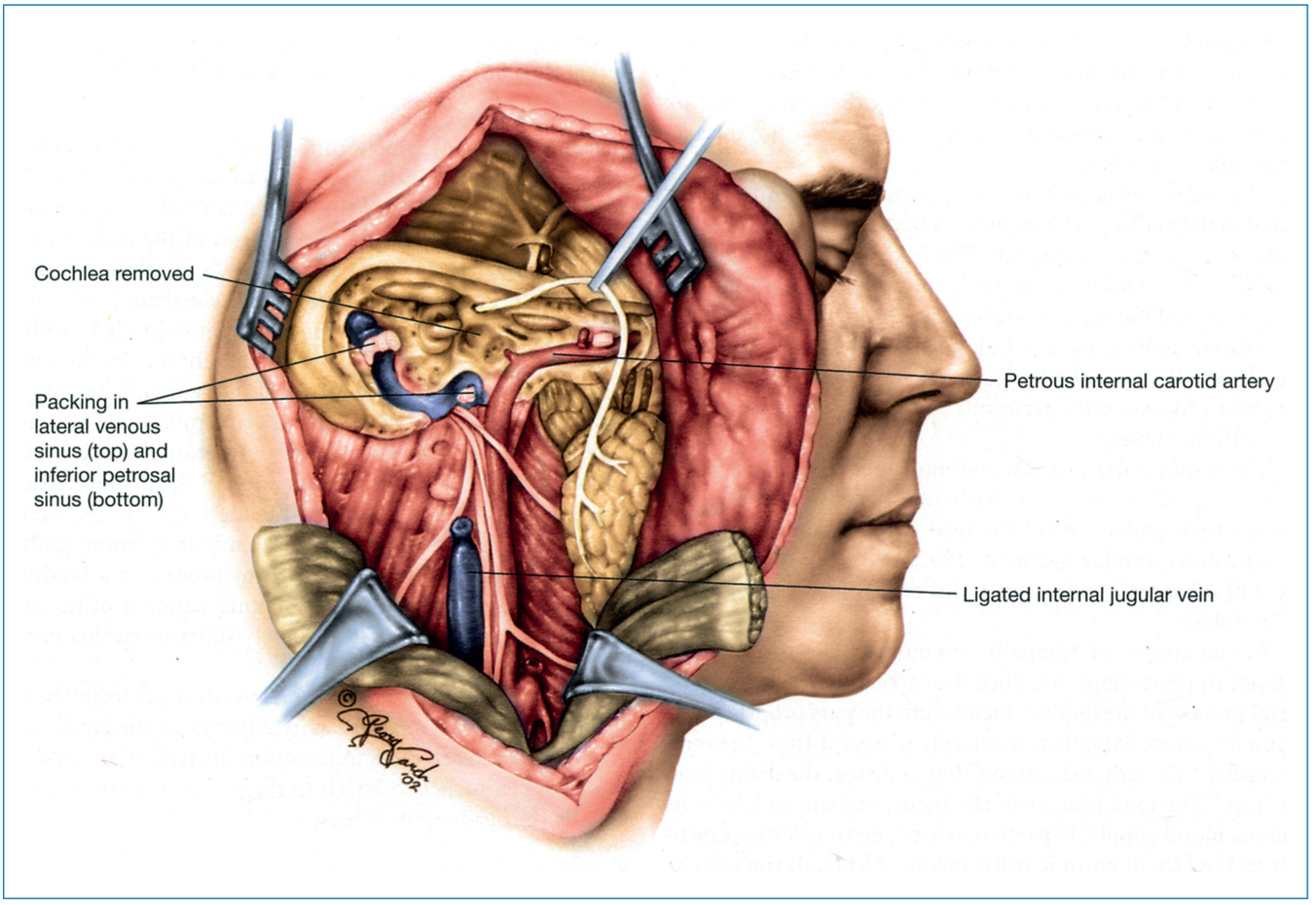

FIGURE 2–10 • With further dissection, the eustachian tube is removed, and the petrous internal carotid artery has been exposed. *After Goldenberg RA. Surgeon's view of the skull base from the lateral approach. Laryngoscope 1984;94:1–21.*

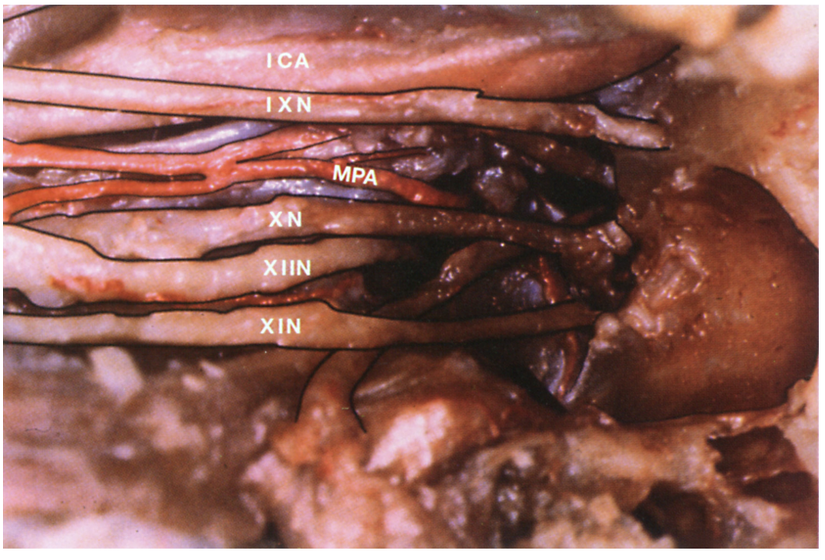

FIGURE 2–11 • Left skull base dissection. Removal of the internal jugular vein and the jugular bulb exposes the exit of the lower cranial nerves from the posterior fossa. (ICA, internal carotid artery; IXN, glossopharyngeal nerve; XN, vagus nerve; XIN, spinal accessory nerve; XIIN, hypoglosal nerve; MPA, posterior meningeal artery) Photo courtesy of John Kveton, MD; *reproduced with permission from Kveton JF. Anatomy of the jugular foramen: the neurotologic perspective. Op Tech ORL-HNS 1996;7:95–8.*

processes. The lateral process has a cartilaginous "cap" that imperceptibly merges with the pars propria of the tympanic membrane. The anterior ligament of the malleus, extending from the anterior process, passes through the petrotympanic fissure and, with the posterior incudal ligament, creates the axis of ossicular rotation.

The incus, the largest of the three ossicles, is immediately medial to the malleus. The incus has a body and three processes: a long, a short, and a lenticular. The body of the incus articulates with the head of the malleus in the epitympanum. The short process of the incus is anchored in the incudal fossa by the posterior incudal ligament. The long process extends inferiorly, roughly paralleling and lying posterior to the manubrium. The lenticular process, at the terminus of the long process, articulates with the stapes.

The stapes is the smallest and most medial of the ossicles. Its head articulates with the lenticular process of the incus, whereas its footplate sits in the oval window, surrounded by the stapediovestibular ligament. The arch of the stapes, composed of an anterior and a posterior crus, links the head and the footplate.

In the course of tympanic membrane elevation, as for instance in tympanoplasty, since the cartilaginous "cap" of the lateral process of the malleus blends into the pars propria of the drum, it is more expedient to sharply dissect it from the malleus rather than tediously attempting to dissect the drum from the "cap." The long process of the incus, perhaps owing to its tenuous blood supply, is particularly prone to osteitic resorption in the face of chronic otitis media. Although the ossicles are held in position by their ligaments and tendons, the force of injudicious surgical manipulation can easily overcome these restraints, resulting in subluxation or complete luxation. When dissecting disease from the stapes, one should parallel the plane of the stapedius tendon, in a posterior to an anterior direction, so that the tendon resists displacement of the stapes.

Middle Ear Muscles

The tensor tympani muscle, innervated by the trigeminal nerve, originates from the walls of its semicanal, greater wing of the sphenoid, and cartilage of the eustachian tube. The tendon of the tensor tympani muscle sweeps around the cochleariform process and across the tympanic cavity to attach to the medial aspect of the neck and manubrium of the malleus.

The medial pull of the tensor tympani muscle is ordinarily opposed by the intact tympanic membrane. In the case of a chronic, substantial perforation of the tympanic membrane, the unopposed action of the tensor tympani muscle can medialize the manubrium, effectively contracting the depth of the tympanic cavity. Forcible lateralization of the malleus, or even sectioning of the tensor tympani tendon, may be required to allow the surgeon to perform tympanic membrane grafting or ossiculoplasty. The cochleariform process is a landmark to the anterior aspect of the tympanic segment of the facial nerve as the nerve runs immediately superior to this process (Figure 2–13).

The stapedius muscle runs in a vertical sulcus in the posterior wall of the tympanic cavity adjacent to the facial nerve, from which it receives its innervation. Its tendon traverses the pyramidal eminence to attach to the posterior crus, and occasionally the head, of the stapes.

Middle Ear Spaces

The tympanic cavity is a sagittally oriented slit that lies immediately medial to the tympanic membrane. Its roof, or tegmen, also serves as part of the floor of the middle cranial fossa,

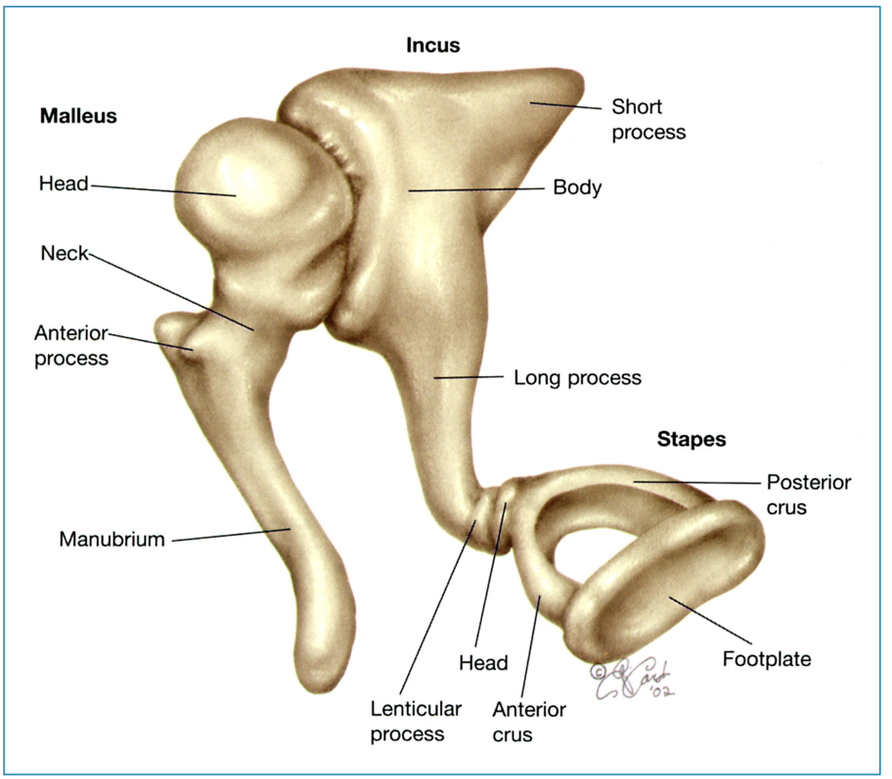

FIGURE 2–12 • The ossicular chain, medial aspect.

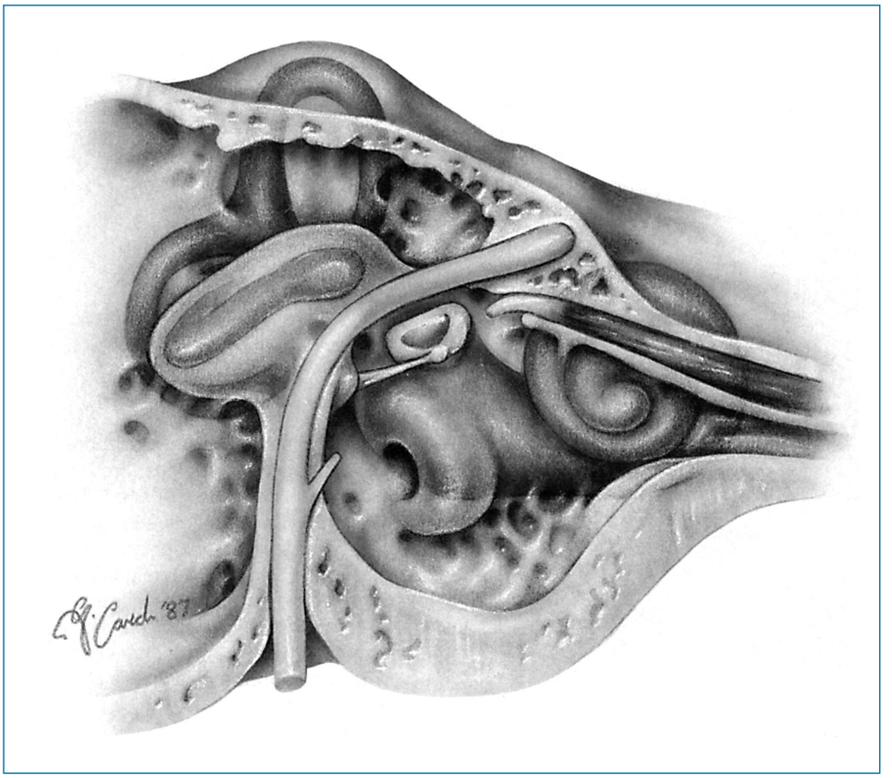

FIGURE 2–13 • The facial nerve is seen in its vertical and tympanic segments. Anterosuperiorly, the facial nerve passes superior to the tensor tympani tendon, which is seen sectioned just after it exits the cochleariform process.

whereas its irregularly contoured floor features the jugular bulb and, posteriorly, the root of the styloid process. The tympanic cavity is in continuity with the eustachian tube anteriorly and with the mastoid air cells via the aditus and antrum. It is traversed by the ossicular chain and is lined with a mucosal epithelium. Planes extended from the tympanic annulus subdivide the tympanic cavity into a mesotympanum, hypotympanum, protympanum, and posterior tympanic cavity. The epitympanum lies above the plane of the anterior and posterior tympanic spines.

Anteriorly, the mesotympanum is dominated by the bulge of the semicanal of the tensor tympani muscle; the tympanic orifice of the eustachian tube is immediately inferior to this bulge (Figure 2–14). Posteriorly, the key anatomic features are the pyramidal eminence and, lateral to it, the chordal eminence. The chordal eminence houses the iter chordae posterius by which the chorda tympani nerve enters the tympanic cavity.

The medial wall (the surgical "floor" of the middle ear) features three depressions: the sinus tympani, oval window niche, and round window niche (Figure 2–15). The sinus tympani is defined by the ponticulus superiorly, the subiculum inferiorly, the mastoid segment of the facial nerve laterally, and the posterior semicircular canal medially; there is substantial variability in the posterior extension (surgical "depth") of the sinus tympani, ranging from "shallow" to "deep." The oval window niche, occupied by the stapes footplate, is located anterosuperior to the ponticulus. The round window niche can be found posteroinferior to the promontory, the bulge created by the basal turn of the cochlea.

The sinus tympani evades direct surgical visualization, which is particularly worrisome in cholesteatoma surgery as it can harbor the nidus of recurrence. Inspection of this region has been somewhat improved by the advent of endoscopes appropriate for otologic surgery. The oval window niche may be the site of a perilymphatic fistula. Similarly, the round window niche may be implicated in perilymph leakage. In assessing the round window, it is important to realize that in the vast majority of cases, the true round window membrane is obscured by some kind of mucosal veil (Figure 2–16); most often, the veil is perforated, giving the false impression of seeing a defect in the round window membrane.[6]

Eustachian Tube

The eustachian tube extends approximately 35 mm from the anterior aspect of the tympanic cavity to the posterior aspect of the nasopharynx and serves to ventilate, clear, and protect the middle ear (see Figures 2–9 and 2–14). The lining mucosa of the tube has an abundance of mucociliary cells, important to its clearance function. The anteromedial two-thirds of the eustachian tube are fibrocartilaginous, whereas the remainder is bony. The tympanic orifice is in the anterior wall of the middle ear, a few millimeters above the floor. In its normal resting position, the tube is closed; opening of the tube is accomplished by the tensor veli palatini muscle, innervated by the trigeminal nerve. A body of fat, the lateral fat pad of Ostmann, abuts the lateral aspect of the fibrocartilaginous tube and aids in maintaining the resting closure of the tube.

Mucosa of the Tympanomastoid Compartment

The medial surface of the tympanic membrane, tympanic cavity, and mastoid air cells are all lined with a mucosal epithelium, reflecting their common heritage from the tubotympanic recess. The predominant cell type varies with location in the

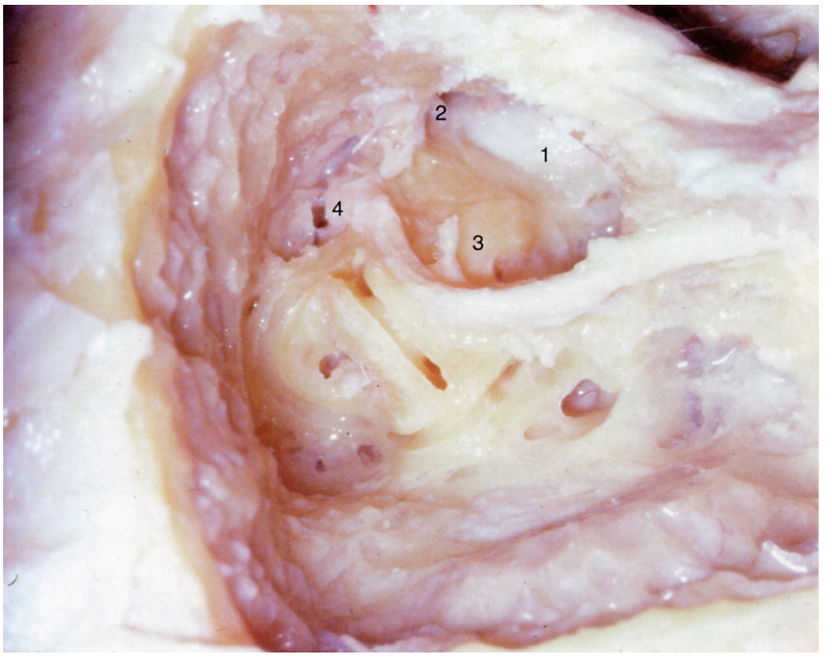

FIGURE 2–14 • Radical mastoid dissection view of a right temporal bone. The three semicircular canals have been opened. The anatomic interrelationships between the internal carotid artery (1), eustachian tube (2), promontory (3), and geniculate ganglion (4) are seen. *Reproduced with permission from Gulya AJ. Gulya and Schuknecht's anatomy of the temporal bone with surgical implications. 3rd ed. New York: Informa Healthcare USA; 2007.*

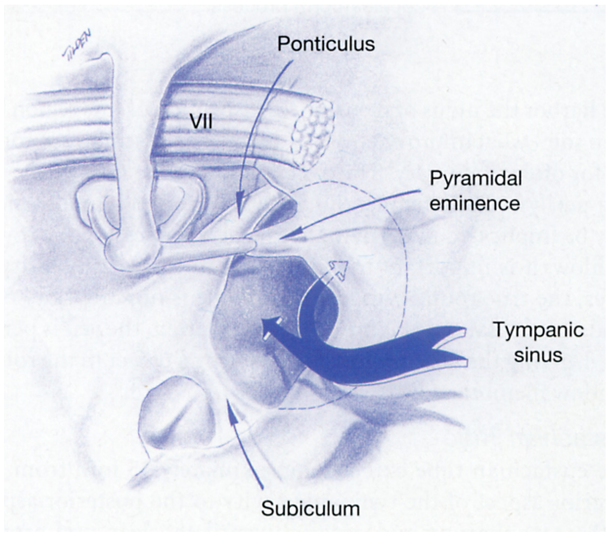

FIGURE 2–15 • The sinus tympani is bordered superiorly by the ponticulus and inferiorly by the subiculum. *Reproduced with permission from Schuknecht HF. Pathology of the ear. Ontario, Canada: Decker; 1974.*

tympanomastoid compartment. Ciliated cells intermingle with secretory cells on the promontory, in the hypotympanum, and in the epitympanum,[7] the mucociliary tracts thus formed act in concert with the mucociliary clearance system of the eustachian tube.

Pneumatization

The extent of pneumatization of the temporal bone varies according to heredity, environment, nutrition, infection, and eustachian tube function. There are five recognized regions of pneumatization: the middle ear, mastoid, perilabyrinthine, petrous apex, and accessory (Figure 2–17). The middle ear region, as described above, is divided into epitympanic, hypotympanic, mesotympanic, protympanic, and posterior tympanic areas. The mastoid region is subdivided into the mastoid antrum, central mastoid, and peripheral mastoid. The bony labyrinth divides the perilabyrinthine region into supralabyrinthine and infralabyrinthine areas. The apical area and the peritubal area comprise the petrous apex region. The accessory region encompasses the zygomatic, squamous, occipital, and styloid areas. There are five recognized air cell tracts. The posterosuperior tract runs at the juncture of the posterior and middle fossa aspects of the temporal bone. The posteromedial cell tract parallels and runs inferior to the posterosuperior tract. The subarcuate tract passes through the arch of the superior semicircular canal. The perilabyrinthine tracts run superior and inferior to the bony labyrinth, whereas the peritubal tract surrounds the eustachian tube.

The anterior petrous apex is pneumatized in only 10 to 15% of specimens studied.[8] Most often, it is diploic; in a small percentage of cases, it is sclerotic.

Troublesome cerebrospinal fluid leakage, persisting after translabyrinthine vestibular schwannoma resection despite apparently adequate tympanomastoid obliteration, has been linked to the presence of peritubal cells that open directly into the eustachian tube anterior to its tympanic orifice.[9]

Inner Ear

The bony labyrinth (see Figure 2–17) houses the sensory organs and soft tissue structures of the inner ear and consists of the cochlea, three semicircular canals, and vestibule. Its bone has three layers: an inner, or endosteal, layer; an outer, or periosteal, layer; and a middle layer consisting of enchondral and

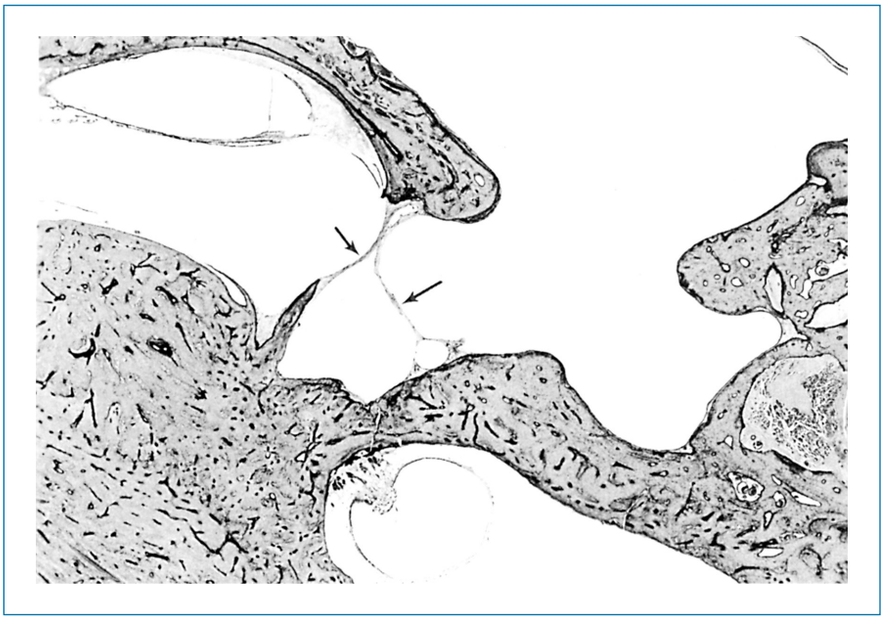

FIGURE 2–16 • The true round window membrane (left arrow) is covered by a veil of mucosa (right arrow). There is a microfissure extending from the medial aspect of the round window niche to the ampulla of the posterior semicircular canal. Right temporal bone; *reproduced with permission from Gulya AJ. Gulya and Schuknecht's anatomy of the temporal bone with surgical implications. 3rd ed. New York: Informa Healthcare USA; 2007.*

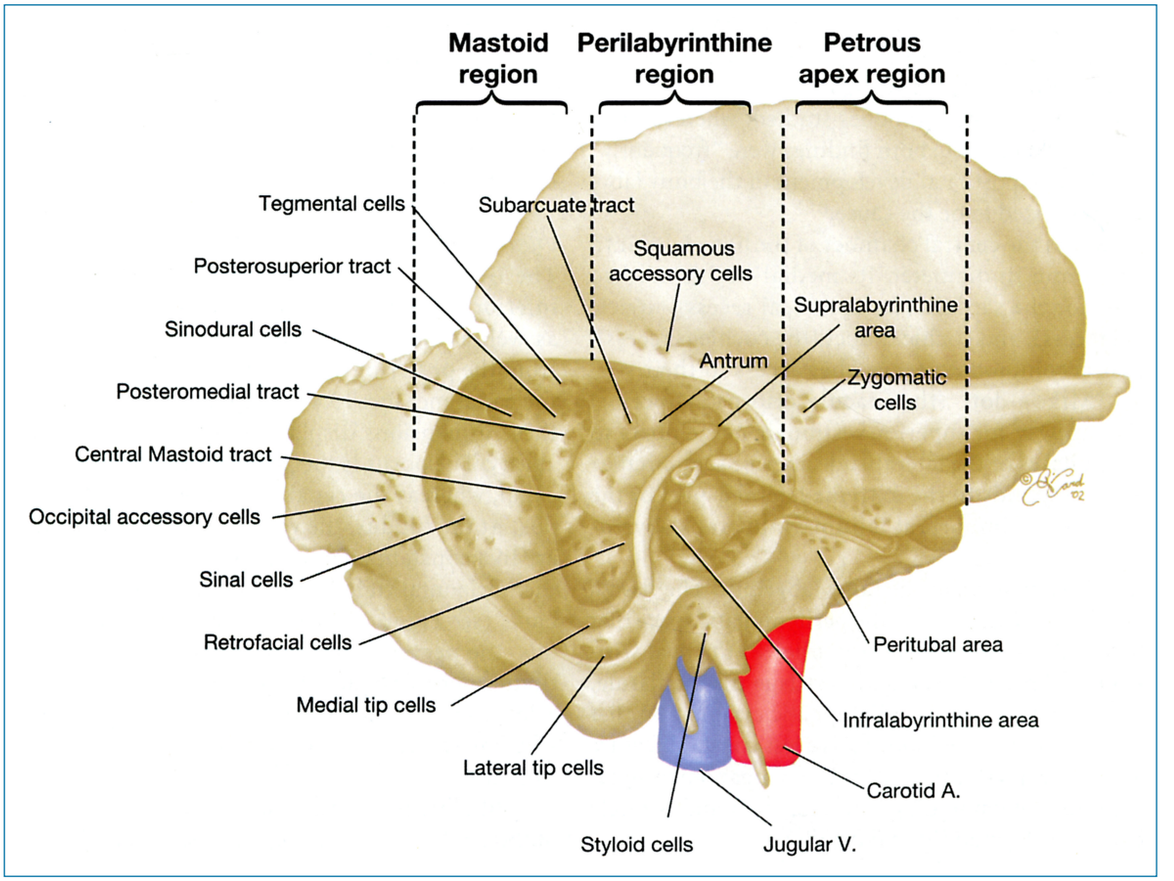

FIGURE 2–17 • Pneumatization of the temporal bone, with regions, areas, and tracts indicated. *After Nadol JB Jr, Schuknecht HF, editors. Surgery of the ear and temporal bone. New York: Raven Press; 1993.*

intrachondrial bone. Intrachondrial bone (globuli interossei) is characterized by cartilage islands, the lacunae of which have a thin bony layer owing to their invasion by osteoblasts.

The cochlea spirals 2½ turns about its central axis, the modiolus, and has a height of 5 mm. The base of the cochlea abuts the fundus of the IAC and is perforated (cribrose), allowing for the passage of cochlear nerve fibers. The apex lies medial to the tensor tympani muscle. The osseous spiral lamina winds about the modiolus and, along with the basilar membrane, separates the scala media (the cochlear duct) from the scala tympani. Adjacent turns of the cochlea are separated by an inter-scalar septum.

The three semicircular canals (see Figure 2–14) are the lateral (horizontal), superior (anterior vertical), and posterior (posterior vertical). The three canals are orthogonally related to one another and arc over a span of 240 degrees. Each canal has an ampullated limb, measuring 2 mm in diameter, and a nonampullated limb, which is 1 mm in diameter. The ampulla is cribrose for passage of nerve fibers. The nonampullated limbs of the posterior and superior canals fuse to form the crus commune. The ampullated and nonampullated limbs all open into the vestibule. The angle formed by the three semicircular canals is the solid angle, whereas the triangle bounded by the bony labyrinth, sigmoid sinus, and superior petrosal sinus is known as Trautmann's triangle.

Thinning, or frank dehiscence, of the bone of the superior semicircular canal is recognized as underlying some cases of sound- and/or pressure-induced vertigo.[10] Such dehiscence has been found in 0.5% of temporal bones studied, whereas thinning was encountered in 1.4%; both findings were "frequently" bilateral.[11] A failure in postnatal development of the bony labyrinth has been theorized to be the cause.[11]

The vestibule is the central chamber of the bony labyrinth and measures 4 mm in diameter. Its medial wall is marked by depressions for the saccule (the spherical recess), utricle (the elliptical recess), and cochlear duct (the cochlear recess). Cribrose areas accommodate nerve fiber access to their sensory organs. "Mike's dot" (the macula cribrosa superior) marks the passageway for superior vestibular nerve fibers to the cristae ampullares of the lateral and superior semicircular canals. As it corresponds to the extreme lateral aspect of the IAC, Mike's dot is an important landmark in translabyrinthine surgery.

There are three fissures of the bony labyrinth. The fissula ante fenestram is an evagination of the perilymphatic space that is invariably found extending anterosuperior to the oval window; in the adult, fibrous tissue and cartilage fill the fissula. The fossula post fenestram is a perilymphatic evagination that extends posterior to the oval window; it is a less constant feature of the temporal bone. Hyrtl's fissure (or the tympanomeningeal hiatus) is a remnant of embryologic development and is rarely present (see Chapter 1 for additional details).

There are two commonly encountered microfissures of the temporal bone. One extends between the round window niche and the ampulla of the posterior semicircular canal (see Figure 2–16). The other runs superior and inferior to the oval window. Both microfissures, or breaks in the endosteal and endochondral layers of the temporal bone, are filled with fibrous tissue and acellular matrix.

A persistent Hyrtl's fissure has been implicated as a route for cerebrospinal fluid leakage into the middle ear.[12] Although the oval and round window microfissures have been hypothesized to be the site of perilymph leakage, evidence refutes this theory.[13]

The membranous (endolymphatic) labyrinth housed within the bony labyrinth consists of the cochlear duct (scala media), the three semicircular ducts and their cristae ampullares, the otolithic organs (the utricle and the saccule), and the endolymphatic duct and sac. Generally interposed between the bony and membranous labyrinths are the connective tissue, blood vessels, and fluid of the perilymphatic space, including the scala tympani, scala vestibuli, perilymphatic cistern of the vestibule, perilymphatic duct, and perilymph spaces surrounding the semicircular ducts.

The endolymphatic duct originates in the medial wall of the vestibule. It first parallels the crus commune and then the posterior semicircular canal as it heads to the endolymphatic sac, anterior and medial to the sigmoid sinus. The endolymphatic sac lies approximately 10 mm inferior and lateral to the porus of the IAC; the sac has an intraosseous portion, which is covered by the operculum, and a more distal intradural portion (see Figure 1–14).

Donaldson's line, a surgical landmark in endolymphatic sac surgery, is derived by extending the plane of the lateral semicircular so that it bisects the posterior semicircular canal and contacts the posterior fossa dura (Figure 2–18); the endolymphatic sac lies inferior to this line. The precise position of the sac shows considerable variability.

Internal Auditory Canal

The IAC is the bony channel that shelters the superior and inferior vestibular, cochlear, facial, and intermediate nerves, as well as the labyrinthine artery and vein, as they course from the posterior cranial fossa to the labyrinth. On average, the canal measures 3.4 mm in diameter and 8 mm in length; these dimensions display considerable interindividual variability. The porus is the posterior cranial fossa opening of the canal, whereas the canal abuts the bony labyrinth at its fundus. At the fundus, the vestibular, facial, and cochlear nerves are in a constant anatomic relationship that is determined by the horizontal (falciform) crest and the vertical crest ("Bill's bar") (see Figure 2–5B). Progressing medially from the fundus, the nerves rotate, with fusion of the cochlear and vestibular nerves (Figure 2–19), so that the facial nerve assumes a location anterior to the cochleovestibular nerve bundle, whereas the cochlear nerve moves to lie inferior to the vestibular nerve.

Bill's bar is a useful landmark in translabyrinthine surgery of the cerebellopontine angle as it separates the superior vestibular nerve from the anteriorly located facial nerve. Although the medial anatomic relationships of the cochlear, vestibular, and facial nerves are useful in vestibular nerve section surgery, these relationships can undergo considerable distortion in the face of a cerebellopontine angle tumor.

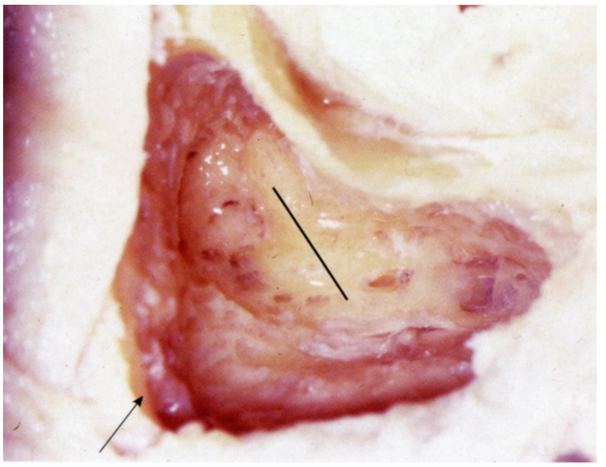

FIGURE 2–18 • Complete mastoidectomy view of a right temporal bone. The lateral and posterior semicircular canals form Donaldson's line (line). The angle of Citelli is indicated (arrow). *Reproduced with permission from Gulya AJ. Gulya and Schuknecht's anatomy of the temporal bone with surgical implications. 3rd ed. New York: Informa Healthcare USA; 2007.*

NEUROANATOMY

Trigeminal and Abducens Nerves

The gasserian ganglion of the trigeminal nerve occupies Meckel's cave on the middle cranial fossa face of the temporal bone, anterolateral to the petrous apex. The abducens (sixth cranial) nerve runs in Dorello's canal beneath the posterior petroclinoid (Gruber's) ligament. Petrous apicitis, with its attendant dural and venous inflammation, can manifest with purulent otorrhea, retro-orbital pain, and abducens palsy.

Facial Nerve

The facial nerve (the seventh cranial nerve) innervates structures derived from Reichert's cartilage. Three nuclei give rise to the fibers of the facial nerve: its motor nucleus in the caudal pons, the superior salivatory nucleus that is dorsal to the motor nucleus, and the nucleus of the solitary tract in the medulla oblongata. The superior aspect of the motor nucleus, innervating the frontalis and orbicularis oculi muscles, receives both crossed and uncrossed input from the motor cortex, whereas the inferior portion receives only ipsilateral input.

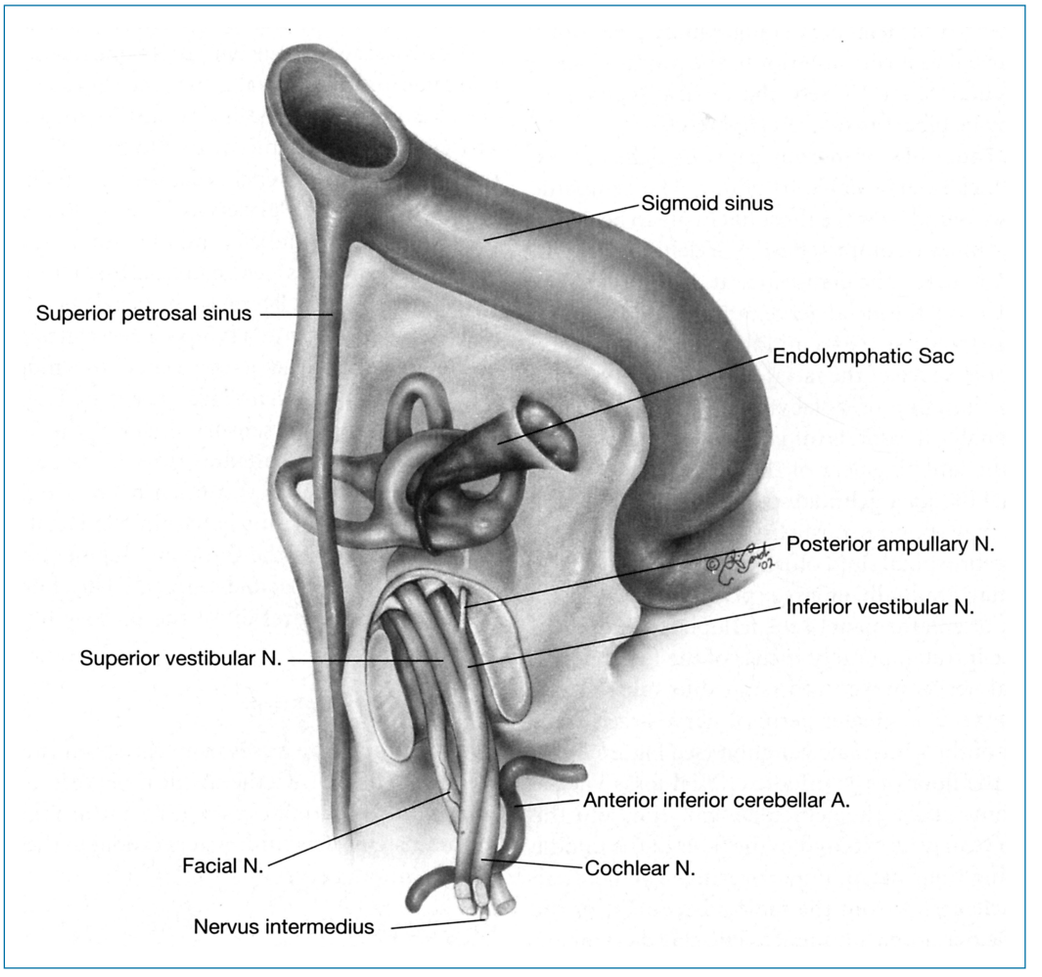

FIGURE 2–19 • The rotation of the facial, cochlear, and vestibular nerves as they traverse the internal auditory canal. *After Nadol JB Jr, Schuknecht HF, editors. Surgery of the ear and temporal bone. New York: Raven Press; 1993.*

Five fiber types make up the trunk of the facial nerve. Its special visceral efferent fibers supply the facial expression, stapedius, stylohyoid, and digastric (posterior belly) muscles. Its general visceral efferent fibers go to the lacrimal, nasal cavity seromucinous, sub-maxillary, and sublingual glands. The taste (sensory) fibers of the facial nerve derive from the anterior two-thirds of the tongue, tonsillar fossae, and posterior palate, whereas its somatic sensory fibers emanate from the EAC and concha. Visceral afferent fibers arise from the mucosa of the nose, pharynx, and palate.

The course of the facial nerve is divided into five segments. Its intracranial segment stretches 24 mm from the pons to the porus of the IAC. The intracanalicular segment traverses the IAC; at the fundus, it occupies the anterosuperior quadrant, where it is joined by the nervus intermedius. The shortest segment is the labyrinthine segment, running 4 mm from the beginning of the fallopian canal to the geniculate ganglion. The tympanic segment is roughly 13-mm long and courses in the medial wall of the tympanic cavity, superior to the cochleariform process and oval window. The mastoid segment spans the 20-mm distance from the second genu (at the lateral semicircular canal) to the stylomastoid foramen.

The facial nerve may follow an anomalous course. One such alternate path takes the tympanic segment of the facial nerve anterior and inferior to the oval window.[14] In another variant, the mastoid segment of the facial nerve bulges more posteriorly and laterally than usual as it runs inferior to the prominence of the lateral semicircular canal.[15] Rarely, the vertical segment of the facial nerve may be bipartite or even tripartite.

The fallopian canal has numerous gaps, or dehiscences, which render the facial nerve liable to injury. The tympanic segment over the oval window is the most likely site to be dehiscent; in one series, this site comprised 66% of dehiscences.[16] In approximately 75% of cases, the dehiscence at the oval window is bilateral.[17] On occasion, the facial nerve can protrude through the gap (Figure 2–20) to present as a middle ear mass.[18]

The subarachnoid space of the facial nerve usually extends no further than the junction of its labyrinthine and tympanic segments.[19] Occasionally, it extends into the geniculate ganglion and, rarely, onto the lateral aspect of the tympanic segment. Gacek theorized that the subarachnoid space extending onto the tympanic segment may spontaneously fistulize into the middle ear, resulting in cerebrospinal fluid otorrhea.[19] Alternatively, he suggested that it may gradually enlarge, presenting as a mass lesion with erosion or enlargement of the fallopian canal.

There are three intratemporal branches of the facial nerve: the greater petrosal nerve, nerve to the stapedius muscle, and chorda tympani nerve. The greater petrosal nerve arises from the anterior aspect of the geniculate ganglion (see Figure 2–14) and emerges onto the floor of the middle cranial fossa via the facial hiatus; in some cases, the geniculate ganglion and the greater petrosal nerve may lie exposed in the floor of the middle cranial fossa, lacking their usual bony covering. The nerve to the stapedius muscle arises from the mastoid segment of the facial nerve near the pyramidal eminence. The chorda tympani nerve, the sensory bundle making up some 10% of the cross-sectional area of the facial nerve, usually separates from the main trunk of the facial nerve approximately 4 mm proximal

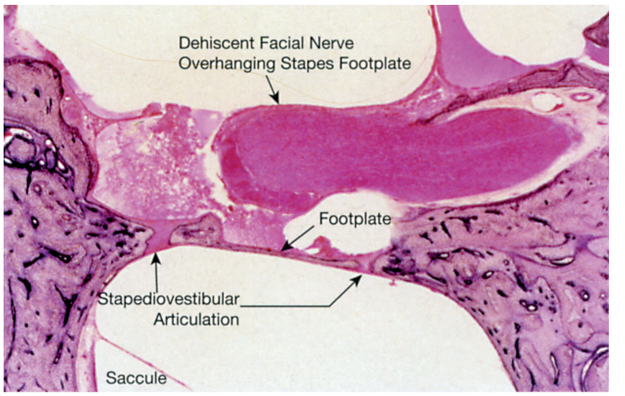

FIGURE 2–20 • The facial nerve is dehiscent at the oval window. *Reproduced with permission from Gulya AJ. Gulya and Schuknecht's anatomy of the temporal bone with surgical implications. 3rd ed. New York: Informa Healthcare USA; 2007.*

to the stylomastoid foramen (Figure 2–21); rarely, the chorda tympani and facial nerves separate extratemporally, and the chorda tympani re-enters the temporal bone via its own canal. Alternatively, the chorda may not separate from the facial nerve until it reaches the level of the lateral semicircular canal. After vertically ascending the temporal bone in a canal that lies lateral and anterior to the facial nerve, the chorda enters the tympanic cavity at the iter chordae posterius. It crosses lateral to the long process of the incus and medial to the malleus to exit the tympanic cavity via the iter chordae anterius (canal of Huguier) and the petrotympanic (glaserian) fissure. Rarely, the chorda may pass lateral to the malleus and the tympanic membrane.

The facial recess (see Figure 2–21) is a triangular area inferior to the incudal fossa, lateral to the facial nerve (vertical segment), and medial to the chorda tympani nerve; it is used in intact canal wall mastoidectomy to gain access to the middle ear.

The nervus intermedius (nerve of Wrisberg) carries the taste, secretory, and sensory fibers of the facial nerve. In the IAC, the nervus intermedius runs as a separate nerve between the facial and superior vestibular nerves. In the temporal bone, the nervus intermedius is within the facial nerve, occupying its dorsal aspect in the tympanic segment and its posterolateral aspect in the mastoid segment. The chorda tympani nerve represents the separation of the sensory fibers at the inferior mastoid segment.

Cochlear Nerve

The cochlear nerve arises from the spiral ganglion neurons. At the fundus of the IAC, the cochlear nerve is in the anteroinferior compartment. It rotates as it heads toward the porus and enters the brainstem a few millimeters caudal to the root entry zone of the trigeminal nerve.

Vestibular Nerves

The superior and inferior vestibular nerves occupy the posterior half of the IAC. The structures innervated by the superior vestibular nerve are the superior and lateral semicircular canals,

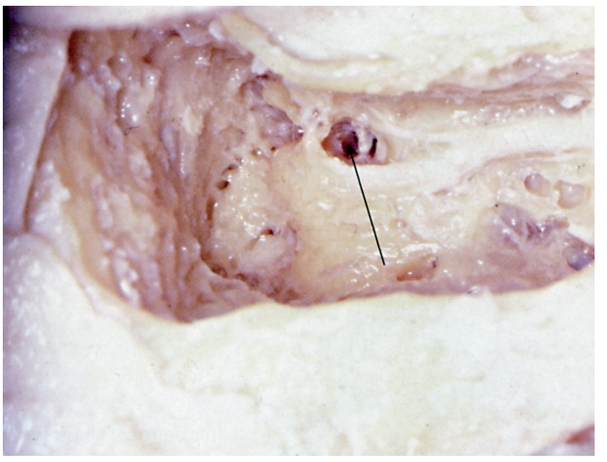

FIGURE 2–21 • The facial recess (arrow) lies between the facial and chorda tympani nerves. The incudostapedial joint is visible just to the right of the arrowhead. *Reproduced with permission from Gulya AJ. Gulya and Schuknecht's anatomy of the temporal bone with surgical implications. 3rd ed. New York: Informa Healthcare USA; 2007.*

utricular macula, and superior portion of the saccular macula. The inferior vestibular nerve innervates the inferior saccular macula and, by its posterior ampullary branch, the posterior semicircular canal. The posterior ampullary nerve separates from the main trunk of the inferior vestibular nerve a few millimeters from the porus of the IAC and traverses the singular canal to the posterior canal ampulla.

Sensory Nerves of the Tympanomastoid Compartment

Jacobson's nerve (the tympanic branch of cranial nerve IX) arises from the inferior (petrosal) ganglion of cranial nerve IX, which is located in the petrosal fossula of the jugulocarotid crest. It enters the tympanic cavity, accompanied by the inferior tympanic artery, through the inferior tympanic canaliculus. Subsequently, the nerve climbs the promontory and medial wall of the tympanic cavity to meet with the caroticotympanic nerves originating from the pericarotid plexus. The union of the preganglionic parasympathetic fibers of Jacobson's nerve and the postganglionic sympathetic caroticotympanic nerves at the tympanic plexus results in the formation of the lesser petrosal nerve. The lesser petrosal nerve heads to the floor of the middle cranial fossa adjacent to, or even within, the semicanal of the tensor tympani muscle. Jacobson's nerve mediates otalgia referred from the pharynx.

Arnold's nerve, the auricular branch of cranial nerve X, has fibers from the facial, glossopharyngeal, and vagus nerves. It originates in the jugular foramen, passes over the dome of the jugular bulb (via the mastoid canaliculus), and enters the fallopian canal. Arnold's nerve has been implicated in herpetic involvement of the EAC in herpes zoster oticus[20] and the cough reflex elicited by manipulation of the skin of the EAC.

VASCULAR ANATOMY

Temporal Bone Arteries

The internal carotid artery enters the temporal bone through the external carotid foramen, located just anteromedial to the styloid process. As it ascends in its intrapetrous segment, it passes first anterior to the tympanic cavity and cochlea and then bends (its "knee") to run medial to the eustachian tube and inferomedial to the semicanal of the tensor tympani muscle (see Figures 2–9 and 2–10). The artery climbs to exit the temporal bone at the internal carotid foramen. Accompanying the artery throughout its intrapetrous course are a venous and a neural (sympathetic) plexus. The bony shell protecting the artery is thin (often less than 0.5 mm thick) and can be dehiscent in 6% of cases.[21] In the course of surgery for chronic otitis media or cholesteatoma, the potential for injuring the internal carotid artery mandates gentle dissection in the medial wall of the eustachian tube.

Aberrant development of the carotid artery (see Chapter 1) can result in an artery that follows an anomalous course lateral and posterior to the vestibular line (a vertical line through the lateral aspect of the vestibule in the coronal plane).

The anterior inferior cerebellar artery (AICA) often extends a loop into the IAC. Its role of such a loop in the generation of symptoms such as tinnitus and vertigo is debatable.[22] Disruption of AICA causes hemorrhage in and infarction of the labyrinth and brainstem.

Temporal Bone Veins

The three dominant sinuses of the temporal bone are the sigmoid (portion of the lateral venous sinus), superior petrosal, and inferior petrosal (Figure 2–22). The lateral venous sinus occupies an S-shaped sulcus in the posterior mastoid—hence the term sigmoid—as it extends from the transverse sinus to the internal jugular vein. This drainage system on the right is larger than that on the left in 75% of cases.[23] The angle between the sigmoid sinus/posterior cranial fossa dura and the middle cranial fossa dura is known as the angle of Citelli (see Figure 2–18).

The superior petrosal sinus drains the cavernous sinus into the lateral venous sinus as it runs in the superior petrosal sulcus at the junction of the posterior and middle fossa dural plates. The inferior petrosal sinus courses in the petro-occipital suture line. It drains the cavernous sinus into the jugular bulb.

Arachnoid granulations (pacchionian bodies) are projections of pia-arachnoid into the venous sinuses and venous lacunae and are extensions of the subarachnoid space. Arachnoid granulations can also be found extending from the arachnoid of the middle and posterior cranial fossae into the adjacent mastoid air cells. Gacek has linked arachnoid granulations to adult-onset spontaneous cerebrospinal fluid otorrhea.[24,25]

The jugular bulb is interposed between the sigmoid sinus and internal jugular vein; in contrast to the thick wall of the sigmoid sinus, which quite readily contracts with bipolar cautery, the thin wall of the bulb does not and is prone to rupture with manipulation. The venous hemorrhage of a torn or incised sigmoid sinus can be controlled with pressure applied via a large square of gelatin sponge (Gelfoam®) surmounted by a neurosurgical cottonoid; several minutes after the bleeding has stopped,

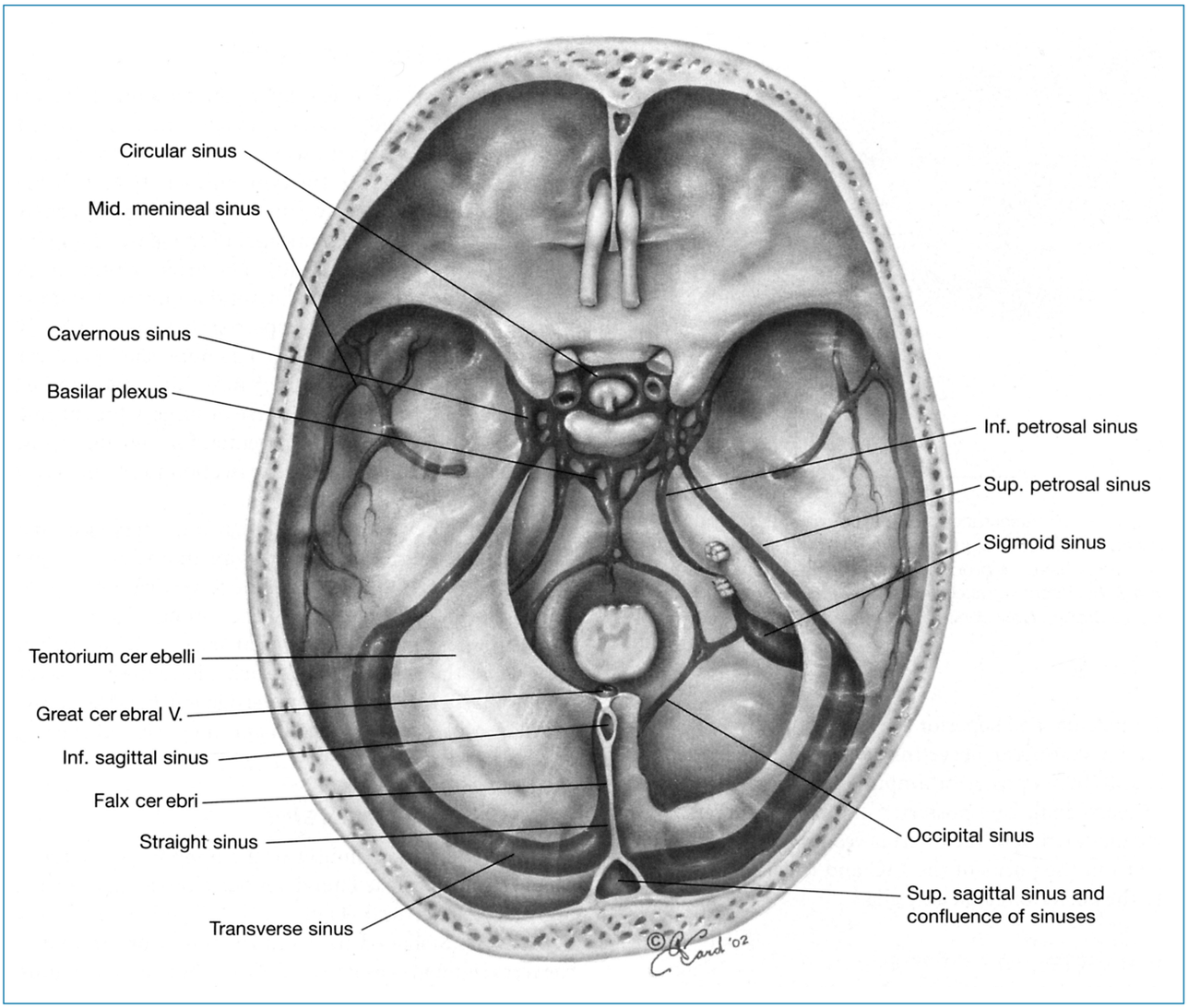

FIGURE 2–22 • The cranium has been opened and its contents removed to reveal the sinuses and related structures.

the cottonoid can be removed safely, and leaving the Gelfoam in place, surgery can be resumed.

The jugular bulb displays considerable variability in its position relative to the facial nerve and in its penetration into the tympanic cavity. A high-riding jugular bulb (one extending to or above the level of the inferior tympanic annulus) has been reported in 3.5 to 5% of temporal bone specimens studied[26,27] and may occur more frequently on the right side.[27] Its bony covering is very thin—only 0.1 to 0.3 mm. An alternate definition of the high-riding jugular bulb encompasses one encroaching to within 2 mm or less on the inferior aspect of the IAC.[28] Using this definition, one study reported that two-thirds of temporal bones from individuals older than 6 years housed a high-riding jugular bulb.[28] A jugular diverticulum is a "venous anomaly" and comprises an "irregular outpouching" of the jugular bulb.[29]

The high-riding jugular bulb may mimic a middle ear vascular mass, such as a glomus tympanicum, and may be the source of hemorrhage in tympanostomy tube insertion. Jugular bulbs reaching as high as the superior aspect of the IAC have been encountered in the course of posterior fossa vestibular schwannoma surgery,[23] rendering exposure of the IAC technically challenging. A jugular diverticulum has been implicated as the etiology of Meniere's disease–like symptoms.[29]

Middle Ear Blood Vessels

The inferior tympanic artery is a branch of the ascending pharyngeal artery (from the external carotid artery). It traverses the inferior tympanic canaliculus with Jacobson's nerve. The inferior tympanic artery is an important arterial feeder of tympanic paragangliomas.

A number of branches from the external carotid artery contribute to the anastomotic network of the tympanic cavity, including the anterior tympanic artery, deep auricular artery, mastoid artery, stylomastoid artery, superficial petrosal artery, and tubal artery.

Labyrinthine Vessels

The majority of the blood supply to the membranous labyrinth stems from the labyrinthine artery, a branch of the AICA. The subarcuate artery arises either as a branch of the labyrinthine artery, or of the AICA, or as multiple branches of both; it passes within the arch of the superior semicircular canal.

Facial Nerve Vessels

The facial nerve has both an intrinsic and an extrinsic vascular system. The extrinsic system consists of the AICA, supplying the intracranial segment of cranial nerve VII; the labyrinthine artery, supplying the intracanalicular segment; the superficial petrosal artery, which supplies the geniculate ganglion and the superior portion of the mastoid segment of the facial nerve; and the stylomastoid artery, which supplies the inferior mastoid segment of the nerve.

The intrinsic network, running within the nerve, is generally thought to be most poorly developed at its labyrinthine segment, in contrast to the tympanic and mastoid segments.[30]

References

1. Gulya AJ. Gulya and Schuknecht's anatomy of the temporal bone with surgical implications. 3rd edition. New York: Informa Healthcare USA; 2007.
2. Kveton JF, Cooper MH. Microsurgical anatomy of the jugular foramen region. Am J Otol 1988;9:109–12.
3. Kveton JF. Anatomy of the jugular foramen: The neurotologic perspective. Op Tech ORL-HNS 1996;7:95–8.
4. Saleh E, Naguib M, Aristegui M, Cokkeser Y, Sanna M. Lower skull base: Anatomic study with surgical implications. Ann Otol Rhinol Laryngol 1995;104:57–61.
5. Aslan A, Falcioni M, Balyan FR, et al. The cochlear aqueduct: An important landmark in lateral skull base surgery. Otolaryngol Head Neck Surg 1998;118:532–6.
6. Nomura Y. Otological significance of the round window. Adv Otorhinolaryngol 1984;33:1–162.
7. Lim DJ. Functional morphology of the lining membrane of the middle ear and eustachian tube. An overview. Ann Otol Rhinol Laryngol 1974;83 Suppl 11:5–22.
8. Lindsay JR. Suppuration in the petrous pyramid. Ann Otol Rhinol Laryngol 1938;47:3–36.
9. Saim L, McKenna MJ, Nadol JB Jr. Tubal and tympanic openings of the peritubal cells: Implications for cerebrospinal fluid otorrhea. Am J Otol 1996;17:335–9.
10. Minor LB, Solomon D, Zinreich JS, Zee DS. Sound- and/or pressure-induced vertigo due to bone dehiscence of the superior semicircular canal. Arch Otolaryngol Head Neck Surg 1998;124:249–58.
11. Carey JP, Minor LB, Nager GT. Dehiscence or thinning of bone overlying the superior semicircular canal in a temporal bone survey. Arch Otolaryngol Head Neck Surg 2000;126:137–47.
12. Gacek RR, Leipzig B. Congenital cerebrospinal fluid otorrhea. Ann Otol Rhinol Laryngol 1979;88:358–65.
13. El Shazly MAR, Linthicum FH Jr. Microfissures of the temporal bone: Do they have any clinical significance? Am J Otol 1991;12:169–71.
14. Hough JVD. Malformations and anatomical variations seen in the middle ear during the operation for mobilization of the stapes. Laryngoscope 1958;68:1337–79.
15. Procter B, Nager GT. The facial canal: Normal anatomy, variations and anomalies. Ann Otol Rhinol Laryngol 1982;91 Suppl 97:33–61.
16. Baxter A. Dehiscence of the fallopian canal: An anatomical study. J Laryngol Otol 1971;85:587–94.
17. Moreano EH, Paparella MM, Zelterman D, Goycoolea MV. Prevalence of facial canal dehiscence and of persistent stapedial artery in the human middle ear: A report of 1000 temporal bones. Laryngoscope 1994;104:309–20.
18. Johnsson L-G, Kingsley TC. Herniation of the facial nerve in the middle ear. Arch Otolaryngol 1970;91:598–602.
19. Gacek RR. Anatomy and significance of the subarachnoid space in the fallopian canal. Am J Otol 1998;19:358–64.
20. Eshraghi AA, Buchman C, Telischi FF. Facial nerve branch to the external auditory canal. American Neurotology Society 2001 Annual Meeting abstracts. http://itsa.ucsf.edu/~ajo/ANS/ANSspr21ab.html (accessed Mar 31, 2001).
21. Moreano EH, Paparella MM, Zelterman D, Goycoolea MV. Prevalence of carotid canal dehiscence in the human middle ear: A report of 1000 temporal bones. Laryngoscope 1994;104:612–18.
22. Makins AE, Nikolopoulus TP, Ludman C, O'Donoghue GM. Is there a correlation between vascular loops and unilateral auditory symptoms? Laryngoscope 1998;108:1739–42.
23. Kennedy DW, El-Sirsy HH, Nager GT. The jugular bulb in otologic surgery: Anatomic, clinical, and surgical considerations. Otolaryngol Head Neck Surg 1986;94:6–15.
24. Gacek RR. Arachnoid granulation cerebrospinal fluid otorrhea. Ann Otol Rhinol Laryngol 1990;99:854–62.
25. Gacek RR. Evaluation and management of temporal bone arachnoid granulations. Arch Otolaryngol Head Neck Surg 1992;118:327–32.
26. Overton SB, Ritter FN. A high placed jugular bulb in the middle ear: A clinical and temporal bone study. Laryngoscope 1973;83:1986–91.
27. Subotic R. The high position of the jugular bulb. Acta Otolaryngol (Stockh) 1979;87:340–4.
28. Rausch SD, Xu W-Z, Nadol JB Jr. High jugular bulb: Implications for posterior fossa neurotologic and cranial base surgery. Ann Otol Rhinol Laryngol 1993;102:100–7.
29. Jahrsdoerfer RA, Cain WS, Cantrell RW. Endolymphatic duct obstruction from a jugular bulb diverticulum. Ann Otol Rhinol Laryngol 1981;90:619–23.
30. Balkany T, Fradis M, Jafek BW, Rucker NC. Intrinsic vasculature of the labyrinthine segment of the facial nerve—Implications for site of lesion in Bell's palsy. Otolaryngol Head Neck Surg 1991;104:20–3.

Acoustics and Mechanics of the Middle Ear

3

Saumil N. Merchant MD / John J. Rosowski, PhD

Two of the primary tasks of the otologic surgeon include: *diagnosis*, the understanding of how pathological variations in external and middle-ear structure lead to hearing loss, and *surgical treatment* of external and middle ears ravaged by disease, such that the reconstructed ear has near-normal mechanical and acoustic function. The authors believe that a basic knowledge of physiology of the normal ear and pathophysiology of the diseased ear is necessary for proper diagnosis and surgical treatment of otologic disorders. This chapter provides a review of some fundamental principles of acoustics that are relevant to sound transmission in normal, diseased and reconstructed middle ears. The review concentrates on middle-ear mechanics and does not cover the physiological maintenance of middle-ear gases or static air pressures. The chapter is meant as a guide rather than an exhaustive treatise, and has been written with clinicians as its primary audience.

HISTORICAL ASPECTS

The histories of otology, audiology and acoustics have been documented by several authors.[1–5] The early events may be summarized as follows.[6]

Early Greek physicians (5th century BC) knew of the tympanic membrane and middle-ear space. The Greeks considered the middle-ear space to be the seat of hearing. Galen (AD 131 to 201) described the auditory nerve but suggested it originated in the middle ear. The Renaissance produced several great anatomists who described the ear in detail. Vesalius, in 1543, described the malleus and incus. In 1546, Ingrassia described the stapes and the oval and round windows. In 1561, Fallopius named the cochlea, the labyrinth, and the canal for the facial nerve. Eustachius described the auditory tube bearing his name in 1564.

These anatomic discoveries formed the basis for tracing the pathway of sound through the ear by Coiter in 1566, and the later more elaborate description of Durverney in 1683. Neither Coiter nor Duverney appreciated the impedance matching function of the middle ear because both thought the inner ear was filled with air. That the labyrinth contained fluid was established by Meckel, who, in 1777, demonstrated that frozen temporal bones were always filled with ice. The microscopic structures of the inner ear were first described by Corti in 1851, followed by Retzius's description of hair cells and their innervation by auditory nerve fibers in 1892.

Helmholtz, in 1868,[7] initiated the period of modern auditory physiology by defining the principles of impedance matching and how the middle ear served this function. Stating the problem of matching the transmission of sound in low-impedance air to the high impedance of the fluid-filled cochlea, Helmholtz conceived of three means by which this pressure transformation takes place: a lever action that resulted from the shape of the drumhead itself, a lever effect of the ossicular chain, and a hydraulic action of the large tympanic membrane acting upon the small stapes footplate.

In the 20th century, many investigators expanded, corrected, or quantified these basic concepts. Notable contributors to our knowledge of middle-ear mechanics include Nobel laureate Georg von Békésy, Ernst Glenn Wever, Merle Lawrence, Juergen Tonndorf, Shyam Khanna, William Peake, Richard Goode, Aage Møller, and Josef Zwislocki. Clinical observations and surgical advances that have stimulated physiologic investigations have included the question of altered sound conduction as a result of middle-ear diseases, and the restoration of hearing in pathologic middle ears through tympanoplasty and stapedectomy procedures.

SOUND AND ITS MEASUREMENT

Sound results when particles of a medium are set into vibration. For example, the vibrating tines of a struck tuning fork produce backward and forward motions of the air particles that surround the tines (Figure 3–1). The particles set in motion by the vibrating tines then push on adjacent air particles, where the push is proportional to the sound pressure, setting the next layer of particles into back and forth motion. The physical disturbance of sound pressure and particle motion, not the particles themselves, propagates through the medium, as succeeding layers of air particles are set into vibration. The *frequency* of the resulting

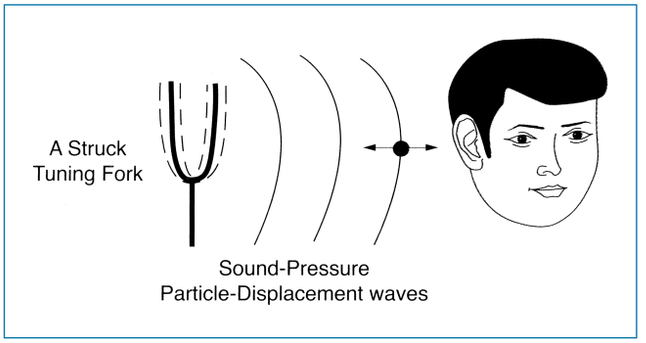

FIGURE 3–1 • The vibrating tines of a struck tuning fork set nearby air particles into motion with a frequency equal to the natural frequency of the fork. The air particles that are set in motion push on adjacent particles and so forth, resulting in a propagating physical disturbance that is perceived as sound. The black dot with the arrow is a hypothetical air particle set into back and forth motion, by the waves (curved lines) propagating from the struck fork.

sound is the number of cycles per second of the back and forth motion of the air particles. The unit of frequency is Hertz (Hz, with 1 Hz = 1 cycle per second). The amplitude of the propagating physical disturbance can be quantified either in terms of the sound pressure acting on the particles or the amplitude of the particle motion. In practice, it is easier to measure pressure variations than to measure motion of the particles; hence, sound pressure is the primary measure of sound.

Sound pressure refers to the magnitude of the temporal variations in pressure produced around ambient static pressure (Figure 3–2). A pressure is a force per area. The international unit of pressure is the pascal (Pa), where 1 Pa = one Newton of force per square meter of area. The quietest sounds heard by a human ear are of very low pressure; the change in pressure associated with sound at the threshold of hearing for a 1,000 Hz tone is about 20 μPa (or two-tenths of a billionth atmospheres). There are many ways to quantify sound pressure, the most common being in terms of the rms or the root of the mean squared deviation in pressure. For a sinusoidal pure tone like that in Figure 3–2A, the sound pressure can be quantified in terms of the peak, peak-to-peak or rms measures of amplitude. In the case of sinusoids, there is a fixed relationship between the three different measures, and for the tone shown in Figure 3–2A, these different measures yield values of 1, 2, or 0.71 Pa, respectively. The intensity or power within a complex sound waveform as illustrated in Figure 3–2B, is not readily quantified by peak measures but is well described by the rms value of the sound pressure. In fact, the rms sound pressure of this complex sound is 0.71 Pa, a value identical to that of the tonal sound pressure shown in Figure 3–2A. In general then, sound pressure measurements are usually quantified in terms of the rms pressure.

The human auditory system is sensitive to a wide range of sound pressures. Conversational speech is typically 100 to 500 times threshold, music often contains sound pressures that are 10,000 times threshold, while jet engines, guns, and fireworks can produce pressures that are more than 1 million times threshold. Because of the ear's sensitivity to pressures that vary by more than a million times, and because the human ear can discriminate fractional changes in pressure, it is common to use a logarithmic scale to grade sound pressures.[8] The decibel (dB, one-tenth of a Bell) is a logarithmic measure of relative energy where 10 dB (1 Bell) represents an increase over a given reference energy level of 1 order of magnitude (ie, 1 common log unit or a factor of 10). The reference level for sound pressure level (SPL) is 2×10^{-5} rms pascals (or Pa), and since energy is proportional to pressure squared:

$$\text{Sound level in dB SPL} = 10\log_{10}\left(\frac{X}{0.00002\,rms\,Pa}\right)^2 = 20\log_{10}\left(\frac{X}{0.00002\,rms\,Pa}\right)$$

where X is the sound pressure in rms pascals and 0.00002 rms Pa is the reference pressure. Different dB sound pressure scales use different reference pressures. For example, the dB Hearing Level scale (dB HL) of the clinical audiogram uses the average sound pressure threshold of the normal population at a given frequency as the reference pressure. The sound pressure level of both sounds shown in Figure 3–2 is 91 dB SPL, where 91 = 20 log10 (0.71/0.00002). The loudness of a sound is a monotonic function of the sound pressure; for mid-level sounds a 20 dB increase in sound pressure produces about a factor of six increase in loudness.[9] The sound pressures of various commonly experienced sounds are noted in terms of rms Pa and dB SPL in Table 3–1.

Sound is a variation in pressure with time. A pure tone, as in Figure 3–2A, is a sound in which the relationship between sound pressure and time can be described by a sine function, eg,

$$p(t) = A\cos(2\pi ft + \phi)$$

where we use the cosine function that is the common standard in engineering applications, $p(t)$ describes the variation in sound pressure with time, A describes the peak amplitude or *magnitude* of the pressure, f is the *frequency* of the sinusoid and ϕ is the *phase*. The phase ϕ determines the time when the pressure is maximum relative to some reference time zero. The relative phases of the sound pressure in the ear canal, and the mechanical and neural responses within the ear are useful in determining the physical and biological processes associated with hearing.[10,11] Also, the relative timing information in the phase is critical when waveforms are combined; two waves of the same frequency added together can sum constructively if they have similar phases, sum to near zero if the waves are out of phase and of identical amplitude, or somewhere in between for intermediate phases. Complex sounds (eg, Figure 3–2B) can be described by the addition of pure tones of different frequencies and different phases. A complex sound can be broken down into its individual components (individual sinusoids with magnitude and phase information) by using a Fourier analysis. While the ear is insensitive to the absolute phase of a single tone, a complex acoustic signal with a fixed number of frequency components of fixed magnitude can sound quite different depending on the relative phases of the components.

While the human ear can hear sound frequencies ranging from 20 to 20,000 Hz, the ear is differentially sensitive to sounds of different frequencies, and measurements of the

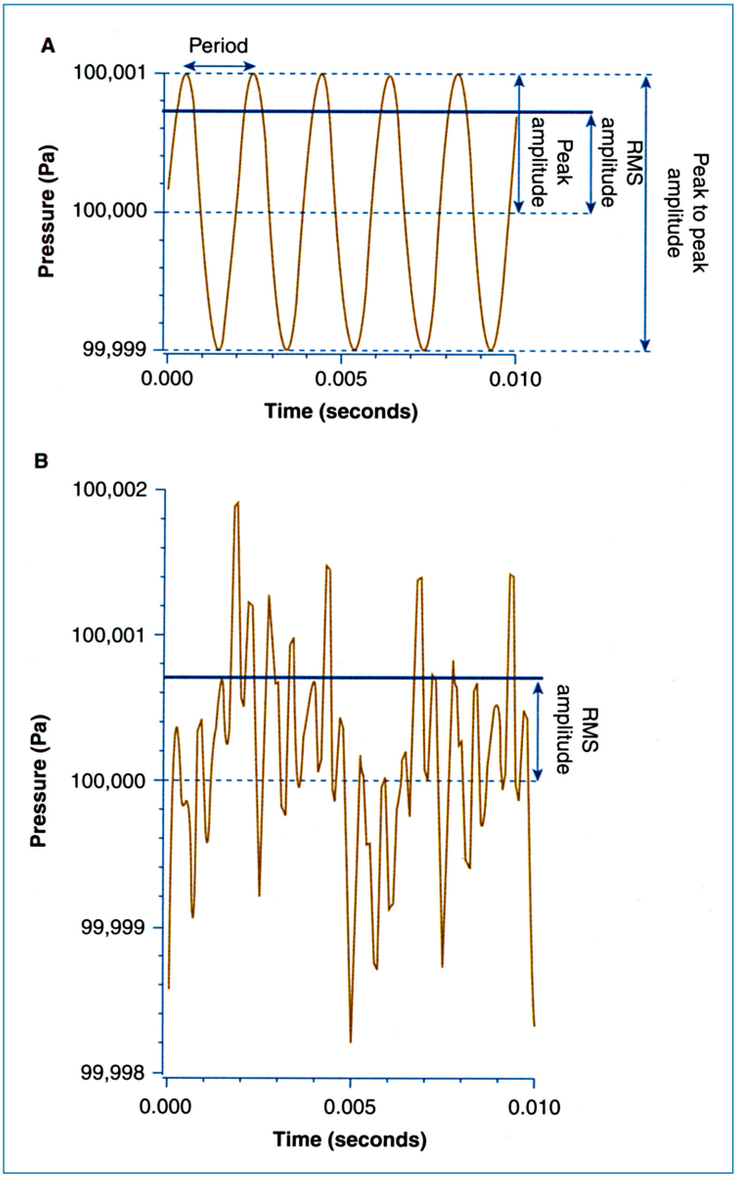

FIGURE 3–2 • Two patterns of temporal variations and air pressure produced by sounds. The schematic in *A,* depicts that produced by a 512-Hz pure tone, while *B,* depicts that produced by a complex sound. The absolute value of pressure is scaled in both plots, and, therefore, the sound-induced variations occur around a static value of 100,000 Pa = 1 atmosphere. The sound pressure corresponds to amplitude of variations around the static value. In both *A* and *B*, while the static atmospheric pressure is 100,000 Pa, the amplitude of the sound pressure is on the order of 1 Pa. *A*, The pressure variations are those of a 512-Hz pure tone. The pressure varies sinusoidally with a period of 1/512 = 0.00195 seconds. The amplitude of pressure variations around the static value can be quantified in terms of the peak-to-peak value of 2 Pa, the peak value of 1 Pa, or the rms (root mean square) value of 0.71 Pa. (The rms value is the square root of the mean of the squared pressure deviations from static values averaged over some time. In the case of a sinusoid, a convenient averaging time is an integral number of periods of the sine wave. With sinusoidal sound pressures, the rms value equals the peak amplitude/$\sqrt{2}$). *B*, The pressure variations are those of a complex sound with many irregular risings and fallings of the sound pressure. With this kind of sound, peak amplitude and peak-to-peak amplitude are poor indicators of the average sound level. However, rms is an excellent measure as long as one specifies an averaging time. In the case depicted, the rms sound pressure was computed over the 0.01 second time window. Note that the sound pressure in *B* has the same rms value as the sound pressure in *A*.

TABLE 3–1 Sound pressures of common sounds

APPROXIMATE SOUND LEVEL		
rms Pa	dB SPL	SOUND SOURCE
0.0001–0.0002	14–20	Just audible whisper
0.002–0.02	40–60	Conversational speech
0.02–0.6	60–90	Noisy room
0.6–20	90–120	Loud music
>20	>120	Gun fire

hearing threshold vary depending on how the sound stimulus is specified. Sound pressure thresholds (the lowest sound pressures that are audible) measured in normal young adults with pure tones of different frequencies under two different measurement conditions are shown in Figure 3–3. The lower curve depicts thresholds determined with subjects in an open space or free field,[12] where the sound pressure measurement was made at the location of the subject's head when the subject was not present. The upper curve is the ANSI (American National Standards Institute[13]) standard measurement of thresholds made under earphones, where the sound pressures are those generated by the earphones in a calibration coupler. The differences between these two curves can be explained by the effect of the human subject on the open sound field, sound gathering by the external ear, the effect of closing the ear canal by earphones and differences in calibration between the two circumstances.[14] Both curves clearly show that normal young adult humans are most sensitive to sound frequencies of 500 to 8,000 Hz. The best frequency differs depending on the measurement circumstance, being 1,500 Hz under earphones and 4,000 Hz in the free field. At higher and lower

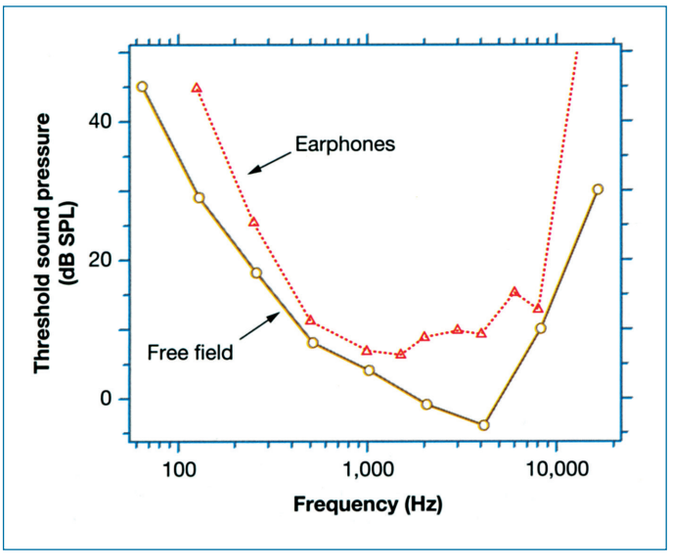

FIGURE 3–3 • Sensitivity of the ear to sounds of different frequencies. The figure depicts measurements of auditory threshold made under earphones (ANSI standards[13]) and those made in the free field (Sivian and White[12]). The mean normal threshold at 1,000 Hz under both measurement conditions is about zero dB SPL.

frequencies, more sound pressure is required to be audible, and the thresholds increase steeply below 500 Hz and above 8,000 Hz.

Clinicians are most interested in how an individual's hearing threshold differs from normal; in practice, normal is defined by the ANSI standard earphone measurements shown in Figure 3–3. A powerful graphical tool for comparing two different functions is to plot their difference. The *clinical audiogram* (Figure 3–4, discussed more in Chapter 8) uses this difference technique by plotting an individual's threshold relative to the ANSI standard normal hearing level. For example, a person whose hearing threshold at 1,000 Hz is 10 dB greater than the ANSI standard is assigned a hearing level of 10 dB at that frequency. In clinical audiograms, threshold sound pressure levels relative to the standard *Hearing Level* are quantified in dB relative to normal at frequencies of octave or half octave intervals. It is important to remember that the normal curve is based on mean hearing thresholds in normal subjects and that there is normal variation (plus or minus 20 dB) around the mean.

The *speed* or *propagation velocity* of sound through a medium determines the *sound wave length* for a given frequency, which is the distance it takes a propagating sound wave to repeat itself. Specifically, the wave length λ equals the propagation velocity divided by sound frequency. The wave length describes how a tone varies in space and the relative size of the wavelength and an object's dimensions determines how sound interacts with the object. If the wave length of a sound is at least five times larger than the largest dimension of an object, the object will have little effect on the sound, ie, as the sound propagates around the object, the sound pressure at the front and back side of the object will be very similar to the sound pressure measured when the object is not present. On the other hand, if the wave length is similar to or smaller than the dimensions of an object, variations in sound pressure will be introduced by the object. In general, as short wave length sound interacts with the object, the sound pressure along the front surface of the object will increase because of reflection of sound, and sound pressure along the back surface will be decreased because the object shields that location from the sound. A common analogy is between light and sound, where in the small wave length case, the object casts a sound shadow.

The size of body and ear structures relative to sound wave length plays a significant role in determining the interaction of the ear with sounds of different frequencies.[14] A 20 Hz sound wave (wave length of 17 m) is affected very little by the head or body. A 200 Hz sound (wave length of 1.7 m) can be effectively scattered by the head and torso so that there is a small gain in sound pressure at the ear. A 2,000 Hz tone (wave length of 17 cm) is diffracted by the head so that there is a doubling of sound pressure on the side of the head directed toward the sound source and a shadow on the opposite side of the head. A 4,000 Hz tone (8.5 cm wave length) is scattered by the pinna such that there is an increase in sound pressure for sound

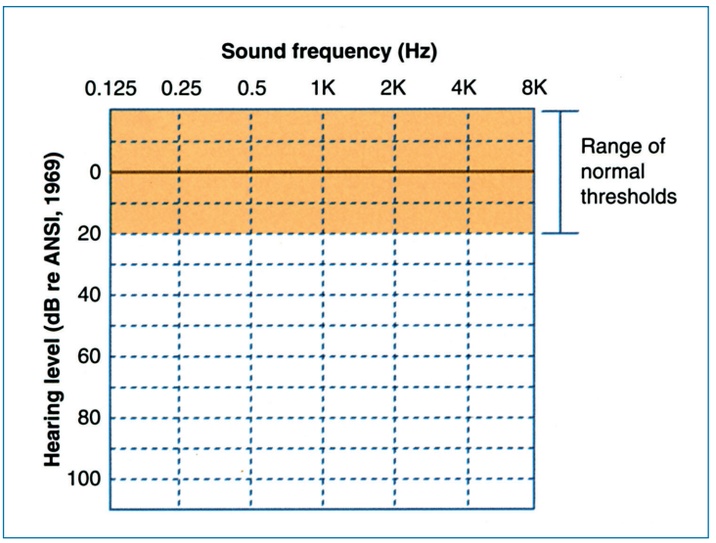

FIGURE 3–4 • Clinical audiogram, where an individual's hearing threshold relative to the ANSI standard normal hearing level is plotted versus frequency. The ordinate scale is inverted so that higher thresholds are plotted lower on the graph.

TABLE 3–2 Wavelengths of sound and body structures with which wave interactions are important

FREQUENCY (Hz)	WAVELENGTH	ANATOMICAL STRUCTURE	STRUCTURAL DIMENSIONS
340	1 m	Torso	0.5 m
2,000	17 cm	Head	10 cm
4,000	8.5 cm	Pinna Ear canal length	4 cm 2.5 cm
20,000	1.7 cm	Diameter of ear canal and tympanic membrane	0.8 cm

sources pointing directly at the meatus and decreases in sound pressure for other directions. Another kind of wave length interaction occurs in the external ear canal; resonances occur within the ear at frequencies where the length of the ear canal and depth of the concha are odd multiples of $\lambda/4$.[14] Table 3–2 lists some of the critical frequencies above which sound wave lengths allow interactions with various parts of the body and ear. In general, the interaction of the structures of the external ear and sound are restricted to sound frequencies of 1,000 Hz and above.

SOUND TRANSMISSION IN THE NORMAL EAR

The Problem of Transferring Air-Borne Sound Power to the Fluids of the Inner Ear: The Air-Fluid Impedance Mismatch

Acoustic signals are transmitted from the air of the external environment to the fluid-filled inner ear. The transmission of sound power at an air–fluid interface depends on the relative impedances of air and fluid. In the case of the inner ear, only about 0.1% of the intensity of an incident sound wave is transmitted to the fluid, and this is equivalent to a 30 dB loss. The external and middle ears act to better match the sound conducting properties of air and cochlear fluid by increasing the sound pressures that reach the inner ear at certain frequencies as described below. The discussion that follows is meant to be an overview, and readers seeking more detailed descriptions are referred to other sources.[15–17]

The External Ear

The external ear, along with the head and body, has a significant influence on the sounds that reach the middle ear. This acoustic function of the external ear, sometimes called the *external ear gain*, can be described by a frequency- and directionally-dependent alteration in the sound pressure at the tympanic membrane when compared to the sound pressure in the free field. As illustrated in Figure 3–5, when a sound source is positioned facing the ear, the external ear produces a gain of as much as 20 dB at 2,500 Hz, with less gain at lower and higher frequencies. As also illustrated in Figure 3–5, this gain results from the combination of sound scattering and diffraction around the head and torso, as well as the acoustic influence of the pinna, concha, ear canal, and middle-ear load impedance. The figure illustrates the frequency dependence of these different contributions and shows how the gains add (in dB terms) to define the total external-ear gain. Not shown in Figure 3–5 is how this external ear gain is directionally dependent for frequencies above 500 Hz. In fact, for sounds coming from the opposite side of the head, the sound pressure at the tympanic membrane can

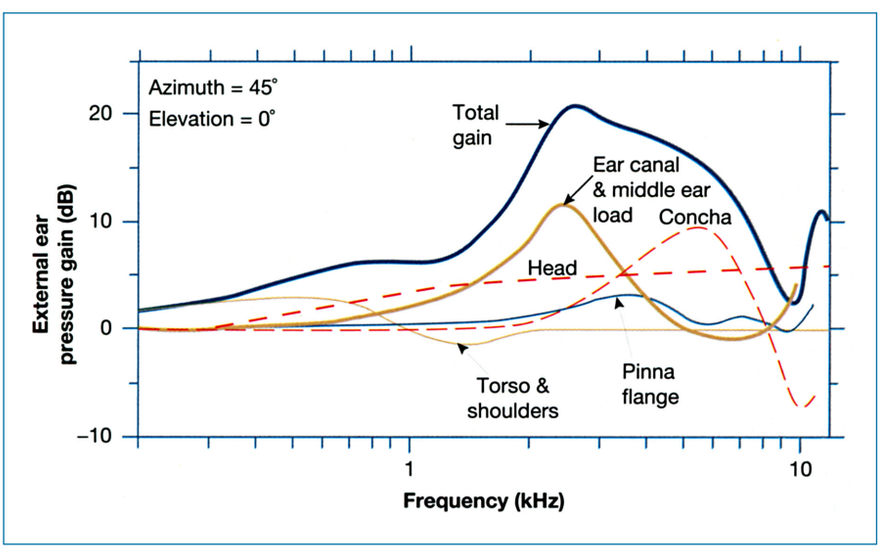

FIGURE 3–5 • Schematic representation of the external ear gain. The total gain and the gain of individual components in dB is plotted versus frequency. The plots describe the gains for a sound source that is positioned on the same horizontal plane as the interaural axis (elevation of 0 degrees) and which is 45 degrees off of the midline towards the ear that is measured (azimuth of 45 degrees). The gains of the different components are all multiplied (added in dB) together to achieve the total gain. *After Shaw.*[14]

be less than the sound pressure in the stimulus (ie, the external ear gain in dB is negative).

The Middle Ear

The middle ear couples sound signals from the ear canal to the cochlea primarily through the action of the tympanic membrane and the ossicular chain. Figure 3–6 is a schematic depicting the important structures in the *transformation* of sound power from the external ear to the inner ear. (Power is a product of pressure and volume velocity. Volume velocity refers to how much particle volume flows through a given area and is equal to the product of the average linear velocity across a surface and surface area. An acoustical transformer increases either pressure or volume velocity, while decreasing the other, thereby equalizing the sound power at the input and output). The middle ear acts as a transformer to increase sound pressure at the footplate relative to that at the tympanic membrane at the expense of a decrease in stapes volume velocity relative to the tympanic membrane volume velocity. The major transformer mechanism within the middle ear is the ratio of the tympanic membrane area to the stapes footplate area (*the area ratio*). The tympanic membrane gathers force over its entire surface and then couples the gathered force to the smaller footplate of the stapes. Since pressure is force per area, and the human tympanic has an area that is 20 times larger than the footplate,[2] if the transformer action of the area ratio is "ideal," the sound pressure applied to the inner ear by the stapes footplate should be 20 times or 26 dB larger than the sound pressure at the tympanic membrane. Another transformer within the middle ear is the ossicular lever: the lever action that results from the different lengths of the rotating malleus and incus arms around the axis of rotation of the ossicles. The axis of rotation is an imaginary line joining the anterior malleal ligament to the incudal ligament that anchors the short process of the incus. The malleus and incus lever arms in humans are nearly the same length. Hence, the ratio of these lengths, which is 1.3,[18] predicts only a small 2 dB increase in sound pressure applied by the stapes to the inner ear. Thus, if these transformers acted ideally, then the *theoretical middle-ear sound pressure gain* is about 28 dB (=26 dB area ratio + 2 dB ossicular lever).

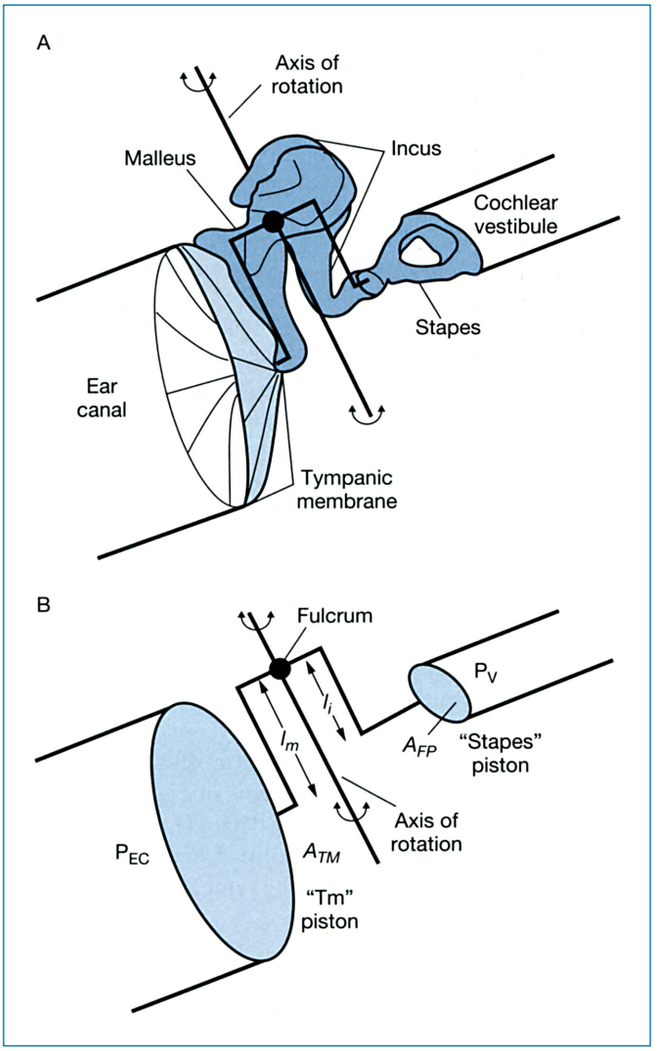

FIGURE 3–6 • Schematics of the tympano-ossicular system (*A*), and a mechanical analog (*B*), depicting important structures in the transformation of sound power from the middle ear to the inner ear. The key transformer within the middle ear is the ratio of the tympanic membrane area (*A*TM) to the area of the stapes footplate (*A*FP). Another transformer is the ossicular lever: this is the lever action due to differing lengths of the manubrium (*l*m) and long process of incus (*l*i) around the axis of rotation of the ossicles. This axis of rotation is an imaginary line joining the anterior malleal ligament to the incudal ligament that anchors the short process of the incus. The total middle-ear sound pressure gain, which is the result of the area ratio and the ossicular lever, can be quantified and measured using the ratio of sound pressure in the vestibule (P_v) to the sound pressure in the ear canal (P_{EC}). As described in the text, the theoretical (ideal) middle ear gain is 28 dB, whereas the actual (measured) middle-ear gain is only about 20 dB.

Measurements of the *actual middle-ear sound pressure gain* of the human middle ear performed in normal temporal bones under physiologic conditions[19] are illustrated in Figure 3–7. The data demonstrate that the pressure gain is frequency dependent, with a maximum gain of only about 20 dB near 1,000 Hz with lower gains at other frequencies. Similar findings have also been reported by other investigators.[20,21] Thus, the measured middle-ear gain is less than the 28 dB gain predicted by the ideal anatomical transformer model of Figure 3–6. The difference between the measured and theoretical gains is the result of several nonideal conditions within the middle ear: (1) The anatomical transformer model assumes that the entire tympanic membrane moves as a rigid body. However, measurements of tympanic membrane motion[22,23] show that portions of the membrane move differently than others. At low frequencies, the entire tympanic membrane moves with the same phase, but the magnitude varies. At frequencies above 1,000 Hz, the patterns of vibration become more complicated with the tympanic membrane breaking up into smaller vibrating portions that vibrate with different phases. This decreases the efficacy of the tympanic membrane as a coupler of sound pressure. (2) The simple transformer model does not account for the forces and pressures needed to stretch the tympanic membrane and ossicular ligaments and accelerate the mass of the middle-ear components. Part of the force generated by a sound pressure in the ear canal is used to move the tympanic membrane and ossicles themselves, and this force is lost before it

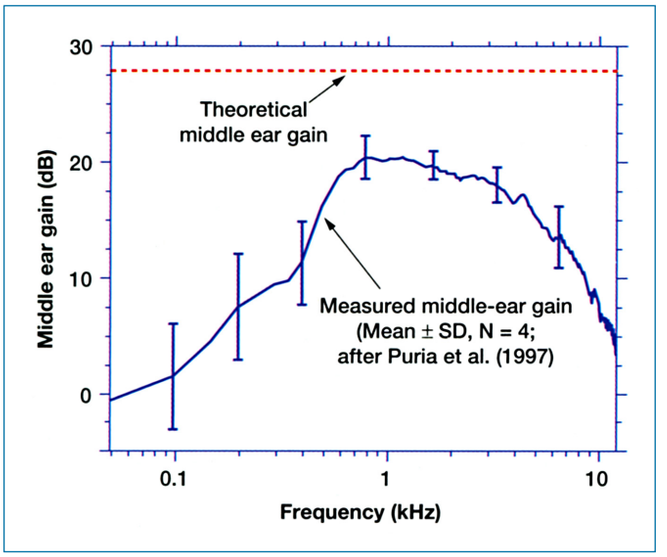

FIGURE 3–7 • Middle-ear sound pressure gain. The dashed line at the top shows the theoretical (ideal) transformer ratio produced by the tympanic membrane to footplate area ratio and the ossicular lever. The theoretical middle-ear gain, which is approximately 28 dB, is independent of frequency. The curve represents the mean ± standard deviation of measurements of middle-ear gain made in 4 normal temporal bones (Puria et al.[19]). The measurements consist of the increase in magnitude of the sound pressure in the cochlear vestibule over the sound pressure at the tympanic membrane. It is evident that the actual middle-ear gain is frequency dependent, and is only about 20 dB at best (around 1,000 Hz).

reaches the cochlea. (3) Other acoustical structures of the ear such as the middle-ear air spaces load the motion of the tympanic membrane and ossicles, and use up some of the pressure increase produced by the middle-ear transformer. (4) The anatomical transformer model implies that the ossicular system acts as a rigid body. In reality, there is slippage in the ossicular system particularly at frequencies above 1,000 to 2,000 Hz, which reduces the motion of the stapes relative to that of the manubrium. This slippage has been associated with translational movement in the rotational axis of the ossicles[24] or flexion in the ossicular joints.[10,25,26]

As will be discussed later, the effective stimulus to the inner ears is a difference in sound pressure between the oval and round windows. The middle ear maximizes this window pressure difference via two mechanisms.[27,28] First, as described above, the tympano-ossicular system preferentially increases the sound pressure at the oval window of the inner ear. At the same time, the intact tympanic membrane reduces the sound pressure in the tympanic cavity by 10 to 20 dB compared to the sound pressure in the ear canal,[29,30] thereby protecting or shielding the round window from the sound in the ear canal. A third function of the middle ear related to the protective function is that the presence of middle-ear air outside the round window permits the window to move freely when the inner ear is stimulated by motion of the footplate. These concepts of middle-ear sound pressure gain, round window protection and round window mobility have important practical implications for tympanoplasty.

The Inner Ear

The cochlea is a coiled tube made of three fluid-filled chambers. The fluid is essentially incompressible, so that any movement of the stapes footplate within the oval window must be accompanied by fluid motion elsewhere. Over the auditory frequency range, the small fluid-filled cochlear and vestibular aqueducts and other connections between the cochlea and cerebrospinal fluid space are effectively closed,[31] and it is the compliant membrane covering the round window that permits large motions of the footplate. When the stapes footplate moves in, the round window moves out. (The footplate and round window have approximately the same volume velocities, but move with opposite phase.) It is this coupling of the round and oval windows by the incompressible cochlear fluids that leads to the importance of the *difference* in sound pressure at the two cochlear windows in stimulating the inner ear.[32,33]

The cochlear partition within the inner ear includes the basilar membrane, the organ of Corti, scala media, and Reissner's membrane. The mechanical properties of the cochlear partition are heavily influenced by the mechanics of the basilar membrane; the latter is narrow, stiff and thick at the base, and it is wider, compliant and thin at the apex. Because the fluid is essentially incompressible, inward motion of the stapes causes a near instantaneous transfer of the motion through the cochlear fluids, resulting in outward motion of the round window. Associated with this displacement of the fluid is a nearly instantaneous pressure distribution across the cochlear partition. The reaction of the cochlear partition with its graded mechanical properties to this pressure distribution, results in a *traveling wave* of cochlear partition displacement.[34] The maximum displacement of this wave is tonotopically organized in a manner consistent with place-dependent differences in partition mechanics. High-frequency sounds produce displacement maxima near the stiff and thick base, while low-frequency sounds produce displacement maxima near the compliant and thin apex.

Because the wave appears to travel from the base towards the apex and also appears to stop just past the location of maximum displacement, there is an asymmetry in the motion of the cochlear partition. All sounds produce some motion of the basal portions of the cochlear partition, while only low-frequency sounds produce significant partition motion in the apex. This asymmetry has implications in our perception of complex sounds (where low-frequency sounds can interfere with our perception of high-frequency sounds, but not vice versa[35]), and has also been suggested to play a role in the sensitivity of the high-frequency base to noise trauma and in presbycusis.[36] Motion of the cochlear partition stimulates hair cells of the organ of Corti, where larger stimuli result from larger motions.

Phase Difference Between the Cochlear Windows

As stated earlier, the cochlea responds to the *difference* in sound pressure between the cochlear windows,[32,33] where the sound pressure at the oval window is a sum of the pressure produced by the tympano-ossicular system and the acoustic pressure within the middle-ear air space. It is important to understand how this difference (the essential stimulus to the inner ear),

depends on the relative magnitude and phase of the individual sound pressures at the two windows. When there is a significant difference in magnitude between the oval- and round-window sound pressures (as in the normal ear and after successful tympanoplasty when the tympano-ossicular system amplifies the pressure acting at the oval window), *differences in phase have little effect* in determining the window-pressure difference.[37,38] The lack of importance of phase when the magnitudes differ is illustrated in Figure 3–8, which shows a hypothetical situation where the magnitude of the oval window sound pressure is ten times (20 dB) greater than the round window sound pressure. The range of possible window-pressure difference is shown by two curves, one with an amplitude of 9 representing the difference when the two window pressures are in-phase (0-degree phase difference) and the other curve with an amplitude of 11 representing the difference when the window pressures are completely out-of-phase (180-degree phase difference). Even with this maximum effect of varying the phase difference, the two curves shown in Figure 3–8 are similar in magnitude, within 2 dB of each other. With larger magnitude differences such as factors of 100 to 1,000 (40–60 dB) that occur in the normal ear and in ears that have undergone successful tympanoplasty, variations in phase have a negligible effect.

However, phase differences can become important under conditions when the magnitudes of the sound pressures at the oval and round windows are similar (eg, with an interrupted ossicular chain). When the individual window pressures are of similar magnitude and similar phase, they tend to cancel each other and produce only a small net window-pressure difference. On the other hand, if the individual window pressures are of similar magnitude but opposite phase, then they will add to each other, resulting in a window-pressure difference that is similar in magnitude to the applied pressures.

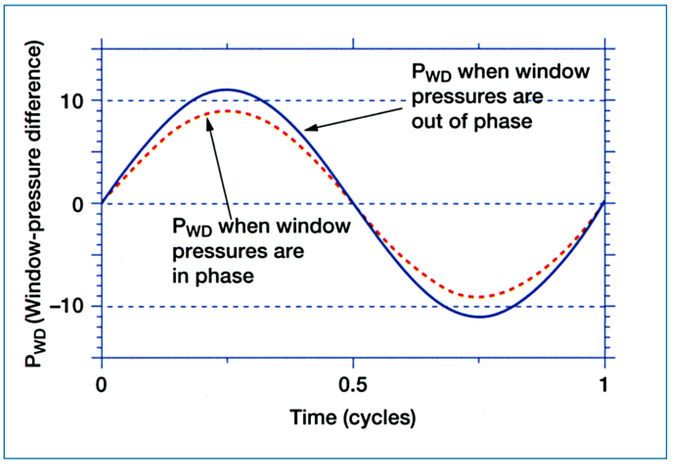

FIGURE 3–8 • Schematic showing that if there is a significant difference in magnitude between window pressures, then differences in phase are of little importance in determining the difference between the two sound pressures. In this specific case, the oval window sound pressure is 10 times (=20 dB) greater than the round window sound pressure. One cycle of the wave form of the window-pressure difference (P_{WD}) is plotted for two circumstances. The dashed line shows P_{WD} when the oval window and round window pressures are in-phase, and the result is a P_{WD} wave of peak amplitude 9 = 10 – 1. The solid line shows P_{WD} when the individual window pressures are completely out-of-phase, and the result is a P_{WD} wave of amplitude 11 = 10 – (– 1). Note that the two P_{WD} pressures differ by less than 2 dB ($20\log_{10}11/9 = 1.7$ dB), even though this phase variation produces the largest possible magnitude difference. Thus, in the normal ear and after successful tympanoplasty when the sound pressure at the oval window is large due to significant ossicular conduction of sound, differences in phase of sound pressures at the oval and round windows have little effect in determining the hearing outcome.

Multiple Pathways for Sound Stimulation of the Inner Ear

The contribution of the middle ear to the window-pressure difference that stimulates the inner ear can be split into several stimulus pathways. A previous section described how the tympano-ossicular system transforms sound pressure in the ear canal to sound pressure at the oval window. This pathway has been termed *ossicular coupling*.[39] There is another mechanism, called *acoustic coupling*,[39] through which the middle ear can stimulate the inner ear (Figure 3–9). Motion of the tympanic membrane in response to ear canal sound creates sound pressure in the middle ear cavity. Because the cochlear windows are separated by a few millimeters, the acoustic sound pressures at the oval and round windows respectively, are similar but *not* identical.[40] Small differences between the magnitudes and phases of the sound pressures outside the two windows result in a small but measurable difference in sound pressure between the two windows. In the normal ear, the magnitude of this acoustically-coupled window pressure difference is small, on the order of 60 dB less than ossicular coupling.[38,40] Hence, ossicular coupling dominates normal middle-ear function and one can

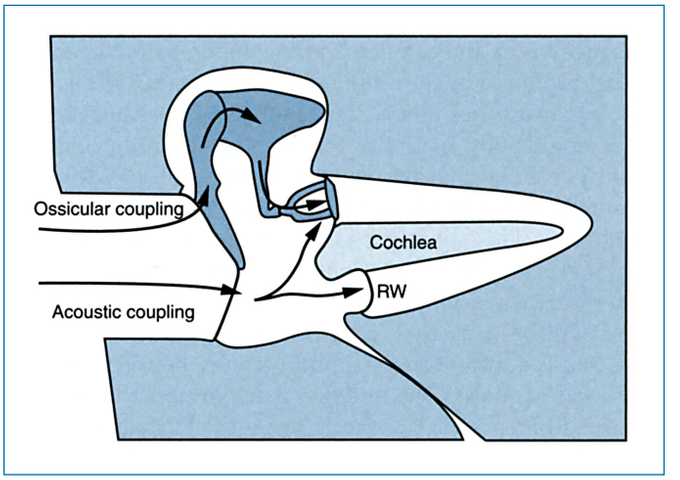

FIGURE 3–9 • Schematic showing the pathways of ossicular coupling and acoustic coupling. Ossicular coupling is produced by the coupled motion of the tympanic membrane, ossicles and stapes footplate. Acoustic coupling results from middle-ear sound pressure that is produced by ear canal sound pressure and motion of the tympanic membrane. Because the cochlear windows are spatially separated, the sound pressures within the middle ear cavity that act at the oval and round windows (RW), respectively, are *not* identical. The small differences between the magnitudes and phases of the two window pressures result in a small but measurable *difference* in sound pressure between the two windows. This difference is called acoustic coupling. In the normal ear, acoustic coupling is quite small and its magnitude is approximately 60 dB less than ossicular coupling.[38,39]

ignore acoustic coupling. However, as will be seen later, acoustic coupling can play an important role when ossicular coupling is compromised as in some diseased and reconstructed ears.

Environmental sound can also reach the inner ear by producing vibrations of the whole body and head, so-called whole body sound conduction.[41] This is a more general process than audiological *bone conduction* where a vibrator acts only on the mastoid portion of the skull. Sound-induced vibrations of the whole body and head can stimulate the inner ear by (1) generating external ear or middle-ear sound pressures via compressions of the ear canal and middle-ear walls, (2) producing relative motions between the ossicles and inner ear, and (3) direct compression of the inner ear and its contents by compression of the surrounding fluid and bone. Little is known about the contribution of *whole body sound conduction* to normal auditory function. However, measurements of hearing loss due to pathology such as congenital aural atresia suggest that the whole body route can provide a stimulus to the inner ear which is about 60 dB smaller than that provided by normal ossicular coupling.[41]

Audiological Bone Conduction

Sound energy transmitted to the skull by a bone vibrator (eg, a tuning fork or the electromagnetic vibrator of an audiometer) sets the basilar membrane in motion and is perceived as sound. Clinical bone conduction testing is used as a means to determine the functionality of the cochlea. The mechanisms by which a bone vibrator can stimulate the inner ear have been described by Tonndorf[42] and others[43,44] and are similar to those described earlier for whole-body sound transmission. It is important to realize that all of the hypothesized bone-conduction mechanisms involve relative motion between the ossicles and inner ear, and that bone-conduction hearing is influenced by pathologies in the external and middle ears. The so-called occlusion effect (easily demonstrated by occlusion of the external ear canal while talking, which results in increased loudness of sound heard in the occluded ear) occurs because vibrations of the ear canal wall produce significant sound pressures in the closed ear canal. Furthermore, a classic pattern in bone conduction audiometry known as the Carhart notch (see Chapter 10) is used to help identify cases of stapes footplate fixation.[45] The mechanical processes that underlie the Carhart notch phenomenon are not well understood. Therefore, the idea that vibrating the skull directly stimulates the cochlea in a manner that is independent of the middle ear is not strictly true.

Middle Ear Muscles

The stapedius and tensor tympani muscles contract under a variety of circumstances including loud sounds, before and during vocalization, tactile stimulation of the head or face, and fight or flight behavioral responses.[46] Such protective contractions reduce the transmission of low-frequency sound through the middle ear but have little effect on high-frequency sound.[2,47,48] Contraction of the stapedius muscle in response to sound is known as the *acoustic reflex*. The reflex is thought to help in speech discrimination (the reflex reduces masking by low-frequency sound of high-frequency stimuli[49,50]), and in protecting the inner ear from acoustic trauma of loud continuous sound.[51] Contractions of the tensor tympani have also been associated with opening of the eustachian tube where the inward motion of the tympanic membrane that results from the contraction produces an overpressure in the middle ear that helps open the tube.[52]

Middle Ear Joints

The incudomalleal and incudostapedial joints add flexibility to the ossicular system, which allows the middle ear to withstand large variations in the static pressure difference across the tympanic membrane without producing damage to the ear. Middle-ear static pressure variations that occur regularly in day-to-day activities (eg, those produced by sneezing and swallowing) generate millimeter-sized motions of the tympanic membrane; such large motions are not transmitted to the stapes due to the flexibility of the incudomalleal and incudostapedial joints.[53,54]

The ossicular joints also permit independent control of tympanic membrane and stapes motion by the middle-ear muscles. Large contractions of the stapedius muscle that cause 0.1 mm changes in position of the stapes head have been shown to have little effect on position of the other ossicles because of sliding in the incudostapedial joint.[55] Similarly, the tensor tympani can pull the malleus inwards by a millimeter or more but has little effect on the stapes because of the incudomalleal joint. There is some data from studies of ossicular motion in animals and human temporal bones to suggest that a consequence of the joint-induced flexibility is a decrease in the high-frequency response of the middle ear.[10,56] There is also evidence that flexion of the incudo-malleolar joint is a major component of the human ossicular response to sound at all frequencies.[25,57]

Investigation of Middle-Ear Mechanics

Broadly speaking, investigations of middle-ear mechanics have employed one or more of four approaches: behavioral and other assessments of hearing in normal and diseased ears, physiologic studies of the middle ears of animals, quantitative physics-based models, and acoustic measurements in cadaveric temporal bones.

The use of animal models to study the middle ear was pioneered by Wever and Lawrence in a series of studies of the effects of middle-ear modifications on cochlear potentials in cats.[2] Other landmark studies include: investigations of middle-ear impedance and ossicular motion,[10,58–61] investigations of the effect of middle-ear muscles,[62] and investigations of simulated pathologies on middle-ear transmission.[63–65] Animal studies continue to provide new insights into middle-ear function, including recent evidence that the ossicles are not completely rigid,[66] evidence of wave-motion in the tympanic membrane itself and within the ossicular chain[67–69] and new evidence of contractile elements within the support of the tympanic membrane.[70]

A "model" of the middle ear is essentially a set of mathematical equations that relate the physical structure of the ear to its acoustic function. The degree and complexity of the association of model elements with anatomic structures varies widely within models, ranging from simple "black-box" models of the ear,[71] through models where simple elements

are associated with specific structures of the ear,[72] to complex three-dimensional finite-element models that include detailed depictions of middle-ear shape and approximations of the mechanical properties of the structural elements.[69,73,74] A wide variety of middle-ear models have been described, dealing with sound transmission in normal as well as in pathological ears. A discussion of such models is outside the scope of this review, and the reader is referred to other sources.[17]

Cadaveric temporal bones (the "temporal bone preparation") are also useful in studying middle-ear mechanics. It has been shown that the mechanical properties of the middle ear in carefully prepared temporal bones are indistinguishable from those measured in living human ears.[75–77] The temporal bones must be in a fresh state, kept moist and static pressure must not be allowed to build up within the middle ear. Besides its utility in studying normal middle-ear function, the temporal bone preparation allows one to make repeated measurements of acoustic and mechanical function after precise modifications that simulate specific pathologies or tympanoplasties. Measurements in such preparations have provided valuable insight into the mechanics of sound transmission in a variety of diseased and reconstructed ears.

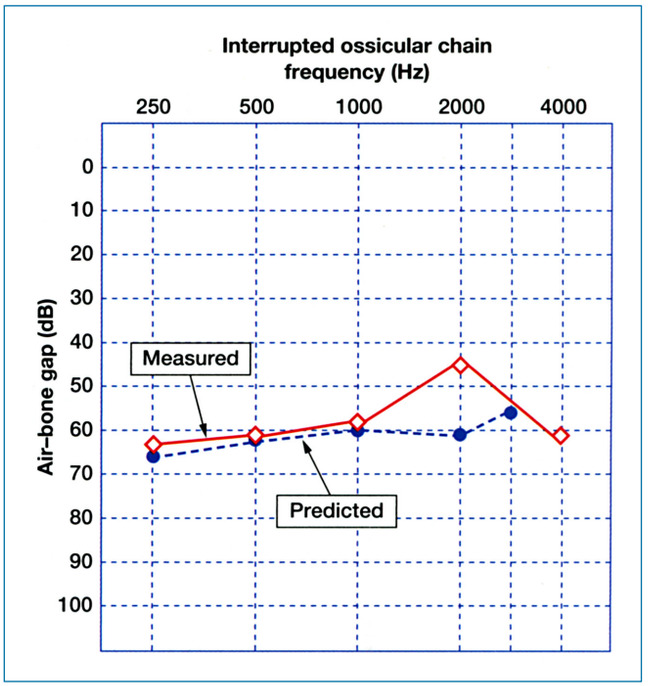

FIGURE 3–10 • Comparison of air–bone gaps measured in eight cases with surgically confirmed complete ossicular chain interruption with an intact tympanic membrane to air–bone gaps predicted on the basis of hearing resulting from acoustic coupling. In this pathological state, there is no ossicular coupling. Since acoustic coupling is about 60 dB smaller than ossicular coupling, the prediction is a 60 dB conductive hearing loss, which is consistent with the measured air–bone gaps. The standard deviation for each of the measured points is about ± 10 dB. *After Peake et al.*[39]

ACOUSTICS AND MECHANICS OF DISEASED MIDDLE EARS

The concepts discussed in the previous section help us to understand sound transmission in various pathological middle-ear conditions. In this review, we have chosen the "air–bone gap" as determined by standard clinical audiometry to describe the loss of middle-ear sound transmission in various pathological conditions. Our choice of the air–bone gap measure is a matter of ease and convenience, since the gap can be easily calculated from a clinical audiogram and it allows one to compare ears with disparate levels of sensorineural function. However, one must remember that the air–bone gap is not always an accurate measure of middle-ear sound transmission loss, because bone conduction thresholds can be influenced by middle-ear pathologies, as mentioned previously.

Ossicular Interruption With an Intact Tympanic Membrane

When there is ossicular interruption in the presence of an intact drum, ossicular coupling is lost and sound input to the cochlea via the middle ear occurs as a result of acoustic coupling.[39] Since acoustic coupling is about 60 dB smaller than ossicular coupling, one would predict that complete ossicular interruption would result in a 60 dB conductive hearing loss. This prediction is consistent with clinical observations as shown in Figure 3–10, where there is good agreement between the predicted and actual air–bone gap as measured in eight surgically confirmed cases of ossicular interruption with an intact tympanic membrane. Note that the consistency of the clinical results with the model of acoustic coupling suggests that stimuli reaching the inner ear through whole body or bone conduction mechanisms in this particular condition are small enough to be ignored.

A special type of ossicular interruption consists of resorption or a break in one of the ossicles and its replacement by connective tissue. An example is resorption of the long process of the incus and its replacement by a band of fibrous tissue in chronic otitis media. Such "partial ossicular interruption" is often associated with an air–bone gap that is greater at high versus low frequencies. It is one of the few types of middle-ear pathologies where the air–bone gap is greater at the high frequencies. The mechanism of hearing loss is probably related to a decrease in the rigidity within the ossicular chain. At low frequencies, a fibrous band seems to be tense enough to allow near-normal sound transmission; however, at higher frequencies, the fibrous band flexes such that motions of the tympanic membrane are not readily coupled to the stapes.

Loss of the Tympanic Membrane, Malleus, and Incus

In cases where the tympanic membrane, malleus, and incus are lost, the conductive hearing loss is on the order of 40 to 50 dB, ie, this condition results in hearing sensitivities that are 10 to 20 dB superior to cases with an intact tympanic membrane and complete ossicular interruption. The 40- to 50-dB loss can be explained by a loss of ossicular coupling together with an enhancement of acoustic coupling by about 10 to 20 dB, as compared to the normal ear.[39] The enhancement of acoustic coupling results from loss of the shielding effect of the tympanic membrane, which in the normal ear attenuates middle-ear sound pressure by 10 to 20 dB relative to ear canal

sound pressure. The air–bone gap predicted by loss of ossicular coupling and enhanced acoustic coupling is similar to that measured in patients as shown in Figure 3–11. The increase in acoustic coupling due to loss of tympanic membrane shielding also explains why the hearing of a patient with an interrupted ossicular chain and an intact drum is improved by 10 to 20 dB when a perforation is created in the tympanic membrane.

Ossicular Fixation

Partial or complete fixation of the stapes footplate (eg, otosclerosis, tympanosclerosis, etc.) results in conductive hearing losses that range from 5 dB to 60 dB depending on the degree of fixation.[78] The losses are greater for the lower frequencies (Figure 3–12). Fixation of the footplate reduces ossicular coupling by hindering stapes motion, resulting in a conductive hearing loss. The amount of hearing loss depends upon the degree of decreased stapes motion. The primary effect of the otosclerotic lesion is an increase in the stiffness of the annular ligament that supports the stapes, where the normal ligament stiffness is a major constraint on the ossicular coupling route in the normal ear. Increases in ligament stiffness should first affect the low-frequency response of the ear, which is consistent with the observation that in early otosclerosis the hearing loss is mainly in the low frequencies.[78]

The conductive hearing loss resulting from fixation of the malleus is determined by the location, extent, and type of pathology causing the fixation.[79] Fixation at the level of the anterior malleal ligament (eg, calcification of the ligament) results in a hearing loss less than 10 dB. More commonly, fixation of the malleus is at the level of its head due to a bony spur that ankyloses the malleus head to the lateral epitympanic wall or to the tegmen tympani.[80] The resulting air–bone gap is small, usually in the range of 15 to 25 dB.[80,81] Malleus ankylosis can also be caused by extensive deposition of fibrous tissue and new bone in the epitympanum as the result of chronic otitis media.[80,82] In such a case, both the malleus and incus are usually fixed in the epitympanum, with an air–bone gap of 30 to 50 dB.[82] The differential effects of location, extent, and type of malleus fixation can be explained on the basis of the mechanics of rotation of the malleus (and incus) about an axis linking the anterior malleal and the posterior incudal ligaments.[79] In such a rotating system, the stiffening torque associated with malleus fixation is proportional to the distance between the fixation and the axis of rotation. When the fixation is at the axis of rotation (the anterior malleal ligament), the fixation-associated stiffening torque is small, whereas when a similar fixation is placed away from the axis of rotation at the malleus head (such as a bony spur), a much larger stiffening torque results.

Tympanic Membrane Perforation

Perforations of the tympanic membrane cause a conductive hearing loss that can range from negligible to 50 dB (Figure 3–13). The primary mechanism of conductive loss due to a perforation is a reduction in ossicular coupling caused by a loss in the sound-pressure difference across the tympanic membrane.[63,83–86] The sound–pressure difference across the tympanic membrane provides the primary drive to the motion of the drum and ossicles. Perforation-induced physical changes such as reduction in

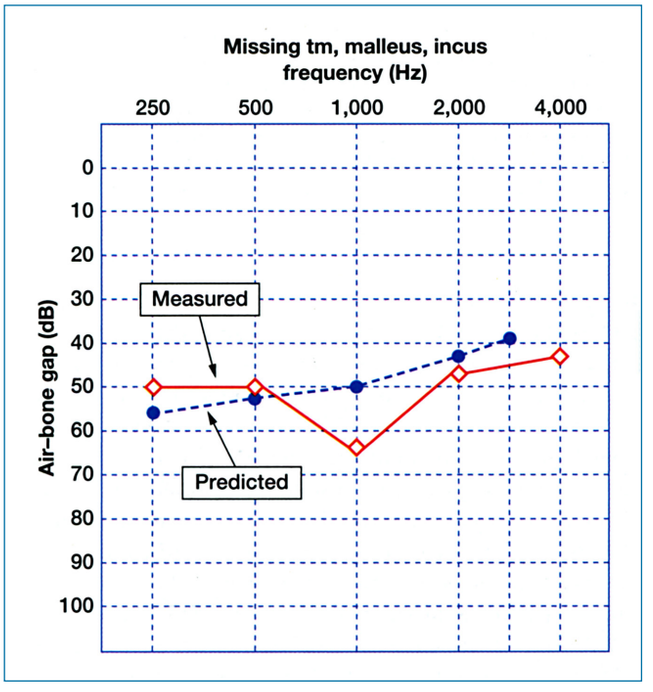

FIGURE 3–11 • Comparison of air–bone gaps measured in 5 cases with missing tympanic membrane (TM), malleus and incus to air–bone gaps predicted on the basis of acoustic coupling. With loss of the tympanic membrane, there is enhancement of acoustic coupling by about 10 to 20 dB compared to the normal ear. The predicted and measured gaps are similar. *After Peake et al.*[39]

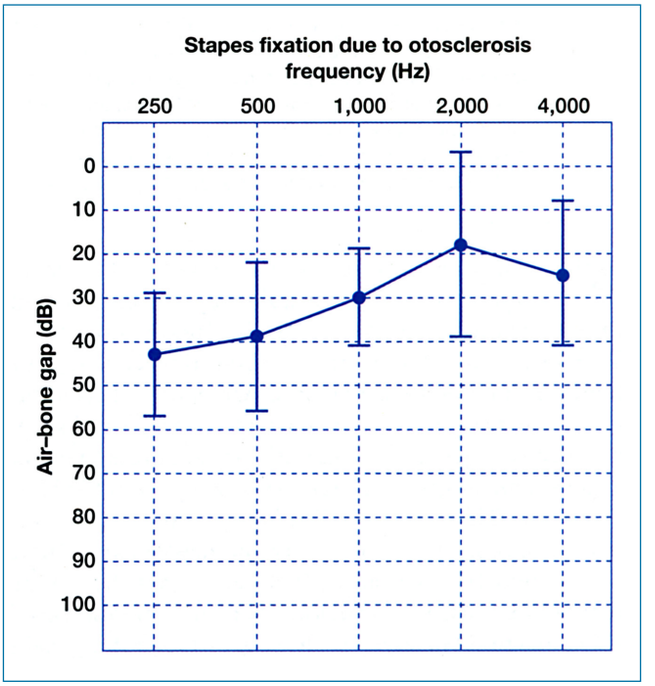

FIGURE 3–12 • Air–bone gaps measured in 75 cases of surgically confirmed stapes fixation of varying degrees due to otosclerosis. The mean ± 1 standard deviation of the air–bone gap at each frequency is shown. The conductive hearing loss is greater for the lower frequencies.

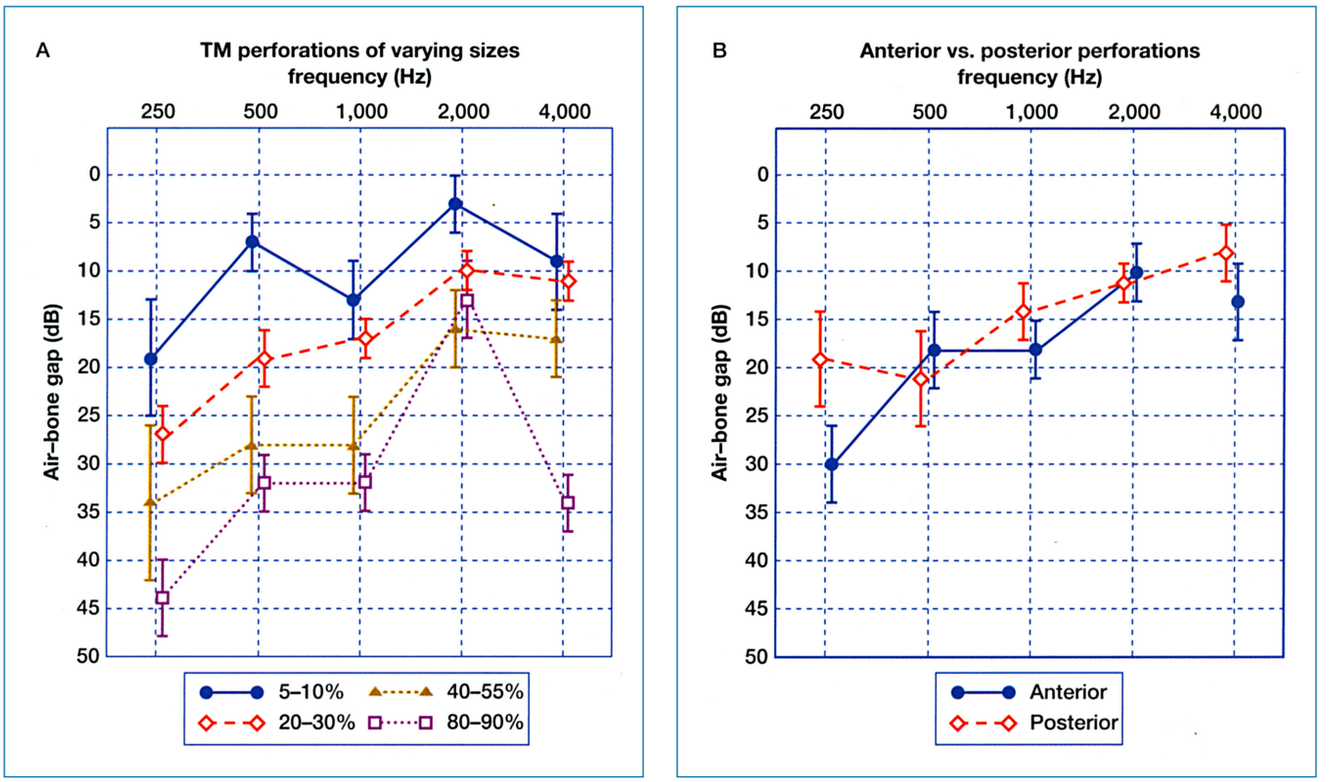

FIGURE 3–13 • Air–bone gaps measured in 42 ears with tympanic membrane perforations. In each case, the conductive hearing loss was caused solely by the perforation, because (1) the ossicular chain was found to be intact and mobile at subsequent tympanoplasty surgery done to repair the perforation, and (2) there was closure of the air–bone gap after the surgery. *A*, Air–bone gaps (mean ± one standard error of mean) are shown for perforations of varying sizes. Perforation size was estimated as a percentage of the area of the tympanic membrane. There were four groups of perforations, based on their size: 5 to 10% (5 ears), 20 to 30% (22 ears), 45 to 55% (6 ears), and 80 to 90 % (9 ears). Air–bone gaps are greater at the lower frequencies, and the gaps increase as the perforations get larger. The largest perforation-induced air–bone gaps are about 40 to 50 dB. *B*, Air–bone gaps (mean ± one standard error of mean) are shown for anterior versus posterior perforations of the same size. The ears of perforation size equal to 20 to 30% of tympanic membrane area from the dataset shown in *A*, were subdivided into anterior (11 ears), and posterior (8 ears) groups, based on location of the perforation with respect to the manubrium. There are no statistically significant differences between the two means at any frequency. (In 3 ears with 20 to 30% perforations, the perforation was directly inferior to the umbo, and they were excluded from the anterior versus posterior analysis.)

tympanic membrane area or changes in coupling of tympanic membrane motion to the malleus do not appear to contribute significantly to the hearing loss caused by a perforation.[84–86]

Perforations cause a loss that depends on frequency, perforation size, and middle-ear air space volume.[84–86] Perforation induced losses are greatest at the lowest frequencies and generally decrease as frequency increases. Perforation size is an important determinant of the loss; larger perforations result in larger hearing losses (Figure 3–13A). The volume of the middle-ear air space (combined tympanic cavity and mastoid air volume) is also an important parameter that determines the amount of hearing loss caused by a perforation; small middle-ear air space volumes result in larger air–bone gaps. Other things being equal, for a given sound pressure in the ear canal and a given perforation, the resulting sound pressure within the middle-ear cavity will vary inversely with middle-ear volume. Hence, the transtympanic membrane sound–pressure difference will be smaller (and the conductive loss correspondingly greater) with smaller middle-ear volumes.[84,87] Identical perforations in two different ears can have conductive losses that differ by up to 20 to 30 dB if the middle-ear air space volumes differ substantially (within normal ears, middle-ear air space volume can range from 2 to 20 cm^3).[88] Thus, a perforation will result in a larger air–bone gap when the mastoid is extremely sclerotic compared to one that is well pneumatized. The dependence of the hearing loss on the middle ear and mastoid air volume can explain the common clinical observation that seemingly identical perforations (in size and location) may produce significantly different degrees of hearing loss. It can also explain the clinical observation that an air–bone gap in a given perforation can vary from time to time in the same ear. For example, the air–bone gap is often smaller when the perforation is dry compared to when it is wet and draining. It is likely that in the infected situation, the volume of air in the middle ear and mastoid is reduced compared to the dry state.

The dependence of perforation-induced hearing loss on the transtympanic membrane sound–pressure difference also suggests that there should be *no* systematic differences in the

air–bone gaps caused by perforations of identical size at different locations. The notion that location of a perforation should not influence the resulting hearing loss is supported by the following evidence-to-date:

1. *Theoretical calculations.* While it has been demonstrated that perforations of the tympanic membrane lead to increases in the sound pressure outside the cochlear windows, since the wave lengths of sound are generally larger than the middle-ear dimensions, the acoustically coupled window-pressure difference should not depend on perforation location.
2. *Experimental data.* Measurements in a temporal bone preparation have shown that the location of a perforation affects neither the resulting loss in sound transmission, nor the magnitude or phase of the sound pressures acting at the oval and round windows.[84–86]
3. *Clinical data.* Figure 3–13B compares air–bone gaps between same-sized perforations situated in anterior versus posterior locations, and there is no significant difference between the two groups. Mehta et al.,[87] in a study of 62 cases, found no significant differences in air–bone gaps at any frequency for perforations in the anterior versus posterior quadrants, after controlling for size of perforation and middle-ear air volumes. We speculate that the common clinical perception that perforations of similar size but different locations produce different hearing losses may result from inter-ear differences in the volume of the middle-ear and mastoid air space.[84–86]

Finally, measurements in temporal bones[40,84–86] demonstrate that tympanic membrane perforations lead to an increase in acoustic coupling by 10 to 20 dB due to loss of the shielding effect of the intact tympanic membrane. The increase in acoustic coupling allows one to predict that the maximum conductive loss following a perforation will be about 40 to 50 dB, which is consistent with clinical observations (Figure 3–13A).

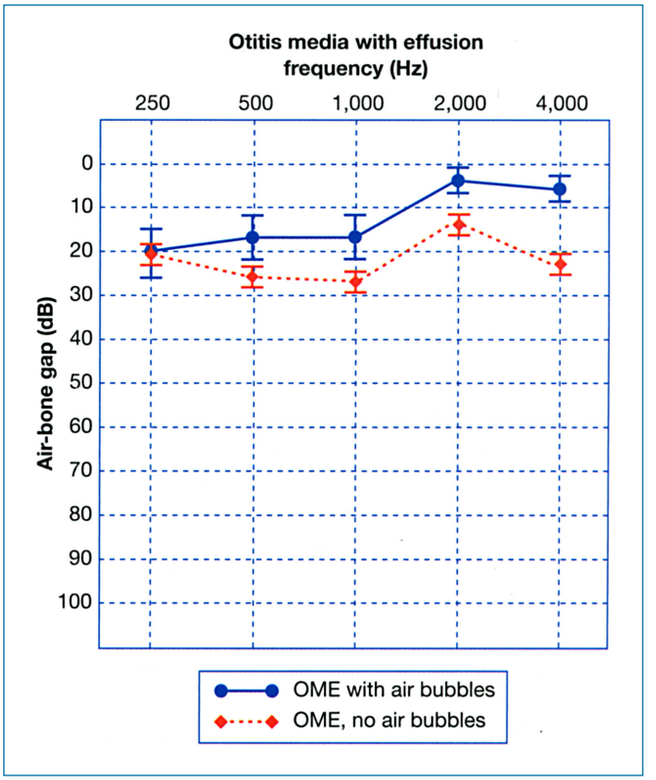

FIGURE 3–14 • Air–bone gaps (mean ± one standard error of mean) measured in 29 adult ears with otitis media with effusion (OME). In each case, the air–bone gap disappeared when the OME resolved, either spontaneously or after myringotomy. Two groups of ears are displayed, based on absence (N = 24) or presence (N = 5) of visible air bubbles behind the tympanic membrane at otoscopy, at the time the air–bone gaps were measured. Ears with air in the tympanic cavity show a smaller conductive loss than ears with no visible air bubbles. The differences between the two groups are statistically significant at the 5% level for 1,000, 2,000, and 4,000 Hz.

Middle Ear Effusion

Fluid in the middle ear, a primary feature of otitis media with effusion (OME), is associated with a conductive hearing loss of up to 30 to 35 dB,[89] though the degree and frequency dependence of individual losses vary (Figure 3–14). The conductive loss occurs because of a reduction in ossicular coupling due to several mechanisms.[90] At frequencies greater than 1,000 Hz, the loss is caused primarily by mass loading of the tympanic membrane by fluid, with decreases in sound transmission of up to 20 to 30 dB. The effect increases as more of the tympanic membrane surface area is covered with fluid. At frequencies below 1,000 Hz, the hearing loss is due to an increase in impedance of the middle-ear air space resulting from reduced middle-ear air volume, and possibly from negative middle-ear static pressure which is often associated with OME. Increasing the viscosity of the middle-ear fluid appears to have rather small effects (less than 5–10 dB) on the overall hearing loss.

Tympanic Membrane Atelectasis

Atelectasis of the tympanic membrane occurring without a tympanic membrane perforation (and in the presence of intact and mobile ossicles) can result in conductive hearing losses that vary in severity from negligible to 50 dB.[37] The conductive loss can be explained on the basis of a reduction in ossicular coupling due to the tympanic membrane abnormality. As long as the area outside the round window remains aerated and is shielded from the sound pressure in the ear canal by the tympanic membrane, the conductive hearing loss caused by the atelectasis should not exceed the amount of middle-ear sound pressure gain in normal ears, ie, air–bone gaps of up to 25 dB. If the atelectasis results in invagination of the tympanic membrane into the round window niche, the protective effect of the tympanic membrane and middle-ear air space on round window motion is lost, and larger 40 to 50 air–bone gaps should result. This prediction is consistent with the amount of acoustic coupling in cases where there is loss of the tympanic membrane, malleus, and incus.

Third Window Lesions of the Inner Ear

The majority of cases demonstrating an air–bone gap are the result of middle-ear pathology affecting the tympanic membrane or ossicular chain. However, there are a number of disorders affecting the inner ear that can result in an apparent conductive hearing loss in the absence of true middle-ear

pathology. Their clinical presentation can mimic otosclerosis or other middle-ear disease. These disorders of the labyrinth produce an air–bone gap by creating a pathologic "third window' in the inner ear (in addition to the two normal windows, the oval and round windows).[91] The third window permits dissipation of air conducted sound energy away from the cochlea, thus resulting in a hearing loss by air conduction. At the same time, the third window improves thresholds for bone conducted sounds or leaves the bone thresholds unchanged. Thus, the net audiometric effect of the third window is a conductive hearing loss (air–bone gap).

The best characterized of these third window lesions is the syndrome of superior canal dehiscence.[92–95] The typical audiometric manifestation is an air–bone gap in the low and middle frequencies below 2,000 Hz, with no gap or only a small gap at higher frequencies. Low-frequency bone conduction thresholds may be at supra-normal levels of up to -20 dB or better.

Besides superior canal dehiscence, a number of disorders of the inner ear can result in pathologic third windows (Table 3–3).[96,97] Such lesions may be anatomically discrete or diffuse. Anatomically discrete lesions may be classified by location: semicircular canals (superior, lateral or, posterior canal dehiscence), bony vestibule (enlarged vestibular aqueduct, other inner ear malformations) or the cochlea (carotid–cochlea dehiscence, X-linked deafness with stapes gusher). An example of an anatomically diffuse lesion is Paget disease which may behave as a distributed third window.

The syndrome of superior canal dehiscence has been used as a prototype to investigate the mechanisms by which an air–bone gap rises in third window lesions. These investigations have included theoretical model analyses,[91,98] measurements in cadaveric human temporal bone preparations,[99] experiments in animal models of superior canal dehiscence,[100,101] and measures of middle-ear sound transmission in patients.[95,102] These studies have suggested the following conceptual mechanism causing the air–bone gap (Figure 3–15). In the normal ear, air conducted sound stimuli entered the vestibule through motion of the stapes. An inward motion of the stapes is accompanied by an equal but outward motion of the round window membrane. The fluid flow between the windows produces a pressure difference between the scala vestibuli and scala tympani, resulting in motion of the cochlear partition, activation of hair cells, and perception of sound. A pathologic third window on the vestibular side of the cochlear partition shunts a portion of the acoustic energy away from the cochlear partition, producing a decrease in sound pressure within the vestibule, thus resulting in a loss of hearing sensitivity to air-conducted sound. The effect of a third window on bone conduction thresholds is less intuitive but can be understood based on the compression of mechanism of bone conduction. In the normal ear, compression of inner-ear fluids by bone conducted sound results in a hearing percept because of an inequality in the impedance between the scala vestibuli side and the scala tympani side of the cochlear partition, which in turn, is due to a difference between the impedance of the oval and round windows, respectively. This inequality leads to a pressure difference across the cochlear partition, resulting in motion of the basilar membrane that leads to the perception of bone-conducted sound. A pathologic third window on the vestibular side of the cochlear partition increases the pressure difference between the two sides of the cochlear partition by lowering the impedance on the vestibuli side, thereby improving the cochlear response to bone conduction. Therefore, supra-normal thresholds for bone conduction may be evident. It should be noted that such improvements of bone conducted thresholds produced by the third window may be masked by an accompanying true sensorineural hearing loss.

It is important to note that the pathologic third window must be on the scala vestibuli side of the cochlear partition to produce an air–bone gap (ie, the window must be in the bony vestibule, in one of the semicircular canals, or in the bony wall of the scala vestibuli of the cochlea). A third window on the scala tympani side, such as an enlarged cochlear aqueduct, is not predicted to result in a conductive hearing loss and may even lead to an improvement in hearing function by increasing the sound pressure difference across the cochlear partition that results from air- and bone-conducted sound.

A number of audiometric clues and tests are available to the clinician for making an accurate diagnosis of an air–bone gap caused by a third window lesion as opposed to a pathological lesion within the middle ear.[93,94,97] A low-frequency air–bone gap with bone conduction thresholds that are better than 0 dB can be a clue. Therefore, it is important to accurately assess audiometric bone conduction thresholds to levels below 0 dB HL. Acoustic reflexes are typically absent in true middle-ear disease, but are generally present in third window lesions. Vestibular evoked myogenic responses are typically absent in patients with true middle-ear pathology but may be larger than normal and present at lower stimulus levels in third window lesions. Vestibular manifestations comprising sound- or pressure-induced vertigo and eye movements may be evident in third window lesions caused by canal dehiscences. When audiometric and other tests suggest that an inner ear

TABLE 3–3 Third-window lesions of the inner ear causing air-bone gaps

1. Anatomical third window
   a. Semicircular canal
      - Superior canal dehiscence
      - Posterior canal dehiscence
      - Lateral canal dehiscence
   b. Vestibule
      - Large vestibular aqueduct syndrome
      - Inner ear malformations causing a dehiscence between internal auditory canal and vestibule
   c. Cochlea
      - Dehiscence between carotid canal and scala vestibuli
      - Inner ear malformations causing a dehiscence between internal auditory canal and scala vestibuli, eg, DFN-3 (X-linked deafness with stapes gusher)
2. Diffuse or distributed third window
   a. Paget disease of the temporal bone

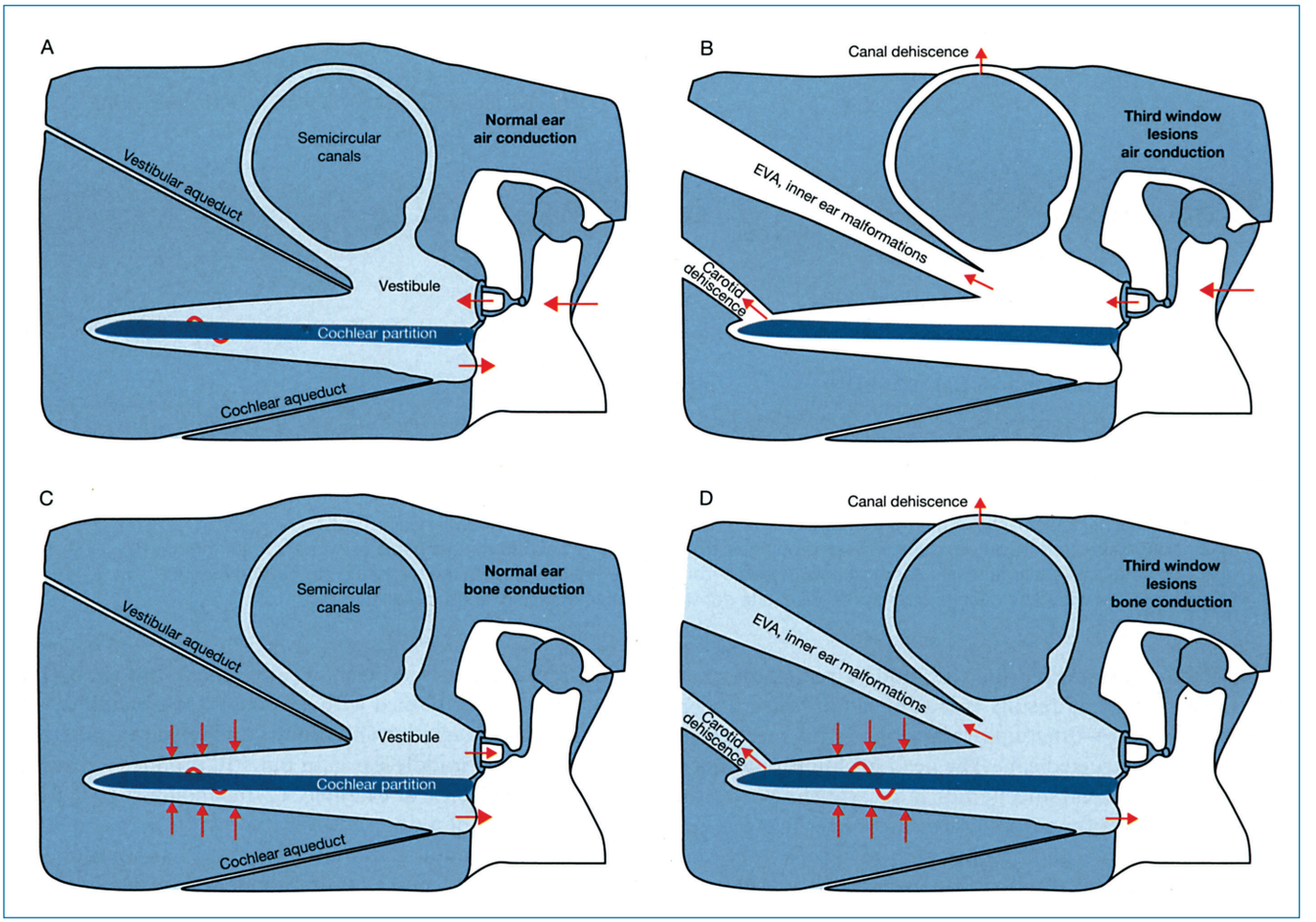

FIGURE 3–15 • Schematic representations of mechanism of air–bone gap in third window lesions. *A*, Normal ear, air conduction. Air-conducted sound stimuli enter the vestibule through motion of the stapes. There is a pressure difference between the scala vestibuli and the scala tympani, resulting in motion of the cochlear partition. The volume velocities of the oval and round windows are equal in magnitude but opposite in phase. *B*, Third-window lesion, air-conduction. It is hypothesized that a third window (in one of the canals, the vestibule or the scala vestibuli) allows a portion of the acoustic energy entering the vestibule through motion of the stapes to be shunted away from the cochlea. The shunting occurs primarily at low frequencies, resulting in a hearing loss by air-conduction. *C*, Normal ear, bone-conduction. Compression of inner ear fluid by bone-conducted sound results in a hearing percept because of an inequality in the impedance between the scala vestibuli side and the scala tympani side of the cochlear partition. This inequality is primarily due to a difference in the impedance between the oval and windows. As a result, there is a pressure difference across the cochlear partition, resulting in motion of the basilar membrane that leads to perception of bone-conducted sound. *D*, Third window lesion, bone-conduction. A third window increases the difference between the impedance on the scala vestibuli side and the scala tympani side of the cochlear partition by lowering the impedance on the vestibuli side, thereby improving the cochlear response to bone-conduction. In patients with healthy cochleae as in superior canal dehiscence, supranormal bone-conduction thresholds may be evident. In other patients with an accompanying true sensorineural hearing as in DFN-3, enlarged vestibular aqueduct (EVA), etc, the improved bone-conduction due to the third window mechanism may not be result in supranormal thresholds. *After Merchant and Rosowski*.[97]

lesion may be responsible for the conductive hearing loss, an appropriate imaging study such as a CT scan will help to make a definitive diagnosis.

ACOUSTICS AND MECHANICS OF RECONSTRUCTED MIDDLE EARS

Though tympanomastoid surgery for chronic otitis media is quite successful in controlling infection with reported success rates in excess of 80 to 90% (Chapter 28), it is well recognized that post-tympanoplasty hearing results are often unsatisfactory, especially with advanced lesions of the ossicular chain or when there is inadequate aeration of the middle ear. Table 3–4 is a summary of postsurgical hearing results from eight large clinical series[103–110] spanning the past three decades that demonstrates results are often less than satisfactory. When the ossicular chain has to be reconstructed, long term closure of the air–bone gap to ≤20 dB occurs in only 40 to 70% of cases when the stapes is intact, and only in 30 to 60% of cases when the stapes superstructure is missing.

TABLE 3–4 Hearing results after ossicular reconstruction: Cases (%) with postoperative air-bone gaps ≤ 20 dB

AUTHORS	NO. OF CASES	MINOR COLUMELLAS, INCLUDING PORPs	MAJOR COLUMELLAS, INCLUDING TORPs
1. Lee and Schuknecht, 1971[103]	936	40	—
2. Pennington, 1973[104]	216	70	—
3. Jackson, Glasscock et al., 1983[105]	417	64	43
4. Brackmann, Sheehy, and Luxford, 1984[106]	1,042	73	55
5. Lau and Tos, 1986[107]	229	54	40
6. Ragheb, Gantz, and McCabe, 1987[108]	455	52	37
7. Colletti et al., 1987[109]	832	48–80*	28–70*
8. Goldenberg, 1992[110]	262	57	58

PORP, partial ossicular replacement prosthesis; TORP, total ossicular replacement prosthesis.
Minor columella refers to an ossicular strut or prosthesis from the stapes head to the tympanic membrane/manubrium.
Major columella refers to an ossicular strut or prosthesis from the stapes footplate to the tympanic membrane/manubrium.
* Results varied with time interval after surgery: results got worse with increasing length of follow-up.

One factor responsible for the modest nature of post-tympanoplasty hearing results is lack of quantitative understanding of structure–function relationships in the mechanical response of reconstructed ears. The need for improved understanding of middle-ear mechanics is clearly shown by the clinical occurrence of many instances in which the structural differences between a good and poor hearing result are not apparent or where seemingly minor variations in structure are associated with large differences in function. For example, Liston et al.,[111] with the use of intraoperative monitoring by auditory evoked responses during ossiculoplasty, found that changes in prosthesis position of 0.5 to 1.0 mm had effects on hearing as large as 20 dB. It is also a common clinical observation that postsurgical ears, which seem identical in structure, can exhibit markedly different degrees of conductive hearing loss. Better quantitative understanding of the factors that determine the hearing response, eg, graft stiffness and tension, and the mechanical properties of the prosthesis, should permit us to understand what are the important structural differences that might account for these seemingly unexplainable results.

Other major factors contributing to unsatisfactory postsurgical hearing results are incomplete knowledge of the biology of chronic middle-ear disease (including pathology of middle-ear aeration and Eustachian tube function), and a lack of control over the histopathological and tissue responses of the middle ear to surgery. These factors are outside the scope of this chapter.

Reconstruction of the Sound Conduction Mechanisms

The goal of tympanoplasty is to restore sound pressure transformation at the oval window by coupling an intact tympanic membrane with a mobile stapes footplate via an intact or reconstructed ossicular chain, and to provide sound protection for the round window membrane by means of a closed, air-containing, mucosa-lined middle ear. As previously mentioned, the mean sound–pressure gain provided by the normal ear is only about 20 dB. Consequently, a mechanically mobile but suboptimal tympanoplasty, combined with adequate stapes mobility, adequate middle-ear aeration and round window sound protection, can result in no middle-ear gain but still produce a relatively good hearing result. For example, a tympanoplasty that gives a middle-ear gain of 5 dB but leaves the middle ear aerated and allows round window motion, will result in an air–bone gap of only 15 dB. (Of course, an immobile, rigid tympanoplasty graft will result in very little stapes motion and much larger hearing losses.) As previously discussed, the magnitude of the ossicularly coupled sound pressure at the oval window is significantly greater than the acoustically coupled sound pressure at the round window in the normal ear and we suspect a similar pressure gain after successful tympanoplasty. Under these circumstances, differences in phase of sound pressures at the oval and round windows have little effect in determining the hearing outcome. Therefore, the goal of a tympanoplasty should be to increase the magnitude of sound pressure at the oval window relative to the round window, *without* regard to phase.

The following subsections attempt to describe the structural parameters that are thought to be important to hearing results after middle-ear surgery.

Aeration of the Middle Ear

Aeration of the middle ear (including the round window) is *critical* to the success of any tympanoplasty procedure. Aeration allows the tympanic membrane, ossicles and round window to move. Clinical experience has shown that nonaerated ears often demonstrate 40-to 60-dB air–bone gaps.[38] The large gap in nonaerated ears occurs because (1) ossicular coupling is greatly reduced and (2) stapes motion is reduced because the round window membrane (which is coupled to the stapes by incompressible cochlear fluids) cannot move freely.

How much air is necessary behind the tympanic membrane (that is, within the middle ear and mastoid)? Model analyses of the effects of varying the volume of the middle ear and mastoid

predict an increasing low frequency hearing loss as air volume is reduced[112] (Figure 3–16). The normal, average volume of the middle ear and mastoid is 6 cc; a combined middle ear and mastoid volume of 0.5 cc is predicted to result in a 10 dB conductive hearing loss. Volumes smaller than 0.5 cc should lead to progressively larger gaps, whereas increases in volume above about 1.0 cc should provide little additional acoustic benefit. Experimental studies[29,113] using a human temporal bone preparation where the middle ear and mastoid volume was reduced progressively show results consistent with the model prediction.

The above predictions of the effect of middle ear and mastoid air volume on the air–bone gap are applicable to those cases where the tympanic membrane is intact. Once there is a perforation of the tympanic membrane, then the volume of the middle ear and mastoid air space has an important bearing on the resulting air–bone gap, as discussed earlier.

Another parameter of the middle-ear air space that can influence middle-ear mechanics is the static air pressure within the space. Experiments in human perception dating back to the 19th century,[114] numerous animal studies[2,59] and measurements of ossicular motion in human temporal bones[115] have demonstrated that middle-ear static pressure can have different effects on sound transmission at different frequencies. Generally, transtympanic membrane static pressure differences produce decreases in sound transmission through the middle ear for frequencies less than 1,000 Hz, and have less effect at higher frequencies. Also, the effect of such static pressure differences are asymmetric with larger decreases observed when the middle-ear pressure is negative relative to that in the ear canal. The mechanisms by which pressure changes reduce middle-ear sound transmission are not well defined, and possible sites of pressure sensitivity include the tympanic membrane, annular ligament, incudo-malleal joint, and suspensory ligaments of the ossicles. Some of these structures are drastically altered as a result of tympanoplasty, and the acoustic effects of negative and positive middle-ear static pressure in reconstructed ears have not been characterized.

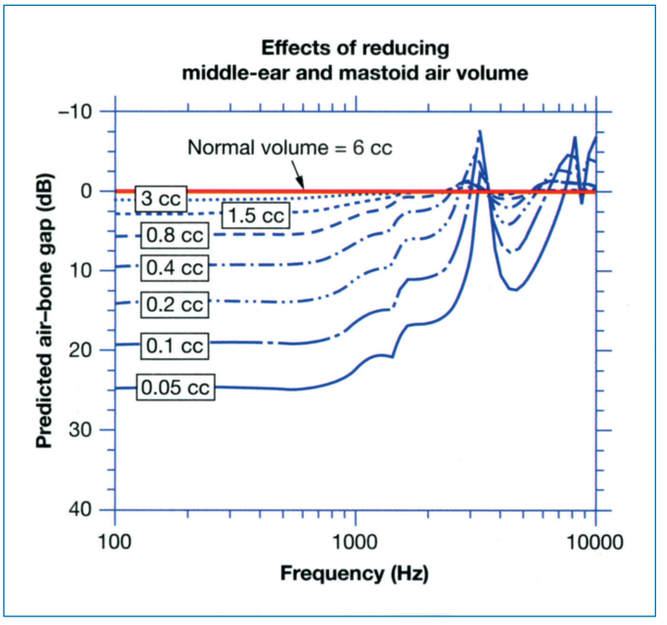

FIGURE 3–16 • Model predictions of the effects of reducing the volume of the middle ear and mastoid. The normal baseline volume is taken to be 6 cc. Note that reduction of the volume to 0.4 cc is predicted to result in an air–bone gap less than 10 dB. Volumes smaller than 0.4 cc are predicted to lead to progressively larger gaps. *After Rosowski and Merchant.*[112]

Tympanoplasty Techniques without Ossicular Linkage: Types IV and V

A type IV tympanoplasty[116] is a surgical option in cases where the tympanic membrane and ossicles are missing, the stapes footplate is mobile and there is a canal wall-down mastoid cavity. Incoming sound from the ear canal impinges directly on the stapes footplate while the round window is shielded from the sound in the ear canal by a tissue graft such as temporalis fascia (Figure 3–17). If the stapes footplate is ankylosed, it is removed and replaced by a fat graft and this arrangement constitutes a type V tympanoplasty.[117] In both type IV and type V procedures, there is no ossicular coupling and residual hearing depends on acoustic coupling.[39,118–120] The introduction of a tissue graft to shield the round window from sound enhances acoustic coupling by increasing the sound pressure difference between the oval and round windows. Model analyses of type IV reconstructions[118,119] suggest that an optimum reconstruction (defined by normal footplate mobility, a sufficiently stiff acoustic graft-shield, and adequate aeration of the round window) results in *maximum* acoustic coupling with a predicted residual conductive hearing loss of only 20 to 25 dB. This optimum result is consistent with the best type IV hearing results (Figure 3–18). These analyses also predict that decreased footplate mobility, inadequate acoustic shielding or inadequate round window aeration can lead to hearing losses as large as 60 dB.

Since the literature demonstrates that less than 50% of ears after type IV surgery have air–bone gaps less than 30 dB,[119] it is clear that many type IV reconstructions are nonoptimum.

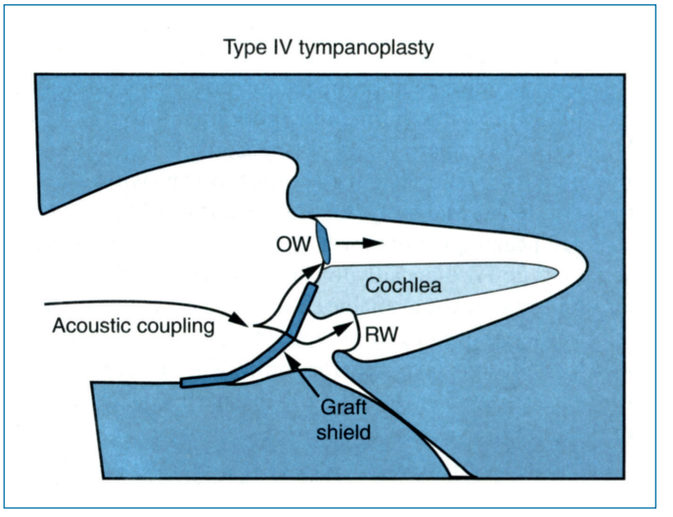

FIGURE 3–17 • Schematic of type IV tympanoplasty. Incoming sound from the ear canal impinges directly on a mobile stapes footplate within the oval window (OW), while the round window (RW) is acoustically protected by a graft-shield. With no ossicular coupling, cochlear stimulation depends on acoustic coupling.

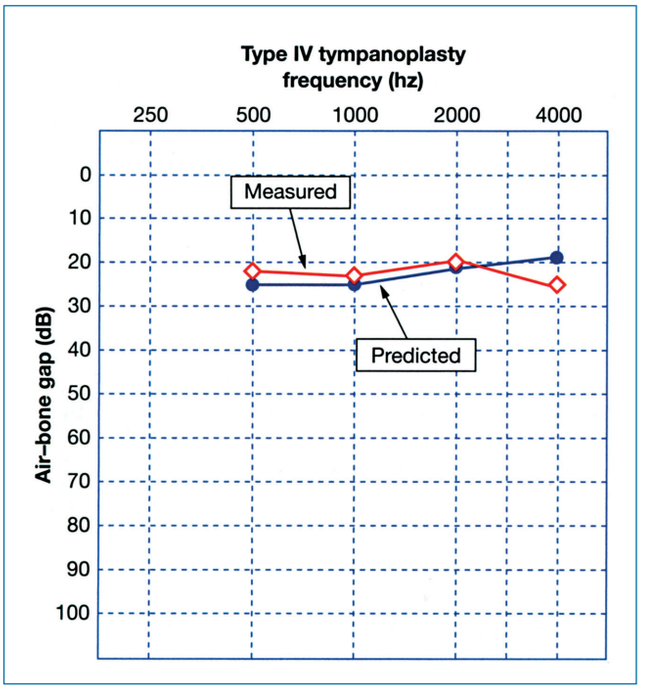

FIGURE 3–18 • Air–bone gaps after type IV tympanoplasty: the best surgical results are compared with a prediction based on "maximum" acoustic coupling. The predicted and measured results are similar, with an air–bone gap of approximately 20 dB. *After Peake et al.*[39]

The following surgical guidelines can be used to optimize the postoperative hearing results: (1) one should preserve normal stapes mobility by covering the footplate with a thin split-thickness skin graft and not a fascia graft (fascia is much thicker than skin and can increase footplate impedance), (2) one should reinforce the round window fascia graft-shield with cartilage or 1 mm thick Silastic™ (reinforcing the graft-shield in this manner increases its stiffness and improves its performance as an acoustic shield), and (3) one should create conditions that promote aeration of the round window niche and preserve mobility of the round window membrane (eg, by preserving all healthy mucosa in the protympanum and hypotympanum).

In a type V tympanoplasty, it is reasonable to assume that the mobility of the fat used to replace the footplate will be greater than that of the normal footplate. Hence, one would predict that the average hearing results for a type V would be better than those for a type IV, especially for low frequencies. This prediction is supported by the available clinical evidence. For example, in a clinical series of 64 cases of type V tympanoplasty[121] 86% of ears with conditions favorable for round window aeration had an air–bone gap smaller than the 20-dB gap that occurs with an optimum type IV.

Tympanoplasty Techniques with Reconstruction or Preservation of Ossicular Linkage: Types I, II, and III

Type I, II, and III tympanoplasty involve reconstruction of the tympanic membrane and/or the ossicular chain. Besides maintenance of middle-ear aeration and static pressure, the postoperative hearing result depends on the efficacies of the reconstructed eardrum and the reconstructed ossicular chain.

Tympanic Membrane Reconstruction

While the tympanic membrane is responsible for most of the middle-ear sound pressure gain, the details of how that gain is achieved are not well understood. Motion of the normal tympanic membrane is complex, especially at frequencies above 1,000 Hz.[22] Clinical observations suggest that surgical techniques that restore or preserve the normal anatomy of the tympanic membrane can lead to good hearing results.[37,38] However, more research is needed to define the optimum acoustic and mechanical properties of reconstructed tympanic membranes. For example: (1) Little is known of the mechanical significance of the arrangements of structural fibers in the tympanic membrane. (2) While it has been argued that the conical shape of the normal tympanic membrane plays an important role in middle-ear function,[7,22] the possible effects of changes in tympanic membrane shape on postoperative hearing results are not understood. (3) While many existing models of tympanic membrane function have been shown to fit some of the available data,[73] there are wide differences in the structure of these models, and little effort has been made to compare their significant differences and similarities. Further, these models generally have not been applied to reconstructed tympanic membranes. Better understanding of the features of tympanic membrane structure that are critical to its function should lead to improved methods for reconstructing the ear drum.

Ossicular Reconstruction

A wide variety of ossicular grafts and prostheses are in use. However, there are limited scientific data on the optimum acoustic and mechanical properties of ossicular prostheses. Factors that can influence the acoustic performance of an ossicular prosthesis include its *stiffness, mass,* and *position,* the *tension* imposed by the prosthesis on the drum and annular ligament, and mechanical features associated with *coupling* of the prosthesis to the drum and stapes.[37,38]

In general, the stiffness of a prosthesis will not be a significant factor as long as the stiffness is much greater than that of the stapes footplate-cochlear impedance. For clinical purposes, prostheses made of ossicles, cortical bone, and many synthetic materials generally meet this requirement.

Model analysis[112] and experimental data[122,123] suggest that an increase in ossicular mass does not cause significant detriment in middle-ear sound transmission. Shown in Figure 3–19 are model predictions of air–bone gaps resulting from increasing the mass of an ossicle strut, relative to the stapes mass, which is 3 mg. Increases up to 16 times are predicted to cause less than 10 dB conductive loss and only at frequencies greater than 1,000 Hz.

The positioning of the prosthesis appears to be important to its function. Measurements in human temporal bone preparations suggest that the angle between the stapes and a prosthesis should be less than 45 degrees for optimal sound transmission.[124,125] There is also evidence that some variations in positioning produce only small changes. For example, while it is ideal to attach a prosthesis to the manubrium, experimental data show that acceptable results can occur with a prosthesis placed against the posterior-superior quadrant of the tympanic

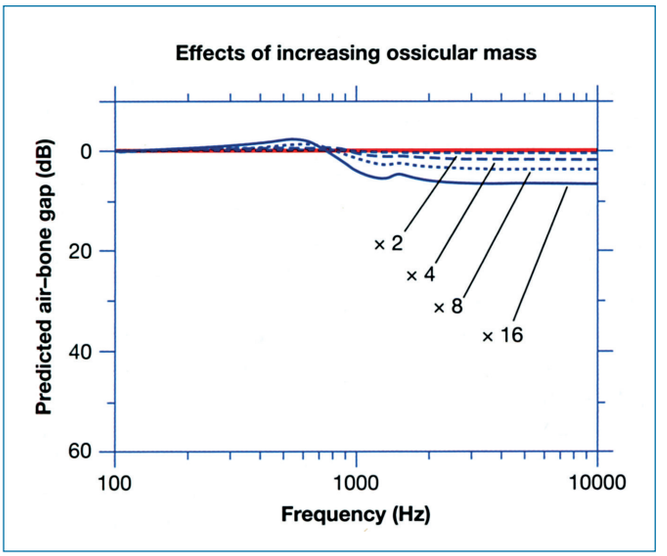

FIGURE 3–19 • Model prediction of the effects of increasing ossicular mass. The mass of an ossicular strut is increased as shown. These increases are relative to the stapes mass which is 3 mg. Increases up to 16 times are predicted to cause less than 10 dB conductive loss and only at frequencies greater than 1,000 Hz. *After Rosowski and Merchant.*[112]

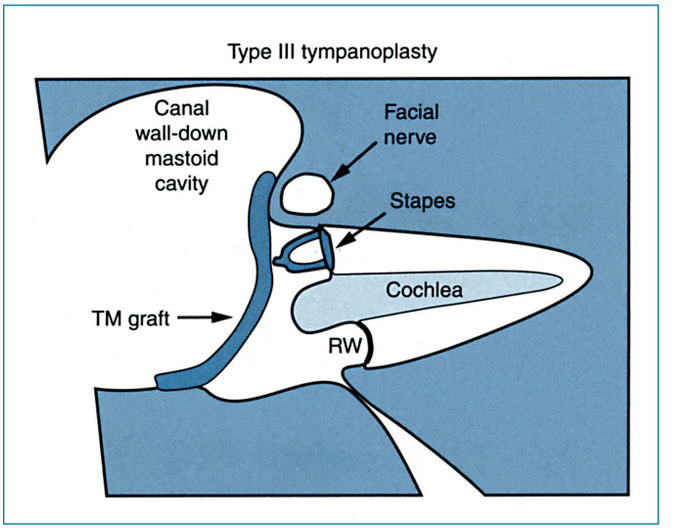

FIGURE 3– 20 • Schematic of type III tympanoplasty, stapes columella. A tympanic membrane (TM) graft, usually temporalis fascia, is placed directly onto the stapes head. The procedure is typically performed in conjunction with a canal-wall-down mastoidectomy. RW, round window.

membrane as long as 3 to 4 mm of the prosthesis's diameter contacts the drum.[126]

The tension the prosthesis creates in the middle ear, which is generally a function of prosthesis length, appears critical in determining the hearing result.[127] The mechanical impedance of biological structures is inherently nonlinear, and measurements such as tympanometry have shown that the tympanic membrane and annular ligament act as linear elements only over the range of small motions (less than 10 micrometers) associated with physiological sound levels. Larger displacements of the ligament and membrane stiffen these structures. The large static displacements produced by a prosthesis that is too long would stretch the annular ligament and tympanic membrane, resulting in a stiffening of these structures, a reduction in tympano-ossicular motion and an air–bone gap. Currently, tension cannot be assessed intraoperatively in an objective fashion; a reliable objective test of this tension would be useful to the otosurgeon.

"Coupling" refers to how well a prosthesis adheres to the footplate or tympanic membrane, and the degree of coupling will determine whether or not there is slippage in sound transmission at the ends of a prosthesis. Thus, a prosthesis transmits sound effectively only if there is good coupling at both ends. Clinical observations indicate that it is rare to obtain a firm union between a prosthesis and the stapes footplate. Hence, inadequate coupling at the prosthesis-footplate joint may be an important cause of a persistent postoperative air–bone gap. The physical factors that control coupling have not been determined in a quantitative manner, and further study of this parameter is warranted.

Type III Tympanoplasty, Stapes Columella

A classical type III or stapes columella tympanoplasty (Figure 3–20) involves placement of a tympanic membrane graft such as temporalis fascia directly onto the stapes head,[116] ie, the ossicular chain is replaced by the single columella of the stapes. This tympanoplasty is typically performed in conjunction with a canal-wall-down mastoidectomy. The hearing results after this procedure vary widely with air–bone gaps ranging from 10 to 60 dB. Large air–bone gaps (40–60 dB) occur as a result of stapes fixation, nonaeration of the middle ear, or both (Figure 3–21). When the stapes is mobile and the middle ear is aerated, the average postoperative air–bone gap is on the order of 20 to 25 dB, suggesting that there is little middle-ear sound pressure gain occurring through the reconstruction. Experimental and clinical studies of the type III stapes columellar reconstruction have shown that interposing a thin disk of cartilage between the graft and the stapes head improves hearing in the lower frequencies by 5 to 10 dB.[128–130] We hypothesize that the cartilage acts to increase the "effective" area of the graft that is coupled to the stapes, which leads to an increase in the middle-ear gain of the reconstructed ear.

Canal Wall-Up Versus Canal Wall-Down Mastoidectomy

In a canal wall-down mastoidectomy, the bony tympanic annulus and much of the ear canal is removed, and the tympanic-membrane graft is placed onto the facial ridge and medial attic wall. This results in a significant reduction in the size of the residual middle-ear air space. However, as long as this air space is greater than or equal to 0.5 cc, the resultant loss of sound transmission should be less than 10 dB (see above). Since the average volume of the tympanic cavity is 0.5 to 1.0 cc,[88] a canal-wall-down procedure should create no significant acoustic detriment, so long as the middle ear is aerated. Indeed, clinical studies comparing the acoustic results of canal-wall-down versus canal-wall-up mastoidectomy have shown no significant differences in hearing between the two conditions.[106,109,130,131]

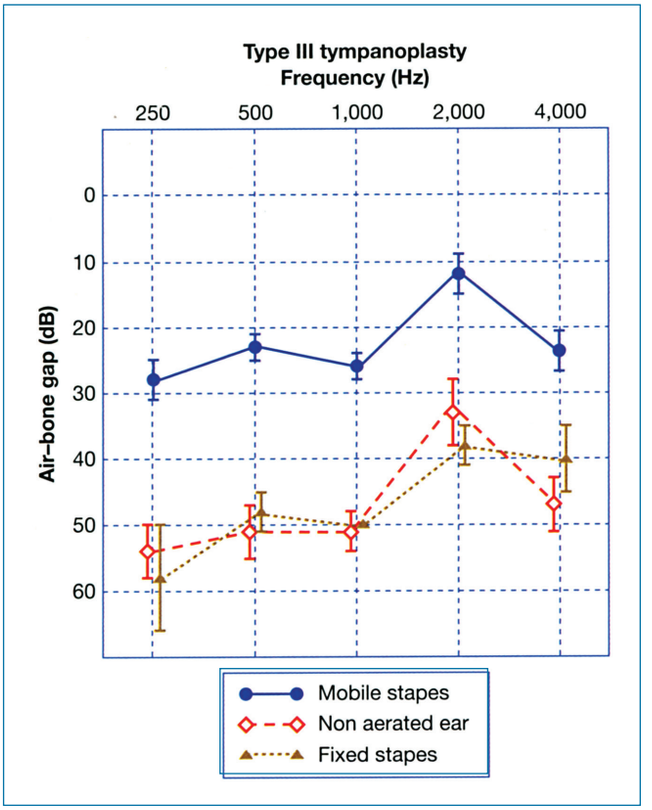

FIGURE 3–21 • Air–bone gaps (mean ± one standard error of mean) measured in 35 ears after canal-wall-down mastoidectomy and type III tympanoplasty with temporalis fascia graft onto stapes head. Results are displayed in three groups: (1) ears with a mobile stapes and an aerated middle ear after surgery, N = 23; (2) ears with a mobile stapes but no aeration of the middle ear postoperatively, N = 10; and (3) ears with an aerated middle ear postoperatively, but a fixed stapes footplate, N = 2. Mobility of the stapes was judged at time of surgery, and aeration of the middle ear was determined on the basis of postoperative CT scan assessments, pneumatic otoscopy and visible motion of the graft during a Valsalva maneuver. The best hearing results (air–bone gaps of 20 to 25 dB) are seen in those cases where the middle ear becomes aerated and the stapes is mobile. Large air–bone gaps of 40 to 60 dB occur as a result of stapes fixation, nonaeration of the middle ear or both.

A canal-wall-down procedure also results in the creation of a large air space lateral to the eardrum, ie, the air space within the mastoid bowl including the external auditory canal. This mastoid bowl and ear canal air space generates resonances which can influence middle-ear sound transmission favorably or unfavourably.[132] The structure-function relationships between the size and shape of the mastoid cavity, and cavity resonances have not been well defined. An improved understanding of this issue may help otosurgeons to configure mastoid cavities in ways that are acoustically beneficial.

Stapedotomy

The output of the middle ear can be quantified by the "volume velocity" of the stapes,[112] where volume velocity is the product of stapes linear velocity and the area of the stapes footplate. After a stapedotomy, the effective area of the footplate is reduced to the area of the prosthesis, thereby reducing the volume velocity produced by a given stapes linear velocity. The reduction in effective footplate area also reduces the area of the cochlear fluid over which the force generated by the stapes is applied. While the reduced footplate area leads to a local increase in pressure over the surface of the prosthesis, the average pressure at the cochlear entrance is reduced. The reduction in stapes volume velocity and cochlear sound pressure lead to a decrease in ossicular coupling and the development of an air–bone gap. The smaller the area of the stapes prosthesis, the greater the air–bone gap. Model predictions of the relationship between piston diameter and residual air–bone gap after stapedotomy were made using a simple lumped element model of the middle ear.[112] This analysis predicted the 0.8-mm piston diameter will produce 5 dB better hearing results than the 0.6-mm piston and 10 dB better results than the 0.4-mm piston. These predictions are in general agreement with (1) experimental temporal bone data,[133] (2) results of finite element modeling data,[134,135] and (3) clinical observations.[136–140] The predictions made in the simple lumped element model[112] assumed that the effective vibrating footplate surface area after a stapedotomy is no more than the area of the lower end of the prosthesis. In cases of partial or total stapedectomy with placement of a tissue graft and a stapes prosthesis, the effective vibrating surface may be greater than the area of the prosthesis alone, and the model predictions may overestimate the air–bone gap.

Conclusions Regarding the Contribution of Middle-Ear Mechanics to Otologic Practice

Till recently, the history of middle-ear surgery has generally progressed with minimal input from basic scientists and engineers who studied the acoustics, mechanics, and physiology of the middle ear. In this chapter, we have made a case for how knowledge of middle-ear mechanics can help the clinician to understand important aspects of present day otologic practice, and how close collaboration between clinicians and basic scientists can lead to improvements in an otologist's diagnostic and surgical capabilities. We have pointed out areas where recent work and new knowledge have produced new guidelines to optimize surgical results (eg, type III and IV tympanoplasty, stapedotomy, some aspects of ossiculoplasty), and also pointed out areas where our knowledge is incomplete and more research is needed (eg, tympanic membrane reconstruction, effect of static pressures, some aspects of ossicular reconstruction). Hopefully, some of these latter areas will be better understood by the time the next edition of this book is produced.

ACKNOWLEDGMENTS

We thank Joseph B. Nadol, Jr., MD, Michael J. McKenna, MD, Steven D. Rauch, MD, and William T. Peake, ScD, for advice and comments on previous versions of this chapter. The authors' efforts were supported by funding from the National Institute on Deafness and Other Communication Disorders of the National Institutes of Health, as well as by Mr. Axel Eliasen and Mr. Lakshmi Mittal.

References

1. Polizter A. Geschichte der Ohrenheilkunde. (2 volumes). Stuggart: F. Enke; 1907–13. (Reprinted, Hildesheim, 1967).
2. Wever EG, Lawrence M. Physiological acoustics. Princeton (NJ): Princeton University Press; 1954.
3. Leicher H, Mittermaier R, Theissing G, editors. Awanglose Abhandlungen aus dem Gebief der Hals-Nasen-Ohren-Heilkunde. Stuttgart: Georg Thieme Verlag; 1960. (English translation: A history of audiology: a comprehensive report and bibliography from the earliest beginnings to the present. Transactions of the Beltone Institute for Hearing Research, 1970.)
4. Hunt FV. Origins in acoustics: The science of sound from antiquity to the age of Newton. New Haven (CT): Yale University Press; 1978.
5. Pappas DG and Kent L. Otology's great moments. Birmingham (UK): Pappas; 2000.
6. Austin DF. Mechanics of hearing. In: Glasscock ME, Shambaugh GE, editors. Surgery of the ear. 4th ed. Philadelphia: WB Saunders; 1990. p. 297–8.
7. Helmholtz HLF. Die Mechanik der Gehörknöchelchen und des Trommelfells. Pflüg Arch ges Physiol 1868;1:1–60.
8. Yost WA. Fundamentals of hearing. New York: Academic Press; 1994.
9. Stevens SS, Davis H. Hearing. New York: Wiley; 1938.
10. Guinan JJ, Peake WT. Middle ear characteristics of anesthetized cats. J Acoust Soc Am 1967;41:1237–61.
11. Ruggero MA, Rich NC, Shivapuja BG, Temchin AN. Auditory-nerve responses to low-frequency tones: Intensity dependence. Auditory Neurosci 1996;2:159–85.
12. Sivian LJ, White SD. On minimum sound audible fields. J Acoust Soc Am 1933;4:288–321.
13. American National Standards Institute. American national standard specifications for audiometers. New York: ANSI; 1970. ANSI-S3.6-1969.
14. Shaw EAG. The external ear. In: Keidel WD, Neff WD, editors. Handbook of sensory physiology. Vol V, Part I: Auditory system. New York: Springer-Verlag; 1974. p. 455–90.
15. Dallos P. The auditory periphery. New York: Academic Press; 1973.
16. Zwislocki J. The role of the external and middle ear in sound transmission. In: Tower DB, editor. The nervous system. Vol 3: Human communication and its disorders. New York: Raven Press; 1975. p. 45–55.
17. Rosowski JJ. Models of external and middle ear function. In: Hawkins HS, McMullen TA, Popper AN, Fay RR, editors. The Springer handbook of auditory research. Vol 6: Auditory computation. New York: Springer-Verlag; 1996. p. 15–61.
18. Kirikae I. The structure and function of the middle ear. Tokyo: University of Tokyo Press; 1960.
19. Puria S, Peake WT, Rosowski JJ. Sound pressure measurements in the cochlear vestibule of human cadaver ears. J Acoust Soc Am 1997;101:2754–70.
20. Kurokawa G, Goode RL. Sound pressure gain produced by the human middle ear. Otolaryngol Head Neck Surg 1995;113:349–55.
21. Aibara R, Welsh J, Puria S, Goode R. Human middle-ear sound transfer function and cochlear input impedance. Hear Res 2001;152:100–9.
22. Tonndorf J, Khanna SM. Tympanic membrane vibrations in human cadaver ears studied by time-averaged holography. J Acoust Soc Am 1972;52:1221–33.
23. Decraemer WF, Khanna SM, Funnell WRJ. Interferometric measurement of the amplitude and phase of tympanic membrane vibrations in cat. Hear Res 1989;38:1–18.
24. Goode RL, Killion M, Nakamura K, Nishihara S. New knowledge about the function of the human middle ear: Development of an improved analog model. Am J Otol 1994;15:145–54.
25. Willi UB, Ferrazzini MA, Huber AM. The incudo-malleolar joint and sound transmission loss. Hear Res 2002;174:32–44.
26. Decraemer WF, Khanna S. Measurement, visualization and quantitative analysis of complete three-dimensional kinematical data sets of human and cat middle ear. In: K Gyo, H Wada, N Hato, T Koike,editors. Middle ear mchanics in research and otology. Singapore:World Scientific; 2004. p. 3–10.
27. Schmitt H. Über die bedeutung der Schalldrucktransformation und der Schallprotektion für die Hörschwelle. Acta Otolaryngol (Stock) 1958;49:71–80.
28. Terkildsen K. Pathologies and their effect on middle ear function. In: Feldman A, Wilber L, editors. Acoustic impedance and admittance: The measurement of middle-ear function. Baltimore: Williams & Wilkins; 1976. p. 78–102.
29. Whittemore KR, Merchant SN, Rosowski JJ. Acoustic mechanisms: Canal wall-up versus canal wall-down mastoidectomy. Otolaryngol Head, Neck Surg 1998;118:751–61.
30. Voss SE, Rosowski JJ, Merchant SN, Peake WT. Acoustic responses of the human middle ear. Hear Res 2000;150:43–69.
31. Gopen Q, Rosowski JJ, Merchant SN. Anatomy of the normal cochlear aqueduct with functional implications. Hear Res 1997;107:9–22.
32. Wever EG, Lawrence M. The acoustic pathway to the cochlea. J Acoust Soc Am 1950;22:460–7.
33. Voss SE, Rosowski JJ, Peake WT. Is the pressure difference between the oval and round windows the effective acoustic stimulus for the cochlea? J Acoust Soc Am 1996;100:1602–16.
34. Bekesy GV. Experiments in hearing. New York: McGraw Hill; 1960.
35. Wegel RL, Lane CE. The auditory masking of one pure tone by another and its probable relation to the dynamics of the inner ear. Physiol Rev 1924;23:266–85.
36. Rosen S, Bergman M, Plester D, El-Mofty A, Satti MH. Presbycusis study of a relatively noise-free population in the Sudan. Ann. Otol. Rhinol. Laryngol. 1962;71:727–43.
37. Merchant SN, Ravicz ME, Puria S, et al. Analysis of middle ear mechanics and application to diseased and reconstructed ears. Am J Otol 1997;18:139–54.
38. Merchant SN, Ravicz ME, Voss SE, Peake WT, Rosowski JJ. Toynbee Memorial Lecture 1997. Middle ear mechanics in normal, diseased and reconstructed ears. J Laryngol Otol 1998;112:715–31.
39. Peake WT, Rosowski JJ, Lynch TJ III. Middle ear transmission: Acoustic versus ossicular coupling in cat and human. Hear Res 1992;57:245–68.
40. Voss SE, Rosowski JJ, Merchant SN, Peake WT. Nonossicular signal transmission in human middle ears: Experimental assessment of the "acoustic route" with perforated tympanic membrane. J Acoust Soc Am. 2007;122:2154–73.
41. Rosowski JJ. Mechanisms of sound conduction in normal and diseased ears. In: Rosowski JJ, Merchant SN, editors. The function and mechanics of normal, diseased and reconstructed middle ears. The Hague, The Netherlands: Kugler; 2000. p. 137–45.

42. Tonndorf J. Bone conduction hearing. In: Keidel WD, Neff WD, editors. Handbook of sensory physiology. Vol V/Part III. Berlin: Springer-Verlag; 1974. p. 37–84.
43. Sohmer H, Freeman S, Geal-Dor M, Adelman C, Savion I. Bone conduction experiments in humans—A fluid pathway from bone to ear. Hear Res 2000;146:81–8.
44. Stenfelt S, Goode RL. Bone-conducted sound: Physiological and clinical aspects. Otol Neurotol 2005;26:1245–61.
45. Carhart R. The clinical application of bone conduction audiometry. Arch Otol 1950;51:798–808.
46. Carmel PW, Starr A. Acoustic and nonacoustic factors modifying middle ear muscle activity in waking cats. J. Neurophysiol 1963;26:598–616.
47. Borg E. A quantitative study of the effect of the acoustic stapedius reflex on sound transmission through the middle ear of man. Acta Otolaryngol (Stock) 1968;66:461–72.
48. Møller AR. The acoustic middle-ear muscle reflex. In: Keidel WD, Neff WD, editors. Handbook of sensory physiology: Auditory system. Vol V/Part I.Berlin: Springer-Verlag; 1974. p. 519–48.
49. Borg E, Zakrisson JE. Stapedius muscle and monaural masking. Acta Oto-Laryngol (Stockh) 1974;94:385–93.
50. Pang XD, Guinan JJ. Effects of stapedius-muscle contractions on the masking of auditory nerve responses. J Acoust Soc Am 1997;102:3576–86.
51. Borg E, Nilsson R, Engstrom B. Effect of the acoustic reflex on inner ear damage induced by industrial noise. Acta Otolaryngol (Stock) 1983;96:361–9.
52. Ingelstedt S, Jonson B. Mechanisms of gas exchange in the normal human middle ear. Acta Otolaryngol (Stock) 1966; Suppl 224: 452–61.
53. Marquet J. The incudo-malleal joint. J Laryngol Otol 1981;95:542–65.
54. Hüttenbrink KB. The mechanics of the middle-ear at static air pressures. Acta Otolaryngol (Stock) 1988; Suppl 451:1–35.
55. Pang XD, Peake WT. How do contractions of the stapedius muscle alter the acoustic properties of the middle ear? In: Allen JB, Hall JL, Hubbard A, Neely ST, Tubis A, editors. Peripheral auditory mechanisms. New York: Springer-Verlag; 1986. p. 36–43.
56. Gyo K, Aritomo H, Goode RL. Measurement of the ossicular vibration ratio in human temporal bones by use of a video measuring system. Acta Otolaryngol (Stock) 1987;103:87–95.
57. Nakajima HH, Ravicz ME, Merchant SN, Peake WT, Rosowski JJ. Experimental ossicular fixations and the middle-ear's response to sound: Evidence for a flexible ossicular chain. Hear Res 2005;204:60–77.
58. Zwislocki J. Analysis of the middle ear function. Part II. Guinea-pig ear. J Acoust Soc Amer 1963;35:1034–40.
59. Møller AR. Experimental study of the acoustic impedance of the middle ear and its transmission properties. Acta Otolaryngol (Stock) 1965;60:129–49.
60. Khanna SM, Tonndorf J. Tympanic membrane vibrations in cats studied by time-averaged holography. J Acoust Soc Am 1972;51:1904–20.
61. Nedzelnitsky V. Sound pressures in the basal turn of the cat cochlea. J Acoust Soc Am 1980;68:1676–89.
62. Nuttall AL. Tympanic muscle effects on middle-ear transfer characteristics. J Acoust Soc Am 1974;56:1239–47.
63. McArdle FE, Tonndorf J. Perforations of the tympanic membrane and their effects upon middle ear transmission. Arch Klin Exp Ohren Nasen Kehlkopfheilkd 1968;192:145–62.
64. Bigelow DC, Swanson PB, Saunders JC. The effect of tympanic membrane perforation size on umbo velocity in the rat. Laryngoscope 1996;106:71–6.
65. Wiederhold ML, Zajtchuk JT, Vap JG, Paggi RE. Hearing loss in relation to physical properties of middle ear effusions. Ann Otol Rhinol Laryngol 1980;89, Supp 68:185–89.
66. Decraemer WF, Khanna SM. Funnell WRJ. Bending of the manubrium in cat under normal sound stimulation. Prog in Biomedl Optics 1995;2329:74–84.
67. Puria S, Allen JB. Measurements and model of the cat middle ear: Evidence of tympanic membrane acoustic delay. J Acoust Soc Am 1998;104:3463–81.
68. Olson L. Observing middle and inner ear mechanics with novel intracochlear pressure sensors. J Acoust Soc Am 1998;103:3445–63.
69. Fay J, Puria S, Decraemer WF, Steele C. Three approaches for estimating the elastic modulus of the tympanic membrane. J Biomech 2005;38:1807–15.
70. Henson OW, Henson MM. The tympanic membrane: highly developed smooth muscle arrays in the annulus fibrosus of mustached bats. J Assoc Research Otolaryngol 2000;1:25–32.
71. Rosowski JJ, Carney LH, Lynch TJ, Peake WT. The effectiveness of external and middle ears in coupling acoustic power into the cochlea. In: Allen JB, Hall JL, Hubbard A, Neely ST, Tubis A,editors. Peripheral auditory mechanisms: proceedings of a conference held at Boston University, Boston, MA, August 13–16, 1985. New York: Springer-Verlag; 1986. p. 3–12.
72. Zwislocki, J. Analysis of the middle-ear function. Part I: Input impedance. J Acoust Soc Amer 1962;34:1514–23.
73. Funnell WRJ, Decraemer WM. On the incorporation of moiré shape measurements in finite-element models of the cat eardrum. J Acoust Soc Am 1996;100:925–32.
74. Gan R, Sun Q, Feng B, Wood MW. Acoustical-structural coupled finite element analysis for sound transmission in human ear pressure distributions. Med Engin Phys. 2006;28:395–404.
75. Rosowski JJ, Davis PJ, Merchant SN, Donahue KM, Coltrera MD. Cadaver middle ears as models for living ears: Comparisons of middle ear input immittance. Ann Otol Rhinol Laryngol 1990;99:403–12.
76. Goode RL, Ball G, Nishihara S, Nakamura K. Laser Doppler Vibrometer (LDV)—A new clinical tool for the otologist. Am J Otol 1996;17:813–22.
77. Chien W, Ravicz ME, Merchant SN, Rosowski JJ. The effect of methodological differences in the measurement of stapes motion in live and cadaver ears. Audiol Neurotol 2006;11:183–97.
78. Schuknecht HF. Stapedectomy. Boston: Little, Brown; 1972.
79. Nakajima HH, Ravicz ME, Rosowski JJ, Peake WT, Merchant SN. Experimental and clinical studies of malleus fixation. Laryngoscope 2005;115:147–54.
80. Schuknecht HF. Pathology of the ear. 2nd edition Philadelphia: Lea & Febiger; 1993.
81. Vincent R, Lopez A, Sperling NM. Malleus-ankylosis: A clinical, audiometric, histologic and surgical study of 123 cases. Am J Otology 1999;20:717–25.
82. Harris JP, Mehta RP, Nadol JB. Malleus fixation: Clinical and histopathologic findings. Ann Otol Rhinol Laryngol. 2002;111:246–54.
83. Kruger B, Tonndorf J. Middle ear transmission in cats with experimentally induced tympanic membrane perforations. J Acoust Soc Am 1977;61:126–32.

84. Voss SE, Rosowski JJ, Merchant SN, Peake WT. How do tympanic membrane perforations affect human middle-ear sound transmission? Acta Otolaryngol (Stockh) 2001;121:169–73.
85. Voss SE, Rosowski JJ, Merchant SN, Peake WT. Middle-ear function with tympanic membrane perforations I: Measurements and mechanisms. J Acoust Soc Am 2001;110:1432–44.
86. Voss SE, Rosowski JJ, Merchant SN, Peake WT. Middle-ear function with tympanic membrane perforations II: A simple model. J Acoust Soc Am 2001;110:1445–52.
87. Mehta RP, Rosowski JJ, Voss SE, O'Neil E, Merchant SN. Determinants of hearing loss in perforations of the tympanic membrane. Otol Neurotol 2006;27:136–43.
88. Molvaer O, Vallersnes F, Kringelbotn M. The size of the middle ear and the mastoid air cell. Acta Otolarygol (Stock) 1978;85:24–32.
89. Fria T, Cantekin E, Eichler J. Hearing acuity of children with otitis media. Arch Otolaryngol 1985;111:10–16.
90. Ravicz ME, Rosowski JJ, Merchant SN. Mechanisms of hearing loss resulting from middle ear fluid. Hear Res 2004;195: 103–1301.
91. Rosowski JJ, Songer JE, Nakajima HH, Brinsko KM, Merchant SN. Clinical, experimental and theoretical investigations of the effect of superior semicircular canal dehiscence on hearing mechanisms. Otol Neurotol 2004;25:323–32.
92. Minor LB, Solomon D, Zinreich JS, Zee DS. Sound- and/or pressure-induced vertigo due to bone dehiscence of the superior semicircular canal. Arch Otolaryngol Head Neck Surg. 1998;124:249–58.
93. Minor LB, Carey JP, Cremer PD, Lustig LR, Streubel SO, Ruckenstein MJ. Dehiscence of bone overlying the superior canal as a cause of apparent conductive hearing loss. Otol Neurotol 2003;24:270–8.
94. Halmagyi GM, Aw ST, McGarvie LA, et al. Superior semicircular canal dehiscence simulating otosclerosis. J Laryngol Otol 2003;117:553–7.
95. Mikulec AA, McKenna MJ, Ramsey MJ, et al. Superior semicircular canal dehiscence presenting as conductive hearing loss without vertigo. Otol Neurotol 2004; 25:121–29.
96. Merchant SN, Nakajima HH, Halpin C, et al. Clinical investigation and mechanism of air–bone gaps in large vestibular aqueduct syndrome. Annals Otol Rhinol Laryngol 2007;116:532–41.
97. Merchant SN, Rosowski JJ. Conductive hearing loss caused by third-window lesions of the inner ear. Otol Neurotol (in press).
98. Songer JE, Rosowski JJ. A mechano-acoustic model of the effect of superior canal dehiscence on hearing in chinchilla. J Acoust Soc Am 2007;122:943–51.
99. Chien W, Ravicz ME, Merchant SN, Rosowski JJ. Measurements of human middle- and inner-ear mechanics with dehiscence of the superior semicircular canal. Otol Neurotol 2007;28:250–57.
100. Songer JE, Rosowski JJ. The effect of superior canal dehiscence on cochlear potential in response to air-conducted stimuli in chinchilla. Hear Res 2005;210:53–62.
101. Songer JE, Rosowski JJ. The effect of superior-canal opening on middle-ear input admittance and air-conducted stapes velocity in chinchilla. J Acoust Soc Am 2006;120:258–69.
102. Rosowski JJ, Nakajima HH, Merchant SN. Clinical utility of laser-Doppler vibrometer measurements in live normal and pathologic human ears. Ear and Hearing 2008;29:3–19.
103. Lee K, Schuknecht HF. Results of tympanoplasty and mastoidectomy at the Massachusetts eye and ear infirmary. Laryngoscope 1971;81:529–43.
104. Pennington CL. Incus interposition techniques. Ann Otol 1973;82:518–31.
105. Jackson CG, Glasscock ME, Schwaber MK, Nissen AJ, Christiansen SG. Ossicular chain reconstruction: The TORP and PORP in chronic ear disease. Laryngoscope 1983;93:981–8.
106. Brackmann DE, Sheehy JL, Luxford WM. TORPS and PORPS in tympanoplasty: A review of 1042 operations. Otolaryngol Head Neck Surg 1984;92:32–7.
107. Lau T, Tos M. Long-term results of surgery for granulating otitis. Amer J Otolaryngol 1986;7:341–5.
108. Ragheb SM, Gantz BJ, McCabe BF. Hearing results after cholesteatoma surgery: The Iowa experience. Laryngoscope 1987;97:1254–63.
109. Colletti V, Fiorino FG, Sittoni V. Minisculptured ossicle grafts versus implants: Long term results. Am J Otol 1987;8: 553–59.
110. Goldenberg RA. Hydroxylapatite ossicular replacement prostheses: A four year experience. Otolaryngol-Head Neck Surg 1992;106:261–9.
111. Liston SL, Levine SC, Margolis RH, Yanz JL. Use of intraoperative auditory brainstem responses to guide prosthesis positioning. Laryngoscope 1991;101:1009–12.
112. Rosowski JJ, Merchant SN. Mechanical and acoustic analysis of middle-ear reconstruction. Am J Otol 1995;16:486–97.
113. Gyo K, Goode RL, Miller C. Effect of middle-ear modification on umbo vibration-human temporal bone experiments with a new vibration measuring system. Arch Otolaryngol Head Neck Surg 1986;112:1262–8.
114. Mach E, J Kessel. Die Function der Trommelhöhle und der Tuba Eustachii. Sitzungsber. Akad Wiss Wein math-nat Cl 1872;66:329–66.
115. Murakami S, Gyo K, Goode RL. Effect of middle ear pressure change on middle ear mechanics. Acta Otolaryngol (Stock) 1997;117:390–5.
116. Wullstein H. The restoration of the function of the middle ear, in chronic otitis media. Ann Otol Rhinol Laryngol 1956;65:1020–41.
117. Gacek RR. Symposium on tympanoplasty. Results of modified type V tympanoplasty. Laryngoscope 1973;83:437–47.
118. Rosowski JJ, Merchant SN, Ravicz ME. Middle ear mechanics of type IV and type V tympanoplasty. I. Model analysis and predictions. Am J Otol 1995;16:555–64.
119. Merchant SN, Rosowski JJ, Ravicz ME. Middle ear mechanics of type IV and type V tympanoplasty. II. Clinical analysis and surgical implications. Am J Otol 1995;16:565–75.
120. Merchant SN, Ravicz ME, Rosowski JJ. Experimental investigation of the mechanics of type IV tympanoplasty. Ann Otol Rhinol Laryngol 1997;106:49–60.
121. Montandon P, Chatelain C. Restoration of hearing with type V tympanoplasty. ORL J Otorhinolaryngol Relat Spec 1991;53:342–5.
122. Gan RZ, Dyer RK, Wood MW, Dormer KJ. Mass loading on the ossicles and middle ear function. Ann Otol Rhinol Laryngol 2001;110:478–85.
123. Bance M, Morris DP, Van Wijhe R. Effects of ossicular prosthesis mass and section of the stapes tendon on middle ear transmission. J Otolaryngol. 2007;36:113–9.
124. Vlaming MSMG, Feenstra L. Studies on the mechanics of the reconstructed human middle ear. Clin Otolaryngol 1986;11:411–22.

125. Nishihara S, Goode RL. Experimental study of the acoustic properties of incus replacement prostheses in a human temporal bone model. Am J Otol 1994;15:485–94.

126. Goode RL, Nishihara S. Experimental models of ossiculoplasty. In: Monsell E, editor. Ossiculoplasty. Otolaryngol Clin North Am 1994;27:663–75.

127. Morris DP, Bance M, van Wijhe RG, Kiefte M, Smith R. Optimum tension for partial ossicular replacement prosthesis reconstruction in the human middle ear. Laryngoscope. 2004;114:305–8.

128. Mehta RP, Ravicz ME, Rosowski JJ, Merchant SN. Middle-ear mechanics of type III tympanoplasty (stapes columella). I. Experimental studies. Otol Neurotol 2003;24:176–85.

129. Merchant SN, McKenna MJ, Mehta RP, Ravicz ME, Rosowski JJ. Middle-ear mechanics of type III tympanoplasty (stapes columella). II. Clinical studies. Otol Neurotol 2003;24:186–94.

130. Merchant SN, Rosowski JJ, McKenna MJ. Tympanoplasty: operative techniques. Otolaryngol Head Neck Surg 2003;14:224–36.

131. Toner JG, Smyth GD. Surgical treatment of cholesteatoma: a comparison of three techniques. Am J Otol. 1990;11:247–9.

132. Goode RL, Friedrichs R, Falk S. Effect on hearing thresholds of surgical modification of the external ear. Ann Otol Rhinol Laryngol 1977;86:441–51.

133. Honda N and Goode RL. The acoustic evaluation of stapedotomy using a temporal bone otosclerosis model. In Gyo K, Wada H, editors. Middle ear mechanics in research and otology. Singapore:World Scientific; 2004. p. 203–8.

134. Koike T, Wada H, Goode RL. Finite-element method analysis of transfer function of middle ear reconstructed using stapes prosthesis. In: Association for Research in Otolaryngology (ARO) Abstracts of the 24th Midwinter Meeting. Mt. Royal, (NJ): Association for Research in Otolaryngology; 2001. p. 221.

135. Bohnke F, Arnold W. Finite element model of the stapes-inner ear interface. Adv Otorhinolaryngol 2007;65:150–4.

136. Smyth GDL, Hassard TH. Eighteen years experience in stapedectomy. The case for the small fenestra operation. Ann Otol Rhinol Laryngol 1978;Suppl 49:3–36.

137. Schuknecht HF, Bentkover SH. Partial stapedectomy and piston prosthesis. In: Snow JB Jr., editor. Controversy in otolaryngology. Philadelphia: WB Saunders; 1980. p. 281–91.

138. Teig E and Lindeman HH. Stapedectomy piston diameter: is bigger better? Otorhinolaryngol Nova 1999; 9:252–6.

139. Sennaroglu L, Unal OF, Sennaroglu G, Gursel B, Belgin E. Effect of teflon piston diameter on hearing result after stapedotomy. Otolaryngol Head Neck Surg 2001;124:279–81.

140. Marchese MR, Cianfrone F, Passali GC, Paludetti G. Hearing results after stapedotomy: role of the prosthesis diameter. Audiol Neurootol 2007;12:221–5.

Auditory Physiology: Inner Ear

4

Veronika Starlinger, MD / Kinuko Masaki, PhD / Stefan Heller, PhD

INTRODUCTION

The cochlea, the mammalian auditory organ, is enclosed by the temporal bone and appears as a snail-shaped osseous structure (*cochlos* is Greek for "snail"). In humans, the cochlea is coiled for about $2^{2}/_{3}$ turns around a central axis, the modiolus. Within the bony cochlea (also known as the osseous labyrinth), three canals, or scalae, are formed by the membranous labyrinth: the central scala media, also known as the cochlear duct, is separated from the scala vestibuli by the Reissner's membrane and from the scala tympani by the basilar membrane (Figure 4–1). The connection of the scala vestibuli with the middle ear occurs via the oval window, which is attached to the stapes footplate. The round window links the scala tympani to the middle ear and is covered by the round window membrane. The scalae vestibuli and tympani merge at the cochlear apex (at the helicotrema); the scala media ends blindly. The scalae vestibuli and tympani are filled with perilymph, an extracellular fluid with high Na^+ and low K^+ concentration, whereas the scala media is filled with endolymph, which is defined by a unique ion composition of high K^+ and low Na^+ concentrations. Cochlear endolymph has a positive electrical potential of approximately +85 mV. This difference in ion composition between perilymph and endolymph and the electrical potential difference provide the energy required for the cochlea's work.

From a physiological viewpoint, three functional units within the cochlea can be distinguished: (1) The organ of Corti represents the "sensor" of the cochlea converting and amplifying mechanical sound stimuli into electrical signals (mechanoelectrical transduction). (2) The stria vascularis is the cochlea's "battery," generating the energy (endocochlear potential) necessary for mechanoelectrical transduction and influencing cochlear fluid homeostasis. (3) The spiral ganglion contains the neurons featuring axons ("electrical wires") that transport the electrical signals from the cochlea to the central nervous system. All three parts are essential for proper function of the cochlea and they will be discussed in detail in this chapter.

THE ORGAN OF CORTI

Overview

The organ of Corti is the auditory receptor organ of the mammalian cochlea. It is named after the 19th century Italian microscopist Alfonso Giacomo Gaspare Corti, who was the first to visualize and to describe this morphologically complex hearing organ.

The organ of Corti comprises two types of sensory receptors, the inner and outer hair cells. About 3,500 flask-shaped inner hair cells are lined up in a single row throughout the entire length of the human cochlear duct. Lateral to the inner hair cell row are three rows of outer hair cells that can be distinguished by their unique cylindrical shape (Figure 4–1B). Both hair cell types contain hair bundles that consist of highly organized actin-filled stereocilia that are graded in height with the most lateral row being the tallest and the most medial row being the shortest. The hair bundles of inner hair cells are organized as a smoothly curved line of two to three rows of stereocilia. Outer hair cell stereociliary bundles are arranged in a shallow V-shape (Figure 4–2). Hair bundles are the mechanosensitive organelles of hair cells. Every hair cell sits atop a phalangeal supporting cell, which for the outer hair cells are called Deiters cells. The inner and outer pillar cells delineate the area between inner and outer hair cells and frame the tunnel of Corti. Other supporting cells embrace the hair cell-bearing part of the organ of Corti. Medially, there are the inner marginal, and laterally, the Hensen's (outer marginal cells), Claudius, and Boettcher cells (Figure 4–1B). Along its entire length, the organ of Corti is covered by the tectorial membrane. This acellular structure is medially attached to the spiral limbus and connects to the hair bundles of outer hair cells.

The Basilar Membrane and Tonotopy

When sound strikes the eardrum, vibration is transmitted to the inner ear via the three middle ear ossicles. Movement of the stapes causes the displacement of the cochlear fluid in the scala

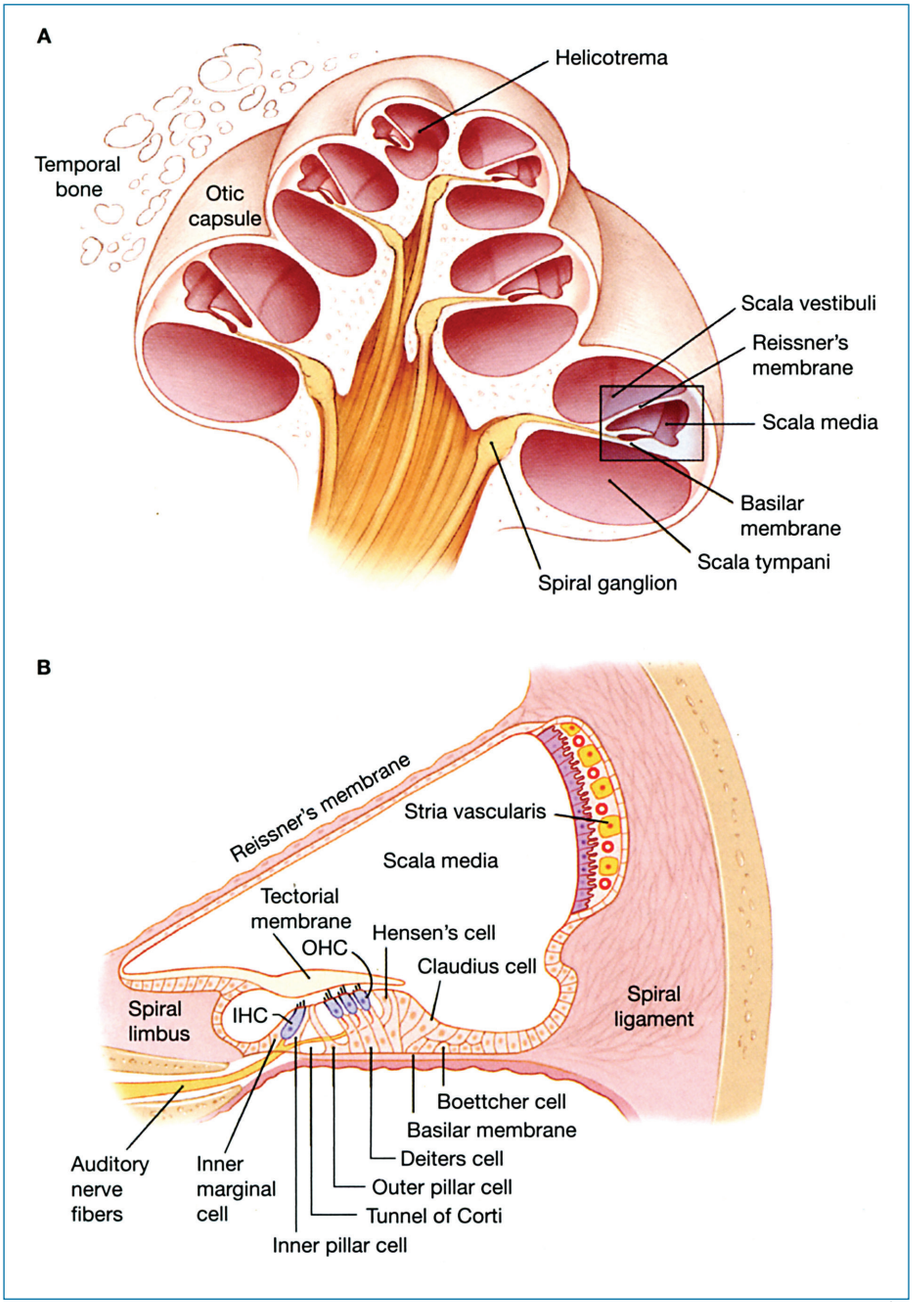

FIGURE 4–1 • Cross-section of the cochlea. *A*, schematic drawing of a cochlear cross-section. The rectangle delineates the area shown in *B*, illustrating a section of the scala media with surrounding structures such as the organ of Corti and the stria vascularis. IHC, inner hair cell; OHC, outer hair cell.

vestibuli. The incompressibility of perilymph causes a pressure gradient between the scala vestibuli and scala tympani, leading to movement of the basilar membrane and the organ of Corti. This displacement can be conceptualized as a travelling wave that moves from base to apex along the basilar membrane.[1] For a pure tone stimulus, the travelling wave reaches a maximum at a characteristic place along the basilar membrane and then decays. The precise location of this maximum depends on the frequency of the stimulus, which is the underlying principle of the tonotopic organization of the cochlea. Characteristic frequency at a specific basilar membrane location is governed by the properties of both the passive components such as extracellular, cellular, and molecular structures at that location (Figure 4–3), as well as the properties of the active system such as the cochlear amplifier (described below). The base of the cochlea is tuned for frequencies as high as 20 kHz in humans and at its apex the organ is sensitive to frequencies as low as 20 Hz. The tonotopic gradient is anatomically manifested not only in a continuous gradient in basilar membrane width but also in changes in hair cell height and the length of cellular structures such as the stereociliary hair bundles.

Inner Hair Cells and Mechanoelectrical Transduction

The cochlear inner hair cells are the linchpins in hearing as they are the sensory cells that convert mechanical stimulation into electrical signals and synaptic activity transmitted to the brain.

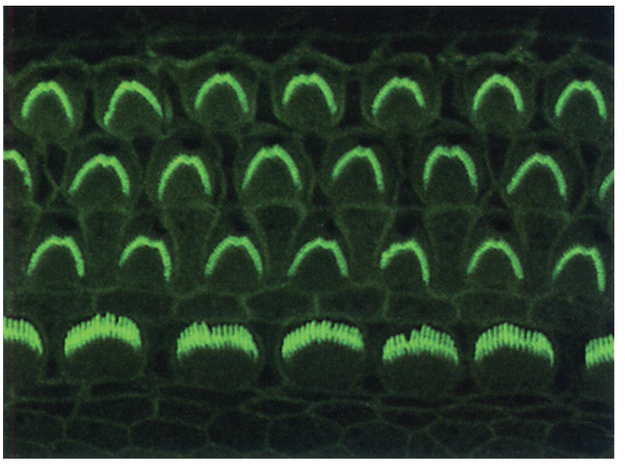

FIGURE 4–2 • Cochlear stereocilia. Shown is a view of the apical surface of a whole-mount preparation of a 150-μm long segment of the mouse organ of Corti. The stereociliary hair bundles are strongly labeled with fluorescein-conjugated phalloidin, which binds to filamentous actin. The curved hair bundles of inner hair cells are visible at the bottom as well as the three rows of V-shaped outer hair cell hair bundles at the top. *Image courtesy of Anthony W. Peng, Stanford University.*

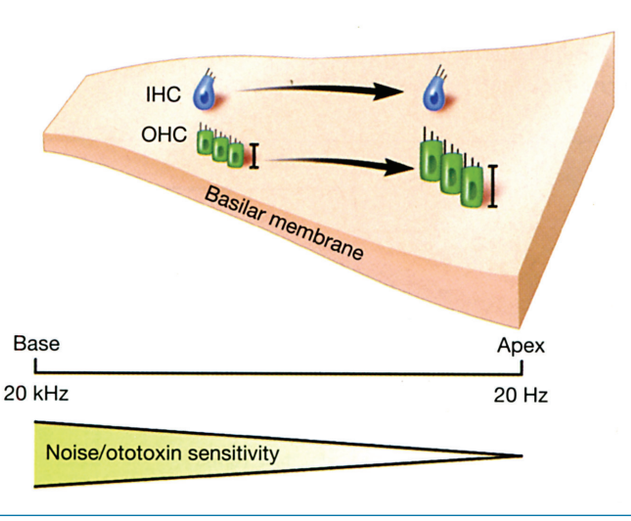

FIGURE 4–3 • Tonotopic organization of the organ of Corti. Schematic drawing of the anatomical changes along the length of the cochlea from base to apex, which include increasing width of the basilar membrane and size of the outer hair cells. These changes contribute to the frequency tuning of the organ of Corti. Likewise, sensitivity to ototoxic insults such as noise or aminoglycosides is highest at the cochlear base and decreases toward the apex.

At the core of this process is the mechanoelectrical transduction that occurs at or near the tips of the stereocilia. This mechanoelectrical transduction apparatus is present in all hair cells and consists of one or more mechanically gated cation channels, closely associated elastic structures, and a tip link that connects the tip of one stereocilium to the side of the next tallest stereocilium (Figure 4–4).[2–4]

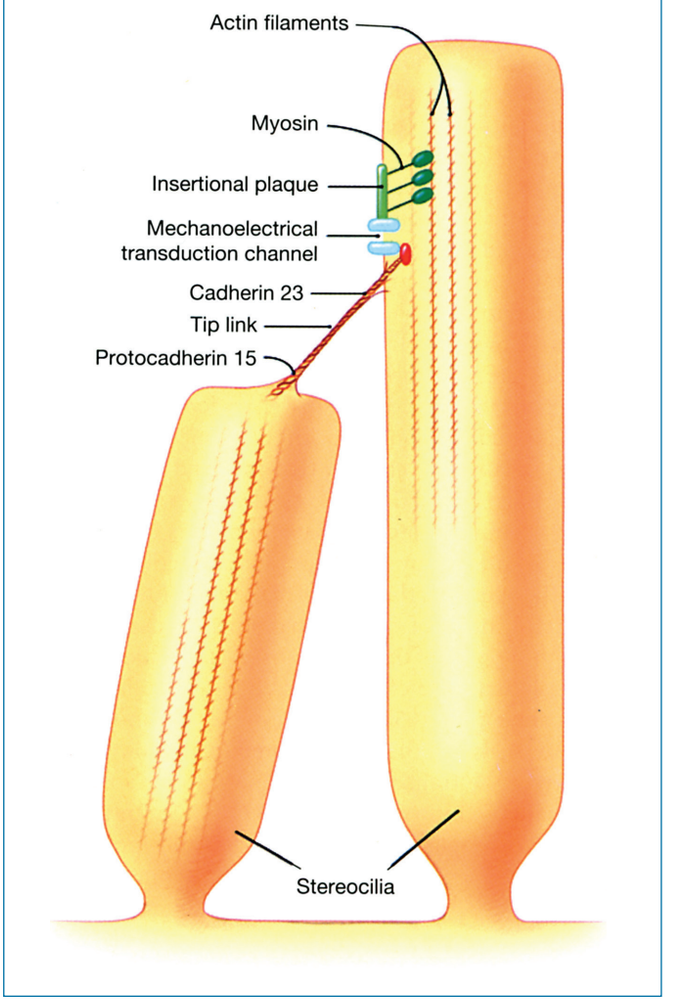

FIGURE 4–4 • Model of the stereociliary mechanoelectrical transduction apparatus. Known and proposed components of the mechanoelectrical transduction apparatus are shown.

Mechanical deflection of the hair cell's stereociliary bundle toward the tallest row of stereocilia leads to shearing motions between adjacent stereocilia.[4] The consequential increase of mechanical tension in the transduction apparatus leads to a conformational change in the transduction channel protein, leading to an increase in the channel open probability, which is about 40 to 50% at rest in the mammalian cochlea. Despite a few candidate proteins, none of the putative components of the hair cell transduction apparatus has been unequivocally linked functionally with the biophysical process of mechanotransduction. The most attractive candidates are cadherin 23 and protocadherin 15, which have been proposed as components of the tip link, and myosin 1c, which is essential for the adaptation process that controls the set point of mechanosensitivity (Figure 4–4). Mutations in the human genes encoding either cadherin 23 or protocadherin 15 cause Usher Syndrome (congenital hearing loss with progressive loss of vision from retinitis pigmentosa).

Upon mechanical stimulation toward the tallest row of stereocilia, K^+ and Ca^{2+} ions enter the hair cell through open mechanoelectrical transduction channels located near the stereociliary

tips. This excitatory deflection leads to depolarization of the cell. When the stereocilia are deflected toward the shorter stereocilia, the transduction channels close, thereby hyperpolarizing the cell. After a sustained excitatory deflection of the hair bundle, the initially large transduction current adapts, which is manifested in a decline of the current that is correlated with the closure of transduction channels (Figure 4–5A). It has been hypothesized that two distinct processes are responsible for this adaptation: rapid reclosure of transduction channels and sliding of a myosin-based motor that is associated with the transduction apparatus (Figure 4–5B and C). Rapid channel reclosure or "fast adaptation" is presumably caused by Ca^{2+} binding to a proposed intracellular site near the channel's gate. The exact underlying mechanism of this process is not yet understood. The second process, "slow adaptation," happens at about a 10 times slower time course than rapid channel reclosure and occurs when the upper insertion point of the tip link slides down the stereocilium. During a sustained stimulus, adaptation leads to a resetting of the resting point, thereby allowing the transduction apparatus to continuously operate at the point of highest sensitivity. It has been proposed that influx of Ca^{2+} through open transduction channels leads to slippage of the myosin-based adaptation motor that continuously strives to crawl toward the stereociliary tip along the actin core (Figure 4–5B). Slippage of the myosin-based motor reduces the tension in the tip link complex and lowers the open probability of the transduction channels, which in turn shuts off the local Ca^{2+} influx. At low local Ca^{2+} concentrations, the myosins of the adaptation motor will effectively move upwards, thereby readjusting the tension in the tip link complex to a point where the open probability of the transduction channels is close to the open probability at rest. Myosin 1c has been put forward as a crucial component of the adaptation motor, which does not preclude the involvement of other myosins in this process.[5]

Outer Hair Cells and Amplification

The outer hair cells play a key role in the amplification of basilar membrane motion. Amplification is necessary for the detection of sounds at low sound pressure levels. The importance of the outer hair cells was illustrated when kanamycin, an ototoxic antibiotic, was used to selectively damage outer hair cells while keeping inner hair cells intact. Outer hair cell loss resulted in elimination of the auditory nerve's low threshold sensitivity and its sharp tuning while not affecting its high threshold characteristics.[6] This observation led to the hypothesis that the outer hair cells are mainly responsible for amplification and sharp tuning of the auditory system.

One mechanism for amplification is somatic electromotility.[7] Isolated outer hair cells have been shown to change their length by 3 to 5% in response to electrical stimulation. When depolarized, outer hair cells contract, whereas they elongate when hyperpolarized. As a result, outer hair cells exert mechanical force that feeds back into movements of the basilar membrane for stimuli up to a few kHz.

Upward stimulation of the basilar membrane, eg, moves the stereocilia in an excitatory direction and depolarizes the outer hair cells, which in turn shorten, further pulling the basilar membrane upward. In this way, outer hair cell electromotility amplifies basilar membrane motion caused by the traveling wave.

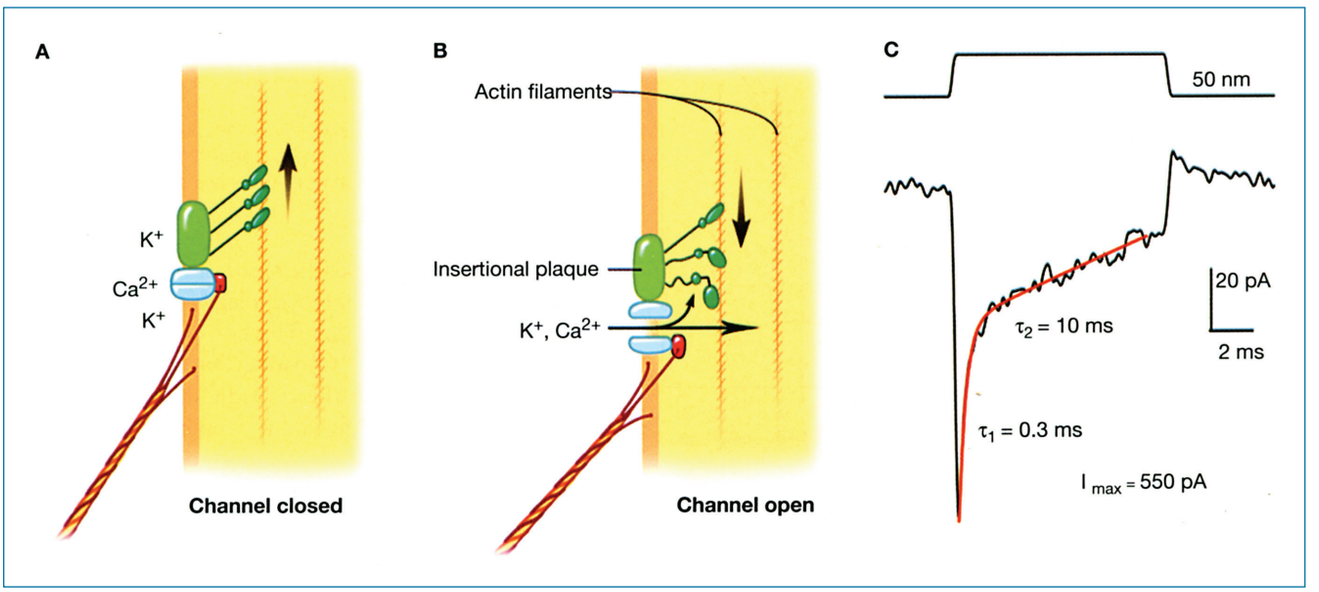

FIGURE 4–5 • Mechanoelectrical transduction. *A*, At rest, approximately 90% of the transduction channels are closed. Myosin-based molecular motors climb toward the stereociliary tips and adjust the tension in the tip link and associated structures to assure that the transduction apparatus operates at the highest sensitivity. *B*, Increased mechanical tension in the tip link and associated structures leads to opening of the transduction channels and incoming cations depolarize the cell. Local increase of the Ca^{2+} concentration affect the myosin motors and result in slippage of the transduction apparatus, thereby decreasing the mechanical tension and open probability of the transduction channels. *C*, Depolarization of a rat outer hair cell in response to a moderate mechanical deflection of 50 nm. Shown is the rapid rise of the receptor potential that is capable of reaching a maximum current of 550 pA in this specific cell, when fully stimulated. The current trace is labeled with the time courses of the fast (τ_1) and slow (τ_2) adaptation. *Data courtesy of Dr. Anthony Ricci, Stanford University.*

Prestin is thought to be the motor protein responsible for somatic electromotility in outer hair cells. Several lines of evidence support this fact.[8] First, cells transfected with prestin were found to be electromotile with magnitudes ranging up to 0.2 μm, showing that prestin is sufficient for motility. Second, prestin is located at the right place, namely in the lateral membrane of outer hair cells. And finally, mouse models with targeted deletion or modifications of prestin affect cochlear sensitivity and demonstrate that prestin is essential for outer hair cell electromotility. Prestin belongs to the SLC26 anion transporter superfamily whose members can mediate the electroneutral exchange of chloride and carbonate across the plasma membrane. The exact mechanism by which this motor works is still debated, but it is conceivable that a motor protein working on the principles of voltage displacement could operate much faster than the classical ATP-driven cellular motors.[9] A current working hypothesis suggests that intracellular anions act as voltage sensors that bind to prestin and trigger conformational changes. Hyperpolarization leads to anions binding to prestin, which causes the surface area of prestin to increase, leading to cell elongation. Depolarization, on the other hand, leads to dissociation of the anion and a decrease in the prestin surface area, leading to cell contraction. At rest, anions are usually bound to prestin; therefore, the protein assumes its longer conformation.

Another likely source of amplification is mediated by active hair bundle movements caused by interplay of mechanotransduction and adaptation. In cochleae of nonmammalian vertebrates, hair bundles are able to generate sustained oscillatory motion and similar net amplification rates as mammalian outer hair cells. Active stereocilia motion is an important amplification mechanism of nonmammalian vertebrates and it is likely that this process is also utilized for amplification or tuning in the mammalian organ of Corti, side-by-side with prestin-driven outer hair cell electromotility.

Tectorial Membrane

The tectorial membrane is an extracellular structure that overlies both the inner and outer hair cells. However, only the tallest stereocilia of the outer hair cells are directly embedded into the underside of the tectorial membrane. The tectorial membrane is attached on its inner edge to the spiral limbus and is loosely connected to the supporting cells such as the Hensen's cells by means of microscopically visible projections called trabeculae. The importance of the tectorial membrane is illustrated by the fact that mutations of tectorial membrane genes such as alpha- and beta-tectorin cause profound hearing loss both in humans and animal models.[10]

Based on anatomic observations, it was initially suggested that the tectorial membrane acts as a simple lever, shearing the hair bundles as the basilar membrane moves up and down. Other cochlear models treated it either as a simple mechanical load or as a resonant system consisting of a mass and spring. Recent findings suggest that the tectorial membrane is more like a resonant gel and is involved in enhancing the frequency selectivity of the cochlea. It is likely that all proposed functions of the tectorial membrane are relevant and because, like most structures in the organ of Corti, it changes its size from base to apex, the tectorial membrane may also contribute to the overall tonotopic organization of the cochlea.

THE STRIA VASCULARIS

Overview

The stria vascularis plays a pivotal role in cochlear homeostasis by generating the endocochlear potential and maintaining the unique ion composition of the endolymph.

The stria vascularis is a highly vascularized, multilayered tissue that is part of the lateral wall of the scala media (Figure 4–1 and 4–6). It is comprised of three distinct cell types: marginal,

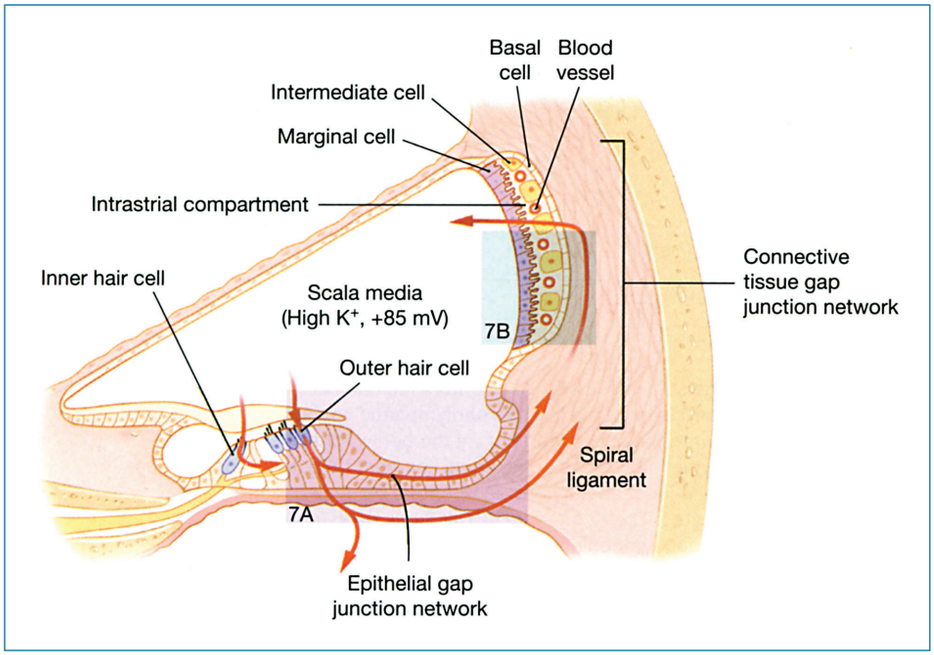

FIGURE 4–6 • Stria vascularis and K^+ circulation. Schematic drawing showing the flow of K^+ from the scala media through hair cells into the perilymphatic spaces as well as through the epithelial gap junction network into the spiral ligament. K^+ from the spiral ligament is transported via the stria vascularis into the scala media. Not shown are other pathways for K^+ out of the scala media, eg through outer sulcus cells and Reissner's membrane. The rectangles outline the areas shown in more detail in Figure 4–7.

intermediate, and basal cells, all of which are essential for its proper function. Tight junctions provide the ionic barriers that demarcate the strial tissue, one at the level of the marginal cells and the other at the level of the basal cells. The extracellular space in between these two barriers is called the intrastrial compartment.[11] As shown in Figure 4–7B, the marginal cells separate the endolymph-filled scala media from the intrastrial compartment that is filled with the intrastrial fluid, whereas the basal cells separate the intrastrial space from the perilymph that surrounds the fibrocytes of the spiral ligament. Intermediate cells as well as blood vessels are embedded in the intrastrial compartment. Gap junctions connect the basal cells with intermediate cells and with the fibrocytes of the spiral ligament, allowing electric coupling as well as exchange of ions and small molecules.[11,12] The regulation of cochlear fluid homeostasis also involves the endolymphatic sac, which responds to endolymph volume disturbances and probably disturbs homeostasis when it malfunctions.[13]

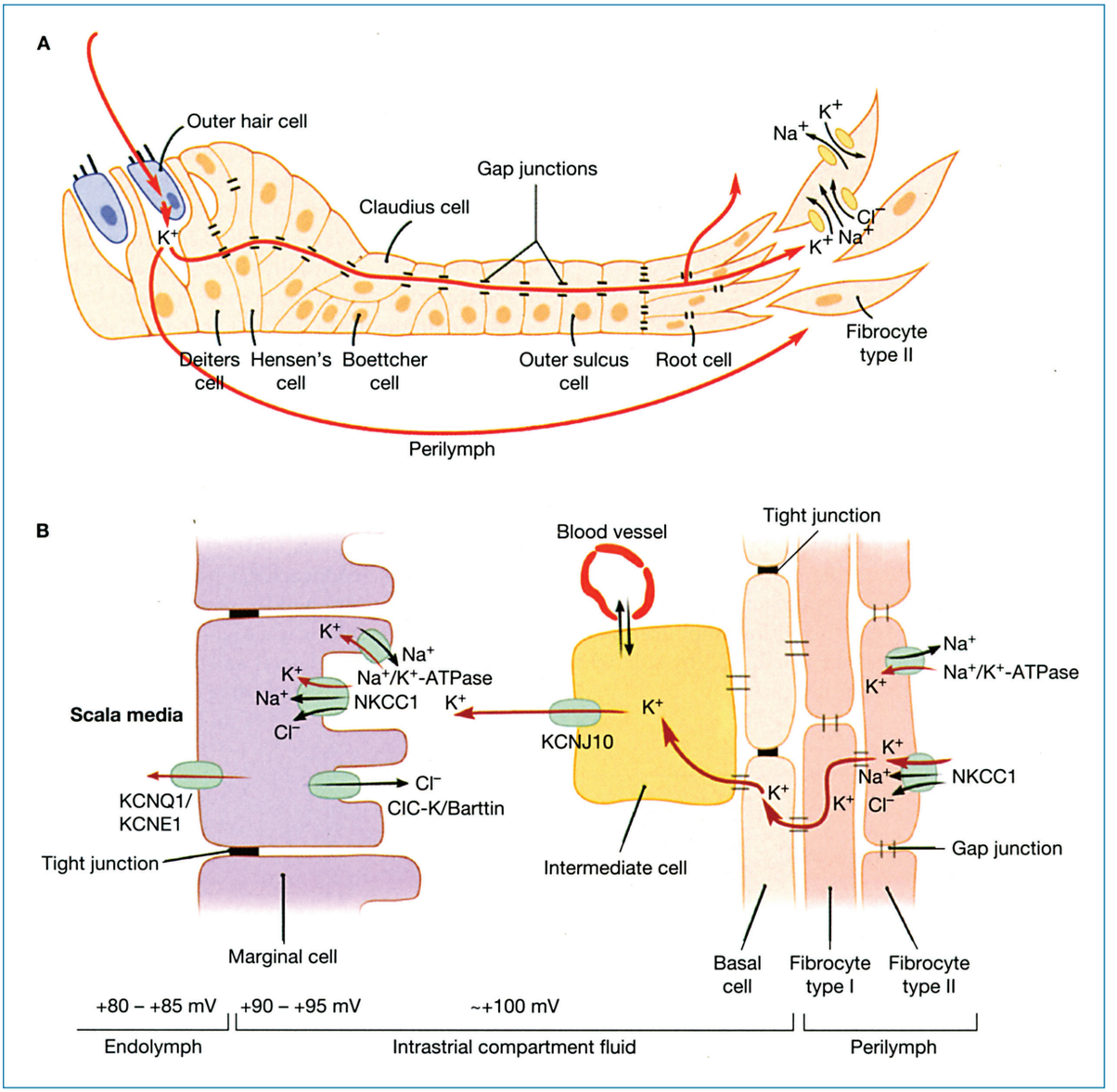

FIGURE 4–7 • K^+ flow through the organ of Corti and the stria vascularis. *A*, K^+ enters the hair cell via the mechanotransduction channels. On its basolateral side K^+ is released into the perilymphatic space via K^+ channels such as the KCNQ4 channel. K^+ can travel toward the spiral ligament via the perilymphatic space and, intracellularly, via the epithelial gap junction network. Type II fibrocytes in the spiral ligament take up K^+ and provide a path to the stria vascularis via the connective tissue gap junction network. *B*, K^+ enters basal and intermediate cells through gap junctions with type I and type II fibrocytes. The K^+ channel KCNJ10 has been identified as important for releasing K^+ into the intrastrial space. The gene encoding KCNJ10 is consequently essential for proper generation of the endocochlear potential. K^+ is efficiently removed from the intrastrial space by marginal cells, which actively take up K^+ via NKCC1 ($Na^+/K^+/ 2Cl^-$) cotransporters and by Na^+/K^+-ATPases. Finally, marginal cells secrete K^+ into the scala media via the KCNQ1/KCNE1 K^+ channel maintaining the high K^+ concentration of the endolymph essential for mechanoelectrical transduction.

Malfunctions in cochlear fluid homeostasis due to disruptions of the endocochlear potential, ionic composition, or its volume regulating mechanisms lead to various forms of hearing impairment in humans and animals.[11,12,14]

Endocochlear Potential and Potassium Homeostasis

Hair cell mechanoelectrical transduction works efficiently due to the large driving force for cations to enter the cell's cytoplasm from the scala media. The ≈ +85 mV endocochlear potential of the endolymph and the chemical K^+ gradient are the principal components of this driving force, which reaches about 130 mV when the hair cell's resting potential of –45 mV is taken into account.[4] Hearing threshold increases approximately 1 dB per mV loss of endocochlear potential.

K^+, the main cation of the endolymph, carries the majority of the electrical charge that generates the endocochlear potential. It is therefore important to understand how K^+ moves through the cochlea. K^+ can enter hair cells through mechanoelectrical transduction channels and it is released through the hair cells' basolateral membranes into the perilymphatic extracellular space (Figures 4–6 and 4–7A). It has been proposed that K^+ can enter supporting cells and move toward the spiral ligament by an extensive gap junction network. Alternatively, K^+ can diffuse extracellularly via the perilymphatic space. Spiral ligament type II and type I fibrocytes take up K^+ and provide an intracellular pathway into the basal and intermediate cells of the stria vascularis (Figures 4–6 and 4–7B). K^+ is released by intermediate cells via KCNJ10 channels into the intrastrial space from which it is actively pumped and cotransported into marginal cells. The marginal cells release K^+ into the scala media.[11,12] The overall K^+ circulation is probably not a true recycling as the perilymphatic and intrastrial spaces do not form an enclosed loop because these compartments are connected to other extracellular spaces as well as to the blood supply.

Malfunctions in several K^+ channels lead to perturbation of cochlear K^+ homeostasis, resulting in hearing impairment (Table 4–1). In mice, loss of the *KCNE1* gene that encodes a K^+ channel subunit expressed by marginal cells causes a phenotype highly similar to human Jervell and Lange–Nielsen syndrome, which is characterized by hearing loss and cardiac arrhythmia. This observation led to the identification of two human genes, *KCNE1* and *KCNQ1*, which both cause Jervell and Lange–Nielsen syndrome when mutated. It is conceivable that KCNQ1 and KCNE1 form the channel that allows secretion of K^+ from marginal cells into the scala media. Another member of the KCNQ family of potassium channels, KCNQ4, is likely involved in basolateral K^+ secretion by hair cells. Mutations in the human *KCNQ4* gene cause nonsyndromic deafness. Other known genetic dysfunctions involve ion transport proteins localized in the basolateral membrane of marginal cells (see below and Table 4–1). Probably the most well-known genes involved in cochlear K^+ homeostasis are the ones that encode connexin proteins. Connexins form the subunits of gap junction channels, which underlie the K^+ circulation networks described for the supporting cells of the organ of Corti, the spiral ligament, and stria vascularis. Mutations in genes encoding human connexins 26, 30, 31, and 43 are responsible for the majority of nonsyndromic hereditary hearing loss.[14]

Cochlear Fluid Homeostasis

Perilymph, endolymph, and intrastrial fluid are the three distinguishable fluids in the cochlea and can be seen as its metabolic support system. The proper ionic composition of these fluids is essential for generation and maintenance of the endocochlear potential. Perilymph and intrastrial fluid are characterized by a high Na^+ concentration and a low K^+ concentration, similar to other extracellular fluids. Endolymph not only has high K^+ and low Na^+ concentrations but also features an unusually low Ca^{2+} concentration compared to other extracellular fluids (Table 4–2).[15] Ca^{2+} ion homeostasis in the cochlea is controlled by ion channels and transporters located in the plasma membranes of its cells, as previously described for K^+.

In the stria vascularis, influx of Na^+ ions accompanies that of K^+ ions from the intrastrial compartment into the marginal cells. The cotransporter NKCC1 makes use of the strong Na^+ gradient to bring Na^+, K^+, and 2 Cl^- ions into the marginal cells. Na^+/K^+-ATPase is responsible for setting up this gradient by pumping Na^+ into the intrastrial space in exchange for K^+. Finally, K^+ leaves marginal cells into the endolymphatic space, driven by the high positive resting potential of marginal cells (Figure 4–7, B). This intricate process maintains a high Na^+ and low K^+ concentration of the intrastrial fluid that facilitates K^+ replenishment into the intrastrial space. Cl^- is transported back to the intrastrial space by ClC-K/Barttin channels. Inhibition of NKCC1 and the Na^+/K^+-ATPase by the loop diuretic furosemide and ouabain, respectively, leads to suppression of the endocochlear potential. Mutations of the Barttin gene, or the mutation of both the ClC-Ka and ClC-Kb subunits of the basolateral Cl^- channels, lead to Bartter's syndrome type 4, characterized by deafness and renal salt wasting (Table 4–1). Na^+ is reabsorbed from the endolymph by outer sulcus and Reissner's membrane cells, which play a role in maintaining the low Na^+ concentration in the scala media.[11,14]

Regulation of endolymphatic Ca^{2+} concentration is also of great importance. Hair cell physiology has revealed that tip links break at very low Ca^{2+} concentrations and that the mechanoelectrical transduction channels are blocked at high Ca^{2+} concentrations.[16,17] Furthermore, Ca^{2+} carries part of the transduction current and plays critical roles in adaptation and possibly in cochlear amplification.[18] Ca^{2+}-permeable channels, Ca^{2+}-ATPases, as well as Na^+/Ca^{2+}-exchangers are found in many cochlear cell types and could be involved in regulating Ca^{2+} efflux from and influx into the endolymph, but specific mechanisms have not been elucidated.

Cochlear fluid volume regulation is equally important for cochlear function and different mechanisms have been postulated.[13,19] Previously, longitudinal and radial flow patterns have been proposed as the underlying principle. Longitudinal flow of endolymph is described as its secretion along the membranous labyrinth with reabsorption in the endolymphatic duct and sac, whereas radial flow is based on local secretion and reabsorption, eg, via the stria vascularis. Under pathological conditions such as an increase or decrease of endolymph volume, longitudinal flow may be relevant. Experimental enlargement of

TABLE 4–1 Genes that alter cochlear K homeostasis when mutated

GENE	ENCODED PROTEIN	PROTEIN LOCALIZATION	PROTEIN FUNCTION	DISEASE
KCNE1	KCNE1	Marginal cells	K^+ channel	Jervell/Lange–Nielsen syndrome
KCNQ1	KCNQ1	Marginal cells	K^+ channel	Jervell/Lange–Nielsen syndrome
KCNQ4	KCNQ4	Outer and inner hair cells	K^+ channel	DFNA2
GJB2	Cx26	Fibrocytes in SL and SLi, epithelia on BM, intermediate and basal cells	Gap junction protein	DFNB1/DFNA3 Hereditary palmoplantar keratoderma with deafness
GJB6	Cx30	Fibrocytes in SL and SLi, supporting cells of the OoC	Gap junction protein	DFNA3
GJB3	Cx31	Fibrocytes in SL and SLi, epithelia on BM	Gap junction protein	DFNA2, AR-nonsyndromic deafness
GJB1	Cx32	Fibrocytes in SL and SLi, epithelia on BM	Gap junction protein	X-linked Charcot-Marie-Tooth and deafness
GJA1	Cx43	Fibrocytes in SL and SLi, epithelia on BM, intermediate and basal cells	Gap junction protein	AR-nonsyndromic deafness
BSND	Barttin	Marginal cells	Cl^- channel	Type 4 Bartter's syndrome

SL, spiral ligament; Sli, spiral limbus; BM, basilar membrane; OoC, Organ of Corti.

TABLE 4–2 Ionic composition of the endo- and perilymph

	COCHLEAR PERILYMPH (mM)	COCHLEAR ENDOLYMPH (mM)
Na^+	148	1.3
K^+	4.2	157
Cl^-	119	132
HCO_3^-	21	31
Ca^{2+}	1.3	0.023
pH	7.3	7.5

Adapted from Lang et al.[15]

the endolymph compartment was found to produce a longitudinal flow toward the base of the cochlea into the endolymphatic sac, decreasing both the volume of fluid and concentration of electrolytes within the cochlear duct. On the other hand, experimental decrease in endolymph compartment volume led to an apically directed flow, increasing fluid volume and electrolyte concentration. The radial flow theory has never been experimentally proven. Today, the prevailing thought is that there is no significant volume flow under physiological conditions. Experiments in animals have shown that markers iontophoresed into the endolymph without volume disturbance move solely by diffusion. The ions in the endolymph, therefore, turn over locally without concomitant volume flow. Similar regulatory mechanisms have been proposed for perilymph homeostasis. A low volume flow inside the cochlea has consequences for intracochlear drug applications where, under physiological conditions, diffusion of compounds inside the fluid-filled compartments appears to limit the equal dosing of potential drugs from base to apex.

On a cellular level, transmembraneous water movement largely depends on pore-like water-permeable channels such as aquaporins. Several aquaporins are found in the inner ear with only a few localized within the endolymph lining epithelium.[20] Lack of aquaporin 4 in mice results in hearing impairment. Other aquaporin knock-out mice either show no inner ear phenotype, are not available to date, or are embryonically lethal, such as aquaporin 2 knock-out mice. Nevertheless, aquaporin 2 is interesting as it is found in the endolymph-lining epithelium of the endolymphatic sac and is regulated by the hormone vasopressin. Animal models have shown that pathologically increased levels of vasopressin lead to a prominent endolymphatic hydrops, a morphological characteristic of Ménière's disease. Besides its potential relevance to the pathogenesis of Ménière's disease, this finding suggests a hormonal influence on inner ear volume regulation.[21] For example, vasopressin has not only been shown to influence the membrane expression of aquaporin 2 but also to increase the activity of epithelial Na^+ channels and the NKCC1 cotransporter found in strial marginal cells and type II fibrocytes of the spiral ligament.

Modulation of these channels could lead to increased K^+ secretion into the endolymph and consequently an osmotic volume movement, resulting in typical hydrops. Similar findings have been reported for another hormone, aldosterone, which increases activity of both epithelial Na^+ channels and Na^+/K^+-ATPase.[22] However, other hormones have an effect opposite to that of vasopression. Glucocorticoids, eg, have been shown to suppress the symptoms of Ménière's possibly due to a decrease of vasopressin production and modulation of the membrane expression of certain aquaporins.[23]

Cochlear fluid homeostasis, ion transport, and endocochlear potential are all required for proper cochlear function. Metabolic blockade or specific inhibitors of ion transport such as ouabain and furosemide rapidly affect this microenvironment and interfere with auditory function by disturbing the cochlea's battery, the endocochlear potential. It has been hypothesized that aging affects long-term maintenance of the endocochlear potential and that lowered metabolic rates of the stria vascularis could play a role in age-related hearing loss.

THE SPIRAL GANGLION

Overview

The spiral ganglion is located in Rosenthal's canal within the modiolus of the cochlea. It contains the cell bodies of afferent neurons, the dendrites of which are excited by neurotransmitters released by organ of Corti hair cells and the axons of which project centrally into the cochlear nucleus located in the brain stem. The majority (approximately 95%) of the afferent fibers are thick and myelinated and originate from type I ganglion neurons (Figure 4–8). These fibers exclusively innervate inner hair cells. The remaining afferent fibers are thin, unmyelinated, and emanate from type II ganglion neurons; these fibers contact outer hair cells. About a dozen type I ganglion neurons innervate each inner hair (converging innervation pattern), whereas the type II afferent nerve fibers divide into multiple branches and contact multiple outer hair cells (diverging innervation pattern). All auditory information is carried to the brain stem by the afferent system. The auditory and the vestibular nerves join each other to form the eighth cranial nerve (the vestibulocochlear nerve).

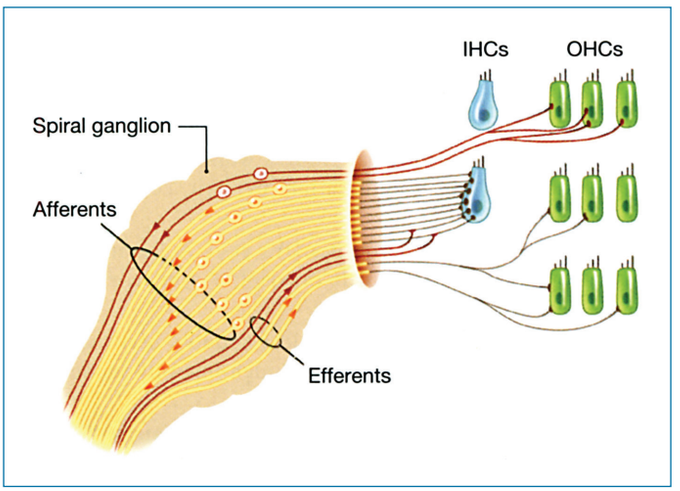

FIGURE 4–8 • Innervation of the organ of Corti. Schematic drawing of afferent and efferent innervation of inner and outer hair cells. Shown from top to bottom are unmyelinated type II afferent and myelinated type I afferent fibers, unmyelinated LOC efferent fibers, and myelinated MOC efferent fibers.

Efferent fibers originate in the brain stem from neurons located in the superior olivary complex and send information to the cochlea by synapsing with outer hair cells as well as with afferent fibers beneath inner hair cells. The efferent system allows the central nervous system to modulate the operation of the cochlea.[24]

The innervation pattern of the organ of Corti clearly underlines the functional differences of the two types of cochlear hair cells.

Neural Processing of Auditory Information and Inner Hair Cell Synapses

Afferent neurotransmitter release by inner hair cells is initiated at their 5 to 30 ribbon-type synapses where local influx of Ca^{2+} through voltage-gated Ca^{2+} channels leads to finely graded fusion of synaptic vesicles at presynaptic sites. The resulting exocytosis of neurotransmitters is, therefore, directly proportional to the presynaptic Ca^{2+} current, which in turn is dependent on voltage changes driven by mechanotransduction. Information coding at the afferent synapse is remarkably accurately, allowing high temporal precision as well as a considerable dynamic range of five orders of magnitude ranging from 0 dB to more than 100 dB.

Each ribbon synapse is composed of a presynaptic dense body (equivalent to the synaptic ribbon of photoreceptor cells) that is surrounded by vesicles containing neurotransmitters, a thickening of the underlying plasma membrane, a synaptic cleft, and the postsynaptic region containing the AMPA-type glutaminergic receptors of the afferent neurons. Glutamate, or a closely related compound, is thought to be the neurotransmitter of the inner hair cell afferents even though other yet unidentified transmitters may also be involved.

The tonotopic organization of the organ of Corti is maintained within the afferent system, where depolarization of inner hair cells at a specific location leads to the excitation of connected afferent spiral ganglion neurons. Each afferent fiber is characterized by a specific tuning curve (Figure 4–9), which describes the sound pressure level of the stimulus needed to elicit a response at a given frequency. An apparent feature of tuning curves is that they show the frequency at which the nerve fiber displays highest sensitivity, its characteristic frequency. Stimuli at higher or lower frequencies relative to the characteristic frequency can also evoke a response but only if presented at higher intensities. The sharpness and thresholds of afferent nerve fiber tuning curves depend on many factors including organ of Corti morphology and active processes associated with cochlear amplification. The activity of the efferent system plays an important role in modulating the afferent nerve characteristics (Figure 4–9). Loss of cochlear amplification, eg, as a result of outer hair cell loss, leads to a broadening of the tuning curve and an increase in the fibers' response thresholds.

The tonotopic organization of the cochlea is the basis for frequency coding in auditory nerve fibers (place coding).

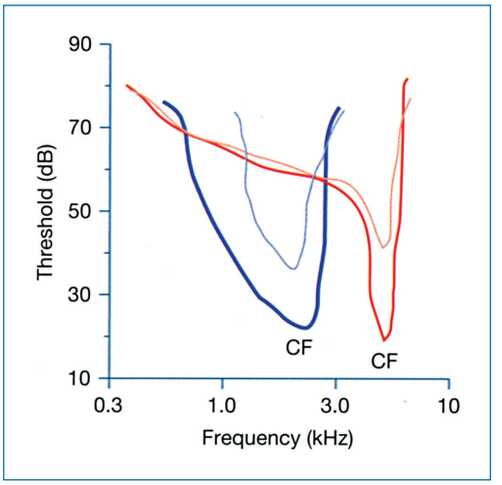

FIGURE 4–9 • Typical tuning curves of auditory nerve fibers. (Thick lines) Tuning curves of auditory nerve fibers with characteristic frequencies of ≈ 2 kHz (blue) and ≈ 5 kHz (red). (Thin lines) Substantial decrease of the auditory threshold in response to stimulation of the MOC system. Changes in the specific shapes of tuning curves depend on the characteristic frequencies (CF) of the individual fibers. *Adapted from Guinan.*[24]

Additionally, frequency is coded by the auditory nerve fibers' discharge characteristics known as phase locking. Here, an auditory nerve fiber fires at a particular phase of the stimulating frequency, which leads to a regular response pattern characterized by spacing of the nerve spikes in equals or multiples of the stimulus wavelength. Phase locking only happens at low frequencies. Above 5 kHz, spike responses of auditory nerve fibers occur at random intervals. Tonotopic organization and phase locking are both important for frequency discrimination. Discharge rates within the auditory nerve fibers are not only determined by the frequency but also by the intensity of the stimulus. As intensity increases, the discharge rate within a single auditory nerve fiber increases. Likewise, the number of auditory nerve fibers activated at a given characteristic frequency increases with intensifying stimuli. This recruitment of more fibers is due to the fact that auditory nerve fibers of the same characteristic frequency have different response thresholds. Furthermore, with increasing stimulus intensity, other afferent nerve fibers of nearby characteristic frequencies are also activated. These physiologically relevant features set some of the complex rules for cochlear implant design and application.

In summary, the frequency-dependent stimulation of cochlear hair cells leads to an increase in inner hair cell synaptic transmission at ribbon synapses. The ensuing excitatory postsynaptic currents in afferent nerve fibers lead to a timed discharge of action potentials in the auditory nerve. The acuity, temporal resolution, and dynamic range of the auditory system is unmatched by any other sensory system.

Efferent Innervation of the Cochlea

Two clearly distinguishable groups of efferent fibers originate in the brain stem.[24] First, myelinated medial olivocochlear (MOC) efferents arise from neurons located around the medial superior olivary nucleus. The MOC efferents project to the contralateral and ipsilateral cochleae, where they form cholinergic synapses with outer hair cells. The second group of fibers are the unmyelinated lateral olivocochlear (LOC) efferents that originate from neurons with small somata located in and around the lateral superior olivary nucleus. The LOC fibers project predominantly to the ipsilateral cochlea where they terminate on the dendrites of afferent type I neurons beneath inner hair cells. LOC efferent synapses are neurochemically complex and utilize cholinergic, GABAergic, and dopaminergic transmission as well as various neuropeptides.

The effects of stimulation of MOC fibers have been studied much more extensively than LOC fiber stimulation. In general, stimulation of the MOC system leads to increased thresholds, which is due to a decrease in the degree of cochlear amplification by outer hair cells (Figure 4–9). This sound-evoked feedback, therefore, decreases sensitivity of the hearing apparatus in situations when the metabolically expensive amplification mechanisms are not needed.

The function of the LOC efferent neurons appears to be more complex. Their direct input on the afferent neurons suggests that they regulate afferent activity, thereby affecting the dynamic range. Lesion studies support this view, where loss of specific neurotransmitters or destruction of cell bodies in the brainstem leads to either enhancement or suppression of auditory nerve response. These LOC feedback effects are slow and usually require minutes to become effective. An additional function of the LOC system is to perform slow integration and adjustment of binaural inputs needed for accurate binaural function and sound localization.[25]

Finally, activity of the MOC and the LOC efferent systems seem to have protective effects against acoustic injury and such a feedback could be important in loud noise environments.[26]

References

1. Raphael Y, Altschuler RA. Structure and innervation of the cochlea. Brain Res Bull 2003;60:397–422.
2. Pickles JO, Comis SD, Osborne MP. Cross-links between stereocilia in the guinea pig organ of Corti, and their possible relation to sensory transduction. Hear Res 1984;15:103–12.
3. Hudspeth AJ, Gillespie PG. Pulling springs to tune transduction: Adaptation by hair cells. Neuron 1994;12:1–9.
4. Hudspeth AJ. How the ear's works work: Mechanoelectrical transduction and amplification by hair cells. C R Biol 2005;328:155–62.
5. Holt JR, Gillespie SK, Provance DW, et al. A chemical-genetic strategy implicates myosin-1c in adaptation by hair cells. Cell 2002;108:371–81.
6. Kiang NY, Liberman MC, Levine RA. Auditory-nerve activity in cats exposed to ototoxic drugs and high-intensity sounds. Ann Otol Rhinol Laryngol 1976;85:752–68.
7. Brownell WE, Bader CR, Bertrand D, de Ribaupierre Y. Evoked mechanical responses of isolated cochlear outer hair cells. Science 1985;227:194–6.
8. Zheng J, Shen W, He DZ, Long KB, Madison LD, Dallos P. Prestin is the motor protein of cochlear outer hair cells. Nature 2000;405:149–55.
9. Ashmore J. Cochlear outer hair cell motility. Physiol Rev 2008;88:173–210.

10. Legan PK, Lukashkina VA, Goodyear RJ, Kossi M, Russell IJ, Richardson GP. A targeted deletion in alpha-tectorin reveals that the tectorial membrane is required for the gain and timing of cochlear feedback. Neuron 2000;28:273–85.
11. Wangemann P. Supporting sensory transduction: Cochlear fluid homeostasis and the endocochlear potential. J Physiol 2006;576:11–21.
12. Hibino H, Kurachi Y. Molecular and physiological bases of the K+ circulation in the mammalian inner ear. Physiol (Bethesda) 2006;21:336–45.
13. Salt AN. Regulation of endolymphatic fluid volume. Ann N Y Acad Sci 2001;942:306–12.
14. Heller S. Application of physiological genomics to the study of hearing disorders. J Physiol 2002;543:3–12.
15. Lang F, Vallon V, Knipper M, Wangemann P. Functional significance of channels and transporters expressed in the inner ear and kidney. Am J Physiol Cell Physiol 2007;293:C1187–208.
16. Assad JA, Shepherd GM, Corey DP. Tip-link integrity and mechanical transduction in vertebrate hair cells. Neuron 1991;7:985–94.
17. Farris HE, LeBlanc CL, Goswami J, Ricci AJ. Probing the pore of the auditory hair cell mechanotransducer channel in turtle. J Physiol 2004;558:769–92.
18. Mammano F, Bortolozzi M, Ortolano S, Anselmi F. Ca^{2+} signaling in the inner ear. Physiol (Bethesda) 2007;22:131–44.
19. Salt AN. Dynamics of inner ear fluids. In: Jahn AF, Santos-Sacchi J, editors. Physiology of the ear. 2nd ed. San Diego, CA: Singular Thompson Learning; 2001. p. 333–55.
20. Beitz E, Zenner HP, Schultz JE. Aquaporin-mediated fluid regulation in the inner ear. Cell Mol Neurobiol 2003;23:315–29.
21. Al-Mana D, Ceranic B, Djahanbakhch O, Luxon LM. Hormones and the auditory system: A review of physiology and pathophysiology. Neuroscience 2008;153:881–900.
22. Dunnebier EA, Segenhout JM, Wit HP, Albers FW. Two-phase endolymphatic hydrops: A new dynamic guinea pig model. Acta Otolaryngol 1997;117:13–9.
23. Fukushima M, Kitahara T, Uno Y, Fuse Y, Doi K, Kubo T. Effects of intratympanic injection of steroids on changes in rat inner ear aquaporin expression. Acta Otolaryngol 2002;122:600–6.
24. Guinan JJ. Physiology of olivocochlear efferents. In: Dallos P, Fay RR, Popper AN, editors. The cochlea. Springer handbook of auditory research. New-York: Springer; 1996. p. 435–502.
25. Darrow KN, Maison SF, Liberman MC. Cochlear efferent feedback balances interaural sensitivity. Nat Neurosci 2006;9:1474–6.
26. Maison SF, Luebke AE, Liberman MC, Zuo J. Efferent protection from acoustic injury is mediated via alpha 9 nicotinic acetylcholine receptors on outer hair cells. J Neurosci 2002;22:10838–46.

Neurophysiology: The Central Auditory System

5

Bradford J. May, PhD / Charles Limb, MD

Sounds are events inhabiting multidimensional space. The identity of each event is mapped by a listener in perceptual coordinates that include pitch, loudness, location, and time. The listener chooses to ignore or attend to the sound by weighing the biological context in which it occurs, where it originates, and what it means. Although this critical information is extracted in an instant without conscious effort, the act of listening requires the simultaneous analysis of multiple acoustic dimensions, and their interactions upon each other. Further increasing the demands of the listening task, the resulting auditory object must maintain a stable identity as it moves within the perceptual coordinate system, for example, by changing pitch or location. Natural auditory events rarely propagate under ideal listening conditions and therefore they also must be separated from environmental effects that are capable of distorting the original waveform with reflection or reverberation. Sounds seldom occur in isolation and therefore must be separated from competing stimuli that may mask or confuse the signal. This chapter will describe how neurons in the central nervous system are endowed with specialized sensitivities to meet the many challenges of auditory information processing and how this exquisitely tuned circuitry may break down after exposure to loud sounds, ototoxic agents, trauma, or the aging process.

A defining feature of the central auditory system is the elaborate neural network that governs sound representation. When sound-driven activity enters the brain by way of the auditory nerve, it is transformed by no less than 12 types of projection neurons in seven major processing centers before converging in the auditory thalamus. By contrast, visual information is conducted from the retina to thalamus without intermediate processing. In part, these differences in computational complexity may be traced back to the most elemental stage of sensory transduction. When light strikes the eye, its color, intensity, and location are unambiguously defined by the photoreceptors that it excites, the magnitude of the excitation, and their position on the retina. When sound propagates to the ear, auditory receptors are selectively excited by sound frequency. All other perceptual dimensions must be computed by integrating coincident activity across neural populations.

This review follows the central representation of sound information from cochlear nucleus to cerebral cortex (Figure 5–1). The descriptions of each of the major auditory nuclei summarize the anatomical pathways and physiological responses that give rise to the perceptual behaviors of normal and hearing impaired listeners. Each description begins with a brief summary of the essential functional characteristics of the processing center. Readers seeking the most general knowledge may quickly peruse this chapter by focusing their attention on this introductory material. Subsequent sections are intended to provide the reader with an understanding of basic concepts and

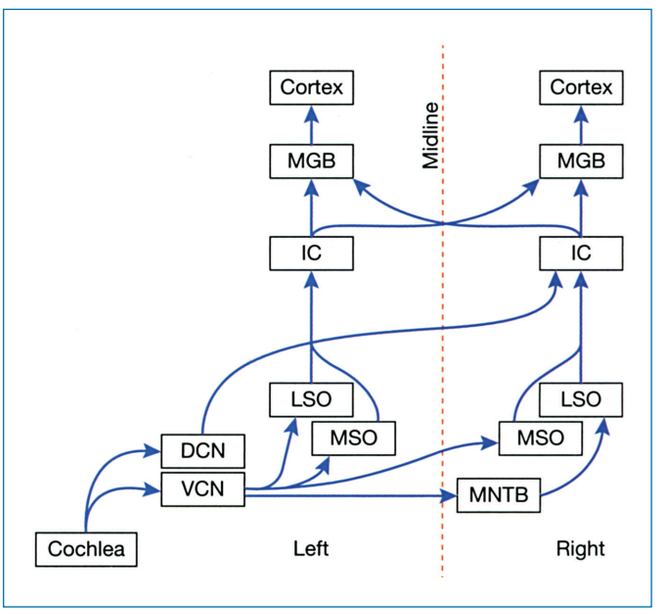

FIGURE 5–1 • Schematic diagram of the ascending pathways of the central auditory system. Principal connections between major nuclei are shown for the left ear. Symmetrical projections for the right ear are not shown. DCN, dorsal cochlear nucleus; IC, inferior colliculus; LSO, lateral superior olive; MGB, medial geniculate body; MNTB, medial nucleus of the trapezoid body; MSO, medial superior olive; VCN, ventral cochlear nucleus.

reference material to guide independent scholarship. Where it is possible, animal research is linked to clinical manifestations of processing disorders.

COCHLEAR NUCLEUS

As described in the accompanying chapter *Auditory Physiology: the Inner Ear*, a complex sound is broken apart into its constituent frequency components by the mechanical tuning of the cochlea. Because acoustic energy is tonotopically distributed along the length of cochlear partition, the discharge rates of individual auditory nerve fibers carry a single piece of the waveform puzzle. The complementary process of reconstructing the auditory signal from a dispersed peripheral representation begins in the cochlear nucleus where parallel streams of ascending information, each with a unique functional role, are established by the convergence patterns of auditory nerve fibers.[1]

The following discussion is organized around the broadest of functional dichotomies: the ventral and dorsal subdivisions of the cochlear nucleus complex. This parcellation was introduced by early anatomical descriptions of the auditory brainstem.[2] It endures because cellular morphology has proven to be an excellent predictor of function at the initial stages of central auditory processing.

VENTRAL COCHLEAR NUCLEUS

The ventral cochlear nucleus (VCN) serves as the primary input for afferent projections to the superior olive, lateral lemniscus, and inferior colliculus (ICC). Auditory information is channeled to each of these structures in discrete pathways that are optimized for the selective coding of local characteristics such as the phase and level of individual frequency components, or more global properties such as amplitude modulations of the stimulus envelope. This functional segregation is derived from striking differences in the synaptic structures, convergence patterns, and intrinsic electrical properties of VCN neurons.[3]

Anatomy

Approximately 30,000 auditory nerve fibers connect the human inner ear to the cochlear nucleus complex.[4] Upon entering the brainstem, the projections bifurcate into an ascending branch that proceeds to the anterior VCN and a descending branch that passes through the posterior VCN and dorsal cochlear nucleus (DCN). Although the systematic arrangement of the projections recapitulates the tonotopic organization of the cochlear partition, the one-dimensional frequency map is transformed into terminal fields. Within each two-dimensional frequency lamina, an orthogonal axis encodes other dimensions of sound.

The termination of the auditory nerve within the cochlear nucleus is obligatory. All sound information must be passed to higher centers by the discharge rates of cochlear nucleus neurons. There are approximately two VCN neurons for every auditory nerve fiber, suggesting a high degree of convergence within the nucleus.[5]

How VCN neurons integrate their multiple auditory nerve inputs is strongly influenced by the physical characteristics of cochlear nucleus synapses.[6] Two basic structures are observed. Neurons with wide-scale integration properties have profuse dendritic fields that are encrusted with the conventional bouton endings of large numbers of auditory nerve fibers. Neurons that faithfully preserve spike patterns in the auditory nerve are driven by large axosomatic endings, the endbulbs of Held.[7] These inputs are few in number but individually powerful enough to evoke postsynaptic activity.

The principal neuronal subtypes of the VCN are distinguished by three general cellular morphologies.[3] Bushy cells have stunted, shrub-shaped primary dendrites, globular or spherical cell bodies, and endbulb synapses. Like most neurons in the central nervous system, multipolar (or stellate) cells have long, relatively unbranched dendrites and bouton synapses. The integration properties of these cells are primarily determined by whether their dendritic fields lie within the plane of frequency laminae or radiate across them. Octopus cells have long, tufted dendrites that emanate from one side of the cell body creating the cephalopodal appearance for which they are named. These cells also receive highly convergent bouton inputs from the auditory nerve.

The cytoarchitecture of the VCN is regionally organized (Figure 5–2).[5] Spherical bushy cells are found in the most anterior subdivision, surrounding the entry point of the auditory nerve. Globular bushy cells occupy an intermediate location within the nucleus, while octopus cells are located in the

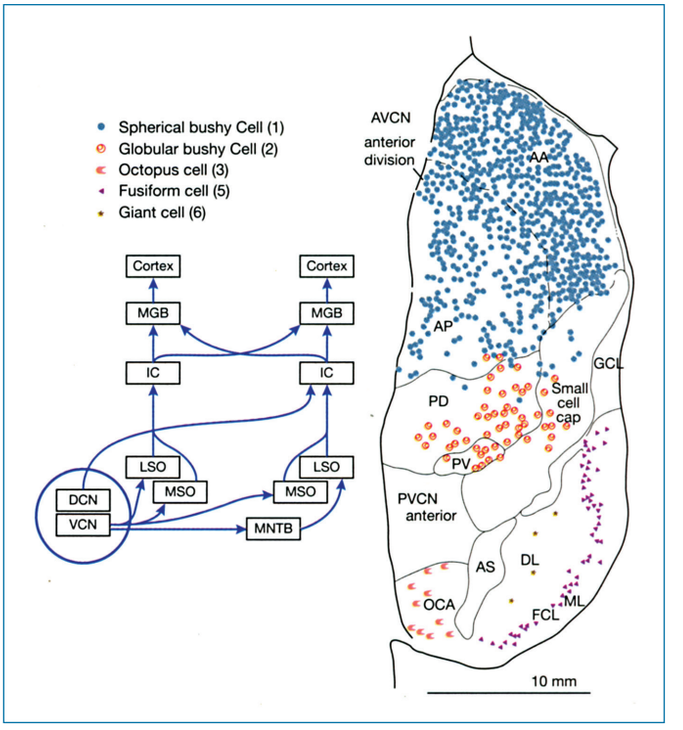

FIGURE 5–2 • Topographical clustering of morphological neuronal classes in the cochlear nucleus complex. See key for symbol identification. Inset shows relative position of the cochlear nucleus within the central auditory pathways. Abbreviations are explained in Figure 5–1. *Adapted with permission from Cant.*[3]

posterior subdivision. Multipolar cells, the most structurally diverse neurons, also show the most dispersed distribution.

Basic Physiological Properties

The regional separation of anatomically defined neuronal populations has allowed physiologists to relate the anatomical specializations of VCN neurons to their sound coding properties. Responses in the anterior nucleus are most likely recorded from bushy cells, while responses in the posterior nucleus are recorded from octopus cells. These inferences have been supported by intracellular experiments that have characterized the physiological properties of cochlear nucleus neurons before filling the cells with labeling material such as horseradish peroxidase (HRP) for later visualization.[8,9]

Single-unit electrophysiological activity in the VCN is typically classified by responses to short tone bursts at a neuron's best frequency (BF: the most sensitive frequency).[10,11] The timing of sound-driven action potentials, or spikes, is recorded and summed in temporal bins over many stimulus presentations to produce a peristimulus time histogram (PSTH). Six major response types can be identified by differences in PSTH shape (Figure 5–3).[1]

Primary-like neurons produce PSTHs that display an onset response that is robust but adapts rapidly to a lower sustained rate. Because primary-like units are found in the anterior subdivision of the VCN, they are assumed to be the functional counterpart of spherical bushy cells. As predicted by the high security endbulbs that bind bushy cells to auditory nerve fibers, the physiological characteristics of primary-like neurons are closely linked to their peripheral inputs.[12]

Primary-like with notch (PLN) neurons are found in regions containing large numbers of globular bushy cells.[13] Their PSTHs show a sharply peaked onset response that is followed by a brief period of inactivity. This "notch" reflects the neuron's refractory period after the onset spike. Primary-like with notch neurons display this property because modified endbulbs synchronize their responses to stimulus onsets.[14,15]

Onset neurons are named for their tendency to fire at stimulus onset and then show little activity for the remainder of the stimulus.[12] Onset-locker responses (onset-L) are typically recorded in the posterior subdivisions of the VCN and have been associated with octopus cell morphologies through intracellular labeling.[8] The precise onset response, broad frequency tuning, and wide dynamic range of onset neurons are consistent with the highly convergent afferent inputs of octopus cells.[16,17]

Onset chopper (onset-C) neurons show less variability than onset-L neurons. Because their spikes occur at regular intervals, onset-C neurons produce a "chopped" PSTH.[10] This response has been attributed to D stellate cells, which are large multipolar cells that send dorsally directed bilateral projections to the VCN.[18] The

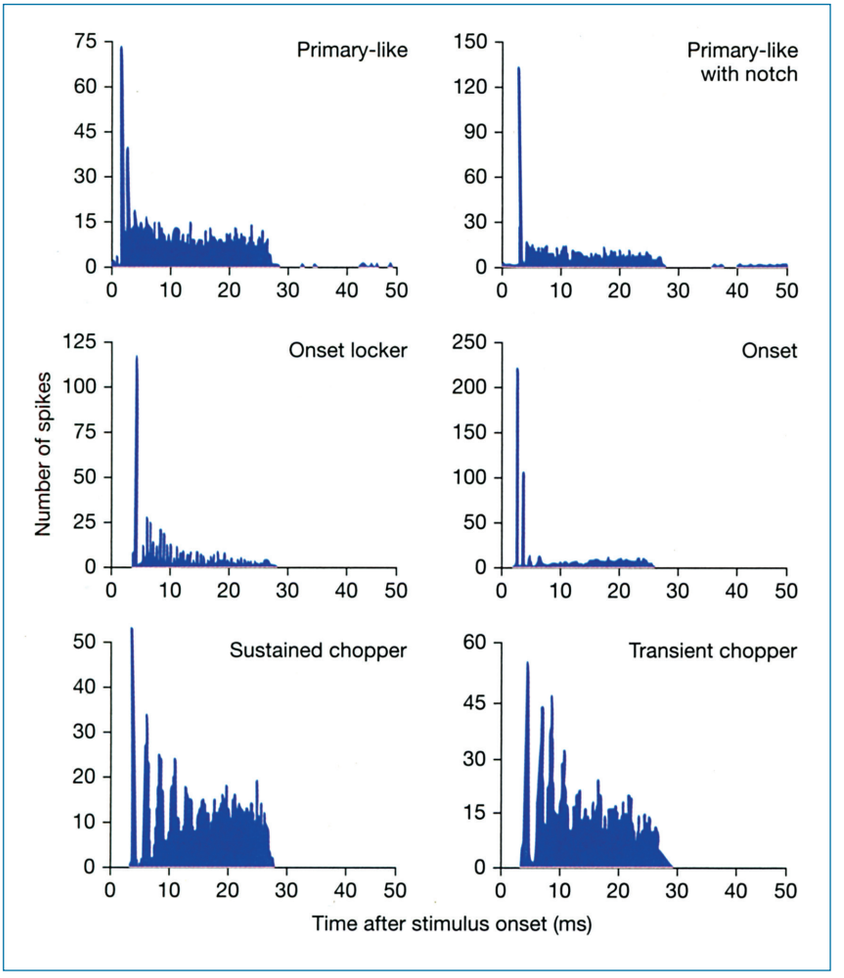

FIGURE 5–3 • Physiological response types in the ventral cochlear nucleus. Peristimulus time histograms for 30-millisecond tone bursts. *Adapted with permission from Rhode and Greenburg.*[1]

neurons have also been called "radiate" neurons because their dendritic fields fan out in three-dimensions integrating auditory nerve inputs across a wide frequency range.[19] They appear to be one source of the glycinergic inhibition that plays an important role in the sound coding properties of the cochlear nucleus.[18,20]

Chopper units are the physiological counterpart of T stellate cells.[1] These smaller multipolar cells project ventrally though the trapezoid body to the contralateral ICC.[3] The neurons are also referred to as "planar" neurons because their dendritic fields are oriented in the plane of frequency laminae.[19] In addition to sharp frequency tuning, chopper units display highly regular discharge rates and therefore produce "chopped" PSTH patterns. By integrating the responses of many auditory nerve fibers, chopper units produce signal representations that are robust across sound level and resistant to the degrading effects of background noise.[21]

Sound Coding in the Ventral Cochlear Nucleus

The diverse physiological patterns of cell populations in the VCN endow neurons with coding abilities that are selectively matched to the acoustic features of complex sounds.[22] With the exception of onset neurons, projection neurons tend to be sharply tuned in frequency. Consequently, as in the auditory nerve, complex spectra with multiple frequency components must be encoded by the discharge rates of many neurons with complementary tuning properties.[23,24]

From the perspective of human auditory experience, the veridical processing of complex spectral shapes is the foundation of speech perception. In the English language, the most rudimentary spectrum is a steady-state vowel. The perceptual identity of a vowel is defined by its formant frequencies,[25] which are high-energy bands within the stimulus. These information-bearing elements are encoded by hundreds of neurons in the auditory nerve and cochlear nucleus that combine to create a surprisingly straightforward representation in which discharge rates are linearly related to the amount of spectral energy within each neuron's range of frequency tuning.[21,26] The shape of the vowel emerges when vowel-driven activity is plotted at the BFs of the neural sample. For example, the vowel /e/, as in "bet," elicits high-discharge rates among neurons with BFs near 0.5 and 1.7 kHz, which are the frequency locations of its first and second formants (Figure 5–4).[25]

Sustained (Figure 5–4A) and transient chopper units (Figure 5–4B) provide excellent rate representations of vowel spectra across a wide range of sound levels.[21,27] It is hypothesized that this enhanced dynamic range reflects the dense convergence of auditory nerve fibers upon multipolar cells. Fibers with high spontaneous rates (SRs) tend to have low thresholds. Chopper units may accentuate these inputs at low sound levels. Conversely, fibers with low SRs have high thresholds, which may dominate chopper responses at high sound levels. A switching circuit for this "selective listening" has been proposed in which high SR inputs are located on distal dendrites and low SR inputs

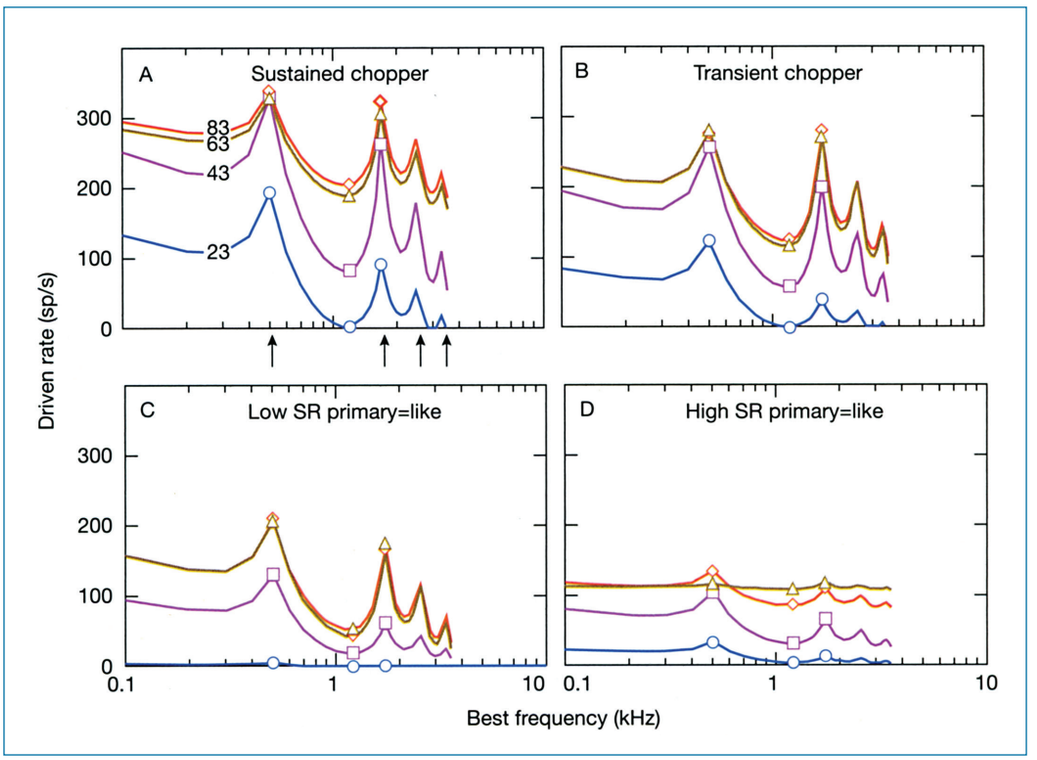

FIGURE 5–4 • Rate representation of the vowel /e/ by cochlear nucleus neurons. The formant frequencies of the vowel are indicated by arrows in *A*. Symbols indicate the average responses of actual neurons to three spectral features that define formant structure. Interpolated points are derived from the linear relationship between the level of those features and the discharge rates that they evoked. Numerical labels indicate the presentation level of the vowel stimuli. SR, spontaneous rates.

near the cell body of the chopper unit.[28] At high sound levels, the activation of intervening inhibitory inputs, possibly from radiate neurons, shunts the saturated high SR inputs away from the cell body. A reciprocal mechanism is not required for low SR inputs because their action is limited by threshold at low sound levels.

The vowel representations of VCN primary-like neurons manifest the dynamic range limitations of their auditory nerve inputs.[21,27] Primary-like neurons with low SRs (Figure 5–4C) provide a poor representation of formant structure at low sound levels because they are not effectively driven by the stimulus. The vowel's structure is apparent at suprathreshold sound levels because the highest discharge rates are restricted to formant-tuned neurons. Primary-like neurons with high SRs (Figure 5–4D) convey a good representation of formant structure at low levels but a featureless profile at high levels because the full complement of neurons responds at maximum driven rates. The threshold and saturation effects of primary-like neurons constrain their ability to encode spectral shapes in terms of discharge rates, but their responses are rich in temporal information.[12,27] In particular, the accurate timing of action potentials is critical for communicating the spatial location of auditory stimuli.

Many natural sounds are brief transients. Onset neurons respond vigorously to these stimuli and may participate in tightly coupled sensorimotor pathways that control acoustic startles and reflexive orientation movements.[29] A binaural comparison of stimulus onset time also exerts strong influences on spatial perception.[30,31] The event need not occur at the beginning of the stimulus. A sharp acoustic transition in the stimulus envelope will evoke similar responses. If the transients are repeated at a fixed rate, the responses of onset neurons will entrain to the period of stimulation. Periodicity is a fundamental characteristic of pitch perception and an essential cue for separating auditory signals from background noise.

Clinical Implications

The analysis of human neurological impairments has been essential for explaining the physiological foundations of higher cognitive function. Current understanding of the localization of speech and language in the human cortex can be traced back to the 19th century descriptions of aphasic patients by Broca[30] and Wernicke.[32] The clinical implications of damage within the pathways that bring information to the cortex have been largely determined by surgical manipulations of experimental animals.

Functional ablations of the VCN have been investigated by lesioning the projections that exit the nucleus by way of the trapezoid body.[33,34] The resulting deficits are as profound as those produced by removal of the cochlea or auditory nerve. If a trapezoid body lesion is made at the ventral midline of the brainstem, outputs from both cochlear nuclei are eliminated and the subject is rendered deaf. If a single lateralized lesion is made, outputs from one VCN are disrupted. Subjects maintain auditory function in one ear but they experience a pervasive loss of directional hearing because the brain is no longer about to make binaural comparisons of localization cues.

Temporary silencing of VCN inputs may have long-lasting clinical implications. During the early stages of development, sound-driven auditory nerve activity is needed to establish normal patterns of connectivity within the cochlear nucleus.[35] If the ear is silenced by conductive loss or sensorineural defects, the endbulbs of Held take on a hypertrophied appearance that is associated with temporal processing deficits. The synapses, and apparently higher cognitive function, may be rescued by swift interventions to restore input to the cochlear nucleus. These animal models may explain why cochlear implantation and hearing aid amplification is most effective when introduced at a young age.[36]

DORSAL COCHLEAR NUCLEUS

The DCN is a center for multisensory integration.[37] The principal output neurons are bipolar in shape and receive bouton endings on basal and apical dendritic arbors. Excitatory inputs from the cochlea are delivered to the basal dendrites. Mixed sources of excitation and inhibition contact the apical dendrites and cell body from the vestibular, cerebellar, and somatosensory nuclei.[38] Because these latter inputs are biased toward the head, neck, and outer ear, it is hypothesized that the cerebellar-like circuitry of the DCN may be involved in acousticomotor behaviors and pinna-based sound localization.[39]

Anatomy

In most mammalian species, the DCN is a three-layered structure (Figure 5–5).[3] The outer molecular layer contains descending inputs from outside the nucleus and their local target

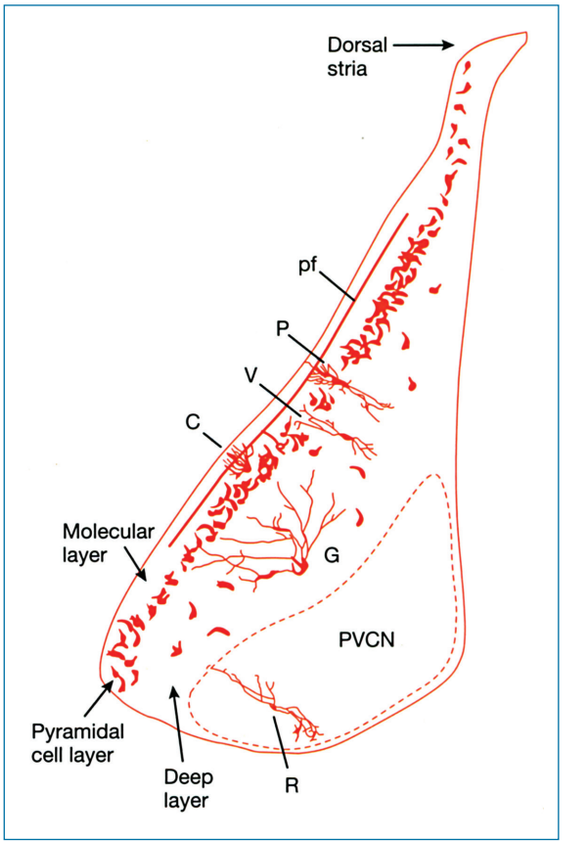

FIGURE 5–5 • Anatomical distribution of primary morphological classes within the layered structure of the dorsal cochlear nucleus. C, cartwheel cell; G, granule cell; P, pyramidal cell; pf, parallel fiber; PVCN, posteroventral cochlear nucleus; R, radiate cell; V, vertical cell. *Adapted with permission from Young and Davis.*[37]

neurons. The diverse sources of these "mossy fibers" have been determined by injecting HRP into the dorsal acoustic stria (DAS), where the fibers enter the nucleus.[38] After this procedure, heavy retrograde labeling is observed in the superior olivary complex because HRP is taken up by the axon collaterals of olivocochlear efferents. Extensive labeling of nonauditory cell groups is noted in the cerebellum and the vestibular nuclei. Retrograde labeling also is found in the lateral cuneate and sensory trigeminal nuclei. In combination, these structures carry proprioceptive information from the upper body, face, and ear.

The multisensory information conveyed to the DCN by mossy fibers is delivered to granule cells.[40] Granule cells are small cell bodies that are found scattered along the molecular layer and in the boundaries that separate the major subdivisions of the cochlear nucleus complex. The axons of granule cells form an array of parallel fibers that traverse the length of the nucleus. These fibers excite pyramidal cells through direct connections with apical dendrites or inhibit them through local interneurons, the cartwheel cells.

The pyramidal cell layer is occupied by the major projection neurons of the DCN.[5] Pyramidal cells, sometimes known as fusiform cells, are regularly arranged along the long axis of the nucleus. They send their apical dendrites into the complex neuropil of the molecular layer where they are contacted by granule and cartwheel cells. They project their basal dendrites into the deep layer where they receive inputs from auditory nerve fibers and additional sources of inhibition. The tonotopic map of the cochlea is transferred to the DCN by the systematic innervation of the dorsal branch of the auditory nerve.[41]

The deep layer of the DCN is inhabited by giant cells and vertical cells.[42] Giant cells are less frequently encountered projection neurons. Their basic physiological properties are similar to those of pyramidal cells, but their deeply located dendrites do not reach into the molecular layer to contact parallel fibers. Vertical cells are inhibitory interneurons. Their narrowband inhibitory influences reflect their alignment within DCN frequency lamina. Additional wideband glycinergic inhibition has been attributed to VCN radiate cells.[19]

Neural Coding of Spectral Cues for Sound Localization

The basic physiological properties of DCN projection neurons are shaped by complex interactions of their numerous excitatory and inhibitory inputs. Whereas VCN representations are linear, narrowly tuned, and distributed, DCN representations are nonlinear, broadly tuned, and integrative. Consequently, the discharge rates of individual pyramidal and giant cells are ideally suited for encoding the spectral shape of complex sounds.[37]

For the cat, which is the most developed animal model of DCN processing, biologically relevant spectral information is derived from the head-related transfer function (HRTF).[43,44] This filter shape describes the directional effects of the head and pinna on a free-field stimulus as it propagates to the ear drum. HRTF-based spectral cues are critical for the accurate localization of sound source elevation.

A prominent feature of the cat's HRTF is a single deep spectral notch, which is a sharp decrease in gain at frequencies between 5 and 20 kHz. When a broadband sound is passed through the transfer function, these frequencies are essentially filtered out of the stimulus. The frequency location of the notch changes systematically as a sound source moves in elevation or azimuth (Figure 5–6A). If these cues are removed from free-field sounds, cats make poorly directed orientation responses.[45]

The neural coding of spectral cues for sound localization has been examined by recording the HRTF-driven discharge rates of DCN projection neurons, which are known as type IV neurons. For best stimulus control, these experiments are performed with simulated spectral notches that are presented through headphones. The notch can be shifted in frequency with digital signal processing techniques to match the tuning of neurons that are encountered along the trajectory of the recording electrode.[46] The goal of these experiments is to mimic the movement of a sound source by manipulating the feature of interest relative to the inhibitory properties of the type IV neuron (Figure 5–6B). When the frequency of the notch is below the BF, the neuron is exclusively excited by the stimulus (Figure 5–6C, plots a and b). A similar response is produced when the notch is above BF (Figure 5–6D, plots d and e). These results are expected given the excitatory effects of broadband noise. However, when the notch coincides with BF, the neuron is strongly inhibited (Figure 5–6C and D, plot c).

The responses of type IV neurons to HRTF shapes are dictated by their nonlinear spectral integration properties.[47] Consequently, the neurons respond selectively to spectral shapes, and not merely the magnitude of individual frequency components. This feature-driven, level-tolerant representation is demonstrated by varying the presentation level of the HRTFs (Figure 5–6C and D). In contrast to the more generalized coding mechanisms of the VCN, major changes in spectral energy have little effect on the polarity of type IV responses to ON-BF and OFF-BF notches.

Clinical Implications

Perceptual abnormalities relating to DCN processing disorders have been investigated in the laboratory by sectioning the DAS (Figure 5–7A). This surgical manipulation eliminates the ascending axonal projections of pyramidal and giant cells en route to the ICC. Unlike lesions of the trapezoid body, lesions of the DAS have little effect on basic patterns of hearing. Absolute thresholds in quiet, and in background noise are not affected by the procedure.[34]

Significant deficits are observed when DAS lesioned cats are tested in localization paradigms that require the identification of sound source elevation.[48,49] Cats make reflexive head movements toward sudden, unexpected sounds. They also can be trained to perform these maneuvers repetitiously to gain access to food rewards. The cat is a natural predator, and the accuracy of these sound-guided responses approaches the limits of human directional hearing (Figure 5–7B).

When the output pathways of the DCN are bilaterally destroyed, cats exhibit clear deficits in localization behavior (Figure 5–7C).[49] Although performance is compromised in both horizontal and vertical dimensions, largest errors are observed in the determination of sound source elevation. These systematic errors confirm that the DCN is an important site for the auditory processing of spectral cues for sound localization. Cats

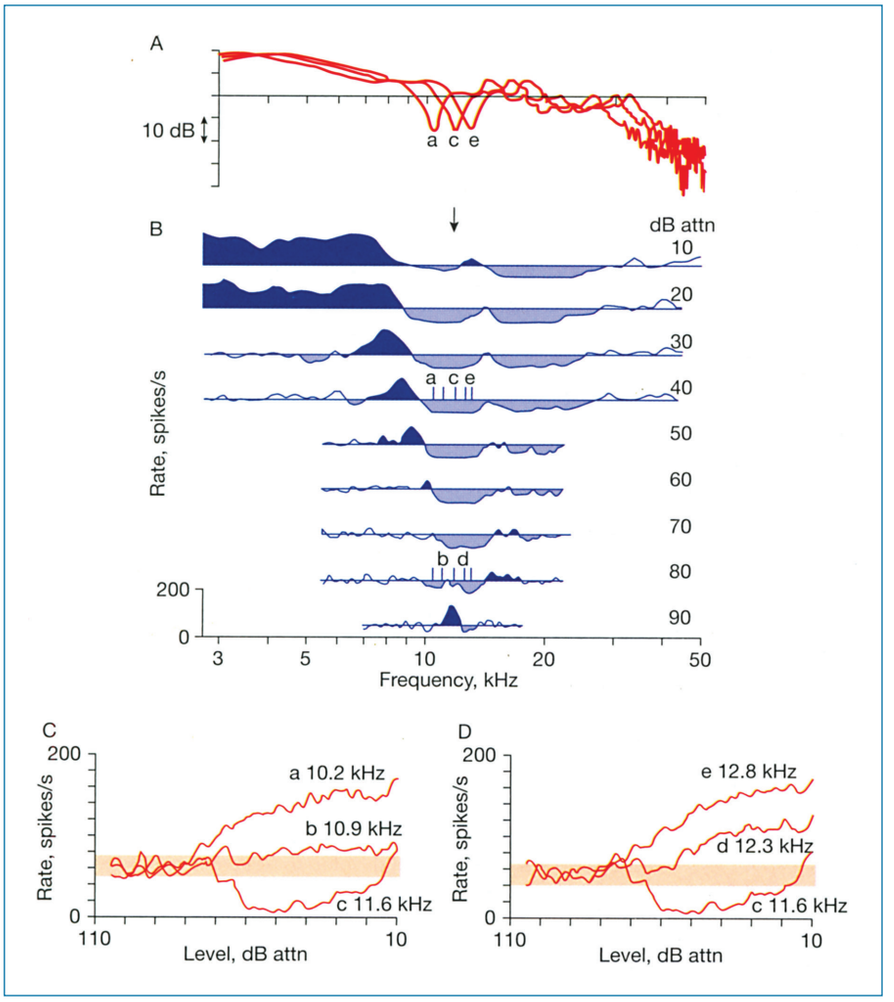

FIGURE 5–6 • Spectral coding in the dorsal cochlear nucleus. *A*, Generic head-related transfer functions of the cat. The biologically relevant spectral notch has been shifted in frequency by changing sampling rate during playback. *B,* The frequency response map of a DCN type IV unit. Letters relate the frequency location of the spectral notch at five sampling rates to the best frequency (BF) of the neuron. Excitatory responses (dark blue fill) are rates that exceed spontaneous activity. Inhibitory responses (light blue fill) are rates that fall below spontaneous activity. *C*, Rate-level functions obtained from the neuron when spectral notches were shifted to the unit's BF (c) or placed below BF (a,b). *D*, Rate-level functions for notches at BF (c) and above BF (d,e). The neuron's spontaneous rates are indicated by shading in *C* and *D*. *Adapted with permission from Young and Davis.*[37]

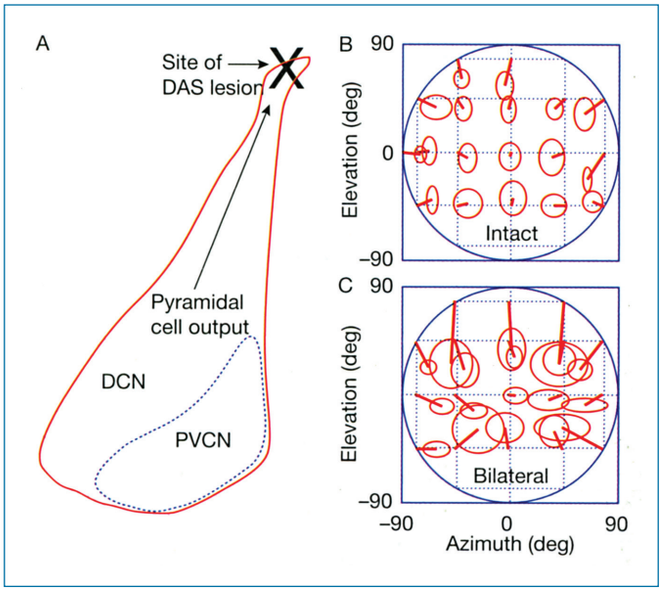

FIGURE 5–7 • Effects of dorsal acoustic stria (DAS) lesions on sound orientation behavior. *A*, Site of lesion. *B*, Accuracy of sound-evoked orientation responses in an intact cat. *C*, Accuracy after bilateral DAS lesions. Line segments connect actual source locations to average response locations. Ellipses indicate the standard deviation of responses in horizontal and vertical dimensions. *Adapted with permission from May.*[49]

with bilateral DAS lesions maintain directional hearing in the horizontal dimension by attending to binaural cues that are processed in the ventral pathways leading to the superior olivary complex.

The absolute silencing of DCN outputs by vascular accident or trauma is rare in human-patient populations. Tinnitus may reflect the less than complete disruption of this delicate circuitry.[50] If current physiological interpretations of tinnitus should prove to be correct, DCN processing deficits represent the most prevalent form of hearing disorder in industrial societies.

There is ample evidence that spontaneous discharge rates in the DCN increase when cochlear inputs are diminished by transient exposure to an intense sound or the long-term effects of aging. Because this hyperactivity mimics the normal auditory response to a physical stimulus, it creates the impression of phantom sound.[51,52]

The functional changes that accompany tinnitus have been extensively studied in animal models that allow controlled induction of the disorder and direct physiological evaluation of its consequences. This analysis has yet to reveal an unequivocal generator site and a unique pathology, but it is clear that candidate structures share common properties. The DCN, ICC, and auditory cortex have each been associated with tinnitus-like behavior.[53,54] These processing centers are

key sites of multisensory integration where inputs from auditory and nonauditory nuclei converge to be acted upon by a constellation of excitatory and inhibitory neurotransmitters. Alterations of any component in this synaptic design have the potential to reorganize the resting and sound-driven properties of the neural circuit.

Neural hyperactivity remains the most influential physiological model of tinnitus. In part, the broad advocacy of this hypothetical mechanism lies in its intuitive simplicity. In addition, global changes in brain activity predict a metabolic signature that can be noninvasively imaged in human tinnitus patients.[55] While it is clear that some animal preparations respond to acoustic overexposure with generalized hyperactivity, important details of the proposed relationship between brain activity and sound perception remain unresolved. The effects may be specific to species, manner of induction, and methods of electrophysiological recording. A more comprehensive explanation of the underlying mechanisms of tinnitus may be gained from a more sophisticated statistical analysis of discharge patterns such as the regularity, synchronization, or long-term fluctuations of spontaneous activity.[56] These properties cannot be adequately described without direct electrophysiological recordings in animal preparations.

SUPERIOR OLIVARY COMPLEX

The superior olivary complex is situated in the ventral brainstem in close proximity to the trapezoid body. It consists of three primary auditory nuclei: the medial superior olive (MSO), lateral superior olive (LSO), and medial nucleus of the trapezoid body (MNTB). Ramon Y Cajal referred to the MSO and LSO as the accessory and superior olives in his classic Golgi studies.[57] These terms are occasionally encountered in modern texts. This central core is surrounded by a cluster of periolivary nuclei of which the lateral nucleus of the trapezoid body (LNTB) is the most prominent.

Ascending projections from both VCNs converge in the superior olivary complex to create binaural representations that are tuned to interaural disparities in time (interaural time differences, ITDs) and sound pressure level (interaural level differences, ILDs). Descending projections from the superior olive modulate cochlear sensitivity and cochlear nucleus inhibitory interactions through the action of olivocochlear efferent neurons.

Medial Superior Olive

The MSO performs a binaural comparison of the timing of sound-evoked discharge rates that reach the brain from the two ears. These temporal disparities are one of two essential cues for azimuthal (left–right) sound localization. The circuitry also plays an important role in spatial masking release, including the well-known "cocktail party effect." When competing auditory signals (eg, multiple talkers at a cocktail party) reach the listener's ear from different directions, spatial information facilitates their separation into distinct auditory objects. This process of "auditory streaming" may reduce the interference between signals by as much as 20 dB. Directional hearing relies heavily on binaural processes that are not available to individuals with unilateral hearing aids, which may explain why the devices perform poorly in complex listening environments.

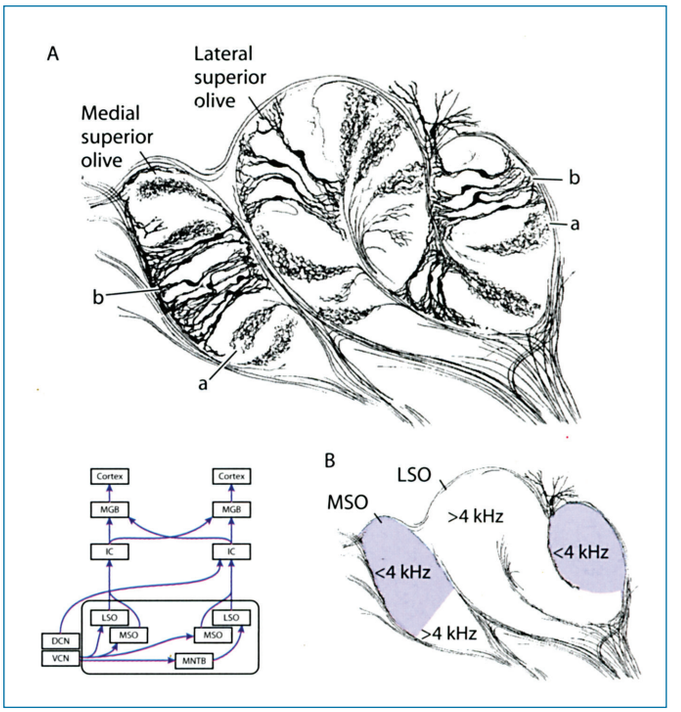

FIGURE 5–8 • The superior olivary complex. *A*, Golgi reconstructions of the lateral and medial superior olives showing bipolar neurons (a) and terminal axonal projections from the cochlear nucleus (b). *B*, Tonotopic map derived from electrophysiological recordings. Shaded regions indicate area devoted to frequencies below 4 kHz, the upper limits of temporal processing. Inset shows relative position of the superior olivary complex within the central auditory pathways. Abbreviations are explained in Figure 5–1. *Anatomical illustrations adapted from Scheibel and Scheibel*[58] *derived from Guinan et al.*[59]

Anatomy

In most mammals, the MSO is a two-dimensional sheet with bipolar dendritic fields (Figure 5–8A). The neurons receive afferent inputs from the ipsilateral VCN on lateral dendrites, and contralateral inputs medially. Because the inputs arise from spherical bushy cells,[60] high security endbulb synapses preserve the timing and frequency tuning of auditory nerve action potentials along their route to the MSO.[61]

The central cell region of the MSO is tonotopically organized along its dorsoventral axis (Figure 5–8B). Unlike the complete cochlear map that is found in the VCN, the MSO is biased toward low frequencies.[62] Although cats are capable of detecting frequencies above 64 kHz, the dorsal half of the feline nucleus is devoted to frequencies below 4 kHz. This frequency bias coincides with the upper limits of temporal coding by auditory neurons.[63]

Matching the delay sensitivity of auditory neurons to biologically relevant cues requires the interaction of a constellation of excitatory and inhibitory inputs, as well as the precisely timed delivery of each component. Results from immunocytochemical studies and intracellular recordings suggest that primary binaural inputs from the VCN are mediated by the excitatory

amino acid glutamate through AMPA and NMDA receptors.[64] The MSO also shows a wide distribution of glycinergic receptors. The injection of retrograde label into the MSO indicates that the inhibitory inputs originate in the MNTB and LNTB.[65] Blocking the inhibition with strychnine compresses the range of temporal tuning shown by MSO neurons.[66]

The ascending projections of MSO neurons are almost exclusively directed ipsilaterally to low-frequency regions of the central nucleus of the ICC.[67] Injections of retrograde label into high-frequency regions has revealed few projections from the ventral subdivision of the MSO, where high-frequency neurons reside.[68]

Physiology

Neurons in the MSO are characterized by their monaural properties, binaural interactions, and ITD sensitivity. The sheet-like neuropil of MSO principal cells and the presence of powerful field potentials make isolation of single-unit activity in the nucleus difficult. Existing descriptions are typically founded on relatively small samples.

In general, MSO neurons show primary-like activity when tested with monaural stimuli. The discharge rates that are elicited by pure tones are irregularly timed, monotonically related to stimulus level, and narrowly tuned in frequency.[69] Responses to sounds in one ear cannot be considered in isolation because MSO neurons are excited by sounds in either ear. This excitatory-excitatory (EE) binaural interaction creates units with preferences for either contralateral or ipsilateral stimuli under monaural conditions.

The most influential model of binaural processing in the MSO is the Jeffress coincidence detector (Figure 5–9).[70] This anatomically based model was developed well before actual physiological recordings in the central auditory system. The key concept of coincidence is the existence of multiple delay lines in the afferent projections to MSO neurons. As a result, any acoustic delay in the interaural timing of a free-field sound is offset by a neural delay that is equal in magnitude but opposite in sign. The neuron with the appropriate delay line receives coincident inputs, which elicit maximum rates because of the EE binaural interaction. This pattern of excitatory ITD sensitivity is called a "peak-type" response. The neuron's delay sensitivity, therefore, represents a place code for the sound's location. It is interesting that, 50 years after the introduction of the Jeffress model, there is now anatomical evidence for coincidence detection circuits in the avian and mammalian MSO.[71, 72]

Lateral Superior Olive

The LSO encodes the ILDs that signal the azimuth of high-frequency sounds. These cues are created by the "sound shadow" of the upper torso, head, and outer ear. Just as opaque objects block the path of light, acoustic reflections from the head produce interference patterns that reduce sound energy as it propagates to the two ears. A lateralized location will generate robust ILD cues because the interference is applied disproportionately to the far ear. The lower frequency limit of the shadowing effect is dictated by the geometry of the head. Larger animals are afforded lower frequency cues because their head attenuates longer acoustic wavelengths. Humans rely heavily on ILD cues at frequencies above 2 kHz.[73]

Anatomy

The LSO is arguably the most visually striking structure in the central auditory system. In cats, the LSO folds upon itself to take on an S-shaped conformation when viewed in transverse section (Figure 5–8A). The complexity and orientation of folding varies greatly in other species, depending on the biological significance of high-frequency sound localization.

The principal cells of the LSO have bipolar dendritic arbors that radiate across the hila of the nucleus. Axodendritic inputs arise from the same spherical bushy cell populations that project to the MSO; however, the inputs are confined to the ipsilateral cochlear nucleus.[3] The immunocytochemistry and morphological features of the synapses suggest that they evoke excitatory influences through the amino acid glutamate.[74]

Ascending inputs from the contralateral cochlear nucleus are relayed to the LSO by neurons in the MNTB. These indirect projections are the axonal tracts of globular bushy cells, which enter the trapezoid body and cross to the contralateral superior olivary complex.[60] Within the MNTB, the projections terminate in large calyceal synapses displaying glutamatergic pharmacological properties.[75] The postsynaptic targets of these projections label intensely for glycine.[76] Consequently, the excitatory input from the contralateral cochlear nucleus is reversed in sign before it reaches the LSO.

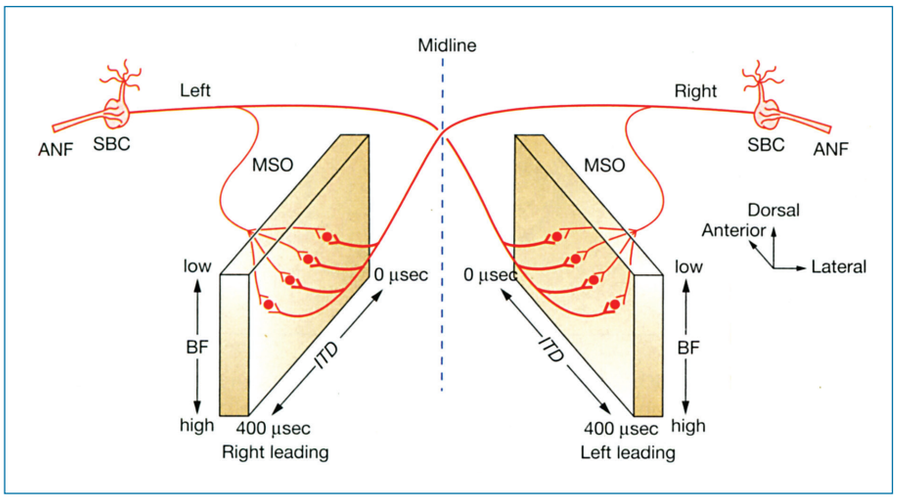

FIGURE 5–9 • The Jeffress coincidence detection model of sound localization. A single contralateral and ipsilateral input to the median superior olive (MSO) is shown. Neural delay lines are created by the arrayed termination pattern of the contralateral projections. ANF, auditory nerve fiber; BF, best frequency; ITD, interaural time difference; SBC, spherical bushy cell. *Adapted with permission from Yin.*[77]

The secure synaptic organization of MNTB principal cells preserves the timing and tuning of its cochlear nucleus inputs. Unlike the diffuse axosomatic endings of the monosynaptic excitatory input from the ipsilateral cochlear nucleus, disynaptic inhibitory inputs from the contralateral cochlear nucleus are delivered directly to the soma and proximal dendrites of LSO neurons.[78] This configuration aids a coincident binaural comparison by offsetting the synaptic delay that is introduced by additional transformations in the MNTB. Although many anatomical properties of the LSO are similar to those seen in the MSO, contralateral inhibition tunes its responses to the relative magnitude, and not timing of sound energy at the two ears.

Physiology

Single-unit recordings in the LSO reveal a tonotopic map with an exaggerated representation of high frequencies (Figure 5–8B). This bias corresponds favorably with the frequency domain of ILD information. Monaural responses to ipsilateral and contralateral stimuli show similar frequency tuning suggesting that underlying binaural comparisons are frequency specific. As expected, given the neurotransmitters of their ascending inputs, LSO neurons display IE binaural interactions. That is, they are inhibited by contralateral stimuli and excited by ipsilateral sounds. Because LSO neurons are maximally inhibited by coincident binaural inputs, they show minimum discharge rates. This inhibitory ITD sensitivity that is call a "trough-type" response.

Most LSO neurons exhibit monotonically increasing rate-level functions when ipsilateral tones are presented under closed-field conditions (Figure 5–10). This monaural response pattern recapitulates the coding of stimulus level by auditory nerve fibers and primary-like neurons in the anteroventral cochlear nucleus. Because monaural responses to contralateral tones are inhibitory, they simply suppress the neuron's spontaneous activity.

The effects of contralateral inhibition are better demonstrated under binaural conditions. To quantify the strength of inhibition, activity is evoked by an ipsilateral excitatory stimulus while a competing contralateral inhibitory stimulus is varied in level. This manipulation simulates the movement of a sound source from an ipsilateral location (lower contralateral levels) to a contralateral location (higher contralateral levels). The resulting rate changes show good agreement between LSO sensitivity and behavioral thresholds for ILD discrimination.[80]

The Acoustic Chiasm

The LSO sends bilateral projections through the lateral lemniscus to the central nucleus of the ICC. Approximately equal numbers of fibers ascend in an ipsilateral and contralateral direction. Tract tracing techniques have localized the source of ipsilateral projections to the lateral limb of the LSO. Contralateral projections originate in the medial limb. This sorting of output by physical location resembles the routing of optic nerve fibers through the optic chiasm. Because a tonotopic gradient is imposed on anatomical locations in the central auditory system, this "acoustic chiasm" separates high frequencies and routes them contralaterally, while low frequencies are sent ipsilaterally.[81]

The projection patterns and neurotransmitter systems of the superior olive enhance the contralateral representation of sound (Figure 5–11). A sound on the left side of the listener will produce bilateral activity in the anterior VCN, MNTB, and the MSO. Neural transmission in these pathways is mediated by excitatory amino acids. The ascending excitatory input carrying high-frequency information from the right LSO crosses to the left ICC.[82,83] Activity in the left LSO is silenced by MNTB inhibition. Both MSOs carry low-frequency information to the mid brain by ipsilateral excitatory projections but these inputs are inhibited in the right ICC by uncrossed glycinergic projections from the low-frequency LSO.[84] The net result of these reciprocal influences

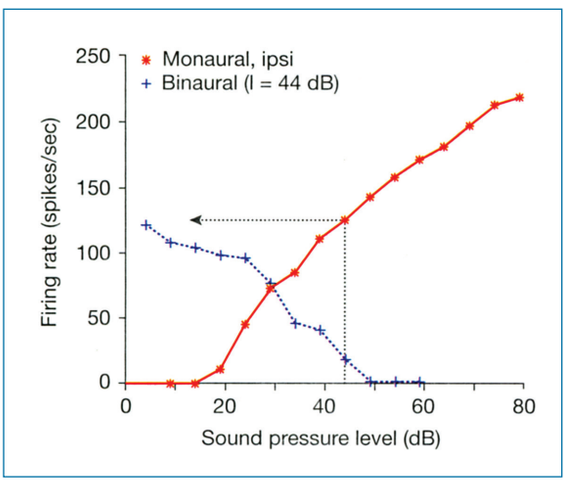

FIGURE 5–10 • Binaural interactions in the lateral super olive. Rate-level functions are compared for monaural ipsilateral tones and binaural tones. Dotted line indicates the firing rate evoked by a monaural ipsilateral tone at a presentation level of 44 dB SPL. This ipsilateral stimulus was fixed during binaural measures. Variations in contralateral tone levels during binaural testing are indicated on the abscissa. *Adapted with permission from Joris and Yin.*[79] SPL, sound pressure level.

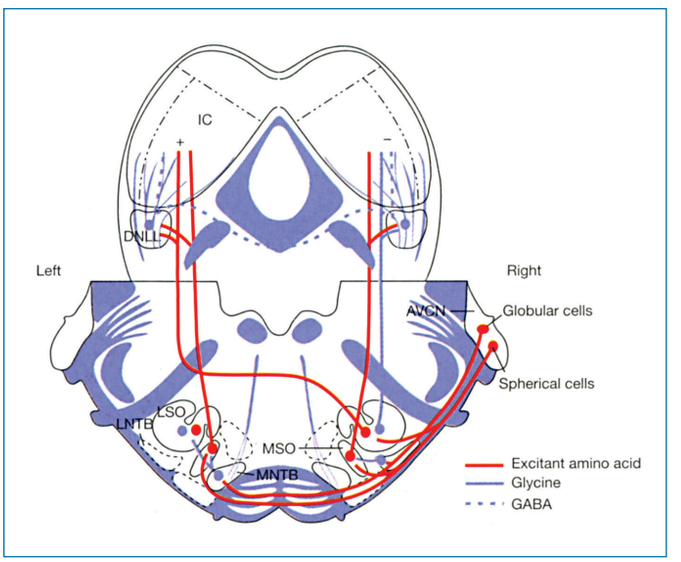

FIGURE 5–11 • The "acoustic chiasm" created by ascending projections from the superior olivary complex. Major connections are shown for the right ear. Putative neurotransmitters are indicated by line style. The strength of the input is represented by line width. *Adapted with permission from Helfert and Aschoff.*[85]

is a complete representation of low and high frequencies in the contralateral ICC. If a unilateral lesion is placed in the ICC or a higher structure in the central auditory system, sound localization deficits are restricted to the contralateral hemifield.[86]

Olivocochlear Efferent Pathway

Decades of research have probed the structure and function of the ascending auditory pathways. The reciprocal descending circuitry at present remains largely unexplored. The exception to this inattention is the olivocochlear efferent pathway, which is a mechanism that gives the brainstem control over the mechanical sensitivity of the auditory periphery. Olivocochlear feedback may play an important role in hearing protection, selective attention, and listening in noise.

Anatomy

Anatomical characteristics suggest that there are two separate olivocochlear systems (Figure 5–12).[87] The thin, unmyelinated axons of the more numerous lateral olivocochlear (LOC) neurons project from lateral regions of the superior olive to the distal processes of auditory nerve fibers. The innervation patterns of LOC fibers are heavily biased toward the ipsilateral cochlea. Medial olivocochlear (MOC) projections originate from cell bodies that are scattered in medial regions of the superior olivary complex. These neurons send thick myelinated axons to the inner ear, where they enter the organ of Corti through the habenulae perforatae, cross the tunnel of Corti, and terminate on the base of outer hair cells. The majority of the fibers project to the contralateral cochlea.

En route to the cochlea, MOC neurons send collateral projections to granule cell areas of the cochlear nucleus.[88] The projections target the dendritic fields of large multipolar cells that reside in the VCN. Because the target neurons are a source of inhibition, this feedback may compensate for efferent-based changes in the dynamic range properties of auditory nerve inputs to the cochlear nucleus. Any reduction in cochlear sensitivity by direct MOC influences may be offset by a reciprocal attenuation of cochlear nucleus inhibition. Consequently, the mechanical tuning of the cochlear partition can be tailored to the ongoing listening environment without a corruption of actual signal levels in higher processing centers.

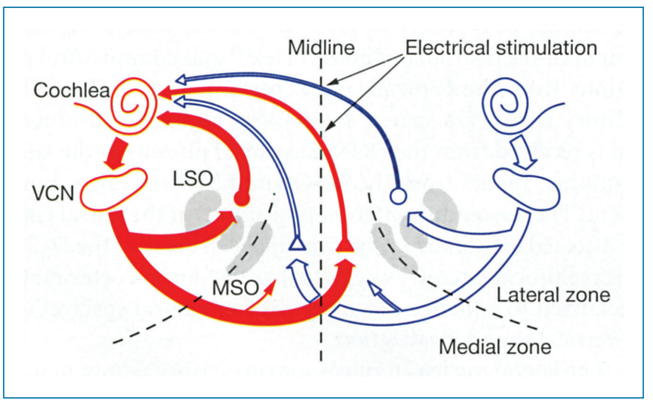

FIGURE 5–12 • The olivocochlear reflex arc. Inputs are shown from both ears, outputs to one ear. The cell bodies of medial olivocochlear efferents are located in the medial zones (triangles). Lateral olivocochlear efferents are located in the lateral zones (circles). The strength of input is indicated by line widths. LSO, lateral superior olive; MSO, medial superior olive; VCN, ventral cochlear nucleus. *Adapted with permission from Warr.*[89]

Physiology

Classical physiological descriptions of olivocochlear function are performed by switching on the system with electrical shocks. The stimulating electrodes are placed on the midline of the IVth ventricle, where crossing fibers of the olivocochlear bundle (OCB) approach the dorsal surface of the medulla (Figure 5–12). This paradigm is assumed to selectively activate the medial efferent system. Electrical stimulation is less effective for the unmyelinated lateral efferent system. In addition, most LOC fibers project to the ipsilateral ear without approaching the site of stimulation.

The effects of olivocochlear feedback can be observed by comparing auditory nerve activity with and without OCB stimulation. The responses have been characterized in terms of compound action potentials (CAPs)[90] or direct single unit recording.[91] In both contexts, OCB stimulation reduces cochlear sensitivity.

Efferent-mediated changes in the dynamic range of the auditory nerve reflect alterations in the active mechanical properties of the cochlea.[92] Outer hair cells display the unique ability to move in response to depolarizing currents.[93] The force generated by this so-called electromotility amplifies and tunes the sound-generated movements of the cochlear partition. The release of acetylcholine by MOC neurons triggers an influx of calcium into the outer hair cells, which opens voltage-gated potassium channels in the cell membranes. The subsequent efflux of potassium hyperpolarizes the cells, making them less sensitive to depolarizing currents that enter through the stereocilia during movements of the basilar membrane. As a result, sound-generated deflections of the stereocilia bundle fail to elicit complementary electromechanical responses.

When sounds occur in the presence of background noise, a listening advantage may be gained by shifting the dynamic range of neural responses to higher levels.[94] Auditory nerve recordings have shown that a sensitive neuron may be driven to its maximum discharge rate by noise alone, leaving no additional response to encode the occurrence of a meaningful auditory event. When sensitivity is reduced by electrically stimulating the OCB, noise no longer saturates the neuron's response and coincident signals are able to evoke further rate increases.

Clinical Implications

Olivocochlear fibers enter the cochlea intermingled with the inferior vestibular nerve. Consequently, when the vestibular nerve is sectioned to alleviate intractable vertigo, the lesioned ear loses both vestibular and olivocochlear function.[95] What is most striking about these patients is the subtlety of their ensuing auditory deficits.[96] A battery of audiological assessments has identified one consistent abnormality. The loss of olivocochlear feedback reduces "selective listening." Under normal circumstances, this process allows an individual to listen to one channel of information while blocking out sounds in other competing channels. Auditory information channels are usually defined by frequency; that is, the subject focuses attention on one tone frequency at the expense of other frequencies. Because olivocochlear feedback is

tuned in frequency, the listener may optimize performance by increasing cochlear sensitivity at the attended frequency and decreasing sensitivity at unattended frequencies. It is also possible to attend to auditory streams that are defined by their location, pitch, or temporal pattern. This ability is critical for separating important sounds from the acoustic clutter of real-world environments. Consequently, individuals with weak olivocochlear feedback tend to show deficits when listening in background noise.[97]

An important consideration for the audiological evaluation of vestibular neurectomy is that the patient populations upon which these studies have been performed are biased toward preexisting Meniere's disease with concomitant hearing loss. Such confounds are avoided in animal studies of olivocochlear function. The existing literature of controlled experimental manipulations has defined three roles for the efferent system: sound protection, listening in noise, and cochlear development. The ability of olivocochlear feedback to reduce acoustic trauma has received the greatest attention in the laboratory.[98]

Two qualities of the MOC pathways allow efferent feedback to be observed noninvasively in human listeners. First, olivocochlear activity may be induced by contralateral sound stimulation. Second, when the feedback is activated, there is a decrease in the magnitude of otoacoustic emissions, which depend on active cochlear processes. An intriguing aspect of these measures is the considerable variation in the strength of olivocochlear feedback among human subjects. Consequently, observers with weaker systems are less able to process sounds in noisy environments,[97] and may be more susceptible to acoustic trauma.[99]

INFERIOR COLLICULUS

The ICC may have the most elaborate neuronal connections of any auditory structure. It is comprised of a central core of sound processing neurons, the central nucleus, and a surrounding belt of polysensory nuclei with less robust sound-driven responses. The acoustic tuning of neurons in the central nucleus reflects the convergence of multiple parallel pathways that are created in the cochlear nucleus. Direct monaural projections originate in the ventral and dorsal subdivisions of the contralateral cochlear nucleus. Indirect binaural projections are routed through the superior olivary complex and nuclei of the lateral lemniscus. These ascending inputs are not simply relayed to higher structures. They are transformed into more selective representations of acoustic information and then delivered to higher processing centers in the auditory thalamus and cortex.

The sharp dichotomy of response patterns in the central and belt regions of the ICC has prompted the distinction of lemniscal pathways (the tonotopic core) versus extralemniscal pathways (the nontonotopic belt). Although auditory physiologists have focused on auditory activity in the lemniscal pathways, many clinicians have directed their attention to the extralemniscal system because disordered interactions of its multimodal inputs may serve as generator sites for audiogenic seizures, abnormal loudness perception, and certain types of tinnitus.[100]

Anatomy

The primary anatomical subdivision of the ICC is the central nucleus (Figure 5–13A).[101] The laminar structure of the ICC is created by incoming projections from the brainstem and the dendrites of disc-shaped principal cells. These fibrodendritic arrays are oriented in parallel creating isofrequency laminae. The cochlear tonotopic map is projected on the dorsal–ventral axis of the nucleus and preserved in its ascending outputs to the auditory thalamus.[102]

In addition to disc-shaped cells, stellate cells represent approximately 25% of the ICC cell population. They have ovoid or stellate dendritic fields that integrate synaptic inputs across isofrequency laminae. Immunostaining indicates that the ICC sends both excitatory and inhibitory projections to the medial geniculate body.[103] Because the number and size of cells that label positively for the inhibitory neurotransmitter gamma-amino butyric acid (GABA) match the characteristics of stellate cells, it is suspected that the neural population is an important source of thalamic inhibition.[104] It is not presently known if the broadband inhibitory influences of stellate cells are localized within particular processing pathways.

The ICC receives direct or indirect inputs from all of the major projection pathways of the cochlear nucleus. Within the ICC, there are regionalized differences in the topography of these inputs. The results of anterograde tracing studies suggest that excitatory inputs from ITD-sensitive MSO neurons and ILD-sensitive LSO neurons remain anatomically segregated (Figure 5–13B).[105] From a functional perspective, the discrete synaptic domains of these two binaural pathways mirror their separate roles in sound localization. Similarly, although the DCN and LSO both project to high-frequency regions, each lamina may be divided into a ventral portion that receives mixed inputs and a dorsal portion that is exclusively innervated by the DCN.[106] This pattern of input may establish functional modules that differ in their accentuation of binaural and monaural coding.

The belt regions of the ICC have been subdivided with varying degrees of complexity. Differences in existing maps of cellular anatomy reflect the histological methods used to identify cytoarchitectural features and connectivity. Most parcellations involve a dorsal cortex and paracentral nuclei of which the lateral or external nucleus is the most prominent.[107]

The dorsal cortex is the target of profuse descending inputs from multiple fields in auditory cortex[108] and commissural projections from the contralateral central nucleus.[109] Ascending auditory inputs are sparse. Incomplete regionalized innervation is received from the DCN and dorsal nucleus of the lateral lemniscus. Inputs from the MSO and LSO are conspicuously absent. The descending efferent projections of the dorsal cortex are directed bilaterally to the principal cell areas of the DCN.[110] This reciprocal circuitry suggests that the dorsal cortex may be specialized to enhance the analysis of monaural spectral cues for vertical sound localization.

The lateral nucleus receives somatosensory representations of the head from the dorsal column and trigeminal nuclei, as well as premotor inputs from components of the basal ganglia.[111] Auditory inputs are dominated by intracollicular projections from the ipsilateral central nucleus. Efferent projections of the lateral nucleus pass to the deep layers of the superior colliculus and cerebellum by way of the pontine nuclei where they may contribute to the integration of acoustically driven motor

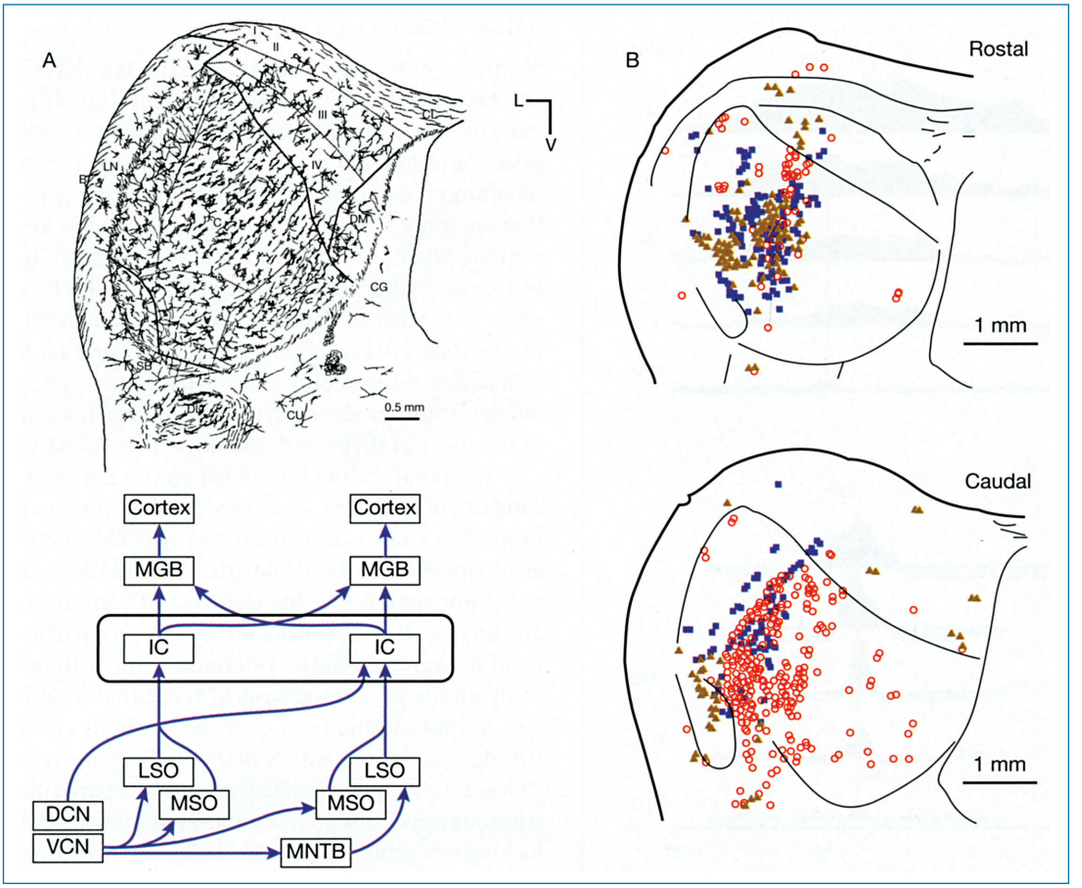

FIGURE 5–13 • Anatomical organization of the cat inferior colliculus. *A*, Laminar structure imposed by the trajectory of axonal projections and the dendritic fields of disc-shaped neurons. *B*, Terminal zones of projections from the superior olive. Excitatory projections from the contralateral LSO dominate rostral locations (filled triangles). Excitatory projections from the ipsilateral MSO are mostly found at caudal locations (open circles). Inhibitory inputs from the ipsilateral LSO are also shown (blue squares). Inset shows relative position of the inferior colliculus within the central auditory pathways. Abbreviations are explained in Figure 5–1. *Adapted with permission from Morest and Oliver*[107] *and Loftus et al.*[105]

behaviors such as startle responses, pinna reflexes, and sound target acquisitions by the head and eyes.[112]

Classification of Sound-Driven Activity in the Central Nucleus

The physiological properties of the central nucleus are strongly modified by barbiturate anesthesia. These influences may be avoided by recording single-unit activity in unanesthetized, decerebrate preparations. The subject's ability to initiate movements and experience pain is eliminated by transecting all fibers entering and exiting the cerebral cortex at the level of the thalamus. A limitation of this approach is that descending feedback systems from cortex are also removed from the neuronal circuitry of the auditory midbrain.

The principal cells of the ICC show three basic response patterns when frequency response maps (FRMs) are recorded in decerebrate cats (Figure 5–14).[113] The most common response has been designated the type-O unit because the neuron's excitatory receptive field is constrained to a small O-shaped island of frequencies near threshold. The remainder of the receptive field is dominated by inhibition. The neurons also tend to be insensitive to ITD cues.[114] These response patterns are reminiscent of monaural projection neurons in the DCN (type IV neurons). Type-O units are silenced when conduction is blocked in the DAS, further supporting a direct link between the DCN and the response type.[115] Type-O units are less commonly encountered in prey species (eg, guinea pigs, mice, gerbils),[116] which implies that they may play a specialized role in the predatory behaviors of the cat. The localization accuracy of cats is far superior to that of the prey upon which they feed.[117]

Type-I units are defined by a narrow I-shaped excitatory receptive field that is surrounded by lateral inhibition. The neurons tend to be tuned to higher frequencies and display trough-type ITD sensitivity. This cluster of physiological characteristics suggests that type-I units are the midbrain target of ascending excitatory projections from the contralateral LSO. Conversely, type-V units show an excitatory receptive field, low-frequency tuning, and peak-type ITD sensitivity. The controlling influences of these neurons are assumed to emanate from the ipsilateral MSO.

The FRM classification scheme is useful for interpreting the functional connections of the ICC. This simple conceptual framework reveals how physiologically defined pathways of the cochlear nucleus remain segregated en route to higher processing levels. It also provides a metric for evaluating

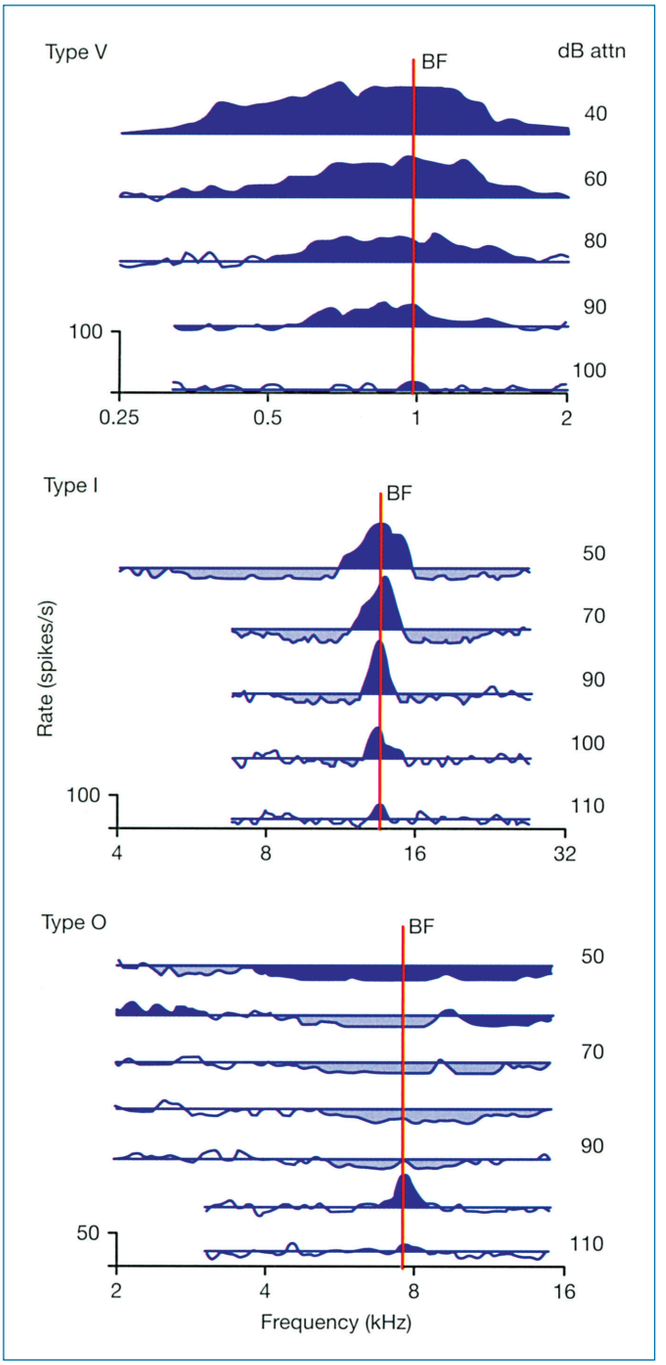

FIGURE 5–14 • Physiological properties of neurons in the central nucleus of the inferior colliculus. The responses were recorded in decerebrate cats. Frequency response maps plot sound-driven discharge rates as a function of pure tone frequency and level. Plotting conventions for frequency response maps are described in Figure 5–6. *Adapted with permission from Ramachandran et al.*[113]

how local transformations impact the quality of information coding. Nevertheless, it is clear from anatomical evidence that the central nucleus is the nexus of the auditory system; ie, the place where discrete representations from multiple input sources are bound together to form perceptual experience.[118]

Information Coding

Studies of information coding in the ICC have examined the representation of simple sound elements (amplitude, frequency, and timing), as well as the more complex constructs that support communication, localization, and perceptual grouping. A common theme in this research is the emergence of responses that are more selective than those observed in lower processing centers. Single-unit responses may be sharply tuned not only to frequency but also to sound pressure level[119] and temporal properties such as amplitude modulation (AM) or frequency modulation (FM).[120] Consequently, in contrast to the population codes of the auditory brainstem, the responses of individual neurons may signify critical biological information that lies in the spectral shape or dynamic patterns of natural sounds.

Temporal coding is founded on the ability of auditory neurons to entrain their discharge rates to time varying acoustic properties such as monaural AM and FM fluctuations as well as binaural temporal disparities. Modulation cues are important information-bearing elements of communication sounds and an essential reference for the segregation of auditory signals from background noise. Interaural time differences, as previously discussed, are the basis of azimuthal sound localization.

Amplitude and frequency modulations are encoded by the timing of action potentials in the auditory nerve and brainstem. At low tone frequencies, neurons fire at a particular phase of the stimulus waveform. In most mammals, the upper limit of phase-locking is reached around 5 kHz. Nevertheless, this mechanism remains in effect at much higher frequencies because discharge rates are synchronized to the envelope fluctuations of complex sounds.

Beyond the upper frequency limits of phase-locking and envelope following responses, temporal coding is constrained by the probabilistic nature of synaptic events. Each synapse adds error to the neural representation of time because of uncertainties in the release of neurotransmitter from the presynaptic neuron and the subsequent generation of action potentials in the postsynaptic neuron. The dedicated temporal pathways that project to the olivary complex minimize this "jitter" by integrating the inputs of multiple auditory nerve fibers and securely transmitting that information through powerful endbulb synapses.

Further synaptic degradation of temporal information may be avoided at high levels of auditory processing by transforming the temporal code into a rate code.[121] Neurons in the ICC are sharply tuned to specific modulation rates just as brainstem neurons are tuned in frequency. Consequently, the neuron acts as a "labeled line" signaling modulation frequency with its relative firing rates and not the temporal structure of its responses.

The ascending projections of the LSO and MSO endow neurons in the central nucleus with binaural temporal tuning. As in the brainstem, the majority of these neurons show peak-type or trough-type responses, which according to the Jeffress Model, may be explained by binaural excitatory and inhibitory interactions (see detailed descriptions in Superior Olivary Complex). A number of neurons, however, show intermediate-type ITD sensitivity.[122,123] The neurons may respond best to intermediate interaural phase disparities or show complex phase–frequency relationships. This temporal pattern is not compatible with the

Jeffress Model and probably reflects the convergence of olivary inputs with different ITD tuning.[124] It is likely that even ICC neurons with less complicated peak-type and trough-type responses integrate multiple inputs from the superior olive because the bandwidth of ITD tuning for both unit types is significantly sharper than their SOC counterparts.[125]

Spectral coding in the ICC is important for monaural sound localization and vocal communication.[126] The receptive fields of ICC neurons may span several octaves creating regions where spectral energy produces either excitatory or inhibitory effects. Sounds with energy at excitatory frequencies evoke strong responses; whereas, sounds with energy at inhibitory frequencies elicit weak responses. The response to a complex spectral shape, such as a broadband noise that has been filtered by the transfer function of the outer ear, is dictated by the balance of this excitation and inhibition.

The functional consequences of the template-matching process are summarized in Figure 5–15, which shows how the spatial tuning of an ICC neuron correlates with the frequency domain of its OFF-BF inhibition. In Figure 5–15A, the neuron's discharge rates are shown for HRTF-filtered noise bursts. The binaural stimuli were presented through headphones to simulate the acoustic effects of the two external ears at 99 different locations in the frontal sound field. Responses to these "virtual" sound locations are shown at four presentation levels. Each response is plotted according to the spectral energy in the contralateral (dominant) ear at the neuron's BF (~12 kHz). The distinguishing feature of the resulting rate-level function

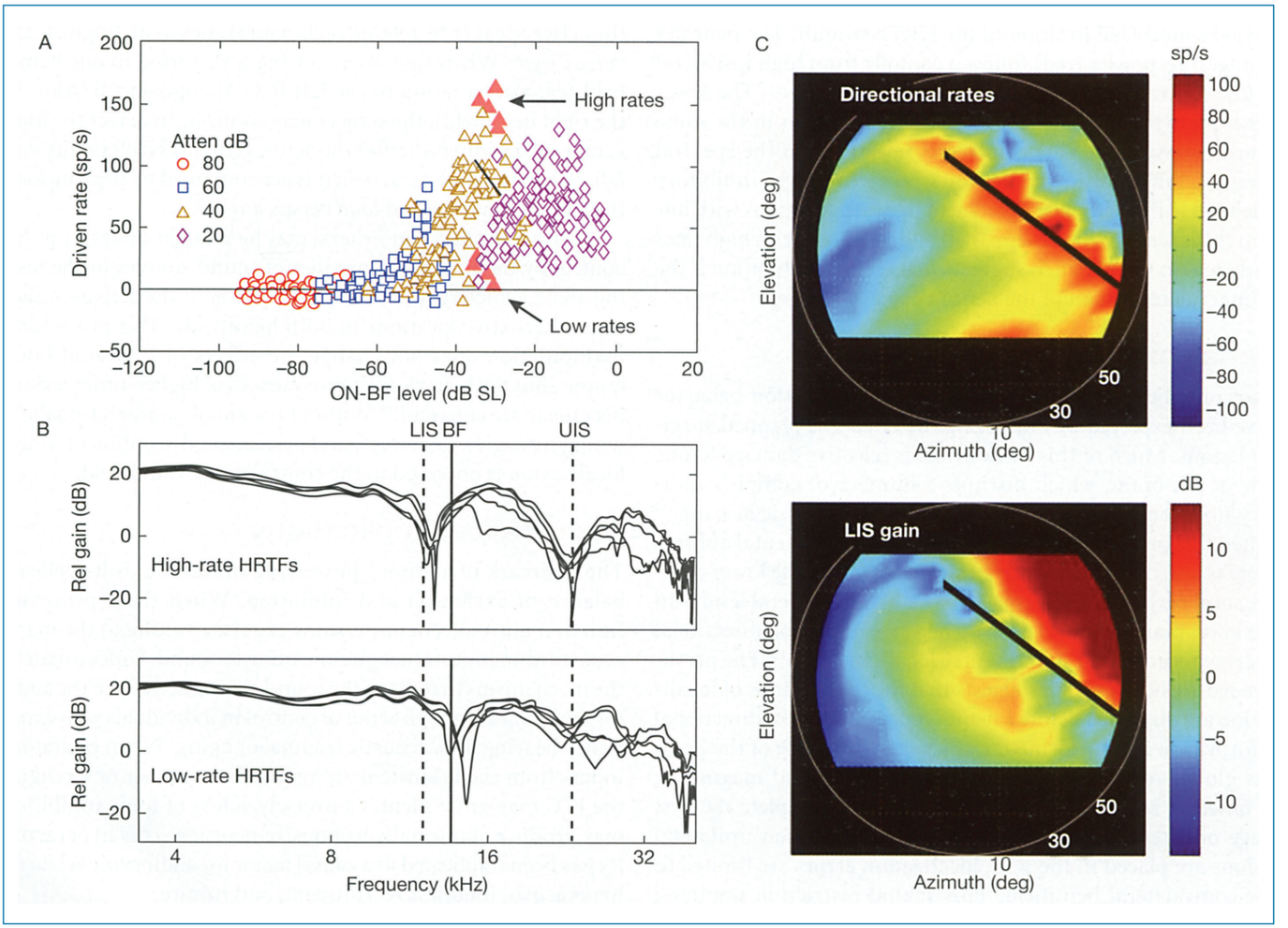

FIGURE 5–15 • Spatial tuning of a single-unit response in the inferior colliculus of a decerebrate cat. *A*, Discharge rates evoked by noise bursts that have been shaped by the cat's head-related transfer functions (HRTFs, see dorsal cochlear nucleus). Responses are shown for 99 locations in the frontal sound field at four presentation levels. Each data point is plotted in terms of spectrum level at the neuron's best frequency (BF). Filled symbols contrast HRTFs with similar ON-BF energy that elicited high versus low discharge rates. *B*, The spectral shapes of high- versus low-rate HRTFs. Vertical lines mark the relative gain of the functions at BF, and at a lower inhibitory sideband (LIS) and an upper inhibitory sideband (UIS). *C*, The role of sideband inhibition in the neuron's directional tuning. In the upper panel, the discharges rates in A are plotted in spatial coordinates. In the lower panel, the gain of the HRTFs at the LIS are plotted in spatial coordinates. Strongest responses (red) are observed where the transfer functions show the weakest gain at inhibitory frequencies. *Adapted with permission from May et al.*[126]

is the extreme variation in responses to HRTFs with similar ON-BF energy. These differences are observed because the neuron is sensitive to spectral features that exist at frequencies well beyond BF.

The HRTF shapes in Figure 5–15B are grouped by their ability to elicit high- or low-discharge rates from the IC neuron, as indicated by filled symbols in Figure 5–15A. Although the transfer functions have similar ON-BF energy, there are consistent differences in the frequency locations of their prominent spectral notches. High-rate HRTFs have notches that fall within lower and upper inhibitory sidebands (vertical dashed lines). Consequently, they produce relatively weak inhibitory responses. The low-rate HRTFs show the opposite polarity. Their spectral notches correspond to the central excitatory region surrounding the neuron's BF (vertical solid line).

The neuron's sensitivity to HRTF shapes is translated to spatial tuning in Figure 5–15C. The upper panel plots the discharge rates in Figure 5–15A, in spatial coordinates that indicate the virtual sound field location of the HRTF stimuli. The neuron's strongest responses (red) follow a contour from high ipsilateral to low contralateral elevations (superimposed line). The lower panel plots the relative gain of the HRTF stimuli in the same coordinate system. This gain refers selectively to the spectral energy falling within the neuron's powerful lower inhibitory sideband (LIS). The close agreement between locations with low gain (blue areas in the lower panel) and locations with high rates (red areas in upper panel) suggests that OFF-BF inhibition is the primary determinant of the neuron's spatial tuning.

Behavior/Ablation Studies

The contributions of the ICC to sound localization behavior have been explored by evaluating the effects of planned surgical lesions. Much of this work involves selective damage to one side of the brain, which disrupts a number of complex auditory functions without completely eliminating basic hearing.[118] When this procedure is performed on an experimental animal, there is a striking dichotomy between lesions of the lower commissural pathways and damage to the ICC. Unilateral lesions in the lower brainstem nuclei have a negative impact on directional hearing regardless of sound source location. [33,86,127,128] The pervasive nature of the deficit suggests that the foundations of localization are disrupted before a neural representation of directional information is fully formed. Damage to either side of the brain has global consequences because the timing and magnitude of binaural responses must be integrated to complete the first stage of directional processing. By contrast, when unilateral lesions are placed in the ICC, localization errors are limited to the contralateral hemifield. This spatial restriction implies a second-stage "distributive" process that biases the higher-order representation of auditory space toward contralateral source locations.[81,129] As previously noted, the acoustic chiasm is the proposed mechanism for the selective lateralized distribution of ascending olivary inputs to the central nucleus. Damage to the lateral lemniscus, therefore, produces similar deficits.

Behavior-ablation studies have relied heavily on free-field testing arenas to characterize the accuracy of directional hearing. In the classic two-alternative forced-choice paradigm, one of two goal boxes is unlocked to allow an animal access to a food reward. The left versus right location of the unlocked receptacle is signaled by the presentation of an auditory stimulus from an attached speaker. The limits of the subject's localization capabilities are measured by varying the angle of separation between the two goal box/speaker combinations. This is a true localization task that requires the subject to identify and approach the sound source for the food reward.

A review of this classic literature leads to the impression that destruction of the commissures of the ICC or cerebral cortex does not radically alter localization behavior.[33,128] Lesions of the trapezoid body may produce striking deficits, but these effects are only observed in some subjects and they tend to be transient.

Subsequent investigations have brought up the possibility that goal-box testing may be confounded by listening strategies that do not require directional hearing.[86] When two sound sources are located in the left and right hemifield of the testing arena, a subject with normal directional hearing may identify the active speaker by relying on binaural cues to distinguish *left* versus *right*. When spatial processing is distorted in one hemifield (eg, after a lesion of the left ICC disrupts localization in the right hemifield), the subject may continue to detect the food source by deciding whether the active goal box is *left* versus *not-left*. When the unilateral deficit is accompanied by hearing loss, the subject may respond *loud* versus *quiet*.

Covarying decision-criteria may be brought under stimulus control by increasing the number of sound sources in the testing arena, which requires the subject to select the active speaker from alternative locations in both hemifields. This procedural manipulation does not change the effects of trapezoid body lesions, but the behavioral consequences of higher-order lesions become more apparent.[86] Without the aid of nondirectional listening strategies, a complete and permanent disruption of sound localization is observed in the contralateral sound field.

Audiological Implications

The hallmark of auditory processing in the ICC is its delicate balance of excitation and inhibition. When these processes function normally, neurons show exquisite tuning to the many acoustic dimensions that give meaning to sound. Unfortunately, the mechanisms that shape the sound-driven activity of the auditory midbrain may spiral out of control in individuals who experience hearing loss, acoustic trauma, or aging. When excitatory inputs from the brainstem are reduced in number or strength, the ICC may grow silent. Conversely, a loss of tonic inhibition may produce abnormally responsive neurons. This hyperactivity has been implicated as a causal factor for audiogenic seizures, hyperacusis, loudness recruitment, and tinnitus.

Immunocytochemical studies[130] have demonstrated a substantial loss of the inhibitory neurotransmitter GABA in the central nucleus of aged rats. The loss is regionally selective. One-third fewer GABA-positive neurons are seen in the ventrolateral portion of the nucleus relative to young controls. Neurochemical analyses confirm that the potassium-evoked release of GABA by this tissue is significantly decreased, while the release of the excitatory neurotransmitter glutamate is up-regulated. These findings suggest that disordered GABAergic transmission in the ICC may contribute to a

number of the audiological abnormalities that accompany neural presbycusis.[131] The effectiveness of GABAergic inhibition is also diminished by experimental manipulations that are known to induce tinnitus.[132,133]

The ICC has been proposed as a site for audiogenic seizures in animal models of epilepsy.[134] At the neural level, the induction of epileptiform activity is observed as a train of prolonged afterdischarges that follow sound stimulation. Insensitivity to endogenous GABA inhibition appears to lie at the core of these abnormal response patterns. When GABA is delivered to an ICC neuron by iontophoresis, the amount of neurotransmitter that is required to suppress activity in epilepsy-prone rats is significantly greater than in normal rats. A reduction of GABA-mediated inhibition also is indicated by the decreased efficacy of agonists such as benzodiazepine. Epileptiform activity may be induced in normal neurons by iontophoresis of bicuculline, a potent antagonist of GABA.

This same loss of central inhibition may lead to the perception of chronic tinnitus.[135] In addition to producing stronger, longer lasting responses to auditory stimuli, downregulation of GABA may increase spontaneous activity in the absence of sound. Because the hyperactivity mimics the sound-driven responses of auditory neurons, it is hypothesized that higher brain centers interpret the activity as sound even though no physical stimulus is present. The ICC may play a prominent role in the phenomenon because of the well-established physiological vulnerability of its inhibitory networks. Like the DCN, another putative generator site for tinnitus, the ICC receives converging inputs from both auditory and nonauditory pathways. One nonauditory function, the initiation of conditioned aversive responses, may be demonstrated with electrical or chemical stimulation of the auditory midbrain.[136] With reduction of central inhibition, these subsystems may potentiate the perceived severity of tinnitus, which often fails to correlate with objective loudness measures.[137]

The hypothesized role of GABA in tinnitus creates the opportunity to pursue pharmacological interventions. Because potentially toxic substances cannot be directly tested in human subjects, researchers must rely on animal models with experimentally induced tinnitus. This approach raises the conundrum, How do you characterize the subjective perception of phantom sound in an animal?[138] Although several behavioral testing procedures exist, the basic strategy is to train the subject to respond to the onset of a silent interval that is created by switching off a continuous background sound. After tinnitus is induced by exposure to a loud sound or a large dose of salicylate, the subject can no longer perform the task because it hears a phantom sound instead of silence. The success of a drug treatment is indicated by the restoration of normal behavioral performance. These paradigms are currently producing promising results with agents that modulate GABAergic transmission.[139]

THE AUDITORY THALAMUS

The auditory thalamus, or medial geniculate body (MGB), is an obligatory relay for the projections of the central nucleus of the ICC. Within the ventral division of the MGB, a rich intrinsic circuitry works in conjunction with descending feedback from cortex and the limbic systems to condition ascending auditory representations before they are passed on to the auditory cortex. In parallel to this tonotopic pathway, diffusely tuned and polysensory inputs from multiple brainstem nuclei converge within the dorsal and medial divisions. Each thalamic region maintains the separate functional identity of these diverse inputs by preferentially innervating distinct cortical areas.

Anatomy

Alternative anatomical parcellations of the MGB have been proposed based on cytoarchitectural structure and patterns of neural connectivity. Most recognize a tripartite scheme that divides the nucleus into a ventral principal cell area, a medial magnocellular area, and a structurally diverse dorsal area.[140,141] The ventral division alone shows robust sound-driven activity.

The major functional connections of the ventral division integrate ascending inputs from the ICC, local inhibitory neurons, and descending projections from the auditory cortex (Figure 5–16A). The thalamic targets of the predominately excitatory projections from the central nucleus of the ICC are large tufted cells that serve as the principal relay neurons, and small stellate cells that are inhibitory interneurons.[142] Because the dendritic fields of bushy cells are oriented in parallel to their afferent inputs, responses within the ventral division maintain the tonotopic organization and basic physiological characteristics of the midbrain. Excitatory outputs from the ventral division are mainly directed to cellular layer IV of A1.[143] The cortical region receiving these inputs sends reciprocal corticothalamic projections back to the ventral division.

As in other sensory relay nuclei of the thalamus, the inhibitory interneurons of the ventral division are organized in synaptic glomeruli (Figure 5–16B).[144] Excitatory inputs from the ICC form a triad synapse with the dendrites of interneurons and MGB principal cells. The synaptic complex is insulated from the surrounding neuropil by glial processes. When inputs from the ICC activate the triad, presynaptic terminals on the dendrites of the interneuron release GABA within the glomerulus.[145] The release of the inhibitory neurotransmitter is regulated by metabotrophic glutamate receptors, which require high input rates for activation and then maintain an active state for relatively long durations. Consequently, the transmission properties of the triad are ideal for modifying the long-term efficacy of midbrain inputs.

The MGB receives as many inputs from the cortex as it does from the ICC. Retrograde labeling suggests that corticothalamic feedback to the ventral MGB originates from small pyramidal cells in layer VI of area AI.[146] Synaptic morphology suggest that the descending projections are excitatory. En route to the dendritic fields of principal cells in the ventral division, the fibers send collaterals to the thalamic reticular nucleus (TRN), a large source of extrinsic GABAergic inhibition.[147] Therefore, cortical feedback has the potential to alter thalamic activity by direct action, or through its indirect influence on inhibitory networks. Additional inhibitory feedback is provided by the limbic system, particularly the mesencephalic reticular formation. This complex circuitry allows cognitive factors such as learning, attention, and state of arousal to activate a subset of thalamic neurons while suppressing others.[148]

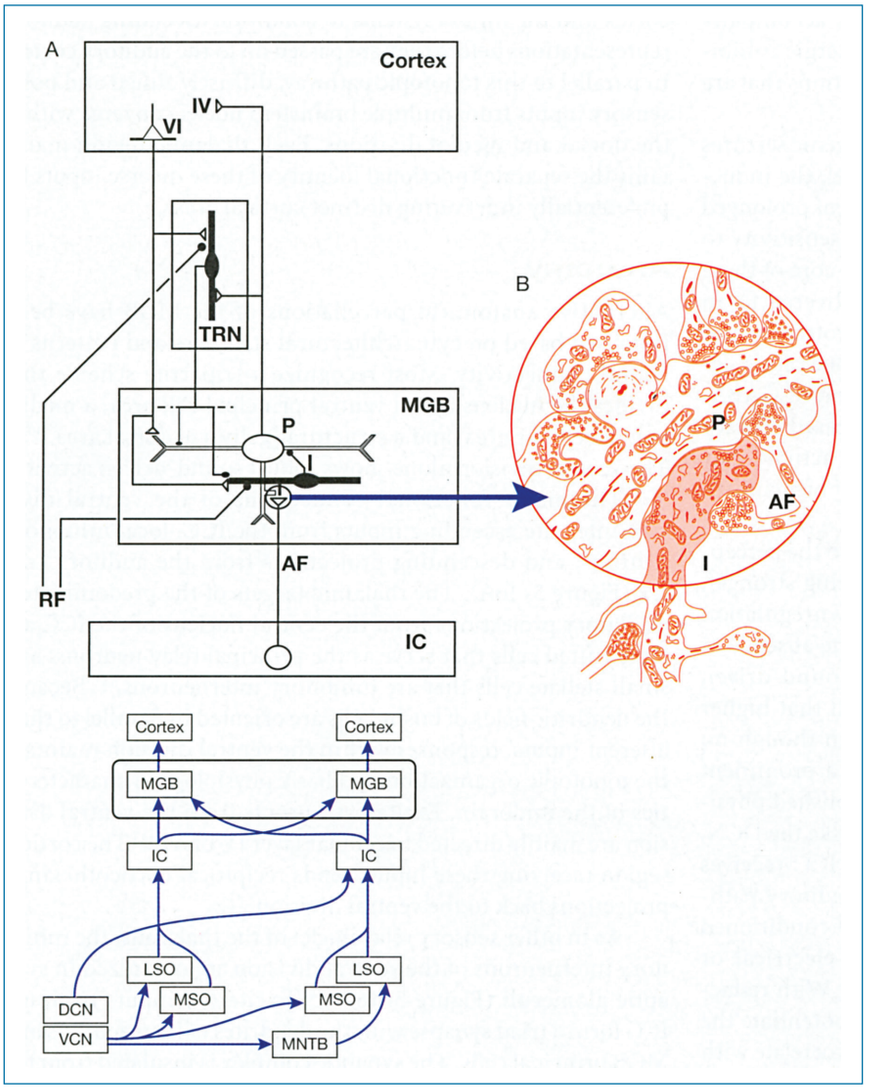

FIGURE 5–16 • Schematic diagram of the major inputs to principal cells in the ventral division of the auditory thalamus. *A*, Neural connections between the inferior colliculus (IC), medial geniculate body (MGB), and auditory cortex. Additional inputs are shown for the thalamic reticular nucleus (TRN) and mesencephalic reticular formation (RF). Cortical layers are identified by Roman numerals. Excitatory synapses are indicated by open triangles; inhibitory synapses, by filled circles. A synaptic glomerulus is encircled in the MGB. *Adapted from de Ribaupierre.*[149] *B*, Anatomical reconstruction of a synaptic glomerulus. The dendritic process of an inhibitory interneuron is shaded to facilitate visualization of triadic circuitry involving the dendrite of the interneuron (I), the dendrite of a thalamic principal cell (P), and an ascending axonal fiber from the inferior colliculus (AF). Inset shows relative position of the MGB within the central auditory pathways. Additional abbreviations are explained in Figure 5–1. *Adapted with permission from Morest.*[150]

Basic Physiology

Principal cells in the ventral division are organized in frequency laminae that reflect the tonotopic projections of the ICC. Within each laminae, the neurons form clusters of cells with similar binaural interactions and integration bandwidths.[151] These functional gradients suggest that parallel streams of information from the midbrain remain segregated in the auditory thalamus.

Detailed comparisons of the existing descriptions of sound-driven activity in the MGB and ICC are made difficult by procedural differences in subject species, testing parameters, and anesthetic state. Although there may be noteworthy changes in specific response patterns, the two structures appear to share fundamental coding properties. Like neurons in the central nucleus, many neurons in the ventral division are tuned in frequency, level, and time. They tend to be activated by sound presentations to either ear, but show a preference for one ear. Low-frequency neurons respond to ITD information in binaural sounds; whereas, high-frequency neurons are sensitive to ILD cues. It is clear that many of these properties are passed to the MGB from the brainstem. How these representations are transformed by local inhibitory networks and modulated by cortical feedback remains a subject of intense scientific interest.[148]

Adaptive Filtering of Biological Signals

The effects of corticofugal feedback on sound processing have been investigated by recording single-unit activity in the ventral division of the MGB during reversible cortical inactivation. When large areas of AI are silenced by cryogenic blockade in anesthetized cats, neurons in the ventral division show decreased spontaneous rates, increased signal-to-noise ratios, and changes in frequency tuning.[152] The selectivity of frequency tuning expands in some neurons and compresses in others. The diversity of the effects of cortical inactivation suggest that corticothalamic projections may operate through direct excitatory influences as well as by suppressing local inhibitory influences via projections from the TRN.

Adaptive filtering may enhance the auditory processing of biologically relevant sounds. For example, the MGB of the mustached bat displays an exaggerated neural representation of frequencies that are most important in the species' biosonar signals. These responses can be increased in magnitude and sharpened

in their selectivity by stimulating matching frequency regions in auditory cortex. The effect is abolished by pharmacological blockade of cortical activity.[153]

Adaptive filtering is not only observed in specialized auditory systems, the magnitude of neural representations also may be modified by experience in more generalized listeners. When repeating tones are paired with noxious shocks, the frequency responses of central auditory neurons shift in frequency to produce an expanded reorganization of the fear-conditioned stimulus.[154] Pharmacological inactivation of auditory cortex abolishes the effect.[155]

Clinical Implication

Anatomical and functional abnormalities of the auditory thalamus have been implicated in language disorders that involve the inability to process rapidly changing speech sounds.[156] These temporal deficits have been related to aberrant thalamic anatomy by postmortem studies of dyslexic brains.[157] Although the MGB is bilaterally symmetrical in normal humans, the left MGB appears smaller in dyslexic brains because there are fewer large projection neurons. It is intriguing that the cortical target of the left MGB; ie, the left hemisphere of the cerebral cortex, is known to play a critical role in speech processing.[158]

Language impairments also have been linked to thalamic abnormalities by electrophysiological measures. Dyslexics show less mismatch negativity (MMN) when tested with rapid speech changes.[159] This electrical potential is evoked when the observer detects the presentation of a deviant stimulus in a repeating background. It is posited that dyslexics exhibit a reduced MMN because they cannot process the rapid change. Implanted electrodes in experimental animals have linked the MMN to activity in the extralemniscal divisions of the MGB.[160]

AUDITORY CORTEX

The auditory cortex receives all incoming sound representations from the thalamus. Whereas the separate subcortical structures are responsible for extracting specific features from acoustic stimuli, the auditory cortex must recombine these parallel information streams into integrated auditory percepts. These diverse perceptual behaviors include the discrimination of sound sources, localization of sound, recognition of voices, interpretation of sounds in a biological context, auditory memory, and training-induced plasticity. Much of our knowledge pertaining to the structure and function of the auditory cortex has been derived from studies in other species, with some of the most intriguing findings stemming from work in nonhuman primates. Given the limitations of experimental animals as a model system for the study of higher cognitive processes, our knowledge of human function has been significantly advanced by indirect measures of neural activity that can be applied to humans, particularly functional neuroimaging.

The technical difficulties of studying in vivo human auditory function are complicated by the broad heterogeneity of the auditory cortex, with its numerous areas and fields, each with their own distinctive anatomy and physiology. Many anatomical approaches have been utilized to define the subregions of the auditory cortex, including cytoarchitectonic and chemoarchitectonic methods, in addition to studies of fiber connectivity involved in thalamocortical, corticocortical, and corticofugal circuitry. Physiological studies based on receptive field properties, determination of BF (or characteristic frequencies), spectral bandwidth of target neurons, and temporal response qualities have also been utilized. As a result of these studies, it has become clearly established that a primary auditory field, often referred to as A1, exists in nearly all species, including humans. Beyond the A1, however, it has been difficult to establish uniform anatomical and functional criteria that are valid across species, or even across individuals of the same species.

Anatomy

The A1, constitutes the first stage of cortical processing for sound.[161] Much of what we know about the anatomy of A1 is based on work in primate models, especially monkeys, and therefore, some as of yet unidentified details may differ in humans. On a histological level, the A1 has several unique features of koniocortex, including densely packed small cells of layer 4, heavily myelinated fibers, and the presence of abundant cytochrome oxidase.[162] As stated earlier, it receives much of its input directly from the ventral subdivision of the thalamus.[163] Functionally, the neurons of the A1 tend to respond to pure tones well, with well-tuned BF ranges, and a tonotopic arrangement of isofrequency bands.[161]

Hackett and Kaas use the term *core* to describe primary or primary-like regions, which includes three areas (A1, rostral or R, and rostrotemporal or RT).[162] These areas appear to be activated in parallel, and each of these core subregions shows distinctive neural connections from other cortical areas. These three regions are organized caudo-rostrally along the plane of the lateral fissure, and have a tonotopic arrangement.[164] In humans, much of Heschl's gyrus (transverse temporal gyrus) consists of auditory core (Figure 5–17).

A cytoarchitecturally distinct *belt* of auditory cortex surrounds the centralized core. This region receives few inputs from the ventral thalamic nucleus (MGV), instead its main thalamic inputs originate in the dorsal (MGD) and medial (MGM) nuclei.[165–169] Neurons in the belt receive almost all of their auditory inputs from the core regions, and do not exhibit primary-like activity. A third *parabelt* region, just ventral to the belt, receives dense connections from the belt, but almost none from the core.[170] The parabelt receives thalamic inputs from the MGD and MGM, and cortical inputs from nonauditory regions adjacent to the superior temporal sulcus. This circuitry may play an important role in polysensory processing (audiovisual interactions). Additional prefrontal connections suggest a role in auditory memory and visuospatial representation.[164]

From the parabelt and belt regions, auditory signals are sent to a fourth level of neural processing within temporal, parietal, and frontal lobes. The implication of these relationships is that many areas of the brain, even those not strictly considered to be auditory processing centers, receive auditory inputs and are crucial for proper auditory processing. Polysensory interactions are critical here, and further work is needed to clarify the exact nature of the neural interactions between auditory and visual cortices. Furthermore, the role of homologous regions of the

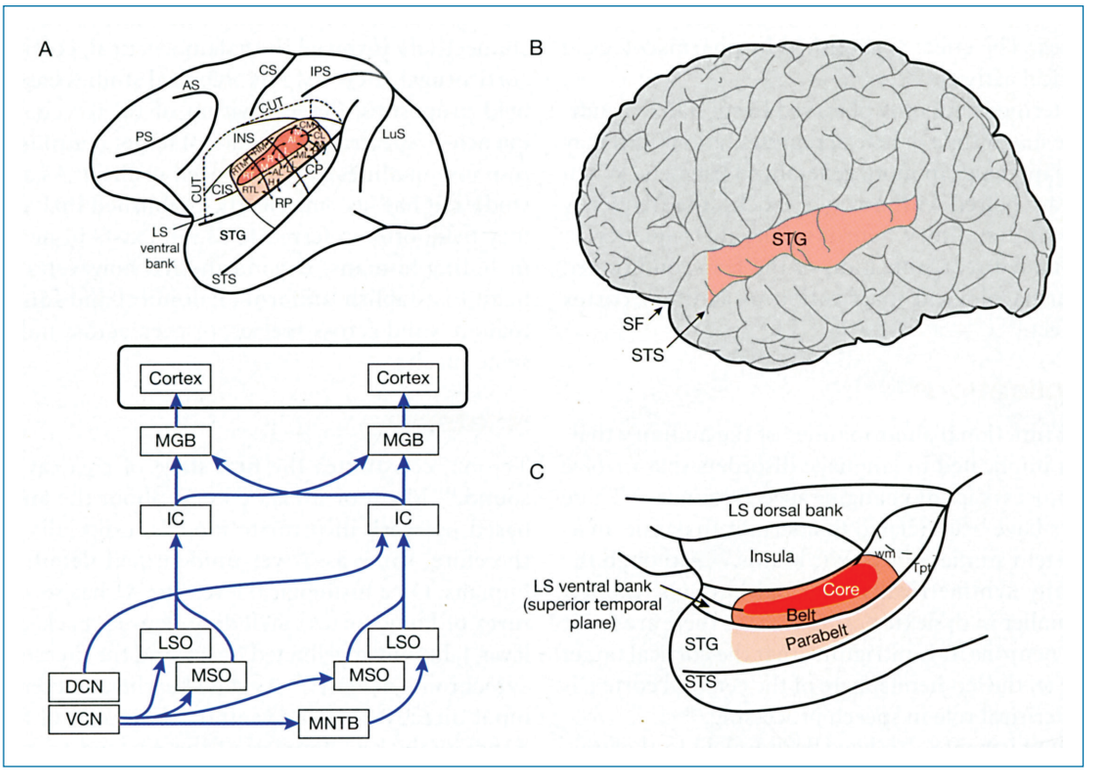

FIGURE 5–17 • *A*, Depiction of auditory cortical regions in the macaque monkey, showing the approximate locations of primary and secondary auditory regions along the left superior temporal plane. *B*, Schematic drawing of left lateral surface of the human brain, with the superior temporal gyrus outlined. The temporal lobe must be reflected laterally to see the contents that lie within the Sylvian fissure. *C*, Schematic drawing of the locations of core, belt and parabelt after reflection of the temporal lobe in primates. Inset shows relative position of the cortex within the central auditory pathways. Abbreviations are explained in Figure 5–1. *Adapted with permission from Hackett et al.,*[162] *Kaas and Hackett,*[171] *and Sweet et al.*[172]

brain connected by the corpus callosum is very poorly understood. In spite of these vagaries, it is the transfer of auditory information in this ascending fashion that ultimately allows humans to have conscious, cognitive perception of incoming auditory input.

Although the descriptions of auditory core, belt, and parabelt regions in monkeys are somewhat clear, our understanding of the human auditory system remains relatively poor, with recent functional imaging studies responsible for much of our current knowledge. In part, this limited understanding can be attributed to the difficulty of interpreting human lesion studies. It is clearly established that the human auditory cortex is concentrated along the superior temporal gyrus (Figure 5–18).

The superior temporal plane—which contains the planum polare, Heschl's gyrus, and planum temporale (from anterior to posterior)—appears to be the locus of the human auditory cortex. This region has notably high variation from person to person, and the parcellation of cortex into Brodmann areas may not apply very well. Within Brodmann's area 41, which corresponds to the anterior transverse temporal area (where A1 is located), a vertical columnar organization of auditory neurons appears to be present (referred to as Te1.1, Te1.0, and Te1.2 medial or posterior to lateral).[173]

As detailed in the first half of this chapter, a substantial amount of processing of auditory information takes place in the brainstem. Therefore, the auditory cortex receives "preprocessed" signals that are then further processed by the core, belt and parabelt regions. The A1 appears to be involved in auditory object identification, as well as integrating spectral and temporal qualities of sounds. Overall, our understanding of non-A1 is sparser in comparison to that of A1, in part due to the fact that most primate studies have utilized electrophysiologic techniques, while most human studies have utilized functional

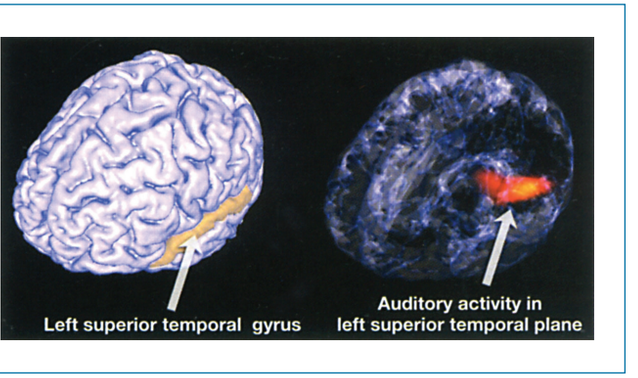

FIGURE 5–18 • Three-dimensional surface rendering of the human brain, showing the anatomical location of the left superior temporal gyrus (left side). Auditory activation within the left superior temporal plane revealed by functional MRI (right side).

neuroimaging methods. The latter approach has low temporal resolution and is complicated by the presence of loud scanner noise. For example, even establishing the exact parameters of the human tonotopic axis has been a challenge, since non-A1 responds weakly to pure tones, while A1 responds transiently. Studies using bandpass filtered stimuli with spectral variations strongly suggest that the human auditory cortex retains a tonotopic axis.[174–176]

The cortical processing of temporal information depends on the transmission rate of the information. In general, sounds can be subdivided into slow-rate (< 30 Hz) and fast-rate temporal structures (> 50 Hz). At slow rates, temporal information is coded directly by neural discharge rates. Both Heschl's gyrus and non-A1 are critical elements for the slow-rate modulations that are integral for processes such as speech envelope detection. At faster rates that outpace the frequency following capability of the neural response, other strategies must be used. Fast-rate (or fine) temporal structure occurs on the scale of milliseconds, and is relevant for issues such as ITDs (important for localization of sound) and important for perception of musical melodies. Several studies have examined how the brain responds to temporal variance of fast rates. Neural responses to regular-interval noise are stronger than for control noise, suggesting that high-frequency patterns trigger specific responses in the A1.[177,178]

It took until the latter half of the 19th century to reach consensus on the idea that sensorimotor functions could be localized to the cerebral cortex. In part, the reluctance to accept the idea of functional localization may have been a reaction to the misinformed theories of phrenologists, who localized sensorimotor function to the shape of the head. In 1861, a patient with expressive aphasia underwent a postmortem autopsy that revealed a left inferior frontal gyrus lesion in a region that has since been named Broca's area.[179] Damage to the posterior superior temporal gyrus in a region commonly referred to as Wernicke's area, leads to a receptive language deficit that is readily apparent clinically.[180] The concept of tonotopicity was identified in the mid 1900s,[181] and many early studies of the specific role of the auditory cortex for frequency discrimination were inconclusive. In 1975, it was discovered that bilateral auditory cortex lesions led to the loss of sound localization abilities.[33] Through a series of ablation experiments in which portions of the neocortex were surgically removed in macaque monkeys, it was determined that bilateral removal of the superior temporal gyrus led to immediate unresponsiveness to sound stimulation with delayed recovery after several months, while unilateral lesions led to contralateral deficits.[182–184] As described earlier, species-specific differences in auditory behavior and neural organization has impeded our understanding of auditory cortex. Critical questions concerning both normal and pathological mechanisms of hearing—remain unanswered.

The ultimate goal of neuroscience is to understand how the brain works. In relationship to the auditory system, the goal is to understand how the central and peripheral auditory systems are able to provide auditory cognition and accurate perception of auditory stimuli. To a certain extent, our current understanding has largely been shaped by approaches that subdivide the central nervous system into smaller subunits and examine the anatomy and physiology of each subunit. Consequently, we know a good deal more about each individual subunit than we do about how the numerous subunits interact with one another. Furthermore, we know relatively little about how the subunits of the auditory systems react with other sensory systems to provide an auditory percept that is correctly interpreted within a practical real-world context.

While it is undoubtedly helpful to break down the study of the auditory system into component features, such as A1 and secondary auditory cortex, this approach has intrinsic limitations that may never lead to a satisfying whole brain model of audition. The notion that auditory function can be specifically "localized" to a particular neuroanatomical region, as discussed briefly above, is likely to be a crude oversimplification. Yet, it is reasonable to consider the function of each subunit in order to be able to interpret how they function within an organic context. For these reasons, the utilization of broad methodologies is to be encouraged, and the development of whole brain mapping strategies, such as functional magnetic resonance imaging (fMRI), should provide important new information as to how auditory regions interact both to one another but perhaps more importantly, to nonauditory regions that ultimately place auditory information in a behavioral context. One of the clear benefits of fMRI is that information from diverse regions of the brain can be accrued simultaneously, allowing us to capture activity in regions of the brain for which we might not necessarily anticipate an obvious relationship to auditory perception. It is important to acknowledge that many classically "nonauditory" regions may play critical roles for the perception or production of complex sounds.

The "What" and "Where" Pathways

Based largely on the principles of parallel cortical processing streams present in the visual system, it has been suggested that auditory processing may possess a similar parallel structure. Specifically, an acoustic signal may be deconstructed during neural processing into separate components that can then be directed toward discrete neural substrates, thereby allowing for the parallel analysis of different aspects of the sound. These pathways have been described as the "what" and "where" pathways of sound, and have been proposed to relate to the identification of a sound's identity (what is it?) and localization of that sound (where is it?). Kraus and Nicol[185] argued that for spoken language, the identity of the speaker and the semantic meaning of the words contained in the spoken message could each be linked to separate brainstem responses that indicate the presence of a subcortical parcellation of information into separate streams akin to visual "what" and "where" processing. In the first behavioral study of the auditory "what" and "where" pathways, Lomber and Malhotra[186] applied the technique of reversible cooling deactivation to selective regions of the cat non-A1. In this study, they found that bilateral deactivation of the posterior auditory fields resulted in sound-localization deficits, while bilateral deactivation of the anterior auditory fields resulted in pattern-discrimination deficits only. These findings support the notion of parallel cortical processing streams within the auditory cortex.

Voice Recognition

In work that also stemmed from studies of facial recognition in the visual system, it has been demonstrated that the human voice is uniquely processed by the auditory system, and is in many ways comparable to an "auditory face" for which humans are specially geared to process and perceive. Given the critical importance of spoken language, these findings are not surprising, yet their demonstration over a series of elegant fMRI findings illustrates the power of these methods to study complex areas of human cognition. Belin et al.[187] reported the identification of voice-selective regions within bilateral STS of the auditory cortex (Figure 5–19). This study utilized fMRI during passive listening to vocal versus nonvocal environmental stimuli, and found greater activation of the STS during vocal stimulation. In addition, the central region of the STS displayed greater activation and selectivity for vocal sounds in comparison to scrambled voice or AM noise. In a follow-up study designed to explore affective/emotional components of vocal stimuli, referred to as paralinguistic vocal information, Belin et al.[188] used fMRI to examine differential responses to speech versus nonspeech vocalizations, and to explore the effect of frequency scrambling on cortical activation. They found that responses to speech versus nonspeech were greater throughout the auditory cortex (including A1) bilaterally, whereas A1 showed little attenuation when listening to frequency-scrambled stimuli as exhibited by the anterior STS. The authors also found that right anterior STS responses to nonspeech vocal sounds exceeded those in response to scrambled versions, suggesting that these regions might be responsible for perception of paralinguistic voice perception.

These human studies were recently confirmed in an fMRI study of monkeys by Petkov et al.,[189] which showed higher activation along the superior temporal plane during perception of species-specific vocalization than during non-species specific vocalizations, indicating that nonhuman primates also contain neural specializations for voice recognition. It should be emphasized that these specializations are different from (but related to) the nonauditory specializations that exist for language perception within the inferior frontal gyrus and inferior parietal lobule.

Nonprimary Pitch Centers

One of the basic elements of auditory processing is the ability to convert the fundamental frequency of a periodic signal into a subjective pitch. Pitch perception is an essential component of music and language perception, and several studies have recently identified the presence of neural centers devoted to the processing of pitch. In an fMRI study of individuals listening to pitches, melodies, and spectrally matched sounds without pitch, Patterson et al.[190] found that only the lateral portion of Heschl's gyrus was activated by pitch, and that the processing of melody recruited auditory neurons that were situated anterolaterally to Heschl's gyrus within the superior temporal gyrus and planum polare. A related study by Penagos et al.[191] utilized fMRI to assess brain activity in response to harmonic tone complexes where pitch varied, but not temporal regularity (ie, periodicity linked to pitch perception). The authors found that pitch information activated an area of non-A1 that overlapped the anterolateral end of Heschl's gyrus, These results suggest that pitch processing may be centered in non-A1.

Single-unit recordings of awake marmoset monkeys have described an area of auditory cortex near the anterolateral border of the A1 that exhibits a strong selectivity for the pitch of pure tones and harmonic tone complexes.[192] This finding extends the notion of a specialized pitch processing center residing outside the A1. Furthermore, the study demonstrates a high degree of congruence in the neural substrate for pitch processing among human and nonhuman primates.

Music Perception and Production

In many ways, the perception and production of music represents the pinnacle of auditory function. An enormously complex acoustic stimulus with an inherent abstractness of meaning is transformed into a unified auditory percept that provides an emotional experience for the listener. The mechanisms by which the brain is able to achieve this remarkable feat are far from understood, yet it is certainly reliant upon the basic auditory circuitry and processing mechanisms outlined throughout this chapter. Multimodal interactions between the brainstem, temporal lobe, and nonauditory centers transform sound into something that may be judged as beautiful or sublime.

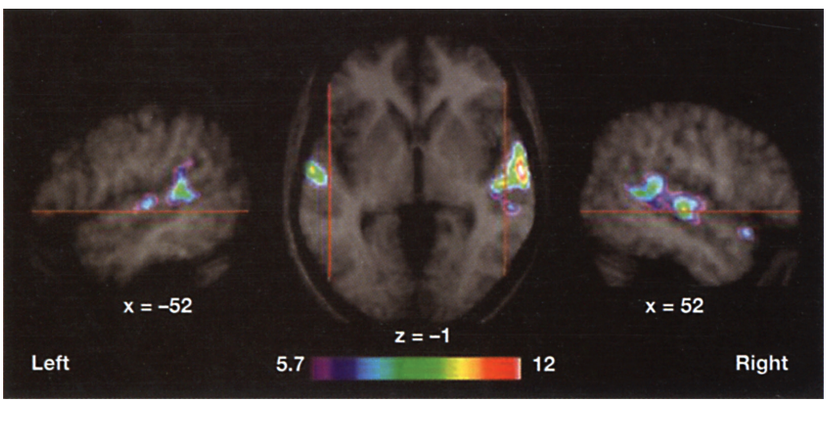

FIGURE 5–19 • Activation maps derived from functional MRI of volunteers listening to vocal stimuli. Activation clusters were identified by a contrast analysis of [Vocal] > [Nonvocal] stimuli. Significant activation along the upper bank of the superior temporal sulcus reveals voice-selective processing areas in human cortex. *Adapted with permission from Belin et al.*[187]

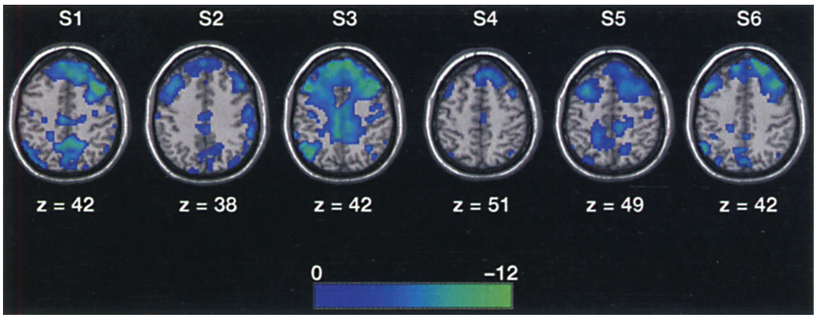

FIGURE 5–20 • Cortical deactivation within six pianists during spontaneous musical improvisation. All subjects show pronounced deactivation during improvisation in comparison to performance of memorized music. The broad region of deactivation is located within the prefrontal cortex, demonstrating the notion that complex auditory tasks show critical changes in nonauditory regions of the brain.

Music has persisted throughout all known historical epochs, and in all human cultures, even though it renders no clear survival benefit. It seems that the pleasure in producing and listening to music is sufficient justification for its persistence throughout history. By using music as a window into the brain, we can begin to understand numerous facets of brain function, under conditions as diverse as extended musical training (plasticity), instrumental performance (complex sensorimotor function), music induced emotion (limbic responses to sound), and spontaneous musical improvisation (neural mechanisms of creativity).

Over the past decade, it has become apparent that the human cortex is uniquely specialized for the processing of music. These observations vary from the hemispheric dominance of spectral versus temporal processing,[193] to links between language and music processing in Broca's area, and on to the detection of musical syntactic expectancies.[194,195] Music that is associated with strong emotional responses (described as "chills down the spine") elicits the same patterns of paralimbic activity that are commonly ascribed to the primitive substrates responsible for aversive or pleasurable reactions.[196] These observations underscore the fact that music, without additional sensory input, can induce changes in the extra-auditory regions that mediate the most basic of human impulses.

In a striking study of central auditory plasticity, Musacchia et al.[197] compared auditory brainstem responses of nonmusicians and highly trained musicians. Responses to speech and music suggest that musicians have earlier and more robust sound-evoked brain activity, superior phase-locking to periodic stimuli, and more sharply tuned temporal/frequency coding. This enhanced performance may be attributable to experience-based modifications of cortical processing that modify sound-driven activity in the brainstem by way of descending projections.

An fMRI study of jazz improvisation, a high level musical task of spontaneous creativity, has revealed unique patterns of brain activity in the prefrontal cortex of professional musicians (Figure 5–20).[198] Improvisation is associated with a focal increase in medial prefrontal activity, and a broad decrease in dorsolateral prefrontal activity. In addition, increased activity is seen in temporal cortices, where responses to simple auditory stimuli are not state dependent. These findings, which may reflect the neural signature of creativity, indicate that the whole brain is involved in the execution of multisensory processes that govern music perception and production.

Whitfield has suggested that the sensory cortices are a site for the formation of the concepts that facilitate the interpretation of external events.[199] In contrast to the auditory brainstem where features are extracted from complex sounds, the auditory cortex assembles these diverse streams of information into unified perceptual objects. The resulting higher-order transformations are shaped as much by a listener's experience, biological context, and behavioral state as they are by ascending sensory inputs. A challenge for future studies of the central auditory system is to move beyond neural representations of the physical dimensions of sound to explorations of the perceptual dimensions of human auditory experience. These questions may be best addressed by physiological approaches that define hearing as the global activity of the brain and not the isolated activity of its localized components.

References

1. Rhode WS, Greenburg S. Physiology of the cochlear nuclei. In: Popper AN, Fay RR, editors. The mammalian auditory pathway: Neurophysiology. New York: Springer-Verlag; 1992. p. 94–152.
2. Lorente de Nó R. The primary acoustic nuclei. New York: Raven Press; 1981.
3. Cant NB. The cochlear nucleus: Neuronal types and their synaptic organization. In: Webster DB, Popper AN, Fay RR, editors. The mammalian auditory pathway: Neuroanatomy. New York: Springer-Verlag; 1992. p. 66–116.
4. Rasmussen GL. Studies of the VIIIth cranial nerve of man. Laryngoscope 1940;50:67–83.
5. Osen KK. Cytoarchitecture of the cochlear nuclei in the cat. J Comp Neurol 1969;136:453–84.
6. Ryugo DK, Fekete DM. Morphology of primary axosomatic endings in the anteroventral cochlear nucleus of the cat: A study of the endbulbs of Held. J Comp Neurol 1982;210:239–57.
7. Held H. Die Cochlea der Säuger und der Vögel, ihre Entwicklung und ihr Bau. In: Bethe A, v Bergman G, Ellinger A, editors. Handbuch der Normalen und Pathologischen Physiologie. Berlin: Springer; 1926. p. 467–534.
8. Rhode WS, Oertel D, Smith PH. Physiological response properties of cells labeled intracellularly with horseradish peroxidase in cat ventral cochlear nucleus. J Comp Neurol 1983;213:448–63.
9. Rhode WS, Smith PH, Oertel D. Physiological response properties of cells labeled intracellularly with horseradish peroxidase in cat dorsal cochlear nucleus. J Comp Neurol 1983;213:426–47.

10. Pfeiffer RR. Classification of response patterns of spike discharges for units in the cochlear nucleus: Tone-burst stimulation. Exp Brain Res 1966;1:220–35.
11. Blackburn CC, Sachs MB. Classification of unit types in the anteroventral cochlear nucleus: PST histograms and regularity analysis. J Neurophysiol 1989;62:1303–29.
12. Rhode WS, Smith PH. Encoding timing and intensity in the ventral cochlear nucleus of the cat. J Neurophysiol 1986;56:261–86.
13. Smith PH, Joris PX, Carney LH, Yin TC. Projections of physiologically characterized globular bushy cell axons from the cochlear nucleus of the cat. J Comp Neurol 1991;304:387–407.
14. Tolbert LP, Morest DK. The neuronal architecture of the anteroventral cochlear nucleus of the cat in the region of the cochlear nerve root: Golgi and Nissl methods. Neuroscience 1982;7:3013–30.
15. Oertel D. Use of brain slices in the study of the auditory system: Spatial and temporal summation of synaptic inputs in cells in the anteroventral cochlear nucleus of the mouse. J Acoust Soc Am 1985;78:328–33.
16. Kane EC. Octopus cells in the cochlear nucleus of the cat: Heterotypic synapses upon homeotypic neurons. Int J Neurosci 1973;5:251–79.
17. Cant NB, Morest DK. The structural basis for stimulus coding in the cochlear nucleus of the cat. In: Berlin CI, editor. Hearing science. San Diego: College-Hill Press; 1984. p. 374–422.
18. Oertel D, Wu SH, Garb MW, Dizack C. Morphology and physiology of cells in slice preparations of the posteroventral cochlear nucleus of mice. J Comp Neurol 1990;295:136–54.
19. Doucet JR, Ryugo DK. Projections from the ventral cochlear nucleus to the dorsal cochlear nucleus in rats. J Comp Neurol 1997;385:245–64.
20. Doucet JR, Ross AT, Gillespie MB, Ryugo DK. Glycine immunoreactivity of multipolar neurons in the ventral cochlear nucleus which project to the dorsal cochlear nucleus. J Comp Neurol 1999;408:515–31.
21. May BJ, Prell GS, Sachs MB. Vowel representations in the ventral cochlear nucleus of the cat: Effects of level, background noise, and behavioral state. J Neurophysiol 1998;79:1755–67.
22. Young ED, Shofner WP, White JA, Robert J-M, Voigt HF. Response properties of cochlear nucleus neurons in relationship to physiological mechanisms. In: Edelman GM, Gall WE, Cowan WM, editors. Auditory function: neurobiological bases of hearing. New York: John Wiley & Sons; 1988. p. 277–312.
23. Kim DO, Molnar CE. A population study of cochlear nerve fibers: Comparison of spatial distributions of average-rate and phase-locking measures of responses to single tones. J Neurophysiol 1979;42:16–30.
24. Sachs MB, Young ED. Encoding of steady-state vowels in the auditory nerve: Representation in terms of discharge rate. J Acoust Soc Am 1979;66:470–9.
25. Peterson GE, Barney HL. Control methods used in the study of the vowels. J Acoust Soc Am 1952;24:175–84.
26. Le Prell GS, Sachs MB, May BJ. Representation of vowel-like spectra by discharge rate responses of individual auditory-nerve fibers. Aud Neurosci 1996;2:275–88.
27. Blackburn CC, Sachs MB. The representations of the steady-state vowel sound /e/ in the discharge patterns of cat anteroventral cochlear nucleus neurons. J Neurophysiol 1990;63:1191–212.
28. Wang X, Sachs MB. Transformation of temporal discharge patterns in a ventral cochlear nucleus stellate cell model: implications for physiological mechanisms. J Neurophysiol 1995;73:1600–16.
29. Davis M, Gendelman DS, Tischler MD, Gendelman PM. A primary acoustic startle circuit: Lesion and stimulation studies. J Neurosci 1982;2:791–805.
30. Berker EA, Berker AH, Smith A. Translation of Broca's 1865 report. Localization of speech in the third left frontal convolution. Arch Neurol 1986;43:1065–72.
31. Heil P. Neuronal coding of interaural transient envelope disparities. Eur J Neurosci 1998;10:2831–47.
32. Wernicke K. The aphasia symptom complex: A psychological study on an anatomical basis. The Hague: Mouton; 1874.
33. Casseday JH, Neff WD. Auditory localization: Role of auditory pathways in brain stem of the cat. J Neurophysiol 1975; 38:842–58.
34. Masterton RB, Granger EM, Glendenning KK. Role of acoustic striae in hearing: Mechanism for enhancement of sound detection in cats. Hear Res 1994;73:209–22.
35. Ryugo DK, Pongstaporn T, Huchton DM, Niparko JK. Ultrastructural analysis of primary endings in deaf white cats: Morphologic alterations in endbulbs of Held. J Comp Neurol 1997;385:230–44.
36. Ryugo DK, Kretzmer EA, Niparko JK. Restoration of auditory nerve synapses in cats by cochlear implants. Science 2005;310:1490–2.
37. Young ED, Davis KA. Circuitry and function of the dorsal cochlear nucleus. In: Oertel D, Fay RR, Popper AN, editors. Integrative functions in the mammalian auditory pathway. New York: Springer-Verlag; 2002. p. 160–206.
38. Adams JC, Warr WB. Origins of axons in the cat's acoustic striae determined by injection of horseradish peroxidase into severed tracts. J Comp Neurol 1976;170:107–21.
39. Kanold PO, Young ED. Proprioceptive information from the pinna provides somatosensory input to cat dorsal cochlear nucleus. J Neurosci 2001;21:7848–58.
40. Manis PB. Responses to parallel fiber stimulation in the guinea pig dorsal cochlear nucleus in vitro. J Neurophysiol 1989;61:149–61.
41. Spirou GA, May BJ, Wright DD, Ryugo DK. Frequency organization of the dorsal cochlear nucleus in cats. J Comp Neurol 1993;329:36–52.
42. Kane ES, Puglisi SG, Gordon BS. Neuronal types in the deep dorsal cochlear nucleus of the cat: I. Giant neurons. J Comp Neurol 1981;198:483–513.
43. Musicant AD, Chan JC, Hind JE. Direction-dependent spectral properties of cat external ear: New data and cross-species comparisons. J Acoust Soc Am 1990;87:757–81.
44. Rice JJ, May BJ, Spirou GA, Young ED. Pinna-based spectral cues for sound localization in cat. Hear Res 1992;58:132–52.
45. Huang AY, May BJ. Sound orientation behavior in cats. II. Mid-frequency spectral cues for sound localization. J Acoust Soc Am 1996;100:1070–80.
46. Young ED, Rice JJ, Spirou GA, Nelken I, Conley RA. Head-related transfer functions in cat: Neural representation and the effects of pinna movement. In: Gilkey RH, Anderson TR, editors. Binaural and spatial hearing in real and virtual environments. Mahwah, NJ: Lawrence Erlbaum Assoc; 1997. p. 475–98.
47. Yu JJ, Young ED. Linear and nonlinear pathways of spectral information transmission in the cochlear nucleus. Proc Natl Acad Sci U S A 2000;97:11780–6.
48. Sutherland DP, Masterton RB, Glendenning KK. Role of acoustic striae in hearing: Reflexive responses to elevated sound-sources. Behav Brain Res 1998;97:1–12.

49. May BJ. Role of the dorsal cochlear nucleus in the sound localization behavior of cats. Hear Res 2000;148:74–87.
50. Kaltenbach JA. Summary of evidence pointing to a role of the dorsal cochlear nucleus in the etiology of tinnitus. Acta Otolaryngol Suppl 2006;556:20–6.
51. Brozoski TJ, Bauer CA, Caspary DM. Elevated fusiform cell activity in the dorsal cochlear nucleus of chinchillas with psychophysical evidence of tinnitus. J Neurosci 2002;22:2383–90.
52. Kaltenbach JA, Afman CE. Hyperactivity in the dorsal cochlear nucleus after intense sound exposure and its resemblance to tone-evoked activity: A physiological model for tinnitus. Hear Res 2000;140:165–72.
53. Bartels H, Staal MJ, Albers FW. Tinnitus and neural plasticity of the brain. Otol Neurotol 2007;28:178–84.
54. Saunders JC. The role of central nervous system plasticity in tinnitus. J Commun Disord 2007;40:313–34.
55. Melcher JR, Sigalovsky IS, Guinan JJ Jr, Levine RA. Lateralized tinnitus studied with functional magnetic resonance imaging: abnormal inferior colliculus activation. J Neurophysiol 2000;83:1058–72.
56. Eggermont JJ. On the pathophysiology of tinnitus; a review and a peripheral model. Hear Res 1990;48:111–23.
57. Ramon Y Cajal S. English translation of new ideas on the structure of the nervous system in man and vetebrates, 1894. Cambridge, MA: The MIT Press; 1990.
58. Scheibel ME, Scheibel AB. Neuropil organization in the superior olive of the cat. Exp Neurol 1974;43:339–348.
59. Guinan JJ, Norris BE, Guinan SS. Single auditory units in the superior olivary complex. II: Locations of unit categories and tonotopic organization. Int J Neurosci 1972;4:147–166.
60. Cant NB, Casseday JH. Projections from the anteroventral cochlear nucleus to the lateral and medial superior olivary nuclei. J Comp Neurol 1986;247:457–76.
61. Smith PH, Joris PX, Yin TC. Projections of physiologically characterized spherical bushy cell axons from the cochlear nucleus of the cat: Evidence for delay lines to the medial superior olive. J Comp Neurol 1993;331:245–60.
62. Tsuchitani C, Boudreau JC. Single unit analysis of cat superior olive S segment with tonal stimuli. J Neurophysiol 1966;29:684–97.
63. Rose JE, Brugge JF, Anderson DJ, Hind JE. Phase-locked response to low-frequency tones in single auditory nerve fibers of the squirrel monkey. J Neurophysiol 1967;30:769–93.
64. Smith AJ, Owens S, Forsythe ID. Characterisation of inhibitory and excitatory postsynaptic currents of the rat medial superior olive. J Physiol 2000;529 (Pt 3):681–98.
65. Cant NB, Hyson RL. Projections from the lateral nucleus of the trapezoid body to the medial superior olivary nucleus in the gerbil. Hear Res 1992;58:26–34.
66. Pecka M, Brand A, Behrend O, Grothe B. Interaural time difference processing in the mammalian medial superior olive: The role of glycinergic inhibition. J Neurosci 2008;28:6914–25.
67. Aitkin L, Schuck D. Low frequency neurons in the lateral central nucleus of the cat inferior colliculus receive their input predominantly from the medial superior olive. Hear Res 1985;17:87–93.
68. Adams JC. Ascending projections to the inferior colliculus. J Comp Neurol 1979;183:519–38.
69. Goldberg JM, Brown PB. Response of binaural neurons of dog superior olivary complex to dichotic tonal stimuli: Some physiological mechanisms of sound localization. J Neurophysiol 1969;32:613–36.
70. Jeffress LA. A place theory of sound localization. J Comp Physiol Psychol 1941;41:35–9.
71. Carr CE, Konishi M. A circuit for detection of interaural time differences in the brain stem of the barn owl. J Neurosci 1990;10:3227–46.
72. Joris PX, Smith PH, Yin TC. Coincidence detection in the auditory system: 50 years after Jeffress. Neuron 1998;21:1235–8.
73. Mills AW. On the minimum audible angle. J Acoust Soc Am 1958;30:237–46.
74. Helfert RH, Juiz JM, Bledsoe SC Jr, Bonneau JM, Wenthold RJ, Altschuler RA. Patterns of glutamate, glycine, and GABA immunolabeling in four synaptic terminal classes in the lateral superior olive of the guinea pig. J Comp Neurol 1992;323:305–25.
75. Barnes-Davies M, Forsythe ID. Pre- and postsynaptic glutamate receptors at a giant excitatory synapse in rat auditory brainstem slices. J Physiol 1995;488 (Pt 2):387–406.
76. Helfert RH, Bonneau JM, Wenthold RJ, Altschuler RA. GABA and glycine immunoreactivity in the guinea pig superior olivary complex. Brain Res 1989;501:269–86.
77. Yin TCT. Neural mechanisms of encoding binaural localization cues in the auditory brainstem. In: Oertel D, Fay RR, Popper AN, editors. Integrative functions in the mammalian auditory pathway. New York: Springer; 2002. p. 99–159.
78. Spangler KM, Warr WB, Henkel CK. The projections of principal cells of the medial nucleus of the trapezoid body in the cat. J Comp Neurol 1985;238:249–62.
79. Joris PX, Yin TCT . Envelope coding in the lateral superior olive. I. Sensitivity to interaural time differences. J Neurophysiol 1995;73:1043–1062.
80. Tollin DJ, Koka K, Tsai JJ. Interaural level difference discrimination thresholds for single neurons in the lateral superior olive. J Neurosci 2008;28:4848–60.
81. Glendenning KK, Masterton RB. Acoustic chiasm: Efferent projections of the lateral superior olive. J Neurosci 1983;3:1521–37.
82. Oliver DL, Shneiderman A. An EM study of the dorsal nucleus of the lateral lemniscus: Inhibitory, commissural, synaptic connections between ascending auditory pathways. J Neurosci 1989;9:967–82.
83. Glendenning KK, Baker BN, Hutson KA, Masterton RB. Acoustic chiasm V: Inhibition and excitation in the ipsilateral and contralateral projections of LSO. J Comp Neurol 1992;319:100–22.
84. Saint Marie RL, Ostapoff EM, Morest DK, Wenthold RJ. Glycine-immunoreactive projection of the cat lateral superior olive: possible role in midbrain ear dominance. J Comp Neurol 1989;279:382–96.
85. Helfert RH, Aschoff A. Superior olivary complex and nuclei of the lateral lemniscus. In: Ehret G, Romand R, editors. The central auditory system. New York: Oxford University Press; 1997. p. 193–258.
86. Jenkins WM, Masterton RB. Sound localization: Effects of unilateral lesions in central auditory system. J Neurophysiol 1982;47:987–1016.
87. White JS, Warr WB. The dual origins of the olivocochlear bundle in the albino rat. J Comp Neurol 1983;219:203–14.
88. Brown MC, Liberman MC, Benson TE, Ryugo DK. Brainstem branches from olivocochlear axons in cats and rodents. J Comp Neurol 1988;278:591–603.
89. Warr WB. Organization of olivocochlear efferent systems in mammals. In: Webster WB, Popper AN, Fay RR, editors. The mammalian auditory pathway: Neuroanatomy. New York: Springer. p. 410–448.

90. Galambos R. Suppression of auditory nerve activity by stimulation of efferent fibers to cochlea. J Neurophysiol 1956;19:424–37.
91. Wiederhold ML, Kiang NY. Effects of electric stimulation of the crossed olivocochlear bundle on single auditory-nerve fibers in the cat. J Acoust Soc Am 1970;48:950–65.
92. Fuchs PA, Murrow BW. Cholinergic inhibition of short (outer) hair cells of the chick's cochlea. J Neurosci 1992;12:800–9.
93. Brownell WE, Bader CR, Bertrand D, de Ribaupierre Y. Evoked mechanical responses of isolated cochlear outer hair cells. Science 1985;227:194–6.
94. Winslow RL, Sachs MB. Effect of electrical stimulation of the crossed olivocochlear bundle on auditory nerve response to tones in noise. J Neurophysiol 1987;57:1002–21.
95. Chays A, Maison S, Robaglia-Schlupp A, Cau P, Broder L, Magnan J. [Are we sectioning the cochlear efferent system during vestibular neurotomy?] Rev Laryngol Otol Rhinol (Bord) 2003;124:53–8.
96. Scharf B, Magnan J, Chays A. On the role of the olivocochlear bundle in hearing: 16 case studies. Hear Res 1997;103:101–22.
97. Micheyl C, Collet L. Involvement of the olivocochlear bundle in the detection of tones in noise. J Acoust Soc Am 1996; 99:1604–10.
98. Rajan R. Effect of electrical stimulation of the crossed olivocochlear bundle on temporary threshold shifts in auditory sensitivity. II. Dependence on the level of temporary threshold shifts. J Neurophysiol 1988;60:569–79.
99. Maison SF, Liberman MC. Predicting vulnerability to acoustic injury with a noninvasive assay of olivocochlear reflex strength. J Neurosci 2000;20:4701–7.
100. Moller AR, Moller MB, Yokota M. Some forms of tinnitus may involve the extralemniscal auditory pathway. Laryngoscope 1992;102:1165–71.
101. Oliver DL, Morest DK. The central nucleus of the inferior colliculus in the cat. J Comp Neurol 1984;222:237–64.
102. Merzenich MM, Reid MD. Representation of the cochlea within the inferior colliculus of the cat. Brain Res 1974;77:397–415.
103. Winer JA, Saint Marie RL, Larue DT, Oliver DL. GABAergic feedforward projections from the inferior colliculus to the medial geniculate body. Proc Natl Acad Sci U S A 1996;93:8005–10.
104. Oliver DL, Winer JA, Beckius GE, Saint Marie RL. Morphology of GABAergic neurons in the inferior colliculus of the cat. J Comp Neurol 1994;340:27–42.
105. Loftus WC, Bishop DC, Saint Marie RL, Oliver DL. Organization of binaural excitatory and inhibitory inputs to the inferior colliculus from the superior olive. J Comp Neurol 2004;472:330–44.
106. Oliver DL, Beckius GE, Bishop DC, Kuwada S. Simultaneous anterograde labeling of axonal layers from lateral superior olive and dorsal cochlear nucleus in the inferior colliculus of cat. J Comp Neurol 1997;382:215–29.
107. Morest DK, Oliver DL. The neuronal architecture of the inferior colliculus in the cat: Defining the functional anatomy of the auditory midbrain. J Comp Neurol 1984;222:209–36.
108. Andersen RA, Knight PL, Merzenich MM. The thalamocortical and corticothalamic connections of AI, AII, and the anterior auditory field (AAF) in the cat: Evidence for two largely segregated systems of connections. J Comp Neurol 1980;194:663–701.
109. Aitkin LM, Phillips SC. The interconnections of the inferior colliculi through their commissure. J Comp Neurol 1984;228:210–16.
110. Malmierca MS, Le Beau FE, Rees A. The topographical organization of descending projections from the central nucleus of the inferior colliculus in guinea pig. Hear Res 1996;93:167–80.
111. Aitkin LM, Kenyon CE, Philpott P. The representation of the auditory and somatosensory systems in the external nucleus of the cat inferior colliculus. J Comp Neurol 1981;196:25–40.
112. King AJ, Jiang ZD, Moore DR. Auditory brainstem projections to the ferret superior colliculus: Anatomical contribution to the neural coding of sound azimuth. J Comp Neurol 1998;390:342–65.
113. Ramachandran R, Davis KA, May BJ. Single-unit responses in the inferior colliculus of decerebrate cats. I. Classification based on frequency response maps. J Neurophysiol 1999;82:152–63.
114. Ramachandran R, May BJ. Functional segregation of ITD sensitivity in the inferior colliculus of decerebrate cats. J Neurophysiol 2002;88:2251–61.
115. Davis KA. Evidence of a functionally segregated pathway from dorsal cochlear nucleus to inferior colliculus. J Neurophysiol 2002;87:1824–35.
116. Le Beau FE, Rees A, Malmierca MS. Contribution of GABA- and glycine-mediated inhibition to the monaural temporal response properties of neurons in the inferior colliculus. J Neurophysiol 1996;75:902–19.
117. Heffner RS, Heffner HE. Sound localization in a predatory rodent, the northern grasshopper mouse (Onychomys leucogaster). J Comp Psychol 1988;102:66–71.
118. Aitkin L. The auditory midbrain: Structure and function in the central auditory pathway. Clifton, NJ: Humana Press; 1986.
119. Semple MN, Aitkin LM. Physiology of pathway from dorsal cochlear nucleus to inferior colliculus revealed by electrical and auditory stimulation. Exp Brain Res 1980;41:19–28.
120. Rees A, Moller AR. Responses of neurons in the inferior colliculus of the rat to AM and FM tones. Hear Res 1983;10:301–30.
121. Rees A, Moller AR. Stimulus properties influencing the responses of inferior colliculus neurons to amplitude-modulated sounds. Hear Res 1987;27:129–43.
122. Rose JE, Gross NB, Geisler CD, Hind JE. Some neural mechanisms in the inferior colliculus of the cat which may be relevant to localization of a sound source. J Neurophysiol 1966;29: 288–314.
123. Yin TC, Kuwada S. Binaural interaction in low-frequency neurons in inferior colliculus of the cat. III. Effects of changing frequency. J Neurophysiol 1983;50:1020–42.
124. McAlpine D, Jiang D, Shackleton TM, Palmer AR. Convergent input from brainstem coincidence detectors onto delay-sensitive neurons in the inferior colliculus. J Neurosci 1998;18: 6026–39.
125. Palmer AR, Kuwada S. Binaural and spatial coding in the inferior colliculus. In: Winer JA, Schreiner CE, editors. The inferior colliculus. New York: Springer; 2005. p. 377–410.
126. May BJ, Anderson M, Roos M. The role of broadband inhibition in the rate representation of spectral cues for sound localization in the inferior colliculus. Hear Res 2008;238:77–93.
127. Masterton RB, Jane JA, Diamond IT. Role of brainstem auditory structures in sound localization. I. Trapezoid body, superior olive, and lateral lemniscus. J Neurophysiol 1967;30:341–59.
128. Moore CN, Casseday JH, Neff WD. Sound localization: The role of the commissural pathways of the auditory system of the cat. Brain Res 1974;82:13–26.
129. Masterton RB. Neurobehavioral studies of the central auditory system. Ann Otol Rhinol Laryngol Suppl 1997;168:31–4.

130. Caspary DM, Milbrandt JC, Helfert RH. Central auditory aging: GABA changes in the inferior colliculus. Exp Gerontol 1995;30:349–60.
131. Caspary DM, Ling L, Turner JG, Hughes LF. Inhibitory neurotransmission, plasticity and aging in the mammalian central auditory system. J Exp Biol 2008;211:1781–91.
132. Bauer CA, Brozoski TJ, Holder TM, Caspary DM. Effects of chronic salicylate on GABAergic activity in rat inferior colliculus. Hear Res 2000;147:175–82.
133. Mossop JE, Wilson MJ, Caspary DM, Moore DR. Down-regulation of inhibition following unilateral deafening. Hear Res 2000;147:183–7.
134. Faingold CL. Role of GABA abnormalities in the inferior colliculus pathophysiology—audiogenic seizures. Hear Res 2002;168:223–37.
135. Bauer CA, Turner JG, Caspary DM, Myers KS, Brozoski TJ. Tinnitus and inferior colliculus activity in chinchillas related to three distinct patterns of cochlear trauma. J Neurosci Res 2008;86:2564–78.
136. Gerken GM. Central tinnitus and lateral inhibition: An auditory brainstem model. Hear Res 1996;97:75–83.
137. Meikle MB, Vernon J, Johnson RM. The perceived severity of tinnitus. Some observations concerning a large population of tinnitus clinic patients. Otolaryngol Head Neck Surg 1984;92:689–96.
138. Jastreboff PJ, Sasaki CT. An animal model of tinnitus: A decade of development. Am J Otol 1994;15:19–27.
139. Brozoski TJ, Spires TJ, Bauer CA. Vigabatrin, a GABA transaminase inhibitor, reversibly eliminates tinnitus in an animal model. J Assoc Res Otolaryngol 2007;8:105–18.
140. Rioch DM. Studies on the diencephalon of carnivora. Part 1. The nuclear configuration of the thalamus, epithalamus, and hypothalamus of the dog and cat. J Comp Neurol 1929;49:1–119.
141. Morest DK. The neuronal architecture of the medial geniculate body of the cat. J Anat 1964;98:611–30.
142. Andersen RA, Roth GL, Aitkin LM, Merzenich MM. The efferent projections of the central nucleus and the pericentral nucleus of the inferior colliculus in the cat. J Comp Neurol 1980;194:649–62.
143. Winer JA, Diamond IT, Raczkowski D. Subdivisions of the auditory cortex of the cat: The retrograde transport of horseradish peroxidase to the medial geniculate body and posterior thalamic nuclei. J Comp Neurol 1977;176:387–417.
144. Jones EG, Rockel AJ. The synaptic organization in the medial geniculate body of afferent fibres ascending from the inferior colliculus. Z Zellforsch Mikrosk Anat 1971;113:44–66.
145. Schwarz DW, Tennigkeit F, Puil E. Metabotropic transmitter actions in auditory thalamus. Acta Otolaryngol 2000;120:251–4.
146. Rouiller EM, Colomb E, Capt M, De Ribaupierre F. Projections of the reticular complex of the thalamus onto physiologically characterized regions of the medial geniculate body. Neurosci Lett 1985;53:227–32.
147. Houser CR, Vaughn JE, Barber RP, Roberts E. GABA neurons are the major cell type of the nucleus reticularis thalami. Brain Res 1980;200:341–54.
148. Suga N, Zhang Y, Yan J. Sharpening of frequency tuning by inhibition in the thalamic auditory nucleus of the mustached bat. J Neurophysiol 1997;77:2098–114.
149. De Ribaupierre F. Acoustical information processing in the auditory thalamus and cerebral cortex. In: Ehret G, Romand R, editors. The central auditory system. New York: Oxford University Press; 1997. p. 317–397.
150. Morest DK. Synaptic relationships of Golgi type II cells in the medial geniculate body of the cat. J Comp Neurol 1975;162:157–193.
151. Rodrigues-Dagaeff C, Simm G, De Ribaupierre Y, Villa A, De Ribaupierre F, Rouiller EM. Functional organization of the ventral division of the medial geniculate body of the cat: Evidence for a rostro-caudal gradient of response properties and cortical projections. Hear Res 1989;39:103–25.
152. Villa AE, Rouiller EM, Simm GM, Zurita P, de Ribaupierre Y, de Ribaupierre F. Corticofugal modulation of the information processing in the auditory thalamus of the cat. Exp Brain Res 1991;86:506–17.
153. Zhang Y, Suga N. Modulation of responses and frequency tuning of thalamic and collicular neurons by cortical activation in mustached bats. J Neurophysiol 2000;84:325–33.
154. Gao E, Suga N. Experience-dependent corticofugal adjustment of midbrain frequency map in bat auditory system. Proc Natl Acad Sci U S A 1998;95:12663–70.
155. Gao E, Suga N. Experience-dependent plasticity in the auditory cortex and the inferior colliculus of bats: Role of the corticofugal system. Proc Natl Acad Sci U S A 2000;97:8081–6.
156. Tallal P. Auditory temporal perception, phonics, and reading disabilities in children. Brain Lang 1980;9:182–98.
157. Galaburda AM, Menard MT, Rosen GD. Evidence for aberrant auditory anatomy in developmental dyslexia. Proc Natl Acad Sci U S A 1994;91:8010–13.
158. Wada JA, Clarke R, Hamm A. Cerebral hemispheric asymmetry in humans. Cortical speech zones in 100 adults and 100 infant brains. Arch Neurol 1975;32:239–46.
159. Kraus N, McGee TJ, Carrell TD, Zecker SG, Nicol TG, Koch DB. Auditory neurophysiologic responses and discrimination deficits in children with learning problems. Science 1996;273:971–3.
160. Kraus N, McGee T, Littman T, Nicol T, King C. Nonprimary auditory thalamic representation of acoustic change. J Neurophysiol 1994;72:1270–7.
161. Luethke LE, Krubitzer LA, Kaas JH. Cortical connections of electrophysiologically and architectonically defined subdivisions of auditory cortex in squirrels. J Comp Neurol 1988;268:181–203.
162. Hackett TA, Preuss TM, Kaas JH. Architectonic identification of the core region in auditory cortex of macaques, chimpanzees, and humans. J Comp Neurol 2001;441:197–222.
163. Kaas JH, Hackett TA, Tramo MJ. Auditory processing in primate cerebral cortex. Current opinion in neurobiology 1999;9:164–70.
164. Hackett TA, Stepniewska I, Kaas JH. Prefrontal connections of the parabelt auditory cortex in macaque monkeys. Brain Res 1999;817:45–58.
165. Imig TJ, Ruggero MA, Kitzes LM, Javel E, Brugge JF. Organization of auditory cortex in the owl monkey (Aotus trivirgatus). J Comp Neurol 1977;171:111–28.
166. Merzenich MM, Brugge JF. Representation of the cochlear partition of the superior temporal plane of the macaque monkey. Brain Res 1973;50:275–96.
167. Morel A, Garraghty PE, Kaas JH. Tonotopic organization, architectonic fields, and connections of auditory cortex in macaque monkeys. J Comp Neurol 1993;335:437–59.
168. Morel A, Kaas JH. Subdivisions and connections of auditory cortex in owl monkeys. J Comp Neurol 1992;318:27–63.

169. Rauschecker JP, Tian B, Hauser M. Processing of complex sounds in the macaque nonprimary auditory cortex. Science 1995;268:111–14.
170. Hackett TA, Stepniewska I, Kaas JH. Subdivisions of auditory cortex and ipsilateral cortical connections of the parabelt auditory cortex in macaque monkeys. J Comp Neurol 1998;394:475–95.
171. Kaas JH, Hackett TA. Subdivisions of auditory cortex and levels of processing in primates. Audiol Neurootol 1998;3:73–85.
172. Sweet RA, Dorph-Petersen KA, Lewis DA. Mapping auditory core, lateral belt, and parabelt cortices in the human superior temporal gyrus. J Comp Neurol 2005;491:270–289.
173. Morosan P, Rademacher J, Schleicher A, Amunts K, Schormann T, Zilles K. Human primary auditory cortex: cytoarchitectonic subdivisions and mapping into a spatial reference system. NeuroImage 2001;13:684–701.
174. Schonwiesner M, von Cramon DY, Rubsamen R. Is it tonotopy after all? Neuroimage 2002;17:1144–61.
175. Talavage TM, Ledden PJ, Benson RR, Rosen BR, Melcher JR. Frequency-dependent responses exhibited by multiple regions in human auditory cortex. Hear Res 2000;150:225–44.
176. Talavage TM, Sereno MI, Melcher JR, Ledden PJ, Rosen BR, Dale AM. Tonotopic organization in human auditory cortex revealed by progressions of frequency sensitivity. J Neurophysiol 2004;91:1282–96.
177. Griffiths TD, Buchel C, Frackowiak RS, Patterson RD. Analysis of temporal structure in sound by the human brain. Nat Neurosci 1998;1:422–7.
178. Griffiths TD, Uppenkamp S, Johnsrude I, Josephs O, Patterson RD. Encoding of the temporal regularity of sound in the human brainstem. Nat Neurosci 2001;4:633–7.
179. Broca P. Remarks on the seat of the faculty of articulate language, followed by an observation of aphema. Bulletin de la societe anatomique de Paris 1861;6:330–57.
180. James W. The principles of psychology. New York: Henry Holt; 1890.
181. Woolsey CN. Organization of cortical auditory system: A review and a synthesis. In: Rasmussen GL, Windle WF, editors. Neural mechanisms of the auditory and vestibular systems. Springfield, IL: Charles C. Thomas; 1960. p. 165–80.
182. Heffner HE, Heffner RS. Unilateral auditory cortex ablation in macaques results in a contralateral hearing loss. J Neurophysiol 1989;62:789–801.
183. Heffner HE, Heffner RS. Effect of restricted cortical lesions on absolute thresholds and aphasia-like deficits in Japanese macaques. Behav Neurosc 1989;103:158–69.
184. Heffner HE, Heffner RS. Cortical deafness cannot account for the inability of Japanese macaques to discriminate species-specific vocalizations. Brain Lang 1989;36:275–85.
185. Kraus N, Nicol T. Brainstem origins for cortical "what" and "where" pathways in the auditory system. Trends Neurosci 2005;28:176–81.
186. Lomber SG, Malhotra S. Double dissociation of "what" and "where" processing in auditory cortex. Nat Neurosci 2008;11:609–16.
187. Belin P, Zatorre RJ, Lafaille P, Ahad P, Pike B. Voice-selective areas in human auditory cortex. Nature 2000;403:309–12.
188. Belin P, Zatorre RJ, Ahad P. Human temporal-lobe response to vocal sounds. Brain Res 2002;13:17–26.
189. Petkov CI, Kayser C, Steudel T, Whittingstall K, Augath M, Logothetis NK. A voice region in the monkey brain. Nat Neurosci 2008;11:367–74.
190. Patterson RD, Uppenkamp S, Johnsrude IS, Griffiths TD. The processing of temporal pitch and melody information in auditory cortex. Neuron 2002;36:767–76.
191. Penagos H, Melcher JR, Oxenham AJ. A neural representation of pitch salience in nonprimary human auditory cortex revealed with functional magnetic resonance imaging. J Neurosci 2004;24:6810–15.
192. Bendor D, Wang X. The neuronal representation of pitch in primate auditory cortex. Nature 2005;436:1161–5.
193. Zatorre RJ, Belin P. Spectral and temporal processing in human auditory cortex. Cereb Cortex 2001;11:946–53.
194. Koelsch S. Significance of Broca's area and ventral premotor cortex for music-syntactic processing. Cortex 2006;42:518–20.
195. Maess B, Koelsch S, Gunter TC, Friederici AD. Musical syntax is processed in Broca's area: An MEG study. Nat Neurosci 2001;4:540–5.
196. Blood AJ, Zatorre RJ, Bermudez P, Evans AC. Emotional responses to pleasant and unpleasant music correlate with activity in paralimbic brain regions. Nat Neurosci 1999;2:382–7.
197. Musacchia G, Sams M, Skoe E, Kraus N. Musicians have enhanced subcortical auditory and audiovisual processing of speech and music. Proc Natl Acad Sci U S A 2007;104:15894–8.
198. Limb CJ, Braun AR. Neural substrates of spontaneous musical performance: An FMRI study of jazz improvisation. PLoS ONE 2008;3:e1679.
199. Whitfield IC. The object of the sensory cortex. Brain Behav Evol 1979;16:129–54.

Vestibular Physiology and Disorders of the Labyrinth

6

Timothy E. Hullar, MD, FACS / Nathan C. Page, MD / Lloyd B. Minor, MD, FACS

The vestibular system collects information about the position and motion of the head. Together with visual and proprioceptive signals, the brain uses this information to coordinate the eyes, head, and body during movement and to give a conscious perception of orientation and motion. Disturbances in this integrative process can lead to dizziness, which is the ninth most common cause of visits to primary care physicians and the most common among patients over 75 years.[1,2] Many of these patients are referred to otologists to determine if a vestibular abnormality accounts for their complaint and to develop a treatment plan. Knowledge of the anatomy and physiology of the vestibular system gives a rational basis for understanding the causes, diagnosis, and treatment of many types of dizziness.

ANATOMIC ORGANIZATION OF THE VESTIBULAR SYSTEM

Dividing the vestibular system into its peripheral and central parts helps to localize pathologies. The periphery is responsible for measuring accelerations of the head. All accelerations can be divided into six components: rotation around an axis lying in each of the three dimensions and linear motion along each of these axes. The periphery consists of the horizontal, superior (also known as anterior), and posterior semicircular canals, which measure rotation, and the utricle and saccule, which measure linear accelerations (Figure 6–1). Each semicircular canal has a synergistic canal in the opposite temporal bone lying approximately parallel to it. The horizontal canals act as a pair, while each superior canal is paired with the posterior canal on the opposite side (Figure 6–2). Linear forces can arise from translation of the head front to back, side to side, or up and down, as well as from the orientation of the head relative to the pull of gravity. The central vestibular system consists of the lateral, medial, superior, and inferior vestibular nuclei and their projections to the thalamus, cortex, cerebellum, descending spinal cord, and extraocular motor nuclei.

Each membranous semicircular canal is filled with endolymph, a potassium-rich extracellular fluid, and is bathed in perilymph, which has the approximate composition of cerebrospinal fluid. The ends of the canals open into the vestibule. Near one end of each membranous canal is a widening known as the ampulla, which contains the crista ampullaris and cupula. The crista ampullaris is a saddle-shaped gelatinous structure along one wall of the membranous canal that contains the sensory hair cells of the vestibular system. The cupula acts as a membranous diaphragm, stretching from the crista to the opposite walls of the canal (Figure 6–3). Because the membranous labyrinth is tethered to the skull, the crista and cupula accelerate with the head as it rotates, but the endolymph's inertia causes it to lag behind. The endolymph accumulates with higher pressure on one side of the cupula than the other, indenting it and bending the hair cells within the crista. When the head ceases to accelerate, the cupula and crista gradually return to their resting positions.

The utricle and saccule, together called the otolith organs, also contain hair cells that bend in response to acceleration of the head. Instead of cristae, however, the sensory epithelium of these organs is covered by flat, kidney-shaped sheets called maculae. One macula lies horizontally against the ceiling of the utricle, whereas the other hangs sagittally on the wall of the saccule. Each macula is a gelatinous matrix into which hair cells project and which is studded with tiny calcium carbonate granules called otoconia.

The maculae of the otolith organs are sensitive to linear accelerations because of the presence of otoconia on their surface. These increase the density of the maculae so that any time the head moves linearly, the heavy maculae lag behind, bending the hair cells embedded in them (Figure 6–4). The utricle primarily senses lateral tilt and translation of the head, whereas the saccule measures front-to-back tilt and translation as well as motion aligned with the pull of gravity.

Hair cells located in the sensory epithelia of the semicircular canals and otolith organs are responsible for coding head acceleration into a modulation in the discharge rate of vestibular afferent fibers. Each hair cell contains a bundle of 50 to 100 stereocilia and one long kinocilium at the edge of each bundle (Figure 6–5). The location of this kinocilium relative to the stereocilia gives each hair cell an intrinsic polarity. In the

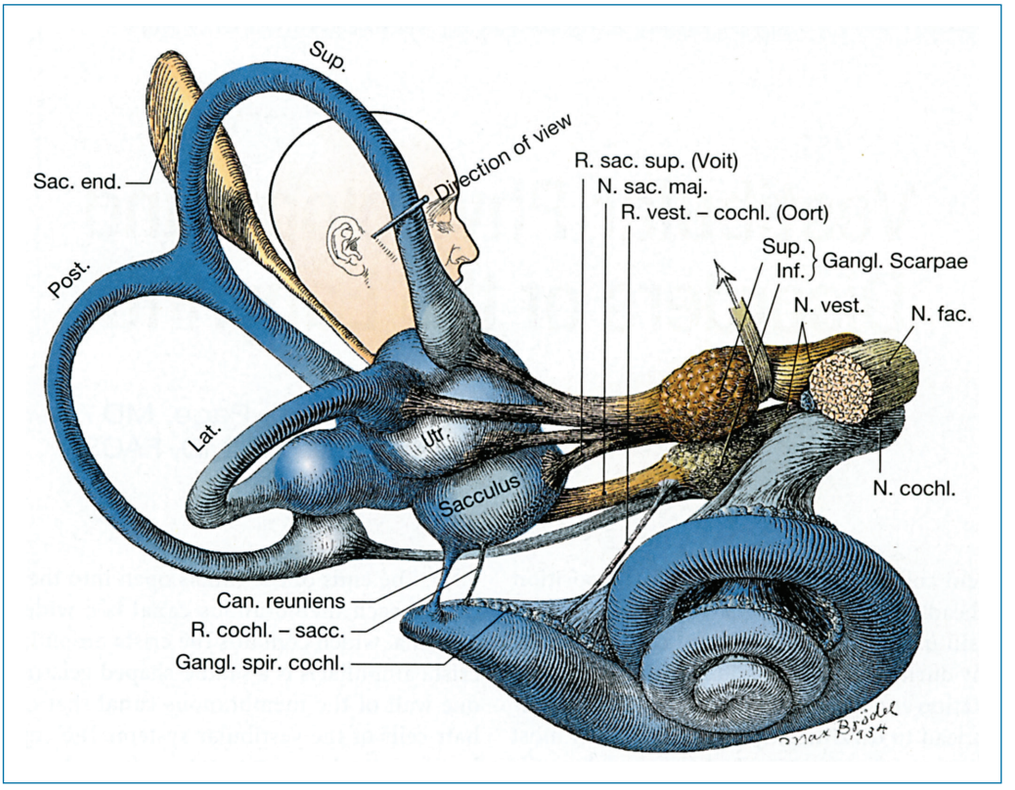

FIGURE 6–1 • Structures of the labyrinth. Structures shown include the utricle (utr.), sacculus, anterior or superior semicircular canal (sup.), posterior semicircular canal (post.), and horizontal or lateral semicircular canal (lat.). The superior vestibular nerve innervates the horizontal and anterior semicircular canals and the utricle. The inferior vestibular nerve innervates the posterior semicircular canal and the saccule. The cell bodies for the vestibular nerves are located in Scarpa's ganglion (Gangl. Scarpae). Drawing from the Brödel Archives, No. 933. *Reproduced with permission of the Department of Art as Applied to Medicine, Johns Hopkins University.*

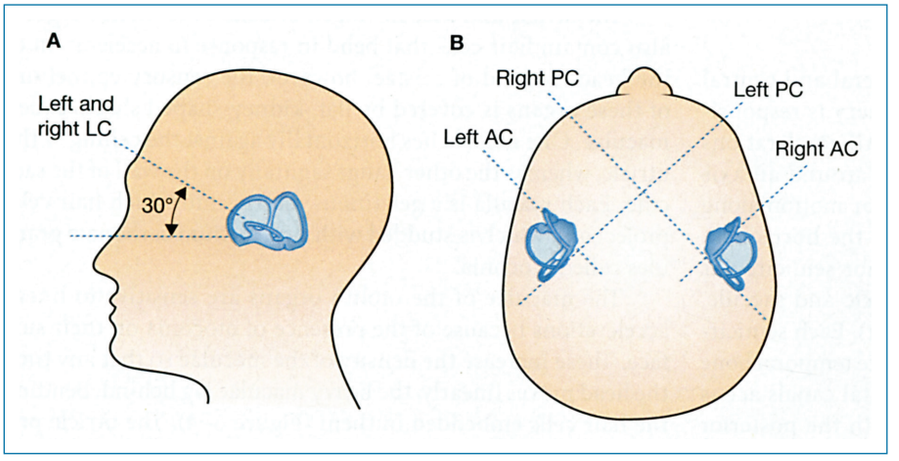

FIGURE 6–2 • Orientation of the semicircular canals. *A*, Horizontal (lateral) semicircular canals. *B*, Anterior (superior) and posterior canals. LC, lateral canal; AC, anterior canal; PC, posterior canal. Relative size of canals exaggerated for clarity. *Reproduced with permission from Barber H, Stockwell C. Textbook of electronystagmography. St. Louis: Mosby; 1976.*

horizontal canals, the kinocilium of every hair cell is located on the side of the ciliary bundle facing the utricle, whereas this arrangement is reversed in the superior and posterior canals. The hair cells of each otolith organ are arranged in two bands along a central stripe called the striola. The kinocilia of the hair bundles in the utricle are oriented toward the striola and those in the saccule face away.[3]

Displacement of a ciliary bundle toward its kinocilium opens potassium channels along the cilia and depolarizes the hair cell from its resting membrane potential of between –50 and –70 mV. The sensitivity of the hair cell can approach 20 mV of depolarization per micrometer of displacement. This depolarization leads to calcium influx at the basal end of the hair cells and increased flow of neurotransmitter into the synapse, whereas displacement in the opposite direction hyperpolarizes the cell and reduces neurotransmitter release.[4] The orientation of the kinocilia of the semicircular canals determines the excitatory direction of the canals. Each horizontal canal is maximally

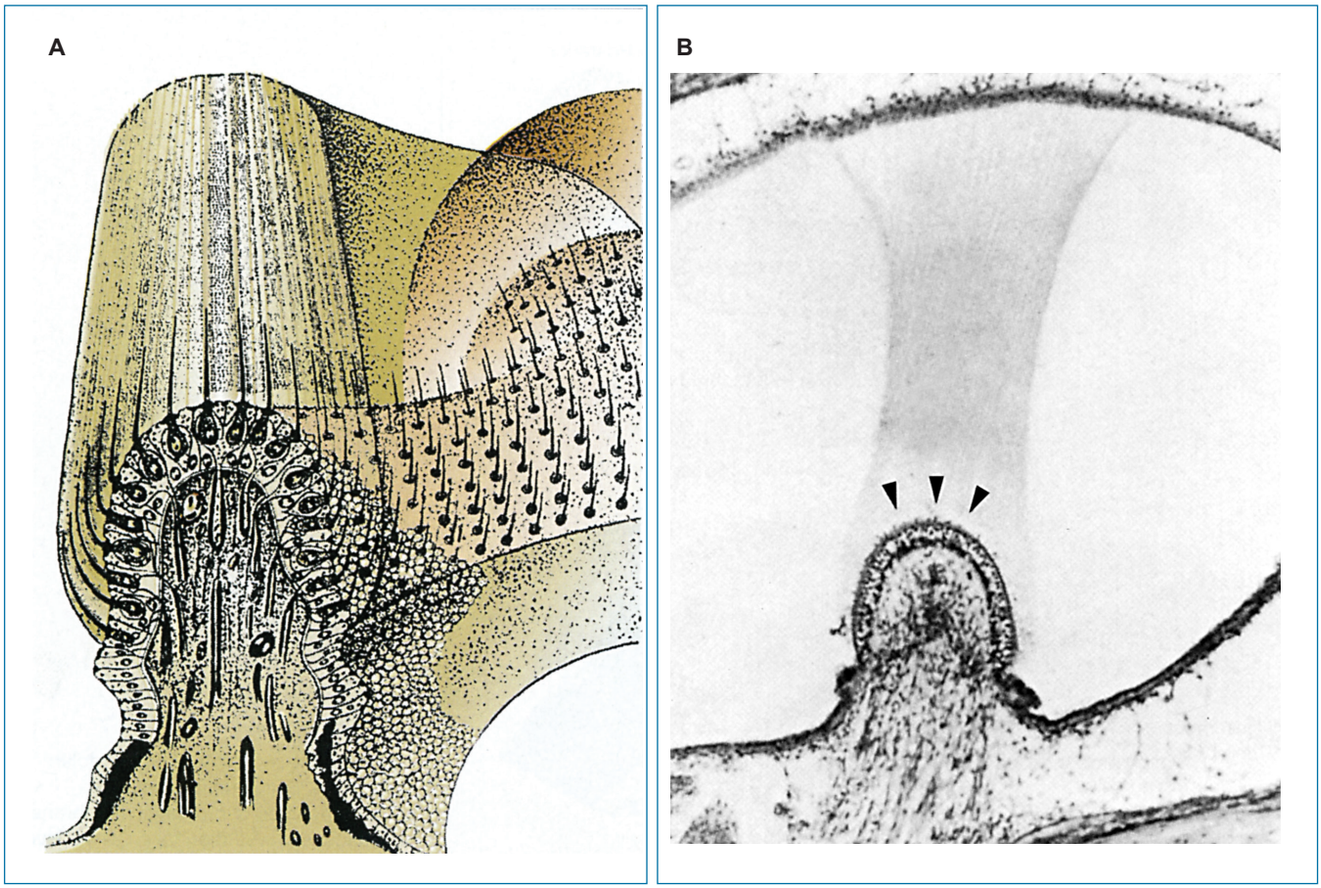

FIGURE 6–3 • Structure of the crista ampullaris and cupula. *A*, Artist's reconstruction of the crista ampullaris. *B*, Transverse section of the crista ampullaris of the monkey. The histologic techniques preserved the attachment of the cupula, which extends from the apex of the crista to the opposite wall of the membranous ampulla. Arrowheads indicate subcupular space. *A*, *Reproduced with permission from Wersäll J, Lundquist PG. In: Graybiel A, editor. Second Symposium on the Role of Vestibular Organs in Space Exploration, NASA SP-115. Washington DC: US Government Printing Office; 1966. B, Reproduced with permission from Igarashi M. In: Graybiel A, editor. Second Symposium on the Role of Vestibular Organs in Space Exploration, NASA SP-115. Washington DC: US Government Printing Office; 1966.*

excited by a rotation toward the side of the canal and inhibited by a rotation in the opposite direction. This results in an excitatory slow-phase movement toward the side opposite the canal and a resetting saccade toward the canal. The superior canal is excited by a rotation downward and to the side, in the plane of the canal. This results in a vertical–torsional nystagmus, with the slow phase of the vertical component upward and the resetting saccade downward. The posterior canal is excited by an upward rotation and to the side, in the plane of the canal, so that the slow phase is downward and the resetting phase upward.

Afferent nerve fibers in the superior vestibular nerve extend from sensory structures in the superior and horizontal canals and the utricle to the vestibular nuclei in the brain stem. The inferior vestibular nerve leads from the posterior semicircular canal and the saccule. In humans, each vestibular nerve is made up of about 25,000 neurons.[5] These neurons are bipolar, with cell bodies located in the vestibular nerve near the brain stem in Scarpa's ganglion. In addition to afferents, about 400 to 600 efferent nerves lead from the vestibular nuclei to hair cells and afferent nerves in each labyrinth. The precise role of these efferents in modulating the physiology of vestibular reflexes is unknown but may be related to adjusting the sensitivity of the vestibular system to an upcoming volitional movement.[6]

Almost all vestibular nerve afferents have a spontaneous or resting discharge rate, with some fibers firing up to approximately 100 spikes/sec.[7] This resting discharge rate enables each afferent to respond both to excitatory and inhibitory stimuli (Figure 6–6). Discharge regularity, measured by the spacing between action potentials of the afferent's discharge, has provided a useful marker for many important physiologic processes. Three groups of vestibular nerve afferents have been identified in mammals based on their responses to motion and their innervation profiles within the sensory epithelia of the labyrinth (Figure 6–7).[8] Bouton-only afferents have terminations exclusively onto type II hair cells in the peripheral zone of the cristae. These afferents are regularly discharging and have low rotational sensitivities. Dimorphic afferents have calyx endings terminating on type I hair cells and bouton endings terminating on type II hair cells. Their physiologic properties vary according to the location within the crista. Those dimorphic afferents

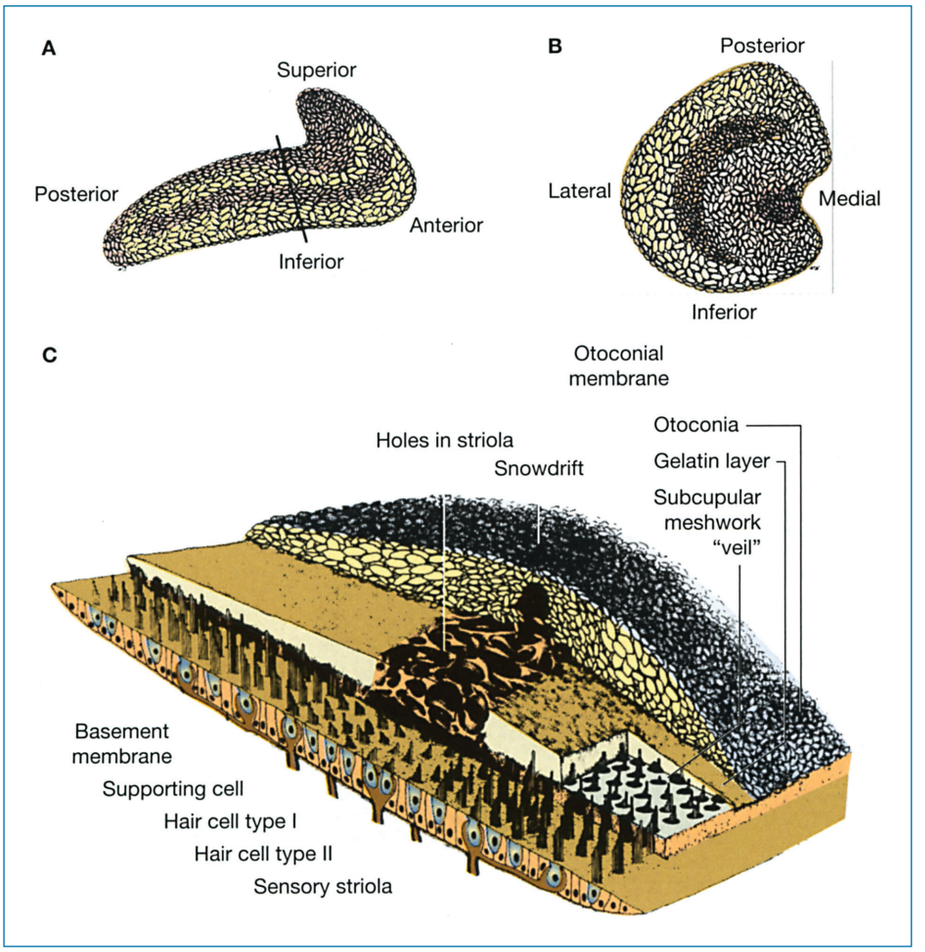

FIGURE 6–4 • Structure of the otolith organs. *A*, Sacculus. *B*, Utriculus. *C*, Composition of otoconial membrane of the saccus in a section taken at the level shown in *A*. *Reproduced with permission from Paparella MM, Shumrick DA, editors. Textbook of Otolaryngology. Vol 1. Philadelphia: WB Saunders; 1980.*

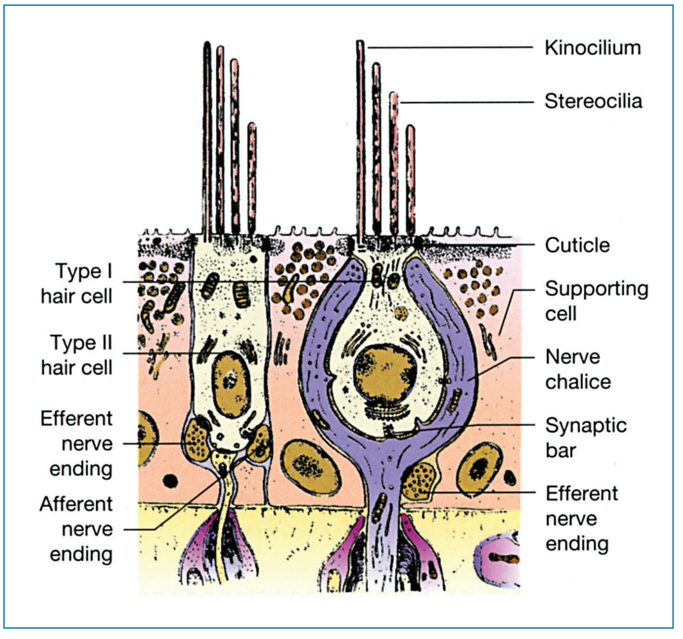

FIGURE 6–5 • Two types of sensory hair cells (types I and II) are found in the mammalian labyrinth. *Reproduced with permission from Wersäll J, Bagger-Sjöback D. In: Kornhuber HH, editor. Handbook of sensory physiology. New York: Springer-Verlag; 1974.*

terminating in the peripheral zone are regularly discharging, whereas those terminating near the central zone are irregularly discharging with higher rotational sensitivity. There is also a group of afferents that terminate exclusively with calyx endings onto type I hair cells in the central zone. The calyx-only afferents are irregularly discharging and have low rotational sensitivities at low stimulus frequencies and high sensitivities at higher frequencies.[9] The function of the different types of fibers may be related to the type of head motion each is coding.[10,11]

In work done over a century ago, Ewald identified two fundamental principles governing the relationship between the labyrinthine receptors and the vestibular reflexes that they mediate.[12] From experiments performed in pigeons, he noted that fenestration of a semicircular canal followed by mechanical stimulation of the membranous canal led to eye and head movements that were in the plane of that canal.

He also noted that excitatory stimuli led to larger amplitude responses than inhibitory stimuli. This is, at least in part, attributable to the resting discharge rate of vestibular nerve afferents and central vestibular neurons. These neurons can be excited up to a firing rate of at least 350 spikes/s but can be inhibited to only 0 spikes/s. Thus, there is a three- to fourfold higher range for excitation in comparison to inhibition. Many central vestibular neurons also have a resting discharge rate, suggesting that their

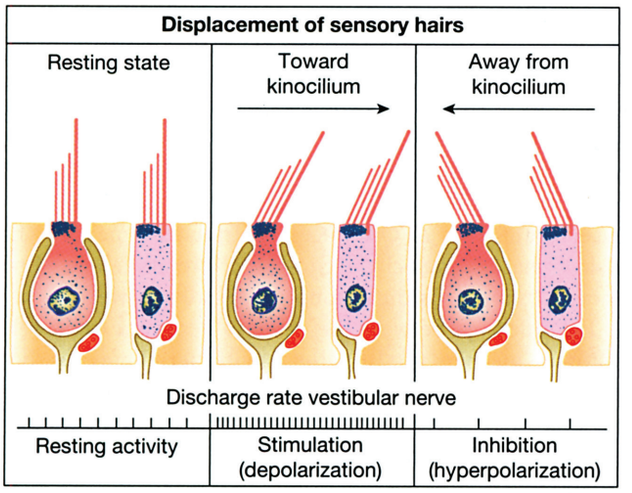

FIGURE 6–6 • Discharge rate of individual vestibular-nerve fibers as a function of the displacement of the cilia. The vestibular nerve afferents fire more frequently when the hair bundles are displaced toward the kinocilia; they fire more slowly when displaced in the opposite direction. *Reproduced with permission from Wersäll J, Lundquist P-G. In: Graybiel A, editor. Second Symposium on the Role of Vestibular Organs in Space Exploration, NASA SP-115. Washington DC: US Government Printing Office; 1966.*

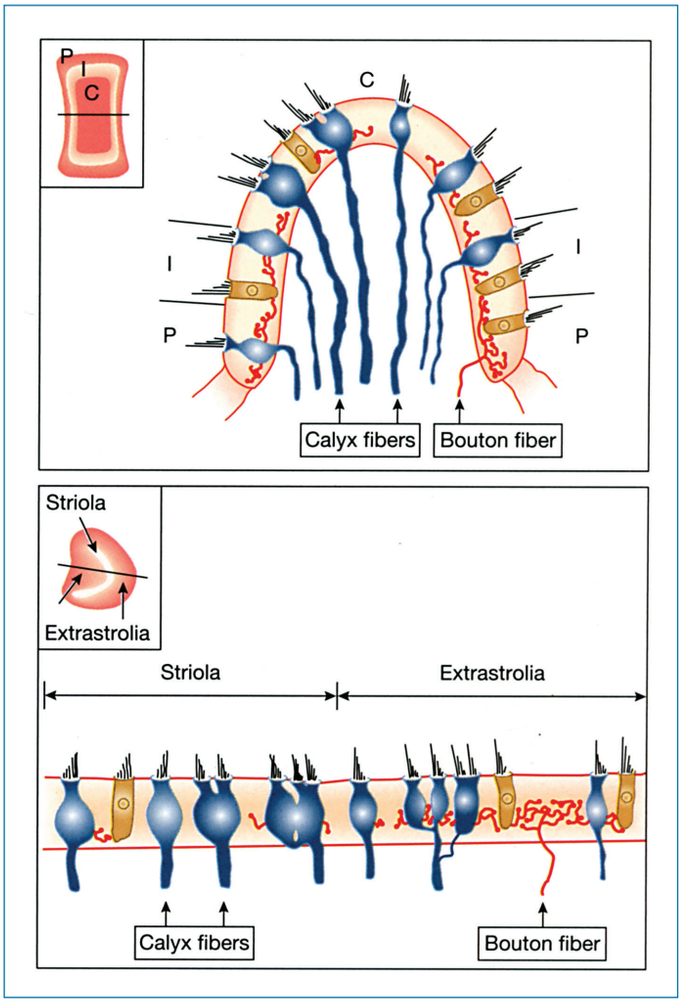

FIGURE 6–7 • Afferent innervation patterns in the mammalian vestibular end-organs. Top, The neuroepithelium of the cristae is divided into central (C), intermediate (I), and peripheral (P) zones, shown in plan in the inset and in cross-section in the main panel. Calyx fibers innervate the central zone, whereas bouton fibers innervate the peripheral zone. Dimorphic fibers are found throughout. Bottom, The macula is divided into the striola and the lateral and medial extrastriola (see inset). Calyx fibers are found in the striola, bouton fibers in the extrastriola, and dimorphs throughout. *Reproduced with permission from Goldberg JM. The vestibular end organs: morphological and physiological diversity of afferents. Curr Opin Neurobiol 1991;1:229–35.*

responses may also contribute to an asymmetry in responses. The first observation, motion of the eyes and head in the plane of the affected canal, is termed Ewald's first law (Figure 6–8). The second observation, excitatory responses are larger than inhibitory ones, is referred to as Ewald's second law. These relationships provide a basis for understanding many of the symptoms and signs that occur after injury to the labyrinth.

CENTRAL PROCESSES INVOLVED IN CONTROL OF VESTIBULAR REFLEXES

The central part of the vestibular system consists of the vestibular nuclei, which integrate information from vision, proprioception via spinal and cervical afferents, and vestibular signals from the labyrinth. These nuclei send projections that extend to the oculomotor system, where they help control eye movements; the muscles of the neck and spine, where they steady the head; and the thalamus and cortex. Central vestibular circuits also include parts of the cerebellum, which is involved in recalibrating the system when necessary.

Vestibular projections to the oculomotor nuclei reflexively maintain a steady image on the retina while the head is turning, tilted, or moving linearly in space. Quantification of these reflexes is the most common way of evaluating vestibular function. The angular vestibulo-ocular reflex (AVOR) is a three-neuron arc consisting of a vestibular afferent neuron, a vestibular interneuron, and an oculomotor neuron innervating the extraocular muscles. The brain interprets stimulation of a particular semicircular canal as motion of the head, and the eyes move reflexively in an equal but opposite amount to compensate. Turning the head to the left, for example, excites the left horizontal semicircular canal, and the eyes track to the right in response. This action leaves the angle of the target relative to the eye unchanged and its image steady on the retina. Similar relationships apply for the posterior and superior canals.

The AVOR is the fastest and one of the most exquisitely accurate reflexes in the body. It has a latency of about 7 milliseconds and produces eye movements that typically have <5% error with respect to rapid head movements.[13] This is critically important during rapid head movements, where even a small time delay might lead to instability of the visual image on the retina. Instability can occur when the image shifts even slightly, more than 2 to 3 degrees/s over the retina.[14] The visual system is unable to provide effective feedback to stabilize

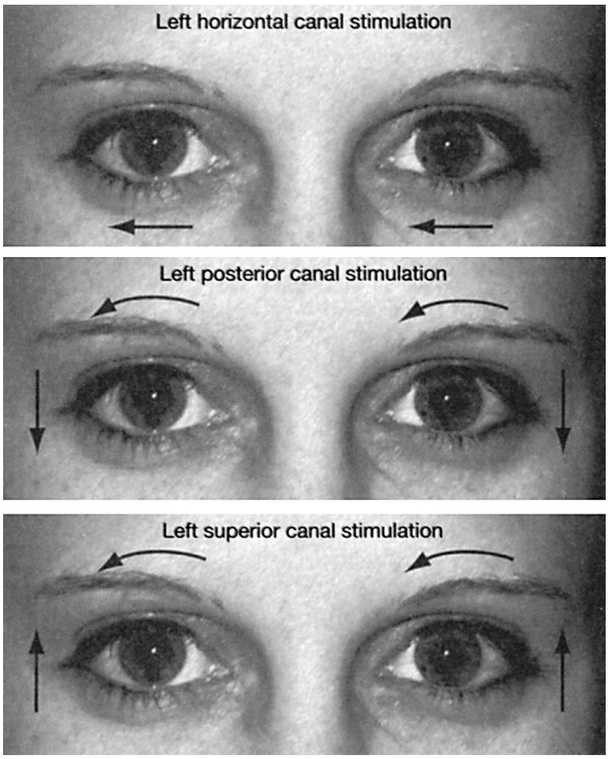

FIGURE 6–8 • Eye movements evoked by excitatory stimulation of individual semicircular canals. The arrows depict the motion of the slow-phase components of the nystagmus. Stimulation of the left horizontal canal results in a horizontal nystagmus with rightward slow phases. A vertical-torsional nystagmus is elicited by excitatory stimulation of either the superior or posterior canals. For the left superior canal, the slow-phase components are directed upward and clockwise with respect to the patient (superior poles of the eyes moving rightward with extorsion of the right eye and intorsion of the left eye). For the left posterior canal, the slow-phase components are the same for torsion but are directed downward in the vertical plane.

gaze during rapid head movements because it has a latency of 50 milliseconds or more. Deficits of the AVOR therefore lead to the symptom of oscillopsia (the apparent motion of objects that are known to be stationary) during rapid head movements. Patients with vestibular loss are less likely to have symptoms of oscillopsia during slower head movements because the visual system can stabilize gaze at lower head velocities.

The oculomotor system must also compensate for linear accelerations (tilt with respect to gravity and linear movements of the head). The linear vestibulo-ocular reflex (LVOR) is responsible for this compensation. Tilting the head side to side evokes ocular counterrolling, which is torsional movement of the eye about the line of sight that partially compensates for the effect of the rotation. Translational motion in which the head is moved laterally, however, requires the eyes to track with horizontal rotations. The otolith organs cannot distinguish between a tilt and a translational movement, so the system must use other information from the semicircular canals and other sensory inputs to decide how to move the eyes.

Several central processes are critical to understanding tests used to diagnose vestibular disorders. Velocity storage is the name given to the process that maintains the sense of rotation even after the rotation has stopped.[15] The neural source of this process is probably located in the vestibular commissure.[16] Signals from the semicircular canals decay away slowly, with a time constant (the time required for the response to decay to 37% of its initial value) of approximately 5 sec. However, the time constant of the AVOR (calculated from the time over which the slow-phase eye velocity declines after a rotation has stopped) in normal subjects is much longer, typically between 12 to 20 sec. The difference between these two values is due to the velocity storage mechanism. In patients with peripheral vestibular dysfunction, the velocity storage mechanism may cease to function. This causes rotation-induced nystagmus, and the conscious perception of rotation, to decay in a shorter period of time than normal.

A second central process whose function is important for measuring vestibular function is the *neural integrator*.[17] The neural integration circuit may be located in the medial vestibular and prepositus hypoglossi nuclei.[18] The neural integrator is the process that provides the signal to hold the eyes away from "primary position" facing straight ahead. When looking away from primary position, the extraocular muscles require a burst of activity to move the eyes to their eccentric position and then a sustained level of discharge that signals the muscles to hold the eye in an eccentric position. In patients with vestibular loss, this process may become dysfunctional and the eyes may drift inappropriately toward primary position.

BEDSIDE EVALUATION OF THE VESTIBULAR SYSTEM

History

A patient's history is often sufficient to identify a likely cause of his or her symptoms. Taking the history of a patient with a complaint related to dizziness should begin in an open-ended fashion, allowing the patient to describe the symptoms with minimal direction from the physician. The process can be facilitated by requesting the patient to complete a questionnaire that asks the patient to describe and respond to queries about symptoms before the first appointment.[19,20] Key elements of the history are described below.

The Nature of the Sensation

Dizziness is a term often used by patients to describe their symptoms in a general way, but categorizing their symptoms more precisely can help determine their cause more accurately. *Vertigo* is an illusory sense of motion when the patient is still. The patient may feel that the motion is internal or that objects in the surroundings are moving or tilting. The sense of motion can be rotatory, linear, or a change in orientation relative to the vertical. Vertigo often indicates a problem within the peripheral vestibular system. Horizontal rotatory movement of objects in the visual surround suggests dysfunction of the semicircular canals, while drop attacks or abnormal sensations of tilt suggest otolith dysfunction. Typical causes of vertigo include benign positional vertigo, viral labyrinthitis, or Ménière's disease, although

other processes such as migraine-related vertigo may also be responsible. *Oscillopsia* is instability of the visual field caused by motion of the head. It is a common complaint in patients with unilateral or, more commonly, bilateral loss of peripheral vestibular function. *Disequilibrium* is the perception of unsteadiness, often with the sensation that a fall may be imminent. This may be related to dysfunction of the vestibular system, but may also be caused by faulty proprioception or other processes responsible for maintaining balance. Migraine-related vertigo, mal de debarquement, side effects of medication, or other conditions such as diabetes may be responsible. *Presyncope* may be related to anxiety, vascular disease, cardiac arrhythmia, or autonomic disorders.

Timing of the Initial Spell

Imbalance occurring shortly after a serious illness requiring hospitalization may be due to exposure to ototoxic antibiotics. Starting or stopping a new prescription or over-the-counter medicine, or changing the strength or dosing schedule of a medication, may lead to new symptoms of dizziness. An upper respiratory infection may precede the onset of symptoms of benign positional vertigo or vestibular neuritis. Trauma or infection can lead to symptoms of endolymphatic hydrops. Stapes surgery followed by episodic dizziness may reflect the development of a perilymphatic fistula. An initial spell of dizziness in a girl nearing menarche may indicate a hormonal influence on balance, often associated with migraine-related imbalance.

Frequency and Duration of Symptoms

Episodic imbalance may be divided into short-, medium-, or long-term events. Short-term symptoms, lasting seconds to minutes, may be caused by autonomic dysfunction or inner ear conditions such as benign positional vertigo, perilymphatic fistula, or semicircular canal dehiscence. Medium-length spells, typically up to 4/ h long, may be due to Ménière's disease. They may also be related to cardiac arrhythmias, transient ischemia, hypoglycemia, or seizure activity. Anxiety disorders may lead to medium-term vertigo. Longer spells, lasting up to days, are more likely to be related to migraine-associated vertigo. Chronic symptoms of dizziness indicate a stable level of dysfunction in any of the systems dedicated to maintaining balance. Unilateral or bilateral peripheral vestibular loss may cause chronic imbalance. It may also be due to dysfunction of other sensory symptoms, such as in patients with peripheral neuropathy. The elderly may suffer from chronic imbalance, as can patients with uncontrolled hypertension or other causes of widespread pathology of the central nervous system such as diffuse brain injury or syphilis. Semicircular canal dehiscence has recently been recognized as a cause of chronic imbalance.

Precipitating or Mitigating Factors

The diagnosis of certain vestibular disorders is strongly suggested from events, stimuli, or movements that trigger symptoms. Benign paroxysmal positional vertigo (BPPV) classically begins on rolling over in bed or tilting the head backward and toward the affected ear. Patients with superior canal dehiscence syndrome experience vertigo and oscillopsia with sound or pressure stimuli. Pressure sensitivity is also common in patients with perilymphatic fistula. Patients with migraine-related vertigo may have symptoms brought on by certain foods, changes in the weather, menses, significant motion stimuli, or exposure to lights or sounds. Seasonal relationships may suggest allergy, which has been linked to Ménière's disease. Migraine patients may benefit from sleep or rest in a darkened quiet room. Patients with BPPV tend to keep their heads as still as possible.

Associated Symptoms

Aural fullness and tinnitus can precede an attack of vertigo in patients with Ménière's disease, a correlation known as Lermoyez's syndrome.[21] Headache or visual symptoms sometimes accompany vestibular migraine. Dysarthria, diplopia, and paresthesias may accompany the vertigo seen in cases of vertebrobasilar insufficiency. Diplopia may be a sign of multiple sclerosis. Dysfunction of other cranial nerves, such as the fifth, seventh, or auditory nerve, may indicate a mass in the cerebellopontine angle or internal auditory canal. Ataxia suggests cerebellar dysfunction, sometimes related to a degenerative condition, but may also be due to the mass effect of a tumor in the cerebellopontine angle. More critically, it may be a manifestation of the lateral medullary syndrome due to brainstem infarct. Sweating, dyspnea, and palpitations often accompany panic attacks. Acute visual changes accompanying imbalance may be due to Cogan's syndrome, which is an otologic emergency affecting hearing, balance, and eyesight, or benign intracranial hypertension. Otosclerosis may cause hearing loss as well as imbalance. Temporomandibular joint disorder may cause headaches, subjective hearing loss, and tinnitus associated with imbalance.

Other Medical Conditions

Thyroid disease, diabetes mellitus, anemia, autoimmune diseases, and vascular or cardiac disease may cause imbalance. Hypoglycemia is a not uncommon cause of dizziness. Many medications, including those used to treat seizures, hypertension, cardiac arrhythmias, and hyperglycemia, can also produce symptoms that mimic peripheral or central vestibular disorders. Anxiety disorders, panic syndromes, and agoraphobia can lead to episodic vertigo that mimics a vestibulopathy. Previous ear surgery or otologic diseases such as cholesteatoma can lead to peripheral vestibular loss, sometimes through creation of a semicircular canal fistula.

Family History

Migraine, Ménière's disease, and otosclerosis can all be related to symptoms of imbalance and sometimes run in families.[22] Syndromic diseases, such as CHARGE syndrome and Usher's syndrome, may be accompanied by vestibular dysfunction. A mutation of the *CACNA1A* gene leads to autosomal-dominant episodic vertigo and ataxia type EA-2.[23]

Examination

The neurotologic examination evaluates components of vestibular and related oculomotor and postural function to identify abnormalities that are characteristic of pathologic entities. One such approach is presented below in an order that would correspond to the actual examination. Much of the examination of peripheral labyrinthine function is dedicated to evaluating semicircular canal function, but tests of otolith function are becoming more commonly used. In both cases, vestibular

function is evaluated primarily by measuring eye movements. The general otolaryngologic examination is a part of the assessment but is not reviewed here.

Inspection for Spontaneous Nystagmus

Vestibulo-ocular reflexes are responsible for maintaining the stability of objects on the retina during head movements. Disorders in their physiology can result in nystagmus and impaired eye movements in response to head movements with consequent loss of visual acuity. Nystagmus is a to-and-fro beating of the eyes with slow and fast components. Spontaneous nystagmus is seen when there is an imbalance in the level of neural activity innervating the extraocular muscles. Vestibular-evoked nystagmus is termed "jerk nystagmus" and comprises a drifting slow phase followed by a rapid resetting motion. The direction of this type of nystagmus is typically named according to its fast phase because that is more obvious to the examiner, but is actually less diagnostically important than the slow phase, which is directly driven by afferent input from the vestibular end-organs. The amplitude of nystagmus is often reduced if a patient is able to fixate on a target. Examination for nystagmus should therefore take place with the patient wearing Frenzel goggles. These are high-diopter glasses, which allow the examiner to see the patient's eyes clearly but minimize the ability to fixate.

"Vestibular nystagmus" is a mixed horizontal-torsional motion of the eye that occurs with a recent vestibular loss. It occurs even if the head is held still and can be dampened by visual fixation. Afferent input to the brain stem is dominated by signal from the normal horizontal canal, which is interpreted by the brain as an ipsilateral turn. The AVOR compensates for this by moving the eye in a slow phase in the opposite direction, which is then reset by a fast phase toward the intact labyrinth. Torsional motion of the eye is provided by the sum of inputs from the intact superior and posterior canals. Because activity of the superior canal induces upward slow phases and the posterior canal induces downward slow phases, no net vertical motion of the eye is seen. Note that in some situations, nystagmus is caused by overstimulation of one labyrinth rather than loss of function of the other. This can occur following surgery on the inner ear or related to an attack of Ménière's disease.[24]

Vestibular nystagmus often changes its amplitude or direction with changes in the direction of gaze. Nystagmus seen in patients with benign positional vertigo related to canalithiasis of the posterior semicircular canal is more vertical when looking away from the involved side and more torsional when looking toward the involved side. This occurs because the eye is more in line with the plane of the posterior canal when looking away and more in line with the axis of the canal when looking toward the pathologic side. Nystagmus may also occur in normal subjects. "Convergence nystagmus" can be brought on voluntarily by focusing on a near target.[25] "Endpoint" nystagmus occurs when gaze is directed to the far limit of the range of motion of the eyes.[26] This may be accentuated in patients intoxicated with alcohol or using some medicines.

Alexander's law describes eye movements seen in patients with an acute unilateral vestibular loss (Figure 6–9). In these patients, the neural integrator is compromised and the eyes tend to drift back to their primary position. This motion combines with the slow phases of vestibular nystagmus caused by asymmetric input from the horizontal canals. The result accentuates the dominant vestibular nystagmus when gaze is directed toward the intact side and reduces it when gaze is directed toward the hypofunctional side.

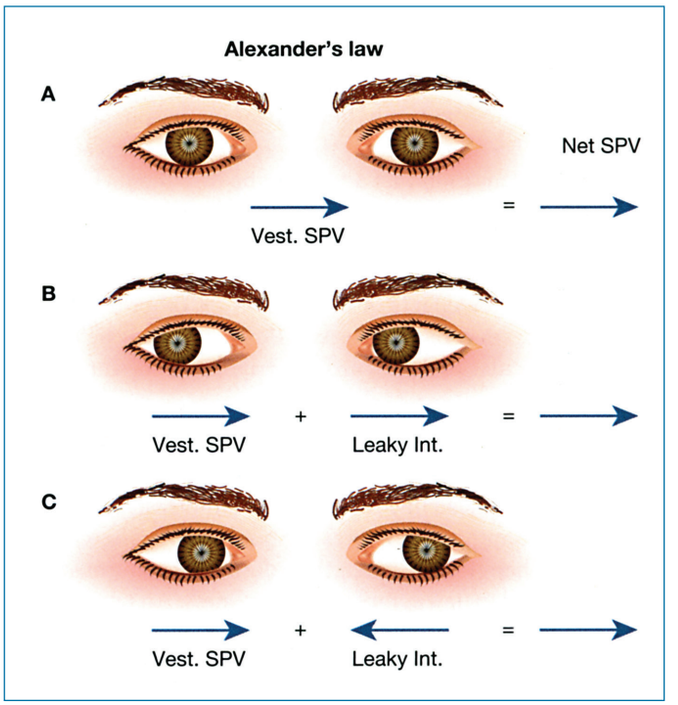

FIGURE 6–9 • Alexander's law. After unilateral vestibular loss, a central process (called the "leaky integrator") contributes to eye motion and nystagmus by allowing the eye to drift to center, regardless of its position. The interaction of this motion and the motion of the eye caused by the imbalance in vestibular activity between the two labyrinths cause nystagmus to be more pronounced when looking away from the lesion. In straight-ahead gaze *A*, the vestibular slow phase alone is manifest. When the eyes look to the direction of the fast phase (right, *B*), the leaky integrator causes the eye to drift to the left. This drift adds to the vestibular slow phase, and the net slow phase velocity (SPV) increases. When the eyes look to the direction of the slow phase (left, *C*), the leaky integrator causes the eye to drift to the right. This drift subtracts from the vestibular slow phase, and the net SPV decreases.

A related finding is seen in patients with Brun's nystagmus. This is seen in patients with a long-standing vestibular loss, such as due to an acoustic neuroma, in whom vestibular nystagmus is less pronounced due to central compensation. When looking toward the intact side, both the functional labyrinth and the loss of the neural integrator add to drive slow phases toward the hypofunctional side. However, when looking toward the hypofunctional side, the effect of the neural integrator letting the eyes drift toward the midline is actually stronger than the remaining, compensated vestibular signal driving their slow phases toward the hypofunctional side. The resulting slow phases are to the intact side and the fast phases beat toward the pathologic side.

Several types of nystagmus are caused by acute or chronic pathologies of the central nervous system. Upbeat or downbeat nystagmus can be caused by alcohol or medicine ingestion or disorders of the brain stem or cerebellum, including Chiari

malformations. "Pendular nystagmus" consists only of slow phases and is often related to brainstem pathology. "Periodic alternating nystagmus," in which the direction of the nystagmus changes approximately every 2 min, is seen with brain stem and cerebellar disease including Chiari malformations. It can be treated with baclofen. "Congenital nystagmus" may appear like vestibular nystagmus, although patients may find a "null point" of gaze where the nystagmus is minimized and preferentially hold their eyes in that position in the orbit. Tourette's syndrome may cause ocular tics that mimic nystagmus. Other types of nystagmus are described in detail elsewhere.[27]

Ocular Tilt Reaction

The ocular tilt reaction is caused by an imbalance in tonic levels of activity along pathways mediating otolith-ocular reflexes. The ocular tilt reaction can occur with lesions anywhere along otolith-ocular pathways: labyrinth or vestibular nerve, vestibular nuclei, medial longitudinal fasciculus, or interstitial nucleus of Cajal. There are three components to the ocular tilt reaction arising from hypofunction of one labyrinth: head tilt toward the lesioned labyrinth, skew deviation with the lower eye being on the side of the lesion, and ocular counter-roll (torsional deviation of the superior poles of the eyes toward the side of the lesion). Patients with skew deviation often complain of vertical diplopia and sometimes torsional diplopia (one image tilted with respect to the other). The alternate cover test is used to detect skew deviation: the examiner covers one eye of the patient with a card and then moves the cover to the patient's other eye while looking for a vertical corrective movement as an index of a vertical misalignment.

Positional Testing

Benign paroxysmal positional vertigo (BPPV) is the most common cause of dizziness in patients who visit an otolaryngologist. It is usually caused by pathology in the posterior semicircular canal, but can affect the horizontal, superior, or multiple canals as well. Diagnosis of BPPV may be determined by the latency, direction, duration, and reversal properties of the nystagmus. The latency and duration of the perception of dizziness during positioning maneuvers, even without visible nystagmus, can also suggest the presence of BPPV. The Dix-Hallpike maneuver for identification of posterior canal BPPV is begun with the patient sitting upright on an examination table. For testing to detect the presence of right posterior canal BPPV, the head is turned 45 degrees, so the chin is toward the right shoulder. The patient is then brought straight back rapidly until the shoulders are flat on the bed and the neck is extended. This position is maintained for at least 30 sec.

Nystagmus due to BPPV typically begins after a latency of 2 to 10 sec, increases in amplitude over about 10 sec, and declines over the next 30 sec. This time course presumably reflects the sinking of the debris in the posterior canal. Posterior canal BPPV results in a vertical–torsional nystagmus with the slow-phase components of the nystagmus directed downward and toward the uppermost ear. The fast-phase vertical component of the nystagmus therefore is toward the forehead and the fast-phase torsional component directs the superior part of the eye toward the ground (Figure 6–8). Because of the orientation of pulling directions for the oblique and vertical recti muscles, the planar characteristics of the nystagmus change with the direction of gaze (when described with respect to an eye-fixed coordinate system): on looking to the dependent ear, it becomes more torsional; on looking to the higher ear, it becomes more vertical.

A horizontal canal (HC) variant of BPPV has also been described.[28] In these patients, a strong horizontal nystagmus builds up over the same time course as for posterior canal BPPV but persist much longer. The standard Dix-Hallpike maneuver may not elicit nystagmus in cases of HC BPPV. Nystagmus can instead be identified by bringing the patient backward into the supine position and then turning the head left or right ear down. The nystagmus seen with HC BPPV may last longer than that seen in posterior canal BPPV.

Nystagmus related to HC BPPV is exclusively horizontal and may beat either downward (geotropic) or upward (ageotropic) regardless of which direction the patient is facing. Geotropic nystagmus may reflect canalithiasis, while ageotropic nystagmus may indicate cupulolithiasis, where debris is stuck to the cupula and symptoms have a quicker onset and last longer following positioning. Geotropic nystagmus tends to be more vigorous than ageotropic nystagmus because geotropic nystagmus may be due to inhibition of the affected canal's afferents and ageotropic nystagmus may be due to their excitation. Anterior canal BPPV has been rarely described and is typified by vertical-torsional nystagmus with fast phases beating toward the patient's chin. This can be initiated with the patient in the standard Dix-Hallpike position, but in that case the involved canal is located in the upper ear.

Symptoms of positional vertigo with a minimal latent period suggest a central cause for dizziness. Sustained symptoms produced during testing for posterior canal BPPV may indicate a Chiari malformation or vertebrobasilar insufficiency worsened by neck extension. A central lesion is most likely when positional nystagmus is purely vertical or purely torsional or if there is a sustained unidirectional horizontal positional nystagmus of high enough intensity to be observed without Frenzel lenses. Multiple sclerosis can cause positional nystagmus, but limitations of eye movements due to internuclear ophthalmoplegia can sometimes mask its effects.[29] Brief symptoms on arising may be associated with orthostatic hypotension. A sustained, usually horizontal, positional nystagmus of low velocity is a common finding in patients with central or peripheral vestibular lesions and may also be present in asymptomatic human subjects.[30] Positional testing may also exacerbate a spontaneous nystagmus.[30] Alcohol intoxication is a common cause of positional nystagmus.[31]

Postheadshaking Nystagmus

Postheadshaking nystagmus (HSN) occurs in patients with imbalance in dynamic vestibular function. With Frenzel lenses in place, the patient is instructed to shake the head vigorously about 30 times side to side with the chin placed about 30 degrees downward to bring the horizontal canal into the plane of rotation. Head shaking is stopped abruptly, and the examiner looks for any nystagmus. Normal individuals usually have no or occasionally just a beat or two of post-HSN. With a unilateral loss of labyrinthine function, however, there is usually

a vigorous nystagmus with slow-phase components initially directed toward the lesioned side.[32]

The initial phase of HSN arises because there is asymmetry of peripheral inputs during high-velocity head rotations: more activity is generated during rotation toward the intact side than toward the affected side. This asymmetry leads to an accumulation of activity within central velocity storage mechanisms during head shaking. Nystagmus following head shaking reflects discharge of that activity. The amplitude and duration of the initial phase of HSN are dependent on the state of the velocity storage mechanism. Because velocity storage is typically ineffective during the immediate period after an acute unilateral vestibular loss, the primary phase of HSN may be absent or attenuated in these circumstances.[33]

Head Thrust Test

The head thrust (or "head impulse") test allows examination of individual semicircular canals during vigorous motion. Brief, high-acceleration rotations of the head in the horizontal plane are applied while instructing the patient to look carefully at the examiner's nose. An AVOR of abnormally low amplitude will be evoked in response to head thrusts in the excitatory direction of a lesioned or hypoactive canal. For the horizontal canals, a rightward head thrust therefore tests the right horizontal canal and a leftward head thrust tests the left horizontal canal.[34] A corrective saccade, required to bring the eyes back to the intended point of fixation, is seen in such cases (Figure 6–10).[35] Corrective saccades observed in head thrust responses from patients with vestibular hypofunction can, with mechanisms of vestibular compensation, occur during the head movement and lead to an eye movement response that appears relatively normal on clinical examination. The sensitivity of the test can be improved by beginning each head movement with the patient's eyes in primary gaze position and moving the head at random intervals and order to the right and left. The test can also be used to detect dysfunction in each of the vertical canals by delivering the head thrusts in approximately the plane of the left anterior–right posterior or right anterior left posterior canals.[36]

Dynamic Visual Acuity

Vestibular dysfunction typically causes a pronounced loss of visual acuity during head movement. The patient reads a Snellen chart with the head stationary and visual acuity is recorded. Acuity is then checked during horizontal head oscillations at a frequency of about 2 Hz. Subjects with corrective lenses are instructed to wear their glasses or contact lenses during this testing. Subjects with normal vestibular function typically show no more than a one-line decline during head movement but those with vestibular hypofunction (particularly bilateral hypofunction) may show up to a five-line decline in acuity.[37] Predictive mechanisms during repetitive, sinusoidal oscillations of the head may augment performance during this test and obscure

FIGURE 6–10 • Eye movements during head thrust test. Testing left horizontal canal by performing head thrust to subject's left. Top: normally functioning left horizontal canal drives eyes to right immediately following the thrust. Bottom: hypofunctional left horizontal canal fails to drive eyes to right. A catchup saccade brings them into position after a delay.

the identification of a deficit.[38] Computerized presentations of visual stimuli in a laboratory setting may avoid this problem.[39]

Other Bedside Tests of Vestibulo-Ocular Function

Changes in relative pressure between the middle and inner ears may induce nystagmus. A Valsalva maneuver with the glottis closed increases intracranial pressure, while a maneuver with the glottis open (blowing against a pinched nose) increases middle ear pressure. Nystagmus is best observed using Frenzel lenses or while examining small blood vessels on the sclera using an obliquely directed microscope. Similar symptoms may also be elicited by tragal compression or insufflation with a pneumatic otoscope or Siegle's speculum. Nystagmus induced during these maneuvers may reflect craniocervical junction anomalies such as Arnold–Chiari malformation, superior canal dehiscence syndrome, perilymph fistula, or compression of the vestibular nerve by tumor.[27]

Patients with pressure-induced eye movements may also have symptoms in response to sound. This may be evaluated by observing the eyes under Frenzel lenses when giving pure tones from 500 to 4,000 dB at intensities of 100 to 110 dB. Tullio's phenomenon is the occurrence of vestibular symptoms and eye movements with sound. Hennebert's sign is the occurrence of these symptoms and signs with motion of the tympanic membrane and ossicular chain. These signs have recently been documented in patients with superior canal dehiscence syndrome.[40, 41] The evoked eye movements in this syndrome align with the plane of the affected superior canal.(Figure 6–8).[42] Patients with superior canal dehiscence may also have eye movements induced by bone conducted vibrations. Otitic syphilis, Ménière's disease, and perilymph fistula have also been reported to cause these signs, although the specific features of their evoked eye movements have not been well characterized.

Hyperventilation may induce symptoms in patients with anxiety or phobic disorders but does not usually produce nystagmus. Patients with demyelinating lesions of the vestibular nerve (such as that caused by a vestibular schwannoma), or compression by a small blood vessel, or central lesions such as those related to multiple sclerosis may show hyperventilation-induced nystagmus.[43] Hyperventilation reduces pCO_2, which leads to an increase in serum and cerebrospinal fluid (CSF) pH. This relative alkalosis increases the binding of extracellular calcium to albumin and leads to an increase in the discharge rate and conduction in partially demyelinated axons.

Bedside Examination of Posture and Gait

Vestibulospinal reflexes maintain posture with respect to gravity and assist vestibulo-ocular reflexes by producing contraction of neck muscles that compensate for externally applied motion to the neck or body. Disorders of vestibulospinal reflexes can result in tilt of the head, abnormal posture, or ataxia. Other causes of similar symptoms may be dysfunctional proprioceptive inputs, visual inputs, or the inability to combine multiple sensory cues accurately. Static imbalance in vestibulospinal reflexes may be identified from a Romberg test, tandem walking, stepping tests, and evaluation of pastpointing. Romberg's test is used to assess sway with feet together and tandem, with eyes both open and closed. Falls during tandem walking or a positive Fukuda stepping test (turning while marching in place for 30 sec with eyes closed) are signs of vestibulospinal asymmetry due to vestibular lesions.[44] Pastpointing of the arms to previously seen targets with eyes closed may also be a sign of vestibulospinal imbalance. Dynamic vestibulospinal function is assessed by observing postural stability during rapid turns or in response to external perturbations imposed by the examiner (ie, a gentle shove forward, backward, or to the side).

Patients with vestibular dysfunction may rely largely on proprioceptive feedback for maintaining balance. Patients with this compensatory strategy often suffer from significantly increased sway when performing a Romberg test on a block of foam to reduce proprioceptive input from the feet and ankles. Patients with a compensatory strategy that depends on visual inputs may be unable to walk steadily with their eyes closed. The ability to combine multisensory cues can be tested at the bedside as part of the "Clinical Test of Sensory Integration and Balance," where both visual and proprioceptive cues are modified simultaneously similar to platform posturography.[45]

LABORATORY TESTES OF VESTIBULAR FUNCTION

Quantitative tests of physiologic processes under vestibular control can be an important adjunct to the history and clinical examination, but diagnoses are rarely made solely on their results. Laboratory tests are best used selectively to evaluate a patient suspected of particular conditions rather than applied to all patients. Many laboratory tests of vestibular function use electronystagmography (ENG) to record eye movements during various vestibular and oculomotor tests. The quantitative information from ENG enables the clinician to monitor progression of or recovery from disorders affecting vestibulo-ocular control. Three techniques can be used for recording eye movements: electro-oculography (EOG), infrared video image analysis, and magnetic search coil techniques.

Electro-oculography techniques are based on the corneoretinal potential (difference in electrical charge potential between the cornea and the retina). Movement of the eye relative to surface electrodes on the face produces an electrical signal corresponding to eye position. Horizontal eye movements can typically be resolved to an accuracy of 0.5 degrees, which is not as great as the sensitivity of direct visual inspection by a trained examiner (approximately 0.1 degrees). Examination of small-amplitude eye movements either directly or with the aid of Frenzel lenses or an ophthalmoscope is therefore important for identification of low-amplitude nystagmus. Torsional eye movements cannot be measured with EOG. Recently developed video imaging techniques are used instead of EOG in many clinical laboratories. In principle, infrared video recordings allow eye movements to be recorded in three dimensions and with an accuracy that is comparable to or greater than that achieved with EOG. Although algorithms and procedures are improving, there are still some patients for whom image fitting and analysis do not work properly.

The gold standard measurement of eye movements is the magnetic search coil technique.[46] This is based on the principle that changes in voltage are induced in a conductor moving relative to a magnetic field (Faraday's law). In humans, a minute

wire is imbedded in a Silastic annulus that is inserted surrounding, but not actually touching, the cornea. Eye movements in three dimensions can be resolved to an accuracy of about 0.02 degrees. The main disadvantages of search coil recordings for general clinical use is the level of expertise required to set up the apparatus, conduct the recording sessions, and analyze the data. It can also be irritating to the eye and poses a hazard of corneal abrasion and is used only in specialized research laboratories.

Assessment of Spontaneous Nystagmus and Oculomotor Function

Eye movements are recorded with eyes closed and with eyes opened and while viewing a stationary visual target. Spontaneous nystagmus and the effects of visual fixation on this nystagmus are noted. The patient then looks to the left, right, up, and down so that a positional nystagmus can be detected.

Saccades are assessed by instructing the patient to fixate (eyes moving while keeping the head stationary) on a series of randomly displayed dots or lights at eccentricities of 5 to 30 degrees. The latency, velocity, and accuracy of saccades are analyzed. Defects in saccades may consist of prolonged latencies, abnormal velocities, and over- or under-shooting the target. These defects may be caused by muscular pathology such as myesthenia gravis, oculomotor paresis, multiple sclerosis, Huntington's disease, pathology in the brainstem or cerebellar vermis, or attentional lesions in the cerebellar hemispheres. Smooth pursuit eye movements are recorded while the patient is tracking a target that moves horizontally with a sinusoidal waveform at a low frequency (0.2–0.7 Hz) with a position amplitude of 20 degrees in each direction. Problems with smooth pursuit indicate a cerebellar pathology. Optokinetic testing is generally performed with the subject surrounded by a visual scene that moves in one direction at velocities of 30 to 60 degrees/sec. The optokinetic response is a nystagmus in the plane of motion of the visual scene. The slow-phase abnormalities on optokinetic tests parallel those detected with smooth pursuit testing, whereas abnormalities of the fast components of optokinetic nystagmus are correlated with those detected on saccade testing.

Caloric Testing

Evaluation of nystagmus induced by warm or cold water irrigation of the external canals has been used to measure vestibular function since the beginning of the twentieth century.[47] This test allows one labyrinth to be studied independently of the other. The stimuli can be applied relatively easily with techniques that are commonly available.

Bárány proposed that caloric nystagmus was the result of a convective movement of endolymph in the horizontal semicircular canal.[47] The convective flow mechanism is based on warm (44°C) or cold (30°C) water (or air) in the external auditory canal, creating a temperature gradient from one side of the horizontal canal to the other. This temperature gradient results in a density difference within the endolymph of the canal. When the horizontal canal is oriented in the plane of gravity (by elevating the head 30 degrees from the supine position or 60 degrees backward from the upright position), there is a flow of endolymph from the region with more dense fluid to the region with less dense fluid. This convective flow of endolymph leads to a deflection of the cupula and a change in the discharge rate of vestibular nerve afferents (Figure 6–11).

Endolymph will flow toward the ampulla of the horizontal canal (resulting in an increase in afferent discharge rate) for warm irrigations and away from the ampulla (resulting in a decrease in afferent discharge rate) for cold irrigations. This simple theory accounts for the dependence of the nystagmus direction on temperature and orientation of the head relative to gravity. Warm irrigations provoke a nystagmus with a slow phase away from the irrigated ear and a fast phase toward the irrigated ear, while nystagmus following irrigation with cold water is oriented in the opposite direction. Two lines of evidence support the existence of an additional, nonconvective component to the caloric response. First, caloric nystagmus can be elicited in the microgravity environment of orbital spaceflight under conditions in which there is no convection.[48] Second, caloric

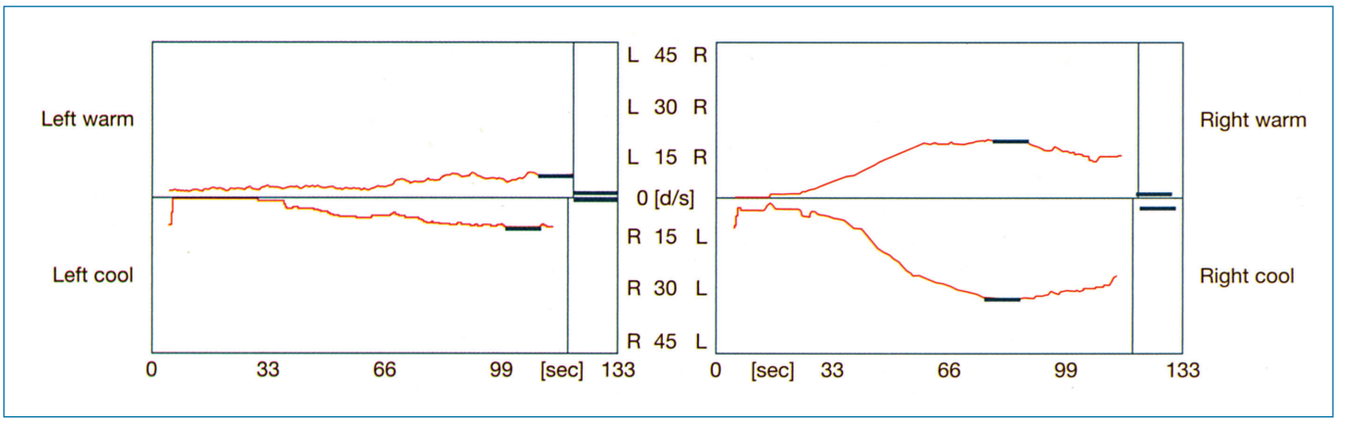

FIGURE 6–11• Caloric stimulation. Tracings represent slow-phase eye velocity following irrigation of a 49 year old female patient presenting with dizziness. Approximately 1 min is required to heat the inner ear enough to reach maximal stimulation. Both warm and cool responses on left are reduced. Jongkee's formulas reveal a 49% left weakness and a 17% left directional preponderance, with a total eye speed of 61 deg/sec. MRI suggested a meningioma in the cerebellopontine angle.

nystagmus can be elicited in animals whose canals are plugged, although the response is reduced to 30% of that obtained before plugging.[49] A direct effect of temperature on vestibular hair cells and/or afferent nerve fibers is the most likely source of the non-convective component.

The conventional Fitzgerald-Hallpike technique for caloric stimuli consists of a single temperature irrigation for 60 to 90 sec.[50] Such stimuli result in a change in temperature in the temporal bone that lasts for 10 to 20 min. This prolonged warming or cooling of the temporal bone following a single-temperature irrigation makes it necessary to allow at least 10 minutes between successive irrigations. Biphasic caloric irrigations can be used to achieve roughly the same levels of eye velocity as noted with a single-temperature irrigation while substantially reducing the duration of the change in the temperature of the temporal bone.[51]

Responses to caloric tests are analyzed by calculating the velocity of each of the slow-phase components of the nystagmus. The maximum response for each irrigation is then determined based on the three to five slow-phase components with the highest velocity. Data are interpreted in terms of unilateral weakness (UW) and directional preponderance (DP) according to formulae described by Jongkees and colleagues, where R and L indicate right and left and W and C indicate warm and cold irrigations; values are velocity of slow-phase responses in degrees per second:[52]

$$\text{Unilateral weakness} = \frac{(RW + RC) - (LW + LC)}{(RW + RC + LW + LC)} \times 100\%$$

$$\text{Directional preponderance} = \frac{(RW + LC) - (LW + RC)}{(RW + LC + LW + RC)} \times 100\%$$

Normative values are established for each laboratory, with a UW greater than 20% and a DP of greater than 25% usually considered significant. Unilateral weakness is a sign of decreased responsiveness of the horizontal canal or the ampullary nerve that provides its innervation. In patients with reduced caloric responses, ice water may be used to elicit a response. This is a particularly provocative stimulus, however, and may cause nausea or vomiting in subjects with preserved function. Directional preponderance is commonly seen in patients with spontaneous nystagmus. Patients with minimal caloric responses may truly have bilaterally reduced vestibular function, but other possibilities such as cerumen impaction and variations in technique must also be considered. Caloric responses may also be affected by blink artifacts or blepharospasm. Rotational chair testing is advised for patients with bilaterally diminished calorics.

Rotatory Tests

Head rotation is the "natural" stimulus for the AVOR. Passive, whole-body rotations can be used to deliver consistent, reproducible rotational stimuli while eye movements are recorded. Standard clinical tests typically involve low-frequency sinusoidal rotations or rapid angular accelerations or decelerations ("steps" of head velocity) about an earth-vertical axis. Rotatory testing is particularly important in several situations. It can define the extent of disease in a patient with bilaterally reduced calorics. It can increase the sensitivity of caloric testing by identifying abnormalities in the vestibulo-ocular system of patients with imbalance but without abnormal caloric exams. Alternatively, caloric examination can sometimes pick up pathology that rotational chair misses, although this is sometimes a false-positive finding due to problems with head conduction as a result of the obstruction of the external ear or poor testing technique.

Rotational chair testing takes place in a darkened room. The head is held stationary on the body to prevent proprioceptive feedback from cervical receptors. The chair is moved sinusoidally at low frequencies, typically 0.01 Hz, up to higher frequencies, usually about 1 Hz as the eye velocity is recorded (Figure 6–12). Multiple cycles of each frequency are used. The results allow the gain, or sensitivity, of the vestibulo-ocular reflex to be quantified (in degrees/s of eye movement divided by degrees/s of head movement). The normal gain is approximately 0.4 at lower frequencies and rises to 0.6 at higher frequencies. Abnormally low gain may be due to unilateral or bilateral vestibular dysfunction but, especially when calorics are normal, may be due to the patient's loss of alertness. A patient's gain may be higher when turning in one direction than when turning in the other direction. The difference in gains is termed directional asymmetry. Directional asymmetry may reflect a weakness of one labyrinth (with a reduced gain when turning toward the dysfunctional side) or an asymmetric lesion in the central vestibular pathways. In cases of unilateral vestibular hypofunction, the stimulus velocity has to reach a peak velocity of 150 to 300 degrees/s to observe an asymmetry between responses for rotations toward in comparison with those away from the side of the lesion.[53]

Although the velocity profiles of the slow phases of the nystagmus follow the sinusoidal movements of the head, they do not correspond exactly in time. This phase shift between the head rotation and the eye response is due in part to the velocity storage mechanism. It is measured in degrees, with a perfectly compensatory AVOR (where the eyes move in perfect opposition to head movement) having a phase shift by convention of 0 degrees. If the eyes reach their maximum velocity slightly before the head does, the reflex shows a phase lead, typically of about 30 degrees at lower frequencies in normal subjects. This phase lead is related to the velocity storage mechanism. Patients with loss of vestibular function have a reduced time constant of the velocity storage mechanism, leading to an abnormally high phase lead at low frequencies.[54]

Another way to measure the gain and time constant of the vestibular system is to perform steps of velocity in the rotational chair (Figure 6–13). In these tests, the patient is accelerated to a steady speed, often of 60 degrees/s. After rotating long enough to have the sensation of rotation fade away (as the velocity storage system discharges), the chair is abruptly stopped and the patient has a sudden feeling of rotation (in the direction of the force used to decelerate the chair, opposite its original direction of rotation). The gain of the system is measured by the slow-phase eye velocity immediately after the chair stops and the time constant is measured by the time it takes for the eye velocity to drop to 37% of its initial value.

The AVOR can also be evaluated from eye movement responses to head-on-body rotations that are actively generated by the patient.[55] Recent evidence suggests that repetitive,

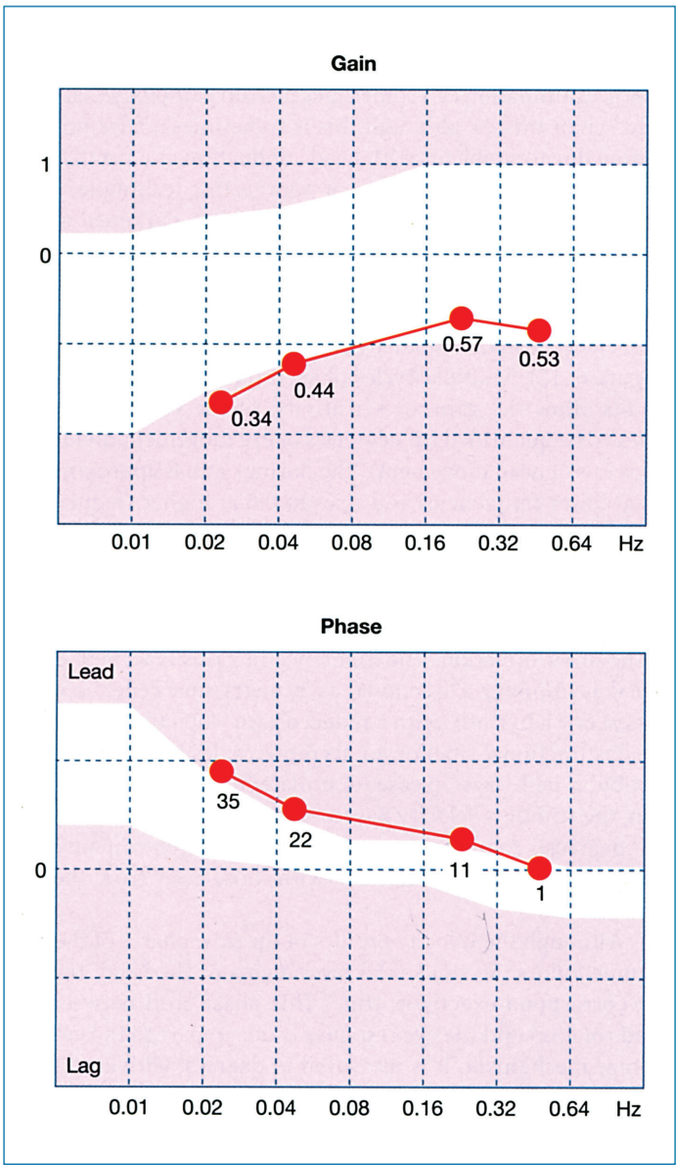

FIGURE 6–12 • Sinusoidal rotational velocity. Bilaterally deficient patient has decreased gain (falling below white band) and increased phase lead (falling above white band) at lower frequencies (0.01–0.04 Hz).

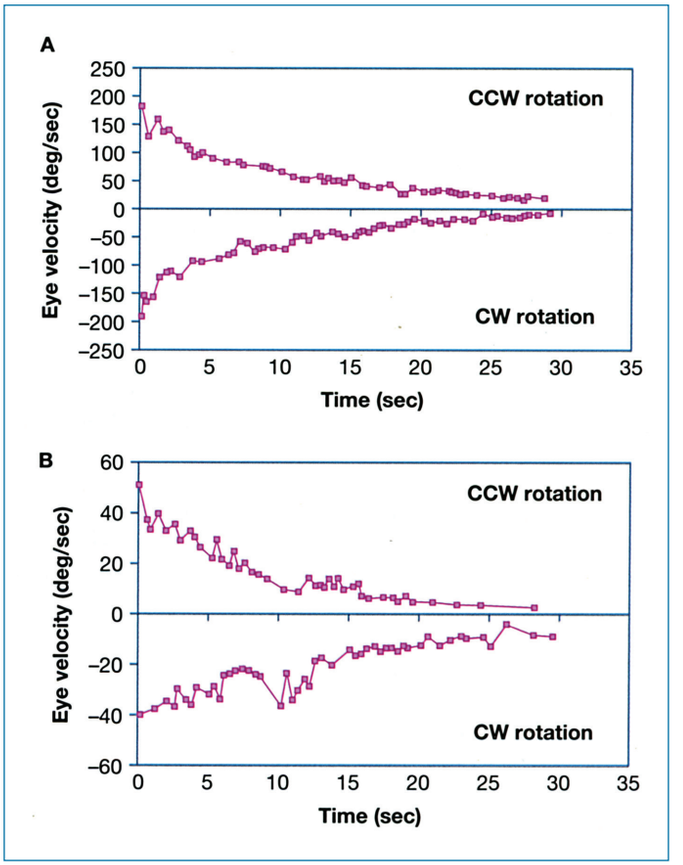

FIGURE 6–13 • Step of rotational velocity. Chair turning at 100 deg/s undergoes an abrupt stop. Normal responses shown in top panel, with a gain of 0.75 (measured as deg/s of eye velocity divided by deg/s of head velocity at the time the chair is stopped) and a time constant of 21 sec. Bilaterally deficient patient shown below, with gain of 0.4 and a time constant of 7 sec.

predictive rotational stimuli may lead to eye movement responses that arise from extralabyrinthine mechanisms (such as prediction or signals from neck proprioception).[56] Thus, the sensitivity of these tests in the identification of vestibular hypofunction may be lower than for those tests that use passive, unpredictable stimuli.

Posturography

Techniques for assessment of postural control in patients have developed in an attempt to provide quantitative measurements of processes that maintain upright stance under static and dynamic conditions.[57] These tests have conceptual appeal because they evaluate the major sensory systems (vestibular, visual, and somatosensory) that are important for maintaining balance.

The postural tests used most commonly include assessment of postural responses to platform movements and determination of effects of manipulations of visual and somatosensory information on balance while standing. The most commonly used posturography paradigm is termed the sensory organization test (SOT). This test includes six conditions selectively depriving the subject of modalities contributing to balance. The subject's balance is disrupted by blindfolding; allowing the platform to move "sway-referenced" along with the patient's center of gravity, reducing proprioceptive feedback; or moving the visual surround to remain fixed with respect to the patient as the center of gravity sways (sway-referenced vision). This last condition provides a conflicting stimulus, where vision indicates that no movement is occurring but vestibular and proprioceptive receptors indicating that it has (Figure 6–14).

The "equilibrium score" measures the patient's passive sway when standing upright in each of the six conditions. An "equilibrium score" of 100% indicates no sway and 0% indicates sway up to the theoretical limits of stability before falling. Normal equilibrium scores drop with increasing age. Patients who perform poorly on the "eyes closed, stable surface" condition may have loss of proprioceptive function; those who perform poorly on the "eyes open, sway-referenced surface" may have loss of

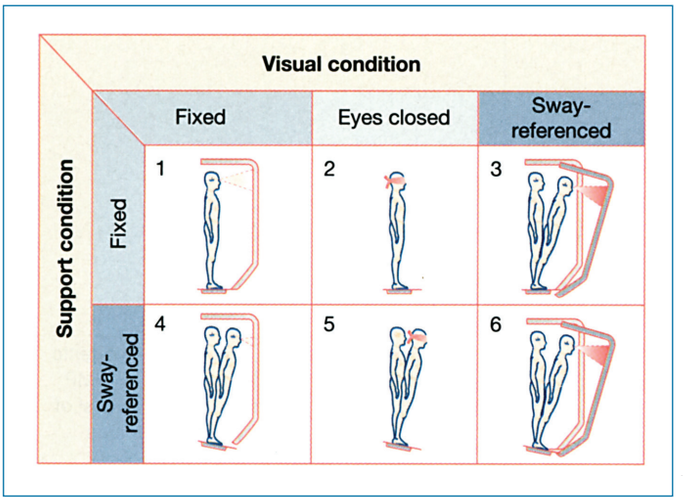

FIGURE 6–14 • Sensory organization test (SOT). Conditions 1–3 are on a stable surface; conditions 4–6 are sway-referenced. Conditions 1 and 4 are with a stable visual background, 2 and 5 are with no visual feedback, and 3 and 6 are with conflicting (sway-referenced) visual feedback.

visual contribution to balance; those who perform poorly on the "eyes closed, sway-referenced surface" may have vestibular problems, and those who perform better with their eyes closed than during "sway-referenced vision" conditions may have difficulty handling conflicting visual stimuli.

The SOT can also quantify the degree to which a subject relies on ankle motion versus hip motion to move the center of gravity to maintain balance. In normal subjects, small alignments are made by ankle movements and larger-amplitude alignments are made by hip movements. The degree to which a subject relies on each strategy is correlated with the shear force on the feet measured by the footplate. Hip dependence may occur with peripheral neuropathies that prevent the ankle joint from providing enough feedback to maintain balance. There are specifically defined clinical situations in which computerized postural assessment can have an effect on treatment outcome:[58] (1) planning a course of vestibular rehabilitation and monitoring response to this rehabilitation program in patients with vestibular hypofunction, central nervous system disorders that affect balance, or processes that require a procedure to ablate vestibular function in one ear; (2) determination of the need for procedures that remove CSF (eg, high-volume CSF drainage with lumbar punctures or a shunt) in patients with disequilibrium or gait disturbances caused by processes that result in abnormal CSF pressure dynamics; and (3) documentation of postural responses when there is suspected malingering, exaggeration of disability for compensation, or conversion disorder. Platform posturography may also be useful in evaluating a patient for proprioceptive loss and may allow cerebellar degeneration to be detected.

Evaluation of Otolith Function

Subjective Visual Vertical

The perception of the orientation of a laser-projected bar of light relative to the earth-vertical or earth-horizontal planes when subjects are in an otherwise dark room is dependent on vestibular function. The alignment of the subjective visual vertical and subjective visual horizontal has been shown to be tilted toward the lesioned side in cases of unilateral vestibular hypofunction.[59] In acute peripheral vestibular lesions, the tilt of the perception of verticality often initially measures 7 to 12 degrees. In cases of long-standing unilateral vestibular loss, the subjective visual vertical either returns to normal or remains tilted only by 2 to 3 degrees toward the side of the lesion.[60]

A modification of the test for subjective visual vertical allows the function of each ear to be tested independently. The patient is positioned in the rotational chair so that one labyrinth is on the axis of rotation and the other is slightly off-axis. In this position, centripetal force will activate the off-axis labyrinth but not the on-axis labyrinth. When the pathologic ear is off-axis, no change in the subjective vertical is elicited by rotation .[61]

Vestibular-Evoked Myogenic Potential Responses

Vestibular-evoked myogenic potential (VEMP) responses are short-latency responses measured from tonically contracting sternocleidomastoid muscles that relax in response to ipsilateral presentation of loud clicks (Figure 6–15).[62,63] These responses are thought to be of vestibular origin because they disappear after vestibular neurectomy and are still present in patients with absent hearing but intact vestibular function.[64,65] The inferior vestibular nerve has been implicated in the responses because all patients who developed posterior canal BPPV after vestibular neuritis had intact VEMP responses, whereas VEMP responses were absent in most patients after vestibular neuritis who did not develop similar symptoms of posterior canal BPPV.[66] Further work has indicated that VEMP responses probably originate in the sacculus. Vestibular-evoked myogenic potential responses can also be elicited from periocular sites, presumably related to electrical activity in the extraocular musculature in response to sound. These "oVEMP" responses have been shown to change their responsiveness in the case of superior canal dehiscence.[67] The threshold for eliciting a VEMP response is reduced in patients with superior canal dehiscence.[68] VEMP responses may be changed in patients with Ménière's disease.[69]

Audiometric Testing

Audiograms can be useful in diagnosing several causes of dizziness. Semicircular canal dehiscence often manifests with a supranormal bone-conduction line, particularly at low frequencies, with an air–bone gap.[70] Stapedial reflexes are normal. Similar findings are sometimes described in patients with enlarged vestibular aqueduct, who may become profoundly imbalanced following head trauma.[71] Patients with otosclerosis usually have conductive hearing loss with absent stapedial reflexes. Sensorineural loss is often found in patients with vestibular schwannoma. Hearing loss associated with Ménière's disease is typically low-frequency and typically varies over time. This finding can help distinguish Ménière's disease from vestibular migraine, conditions which often manifest with similar symptoms but whose treatments are generally distinct. However, migraine may also be related to hearing loss.[72] In later stages of the disease, the level of hearing loss tends to remain stable. Perilymphatic fistulas can also manifest with varying levels of hearing loss.

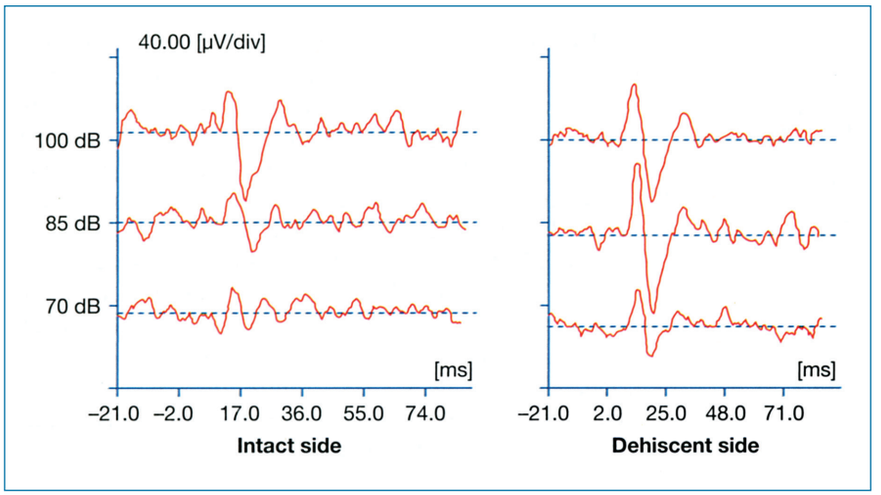

FIGURE 6–15 • Vestibular-evoked myogenic response. Both sides demonstrate a VEMP response to a click at a presentation level of 100 dB SPL. The dehiscent side remains sensitive even at lower amplitudes of stimulation.

FIGURE 6–16 • Temporal bone CT scan from patient with superior canal dehiscence syndrome. Patient's responses shown in Figure 4–9. Projection of the CT image of the right temporal bone into the plane of the superior canal. A dehiscence measuring 3.7 mm in length is noted overlying the superior canal (arrows). *Reproduced with permission from Minor LB, Cremer PD, Carey JP, and colleagues. Symptoms and signs in superior canal dehiscence syndrome. Ann NY Acad Sci 2001;942: 259–273.*

Electrocochleography is an audiometric test that is sometimes used for diagnosing Ménière's disease. However, Ménière's is diagnosed based on clinical criteria, which are not closely matched by results of electrocochleography so its utility in identifying patients with Ménière's is limited.[73]

Radiologic and Serologic Tests

Computerized tomography is commonly used to evaluate patients with sound- or pressure-induced nystagmus. Dehiscence of the superior or posterior canals into the intracranial space as well as dehiscences of the horizontal canal into the middle ear (such as caused by cholesteatoma) may be visualized (Figure 6–16). Congenital dysplasia of the semicircular canals, enlarged vestibular aqueduct, and temporal bone fractures are also visualizable on CT scan.

MRI can be used to visualize tumors of the internal auditory canal, cerebellopontine angle, and brain. It can also indicate other central pathologies underlying symptoms of dizziness such as cerebellar degeneration, stroke, or multiple sclerosis. It may also indicate pathology of the temporal bone such as labyrinthine dysmorphisms and enlarged vestibular aqueduct or of the posterior fossa such as Arnold–Chiari malformation.

Serologic tests are of limited use for diagnosing patients with imbalance. Two notable exceptions are syphilis and Cogan's syndrome. In patients with episodic imbalance consistent with endolymphatic hydrops, or with a high likelihood of sexually transmitted disease, syphilis testing is appropriate.[74] In patients with abrupt onset of ocular symptoms with imbalance, testing for inflammatory markers of Cogan's syndrome is imperative as prompt initiation of treatment can be critical in controlling potentially life-threatening complications.[75]

DISORDERS AFFECTING VESTIBULAR FUNCTION

In this section, we review some of the more common vestibular disorders with an emphasis on their pathophysiology. This brief overview of labyrinthine abnormalities can be supplemented by other sources that address these and other peripheral and central vestibular disturbances in greater detail.

Benign Paroxysmal Positional Vertigo

Benign paroxysmal positional vertigo is the most common cause of vertigo arising from labyrinthine dysfunction.[76] It is characterized by rotatory vertigo brought on when the head is rolled to the side, as when turning over in bed, and backward with a sideways tilt, as when getting out of bed or walking up stairs. In order of frequency, known causes of BPPV include head trauma, middle ear infection, viral labyrinthitis, ear surgery, or bed rest. Half of occurrences have no clear precipitating event. BPPV occurs in children and in adults, although the incidence increases with age. Among those cases without a clear cause,

the average age of onset was in the sixth decade, with females outnumbering males two to one.[77] Signs of BPPV may be present in up to 10% of the elderly, including those without specific complaints of imbalance.

Vertigo typically begins after a latent period—up to 20 sec after positioning the head—and continues for less than a minute before subsiding. It is provoked by the Dix-Hallpike maneuver, in which a patient is moved rapidly from a sitting to a supine position, head turned sharply to the side and shoulders hanging off the end of the examination table. Symptoms lessen if the head is repeatedly placed in the offending position. Knowledge of the anatomy and physiology of the labyrinth has allowed practitioners to develop a working theory for the cause of these symptoms and effective maneuvers to reverse them. Indeed, this sometimes crippling disease can often be completely cured in a single office visit.

In his original description of BPPV, Bárány[78] noted that if a patient's eyes were directed away from the affected ear, they tended to move with a vertical nystagmus (beating upward), whereas if they looked toward the affected ear, they moved with a torsional nystagmus (beating with the superior poles of the eyes directed toward the downward ear). These eye movements are identical to those expected from a stimulation of the posterior semicircular canal, leading this canal to be considered the source of pathology although it can affect the horizontal and superior canals as well.[79]

The actual mechanism of stimulation of the posterior semicircular canal has been confirmed with the observation of free-floating debris in the canal during surgery on a patient with BPPV, an occurrence that is now termed canalithiasis.[80] With the head tilted and hanging over the side of the table, free-floating debris in the posterior canal falls away from the cupula, drawing it away from the ampulla as the debris sinks.[81] The brain interprets that this deflection is caused by rotation of the head around the axis of the canal and creates a compensatory motion of the eyes—motion that is seen as nystagmus when a patient with BPPV is placed in the Dix-Hallpike position.

In addition to explaining the direction of nystagmus in BPPV, canalolithiasis also explains its time course: the sludgy debris in the posterior canal takes some time to begin sliding down the wall of the membranous canal after the head assumes a new position and requires about 1 min before coming to rest at the most dependent part of the canal and terminates the episode of vertigo. Repeated motion of the debris may allow some of it to escape through the open end of the canal, causing the signs and symptoms of posterior canal BPPV to wane with serial testing; this process may also explain the resolution of BPPV in some patients.

Current therapy for BPPV involves repositioning maneuvers that, in cases of canalolithiasis, use gravity to move canalith debris out of the affected semicircular canal and into the vestibule. For posterior canal BPPV, the maneuver developed by Epley[82] and later modified[83] is particularly effective. The maneuver begins with placement of the head into the Dix-Hallpike position that evokes vertigo. The posterior canal on the affected side is in the earth-vertical plane with the head in this position. After the initial nystagmus goes away, there is a 180-degree roll of the head (in two 90-degree increments, stopping in each position until any nystagmus resolves) to the position in which the offending ear is up (ie, the nose is pointed at a 45-degree angle toward the ground in this position). The patient is then brought to the sitting upright position (Figure 6–17). The maneuver is likely to be successful when nystagmus of the same direction continues to be elicited in each of the new positions (as the debris continues to move away from the cupula). The maneuver is repeated until no nystagmus is elicited. This treatment is typically effective in up to 90% of cases in eliminating BPPV.[84] The Semont maneuver moves the otoconial debris through the labyrinth in a manner similar to the Epley maneuver with similar efficacy.[85]

A horizontal canal variant of BPPV has also been identified.[86] The nystagmus typically has a longer duration than that noted with posterior canal BPPV. The direction may beat toward (geotropic) or away from (ageotropic) the downward ear. In cases that involve geotropic nystagmus, lying on one side with the affected ear up for about 12 h eliminates the disorder in most cases. Debris embedded in the cupula or in the canal relatively close to the ampulla may cause ageotropic nystagmus. A repositioning maneuver consisting of a "log roll" of the supine patient may sometimes be effective.[87] A superior canal variant of BPPV has also been described. It is very rare and difficult to treat successfully. Treatment with repositioning maneuvers for BPPV of any canal may direct otoconial debris into previously unaffected canals, necessitating a change in appropriate maneuvers.

Vestibular Migraine

Vestibular migraine is an increasingly recognized cause of episodic imbalance. Up to 25% of patients with migraine headaches have vertigo.[88] Vertigo may occur as an aura related to a migraine headache or may occur in isolation. Symptoms are typically brought on by strong visual or vestibular stimuli but may be provoked by other factors such as changes in the weather, menses,[89] or, quite commonly, particular foods, especially those containing caffeine. Symptoms typically last hours to days, which helps distinguish it from Ménière's disease whose symptoms generally resolve after a few hours.

Twenty-one percent of patients with vestibular migraine have reduced responses on vestibular testing.[90] Hearing loss may occur in patients with vestibular migraine.[91] It may occur in conjunction with BPPV[92] or in patients with symptoms of Ménière's.[93] Patients previously diagnosed with other conditions, in particular Ménière's disease, may in fact best be understood to have a migraine-related process. Children with paroxysmal vertigo of childhood, which typically occurs in patients 4 to 8 years old, may develop more typical symptoms of migraine as they age.[94,95] A positive family history is common in patients with migraine-like symptoms. Many patients who are now understood to have vestibular migraine carry a previous diagnosis of Ménière's disease.

Semicircular Canal Dehiscence Syndrome

A syndrome of vertigo and oscillopsia induced by loud noises or by stimuli that change middle ear or intracranial pressure has recently been defined in patients with a dehiscence of bone

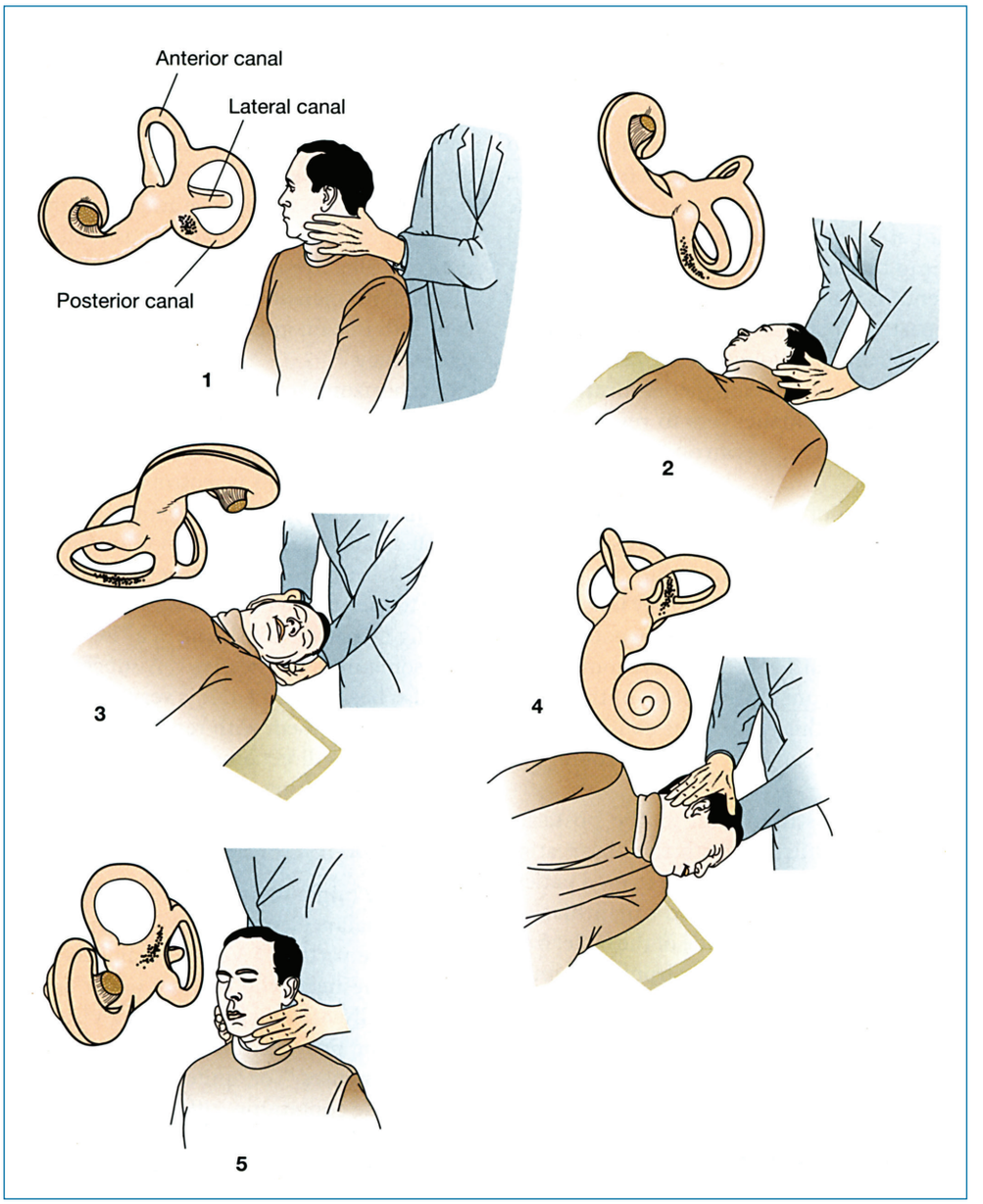

FIGURE 6–17 • Canalith repositioning maneuver for treatment of benign paroxysmal positional vertigo (BPPV) affecting the posterior canal. Panel 1 shows a patient with right posterior canal BPPV. The patient's head is turned to the right at the beginning of the canalith repositioning maneuver. The inset shows the location of the debris near the ampulla of the posterior canal. The diagram of the head in each inset shows the orientation from which the labyrinth is viewed. In panel 2, the patient is brought into the supine position with the head extended below the level of the bed. The debris falls toward the common crus as the head is moved backward. In panel 3, the head is moved approximately 180 degrees to the left while keeping the neck extended with the head below the level of the gurney. Debris enters the common crus as the head is turned toward the contralateral side. In panel 4, the patient's head is further rotated to the left by rolling onto the left side until the patient's head faces down. Debris begins to enter the vestibule. In panel 5, the patient is brought back to the upright position. Debris collects in the vestibule. *Illustration by David Rini.*

overlying the superior semicircular canal.[40,41] These patients may also experience chronic disequilibrium. The dehiscence creates a third mobile window into the inner ear, thereby allowing the superior canal to respond to sound and pressure stimuli. The evoked eye movements in this syndrome align with the affected superior canal (Ewald's first law).[42] Loud sounds, positive pressure in the external auditory canal, and Valsalva's maneuver against pinched nostrils stimulate the canal and produce a nystagmus that has slow-phase components that are directed upward with torsional motion of the superior pole of the eye away from the affected ear. Conversely, negative pressure in the external canal, Valsalva's maneuver against a closed glottis, and jugular venous compression can cause oppositely directed eye movements (slow-phase components directed downward

with torsional motion of the superior pole of the eye toward the affected ear). These eye movement findings have been documented with three-dimensional search coil techniques and can be readily observed on clinical examination. Frenzel lenses should be used for this examination because visual fixation can lead to suppression of the evoked eye movements.

Patients with superior canal dehiscence syndrome have abnormally low thresholds for VEMP responses in the affected ear.[68] Patients often have supranormal bone line and a low-frequency conductive hearing loss with intact stapedial reflexes.[70,96] Temporal bone CT scans in patients with superior canal dehiscence syndrome reveal an absence of bone overlying the affected canal. It is important to remember, however, that a thin but intact layer of bone can appear as a dehiscence on a CT scan because of partial volume averaging. The specificity of temporal bone CT in the diagnosis of superior canal dehiscence syndrome can be improved with the use of reconstructed slice thickness of 0.5 mm or less and projection of images into the plane of the superior canal (Figure 6–11). The diagnosis of this syndrome depends on clinical symptoms and radiographic evidence of dehiscence. Similar symptoms may also be elicited in patients with a dehiscence in the posterior or horizontal canal.

Vestibular Neuritis

Vertigo associated with vestibular neuritis begins suddenly, may last for days with gradual resolution, and is frequently incapacitating early in its course. In support of an infectious etiology is the occurrence of cases around the same time within households or in association with upper respiratory infections. A vascular etiology has been suspected because the condition often spares the inferior division of the vestibular nerve, which is supplied by the posterior vestibular artery while the superior division of the vestibular nerve is supplied by the anterior vestibular artery.

Signs of unilateral vestibular hypofunction are readily apparent early in the course of the illness. These signs include a spontaneous nystagmus with horizontal and torsional slow components that are directed toward the ear with hypofunction and fast components directed oppositely. The horizontal eye velocity of this nystagmus frequently increases in amplitude when patients look in the direction of the fast component. It can be suppressed by looking at a stationary object, whereas the torsional eye velocity (rotation about the line of sight) of the nystagmus is not affected by this maneuver.

The vertigo and nystagmus in such a lesion of the cerebellum can be similar to that observed in vestibular neuritis.[97] It is important that these be distinguished, as a stroke involving the inferior cerebellum can lead to swelling, brain stem compression, and death unless there is prompt neurosurgical intervention. One key distinguishing feature is the degree of postural instability. Patients with cerebellar hemorrhage or infarction are typically unable to walk and are very unstable when standing. Patients with vestibular neuritis, in contrast, are likely to have an unsteady gait, but they can walk. Appropriate imaging such as a magnetic resonance imaging scan of the brain and posterior fossa should be obtained when there is suspicion that the symptoms may arise from an abnormality affecting the cerebellum or brain stem.

Recovery of balance reflexes following vestibular neuritis occurs through three mechanisms: spontaneous return of vestibular function in the affected ear (in about 50% of cases), vestibular adaptation, and substitution of other sensory or motor strategies. Vestibular adaptation involves recalibration of motor responses to diminished signals from a labyrinth. Some examples of substitution strategies include rapid eye movements in response to head movements toward the lesioned labyrinth and use of visual and proprioceptive information to maintain postural stability after loss of vestibular function.

Chemical Vestibulopathy

Vestibular neuritis leads to signs of an unequal level of activity between the two labyrinths, vestibular hypofunction resulting from chemical toxicity (often an aminoglycoside such as gentamicin administered intravenously) is commonly bilateral and symmetric.[98] Vestibulotoxicity is often noted without accompanying injury to the auditory system and can occur even when serum peak and trough levels are within appropriate ranges.[99] Patients typically do not experience vertigo, although oscillopsia with head movements and disequilibrium are commonly noted.

Ménière's Disease

Ménière's disease is characterized by episodic vertigo, tinnitus, fluctuating sensorineural hearing loss, and aural fullness (a pressure sensation deep within the ear). In contrast to the vertigo in BPPV, which typically lasts for only seconds during a single episode, the vertigo in an attack of Ménière's disease has a duration that varies from 30 min to several hours. It typically affects one ear, although bilateral involvement has been reported in 2 to 78% of cases.[100] Females are more often affected than males, and early middle age is a typical age of onset. An incidence of 15 per 100,000 and a prevalence of 218 per 100,000 have been reported.[101] Ménière's disease typically accounts for about 10% of the visits to clinics specializing in vestibular disorders.[76]

Abnormalities in the production and/or resorption of endolymph are thought to underlie the histopathologic changes that are seen in the cochlea and labyrinth of ears affected with Ménière's disease. Most cases are presumed to be idiopathic, although the clinical syndrome can follow infections affecting the inner ear such as mumps or measles, syphilis, or meningitis. Symptoms may also begin following head trauma. Antibodies to a 68-kDa protein (heat shock protein 70) have been noted in patients with Ménière's disease but the clinical utility of serologic testing for this marker is uncertain.[102]

Endolymphatic hydrops, the classic abnormality noted in Ménière's disease, is characterized by dilatation of the endolymphatic spaces with periodic rupture of the membranes that separate endolymphatic from perilymphatic compartments. Although endolymphatic hydrops is a consistent finding in the temporal bones of patients in whom a diagnosis of Ménière's disease had been made, it is not a specific finding as these pathologic changes have been noted in patients with no premorbid symptoms or signs suggestive of Ménière's disease.[103]

Attacks of vertigo are frequently the most disabling symptom in Ménière's disease. The vertigo may be rotatory, in which case semicircular canal dysfunction is suspected, or may consist of a precipitous sensation of being pulled toward one side, as might result from a sudden change in otolith activity. The nystagmus during an episode of vertigo may be "excitatory" with respect to the involved labyrinth (with slow components directed away from the affected ear), although clinical examination between episodes of vertigo may reveal signs of vestibular hypofunction. The hearing loss in Ménière's disease is commonly more severe for the low frequencies.

Low-salt diets and diuretics control episodes of vertigo in most patients. Intratympanic or oral steroids have also been shown to be useful.[104] Opening the endolymphatic sac on the affected side is used by some practitioners, although its effectiveness is in doubt. Refractory cases with unilateral involvement can be managed with procedures that ablate vestibular function in the affected ear. Selective sectioning of the vestibular nerve (when there is useful hearing remaining) and labyrinthectomy (when hearing is absent) have been the procedures of choice. More recent studies have demonstrated that vertigo can be controlled in most patients, with a low risk of hearing loss, by injecting gentamicin into the middle ear.[105] Recent studies have shown that a single intratympanic injection of gentamicin is effective in achieving control of vertigo in most cases.[106] Patients requiring cochlear implantation as a result of hearing loss due to Ménière's have been reported to have fewer attacks of vertigo following surgery.[107]

Vestibular Schwannoma

Vestibular schwannoma may present with imbalance, although typically the slow growth of the tumor allows compensation to occur and symptoms to be minimal. Frank vertigo affects a small percentage of patients, but vague imbalance is much more common. Vestibular schwannomas tend to occur on the superior vestibular nerve. Because this nerve carries fibers from the horizontal canal, standard caloric responses are often abnormal in patients. However, because VEMP responses are due to saccular reflexes carried by the inferior vestibular nerve, they may be preserved. Eye movements typical of posterior fossa mass lesions include Brun's nystagmus and nystagmus with lateral gaze that follows Alexander's law (Figure 6–9).

Vascular Disease

Both central and peripheral symptoms of imbalance may occur in patients with vertebrobasilar insufficiency. Sixty-two percent of patients with vertebrobasilar insufficiency have vertigo and 26% have paresis of the horizontal canal.[108] Transient ischemic attacks involving the posterior circulation may manifest as vertigo lasting for several minutes, with other neurologic symptoms appearing in more severe lesions. Patients with other types of vertigo are usually able to walk despite their symptoms, but those with serious brain stem lesions can be distinguished because they are often too ataxic to ambulate. Like patients with migraine, patients with vascular insufficiency may be more susceptible to BPPV. Several inflammatory conditions may affect the posterior circulation and cause dizziness, including Cogan's syndrome (which typically presents along with visual symptoms) and Susac's syndrome (which includes symptoms of encephalopathy).

References

1. Kroenke K, Arrington ME, Mangelsdorff AD. The prevalence of symptoms in medical outpatients and the adequacy of therapy. Arch Intern Med 1990;150:1685–89.
2. Kroenke K, Mangelsdorff AD. Common symptoms in ambulatory care: Incidence, evaluation, therapy, and outcome. Am J Med 1989;86:262–6.
3. Wersäll J, Bagger-Sjoback D. Morphology of the vestibular sense organ. In:. Vestibular system. part I: Basic mechanisms. Berlin: Springer; 1974. p. 123–70.
4. Precht W. Vestibular mechanisms. Annu Rev Neurosci 1979;2:265–89.
5. Park J, Tang Y, Lopez I, Ishiyama A. Age-related change in the number of neurons in the human vestibular ganglion. J Comp Neurol 2001;431:437–43.
6. Highstein SM, Baker R. Action of the efferent vestibular system on primary afferents in the toadfish. Opsanus tau. J Neurophysiol 1985;54:370–84.
7. Goldberg JM, Fernandez C. Physiology of peripheral neurons innervating semicircular canals of the squirrel monkey I. Resting discharge and response to constant angular accelerations. J Neurophysiol 1971;34:635–60.
8. Baird RA, Desmadryl G, Fernandez C, Goldberg JM. The vestibular nerve of the chinchilla. II. Relation between afferent response properties and peripheral innervation patterns in the semicircular canals. J Neurophysiol 1988;60:182–203.
9. Hullar TE, Della Santina CC, Hirvonen TP, et al. Responses of irregularly discharging chinchilla semicircular canal vestibular-nerve afferents during high-frequency head rotations. J Neurophysiol 2005;93:2777–86.
10. Hullar TE, Lasker DM, Carey JP, Minor LB. Responses of irregular vestibular nerve afferents to high-frequency rotations. J Vestib Res 2002;11:176.
11. Sadeghi SG, Chacron MJ, Taylor MC, Cullen KE. Neural variability, detection thresholds, and information transmission in the vestibular system. J Neurosci 2007;27:771–81.
12. Ewald JR. Physiologische Untersuchungen über das Endorgan des Nervus Octavus. Wiesbaden, Germany: Bergmann; 1892.
13. Tabak S, Collewijn H, Boumans LJJM, Van der Steen J. Gain and delay of human vestibulo-ocular reflexes to oscillation and steps of the head by a reactive torque helmet I. Normal subjects. Acta Otolaryngol 1997;117:785–95.
14. Burr DC, Ross J. Contrast sensitivity at high velocities. Vision Res 1982;22:479–84.
15. Raphan T, Matsuo V, Cohen B. Velocity storage in the vestibulo-ocular reflex arc (VOR). Exp Brain Res 1979;35:229–48.
16. Katz E, Vianney de Jong JMB, Buttner-Ennever JA, Cohen B. Effects of midline section on the velocity storage and the vestibulo-ocular reflex. Exp Brain Res 1991;87:505–29.
17. Arnold DB, Robinson DA. The oculomotor integrator: Testing of a neural network model. Exp Brain Res 1997;113:57–74.
18. Cannon SC, Robinson DA. Loss of the neural integrator of the oculomotor system from brain stem lesions in monkey. J Neurophysiol 1987;57:1383–409.
19. Zee DS, Fletcher WA. Bedside examination. In: Baloh RW, Halmagyi GM, editors. Disorders of the vestibular system. New York: Oxford University Press; 1996. p. 178–90.

20. Halmagyi GM, Cremer PD. Assessment and treatment of dizziness. J Neurol Neurosurg Psychiatry 2000;68:129–34.
21. Lermoyez M. Le vertige qui fait entendre (angiospasme labyrinthique). Presse Medicale 1919;27:1–3.
22. Cha YH, Kane MJ, Baloh RW. Familial clustering of migraine, episodic vertigo, and Ménière's disease. Otol Neurotol 2008;29:93–6.
23. Jen JC, Graves TD, Hess EJ, et al. Primary episodic ataxias: Diagnosis, pathogenesis and treatment. Brain 2007;130: 2484–93.
24. McClure JA, Copp JC, Lycett P. Recovery nystagmus in Ménière's disease. Laryngoscope 1981;91:1727–37.
25. Hotson JR. Convergence-initiated voluntary flutter: A normal intrinsic capability in man. Brain Res 1984;294:299–304.
26. Abel LA, Parker L, Daroff RB, Dell'Osso LF. End-point nystagmus. Invest Ophthalmol Vis Sci 1978;17:539–44.
27. Leigh R, Zee D. The neurology of eye movements. New York: Oxford University Press; 2006.
28. Baloh RW, Jacobson KJ, Honrubia V. Horizontal semicircular canal variant of benign positional vertigo. Neurology 1993;43:2542–49.
29. Katsarkas A. Positional nystagmus of the "central type" as an early sign of multiple sclerosis. J Otolaryngol 1982;11:91–3.
30. McAuley JR, Dickman JD, Mustain W, Anand VK. Positional nystagmus in asymptomatic human subjects. Otolaryngol Head Neck Surg 1996;114:545–53.
31. Fetter M, Haslwanter T, Bork M, Dichgans J. New insights into positional alcohol nystagmus using three-dimensional eye-movement analysis. Ann Neurol 1999;45:216–23.
32. Hain TC, Fetter M, Zee DS. Head-shaking nystagmus in patients with unilateral peripheral vestibular lesions. Am J Otolaryngol 1987;8:36–47.
33. Fetter M, Zee DS, Koenig E, Dichgans J. Head shaking nystagmus during vestibular compensation in humans and rhesus monkeys. Acta Otolaryngol 1990;110:175–81.
34. Halmagyi GM, Curthoys IS, Cremer PD, et al. The human horizontal vestibulo-ocular reflex in response to high-acceleration stimulation before and after unilateral vestibular neurectomy. Exp Brain Res 1990;81:479–90.
35. Tian J, Crane BT, Demer JL. Vestibular catch-up saccades in labyrinthine deficiency. Exp Brain Res 2000;131:448–57.
36. Cremer PD, Halmagyi GM, Aw ST, et al. Semicircular canal plane head impulses detect absent function of individual semicircular canals. Brain 1998;121:699–716.
37. Kasai T, Zee DS. Eye-head coordination in labyrinthine-defective human beings. Brain Res 1978;144:123–41.
38. Tian JR, Shubayev I, Demer JL. Dynamic visual acuity during transient and sinusoidal yaw rotation in normal and unilaterally vestibulopathic humans. Exp Brain Res 2001;137: 12–25.
39. Herdman SJ, Tusa RJ, Blatt P, et al. Computerized dynamic visual acuity test in the assessment of vestibular deficits. Am J Otol 1998;19:790–6.
40. Minor LB, Solomon D, Zinreich JS, Zee DS. Sound- and/or pressure-induced vertigo due to bone dehiscence of the superior semicircular canal. Arch Otolaryngol Head Neck Surg 1998;124:249–58.
41. Minor LB. Superior canal dehiscence syndrome. Am J Otol 2000;21:9–19.
42. Cremer PD, Minor LB, Carey JP, Della Santina CC. Eye movements in patients with superior canal dehiscence syndrome align with the abnormal canal. Neurology 2000;55:1833–41.
43. Minor LB, Haslwanter T, Straumann D, Zee DS. Hyperventilation-induced nystagmus in patients with vestibular schwannoma. Neurology 1999;53:2158–68.
44. Fukuda T. The stepping test: Two phases of the labyrinthine reflex. Acta Otolaryngol 1958;50:95–108.
45. Shumway-Cook A, Horak FB. Assessing the influence of sensory interaction of balance. Suggestion from the field. Phys Ther 1986;66:1548–50.
46. Robinson DA. A method of measuring eye movement using a scleral search coil in a magnetic field. IEEE Trans Biomed Eng 1963;10:137–45.
47. Bárány R. Untersuchungen über den vom Vestibularapparat des Ohres reflektorisch ausgelösten rythmischen Nystagmus und seine Begleiterscheinungen. Mschr Ohrenheilkd 1906;40: 193–297.
48. von Baumgarten R, Benson A, Berthoz A, et al. Effects of rectilinear acceleration and optokinetic and caloric stimulations in space. Science 1984;225:208–12.
49. Paige GD. Caloric responses after horizontal canal inactivation. Acta Otolaryngol 1985;100:321–7.
50. Fitzgerald G, Hallpike CS. Studies in human vestibular function: I. Observations on the directional preponderance ("Nystagmusbereitschaft") of caloric nystagmus resulting from cerebral lesions. Brain 1942;65:115–37.
51. Proctor LR, Dix RC. New approach to caloric stimulation of the vestibular receptor. Ann Otol Rhinol Laryngol 1975;84: 683–94.
52. Jongkees LBW, Maas JPM, Philipszoon AJ. Clinical nystagmography: A detailed study of electronystagmography in 341 patients with vertigo. Pract Otorhinolaryngol 1962;24:65–93.
53. Baloh RW, Jacobson KM, Beykirch K, Honrubia V. Horizontal vestibulo-ocular reflex after acute peripheral lesions. Acta Otolaryngol Suppl 1989;468:323–7.
54. Baloh RW, Honrubia V, Yee RD, Hess K. Changes in the human vestibulo-ocular reflex after loss of peripheral sensitivity. Ann Neurol 1997;16:222–28.
55. Hoffman DL, O'Leary DP, Munjack DJ. Autorotation test abnormalities of the horizontal and vertical vestibulo-ocular reflexes in panic disorder. Otolaryngol Head Neck Surg 1994;110:259–69.
56. Wiest G, Demer JL, Tian J, Crane BT, et al. Vestibular function in severe bilateral vestibulopathy. J Neurol Neurosurg Psychiatry 2001;71:53–7.
57. Nashner LM, Black FO, Wall III C. Adaptation to altered support and visual conditions during stance: patients with vestibular deficits. J Neurosci 1982;2:536–43.
58. Minor LB. Utility of posturography in management of selected conditions that cause dizziness. Am J Otol 1997;18:113–5.
59. Curthoys IS, Dai MJ, Halmagyi GM. Human ocular torsional position before and after unilateral vestibular neurectomy. Exp Brain Res 1991;85:218–25.
60. Tabak S, Collewijn H, Boumans LJJM. Deviation of the subjective vertical in long-standing unilateral vestibular loss. Acta Otolaryngol 1997;117:1–16.
61. Clarke AH, Schonfeld U, Hamann C, Scherer H. Measuring unilateral otolith function via the otolith-ocular response and the subjective visual vertical. Acta Otolaryngol Suppl 2001;545:84–7.

62. Colebatch JG, Halmagyi GM, Skuse NF. Myogenic potentials generated by a click-evoked vestibulocollic reflex. J Neurol Neurosurg Psychiatry 1994;57:190–7.
63. Ferber-Viart C, Dubreuil C, Duclaux R. Vestibular evoked myogenic potentials in humans: A review. Acta Otolaryngol 1999;119:6–15.
64. Colebatch JG, Halmagyi GM. Vestibular evoked potentials in human neck muscles before and after unilateral vestibular deafferentation. Neurology 1992;42:1635–6.
65. Matsuzaki M, Murofushi T, Mizuno M. Vestibular evoked myogenic potentials in acoustic tumor patients with normal auditory brainstem responses. Eur Arch Otorhinolaryngol 1999;256:1–4.
66. Murofushi T, Halmagyi GM, Yavor RA, Colebatch JG. Absent vestibular evoked myogenic potentials in vestibular neurolabyrinthitis. An indicator of inferior vestibular nerve involvement? Arch Otolaryngol Head Neck Surg 1996;122:845–8.
67. Todd NP, Rosengren SM, Aw ST, Colebatch JG. Ocular vestibular evoked myogenic potentials (OVEMPs) produced by air- and bone-conducted sound. Clin Neurophysiol 2007;118:381–90.
68. Streubel SO, Cremer PD, Carey JP, et al. Vestibular-evoked myogenic potentials in the diagnosis of superior canal dehiscence syndrome. Acta Otolaryngol Suppl 2001;545:41–9.
69. Timmer FC, Zhou G, Guinan JJ, Kujawa SG, et al. Vestibular evoked myogenic potential (VEMP) in patients with Ménière's disease with drop attacks. Laryngoscope 2006;116:776–9.
70. Mikulec AA, McKenna MJ, Ramsey MJ, Rosowski JJ, et al. Superior semicircular canal dehiscence presenting as conductive hearing loss without vertigo. Otol Neurotol 2004;25:121–9.
71. Merchant SN, Nakajima HH, Halpin C, Nadol JB, Jr., et al. Clinical investigation and mechanism of air–bone gaps in large vestibular aqueduct syndrome. Ann Otol Rhinol Laryngol 2007;116:532–41.
72. Bernard PA, Stenstrom RJ. Fluctuating hearing losses in children can be migraine equivalents. Int J Pediatr Otorhinolaryngol 1988;16:141–8.
73. Kim HH, Kumar A, Battista RA and Wiet RJ. Electrocochleography in patients with Ménière's disease. Am J Otolaryngol 2005;26:128–131.
74. Yimtae K, Srirompotong S, Lertsukprasert K. Otosyphilis: a review of 85 cases. Otolaryngol Head Neck Surg 2007;136:67–71.
75. Haynes BF, Kaiser-Kupfer MI, Mason P, Fauci AS. Cogan syndrome: Studies in thirteen patients, long-term follow-up, and a review of the literature. Medicine 1980;59:426–41.
76. Nedzelski JM, Barber HO, McIlmoyl L. Diagnosis in a dizziness unit. J Otolaryngol 1986;15:101–4.
77. Katsarkas A. Paroxysmal positional vertigo: an overview and the deposits repositioning maneuver. Am J Otol 1995;16:725–30.
78. Bárány R. Diagnose von Krankheitserscheinungen im Bereiche des Otolithenapparates. Acta Otolaryngol Suppl 1921;2: 434–7.
79. Cohen B, Suzuki J-I, Bender MB. Eye movements from semicircular canal nerve stimulation in the cat. Ann Otol Rhinol Laryngol 1964;73:153–69.
80. Parnes LS, McClure JA. Free-floating endolymph particles: A new operative finding during posterior semicircular canal occlusion. Laryngoscope 1992;102:988–92.
81. Epley JM. New dimensions of benign paroxysmal positional vertigo. Otolaryngol Head Neck Surg 1980;88:599–605.
82. Epley JM. The canalith repositioning procedure: for treatment of benign paroxysmal positional vertigo. Otolaryngol Head Neck Surg 1992;107:399–404.
83. Herdman SJ, Tusa RJ, Zee DS, et al. Single treatment approaches to benign paroxysmal positional vertigo. Arch Otolaryngol Head Neck Surg 1993;119:450–4.
84. Lynn S, Pool A, Rose D, et al. Randomized trial of the canalith repositioning procedure. Otolaryngol Head Neck Surg 1995;113:712–20.
85. Semont A, Freyss G, Vitte E. Curing the BPPV with a liberatory maneuver. Adv Otorhinolaryngol 1988;42:290–3.
86. McClure JA. Horizontal canal BPV. J Otolaryngol 1985;14: 30–5.
87. Fife T. Recognition and management of horizontal canal benign positional vertigo. Am J Otol 1998;19:345–51.
88. Kayan A, Hood J. Neuro-otological manifestations of migraine. Brain 1984;107:1123–42.
89. Grunfeld E, Price C, Goadsby P, Gresty M. Motion sickness, migraine, and menstruation in mariners. Lancet 1998; 351:1106.
90. Cutrer FM, Baloh RW. Migraine-associated dizziness. Headache 1992;32:300–04.
91. Viirre ES, Baloh RW. Migraine as a cause of sudden hearing loss. Headache 1996;36:24–8.
92. Ishiyama A, Jacobson KM, Baloh RW. Migraine and benign positional vertigo. Ann Otol Rhinol Laryngol 2000;109: 377–80.
93. Rassekh CH, Harker LA. The prevalence of migraine in Ménière's disease. Laryngoscope 1992;102:135–8.
94. Lanzi G, Balottin U, Fazzi E, et al. Benign paroxysmal vertigo of childhood: A long-term follow-up. Cephalgia 1999;14:458–60.
95. Basser L. Benign paroxysmal vertigo of childhood. Brain 1964;87:141–52.
96. Minor LB. Clinical manifestations of superior semicircular canal dehiscence. Laryngoscope 2005;115:1717–27.
97. Hotson JR, Baloh RW. Acute vestibular syndrome. N Engl J Med 1998;339:680–5.
98. Minor LB. Gentamicin-induced bilateral vestibular hypofunction. JAMA 1998;279:541–4.
99. Halmagyi GM, Fattore CM, Curthoys IS, Wade S. Gentamicin vestibulotoxicity. Otolaryngol Head Neck Surg 1994;111: 571–4.
100. Balkany TJ, Sires B, Arenberg IK. Bilateral aspects of Ménière's disease: An underestimated clinical entity. Otolaryngol Clin North Am 1980;13:603–9.
101. Wladislavosky-Waserman P, Facer GW, Bahram M, Kurland LT. Ménière's disease: a 30-year epidemiologic and clinical study in Rochester, MN. 1951–1980. Laryngoscope 1984;94: 1098–102.
102. Rauch SD, San Martin J, Moscicki RA, Bloch KJ. Serum antibodies against heat shock protein 70 in Ménière's disease. Am J Otol 1995;16:648–52.
103. Rauch SD, Merchant SN, Thedinger BA. Ménière's syndrome and endolymphatic hydrops: double-blind temporal bone study. Ann Otol Rhinol Laryngol 1989;98:873–83.

104. Boleas-Aguirre MS, Lin FR, Della Santina CC, et al. Longitudinal results with intratympanic dexamethasone in the treatment of Ménière's disease. Otol Neurotol 2008;29:33–8.

105. Minor LB. Intratympanic gentamicin for control of vertigo in Ménière's disease: Vestibular signs that specify completion of therapy. Am J Otol 1999;20:209–12.

106. Driscoll CLW, Kasperbauer JL, Facer GW, et al. Low-dose intratympanic gentamicin and the treatment of Ménière's disease: Preliminary results. Laryngoscope 1997;107:83–9.

107. Lustig LR, Yeagle J, Niparko JK, Minor LB. Cochlear implantation in patients with bilateral Ménière's syndrome. Otol Neurotol 2003;24:397–403.

108. Grad A, Baloh RW. Vertigo of vascular origin: Clinical and electronystagmographic features in 84 cases. Arch Neurol 1989;46:281–4.

Genetics in Otology and Neurotology

7

Anil K. Lalwani, MD / Anand N. Mhatre, PhD

The success of the human genome project in sequencing of the entire human genome has directly impacted our understanding of otologic and neurotologic disorders. Specifically, we have gained insights into the molecular mechanisms of hearing impairment, vestibular schwannomas, and glomus tumors. In this chapter, the principles of Mendelian genetics are reviewed and our understanding of the aforementioned diseases is summarized.[1]

PRINCIPLES OF MENDELIAN GENETICS

Autosomal Dominant Inheritance

In autosomal dominant disorders, the transmission of a rare allele of a gene by a single heterozygous parent is sufficient to generate an affected child (Figure 7–1A). A heterozygous parent can produce two types of gametes. One gamete carries the mutant form of the gene of interest and the other the normal form. Each of these gametes then has an equal chance of being used in the formation of a zygote. Thus, the chance that an offspring of an autosomal dominant affected parent will itself be affected is 50%. Equal numbers of affected males and females are expected for an autosomal dominant trait, and roughly half of the offspring of an affected individual will be affected. If male-to-male transmission of the trait is observed, the possibility that the trait is X-linked can be eliminated.

If the mutant phenotype is always expressed in individuals carrying the disease allele, then its penetrance is said to be complete; otherwise, it is incomplete. Where penetrance of the affected gene is complete, or 100%, the pattern of its inheritance may be discerned in a relatively straightforward manner. Complete penetrance of the dominant allele results in expression of the disease phenotype in all carriers of that allele without skipping generations. However, with incomplete penetrance of the affected gene, the inheritance pattern of the affected trait becomes relatively harder to discern, ie, one cannot easily distinguish between dominant inheritance with reduced penetrance and more complicated modes of inheritance. The failure of the gene to express itself may be owing to a variety of reasons. The most common rationale put forth to explain reduced penetrance is the effect of genetic background. Factors such as genetic redundancy, presence of more than one gene for the performance of a given function, and modifiers affect a variety of genes. Incomplete penetrance can also be seen in traits that are inherited in an autosomal recessive, X-linked recessive, and X-linked dominant manner.

Variable expression of different aspects of syndromes is common. Some aspects may be expressed in a range encompassing mild to severe forms and/or different combinations of associated symptoms may be expressed in different individuals carrying the same mutation within a single pedigree. An example of variable expressivity is seen in families transmitting autosomal dominant Waardenburg's syndrome. Within the same family, some affected members may have dystopia canthorum, white forelock, heterochromia irides, and hearing loss, whereas others with the same mutation may only have dystopia canthorum.

Autosomal Recessive Inheritance

An autosomal recessive trait is characterized by having two unaffected parents who are heterozygous carriers for mutant forms of the gene in question, but in whom the phenotypic expression of the mutant allele is masked by the normal allele. These heterozygous parents (A/a) can each generate two types of gametes, one carrying the mutant copy of the gene (a) and the other having a normal copy of the gene (A). Of the four possible combinations of these two gamete types from each of the parents, only the offspring that inherits both mutant copies (a/a) will exhibit the trait. Of the three remaining possibilities, all will have a normal hearing phenotype, but two of the three will be heterozygous carriers for the mutant form of the gene, similar to the carrier parents. A typical recessive pedigree with affected members in a single generation (horizontal pattern), showing a consanguineous mating between cousins, is depicted in Figure 7–1B.

X-Linked Inheritance

In humans, females have 22 pairs of autosomes and a pair of X chromosomes (46XX), and males have 22 autosomes, one X chromosome, and one Y chromosome (46XY). Accordingly,

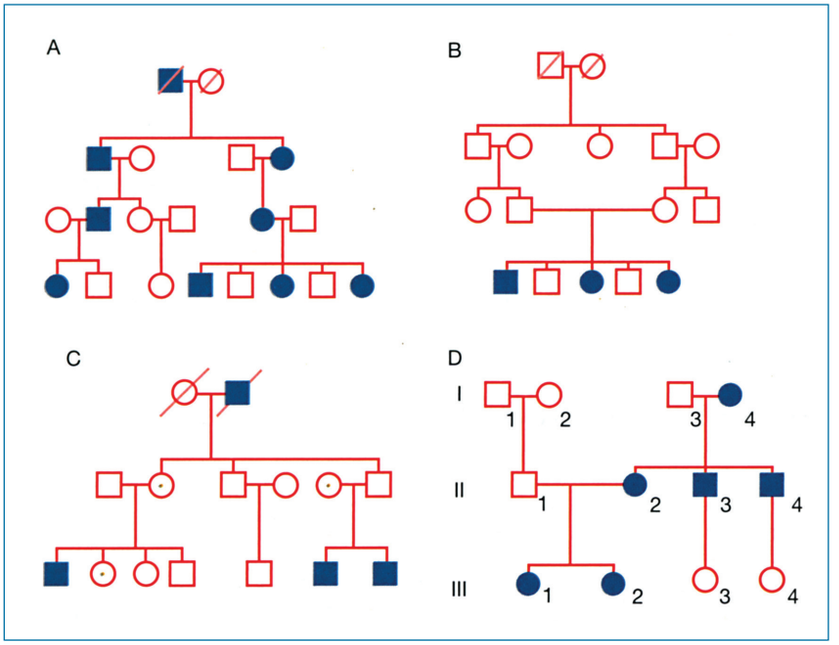

FIGURE 7–1 • Patterns of inheritance. Pedigrees showing autosomal dominant *A*, autosomal recessive *B*, X-linked *C*, and mitochondrial inheritance *D*. Autosomal dominant inheritance is characterized by vertical transmission in contrast to the horizontal pattern seen in recessive inheritance; transmission of recessive disease is more common in consanguineous mating depicted in the pedigree. In X-linked diseases, the unaffected carrier mothers (depicted as a *dot* in the center of the square or the circle) have affected and unaffected sons, whereas all daughters are unaffected. On the other hand, affected fathers only have unaffected children. Mitochondrial diseases can only be transmitted from the mother as mitochondrial DNA is present only in the egg.

males always receive their Y chromosome from their father and their X chromosome from their mother, whereas females receive one of their X chromosomes from each of their two parents. Because males have one copy of the X chromosome, they are hemizygous for genes on the X chromosome, and the X chromosome is active in all of their nucleated cells. In general, only one of the two X chromosomes carried by a female is active in any one cell, whereas the other is rendered inactive by a natural process known as lyonization. This random inactivation process makes all females who are heterozygous for X-linked traits mosaic at the tissue level, resulting in variable expression of the mutant gene. Diseases that are rarely expressed clinically in heterozygous females are called X-linked recessive. In female tissues, various proportions of cells may exist in which one or the other of two alleles for an X-linked locus is expressed. Occasionally, a carrier female may manifest some symptoms of an X-linked recessive disorder owing to this mosaicism if she, by chance, has an abundance of cells with the mutant allele being expressed. Transmission of an X-linked recessive trait in a pedigree is illustrated in Figure 7–1C.

VARIATIONS ON MENDELIAN PRINCIPLES

Mendel established the two fundamental principles of genetics: segregation of genes and their independent assortment. These principles refer to processes that occur in the formation of germ cells known as meiosis. Segregation refers to separation of homologous genes, representing the paternal and the maternal contribution to the individual's genotype, into two separate daughter cells. Thus, the diploid genome is reduced to the haploid state in the germ cells. The principle of independent assortment states that segregation of one gene occurs independently of other genes. These principles have served well for analysis and understanding of the inheritance of traits through a single locus. However, a number of variations on these principles do exist, some of which have already been stated implicitly above. These variations and their underlying principles have contributed toward increasing our understanding of the genetic etiology of disease.

Linkage and Recombination

Not all genes assort independently of each other. This variation of the Mendelian principle was initially identified by Thomas Morgan through analysis of transmission of selected traits in fruit flies. Experiments showed inheritance of specific pairs of alleles in a combination not present in the parental phenotype. This new combination of alleles was considered to result from crossing over and exchange of genetic material between two homologous chromosomes, known as homologous recombination, yielding the new combination of alleles not present in the original parental chromosomes. Analysis of recombination frequencies between two traits considered to be controlled by genes residing on the same linkage group, that is, the same chromosome, provided two essential concepts that led to the development of the genetic map: genes are arranged in a linear order and the frequency with which two alleles are inherited together is a function of the relative physical distance to each other. Thus, the closer the two genes, the greater the chance that they will remain linked post meiosis. The relative chromosomal positions of genes may be readily mapped through the application of these principles of linkage and recombination to generate genetic maps. The genetic distance between two linked genes as measured through the frequency of recombinants between the two alleles is measured in centiMorgans (cM); eg, two loci are one cM apart on the genetic map if there is a 1% chance of a recombination between them in meiosis. Thus, genes that are far apart on a chromosome will assort in an apparently independent manner, whereas genes that are close together will tend to remain linked postmeiosis.

Mitochondrial Inheritance

Not all genes are equally inherited from both parents. The extranuclear mitochondrial genome is inherited solely through the mother. Male mitochondria are not contributed to newly formed zygotes. This inheritance pattern gives rise to pedigrees in which all of the children of an affected mother may be affected and none of the children of an affected father will be affected (Figure 7–1D). In practice, the expression of mitochondrially inherited disorders is often variable and may be incompletely penetrant. If all of the mitochondria transmitted by the mother are of the same genotype, it is called homoplasmia; if there are genetic differences between them, it is called heteroplasmia.

Genomic Imprinting

The manifestation of some genetic diseases depends on the sex of the transmitting parent. This occurrence is considered to result from genomic imprinting. This phenomenon runs counter to the teachings of Mendelian genetics that emphasize equal contribution from paternal and maternal genes, with the obvious exception of genes on the sex chromosomes. Thus, in certain instances, despite the presence of both the paternal and maternal alleles, only one of the parental alleles is expressed. This differential expression of the parental alleles is detected in certain disease states when inheritance of that disorder is dependent on the sex of the parent who transmits the mutant gene. The gene-specific imprinting is presumed to be the consequence of reversible "epigenetic" modification of the parental allele during gametogenesis, leading to its differential expression. The precise mechanism of imprinting and its evolutionary significance remain unknown. Hypermethylation of the imprinted gene represents one possible mechanism.

Genomic imprinting at the level of a specific gene has been identified in familial cases of nonchromaffin paragangliomas (PGs; benign tumors of the paraganglionic cells, also known as glomus tumors). Although benign, their enlargement can cause deafness and/or facial palsy. Familial PGs have shown an autosomal dominant inheritance with genomic imprinting of the maternal allele. Thus, the transmission of the disease occurs via the affected paternal allele and not the maternal allele.

Multifactorial Inheritance

An expression of a phenotype, the outcome of which is determined by a single gene, is termed a Mendelian trait. Its pattern of transmission within a pedigree can be readily discerned in most cases, as described above. On the other hand, most common human diseases and traits show irregular inheritance patterns. These traits are considered to be determined from the action of multiple genes and/or nongenetic factors. A phenotype that is an outcome of both genetic and environmental factors is called a multifactorial, or complex, trait. The low proportion of Mendelian traits relative to the number of multifactorial traits in humans is better illustrated by considering the proportion of total number of Mendelian traits known (approximately 6,000 according to McKusick's Mendelian Inheritance in Man) to the total number of genes that are estimated to exist (approximately 30,000). It should be emphasized that classification of Mendelian traits as being "determined" by single genes is an oversimplification. As more Mendelian disorders are identified and their phenotypes investigated, their phenotypic variability and complexity are becoming increasingly clear, and, concomitantly, their distinction from complex or multifactorial traits is becoming increasingly blurred. Phenotype variability or variable expression seen in a single gene disorder such as Waardenburg's syndrome may reflect interaction of that major gene, such as PAX3, with "modifier" genes. Identification of these modifier genes has important implications for the understanding and treatment of Mendelian disorders with variable expressivity.

The relatively irregular mode of inheritance that characterizes a multifactorial trait is presumed to result from interaction of multiple genes (polygenic). This interaction is apparently distinct from that presumed for Mendelian traits. But this distinction may be at a quantitative rather than a qualitative level. For example, instead of a predominant influence or effect of one gene on expression of the phenotype, the multifactorial trait is characterized by a number of genes with equivalent influence or effect. The genetic component of multifactorial traits is referred to by terms such as increased risk, predisposition, or susceptibility. Because of their complexity, the factors that contribute to the multifactorial traits are poorly defined. Several well-studied diseases, such as cardiovascular conditions and diabetes, as well as distinct behavioral disorders, are classified as multifactorial. The influence of nongenetic factors, eg, environmental agents or stochastic processes during development, on a variety of traits is also clearly illustrated in the studies of identical twins.

GENETICS OF HERRING LOSS

Hearing loss is the most common form of sensory impairment in humans. Nearly 10% of the US population or 30 million Americans have significant auditory dysfunction. For some, the hearing loss is present at the beginning of life. The prevalence of permanent, moderate-to-severe sensorineural hearing loss (SNHL) is estimated to be between 1 and 3 per 1,000 live births.[2,3] Prelingual deafness, in contrast to late-onset hearing loss, can be devastating to the child. Significant delays in the acquisition of speech and language, as well as other developmental childhood milestones, can occur without adequate rehabilitation. The predominant etiology of hearing impairment in children has evolved with advances in medical knowledge and therapeutics. Historically, infectious disorders such as otitis media, maternal rubella infections, and bacterial meningitis, as well as environmental factors such as intrauterine teratogenic exposure or ototoxic insult, were the dominant causes of congenital and acquired hearing losses. The introduction of antibiotics, vaccines, and improved knowledge and enhanced awareness about teratogens has led to a decline in hearing loss resulting from infections and environmental agents. Currently, more than half of all childhood hearing impairment is thought to be hereditary. As a result of advances in clinical and basic medical research, significant progress has been made in understanding the causes of hereditary hearing impairment (HHI).

Classification

When SNHL occurs in isolation, it is called nonsyndromic.[4] On the other hand, hearing loss accompanied by other systemic disturbance is termed syndromic. Two-thirds of HHI is nonsyndromic, whereas the remaining one-third is syndromic. Over 1,100 syndromes are associated with otologic manifestations. Nonsyndromic HHI is further classified by the mode of inheritance. The majority of HHI is inherited in an autosomal recessive fashion (80%), with the autosomal dominant mode of inheritance being less common (15–18%).[5] Rare modes of transmission include X-linked and mitochondrial transmission, which account for the remaining 2% of hearing impairment.

Auditory Phenotype in HHI

Clinically, HHI can be described by several characteristics of the hearing loss: severity of hearing impairment, age of onset, type of hearing impairment, frequencies involved, unilateral/bilateral, stable/progressive, and syndromic/nonsyndromic. In general, recessive HHI tends to be more severe than dominantly inherited hearing impairment. Recessive HHI is predominantly congenital or prelingual in onset, whereas dominant HHI is delayed or postlingual. In contrast to the profound hearing loss associated with recessive deafness, autosomal dominant hearing loss is less severe and progresses with age. Many dominant hearing impairments progress at the rate of about 1 dB/year. Recessive deafness usually affects all frequencies equally. Although there are some types that have predominantly low-frequency or flat hearing loss, dominant hearing impairment more commonly affects the high frequencies, mimicking presbycusis. The frequencies involved in syndromic forms of hearing impairment are variable. Nonsyndromic hearing impairment is usually symmetric. In contrast, syndromic HHI can be unilateral or bilateral and symmetric or asymmetric.

Molecular Genetics of HHI

Rapid progress has been made in the identification of genes responsible for syndromic and nonsyndromic hereditary hearing impairment. In syndromic hearing impairment, more than 100 genes have been identified since 1990, showing a large heterogeneity even in the same type of syndromic hearing impairment. For example, Usher's syndrome type I has been associated with 11 different genetic loci; the genes responsible for nine of these loci have been identified (Table 7–1). In nonsyndromic hearing impairment, as of 2008, 57 autosomal dominant, 75 autosomal recessive, 6 X-linked, 2 mitochondrial loci, and 2 modified loci have been mapped on the human genome. In addition, the current count of nearly 50 nonsyndromic genes identified since 1994 will continue to rapidly increase (Table 7–2; Hereditary hearing loss homepage: http://webh01.ua.ac.be/hhh/).

The identified deafness genes play a variety of different roles in cellular physiology (see Tables 7–1 and 7–2). The responsible genes include cytoskeletal proteins important in maintaining cellular structure, division, and intracellular transport; transcription factors that regulate the expression of other genes; ion channels important in the transport of sodium, potassium, chloride, and iodine; developmental genes that regulate morphogenesis; and proteins involved in intercellular communications such as gap and tight junctions.

As a result of progress in the genetics of deafness (and genetics in general), several conventional notions have had to be modified. It is now clear that a single gene may cause syndromic or nonsyndromic forms of deafness or may be associated with autosomal dominant or autosomal recessive mode of inheritance. Identification of myosin 7A as the gene responsible for both syndromic and nonsyndromic deafness has led to the abandonment of the "one gene, one disease" dogma. In addition, pendrin mutations cause both Pendred's syndrome and isolated (nonsyndromic) large vestibular aqueduct (LVA). To muddle things further, different mutations in myosin 7A cause both dominant and recessive forms of nonsyndromic deafness. The same is true for connexin 26: it is associated with both a dominant and a recessive mode of transmission. In addition to the disease-causing gene, the patient's genetic background and the role of other modifier genes in determining the clinical severity is now better appreciated. For example, the severity of Waardenburg's syndrome in a given patient will be determined not only by the mutation in the PAX3 gene, but also by the nature of other genes present in the remaining genome.

Several of the genes and gene families are especially important in clinical otology including *GJB* (family of gap junction genes), *SLC26A4*, myosins, and mitochondrial gene 12S ribosomal ribonucleic acid (rRNA) and are discussed below.

GJB2

The apparent genetic heterogeneity of HHI is contrasted by the predominance of *GJB2* (encoding for connexin 26 gap junction protein) as a major cause of inherited and sporadic nonsyndromic deafness. Mutations of *GJB2* are responsible for both recessive (DFNB1—DFN for deafness, B for recessive) and dominant (DFNA3—DFN for deafness, A for dominant) forms of HHI; it is an important contributor to childhood hearing loss, accounting for nearly 50% of congenital recessive sensorineural hearing impairment. Connexin 26 (Cx26) is a member of a family of proteins that are involved in the formation of gap junctions. Connexins are transmembrane proteins that form channels allowing transport of ions or small molecules between adjacent cells. Each connexin subunit contains three intracellular domains and two extracellular domains, crossing the plasma membrane four times. The second intracellular domain contains the cytoplasmic loop. The other two intracellular domains consist of the N terminus and the C terminus.[6] Six connexin subunits join to form a connexon. A pair of connexons, one in each adjacent cell, comes together to form an intercellular channel. The family of connexin proteins plays an important role in normal hearing as mutations in several members of the family are associated with hearing impairment. To date, mutations in Cx26 (*GJB2*), Cx30 (*GJB6*), Cx31 (*GJB3*), Cx32 (*GJB1*), and Cx43 (*GJA1*) have been implicated in hearing loss (Connexin-deafness homepage: http://davinci.crg.es/deafness/). Its expression has been shown in the stria vascularis, basement membrane, limbus, and spiral prominence of the human cochlea.[7] One possible biochemical function of Cx26 has been suggested by studying rat cochlear gap junctions. The organization of gap junctions and information provided by other investigators suggest that

TABLE 7–1 Syndromic hereditary hearing impairment genes

SYNDROME/LOCUS	GENE	FUNCTION
Alport's	*COL4A3*	Cytoskeletal protein
	COL4A4	Cytoskeletal protein
	COL4A5	Cytoskeletal protein
Branchio-oto-renal	*EYA1*	Developmental gene
	SIX1	Developmental gene
Jervell and Lange-Nielsen	*KVLQT1*	Delayed rectifier potassium channel
	KCNE1	Delayed rectifier potassium channel
Norrie's	*NORRIN*	Cell-cell interactions?
Pendred's	*SLC26A4*	Chloride-iodide transporter
Stickler's	*COL2A1*	Cytoskeletal protein
	COL11A1	Cytoskeletal protein
	COL11A2	Cytoskeletal protein
Treacher Collins	*TCOF1*	Nucleolar-cytoplasmic transport
Usher's	*MYO7A*	Cytoskeletal protein
	USH1C	?
	CDH23	Intercellular adherence protein
	PCDH15	?
	SANS	Harmonin associated protein
	USH2A	Cell adhesion molecule
	VLGR1	G-protein coupled receptor
	WHRN	Calmodulin-dependent serine kinase
	USH3	?
	Others	
Waardenburg's type I, III	*PAX3*	Transcription factor
Waardenburg's type II	*MITF, SNAI2*	Transcription factor
Waardenburg's type IV	*EDNRB*	Endothelin-B receptor
	EDN3	Endothelin-B receptor ligand
	SOX10	Transcription factor

they serve as the structural basis for recycling of potassium ions back to the endolymph of the cochlear duct after stimulation of the sensory hair cells.[8,9]

Several studies have demonstrated the prevalence of Cx26 mutations in 50% of individuals with recessive deafness, with a carrier rate as high as 4%.[7,10–15] Currently, approximately 100 different mutations have been identified (Connexin-deafness homepage: http://davinci.crg.es/deafness/). Two single base pair deletions account for nearly half of all mutations in this gene: 35delG and 167delT. The 35delG mutation has been found to be common in several populations and accounts for up to 70% of Cx26 mutant alleles in families from the United Kingdom, France, Italy, Spain, Tunisia, Lebanon, Israel, Australia, Greece, United States, and New Zealand, as well as up to 40% of sporadic cases of congenital deafness in these countries.[12,13,16–20]

The 35delG mutation leads to frameshift, early termination of the nascent protein, and a nonfunctional intracellular domain in the protein.[12,16,21] Alternatively, this mutation may lead to an unstable RNA, leading to its early degradation or absence of its translation into protein. Clinically, homozygous patients with the 35delG mutation show a variable phenotype, ranging from mild to profound hearing impairment. However, most patients with the homozygous 35delG mutation show a severe to profound phenotype.

In contrast, the 35delG mutation may be less common in the Japanese populations in which 235delC is the prevalent

TABLE 7–2 Nonsyndromic hereditary hearing impairment genes

LOCUS	GENE	FUNCTION
Dominant loci		
Unnamed	*CRYM*	Thyroid hormone binding protein
DFNA1	*DIAPH1*	Cytoskeletal protein
DFNA2	*GJB3 (Cx31)*	Gap junctions
DFNA2	*KCNQ4*	Potassium channel
DFNA3	*GJB2 (Cx26)*	Gap junctions
DFNA3	*GJB6 (Cx30)*	Gap junctions
DFNA4	*MYH14*	Class II nonmuscle myosin
DFNA5	*DFNA5*	Unknown
DFNA6/14/38	*WFS1*	Endoplasmic reticulum protein
DFNA8/12	*TECTA*	Tectorial membrane protein
DFNA9	*COCH*	Unknown
DFNA10	*EYA4*	Developmental gene
DFNA11	*MYO7A*	Cytoskeletal protein
DFNA13	*COL11A2*	Cytoskeletal protein
DFNA15	*POU4F3*	Transcription factor
DFNA17	*MYH9*	Cytoskeletal protein
DFNA20/26	*ACTG1*	Cytoskeletal protein
DFNA22	*MYO6*	Unconventional myosin
DFNA28	*TFCP2L3*	Transcription factor
DFNA36	*TMC1*	Transmembrane protein
DFNA39	*DSPP*	Dentin phosphoprotein
DFNA44	*CCDC50*	Effector of EGF signaling
DFNA48	*MYO1A*	Unconventional myosin
Recessive Loci		
Unnamed	*SLC26A5 (prestin)*	Motor protein
DFNB1	*GJB2 (CX26)*	Gap junctions
DFNB2	*MYO7A*	Cytoskeletal protein
DFNB3	*MYO15*	Cytoskeletal protein
DFNB4	*PDS*	Chloride-iodide transporter
DFNB6	*TMIE*	Transmembrane protein
DFNB7/11	*TMC1*	Transmembrane protein
DFNB8/10	*TMPRSS3*	Transmembrane serine protease
DFNB9	*OTOF*	Trafficking of membrane vesicles
DFNB12	*CDH23*	Intercellular adherence protein
DFNB16	*STRC*	Stereocilia protein
DFNB18	*USH1C*	?

Continued

TABLE 7–2 Nonsyndromic hereditary hearing impairment genes (Continued)

LOCUS	GENE	FUNCTION
DFNB21	*TECTA*	Tectorial membrane protein
DFNB22	*OTOA*	Gel attachment to nonsensory cell
DFNB23	*PCDH15*	Morphogenesis and cohesion
DFNB24	*RDX*	Cross-link actin filaments
DFNB28	*TRIOBP*	Cytoskeletal-organizing protein
DFNB29	*CLDN14*	Tight junctions
DFNB30	*MYO3A*	Hybrid motor-signaling myosin
DFNB31	*WHRN*	PDZ domain-containing protein
DFNB36	*ESPN*	Calcium-insensitive actin-bundling protein
DFNB37	*MYO6*	Unconventional myosin
DFNB49	*MARVELD2*	Tight junction protein
DFNB53	*COL11A2*	Collagen protein
DFNB59	*PJVK*	Zinc binding protein
DFNB66/67	*LHFPL5*	Tetraspan membrane protein
X-linked Locus		
DFN3	*POU3F4*	Transcription factor

Cx26 mutation.[22–24] Likewise, in the Ashkenazi Jewish population, the 167delT mutation has been found to be more common than the 35delG mutation, with a carrier rate of 4%.[15]

Of the genes identified to date, Cx26, because of its small size, the single coding exon, frequency of involvement, and predominance of two mutations, lends itself to mutation screening. However, it is unlikely that screening for the two common mutations will be sufficient to identify the vast majority of Cx26 deafness. We screened 154 individuals with SNHL for mutations in Cx26by DNA sequencing and identified 34 patients with mutations for an overall incidence of 22% in the study population.[25] Of all Cx26 mutations, the 35delG mutation accounted for 26%. The 35delG mutation was present in a homozygous state in only four individuals (each of the two chromosomes harbored the 35delG mutation) and heterozygous in six individuals (only one chromosome had the 35delG mutation). Herein lies the fundamental problem with screening for only 35delG: only 4 of 34 individuals (12%) with Cx26 mutations, or 154 individuals in total (3%), had a homozygous mutation that would be required to clearly implicate Cx26 as the causative gene. The identification of a single copy of 35delG mutation does not implicate this gene in deafness and may simply reflect the high carrier rate that is present in the population. In this case, the rate of identifying the cause of childhood SNHL by genetic testing is significantly less than radiologic imaging. The predominance of the two common mutations in a heterozygous state (with a second uncommon Cx26 mutation) has been replicated by others.[26,27] Therefore, genetic testing for 35delG and 167delT mutations only, without sequencing the entire *GJB2* gene, is inadequate. *GJB2* testing is now readily available in many laboratories; its role in the management of children with hearing impairment remains to be determined.

SLC26A4 (Pendrin Protein)

Mutations in *SLC26A4* are associated with an isolated LVA (the most common radiologic abnormality associated with childhood deafness), as well as Pendred's syndrome. Vaughan Pendred, while he was working in the Ear, Nose, and Throat Department at Newcastle Royal Infirmary, observed the association between deaf-mutism and goiter in two sisters.[28,29] The first sister appeared to be profoundly deaf and developed goiter at the age of 13 years; the second sister was not completely deaf and also developed a notable thyroid mass at the age of 13. It has been estimated that as much as 10% of all HHI may be attributable to Pendred's syndrome, making it one of the most common syndromic HHI disorders.[30] Goiter may appear at birth, in childhood, or after puberty. The delay in onset, or sometimes absence of goiter can make clinical diagnosis of Pendred's syndrome difficult. Patients are usually euthyroid but can be hypothyroid. The elevation of thyrotropin-releasing hormone suggests a compensatory hypothyroidism.[31] The mild organification defect in Pendred's syndrome can be noted by the partial discharge of iodine in the perchlorate challenge test.[32] The perchlorate ion (ClO_4^-) is a competitor of iodine. When perchlorate is given orally or intravenously following radioactive iodine administration, the perchlorate blocks further uptake of iodine and releases unbound iodine in the thyroid follicular cells. In Pendred's syndrome, in which there is an intrinsic

thyroid organification defect, the perchlorate displaces more iodine than in a normal thyroid gland, leading to a greater iodine "discharge" and a decrease in thyroid radioactivity over time. The hearing loss of Pendred's syndrome is usually congenital and profound. However, there are reports of milder or progressive hearing impairments. Hypoplasia of the cochlea and enlargement of the vestibular aqueduct can be associated with Pendred's syndrome as demonstrated by histologic and radiologic studies.[33,34]

Everett and colleagues identified mutations in the *SLC26A4* (formerly *PDS*) gene on chromosome 7q31 as the cause of Pendred's syndrome.[35] The gene contains 21 exons. The gene product pendrin encodes a 780-amino acid (86-kDa) protein that contains 11 transmembrane domains resembling sulfate transporters.[35] Evidence suggests that pendrin functions as a chloride–iodide anion transport protein.[36] In the mouse inner ear, pendrin localizes to the endolymphatic duct and sac, distinct areas in the utricle and saccule, and the external sulcus region within the cochlea, indicating a possible role in endolymph resorption. Van Hauwe and colleagues noted two particularly frequent missense mutations, L236P (707 T to C) and T416P (1246 A to C); subsequently, a third common mutation, E384G (1151 A to G), has also been identified.[37] Although the gene is too large for screening by direct sequencing, identification of common mutations opens the opportunity for screening for these isolated mutations.

SLC26A4 mutations are also responsible for nonsyndromic hearing loss associated with LVA. The isolated presence of an LVA is one of the most common forms of inner ear anomaly. Genetic studies of families with LVA disorder identified a recessive nonsyndromic locus, DFNB4, that also mapped to the same region as the *SLC26A4* gene.

This discovery led to the evaluation of the *SLC26A4* gene and the subsequent identification of seven pendrin mutations responsible for LVA with nonsyndromic HHI.[38] Like Pendred syndrome, different mutations, V480D, V653A, I490L and G497 S, have been found to be commonly associated with LVA. In a review of our experience, LVA was the most common imaging abnormality detected in children with nonsyndromic SNHL.[39] At least 40% of children with LVA will develop profound SNHL.[40] Patients with LVA are at risk for progressive hearing loss after minor head trauma. Identifying this anomaly influences parent counseling with respect to the dangers of incidental head trauma. In summary, the spectrum of *SLC26A4* mutations and the wide range of phenotypic manifestations show that pendrin is an important participant in ear structural development and in the normal functioning of the inner ear and thyroid. Screening for mutations may play an important role in the diagnosis and management of a child as well as their siblings with hearing impairment.

Myosins

The importance of myosins in inner ear function is manifest in the growing list of unconventional (nonclass II) myosin heavy chain genes pathogenically linked to HHI. These disease genes encode the heavy chains of myosin VI, VII, and XV. The expression of these unconventional myosins is not limited to the cells and the tissues of the inner ear. Yet the expression of their dysfunction is largely restricted to hearing impairment. In the mouse, myosin VI has been identified as the Snell's waltzer gene; the cochlear and vestibular neurosensory epithelium of Snell's waltzer mice degenerates soon after birth. The role of myosin VI in human deafness remains to be determined. Myosin VII has been linked to both rodent and human deafness. Mutations in the gene encoding myosin VIIA are responsible for mouse shaker 1, human Usher's syndrome type 1, and human nonsyndromic hearing impairment DFNB2 and DFNA11. Shaker 1 mice are deaf and have vestibular defects. Mice that are homozygous for mutant shaker 1 allele display disorganized stereocilia. Myosin XV is the largest of all myosin heavy chains, having a molecular weight of 395 kDa. Mutations in myosin XV have been pathogenically linked to DFNB3 in humans and the shaker 2 phenotype in mice.

The unconventional myosins are distributed throughout the mechanosensory hair cells. Moreover, histopathologic study of mouse models of myosin XV dysfunction has been valuable to understanding the consequences of myosin dysfunction on the sensory hair cells. Myosin VI is localized within the actin-rich cuticular plate, as well as in the rootlet actin filaments that descend from the stereocilia into the cuticular plate, suggesting a role in stabilizing the basal attachment of stereocilia.[41,42] Myosin VIIA is localized in the stereocilia and cell body of hair cells.[42] Postulated roles for myosin VIIA include maintaining stereocilia integrity and membrane trafficking in the inner hair cells. On histopathologic evaluation, the inner ears of mouse models of myosin XV dysfunction reveal significantly shortened stereocilia in the sensory hair cells, demonstrating the importance of myosin XV in the maintenance of hair cell structure and thereby its function.

A mutation in a conventional, or class II, myosin, MYH9, has been described. The class II myosins are broadly expressed in skeletal, cardiac, and smooth muscle, as well as nonmuscle tissue and consist of a pair of heavy chains, a pair of light chains, and a pair of regulatory light chains.[43] The N-terminal motor domain is the most highly conserved region of the myosin heavy chain and contains the adenosine triphosphate and actin-binding sites. The apparent molecular weight of the class II myosin heavy chain is 200 kDa. The myosin that mediates skeletal muscle contraction, also known as the sarcomeric myosin, represents the most well-characterized representative of the class II myosin family. Cardiac and smooth muscle cells also express isoforms of class II myosin, distinct from the sarcomeric myosin that mediates contraction in these muscle cells. Mutation in MYH9, a conventional nonmuscle myosin, was described in an American family with autosomal dominant nonsyndromic hereditary hearing impairment (DFNA17) associated with cochleosaccular degeneration.[44–46] The affected members of the DFNA17 family exhibit progressive, postlingual onset hearing loss, a pattern that is observed in the majority of nonsyndromic autosomal dominant HHI. The cosegregation of the mutant MYH9 with nonsyndromic hearing impairment illustrates a biologically significant role for MYH9 in hearing and an organ-specific pathology associated with the mutant allele.

Two other myosin genes have been predicted to have an important role in hearing. Myosin V is an abundant protein of afferent nerve fibers innervating both inner and outer hair

cells.[47] Myosin Ip has been implicated as an effector of adaptation of the hair cell transduction apparatus.[48] The preponderance of myosins is not surprising given the diversity of actin filament systems in the inner ear.[49]

Aminoglycoside Ototoxicity

To date, there are 326 syndromes, disorders, or peculiar phenotypes associated with mutations in the mitochondrial genome.[50] Twenty-one of these disorders have some involvement with SNHL, indicating that the requirement for a healthy population of mitochondria is very important to the cells involved in normal hearing.[51–54] One of the most striking examples of a mitochondrially inherited trait whose expression is environmentally affected is the hearing loss caused by hypersensitivity to aminoglycosides.[51] The aminoglycoside hypersensitivity phenotype is the result of a single base transition of A to G at position 1555 in the mitochondrial 12S rRNA. This mutation causes a portion of the 12S rRNA transcript structure to closely resemble the binding site of aminoglycosides to bacterial rRNA. When an aminoglycoside such as streptomycin is administered to patients carrying this mutation, it binds to the mutant 12S rRNA and prevents it from functioning in the translation of mitochondrially transcribed genes, resulting in the loss of mitochondria in cells and perhaps cell death or impairment of normal function. Screening for this mutation prior to initiation of aminoglycoside therapy may reduce the incidence of ototoxicity.

GENETICS OF NEUROFIBROMATOSIS 2

Neurofibromatosis 2 (NF2) is much rarer than NF1, with an incidence estimated between 1 in 33,000 and 1 in 50,000.[55] Inheritance of NF2 is autosomal dominant, and gene penetrance is over 95%. Neurofibromatosis 2 most frequently presents in the second and third decades of life. The mean age of onset of symptoms from vestibular schwannomas in Kanter and colleagues's series was 20.4 years.[56] Vestibular schwannomas comprise approximately 8% of intracranial tumors and account for approximately 80% of cerebellopontine angle tumors.[57] The majority of vestibular schwannomas are sporadic in occurrence and unilateral, presenting in the fifth decade.

Patients with NF2 with bilateral vestibular schwannomas represent 2 to 4% of all vestibular schwannomas.[58,59]

Neurofibromatosis 2 has often been confused with NF1. The conclusive proof that NF1 and NF2 were distinct disease entities did not occur until 1987. Molecular biologic investigations by Barker and colleagues,[60] among others, showed that the gene responsible for NF1 was located near the proximal long arm of chromosome 17. At the same time, under separate investigation, the gene responsible for NF2 was located on chromosome 22 by Rouleau and colleagues.[61]

Neurofibromatosis 2 results from the inheritance of a mutation in the gene on chromosome 22. The incidence of mutation rate within the NF2 gene has been estimated at 6.5×10^{-6}.[55] In approximately 50% of cases, there is no family history, and these patients represent new germline mutations.[62] Chromosome 22 was first thought to be the likely source of the NF2 gene following cytogenetic studies of meningiomas in 1982.[63] The NF2 gene was subsequently mapped to chromosome 22 by both linkage studies and loss of heterozygosity analysis in 1986 and 1987, respectively.[61,64] In 1993, the NF2 gene, designated merlin or schwannomin, was isolated by two groups working independently.[65,66] The NF2 gene is spread over approximately 100 kb on chromosome 22q12.2 and contains 17 exons. The coding sequence of the messenger RNA is 1,785 bp in length and encodes a protein of 595 amino acids.[65,66] The gene product is similar in sequence to a family of proteins including moesin, ezrin, radixin, talin, and members of the protein 4.1 superfamily. These proteins are involved in linking cytoskeletal components with the plasma membrane and are located in actin-rich surface projections such as microvilli. The N-terminal region of the merlin protein is thought to interact with components of the plasma membrane and the C-terminal with the cytoskeleton.

Merlin or schwannomin is predominantly expressed in the cells of the nervous system and in the lens and is predominantly located in membrane ruffles and cellular protrusions.[67,68] It is currently believed that merlin protein overexpression can inhibit cell growth and that it induces cell surface protrusions and elongation of cells.[68,69] In 1994, Tikoo and colleagues[70] tested merlin's ability to function as a tumor suppressor gene. Following introduction of the NF2 protein into v-Ha-Ras-transformed NIH 3T3 cells, they were able to demonstrate the reversal of the malignant phenotype, thus confirming the tumor suppressor properties of merlin. Although the exact function of the NF2 protein is as yet unknown, the evidence available so far suggests that it is involved in cell–cell or cell–matrix interactions and that it is important for cell movement, cell shape, or communication. Loss of function of the merlin protein therefore could result in a loss of contact inhibition and consequently lead to tumorigenesis.

Mutations involving the NF2 gene have been observed in 22 to 59% of patients with sporadic vestibular schwannoma.[71] Welling and colleagues compared the rate of identification of genetic mutations in sporadic vestibular schwannoma versus patients with NF2 and found a significant difference, 66 to 33%, respectively, while noting that different mutational mechanisms may exist in tumorigenesis.[72] To date, more than 200 mutations of the NF2 gene have been identified, including single base substitutions, insertions, and deletions.[73,74] Most mutations lead to truncation of the C-terminal end of the protein; only 13 missense mutations have been identified.[74] NF2 gene defects have been detected in other malignancies including meningiomas, malignant mesotheliomas, melanomas, and breast carcinomas.[64,75–78]

Genotype–phenotype correlation studies suggest that mutations in the NF2 gene are associated with variable phenotypic expression. Ruttledge and colleagues found that mutations in the NF2 gene that result in protein truncation are associated with a more severe clinical presentation of NF2 (Wishart), whereas missense and splice site mutations are associated with a milder (Gardner) form of the disease.[79] Similarly, Parry and colleagues have reported that retinal abnormalities were associated with the more disruptive protein truncation mutations of the NF2 gene.[80] Both studies showed intrafamilial variability of phenotypic expression.

Although mutations in the NF2 gene play a dominant role in the biology of vestibular schwannoma, it is also possible that

other genetic loci contribute to the development of vestibular schwannoma. In addition, NF2 gene mutations are not uniformly identified in patients with vestibular schwannoma, and published genotype–phenotype correlations are variable, which suggests that other genetic loci may contribute to the genesis of vestibular schwannoma and the ultimate phenotype of affected individuals.[79,80]

The identification of the gene responsible for NF2 has significantly advanced our understanding of the molecular pathology and factors responsible for the clinical heterogeneity among patients with NF2. Understanding the function of merlin in tumor formation will lead to the development of novel therapies, which may eventually alleviate the suffering associated with NF2.

GENETICS OF FAMILIAL PARAGANGLIOMAS (PG)

With the exception of the genes located on the sex chromosomes (X and Y), we inherit two copies of every gene. In most cases, both the maternal and the paternal copy of the gene are active. Therefore, when inheriting a disease that is transmitted in an autosomal dominant fashion, it usually does not matter which parent passes down the single mutated gene for the child to be affected. However, there are many genes in which only the paternal or maternal copy is active or functional and the inactive gene is said to be imprinted. Imprinted genes are normally involved in embryonic growth and behavioral development, but occasionally they also function inappropriately as oncogenes or tumor suppressor genes.

Familial PG is inherited in an autosomal-dominant manner with maternal imprinting. Therefore, when an individual inherits the PG gene from the mother (regardless of whether she herself is affected), that child is unaffected and becomes a silent carrier of the mutated gene. On the other hand, when a child inherits the PG gene from the father, the offspring will have PGs regardless of the affected status of the father. Subsequently, the affected/unaffected child harboring the abnormal PG gene will be able to pass the gene to his/her children; he/she will have affected children only if the transmitting parent is a father. This unusual form of incomplete genetic penetrance is caused by sex-specific gene modification during gametogenesis.[81]

Because of the unusual pattern of inheritance outlined above, it is difficult to determine whether every case of "sporadic" PGs is, in fact, sporadic or a hereditary tumor camouflaged as sporadic. In all likelihood, many sporadic tumors are probably familial and the incidence of hereditary tumors considerably higher than just 1 in 10 PGs. Similar to their familial counterparts, sporadic tumors also demonstrate loss of heterozygosity at PGL1 and PGL2. Bikhazi and colleagues demonstrated loss of heterozygosity to be present in 38% of sporadic cases of carotid body tumors and glomus tumors when tested with markers located at PGL1 and PGL2.[82] This indirectly suggests that one-third of sporadic tumors may indeed be inherited. Similar to NF2, sporadic and familial PGs likely have a common genetic etiology.

The quest for the identification of genes responsible for PG has been greatly aided by the human genome project and the availability of large families with inherited PG. This has led to the delineation of at least three different genes associated with PG.

The First Locus: PGL1

Genetic linkage analysis of a large Dutch family with hereditary PG mapped a gene called *PGL1* to the short arm of chromosome 11, 11q22-q23.[83,84] This finding was confirmed in North American families and further localized to 1 1q23.[85,86] Tumor cells from affected individuals with the PGL1 mutation revealed preferential loss of maternal DNA from chromosome 1 1q harboring the *PGL1* gene, providing genetic support for maternal imprinting. The phenomenon where DNA is deleted is termed a loss of heterozygosity.[85,87] This loss of heterozygosity associated with tumor formation strongly suggests that *PGL1* is a tumor suppressor gene. In the tumor suppressor hypothesis, tumor formation requires the loss of both functional copies of a tumor suppressor gene, since a single functioning copy of the tumor suppressor gene is sufficient to prevent tumors. The NF2 and retinoblastoma genes are examples of tumor suppressor genes. The loss of function of one tumor suppressor gene by inheritance of a mutated allele and a subsequent random mutation of the second allele results in tumorigenesis.[88] This phenomenon, described by Knudson,[88] is known as the "two-hit" hypothesis. In familial PG, like NF2, the inherited first "hit" predisposes the individual to multicentric tumors owing to multiple random second "hits."

The gene responsible for *PGL1* was cloned within the large chromosomal span of 11q23 by screening a candidate gene involved in oxygen metabolism located in this area.[89] This gene, known as *SDHD* (for succinate-ubiquinone oxidoreductase subunit D), encodes a small subunit of mitochrondrial cytochrome b (cybS) involved in Krebs cycle aerobic metabolism.[89] Using five families with hereditary PG, single base pair mutations leading to a loss of function of the *SDHD* gene product were identified. A nonsense mutation was found in two families leading to early truncation in the formation of the *SDHD* protein and consequently the loss of cybS production. The other three families showed evidence of missense mutations with change of a single amino acid, presumably dramatically altering cybS conformation, rendering it nonfunctional. Interestingly, typical postgametogenesis maternal imprinting was not found since biallelic expression of both the maternal and the paternal gene was found in somatic tissues. It appears that only when the normal maternal allele is later imprinted or lost that the mutated paternal allele encoding the mutated *SDHD* leads to tumor formation owing to a loss of tumor suppressor activity. The discovery of this gene will undoubtedly lead to more efficient efforts in screening family members at risk for heritable PG.

The Second Locus: PGL2

Mapping of another large, unrelated Dutch family with hereditary PGs has revealed a second locus, *PGL2*, found on the short arm of chromosome 11. This locus at chromosome 11 q13 harbors another gene for PG that by genetic mapping is clearly distinct from *PGL1*.[90,91]

The Third and Fourth Nonimprinted Loci: PGL3 and PGL4

A large German family with hereditary PG has revealed a third locus, PGL3.[92] Markers flanking the 11q23 and 11q13 loci associated with *PGL1* and *PGL2* excluded linkage to this area. Inheritance in this family was also autosomal-dominant, similar to *PGL1* and *PGL2*, but there was no evidence of maternal imprinting. This family was mapped to chromosome 1q21. Subsequently, as mutations in *SDHD* had been identified as the cause of type 1 PG, Niemann and Muller investigated *SDHC* in this family.[93] They found a G-to-A transition in exon 1 of *SDHC* in all affected members but not in unaffected members. The mutation destroyed the start codon ATG of the gene at nucleotide position 958. In mitochondrial complex II, *SDHA* and *SDHB* constitute the catalytic domains and are anchored in the inner mitochondrial membrane by subunits *SDHC* and *SDHD*. Screening for alterations within *SDHB* identified mutations associated with *PGL4*; mutations in *SDHB* are also associated with malignant pheochromocytoma. *PGL3* and *PGL4* are not maternally imprinted.

Genetic Screening

Rapid advances in molecular genetics and biology have allowed the practicing otolaryngologist insight into the etiology of a rare, yet well-described tumor of the head and neck. On evaluation of a patient with a PG, an extended family history should be elicited to identify additional members with evidence of head and neck tumors suspicious for PG. If hereditary PG is suspected, a detailed family pedigree should be obtained and the patient's family should be offered genetic screening. If the pedigree is sufficiently large, it could be determined by genetic linkage analysis if the family's PGs map to either *PGL1* or *PGL2*. Based on the genetic data, individuals harboring the affected chromosome and thus at risk for tumor formation could be identified. Individuals with a transmitted paternal allele who are at risk for PG should be aggressively followed both clinically and radiologically on a regular basis and offered genetic counseling. Those who have inherited the affected gene through maternal transmission should be advised of the clinically silent carrier state and be offered genetic counseling. Those with a noncarrier state can be advised that no increased risk for tumor development is present over the general population.[94]

Alternatively, the DNA extracted from the patient's blood could be directly tested for mutation in *SDHD* using polymerase chain reaction and direct DNA sequencing. If a mutation is identified, the family members could then be tested to see if they too harbor the mutation and therefore are at risk for tumor formation. It is hoped that genetic screening will lead to earlier identification of tumors to reduce the morbidity and mortality associated with its natural history and treatment. Ultimately, identification of the genetic alteration involved in both hereditary and sporadic PGs should lead to opportunities for genetic manipulation of tumor growth.

SUMMARY

A basic understanding of genetics is crucial to the practicing otologist and neuro-otologist. Genetic screening and genetic testing have already permeated into our daily practice. In the very near future, gene-based therapies too will dramatically change how we treat hearing loss and tumors of the temporal bone and cerebellopontine angle.

References

1. Lalwani AK, Lynch E, Mhatre AN. Molecular genetics: A brief overview. In: Lalwani A, Grundfast K, editors. Pediatric otology and neurotology. Philadelphia: Lippincot-Raven; 1998. p. 49–86.
2. Brookhouser P. Sensorineural hearing loss in children. Pediatr Clin North Am 1996;43:1195–216.
3. Mehl A, Thomson V. Newborn hearing screening: The great omission. Pediatrics 1998;101:e4.
4. Kheterpal U, Lalwani AK. Nonsyndromic hereditary hearing impairment. In: Lalwani A, Grundfast K, editors. Pediatric otology and neurotology. Philadelphia: Lippincott-Raven; 1998. p. 313–40.
5. Mhatre AN, Lalwani AK. Molecular genetics of deafness. Otolaryngol Clin North Am 1996;29:421–35.
6. Yaeger M, Nicholson BJ. Structural of gap junction intercellular channels. Curr Opin Struct Biol 1996;6:183–92.
7. Kelsell DP, Dunlop J, Stevens HP, et al. Connexin 26 mutations in hereditary non-syndromic sensorineural deafness. Nature 1997;387:80–3.
8. Kikuchi T, Adams JC, Paul DL, Kimura RS. Gap junction systems in the rat vestibular labyrinth: Immunohistochemical and ultrastructural analysis. Acta Otolaryngol (Stockh) 1994; 114:520–8.
9. Kikuchi T, Kimura RS, Paul DL, Adams JC. Gap junctions in the rat cochlea: Immunohistochemical and ultrastructural analysis. Anat Embryol 1995;191:101–18.
10. Guilford P, Ben Arab S, Blanchard S, et al. A non-syndromic form of neurosensory recessive deafness maps to the pericentromeric region of chromosome 13q. Nat Genet 1994;6:24–8.
11. Van Camp G, Willems PJ, Smith RJH. Nonsyndromic hearing impairment: Unparalleled heterogeneity. Am J Hum Genet 1997;60:758–64.
12. Zelante L, Gasparini P, Estivill X, et al. Connexin 26 mutations associated with the most common form of non-syndromic neurosensory autosomal recessive deafness (DFNB1) in Mediterraneans. Hum Mol Genet 1997;6:1605–9.
13. Kelley PM, Harris DJ, Comer BC, et al. Novel mutations in the connexin 26 gene (GJB2) that cause autosomal recessive (DFNB1) hearing loss. Am J Hum Genet 1998;62:792–9.
14. Cohn ES, Kelley PM. Clinical phenotype and mutations in connexin 26 (DFNB 1/GJB2), the most common cause of childhood hearing loss. Am J Med Genet 1999;89:130–6.
15. Morell RJ, Kim HJ, Hood LJ, et al. Mutations in the connexin 26 gene (GJB2) among Ashkenazi Jews with nonsyndromic recessive deafness. N Engl J Med 1998;339:1500–5.
16. Denoyelle F, Weil D, Maw MA, et al. Prelingual deafness: High prevalence of a 30delG mutation in the connexin 26 gene. Hum Mol Genet 1997;6:2173–7.
17. Estivill X, Fortina P, Surrey S, et al. Connexin 26 mutations in sporadic and inherited sensorineural deafness. Lancet 1998;351:394–8.
18. Lench N, Houseman M, Newton V, et al. Connexin 26 mutations in sporadic non-syndromal sensorineural deafness. Lancet 1998;351:415.

19. Antoniadi T, Rabionet R, Kroupis C, et al. High prevalence in the Greek population of the 35delG mutation in the connexin 26 gene causing prelingual deafness. Clin Genet 1999;55:381–2.
20. Sobe T, Vreugde S, Shahin H, et al. The prevalence and expression of inherited connexin 26 mutations associated with nonsyndromic hearing loss in the Israeli population. Hum Genet 2000;106:50–7.
21. Carrasquillo MM, Zlotogora J, Barges S, Chakravarti A. Two different connexin 26 mutations in an inbred kindred segregating non-syndromic recessive deafness: Implications for genetic studies in isolated populations. Hum Mol Genet 1997;6: 2163–72.
22. Fuse Y, Doi K, Hasegawa T, et al. Three novel connexin 26 gene mutations in autosomal recessive non-syndromic deafness. Neuroreport 1999;10:1853–7.
23. Abe S, Usami S, Shinkawa H, et al. Prevalent connexin 26 (GJB2) mutations in Japanese. J Med Genet 2000;37:41–3.
24. Kudo T, Ikeda K, Kure S, et al. Novel mutations in the connexin 26 gene (GJB2) responsible for childhood deafness in the Japanese population. Am J Med Genet 2000;90:141–5.
25. Lin D, Goldstein JA, Mhatre AN, et al. Assessment of denaturing high-performance liquid chromatography (DHPLC) in screening for mutations in connexin 26. Hum Mutat 2001;18(1):42–51.
26. Denoyelle F, Marlin S, Weil D, et al. Clinical features of the prevalent form of childhood deafness, DFNB 1, due to a connexin-26 gene defect: Implications for genetic counselling. Lancet 1999;353:1298–303.
27. Marlin S, Garabedian EN, Roger G, et al. Connexin 26 gene mutations in congenitally deaf children: Pitfalls for genetic counseling. Arch Otolaryngol Head Neck Surg 2001;127:927–33.
28. Pendred V. Deaf mutism and goitre. Lancet 1896;11:532.
29. Smith RE. Pendred's syndrome. A historical note. Guys Hosp Rep 1969;118:519–21.
30. Batsakis JG, Nishiyama RH. Deafness with sporadic goiter: Pendred's syndrome. Arch Otolaryngol 1962;76:401–6.
31. Gomez-Pan A, Evered DC, Hall R. Pituitary-thyroid function in Pendred's syndrome. BMJ 1974;2:152–3.
32. Fraser GR, Morgans ME, Trotter WR. The syndrome of sporadic goiter and congenital deafness. Q J Med 1960;29:279–95.
33. Cremers CW, Admiraal RJ, Huygen PL, et al. Progressive hearing loss, hypoplasia of the cochlea and widened vestibular aqueducts are very common features in Pendred's syndrome. Int J Pediatr Otorhinolaryngol 1998;45:113–23.
34. Phelps PD, Coffey RA, Trembath RC, et al. Radiological malformations of the ear in Pendred's syndrome. Clin Radiol 1998;53:268–73.
35. Everett LA, Glaser B, Beck JC, et al. Pendred's syndrome is caused by mutations in a putative sulphate transporter gene (PDS). Nat Genet 1997;17:411–22.
36. Scott DA, Wang R, Kreman TM, et al. The Pendred's syndrome gene encodes a chloride-iodide transport protein. Nat Genet 1999;21:440–3.
37. Van Hauwe P, Everett LA, Coucke P, et al. Two frequent missense mutations in Pendred's syndrome. Hum Mol Genet 1998;7:1099–104.
38. Usami S, Abe S, Weston MD, et al. Non-syndromic hearing loss associated with enlarged vestibular aqueduct is caused by PDS mutations. Hum Genet 1999;104:188–92.
39. Scott DA, Wang R, Kreman TM, et al. Functional differences of the PDS gene product are associated with phenotypic variation in patients with Pendred's syndrome and non-syndromic hearing loss (DFNB4). Hum Mol Genet 2000;9:1709–15.
40. Mafong DD, Shin EJ, Lalwani AK. Utility of laboratory evaluation and radiologic imaging in the diagnostic evaluation of children with sensorineural hearing loss. Laryngoscope 2002;112:1–7.
41. Avraham KB, Hasson T, Sobe T, et al. Characterization of unconventional MYO6, the human homologue of the gene responsible for deafness in Snell's waltzer mice. Hum Mol Genet 1997;6:1225–31.
42. Hasson T, Walsh J, Cable J, et al. Effects of shaker-1 mutations on myosin-VIIa protein and mRNA expression. Cell Motil Cytoskeleton 1997;37:127–38.
43. Sellers JR. Myosins: a diverse superfamily. Biochim Biophys Acta 2000;1496:3–22.
44. Lalwani AK, Linthicum FH, Wilcox ER, et al. A three-generation family with late-onset, progressive hereditary hearing impairment and cochleosaccular degeneration. Audiol Neurootol 1997;2:139–54.
45. Lalwani AK, Luxford WM, Mhatre AN, et al. A new locus for nonsyndromic hereditary hearing impairment (DFNA17) maps to chromosome 22 and represents a gene for cochleosaccular degeneration. Am J Hum Genet 1999;64:318–23.
46. Lalwani AK, Goldstein JA, Kelley MJ, et al. Human nonsyndromic deafness DFNA17 is due to a mutation in nonmuscle myosin MYH9. Am J Hum Genet 2000;67:1121–8.
47. Coling DE, Espreafico EM, Kachar B. Cellular distribution of myosin-V in the guinea pig cochlea. J Neurocytol 1997;26:113–20.
48. Gillespie PG. Deaf and dizzy mice with mutated myosin motors. Nat Med 1996;2:27–9.
49. Tilney LG, Derosier DJ, Mulroy MJ. The organization of actin filaments in the stereocilia of cochlear hair cells. J Cell Biol 1980;86:244–59.
50. Wallace DC. Mitochondrial DNA mutations in diseases of energy metabolism. J Bioenerg Biomembr 1994;26:241–50.
51. Prezant TR, Agapian JV, Bohlman MC, et al. Mitochondrial ribosomal RNA mutation associated with both antibiotic-induced and non-syndromic deafness. Nat Genet 1993;4:289–94.
52. van den Ouweland JM, Lemkes HH, Trembath RC, et al. Maternally inherited diabetes and deafness is a distinct subtype of diabetes and associates with a single point mutation in the mitochondrial tRNA(Leu[UUR]) gene. Diabetes 1994;43:746–51.
53. Ballinger SW, Shoffner JM, Hedaya EV, et al. Maternally transmitted diabetes and deafness associated with a 10.4 kb mitochondrial DNA deletion. Nat Genet 1992;1:11–5.
54. Katagiri H, Asano T, Ishihara H, et al. Mitochondrial diabetes mellitus: Prevalence and clinical characterization of diabetes due to mitochondrial tRNA(Leu[UUR]) gene mutation in Japanese patients. Diabetologia 1994;37:504–10.
55. Evans DGR, Huson SM, Donnai D, et al. A genetic study of type 2 neurofibromatosis in the United Kingdom. 1. Prevalence, mutation rate, fitness and confirmation of maternal transmission effect on severity. J Med Genet 1992;29:841–6.
56. Kanter WR, Eldridge R, Fabricant R, et al. Central neurofibromatosis with bilateral acoustic neuroma: Genetic, clinical and

biochemical distinctions from peripheral neurofibromatosis. Neurology 1980;30:851–9.

57. King TT, Gibson WPR, Morrison AW. Tumors of the VIIIth cranial nerve. Br J Hosp Med 1976;16:259–72.
58. Abaza MM, Makariow EV, Armstrong M, Lalwani AK. Growth rate characteristics of acoustic neuromas associated with neurofibromatosis type 2. Laryngoscope 1996;106:694–9.
59. Lalwani AK, Abaza MM, Makariow EV, Armstrong M. Audiologic presentation of vestibular schwannomas in neurofibromatosis type 2. Am J Otol 1998;19:352–7.
60. Barker D, Wright E, Nguyen L, et al. Gene for von Recklinghausen neurofibromatosis is in the pericentromeric region of chromosome 17. Science 1987;236:1100–2.
61. Rouleau G, Seizinger VR, Ozelius LG, et al. Genetic linkage analysis of bilateral acoustic neurofibromatosis to a DNA marker on chromosome 22. Nature 1987;329:246–8.
62. Evans DG, Huson SM, Donnai D, et al. A genetic study of type 2 neurofibromatosis in the United Kingdom. II. Guidelines for genetic counselling. J Med Genet 1992;29:847–52.
63. Zang KD. Cytological and cytogenetics studies on human meningioma. Cancer Genet Cytogenet 1982;6:249–74.
64. Seizinger BR, Martuza RL, Gusella JF. Loss of genes on chromosome 22 in tumorigenesis of human acoustic neuroma. Nature 1986;322:644–7.
65. Rouleau GA, Merel P, Lutchman M, et al. Alteration in a new gene encoding a putative membrane-organizing protein causes neurofibromatosis type 2. Nature 1993;363:515–21.
66. Trofatter JA, MacCollin MM, Rutter JL, et al. A novel moesin-, ezrin-, radixin-like gene is a candidate for the neurofibromatosis 2 tumor suppressor. Cell 1993;72:791–800.
67. Gonzalez-Agosti C, Xu L, Pinney D, et al. The merlin tumor suppressor localises preferentially in membrane ruffles. Oncogene 1996;13:1239–47.
68. Vaheri A, Carpen O, Heiska L, et al. The ezrin protein family: membrane cytoskeleton interactions and disease associations. Curr Opin Cell Biol 1997;9:659–66.
69. Lutchman M, Rouleau GA. The neurofibromatosis type 2 gene product, schwannomin, suppresses growth of NIH 3T3 cells. Cancer Res 1995;55:2270–74.
70. Tikoo A, Varga M, Ramesh V, et al. An anti-RAS function of neurofibromatosis type 2 gene product. J Biol Chem 1994;269: 23389–90.
71. Irving RM, Moffat DA, Hardy DG, et al. Molecular genetic analysis of the mechanism of tumorigenesis in acoustic neuroma. Arch Otolaryngol Head Neck Surg 1993;119:1222–8.
72. Welling DB, Guida M, Goll F, et al. Mutational spectrum in the neurofibromatosis type 2 gene in sporadic and familial schwannomas. Hum Genet 1996;98:189–93.
73. Merel P, Hoang-Xuan K, Sanson M, et al. Predominant occurrence of somatic mutations of the NF2 gene in meningiomas and schwannomas. Genes Chromosomes Cancer 1995;13:211–6.
74. Kluwe L, Mautner VF. A missense mutation in the NF-2 gene results in moderate and mild clinical phenotypes of neurofibromatosis type 2. Hum Genet 1996;97:224–7.
75. Bianchi AB, Hara T, Ramesh V, et al. Mutations in transcript isoforms of the neurofibromatosis 2 gene in multiple human tumour types. Nat Genet 1994;6:185–92.
76. Bianchi AB, Mitsunaga SI, Cheng JQ, et al. High frequency of inactivating mutations in the neurofibromatosis type 2 gene (NF2) in primary malignant mesotheliomas. Proc Natl Acad Sci U S A 1995;92:10854–8.
77. Ruttledge MH, Sarrazin J, Rangaratnam S, et al. Evidence for the complete inactivation of the NF2 gene in the majority of sporadic meningiomas. Nat Genet 1994;6:180–4.
78. Sekido Y, Pass H, Bader S, et al. Neurofibromatosis type II (NF-2) gene is somatically mutated in mesothelioma but not in lung cancer. Cancer Res 1995;55:1227–31.
79. Ruttledge MH, Andermann AA, Phelan CM, et al. Type of mutation in the neurofibromatosis type 2 gene (NF2) frequently determines severity of disease. Am J Hum Genet 1996;59:331–42.
80. Parry DM, MacCollin MM, Kaiser-Kupfer MI, et al. Germ-like mutations in the neurofibromatosis 2 gene: correlation with disease severity and retinal abnormalities. Am J Hum Genet 1996; 59:529–39.
81. Hall JG. Genomic imprinting: review and relevance to human diseases. Am J Hum Genet 1990;46:857–73.
82. Bikhazi PH, Messina L, Mhatre AN, et al. Molecular pathogenesis in sporadic head and neck paraganglioma. Laryngoscope 2000;110:1346–8.
83. Heutink P, van der Mey AG, Sandkuijl LA, et al. A gene subject to genomic imprinting and responsible for hereditary paragangliomas maps to chromosome 1 1q23-qter. Hum Mol Genet 1992;1:7–10.
84. Heutink P, van Schothorst EM, van der Mey AG, et al. Further localization of the gene for hereditary paragangliomas and evidence for linkage in unrelated families. Eur J Hum Genet 1994;2:148–58.
85. Baysal BE, Farr JE, Rubinstein WS, et al. Fine mapping of an imprinted gene for familial nonchromaffin paragangliomas, on chromosome 11q23. Am J Hum Genet 1997;60:121–32.
86. Milunsky J, DeStefano AL, Huang XL, et al. Familial paragangliomas: linkage to chromosome 11q23 and clinical implications. Am J Med Genet 1997;72:66–70.
87. Devilee P, van Schothorst EM, Bardoel AF, et al. Allelotype of head and neck paragangliomas: allelic imbalance is confined to the long arm of chromosome 11, the site of the predisposing locus PGL. Genes Chromosomes Cancer 1994;11:71–8.
88. Knudson AG Jr. Genetics of human cancer. J Cell Physiol Suppl 1986;4:7–11.
89. Baysal BE, Ferrell RE, Willett-Brozick JE, et al. Mutations in SDHD, a mitochondrial complex II gene, in hereditary paraganglioma. Science 2000;287:848–51.
90. Mariman EC, van Beersum SE, Cremers CW, et al. Analysis of a second family with hereditary non-chromaffin paragangliomas locates the underlying gene at the proximal region of chromosome 1 1q. Hum Genet 1993;91:357–61.
91. Mariman EC, van Beersum SE, Cremers CW, et al. Fine mapping of a putatively imprinted gene for familial non-chromaffin paragangliomas to chromosome 11q13.1: evidence for genetic heterogeneity. Hum Genet 1995;95:56–62.
92. Niemann, S, Steinberger D, Muller U. PGL3, a third, not maternally imprinted locus in autosomal dominant paraganglioma. Neurogenetics 1999;2:167–70.
93. Niemann S, Muller U. Mutations in SDHC cause autosomal dominant paraganglioma, type 3. Nat Genet 2000;26:268–70.

94. Bikhazi PH, Roeder E, Attaie A, et al. Familial paragangliomas: The emerging impact of molecular genetics on evaluation and management. Am J Otol 1999;20:639–43.

Recent Review Articles of Interest

Kochhar A, Hildebrand MS, Smith RJ. Clinical aspects of hereditary hearing loss. Genet Med. 2007;9(7):393–408.

Brown SD, Hardisty-Hughes RE, Mburu P. Quiet as a mouse: Dissecting the molecular and genetic basis of hearing. Nat Rev Genet. 2008;9(4):277–90.

Welling DB, Packer MD, Chang LS. Molecular studies of vestibular schwannomas: A review. Curr Opin Otolaryngol Head Neck Surg. 2007;15(5):341–6.

Mittendorf EA, Evans DB, Lee JE, Perrier ND. Pheochromocytoma: Advances in genetics, diagnosis, localization, and treatment. Hematol Oncol Clin North Am 2007;21(3):509–25.

Tumor Biology 8

D. Bradley Welling, MD, PhD, FACS / Mark D. Packer, MD

INTRODUCTION

Recent advances in molecular biology have led to a better understanding of the etiology of many cranial base tumors. The development of new treatment options with improved outcomes and decreased morbidity by growth stabilization, or possible prevention is the goal of understanding the cellular mechanisms involved in the tumorigenesis. Indeed trials of several therapeutic agents targeting known pathways are underway.

As an example of the recent advances in this field, vestibular schwannomas (VS) will be highlighted. VS generally arise as sporadic unilateral tumors of the internal auditory canal (IAC) and the cerebellopontine angle (CPA); however, they are also found bilaterally as the hallmark of the inherited genetic disorder Neurofibromatosis 2 (NF2) [Online Mendelian Inheritance in Man (OMIM) #101000]. The NF2 syndrome is the autosomal-dominant manifestation of a biallelic mutation of the human chromosome 22, which gives rise to VS, as well as meningiomas, ependymomas, and presenile cataracts.

Fundamental understanding of the underlying molecular events leading to tumor formation began when the neurofibromatosis type 2 tumor suppressor gene (*NF2* gene) was identified and mutations confirmed in the VS or the germline.[1–3] The clinical characteristics of VS and NF2 syndromes have both been related to alterations in the *NF2* gene. The clinical manifestations of NF2 associated with various mutations have been described and signaling pathways affected by merlin, the product of the *NF2* gene, are becoming better understood.

For purposes of this chapter and elsewhere in the literature, abbreviations are as follows: "NF2" is used to indicate the human disease of neurofibromatosis type 2; the italicized "*NF2*" represents the human neurofibromatosis type 2 gene; and "*Nf2*" indicates the homolog or similar gene expressed in rodents. The mouse *Nf2* gene and the human *NF2* gene share greater than 98% amino acid homology, thus making the mouse a very relevant model for study. Interestingly, chickens have 94% and drosophila 50% human amino acid homology as well.[4]

The nomenclature $nf^{+/+}$ is wild type or normal nf gene. $nf^{-/-}$ refers to the absence of both alleles (homozygosity) and $nf^{+/-}$ refers to a heterozygosity or one allele only being nonfunctional.

Vestibular schwannomas can be grouped into unilateral sporadic solid VS or bilateral NF2-associated schwannomas. VS with true cysts or cystic schwannomas present a unique and aggressive phenotype, which may distinguish it from the more benign solid unilateral sporadic schwannoma. Mutations in the *NF2* gene have been identified in all three tumor types, but at the molecular level, the tumors are only beginning to be distinguished from each other.[5,6]

Schwannomas most commonly present as solitary tumors and constitute 95% of all VS. Sporadic unilateral VS occur in approximately 10 to 20 persons per million per year.[7,8] However, the true incidence may be higher, as highlighted by Anderson et al.[9] who demonstrated an incidence of 7 unsuspected schwannomas per 10,000 brain MRI studies (0.07%) or 70 per million. Sporadic tumors usually occur in the 4th and 5th decades with a mean presentation at about 50 years of age. Although histologically benign, schwannomas can compress the brain stem, leading to hydrocephalus, herniation, and death. Most commonly, however, they are associated with hearing loss, tinnitus, imbalance, facial paralysis, and facial paresthesias (see Figure 37–4).

NF2 [OMIM #101000] is clinically an autosomal-dominant disease that is highly penetrant.[10] NF2–associated tumors account for about 5% of all VS. Patients who inherit an abnormal copy of the *NF2* tumor suppressor gene have a 95% chance of developing bilateral VS (see Figure 37–2). However, about one half of patients have no family history of NF2, and thus as founders, they represent new germline mutations that were not inherited. Other disease features of NF2 include intracranial meningiomas, ependymomas, spinal schwannomas, and presenile lens opacities.[11–14] The onset of symptoms is usually between 11 and 30 years of age, but for some patients, the symptoms may present in their 5th or 6th decade. The incidence is estimated at between 1 in 33,000 and 1 in 40,000.[15,16] NF2 is not to be confused with neurofibromatosis type 1 (NF1) or von Recklinghausen's disease [OMIM #162200]. NF1, which is associated with multiple peripheral neurofibromas, is caused by a mutation in the *NF1* tumor suppressor gene on chromosome 17.

The spectrum of phenotypic expression in NF2 varies widely. In the past, the more severe clinical presentations were termed the Wishart type.[17] In addition to bilateral VS, patients often suffered from associated spinal tumors with a typical onset of symptoms in the late teens or early twenties. The less severe phenotypes have been termed the Gardner type with a later onset of bilateral schwannomas and fewer associated intracranial or spinal tumors.[18] In truth, the spectrum of disease does not always allow a clear distinction, but rather follows a continuum.

Occasionally segmental or mosaic categories of NF2 are also included to describe another classification of NF2.[19] The cause of segmental NF2 may be due to somatic mosaicism where a mutation occurs later in embryogenesis rather than in the germline DNA; therefore, only a portion of the patients' cells carry the mutation, and the disease is manifested in limited areas of the body.[20,21] In contrast, patients with familial NF2 inherit one mutation from a parent at conception and all cells carry one mutant allele. Kluwe et al.[21] estimated that mosaicism may account for 25% of the NF2 cases of any subtype among patients whose parents did not display the disease. Patients with somatic mosaicism can display bilateral VS if the postzygotic mutation occurred early in embryogenesis. However, they may also display an atypical presentation, or segmental NF2, in which the patient has a unilateral vestibular schwannoma and an ipsilateral, additional intracranial tumor, such as a meningioma, if the postzygotic mutation occurred later in development.[22] Unlike the traditional forms of NF2, the risk of passing NF2 caused by mosaicism to future offspring is low.

CYSTIC SCHWANNOMAS

Cystic VS are a particularly aggressive group of unilateral, sporadic schwannomas, which invade the surrounding cranial nerves, splaying them throughout the tumors. Cystic VS are associated with either intratumoral or extratumoral cysts, which develop in the loosely organized Antoni B tissues. In addition, a higher degree of nuclear atypia is seen in cystic tumors.[23,24] Careful distinction must be drawn between the truly cystic schwannomas and the very common heterogeneous schwannomas, which are not as aggressive in their clinical behavior. On magnetic resonance imaging (MRI), truly cystic regions of the tumors are hyperintense on T2-weighted images, and the cysts do not enhance with gadolinium administration. The noncystic component of the cystic tumors enhances with gadolinium in a manner similar to the unilateral and NF2-associated schwannomas (see Figure 37–5A and B). Cystic tumors may grow rapidly and are difficult to manage due to the high rate of hearing loss, facial nerve paralysis, and recurrence that occurs after surgical removal.[25] When compared to solid tumors of a similar size, the rate of complete facial nerve paralysis (House–Brachmann grade VI) with surgical removal of cystic tumors was 41%, as compared to 27% for that of solid unilateral schwannomas.[26] Cystic tumors are also more likely to have continued growth and facial nerve paralysis when treated with stereotactic radiation therapy than either the unilateral spontaneous or NF2-associated schwannomas.[27,28]

Although the effectiveness of treatment with current surgical and radiation treatments for VS are generally good, treatment-related morbidity continues to be problematic. A brief review of the recent discoveries and advances in the molecular biology of VS will follow.

The NF2 Gene

The *NF2* gene was localized to chromosome 22 band q12 through genetic and physical mapping (Figure 8–1A to C).[29,30] Positional cloning studies led to the discovery of the *NF2* gene in 1993 by two independent groups, Rouleau et al.[2] and Trofatter et al.[1] The gene was found to be frequently mutated in NF2-related VS. Since that time, mutations in the *NF2* gene have been found not only in NF2-associated tumors but also in sporadic unilateral schwannomas and cystic schwannomas.[3,31–37] Additionally, mutations within the *NF2* gene have been frequently identified in meningiomas and occasionally identified in other tumor types such as mesotheliomas.[35–43]

Human NF2 Mutations and Their Clinical Correlation

Specific *NF2* mutations in VS have been characterized in sporadic unilateral schwannomas and NF2-associated schwannomas.[3,32–36,38,44–58] The frequency, type, and distribution of *NF2* mutations were shown to be different between the sporadic and familial NF2 tumors.[3] Point mutations accounted for the majority of mutations identified in NF2 patients, whereas small deletions accounted for the majority of mutations found in the sporadic unilateral tumors.[46,47,55]

Two groups have recently published large data bases of NF2 mutations. Ahronowitz et al.[59] presented a meta-analysis of 1,070 small genetic changes detected primarily by exon scanning including 42 intragenic changes of 1 whole exon or larger, and 29 whole gene deletions and gross chromosomal rearrangements. Overall, somatic events detected by tumor analysis showed a significantly different genetic profile than constitutional events detected in the patients leukocytes. Over half of the mutations detected in tumors were frameshift mutations. The deletion of a single nucleotide (A < T < C < or G) from a gene can have a particularly disrupting affect because all of the codons downstream from the mutation are changed. In comparison constitutional or system wide inherited changes were primarily nonsense and splice site mutations (see Figure 8–2A to C).[60] Somatic events also differed markedly in meningiomas where most mutations were within the 5-prime four, ezrin, radixin, and moesin (FERM) domain of the transcript with a complete absence of mutations in exons 14 and 15. Less than 10% of small alterations were nontruncating or lesions, which would not completely destroy the protein. These changes were clustered in exons 2 and 3, suggesting that this region may be especially crucial to tumor suppressor activity in the protein. We and others have shown a frequent pattern of mutation changing arginine codons (CGA) to the thymine stop codon (TGA) (This type of "stop" codon not only terminates the transcription of mRNA, but often results in degradation of the mRNA already transcribed.) in both VS and meningiomas, causing a truncating lesion.[3,60] The chemical bonds associated with the configuration

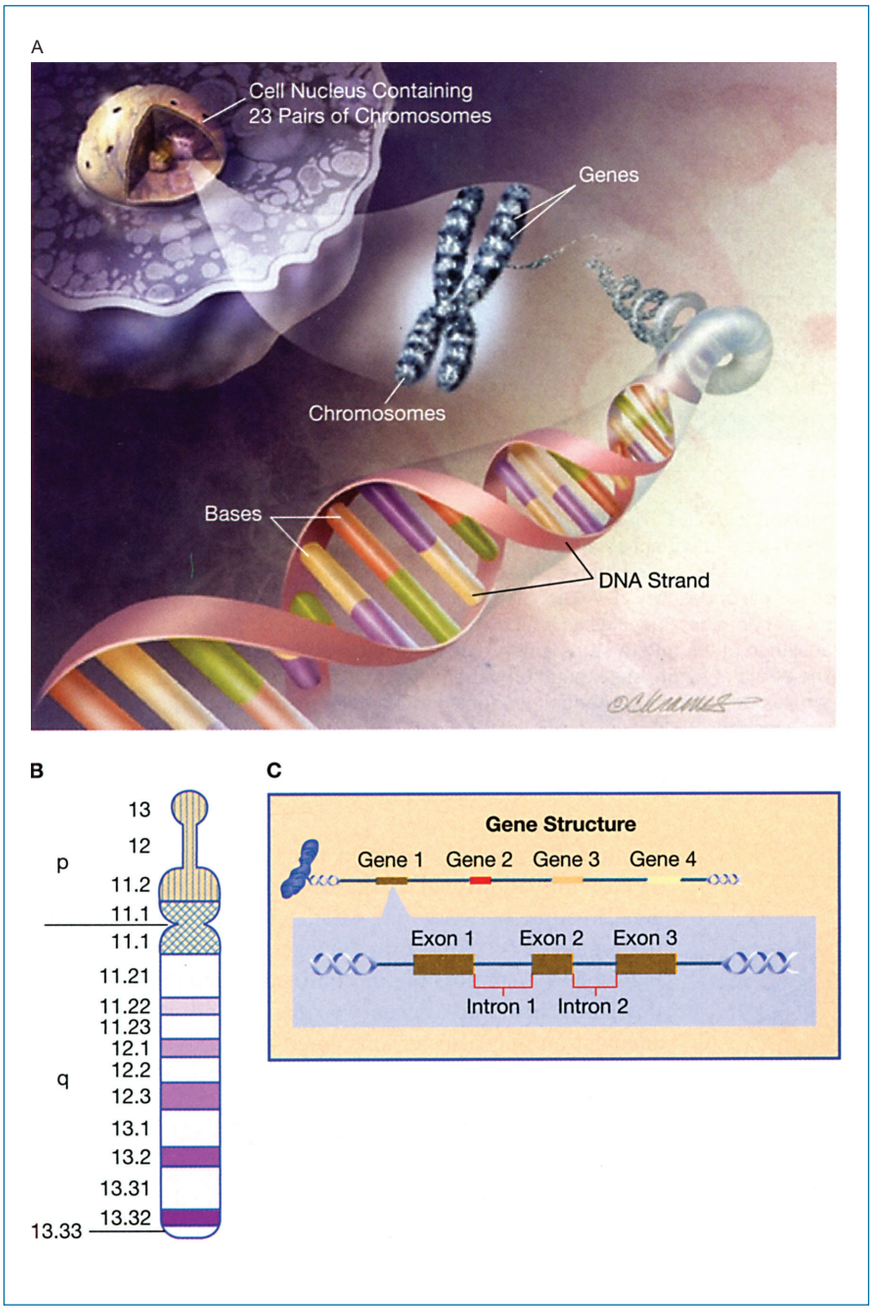

FIGURE 8–1 • *A*, Picture indicating the relationship of chromosomes, genes, and DNA nucleotide bases. *B*, Diagram of one arm of chromosome 22, depicting the p and q segments of the chromosome. *C*, A model of a human gene. The information contained in the gene and used for synthesis of the protein is split between exons (which code for the protein) and introns (noncoding sequences).

of these nucleotides make them less stable and more likely to undergo spontaneous mutation not only in NF2 but many other tumors as well. No mutations have been reported in exons 16 and 17, and few were noted in exon 9.

Studies to determine if genotype could be a predicator of disease severity showed that deletions that caused truncation of the NF2 protein have a more severe phenotype in NF2 pedigrees,[46,47,55] while missense mutations (see Figure 8–2) or small in-frame insertions in the *NF2*-coding region have been reported to associate with a mild phenotype.[3,35,36,54,56,57] However, exceptions are common as some missense mutations have been associated with severe phenotypes. It would appear that the location of the mutation within the gene may be important as missense mutations within the α-helical domain of the NF2 protein (see Figure 8–3) appear to associate with a less severe phenotype than those within the conserved ERM domain.[61] This lack of genotype–phenotype correlation was also seen for large deletions, which could give rise to mild phenotypes as well as the previously reported severe disease expression.[62] Clinical studies indicate that the phenotypic expression is more closely related within families than between families, but even within families, variability exists.[63] When statistically analyzed, the age of onset of NF2, the age at onset of hearing loss, and the number of intracranial meningiomas, were all found to have a significant intrafamilial correlation.[64] It is not known whether this variability occurs by chance, by epigenetic phenomena, or by modifying genes at other loci.[65] Epigenetic phenomena are not caused by a change in the coding sequence of the DNA but

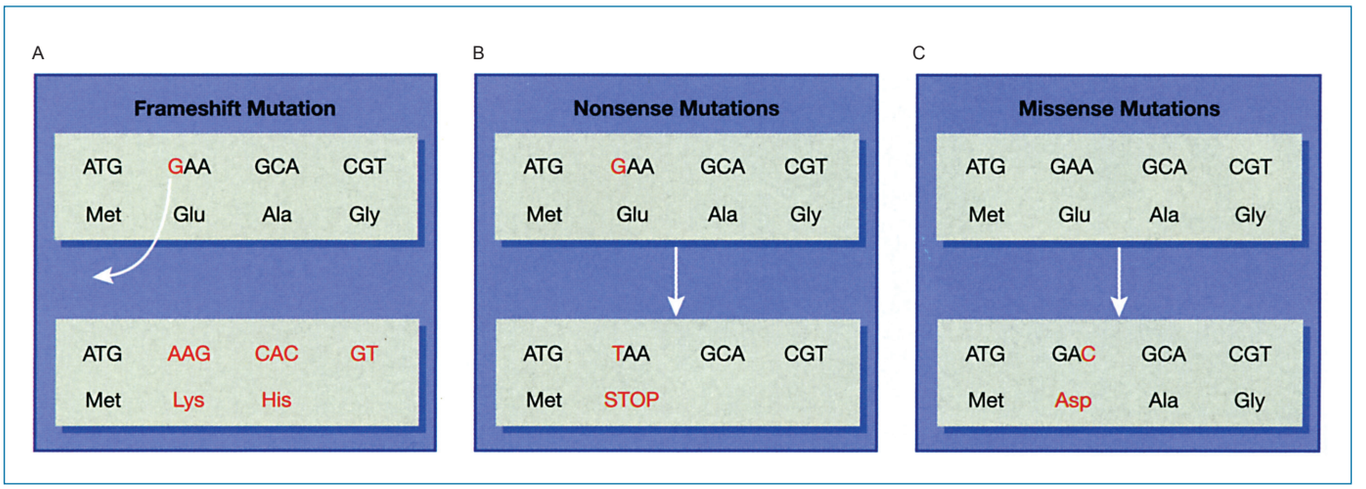

FIGURE 8–2 • *A*, The deletion of a single nucleotide (A, T, C, or G) from a gene can have a particularly disrupting affect on the gene because the deletion of one nucleotide changes all of the codons downstream from the change, resulting in a frameshift mutation. The deletion of the "G" base changes the downstream coding such that instead of coding for…Glu-Ala-Gly, the mutated gene now codes for…Lys-His… downstream from the mutation. *B*, A nonsense mutation is one that converts a codon that specifies an amino acid into a termination codon. This results in a shortened protein, since the translation of the mRNA stops at this new termination codon and not the correct one which if further downstream. The effect of a nonsense mutation depends on how much of the protein is lost. *C*, A point mutation or change of a single nucleotide can change a codon so that a different protein is specified. This is called a missense mutation, since the wrong amino acid is specified. The protein coded by the gene therefore has a change to a single amino acid. This often has no significant effect on the protein, as most can tolerate a few amino acid changes without their biological function changing.

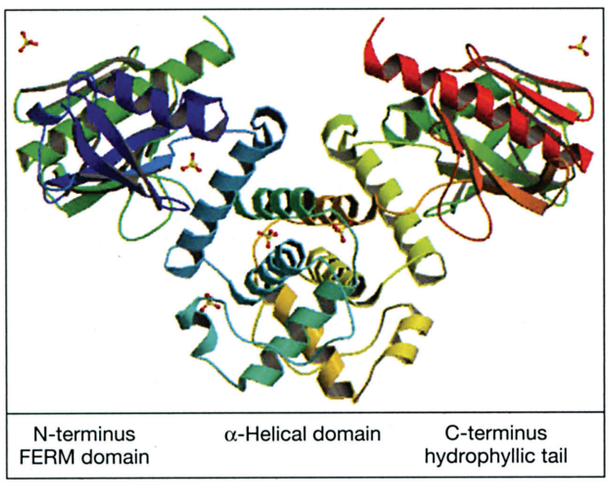

FIGURE 8–3 • The NF2 protein is divided into three general sections. The FERM domain is followed by an alpha-helical domain and a hydrophilic tail.[4] Merlin can dimerize with itself and heterodimerize with other ERM family proteins. *From Shimizu T, Seto A, Maita N, et al. (2002). Structural basis for neurofibromatosis type 2. Crystal structure of the merlin FERM domain. J. Biol. Chem. 277;(12):10332–6. doi:10.1074/jbc.M109979200. PMID 11756419*

rather alter the gene expression during gene development or cell proliferation. An example would be methylation of segments of the promoter region of the *NF2* gene, which suppress the expression of the gene. The *NF2*-coding region encompasses 17 exons spanning 90 kilo base-pairs (kBp) of DNA on chromosome 22.[1,2,66] By extensive screening of the entire *NF2* gene, Zucman-Rocci et al.[66] reported an 84% mutation detection rate in VS. Thus, additional mechanisms for inactivation of the *NF2* gene in some patients may exist. Mutation or methylation in the regulatory region of the *NF2* gene has been suggested (see Figure 8–4) as a possible mechanism of gene inactivation.[67–69] Posttranscriptional alternative splicing and differential polyadenylation may also be considered as possible means of inactivating the *NF2* gene.[68] Polyadenylation refers to the variable number of adenines that are attached at the 3′ end of the mRNA which may play a role in the way a gene is regulated. Alternative splicing refers to different patterns of splicing of exons which occurs, in this case the NF2 gene, resulting in differing isoforms of the gene. The two most common isoforms of NF2 have either exon 16 or exon 17 spliced out.

The NF2 Protein: Structure and Function

The *NF2* gene product is named merlin, for moesin-ezrin-radixin like protein, or *schwannomin*, a name derived from schwannoma.[1,2] For simplicity, the NF2 protein is referred to as "merlin" in this chapter. The *NF2* gene is transcribed into multiple RNA species by alternative splicing. Isoforms I and II are the two major RNA isoforms expressed in the cell. Isoform I encodes a 595-amino-acid protein and has exon 16 spliced out. Isoform II, containing all 17 exons, differs from isoform 1 only at the C-terminus. Insertion of exon 16 into the mRNA provides a new stop codon, resulting in a 590-amino-acid protein that is identical to isoform I over the first 579 residues. Intriguingly, only isoform I possess growth suppression activity.[70]

Merlin shares a high degree of homology to the erythrocyte protein 4.1-related superfamily of proteins, which act to

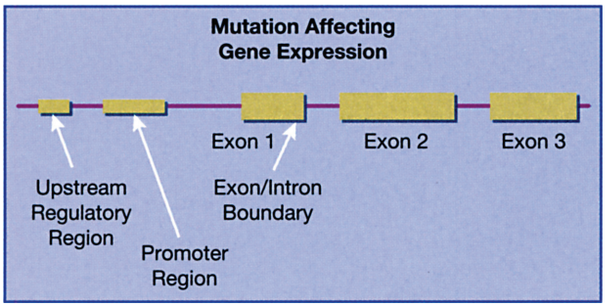

FIGURE 8–4 • Mutations can occur upstream of the gene itself in the promoter or regulatory regions or at the boundries between introns and exons (splice sites). Mutations in the promoter or regulatory regions may lead to over- or underexpression of the gene while mutations in the intron/exon boundaries may lead to aberrant splicing. Aberrant splicing might delete part of the resulting protein, add a new section of amino acids, or result in a frameshift.

link the actin cytoskeleton to the plasma membrane.[1,2] In particular, three proteins, ezrin, radixin, and moesin, referred to as the ERM family, share a great deal of structural similarity with merlin.[71,72] The proteins belonging to this family have a similar N-terminal globular domain, also known as the FERM domain, followed by an α-helical stretch, and finally a charged carboxyl-terminus.[72–74] The key functional domains of merlin may lie within the highly conserved FERM domains and the unique C-terminus of the protein. The ERM proteins have been shown to be involved in cellular remodeling involving the actin cytoskeleton.[75] These proteins bind actin filaments in the cytoskeleton via a conserved C-terminal domain and possibly via a second actin-binding site in the N-terminal half of the protein.[76,77]

Like the ERM proteins, merlin is expressed in a variety of cell types where it localizes to the areas of membrane remodeling, particularly membrane ruffles, although its precise distribution may differ from the ERM proteins expressed in the same cell.[78] Membrane ruffling is related to the interaction between the cytoskeleton with the cell body and the cell membrane. Schwannoma cells from NF2 tumors show dramatic alterations in the actin cytoskeleton and display abnormalities in cell spreading as well.[79] These results suggest that merlin may play an important role in regulating both the actin cytoskeleton-mediated processes and cell proliferation.[80] However, it should be noted that merlin has a growth suppression role, while other ERM-family members seem to facilitate cell growth.

Merlin Acts as a Tumor Suppressor

Overexpression of the *NF2* gene in mouse fibroblasts or rat schwannoma cells limits cell growth[57,81,82] and suppresses cell transformation by the ras oncogene.[83] Without the *NF2* gene overexpressed, transformation occurs when a cancer-causing protein, ras, allows the cellular proliferation machinery to become activated without proper regulatory mechanisms in place, causing malignant tumor growth. The growth control of certain Schwann cells and meningeal cells is lost in the absence of *NF2* function, suggesting that *NF2* mutations and merlin deficiency disrupt some aspect of intracellular signaling that leads to cellular transformation. Together, these findings demonstrate merlin's ability to act as a growth suppressor.

Nf2 knockout mouse models, which are either heterozygous or homozygous for the *Nf2* gene in the germline, have been created.[84,85] Heterozygous *Nf2* knockout mice go on to develop osteosarcomas, and less often, fibrosarcomas or hepatocellular carcinomas.[84] Metastatic disease is common in this model. Genetic analysis shows that nearly all of these malignant tumors are missing both *Nf2* alleles. Tumor growth in the absence of both *Nf2* alleles indicates that the *Nf2* gene possesses a classical tumor suppressor function. However, none of the heterozygous *Nf2* mice develop tumors or clinical manifestations associated with human NF2. The *Nf2* gene also plays an important role during early embryogenesis. Homozygous *Nf2* mutant mice, which are missing both *Nf2* alleles, die at approximately 7 days of gestation from a gastrulation defect or failure of inward migration of cells. Merlin is important in cell migration as we and others have shown during embryogenesis.[85,86]

By engineering mice whose Schwann cells have exon 2 excised from both *Nf2* alleles, conditional homozygous *Nf2* knockout mice have been produced, which display some characteristics of NF2 including schwannomas, Schwann cell hyperplasia, cataracts, and osseous metaplasia.[87] A conditional knockout model is engineered by inserting a regulatory mechanism into the gene, allowing the investigator to choose the time at which the desired gene (in this case *Nf2)* will be knocked out. Although these results are in favor of the argument that loss of merlin is sufficient for schwannoma formation in vivo, none of the tumors observed in these conditional knockout mice were found on the vestibular nerve. This is in contrast to those VS commonly found in patients with NF2.

Biallelic *NF2* inactivation is also frequently found in sporadic and in NF2-associated meningiomas. By engineering mice whose arachnoidal cells have exon 2 excised from both *Nf2* alleles, homozygous $Nf2^{-/-}$ mice show a range of meningioma subtypes histologically similar to the human tumors.[88] Taken together, these results demonstrate a tumor suppressor function for merlin in both Schwann cells and arachnoidal cells.

Merlin Signaling and Regulation

Merlin overexpression (see Figure 8–5), unlike the other members of the ERM protein family, causes growth suppression. In addition to the actin cytoskeleton, merlin has been shown to associate with cell membrane domains, which are highly enriched in signaling molecules that regulate cellular responses to proliferative and antiproliferative stimuli.[89] Vestibular schwannoma cells with *NF2* inactivation have dramatic alterations in cell spreading.[79] To date, several proteins that are likely to interact with merlin have been identified including the ERM proteins, CD44, F-actin, paxillin, microtubules, βII-spectrin, β1-integrin, β-fodrin, the regulatory cofactor of Na^+–H^+ exchanger (NHE-RF), SCHIP-1, hepatocyte growth factor-regulated tyrosine kinase substrate (HRS), p21-activated kinase 1 and 2 (Pak1 and Pak2), Rac1, the RIB subunit of protein kinase A, components of cadherin-mediated cell junctions, PIKE-L [phosphatidylinositol

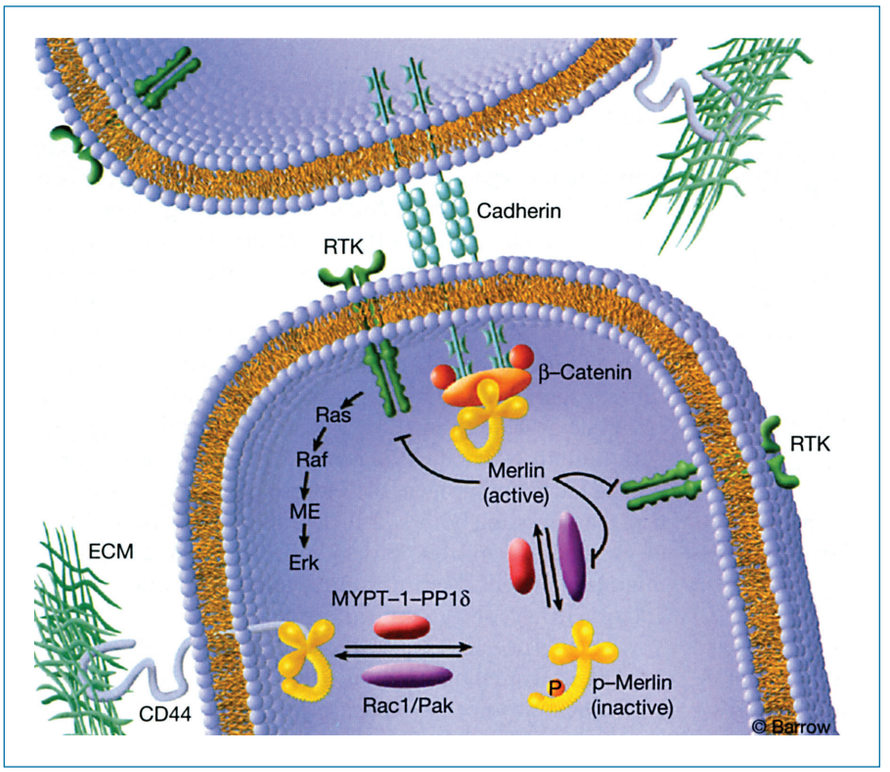

FIGURE 8–5 • Schematic diagram of merlin action. This diagram shows how Rac1 and Pak help convert the merlin protein from a closed conformation to an open conformation by phosphorylation of the protein. Consequently, merlin, in its open conformation, can interact with CD44 and facilitate linking the actin cytoskeleton to the cell membrane. p21-activated kinase 2 (Pak2) has been shown to phosphorylate merlin at serine 518 and inactivates its function. Merlin is activated by dephosphorylation by myosin phosphatase (MYPT-1-PP1δ).

3-kinase (PI3-kinase) enhancer], and erbin (erbB2-interacting protein).[82,90–107]

Presently, how all of these protein–protein interactions relate to the tumor suppressor activity of merlin is largely not understood. The association of merlin with CD44 and β1-integrin raises the possibility that merlin might function as a molecular switch in the signaling pathways. CD44 is a transmembrane hyaluronic acid receptor implicated in cell–cell adhesion, cell–matrix adhesion, cell motility, and metastasis.[90,101] Merlin mediates contact inhibition of cell growth through signals from the extracellular matrix. At high cell density, merlin becomes hypophosphorylated and inhibits cell growth in response to hyaluronate, a mucopolysaccharide that surrounds cells.[108] At low cell density, merlin is phosphorylated, growth permissive, and exists in a complex with ezrin, moesin, and CD44. These data indicate that merlin and CD44 form a molecular switch that specifies cell growth arrest or proliferation.

Lallemand et al.[105] showed that in *Nf2*$^{-/-}$ mouse embryo fibroblasts, *Nf2* deficiency led to piling-up of cells, hyperproliferation, and defective cadherin-mediated cell–cell interactions. When functioning normally, these interactions terminate proliferation by contact inhibition through specialized connections called adherens junctions. Furthermore, merlin colocalizes and interacts with and causes maturation of these adherens junction components in confluent or touching wild-type cells. Stated simply, when normal Schwann cells contact each other, special signaling through these junctions stops further growth. In the absence of merlin, the adherens junctions are immature and do not stop the schwannoma cells from terminating their growth when they contact each other. These results indicate that merlin functions as a tumor suppressor at least in part by controlling cadherin-mediated cell–cell contact.[109]

Merlin's function is regulated by phosphorylation.[106,110] Rac1, a member of the RhoGTPase family, has been demonstrated to promote phosphorylation of merlin, thereby inactivating its growth suppressor mechanism.[111,112] Among the effectors of Rac1 and Cdc42 GTPases, members of the p21-activated kinase (PAK) family have demonstrated interactions with merlin. Specifically, (Pak2) has been shown to phosphorylate merlin at serine 518 and inactivate its function.[89,104,113,114] Kissil et al.[114] also reported an interaction between merlin and Pak1, and merlin could inhibit the activation dynamic of Pak1. Loss of merlin expression leads to the inappropriate activation of Pak1, while overexpression of merlin results in the inhibition of Pak1 activity. Conversely, Merlin is activated by dephosphorylation at serine 518, which occurs on serum withdrawal or on cell–cell or cell–matrix contact.[108] Although the members of the PAK family have been implicated in various cellular processes, such as cytoskeletal reorganization and apoptotic signaling, their exact roles and functions have not been clearly defined. Jin et al.[115] identified the myosin phosphatase (MYPT-1-PP1δ) as a merlin phosphatase. Interestingly, the cellular MYPT-1-PP1δ-specific inhibitor, CPI-17, could cause decreased merlin activity by merlin phosphorylation, Ras activation, and transformation. These results implicate MYPT-1-PP1δ and CPI-17 as important regulatory components in the merlin tumor suppressor pathway.

Merlin's Growth Regulatory Function Is Related to Its Conformation and Protein-Protein Interactions

The activities of the ERM proteins are controlled by self-association of the proteins' N-terminal and C-terminal regions.[116,117] The ERM proteins can exist in the "closed"

conformation, where the N- and C-terminal regions undergo an intramolecular interaction, thus folding the protein to mask the conserved actin-binding site (Figure 8–3). The molecule can be converted to the "open" conformation in which the intramolecular interaction is disrupted by signals such as phosphorylation or treatment with phosphoinositides.[104,114,118]

Merlin's ability to function as a growth regulator is also related to its ability to form such intramolecular associations.[119] Two such interactions have been identified. The first interaction is between residues that fold the N-terminal end of the protein onto itself, while the second interaction folds the entire protein so that there is contact between N- and C-terminal ends of the protein.[82,119,120] In a fashion similar to the ERM proteins, merlin may cycle between the "open" and "closed" conformations that differentially determine whether it binds with the ERM proteins or other molecules to transduce merlin's growth inhibition signal.[121] In addition, the association between merlin and HRS, a substrate implicated in the signaling pathway initiated by hepatocyte growth factor (HGF) binding to the c-met receptor,[122] appears to be regulated by merlin folding.[120] These results suggest that the ability of merlin to cycle between the "open" and "closed" conformations may integrate CD44 and HGF signaling pathways. All of these findings are relevant to growth regulation. Also, merlin can exert its activity by inhibiting phophotidyl inositol 3-kinase (PI3-kinase) through binding to PIKE-L, a brain-specific GTPase that binds to PI3-kinase and stimulates its lipid kinase activity.[106] This finding suggests that PIKE-L is an important mediator of merlin growth suppression. Along this notion, we have found that the PI3-kinase/Akt pathway is activated in VS.[123]

The NF2 Gene Promoter

Characterization of the *NF2* regulatory regions is important for screening for mutations in both spontaneous and familial tumors in which no mutation was found in the *NF2*-coding region. We have shown that transcription of the *NF2* gene is initiated at multiple start sites and multiple regions in the *NF2* promoter are required for full *NF2* promoter activity.[68,124] Both positive and negative regulatory elements required for transcription of the *NF2* gene have been found in the 5′ flanking region of the promoter (see Figure 8–4). In particular, a sequence rich in guanine and cytosine nucleotide bases located in the proximal regulatory region, which can be bound by the Sp1 transcription factor, serves as a positive regulatory element.[68] This region is the area of the gene adjacent to 5′ of the coding region which regulates, either positively or negatively, the translation of the DNA into messenger RNA as we have described. Both the 5′ and 3′ flanking regions of the human *NF2* locus are G/C-rich and could serve as a target for gene methylation and inactivation as a form of therapy.[67,68]

We have also shown that a 2.4-kb human *NF2* promoter could direct where the NF2 gene expression would occur as early as embryonic day 5.5.[86] During early development, strong *NF2* promoter activity was detected in the developing brain and in sites containing migrating cells including the neural tube closure and branchial arches. (Figure 8–6). Interestingly, a transient change of *NF2* promoter activity during neural crest cell migration was noted. While little promoter activity was detected in premigratory neural crest cells at the dorsal ridge region of the neural fold, significant activity was seen in the neural crest cells already migrating away from the dorsal neural tube. In addition, we detected considerable *NF2* promoter activity in various NF2-affected tissues such as the acoustic and trigeminal ganglia, spinal ganglia, optic chiasma, the ependymal cell-containing tela choroidea, and the pigmented epithelium of the retina. The *NF2* promoter expression pattern during embryogenesis suggests a specific regulation of the *NF2* gene during neural crest cell migration and further supports the role of merlin in cell adhesion, motility, and proliferation during development.[86]

Alternatively Spliced NF2 mRNA Isoforms in Vestibular Schwannomas and Other Cell Types

The *NF2* gene undergoes alternative splicing in the coding exons.[38,47,68,125–130] Multiple alternatively spliced *NF2* transcripts have been identified in various human cells. The most common isoforms in these cells were isoforms II (containing all 17 exons) and isoform I (without exon 16). We have also examined the expression of alternatively spliced *NF2* mRNA isoforms in VS. Cloning and sequencing analysis showed that the expression pattern and relative frequency of the alternatively spliced *NF2* transcripts in VS appeared to be different from those detected in other human cell types. In addition to isoforms I and II, these schwannomas expressed a high percentage of the *NF2* isoform lacking exons 15 and 16. These alternatively spliced *NF2* transcripts could encode different protein products (unpublished data).

Presently, the role of alternative splicing of *NF2* mRNA is not well understood. It is possible that the functional contribution of the *NF2* tumor suppressor may require a balanced expression of various isoform proteins in Schwann cells and/or other cell lineages.[68,131] Alternative splicing may be another mechanism for Schwann cells to inactivate merlin function and/or to generate isoforms that have additional properties conducive to tumor formation.

Immunohistochemical Markers of Growth in Vestibular Schwannomas: Clinical Correlation

Attempts to correlate clinical parameters with immunohistologic evaluation of protein expression in VS have been performed. An increase in Ki-67, a protein, which is an index of nuclear proliferation, was shown to correlate with the growth of solid schwannomas on MRI.[132,133] Higher rates of tumor recurrence have also been suggested in tumors with an increased rate of nuclear proliferation and mitotic indexes, although the supporting data for this claim was not conclusive.[134] Positron emission tomography (PET) scanning has been conducted to assess the metabolic activity of VS preoperatively and to assess the metabolic activity with the proliferation index, Ki-67. However, no correlation was found. Additionally, there was no correlation between 18-fluorodeoxyglucose (FDG) uptake (indicator of metabolic activity in tissues) and Ki-67 expression measured by immunostaining.[135] This is most likely because VS are slow

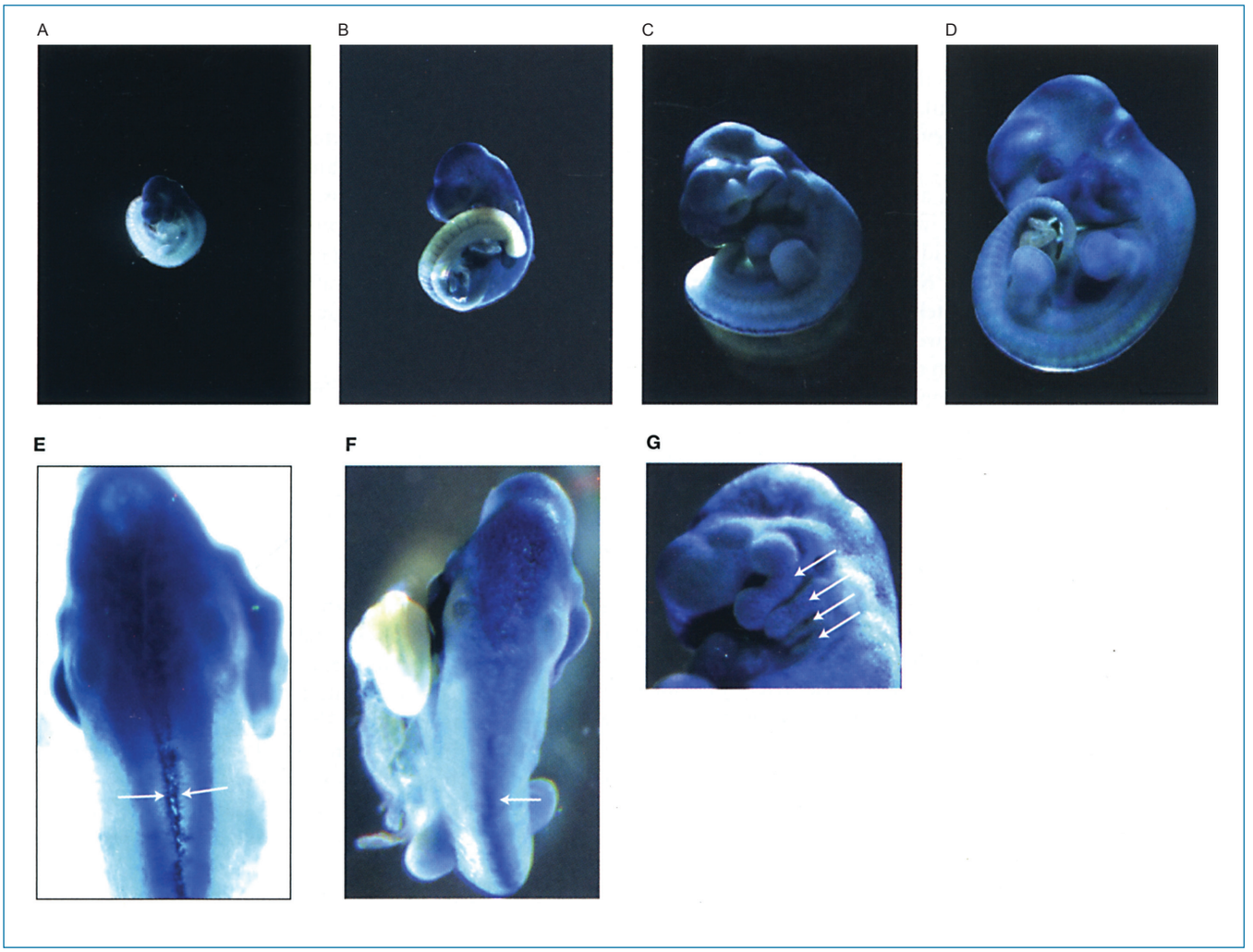

FIGURE 8–6 • *NF2* promoter expression in neural tube and neural crest. Lateral views of whole-mount X-gal-stained transgenic mouse embryos at various days p.c. *A*, E9.5, *B*, E10.5, *C*, E12.5, and *D*, E14.5. Scale bar 400 m. The most intense β-gal expression was detected along the dorsal closure (arrows) of neural tube in *E*, E9.5 and *F*, E10.5, transgenic embryos. Strong β-gal expression was also seen in the branchial arches I–IV (arrows) of the *G*, E10.5 embryo.

growing tumors with less than five percent of tumor cells being in S-phase or active division (Figure 8–7).[136]

Another possible marker for tumor growth is the transforming growth factor β1 (TGF-β1). Immunostaining for TGF-β1 was positive in 96% of blood vessels within schwannomas and in 84% of schwannoma tissue samples; however, no direct correlation with tumor growth was found.[137] Immunohistochemical association of β1-integrin with merlin has been demonstrated, but has not been related directly to tumor phenotypes.[95] Cystic schwannomas are associated with a 36-fold decrease in nuclear proliferation as measured with Ki-67 staining when compared to solid tumors, suggesting that the rapid clinical growth seen in cystic schwannomas is related to the accumulation of cyst formation but not by an actual increase in the growth rate of tumor cells.[138,139] Also, NF2-associated schwannomas have been shown to have an increased proliferation index by Ki-67 and proliferating cell nuclear antigen (PCNA) immunostaining, when compared to unilateral solid schwannomas.[140,141] PCNA is a proliferation index marker and is important in cell division.

Recently, we detected higher levels of cyclin D_3 expression, which is associated with G_1 cell-cycle progression, in 5 of 10 VS, compared to Schwann cells in adjacent normal vestibular nerve.[142] In contrast, expression of the cyclin D_1 protein, which controls Schwann cell differentiation, was not detected in any of the schwannomas examined. These results suggested a possible role for cyclin D_3 in the growth of some VS cells.

Taken together, these studies demonstrate relatively little correlation between clinical growth as assessed by MRI scans, historical data, and nuclear growth indexes in solid unilateral and *NF2*-associated schwannomas. Cystic tumor growth appears to occur via a different mechanism. Although the defective *NF2* gene is the underlying common denominator in tumor formation of all three tumor types, other differences at the molecular level likely account for the variable clinical presentations of these tumors.

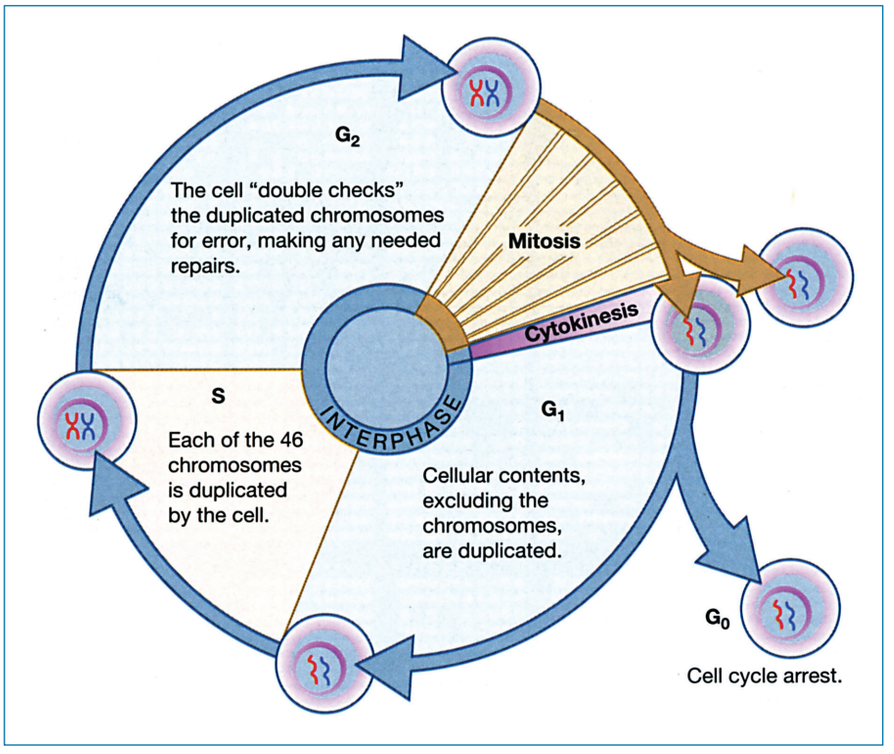

FIGURE 8–7 • Cell cycle revisited. During G1 phase, the cell grows. In S phase, the cell copies its chromosomes so that each chromosome now consist of two sister chromatids. During G2, the cell prepares for division and in M phase, the cell separates into two new cells (cytokinesis). www.le.ac.uk/ge/genie/vgec/sc/cellcycle.html. *From University of © Clinical Tools. Inc. Leicester.*

Identifying Deregulated Genes in Vestibular Schwannomas

To further elucidate the growth pathways in VS, the gene expression profiles have been studied. The study of large-scale gene expression profiles utilizing cDNA microarrays allows examination of the so-called transcriptome of a tissue, and gives a means of exploring a broad view of the basic biology of tumors.[143,144] cDNA is complimentary DNA, synthesized from a mature mRNA template. A microarray consists of thousands of "spots" of DNA attached to a solid surface, each containing a small amount of a specific DNA sequence corresponding to certain genes. A cDNA sample of interest is added to the microarray and allowed to hybridze. Hybridization of the sample and DNA on the array is detected and quantified using fluorescence. Using the technology of microarrays, gene expression profiles can be created in which the activity or expression of thousands of genes can be measured at once, creating a global picture of cellular function. By comparing gene expression profiles between the tumor and normal tissues, deregulated genes in the tumors tissues can be identified.[5,145] We studied gene regulation in VS using cDNA microarray analysis and found 42 genes, which were significantly upregulated including osteonectin, endoglin, and Rho B, when compared to normal vestibular nerve tissues.[5,145] Additionally, multiple genes were found to be significantly downregulated in the majority of VS examined. Of these genes, a putative tumor suppressor gene LUCA-15 was downregulated in 7 of 8 schwannomas studied (Figure 8–8).

Osteonectin is a secreted glycoprotein that interacts with extracellular matrix proteins to decrease adhesion of cells from the matrix, thereby inducing a biological state conducive to cell migration. Endoglin, a TGF-β receptor-binding protein was found to be significantly upregulated in all of the solid tumors but not in any of the cystic tumors examined. It is likely that the increased endoglin expression may induce downstream signaling proteins, somehow leading to an aggressive cystic phenotype.[5] An example of a deregulated signaling pathway suggested by the microarray data is the retinoblastoma protein (pRb)-cyclin dependent kinase (CDK) pathway.[145] Among genes involved in G_1-S progression (see Figure 8–7). CDK2 was found to be downregulated in 7 of 8 tumors. In addition, upregulation of transforming factor RhoB was found in all of the schwannomas examined.[5] Further examination of these deregulated genes as potential downstream targets of the *NF2* tumor suppressor should provide us with targets for pharmacotherapeutic interventions.

Environmental Exposures

There is evidence that radiation may be associated with the induction of vestibular schwannoma growth. While other sites and tumors also show propensity for growth in response to environmental exposures, the vestibular nerve appears to contain an increased sensitivity for tumor growth as compared to other regions within the central nervous system or elsewhere.

Evans and colleagues note an 18.8-fold increased relative risk of schwannoma induction and a 9.5-fold increased relative rate of meningioma induction following radiation doses of 2.5 Gy from the treatment of tinea capitis, adeno-tonsillar disease, and capillary hemangiomas.[146] The radiobiologic effect was dose-dependent similar to the tissue effect and tumor growth response observed in post-WWII Japan. Preston and

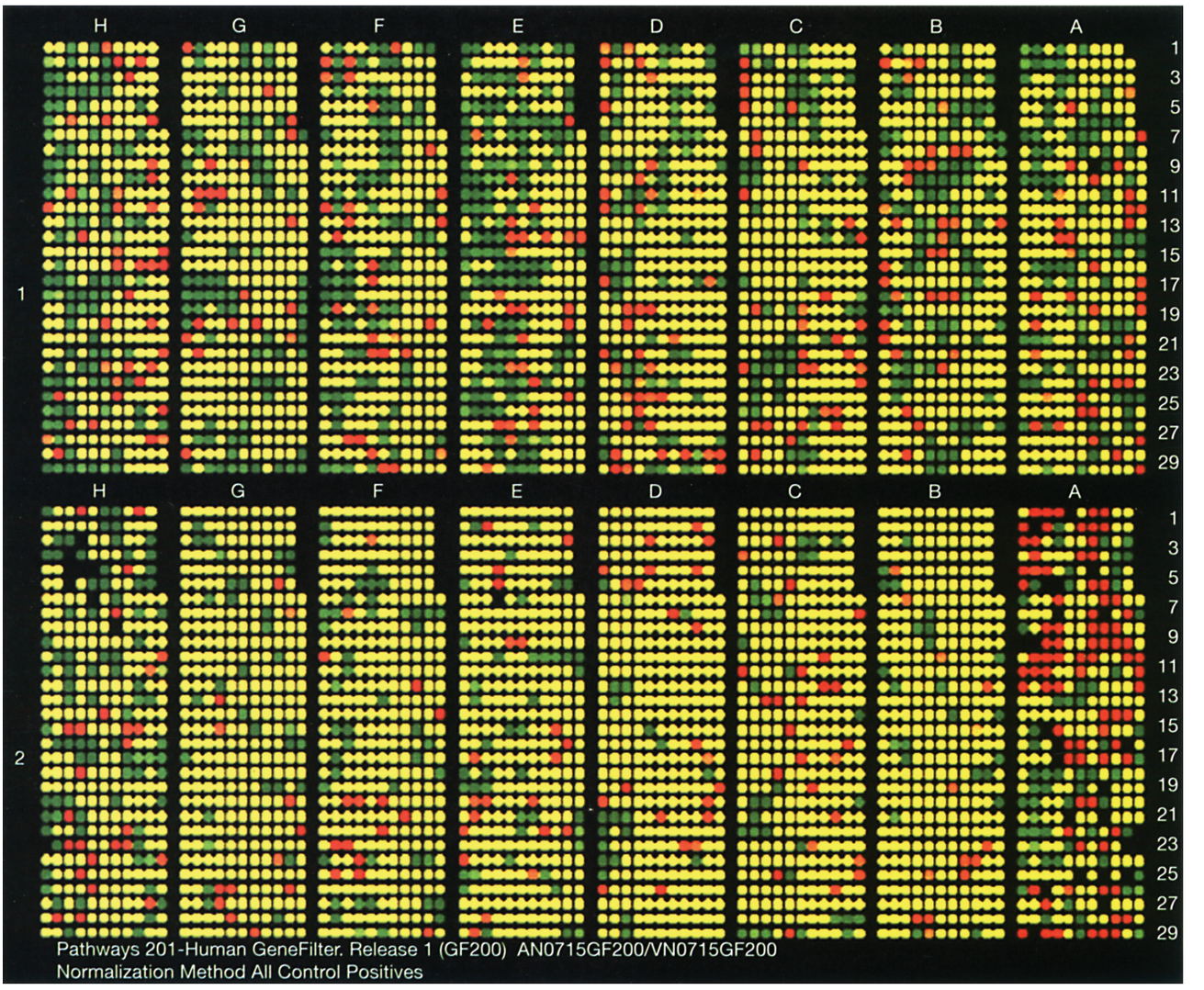

FIGURE 8–8 • cDNA microarray comparison of gene expression of a vestibular schwannoma and adjacent normal vestibular nerve (gene filter 200, Research Genetics, Huntsville, AL). The phosphor image shows red genes overexpressed in the tumor and green genes overexpressed in the vestibular nerve. Yellow images are genes that are nearly equally expressed in both tissues. *From Welling. Otol Neurotol, Volume 23(5).September 2002;736–748.*

colleagues[147] showed that VS were the most abundant intracranial tumors encountered, with a high propensity for Schwann cell mutation in response to radiation damage.

Overall, the risk of tumors induced by therapeutic radiation appears to be approximately 0.1 to 3% after 30 years.[146,148] In light of the 33 to 40% lifetime risk of malignancy in the general population, Evans[146] argues that the benefits of single-dose radiation treatment for VS may be justified for those with documented tumor growth that refuse surgery, or for the elderly or infirm. However, patients with NF2, in particular, are the disproportionate recipients of radiation-induced malignant tumors. Although only 7% of patients with VS have NF2, 50% of malignant changes induced by stereotactic irradiation of VS occur in NF2 patients. Evans strongly cautions the use of radiation treatment for benign tumors in childhood and in tumor-prone conditions such as neurofibromatosis. We concur.

Cellular Telephone Risk

Several studies addressed the risk of cellular telephone use and the formation of VS presumably secondary to electromagnetic radiation over a long exposure period. Hardell et al.[149] reviewed 13 case-controlled studies and found 9 case control studies to have reported patients with over 10 years of cellular telephone use. They concluded that the odds ratios for ipsilateral cellphone use and the development of VS was 2.4 (95% confidence interval 1.1–5.3). A consistent pattern emerges from the case-controlled studies of increased risk for vestibular schwannoma and also glioma with risk elevation greatest for high-grade gliomas associated with unilateral long-term exposure.[149,150]

Genetic Screening for NF2

A parent with NF2 has a 50% chance of passing the affected *NF2* allele along to their offspring if (1) their spouse does not have NF2 and if (2) they do not have a mosaic form of NF2. (Mosaicism occurs when a mutation in the NF2 gene occurs after an embryo has undergone several sets of cell division. Therefore only a portion of the child's cells carry a mutation in the NF2 gene.) A child who inherits an abnormal copy of the *NF2* tumor suppressor gene has a 95% chance of developing bilateral VS.

Because early intervention is very important in clinical outcome, genetic and clinical screening for at-risk patients is advocated. We feel that routine clinical and imaging examinations are mandatory for those who are at-risk to develop NF2. This includes anyone with a first-degree relative with NF2, patients under 30 years old with a unilateral VS, or any patient with multiple intracranial, spinal, or peripheral skin tumors that are associated with NF2. Any offspring of patients with NF2 should have annual ophthalmology examinations starting soon after birth since cataracts can begin at a very early age. Annual neurology examinations should be started at 7 years of age or earlier if neurologic deficits are noted. We recommend bi-annual audiograms and annual MRI evaluations beginning at age 7. Others have recommended starting a similar screening process at 10 years of age with an MRI every other year and annually once a tumor is found.[151]

Mutation screening for the first-degree relatives of NF2 patients is recommended when the probands' mutation has been identified either from a schwannoma or from leukocyte screening.[151,152] A proband is the person who is being studied in whom the disease is first clinically detected. Other family members at risk can be identified and screened for developing NF2 or receive appropriate genetic counseling. Patients who are first-degree relatives of NF2 patients where the mutation in the *NF2* gene has not been identified may have more ambiguity regarding the screening of their *NF2* gene for mutations if no mutation is localized. Appropriate audiometric testing and neural imaging needs to be carried out as false negatives in mutation screening can occur in up to 25% of patients. Taking this fact into consideration, we feel that annual MRI screening and biannual audiometric testing would still be needed for children older than 7 years of age who had a negative test. Additionally, if a mutation was detected during DNA sequencing, we would still recommend annual MRIs and biannual audiometric testing in order to detect the development of VS at the earliest possible stage. Early detection in NF2 does make a significant difference in the ability to successfully preserve hearing and facial nerve function.

When an *NF2* mutation has already been identified in an affected family member, screening additional first degree family members for the same mutation is considerably less costly and is recommended. The sensitivity of genetic testing in this circumstance is extremely high since the DNA being screened can be directly compared to the known mutation in the affected family member. In this case, knowing with near certainty that a child does not carry a *NF2* mutation can avoid the frequent MRI examinations that would otherwise be required.[44,153] Therefore, if a family has multiple members (more than two people) diagnosed with NF2 and mutation testing has not been performed, it may be worthwhile to identify the mutation in at least one family member so that future family members can be screened. This is most effectively done when tumor tissues are available for mutation screening. However, biopsy for genetic diagnosis alone is not suggested if tumor removal is otherwise not indicated as clinical screening protocols are also effective.

Potential Drug Treatments

As the understanding of merlin and its interacting partners is better understood, new means of targeting these pathways for intervention in schwannoma cells is occurring. Some treatments are aimed at restoring the wild-type merlin protein to the mutant cells, while other strategies attempt to block the proliferation of schwannoma cells by blocking its growth pathways or by increasing programmed cell death or apoptosis. For example, Messerli et al.[154] showed effective reduction of schwannoma growth in both a transgenic and a xenograft mouse model by injecting wild-type merlin packaged in an oncolytic recombinant herpes simplex virus vector in the tumor as noted in the text directly. The vehicle for delivery was a replication-competent herpes simplex virus, which has tumoricidal properties. There were no apparent toxicities with the injection of the oncolytic vector. A paradigm for the use of oncolytic vectors to reduce the volume of benign tumors when surgical resection may cause nerve damage is suggested.

Hansen et al.[155] and Doherty et al.[156] demonstrated cell surface human epidermal growth factor, also known as erythroblastic leukemia viral oncogene homolog 2 or ErbB2 receptors as possible targets for VS cell growth inhibition. Blocking the ligand or interacting proteins, which activates this receptor by treatment with blocking antineuregulin antibodies, also inhibited schwannoma cell proliferation. ErbB2 is a tyrosine kinase receptor, a common cellular switch, on the VS cell surface, which triggers the MAPK kinase cascade, a process that leads sequentially to nuclear activation of cell division. One of its ligands, neuregulin-1, is a growth factor produced by schwannoma cells, thus creating an autocrine feedback loop; the schwannomma cells cause further stimulation of schwannoma growth.

Plotkin et al. (Children's Tumor Foundation meeting, June 2008, Bonita Springs, FL) showed that epidermal growth factor receptor (EGFR) blockade with erlotanib HCl was tolerated and showed radiographic and audiometric response to treatment in a patient with NF2 in short follow-up. Although hepatotoxicity may limit this agent's use, other trials with EGFR and ErbB inhibitors are expected.

Several investigators demonstrated that intervention at the intracellular proliferation pathways, specifically the MAPK pathway and the phosphatidylinositol 3-kinase (PI3K) pathway, respectively, may also result in schwannoma growth suppression. Nakai et al.[112] showed that merlin is involved in suppression of Rac signaling, and cultured schwannoma cells contain elevated, GTP-bound, active Rac. Application of a Rac-specific inhibitor, the chemical compound NSC23766, to schwannoma cells restored neuronal interaction. The data support the significance of regulated Rac signaling in mediating Schwann cell–axon interaction and suggest controlling Rac activity as a possible therapy for schwannomas.

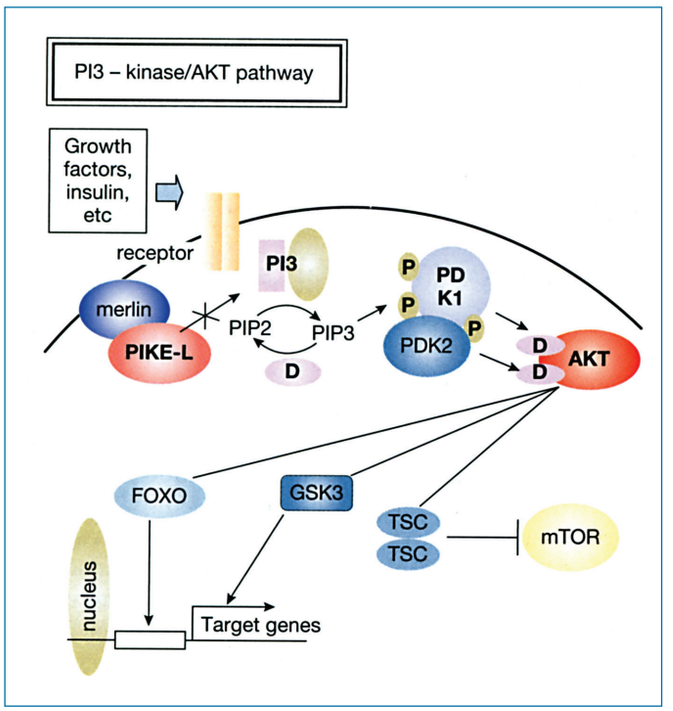

FIGURE 8–9 • PI3K/AKT signaling. Insulin and other growth factors activate cell surface tyrosine kinase receptors that stimulate PI3K activity. PI3K converts PIP2 to PIP3. PTEN is a negative regulator of the AKT pathway that catalyzes the conversion of PIP3 back to PIP2. PDK1 and PDK2 maximally activate AKT. Phosphorylation of downstream effectors of the AKT pathway inhibit these proteins. Existing as a complex, TSC1 and TSC2 normally inhibits mTOR activity. However, when TSC2 is phosphorylated by AKT, it dissociates from TSC1, and mTOR becomes active. Active GSK and FOXO function within the nucleus as transcriptional regulators that activate genes promoting apoptosis. Merlin, the NF2 gene product, can bind PIKE-L and inactivate PI3K. A small molecule PDK1 inhibitor can inhibit phosphorylation of AKT at the 308 site. PNAS 2004

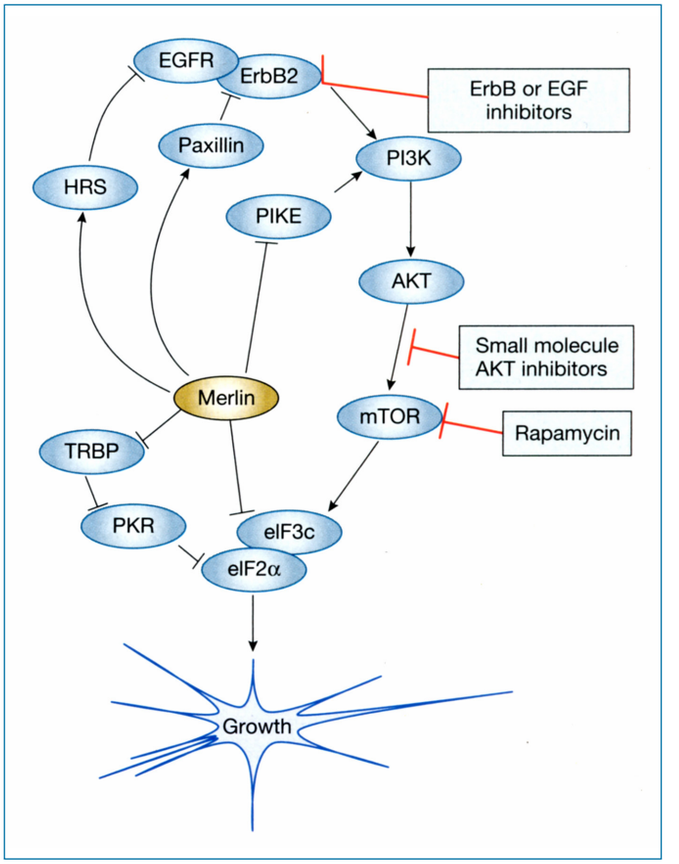

FIGURE 8–10 • Alternative pathways. In this schematic in a recent review by Dan Scoles, Merlin's interaction with the ErbB2—Paxillin complex, PIKE, and eIF3c, effect of NGB and merlin on cyclin D1 expression, and functional consequences of merlin loss on proliferation mediated by these interaction suggest that signaling in the ErbB2–PI3kinase–mTOR–eIF3c–cyclin D1 pathway may contribute to NF2 pathogenesis. PIKE-L is free to enhance PI3K which leads to complete phosphorylation and activation of PDK1 and PDK2, which in turn activate the cells mitotic machinery. Drugs targeting this pathway therefore may be useful for inhibition of NF2 tumors with overactive mTOR signaling, including trastuzumab (herceptin, LY294002, AKT inhibitors, UCN-01, Rad-001, CCI-779, and AP23573, and small molecule AKT pathway and histone deacetylase inhibitors. HSP90 inhibitor 17AAG (17-allylamino-17-desmethoxygeldanamycin) may affect Akt and C-Raf, Cdk4 and Cyclin D-1. (NexGenix)

Jacob et al.[123] demonstrated the activation of the PI3-kinase/AKT pathway in human schwannomas. It has been shown that merlin can inhibit PI3-kinase through its binding to the PI3-kinase enhancer-L (PIKE-L). PIKE-L is a GTPase which binds to and stimulates PI3K. (Figure 8–9) The suppression of PI3-kinase activity results from merlin disrupting the binding of PIKE-L to PI3-kinase. Our recent studies using cultured schwannoma cells further suggest that both an AKT pathway inhibitor as well as a histone deacetylase inhibitor could suppress schwannoma cell growth by blocking the PI3-kinase pathway. Utilizing a quantifiable xenograft model for VS we are currently testing the efficacy of these novel compounds.

Transduction of growth factor stimulation of the mammalian target of rapamycin (mTOR) signaling pathway ultimately results in stimulation of protein synthesis and entry into the G1 phase of the cell cycle. Decreased phosphatase and tensin homolog gene (PTEN), a human gene that acts as a tumor suppressor gene, manifests as AKT and mTOR activation stimulating growth. Additionally hypoxia inducible factors HIF-1 alpha, and HIF-2 alpha show increased expression and account for enhanced angiogenesis with mTOR activation. This may lead to the necessary blood vessel supply to schwannomas. AKT and mTOR activation have been noted in VS. The immunosuppressant, rapamycin, inhibits mTOR and induces G1 arrest and apoptosis. Newer mTOR inhibitors, such as temsirolimus, have shown good effect in the treatment of renal cell carcinoma alone and in combination with other agents. (Figure 8–10)

A novel treatment approach has been proposed and is being evaluated in benign tumors. Nonsense mutations account for up to 39% of NF2 related VS and 23% of mutations leading to unilateral sporadic tumors. These mutations are related to a dominant C to T transition, replacing arginine with a premature termination codon (PTC) within the developing protein molecule as mentioned earlier. PTC 124 is a low-molecular-weight compound that shows an ability to "read through" premature termination codons while still responding to true stops, allowing for synthesis of a full protein product (Figure 8–11). It is showing promise in phase II trials of nonsense mutations in

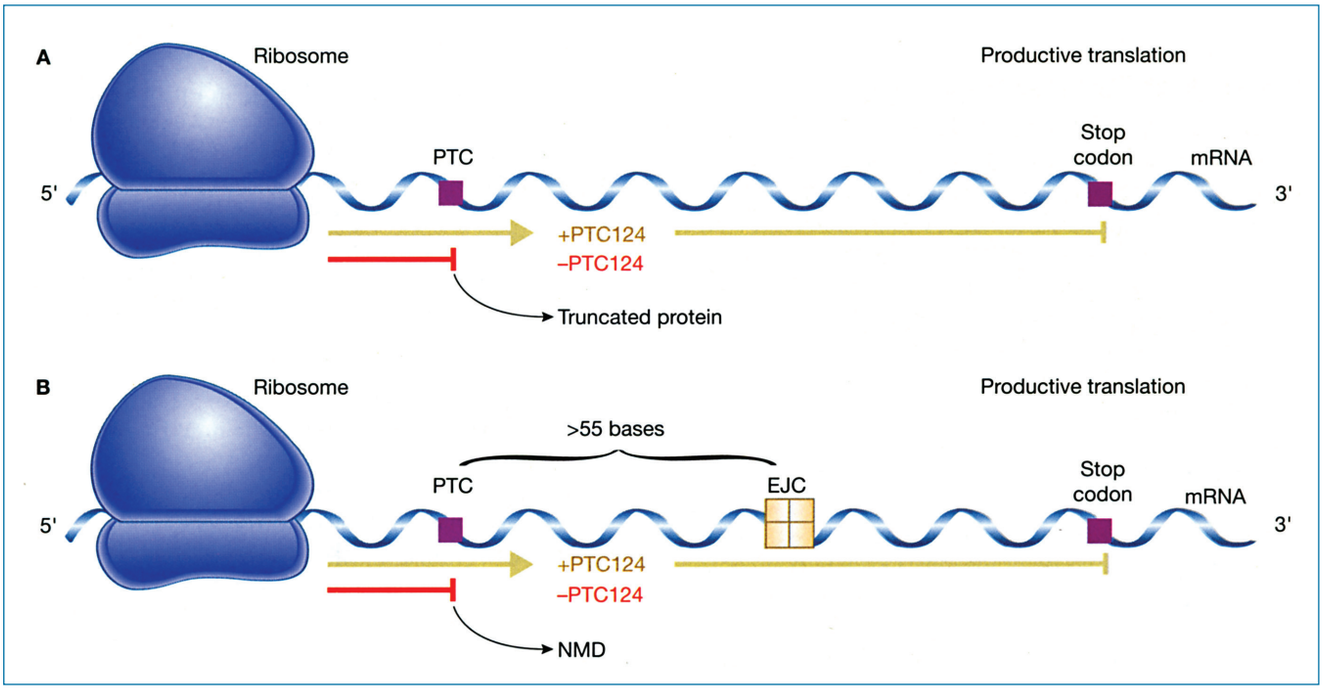

FIGURE 8–11 • Possible mechanisms of PTC124-enhanced translation. *A*, PTC124 could directly suppress termination of "productive" protein translation at a premature termination codon (PTC), leading to increased levels of functional full-length proteins. *B*, Alternatively, PTC124 might suppress the identification of PTCs in "pioneer" translation, thereby preventing nonsense-mediated mRNA decay (NMD), which is induced if a ribosome hits a stop codon more than 55 bases upstream of an exonjunction complex (EJC). This would lead to the stabilization of PTC-containing mRNAs, allowing their translation, presumably through the mechanism shown in View *A*. The work of Welch et al. supports the model depicted in View *A*.

genetically compatible patients with Duchenne's muscular dystrophy and cystic fibrosis.[157,158] Because PTC 124 is a genetically dependant therapeutic as opposed to a disease-specific agent, it holds promise for genetically screened patients displaying nonsense-related tumors.

Angiogenesis inhibitors such as Avastin (Bevacizumab) have been used alone or in combination for treatment of colorectal, and lung and prostate carcinomas.[159–162] It acts by inhibiting vascular endothelial growth factor (VEGF), and is used in several combination treatment protocols. Avastin has anecdotally shown temporary suppression of VS growth. Its temporary effect on tumor growth reduction, the potential side effects of leukopenia, and bleeding limit its use in surgical patients, and it is currently considered a temporizing agent. PTC 299 similarly blocks angiogenesis, but by inhibiting the production of VEGF. It has been shown to be effective against cancer cell lines including breast, cervical, colorectal, gastric, lung, ovarian, pancreatic, prostate, and renal cell carcinomas, fibrosarcoma, melanoma, and neuroblastoma. Animal studies have documented its efficacy in reducing VEGF in tumor and serum, decreasing blood vessel density in tumor, and substantially impeding tumor progression by itself and as a component of combined therapy with other antitumor agents or Avastin. Tolerance in phase I studies has been acceptable, and phase II trials in breast cancer are commencing (unpublished data).

The medical treatment of slow growing benign tumors must maintain efficacy over decades of potential treatment. Perhaps combined modality treatments might be considered. Two agents we are currently studying (a histone deacytelase inhibitor and an AKT pathway inhibitor) have shown capacity to modulate radiation response in an additive fashion. By sensitizing targeted tissues, radiation doses could be lowered to optimistically promote killing effect of tumor cells, reduce adverse effect on surrounding structures, preserve physiologic function, and decrease the risk of tumor promotion or malignant transformation.

Schwannomatosis (OMIM #162091), a recently defined form of neurofibromatosis, is characterized by multiple schwannomas but this condition distinctly lacks any VS. Patients with schwannomatosis frequently present with intractable pain rather than cranial nerve deficits. They do not develop other intracranial tumors or malignancies. MacCollin et al.[163] noted that about one-third of patients with schwannomatosis had tumors in an anatomically limited distribution, such as a single limb, several contiguous segments of spine, or one half of the body. Sporadic cases of schwannomatosis are as common as NF2, but few cases of familial schwannomatosis have been identified in contradistinction to NF1 and NF2, which are autosomal-dominant and highly penetrant. The underlying molecular disruption in schwannomatosis is a pattern of somatic *NF2* gene inactivation incompatible with NF1 or NF2, associated with alterations in

the SMARCB1 (hSnf5/INI1) tumor suppressor gene in familial disease.[164,165]

Genetics of Paragangliomas

Paragangliomas of the head and neck are rare, mostly benign tumors. The hereditary paraganglioma syndromes are autosomal-dominant conditions with increased risk for multifocal tumors of the sympathetic and parasympathetic neuroendocrine systems. Approximately 30% of paraganglioma patients harbor a germline mutation, which is carried by all of the cells of the body (as opposed to a somatic mutation, which is only found in the tumor tissues). In more than a third of these patients, there is no prior family history thus representing new mutations.

Ten to 15% of paragangliomas are caused by mutations in the succinate dehydrogenase (SDH) genes or its anchoring subunits B, C, or D.[166] They may be hormone secreting. Malignant paragangliomas have been particularly associated with mutations in SDHB, but have also been reported in SDHD.[167] The succinate dehydrogenase genes provide a protein that is a small part of the cytochrome *b* complex in the mitochondrial complex II, one of the five protein assemblies or complexes that form the electron transport chain. By production of reactive oxygen molecules, this pathway is considered important in the signaling and detection of oxygen tension. The gene encoding SDHD consist of 4 exons and yields 159 amino acid polypeptides.[168]

Other mutations found to be associated with paragangliomas include the prolyl hydroxylase domain (PHD) proteins, which play a major role in regulating the hypoxia-inducible factor (HIF) that induces expression of genes involved in angiogenesis, erythropoiesis, and cell metabolism, proliferation, and survival. Mutations in the prolyl hydroxylase domain 2 gene (PHD2) have recently been described in a patient with erythrocytosis and recurrent paragangliomas.[169]

SUMMARY

The discovery of molecular mechanisms underlying VS formation is moving forward. Understanding merlin's function and its interactions with other proteins and signaling pathways, and regulation of the *NF2* gene will eventually lead to the development of novel treatments for VS. Ultimately, drug therapies will be designed to stop schwannoma progression. This will offer alternatives to the current options of untreated observation of tumor growth, stereotactic radiation, or surgical removal.

References

1. Trofatter JA, MacCollin MM, Rutter JL, et al. A novel moesin-, ezrin-, radixin-like gene is a candidate for the neurofibromatosis 2 tumor-suppressor. Cell 1993;72:791–800.
2. Rouleau GA, Merel P, Lutchman M, et al. Alteration in a new gene encoding a putative membrane-organizing protein causes neurofibromatosis type 2. Nature 1993;363:515–21.
3. Welling DB, Guida M, Goll F, et al. Mutational spectrums in the neurofibromatosis type 2 gene in sporadic and familial schwannomas. Hum Genet 1996;98:189–93.
4. Chen Y, Gutmann DH, Haipek CA, et al. Characterization of chicken Nf2/merlin indicates regulatory roles in cell proliferation and migration. Dev Dyn 2004;229:541–54.
5. Welling DB, Lasak JM, Akhmametyeva E, et al. cDNA microarray analysis of vestibular schwannomas. Otol Neurotol 2002 Sep;23(5):736–48.
6. Chang LS, Jacob A, Lorenz M, et al. Growth of benign and malignant schwannoma xenografts in severe combined immunodeficiency mice. Laryngoscope 2006 Nov;116(11):2018–26.
7. Tos M, Thomsen J, Charabi S. Incidence of acoustic neuromas. Ear Nose Throat J 1992;71:391–3.
8. Howitz MF, Johansen C, Tos M, et al. Incidence of vestibular schwannoma in denmark, 1977–95. Amer J Otol 2000;21:690–4.
9. Anderson TD, Loevner LA, Bigelow DC, Mirza N. Prevalence of unsuspected acoustic neuroma found by magnetic resonance imaging. Otolaryngol Head Neck Surg 2000;122:643–6.
10. Bull World Health Org. Prevention and control of neurofibromatosis: memorandum from a joint WHO/NNFF meeting. 1992;70:173–82.
11. Fontaine B, Rouleau GA, Seizinger BR, et al. Molecular genetics of neurofibromatosis 2 and related tumors (acoustic neuroma and meningioma). Ann NY Acad Sci 1991;615:338–43.
12. Kaiser-Kupfer M, Freidlin V, Datiles MB, et al. The association of posterior capsular lens opacities with bilateral acoustic neuromas in patients with neurofibromatosis type 2. Arch Ophthalmol 1989;107:541–4.
13. Kanter WR, Eldridge R, Fabricant R, et al. Central neurofibromatosis with bilateral acoustic neuroma: Genetic, clinical and biochemical distinctions from peripheral neurofibromatosis. Neurology 1980;30:851–9.
14. Martuza RL, Eldridge R. Neurofibromatosis 2 (bilateral acoustic neurofibromatosis). New Engl J Med 1988;318:684–8.
15. Evans DGR, Huson SM, Donnai D, et al. A clinical study of type 2 neurofibromatosis. Q J Med 1992;84:603–18.
16. Evans DGR, Huson SM, Donnai D, et al. A genetic study of type 2 neurofibromatosis in the united kingdom. I: prevalence, mutation rate, fitness, and confirmation of maternal transmission effect on severity. J Med Genet 1992;29:841–6.
17. Wishart JH. Case of tumors in skull, dura mater, and brain. Edinburgh Med Surg J 1822;18:393–7.
18. Gardner WJ, Frazier CH. Bilateral acoustic neurofibromatosis: a clinical study and field survey of a family of five generations with bilateral deafness in thirty-eight members. Arch Neurol Psychiatry 1930;23:266–302.
19. Evans DGR, Wallace AJ, Wu CL,et al. Somatic mosaicism: a common cause of classic disease in tumor-prone syndromes? Lessons from type 2 neurofibromatosis. Am J Hum Genet 1998;63:727–36.
20. Ruggieri M, Huson SM. The clinical and diagnostic implications of mosaicism in neurofibromatosis. Neurology 2001;56:1433–43.
21. Kluwe L, Mautner VF, Heinrich B, et al. Molecular study of frequency of mosaicism in neurofibromatosis 2 patients with bilateral vestibular schwannomas. J Med Genet 2003;40:109–14.
22. Moyhuddin A, Baser ME, Watson C, et al. Somatic mosaicism in neurofibromatosis 2: Prevalence and risk of disease transmission to offspring. J Med Genet 203;40:459–63.
23. Kameyama S, Tanaka R, Kawaguchi T, et al. Cystic acoustic neurinomas: studies of 14 cases. Acta Neurochir 1996;138:695–9.
24. Charabi S, Tos M, Thomsen J, et al. Cystic vestibular schwannoma-clinical and experimental studies. Acta Otolaryngol (Suppl) 2000;543:11–3.

25. Charabi S, Tos M, Borgesen SE, Thomsen J. Cystic acoustic neuromas. Results of translabyrinthine surgery. Arch Otolaryngol Head Neck Surg 1994;120:1333–8.
26. Fundova P, Charabi S, Tos M,Thomsen J. Cystic vestibular schwannoma: surgical outcome. J Laryngol Otol 2000;114:935–9.
27. Pendl G, Ganz JC, Kitz K, Eustacchio S. Acoustic neuromas with macrocysts treated with gamma knife radiosurgery. Stereotact Funct Neurosurg 1995;66 (Suppl 1):103–11.
28. Shirato H, Sakamoto T, Takeichi N, et al. Fractionated stereotactic radiotherapy for vestibular schwannoma (VS): comparison between cystic-type and solid-type VS. Int J Radiat Oncol Biol Phys 2000;48:1395–401.
29. Rouleau GA, Wertelecki W, Haines JL, et al. Genetic linkage of bilateral acoustic neurofibromatosis to a DNA marker on chromosome 22. Nature 1987;329:246–8.
30. Wertelecki W, Rouleau GA, Superneau DW, et al. Neurofibromatosis 2: clinical and DNA linkage studies of a larger kindred. New Engl J Med 1988;319:278–83.
31. Welling DB. Clinical manifestations of mutations in the neurofibromatosis type 2 gene in vestibular schwannomas (acoustic neuromas). Laryngoscope 1998;108:178–89.
32. Jacoby LB, MacCollin MM, Barone R, et al. Frequency and distribution of NF2 mutations in schwannomas. Genes Chrom Cancer 1996;17:45–55.
33. Irving RM, Harada T, Moffat DA, et al. Somatic neurofibromatosis type 2 gene mutations and growth characteristics in vestibular schwannoma. Amer J Otol 1997;18:754–60.
34. Lekanne Deprez RH, Bianchi AB, Groen NA, et al. Frequent NF2 gene transcript mutations in sporadic meningiomas and vestibular schwannomas. Am J Hum Genet 1994;54:1022–9.
35. Merel P, Hoang-Xuan K, Sanson M, et al. Predominant occurrence of somatic mutations of the NF2 gene in meningiomas and schwannomas. Genes Chrom Cancer 1995;13:1211–6.
36. Merel P, Khe HX, Sanson M, et al. Screening for germ-line mutations in the NF2 gene. Genes Chrom Cancer 1995;12:117–27.
37. Lasota J, Fetsch JF, Wozniak A, et al. The neurofibromatosis type 2 gene is mutated in perineurial cell tumors: A molecular genetic study of eight cases. Am J Pathol 2001;158:1223–9.
38. Bianchi AB, Hara T, Ramesh V, et al. Mutations in transcript isoforms of the neurofibromatosis 2 gene in multiple human tumour types. Nat Genet 1994;6:185–92.
39. Bianchi AB, Mitsunnaga SI, Cheng JQ, et al. High frequency of inactivating mutations in the neurofibromatosis type 2 gene (NF2) in primary malignant mesotheliomas. Proc Natl Acad Sci USA 1995;92:10854–8.
40. Ruttledge MH, Sarrazin J, Rangaratnam S, et al. Evidence for the complete inactivation of the NF2 gene in the majority of sporadic meningiomas. Nat Genet 1994;6:180–4.
41. Sekido Y, Pass HI, Bader S, et al. Neurofibromatosis type 2 (NF2) gene is somatically mutated in mesothelioma but not in lung cancer. Cancer Res 1995;55:1227–31.
42. Deguen B, Goutebroze L, Giovannini M, et al. Heterogeneity of mesothelioma cell lines as defined by altered genomic structure and expression of the NF2 gene. Int J Cancer 1998;77:554–60.
43. Sanson M, Marineau C, Desmaze C, et al. Germline detection in a neurofibromatosis type 2 kindred inactivates the NF2 gene and a candidate meningioma locus. Hum Mol Genet 1993;2:1215–20.
44. MacCollin M, Mohney T, Trofatter JA, et al. DNA diagnosis of neurofibromatosis 2. altered coding sequence of the merlin tumor suppressor in an extended pedigree. JAMA 1993;270:2316–20.
45. MacCollin MM, Ramesh V, Jacoby LB, et al. Mutational anaylsis of patients with neurofibromatosis 2. Am J Hum Genet 1994;55:314–20.
46. Irving RM, Moffat DA, Hardy DG, et al. Somatic NF2 gene mutations in familial and non-familial vestibular schwannoma. Hum Mol Genet 1994;3:347–50.
47. Jacoby LB, MacCollin MM, Louis DN, et al. Exon scanning for mutation of the NF2 gene in schwannomas. Hum Mol Genet 1994;3:413–9.
48. Jacoby LB, Jones D, Davis K, et al. Molecular analysis of the NF2 tumor-suppressor gene in schwannomatosis. Am J Hum Genet 1997;61:1293–302.
49. Sainz J, Figueroa K, Baser ME, et al. High frequency of nonsense mutations in the NF2 gene caused by C to T transitions in five CGA codons. Hum Genet 1995;4:137–9.
50. Sainz J, Figueroa K, Baser ME, et al. Identification of three neurofibromatosis type 2 (NF2) gene mutations in vestibular schwannomas. Hum Mol Genet 1996;97:121–3.
51. Sainz J, Huynh DP, Figueroa K, et al. Mutations of the neurofibromatosis type 2 gene and lack of the gene product in vestibular schwannomas. Hum Mol Genet 1994;3:885–91.
52. Twist EC, Ruttledge MH, Rousseau M, et al. The neurofibromatosis type 2 gene is inactivated in schwannomas. Hum Mol Genet 1994;3:147–51.
53. Bourn D, Carter SA, Mason S, et al. Germline mutations in the neurofibromatosis type 2 tumour suppressor gene. Hum Mol Genet 1994;3:813–6.
54. Bourn D, Evans DGR, Mason S, et al. Eleven novel mutations in the NF2 tumour suppressor gene. Hum Genet 1995;95:572–4.
55. Parry DM, MacCollin MM, Kaiser-Kupfer M, et al. Germ-line mutations in the neurofibromatosis 2 gene: Correlation with disease severity and retinal abnormalities. Am J Hum Genet 1996;59:529–39.
56. Ruttledge MH, Andermann AA, Phelan CM, et al. Type of mutation in the neurofibromatosis type 2 gene (NF2) frequently determines severity of disease. Am J Hum Genet 1996;59:331–42.
57. Gutmann DH, Geist RT, Xu HM, et al. Defects in neurofibromatosis 2 protein function can arise at multiple levels. Hum Mol Genet 1998;7:335–45.
58. Stokowski RP, Cox DR. Functional analysis of the neurofibromatosis type 2 protein by means of disease-causing point mutations. Am J Hum Genet 2000;66:873–91.
59. Ahronowitz I, Xin W, Kiely R, et al. Mutational spectrum of the NF2 gene: A meta-analysis of 12 years of research and diagnostic laboratory findings. Hum Mutat 2007;28:1–12.
60. Baser ME, Contributors to the International NF2 Mutation Database. The distribution of constitutional and somatic mutations in the neurofibromatosis 2 gene. Hum Mutat 2006;27: 297–306.
61. Gutmann DH, Hirbe AC, Haipek CA. Functional analysis of neurofibromatosis 2 (NF2) missense mutations. Hum Mol Genet 2001;10:1519–29.
62. Bruder CE, Hirvela C, Tapia-Paez I, et al. High resolution deletion analysis of constitutional DNA from neurofibromatosis type 2 (NF2) patients using microarray-CGH. Hum Mol Genet 2001;10:271–82.
63. Mautner VF, Baser ME, Kluwe L. Phenotypic variability in two families with novel splice-site and frameshift NF2 mutations. Hum Genet 1996;98:203–6.

64. Zhao Y, Kumar RA, Bader S, et al. Intrafamilial correlation of clinical manifestations in neurofibromatosis 2 (NF2). Genet Epidemiol 2002;23:245–59.
65. Bruder CE, Ichimura K, Blennow E, et al. Severe phenotype of neurofibromatosis type 2 in a patient with a 7.4-MB constitutional deletion on chromosome 22: possible localization of a neurofibromatosis type 2 modifier gene? Genes Chrom Cancer 1999;25:184–90.
66. Zucman-Rossi J, Legoix P, et al. NF2 gene in neurofibromatosis type 2 patients. Hum Mol Genet 1999;7:2095–101.
67. Kino T, Takeshima H, Nakao M, et al. Identification of the cis-acting region in the NF2 gene promoter as a potential target for mutation and methylation-dependent silencing in schwannoma. Genes Cells 2001;6:441–54.
68. Chang LS, Akhmametyeva EM, Wu Y, et al. Multiple transcription initiation sites, alternative splicing, and differential polyadenylation contribute to the complexity of human neurofibromatosis 2 transcripts. Genomics 2002 Jan;79(1):63–76.
69. Gonzalez-Gomez P, Bello MJ, Alonso ME, et al. CpG island methylation in sporadic and neurofibromatosis type 2-associated schwannomas. Clin Cancer Res 2003;9:5601–6.
70. Gutmann DH, Sherman L, Seftor L, et al. Increased expression of the NF2 tumor suppressor gene product, merlin, impairs cell motility, adhesion, and spreading. Hum Mol Genet 1999;8:267–75.
71. Algrain M, Arpin M, Louvard D. Wizardry at the cell cortex. Current Biol 1993;3:451–4.
72. Golovnina K, Blinov A, Akhmametyeva EM, et al. Evolution and origin of merlin, the product of the *neurofibromatosis type 2* (NF2) tumor-suppressor gene. BMC Evol Biol 2005;5:69–86.
73. Chishti AH, Kim AC, Marfatia SM, et al. The FERM domain: a unique module involved in the linkage of cytoplasmic proteins to the membrane. TIBS 1998;23:281–2.
74. Shimizu T, Seto A, Maita N, et al. Structural basis for neurofibromatosis type 2 crystal structure of the merlin FERM domain. J Biol Chem 2002;277:10332–6.
75. Bretscher A, Chambers D, Nguyen R, et al. ERM-merlin and EBP50 protein families in plasma membrane organization and function. Ann Rev Cell Dev Biol 2000;16:113–43.
76. Turunen O, Wahlstrom T, Vaheri A. Ezrin has a COOH-terminal actin-binding site that is conserved in the ezrin protein family. J Cell Biol 1994;126:1445–53.
77. Roy C, Martin M, Mangeat P. A dual involvement of the amino-terminal domain of ezrin in F- and G-actin binding. J Biol Chem 1997;272:20088–95.
78. Gonzalez-Agosti C, Xu L, Pinney D, et al. The merlin tumor suppressor localizes preferentially in membrane ruffles. Oncogene 1996;13:1239–47.
79. Pelton PD, Sherman LS, Rizvi TA, et al. Ruffling membrane, stress fiber, cell spreading and proliferation abnormalities in human schwannoma cells. Oncogene 1998;17:2195–209.
80. Deguen B, Merel P, Goutebroze L, et al. Impaired interaction of naturally occurring mutant NF2 protein with actin-based cytoskeleton and membrane. Hum Mol Genet 1998;7:217–26.
81. Lutchman M, Rouleau GA. The neurofibromatosis type 2 gene product, schwannomin, suppresses growth of NIH 3T3 cells. Cancer Res 1995;55:2270–4.
82. Sherman L, Xu HM, Geist RT, et al. Interdomain binding mediates tumor growth suppression by the NF2 gene product. Oncogene 1997;15:2505–9.
83. Tikoo A, Varga M, Ramesh V, et al. An anti-ras function of neurofibromatosis type 2 gene product (NF2/merlin). J Biol Chem 1994;269:23387–90.
84. McClatchey AI, Saotome I, Mercer K, et al. Mice heterozygous for a mutation at the NF2 tumor suppressor locus develop a range of highly metastatic tumors. Genes Dev 1998;12:1121–33.
85. McClatchey AI, Saotome I, Ramesh V, et al. The NF2 tumor suppressor gene product is essential for extraembryonic development immediately prior to gastrulation. Genes Dev 1997;11:1253–65.
86. Akhmametyeva EM, Mihaylova MM, Luo H, et al. Regulation of the neurofibromatosis 2 gene promoter expression during embryonic development. Dev Dyn 2006 Oct;235(10):2771–85.
87. Giovannini M, Robanus-Maandag E, van der Valk M, et al. Conditional bialleic *Nf2* mutation in the mouse promotes manifestations of human neurofibromatosis type 2. Genes Dev 2000;14:1617–30.
88. Kalamarides M, Niwa-Kawakita M, Leblois H, et al. *Nf2* gene inactivation in arachnoidal cells is rate-limiting for meningioma development in the mouse. Genes Dev 2002;16:1060–5.
89. Shaw RJ, Paez JG, Curto M, et al. The NF2 tumor suppressor, merlin, functions in rac-dependent signaling. Dev Cell 2001;1:63–72.
90. Sherman L, Sleeman J, Herrlich P, et al. Hyaluronate receptors: key players in growth, differentiation, migration and tumor progression. Curr Opin Cell Biol 1994;6:726–33.
91. Takeshima H, Izawa I, Lee PS, et al. Detection of cellular proteins that interact with the NF2 tumor suppressor gene product. Oncogene 1994;9:2135–44.
92. Sainio M, Zhao F, Heiska L, et al. Neurofibromatosis 2 tumor suppressor protein colocalizes with ezrin and CD44 and associates with actin-containing cytoskeleton. J Cell Sci 1997;110:2249–60.
93. Huang L, Ichimaru E, Pestonjamasp K, et al. Merlin differs from moesin in binding to F-actin and in its intra- and intermolecular interactions. Biochim Biophys Res Comm 1998;248:548–53.
94. Murthy A, Gonzalez-Agosti C, Cordero E, et al. NHE-RF, a regulatory cofactor for na(+)-H+ exchange, is a common interactor for merlin and ERM (MERM) proteins. J Biol Chem 1998;273:1273–6.
95. Obremski VJ, Hall AM, Fernandez-Valle C. Merlin, the neurofibromatosis type 2 gene product, and b1 integrin associate in isolated and differentiating schwann cells. J Neurobiol 1998;37:487–501.
96. Scoles DR, Huynh DP, Morcos PA, et al. Neurofibromatosis 2 tumor suppressor schwannomin interacts with bII-spectrin. Nat Genet 1998;18:354–9.
97. Xu HM, Gutmann DH. Merlin differentially associates with the microtubule and actin cytoskeleton. J Neurosci Res 1998;51:403–15.
98. Fernandez-Valle C, Tang Y, Ricard J, et al. Paxillin binds schwannomin and regulates its density-dependent localization and effect on cell morphology. Nat Genet 2000;31:354–62.
99. Gonzalez-Agosti C, Wiederhold T, Herndon ME, et al. Interdomain interaction of merlin isoforms and its influence on intermolecular binding to NHE-RF. J Biol Chem 1999;274:34438–42.
100. Goutebroze L, Brault E, Muchardt C, et al. Cloning and characterization of SCHIP-1, a novel protein interacting specifically with spliced isoforms and naturally occurring mutant NF2 proteins. Mol Cell Biol 2000;20:1699–712.

101. Herrlich P, Morrison H, Sleeman J, et al. CD44 acts both as a growth and invasiveness-promoting molecule and as a tumor-suppressing cofactor. Ann NY Acad Sci 2000;910:106–18.
102. Scoles DR, Huynh DP, Chen MS, et al. The neurofibromatosis 2 tumor suppressor protein interacts with hepatocyte growth factor-regulated tyrosine kinase substrate. Hum Mol Genet 2000;9:1567–74.
103. Gronholm M, Vossebein L, Carlson CR, et al. Merlin links to the cAMP neuronal signaling pathway by anchoring the R1 beta subunit of protein kinase A. J Biol Chem 2003;278:41167–72.
104. Kissil JL, Wilker EW, Johnson KC, et al. Merlin, the product of the NF2 tumor suppressor gene, is an inhibitor of the p21-activated kinase, PAK1. Mol Cell 2003;12:841–9.
105. Lallemand D, Curto M, Saotome I, et al. NF2 deficiency promotes tumorigenesis and metastasis by destabilizing adherens junctions. Genes Dev 2003;17:1090–100.
106. Rong R, Tang X, Gutmann DH, et al. Neurofibromatosis 2 (NF2) tumor suppressor merlin inhibits phosphatidylinositol 3-kinase through binding to PIKE-L. Proc Natl Acad Sci USA 2004;101:18200–5.
107. Rangwala R, Banine F, Borg JP, Sherman LS. Erbin regulates mitogen-activated protein (MAP) kinase activation and MAP kinase-dependent interactions between merlin and adherens junction protein complexes in schwann cells. J Biol Chem 2005;280:11790–7.
108. Morrison H, Sherman LS, Legg J, et al. The NF2 tumor suppressor gene product, merlin, mediates contact inhibition of growth through interactions with CD44. Genes Dev 2001;15:968–80.
109. Flaiz C, Utermark T, Parkinson DB, et al. Impaired intercellular adhesion and immature adherens junctions in merlin-deficient human primary schwannoma cells. Glia 2008;56:506–15.
110. Surace EI, Haipek CA, Gutmann DH. Effect of merlin phosphorylation on neurofibromatosis 2 (NF2) gene function. Oncogene 2004;23:580–7.
111. Okada T, Lopez-Lago M, Giancotti FG. Merlin/NF-2 mediates contact inhibition of growth by suppressing recruitment of rac to the plasma membrane. J Cell Biol 2005;171:361–71.
112. Nakai Y, Zheng Y, MacCollin MM, Ratner N. Temporal control of rac in schwann cell–axon interaction is disrupted in NF2-mutant schwannoma cells. J Neurosci 2006;26:3390–5.
113. Xiao GH, Beeser A, Chernoff J, et al. P21-activated kinase links Rac/Cdc42 signaling to merlin. J Biol Chem 2002;277:883–6.
114. Kissil JL, Johnson KC, Eckman MS, et al. Merlin phosphorylation by p21-activated kinase 2 and effects of phosphorylation on merlin localization. J Biol Chem 2002;277:10394–9.
115. Jin H, Sperka T, Herrlich P, Morrison H. Tumorigenic transformation by CPI-17 through inhibition of a merlin phosphatase. Nature 2006;442:576–9.
116. Bretscher A, Reczek D, Berryman M. Ezrin: a protein requiring conformational activation to link microfilaments to the plasma membrane in the assembly of cell surface structures. J Cell Sci 1997;110:3011–8.
117. Tsukita S, Yonemura S, Tsukita S. ERM proteins: Head-to-tail regulation of actin-plasma membrane interaction. TIBS 1997;22:53–8.
118. Hirao M, Sato N, Kondo T, et al. Regulation mechanism of ERM (ezrin/radixin/moesin) protein/plasma membrane association: possible involvement of phosphatidylinositol turnover and rho-dependent signaling pathway. J Cell Biol 1996;135:37–51.
119. Gutmann DH, Haipek CA, Hoang Lu K. Neurofibromatosis 2 tumor suppressor protein, merlin, forms two functionally important intramolecular associations. J Neurosci Res 1999;58:706–16.
120. Gutmann DH, Haipek CA, Burke SP, et al. The *NF2* interactor, hepatocyte growth factor-regulated tyrosine kinase substrate (HRS), associates with merlin in the 'open' conformation and suppresses cell growth and motility. Hum Mol Genet 2001;10:825–34.
121. Pearson MA, Reczek D, Bretscher A, et al. Structure of the ERM protein moesin reveals the FERM domain fold masked by an extended actin binding tail domain. Cell 2000;101:259–70.
122. Komada M, Kitamura N. Growth factor-induced tyrosine phosphorylation of hrs, a novel 115-kilodalton protein with a structurally conserved putative zinc finger domain. Mol Cell Biol 1995;15:6213–21.
123. Jacob A, Lee TX, Neff BA, et al. Phosphatidylinositol 3 kinase/AKT pathway activation in human vestibular schwannoma. Otol Neurotol 2008;29:58–68.
124. Welling DB, Akhmametyeva EM, Daniels RL, et al. Analysis of the human neurofibromatosis type 2 gene promoter and its expression. Otolaryngol Head Neck Surg 2000 Oct;123(4):413–8.
125. Arakawa H, Hayashi N, Nagase H, et al. Alternative splicing of the NF2 gene and its mutation analysis of breast and colorectal cancers. Hum Mol Genet 1994;3:565–8.
126. Hitotsumatsu T, Kitamoto T, Iwaki T, et al. An exon 8-spliced out transcript of neurofibromatosis 2 gene is constitutively expressed in various human tissues. J Biochem 1994;116:1205–7.
127. Koga H, Araki N, Takeshima H, et al. Impairment of cell adhesion by expression of the mutant neurofibromatosis type 2 (NF2) gene which lacks exons in the ERM-homology domain. Oncogene 1998;17:801–10.
128. Nishi T, Takeshima H, Hamada K, et al. Neurofibromatosis 2 gene has novel alternative splicing which control intracellular protein binding. Int J Oncol 1997;10:1025–9.
129. Pykett MJ, Murphy M, Harnish PR, et al. The neurofibromatosis type 2 tumor suppressor gene encodes multiple alternatively spliced transcripts. Hum Mol Genet 1994;3(559):564.
130. Schmucker B, Tang Y, Kressel M. Novel alternatively spliced isoforms of the neurofibromatosis type 2 tumor suppressor are targeted to the nucleus and cytoplasmic granules. Hum Mol Genet 1999;8:1561–70.
131. Giovannini M, Robanus-Maandag E, Niwa-Kawakita M, et al. Schwann cell hyperplasia and tumors in transgenic mice expressing a naturally occurring mutant NF2 protein. Genes Dev 1999;13:978–86.
132. Labit-Bouvier C, Crebassa B, Bouvier C, et al. Clinicopathologic growth factors in vestibular schwannomas: A morphological and immunohistochemical study of 69 tumours. Acta Otolaryngol 2000;120:950–4.
133. Niemczyk K, Vaneecloo FN, Lecomte MH, et al. Correlation between ki-67 index and some clinical aspects of acoustic neuromas (vestibular schwannomas). Otolaryngol Head Neck Surg 2000;123:779–83.
134. Light JP, Roland JT, Jr, Fishman A, et al. Atypical and low-grade malignant vestibular schwannomas: Clinical implications of proliferative activity. Otol Neurotol 2001;22:922–7.
135. Chen JM, Houle S, Ang LC, et al. A study of vestibular schwannomas using positron emission tomography and monoclonal antibody ki-67. Am J Otol 1998;19:840–5.

136. Kesterson L, Shelton C, Dressler L, et al. Clinical behavior of acoustic tumors. A flow cytometric analysis. Arch Otolaryngol Head Neck Surg 1993;119:269–71.
137. Cardillo MR, Filipo R, Monini S, et al. Transforming growth factor-b1 expression in human acoustic neuroma. Am J Otol 1999;20:65–8.
138. Charabi S, Mantoni M, Tos M, et al. Cystic vestibular schwannomas: neuroimaging and growth rate. J Laryngol Otol 1994;108:375–9.
139. Charabi S, Klinken L, Tos M, Thomsen J. Histopathology and growth pattern of cystic acoustic neuromas. Laryngoscope 1994;104:1348–52.
140. Antinheimo J, Haapasalo H, Seppala M, et al. Proliferative potential of sporadic and neurofibromatosis 2-associated schwannomas as studied by MIB-1 (ki-67) and PCNA labeling. J Neuropathol Exp Neurol 1995;54:776–82.
141. Aguiar PH, Tatagiba M, Samii M, et al. The comparison between the growth fraction of bilateral vestibular schwannomas in neurofibromatosis 2 (NF2) and unilateral vestibular schwannomas using the monoclonal antibody MIB1. Acta Neurochir 1995;134:40–5.
142. Neff BA, Oberstien E, Lorenz M, et al. Cyclin D(1) and D(3) expression in vestibular schwannomas. Laryngoscope 2006 Mar;116(3):423–6.
143. Bassett DEJ, Eisen MB, Boguski MS. Gene expression informatics—it's all in your mind. Nat Genet 1999;21:51–5.
144. Lockhart DJ, Winzeler EA. Genomics, gene expression, and DNA arrays. Nature 2000;405:827–36.
145. Lasak JM, Welling DB, Akhmametyeva EM, et al. Retinoblastoma-cyclin-dependent kinase pathway deregulation in vestibular schwannomas. Laryngoscope 2002 Sep;112(9):1555–61.
146. Evans DGR, Birch JM, Ramsden RT, et al. Malignant transformation and new primary tumours after therapeutic radiation for benign disease: substantial risks in certain tumour prone syndromes. J Med Genet 2006;43:289–94.
147. Preston DL, Ron E, Yonehara S, et al. Tumors of the nervous system and pituitary gland associated with atomic bomb radiation exposure. J Natl Cancer Inst 2002;94:1555–63.
148. Schneider AB, Ron E, Lubin J, et al. Acoustic neuromas following childhood radiation treatment for benign conditions of the head and neck. Neuro Oncol 2008;10:73–8.
149. Hardell L, Carlberg M, Soderquist F, Mild KH. Meta-analysis of long-term mobile phone use and the association with brain tumors. Int J Oncol 2008;32:1097–103.
150. Hardell L, Carlberg M, Soderquist F, et al. Long-term use of cellular phones and brain tumours: Increased risk associated with use for > or = 10 years. Occup Environ Med 2007;64:626–32.
151. Evans DGR, Sainio M, Baser ME. Neurofibromatosis type 2. J Med Genet 2000;37:897–904.
152. Neff BA, Welling DB. Current concepts in the evaluation and treatment of neurofibromatosis type II. Otolaryngol Clin North Am 2005 Aug;38(4):671,684, ix.
153. Evans DG, Baser ME, O'Reilly B, et al. Management of the patient and family with neurofibromatosis 2: A consensus conference statement. Br J Neurosurg 2005;19:5–12.
154. Messerli SM, Prabhakar S, Tang Y, et al. Treatment of schwannomas with an oncolytic recombinant herpes simplex virus in murine models of neurofibromatosis type 2. Hum Gene Ther 2006;17:20–30.
155. Hansen MR, Roehm PC, Chatterjee P, Green SH. Constitutive neuregulin-1/ErbB signaling contributes to human vestibular schwannoma proliferation. Glia 2006;53:593–600.
156. Doherty JK, Ongekeko W, Crawley B, et al. ErbB and nrg potential targets for vestibular schwannoma pharmacotherapy. Otol Neurotol 2008;29:50–7.
157. Welch EM, Barton ER, Zhuo J, et al. PTC124 targets genetic disorders caused by nonsense mutations. Nature 2007;447:87–91.
158. Schmitz A, Famulok M. Chemical biology: ignore the nonsense. Nature 2007;447:42–3.
159. Pirker R, Filipits M. Targeted therapies in lung cancer. Curr Pharm Des 2009;15:188–206.
160. Aragon-Ching JB, Dahut WL. The role of angiogenesis inhibitors in prostate cancer. Cancer J 2008;14:20–5.
161. Ranieri G, Patruno R, Ruggieri E, et al. Vascular endothelial growth factor (VEGF) as a target of bevacizumab in cancer: from the biology to the clinic. Curr Med Chem 2006;13:1845–57.
162. Chase JL. Clinical use of anti-vascular endothelial growth factor monoclonal antibodies in metastatic colorectal cancer. Pharmacotherapy 2008;28:23S–30S.
163. MacCollin MM, Chiocca EA, Evans DGR, et al. Diagnostic criteria for schwannomatosis. Neurology 2005;18:38–45.
164. Boyd C, Smith MJ, Kluwe L, et al. Alterations in the SMARCB1 (INI1) tumor suppressor gene in familial schwannomatosis. Clin Genet 2008;74:358–66.
165. Sestini R, Bacci C, Provenzano A, et al. Evidence of a four-hit mechanism involving SMARCB1 and NF2 in schwannomatosis-associated schwannomas. Hum Mutat 2008;29:227–31.
166. Papaspyrou K, Rossmann H, Fottner C, et al. Malignant paraganglioma caused by a novel germline mutation of the succinate dehydrogenase D-gene: A case report. Head Neck 2008;30:964–9.
167. Marvin ML, Bradford CR, Sisson JC, Gruber SB. Diagnosis and management of hereditary paraganglioma syndrome due to the F933>X67 SDHD mutation. Head Neck 2009;31:689–94.
168. Mhatre AN, Lalwani AK. Molecular genetics in neurotology. In: Jackler RK, Brackmann DE, editors. Neurotology. Philadelphia, PA: Ellsevier Mosby; 2005.
169. Ladroue C, Carcenac R, Leporrier M, et al. PHD2 mutation and congenital erythrocystosis with paraganglioma. N Engl J Med 2008;359:2685–92.